CHERT AND DOLOMITE IN THE AMURI LIMESTONE GROUP AND WOOLSHED FORMATION, EASTERN MARLBOROUGH, NEW ZEALAND.

A thesis
submitted in partial fulfilment
of the requirements for the degree
of
Doctor of Philosophy
at the
University of Canterbury
by

MARK JOHN FREDERICK LAWRENCE

University of Canterbury
1989

with 11 separate items in back pocket.

ABSTRACT

Chert and dolomite in sediments of coastal Marlborough occur in the detrital units of the Upper Iwitahi Group (Woolshed Formation (WF) and Claverley Sandstone - Late Cretaceous), and in Late Cretaceous - Early Tertiary micritic sediments (foraminiferal nannofossil oozes) of the Amuri Limestone Group (ALG). All sediments were deposited in a NW-SE trending trough. Chert and dolomite are generally restricted to what was the deepest part of the basin. There is a greater volume of chert than dolomite.

Two chronologically and stratigraphically separated types of dolomite occur: concretions of aphanitic dolomite in the WF, and phaneritic, rhombic dolomite in beds, lenses, or disseminated in chert or micrite in the ALG. Both dolomite types are moderately well ordered but Ca-rich. Isotopic and elemental analyses indicate all dolomites formed in wholly marine sediments at temperatures <60°C, in association with sulphate reduction, in the upper sediment column. Concretions formed from the dolomitization of early diagenetic calcite whereas in the ALG primary depositional carbonate was dolomitized. Mg^{2+} was supplied by seawater, with dolomite formation restricted by the presence of dissolved SO_4^{2-}.

Chert formation in the WF is limited. Most chertification occurs in the lower ALG. Chert consists predominantly of quartz with rare opal-CT. SiO_2 concentrations are usually $\geq$90 weight% with all other elements forming trace components, except in detrital-rich cherts where SiO_2 concentrations may be <90 weight percent. The chert chemistry is consistent with replacement of primary carbonate and the expulsion of carbonate-bound elements from the site of chert formation, effectively diluting noncarbonate-bound insoluble residue. Formation was by precipitation of either opal-CT or quartz depending on SiO_2 saturation conditions. Isotopic analyses indicate formation temperatures similar to those of dolomite. The SiO_2 was initially derived from biogenic sources but large amounts are inferred to have been derived from the underlying WF. Clay mineral transformations in the WF produced SiO_2-rich pore waters through which ALG sediments are thought to have compacted. Initiation of silica deposition resulted from localized oxidation of the H_2S produced by SO_4^{2-} reduction. Initially deposited silica provided sites for further chertification.

Evidence for early chertification (such as differential compaction) have lead to development of a combined model for dolomite and chert formation in association with SO_4^{2-} reduction. Although chert and dolomite both commenced nucleation early, the initial rate of dolomite crystallization exceeded that of silica. The extent of dolomitization was governed by the SO_4^{2-} concentration in pore waters and by the availability of Mg^{2+}. Where SO_4^{2-} concentrations were too high no dolomite formed, only calcite recrystallized. Chertification, although slower than dolomitization, continued after the cessation of dolomite formation, chertifying undolomitized beds or parts of beds, and the matrix between dolomite crystals. The extent of chertification was governed by the availability of SiO_2. This model of contemporaneous chert and dolomite formation explains the alternation of chert and dolomite beds, the dissemination of dolomite in chert, and the distribution of chert and dolomite.

TABLE OF CONTENTS

CHAPTER 4 - DOLOMITE PETROLOGY AND GEOCHEMISTRY

APPENDIX 1 - METHODOLOGY

APPENDIX 2 - DESCRIPTION OF LITHOLOGIES

APPENDIX 3 - DESCRIPTION OF PETROGRAPHY, MINERALOGY AND GEOCHEMISTRY OF LIMESTONES

APPENDIX - 4 DESCRIPTION OF PETROGRAPHY, MINERALOGY, AND GEOCHEMISTRY OF DETRITAL SEDIMENTS

APPENDIX 5 - DESCRIPTION OF PETROGRAPHY, MINERALOGY, AND GEOCHEMISTRY OF DOLOMITES

APPENDIX 7 - LITERATURE REVIEW

APPENDIX 11 - WHOLE ROCK CHERT AND DETRITAL SEDIMENT DATA

LIST OF FIGURES

LIST OF TABLES

CHAPTER 1

INTRODUCTION

1.1. AIMS AND OBJECTIVES

Although a number of authors have worked on the Amuri Limestone, many aspects of its geology are neither adequately described nor fully understood. The Amuri Limestone is an important and distinctive geological unit in the Cretaceous-Cenozoic stratigraphy of Marlborough. As such it is important to the NZ Geological Survey's Cretaceous-Cenozoic Project (CCP). The objectives of the CCP are (Officers of the New Zealand Geological Survey 1985, p12) *"to investigate and interpret the sedimentary rock succession to a uniform standard, to provide a data base of high quality for future hydrocarbon and sedimentary mineral exploration, and to pinpoint aspects of New Zealand's later geological history and earth resources needing further detailed investigation."* To this end the New Zealand Geological Survey (a division of the Department of Scientific and Industrial Research) established a research contract in the early 1980's to study the stratigraphy, structure, and geochemical and paleoenvironmental aspects of the Amuri Limestone in Marlborough. The study was envisaged as a co-operative project between the New Zealand Geological Survey and the University of Canterbury Geology Department. For a number of reasons the project was split in two; the first which encompassed the stratigraphy and paleoenvironmental interpretations was carried out by Morris (1987). The second, which is the subject of this thesis, is a study of the chert and dolomite in the Amuri Limestone. During the course of study, it became appropriate to include the upper part of the underlying unit (i.e. the Woolshed Formation).

The aims of the study are:

i) To describe the geographic distribution of chert and dolomite, modes of occurrence, and stratigraphic relationships.
ii) To document the mineralogy and geochemistry of the chert and dolomite.
iii) To develop an integrated model for the genesis of chert and dolomite.

1.2. LOCATION AND PHYSIOGRAPHY

The field area extends from Haumuri Bluffs and Oaro in the south to Cape Campbell in the north [Figure 1.1]. The western boundary is at the base of the inland Kaikoura Range [Figure 1.1]. Areas visited are confined to

Figure 1.1 Location of field area.

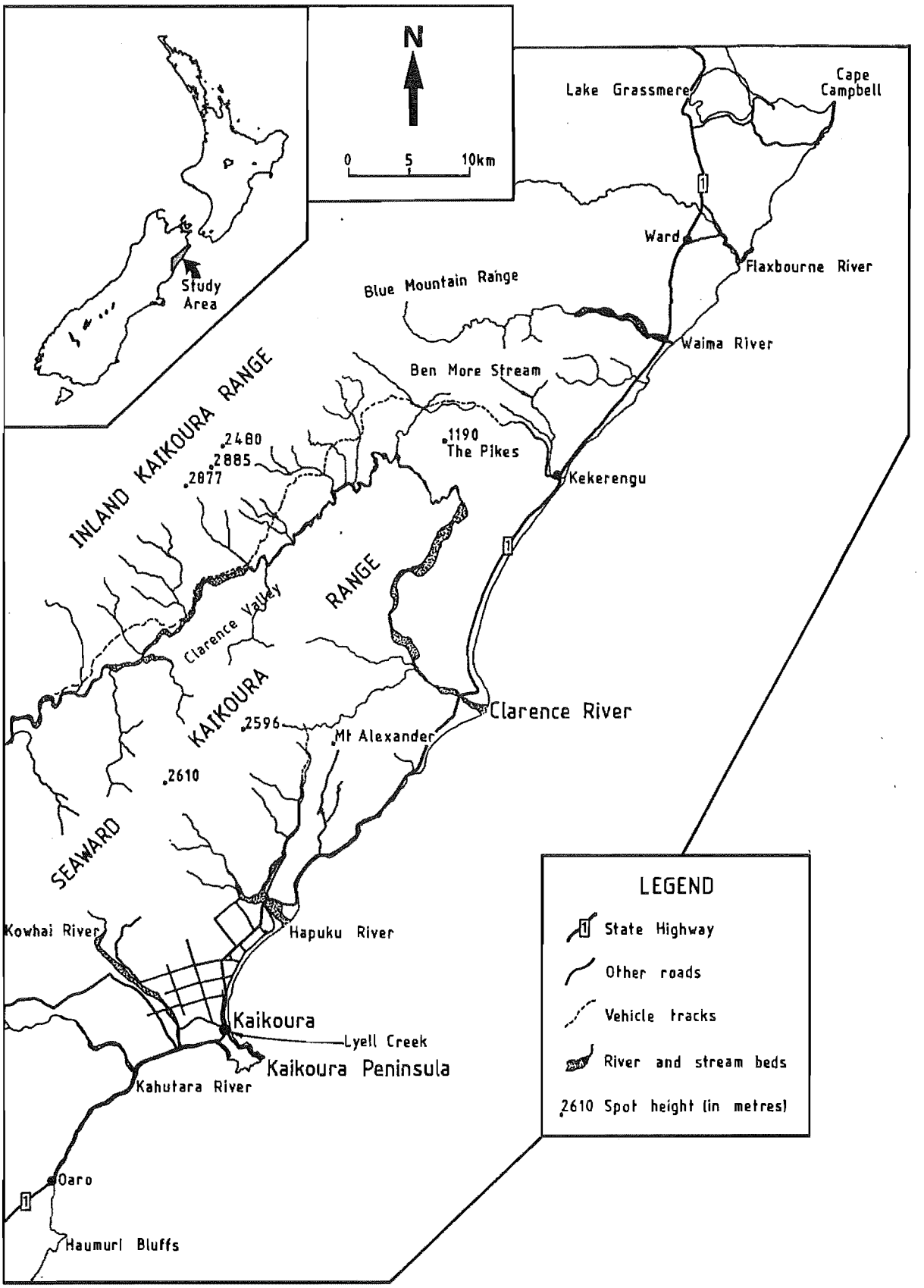
N
0 5 10km
Study Area
Lake Grassmere
Cape Campbell
Ward
Flaxbourne River
Blue Mountain Range
Waima River
Ben More Stream
1190
The Pikes
Kekerengu
INLAND KAIKOURA RANGE
2480
2885
2877
RANGE
Clarence Valley
KAIKOURA
2596
Mt Alexander
Clarence River
2610
SEAWARD
Kowhai River
Hapuku River
Kaikoura
Lyell Creek
Kaikoura Peninsula
Kahutara River
Oaro
Haumuri Bluffs
LEGEND
State Highway
Other roads
Vehicle tracks
River and stream beds
2610 Spot height (in metres)

the limits of the Amuri Limestone as shown in Figure 1.2.

The physiography of the field area is dominated by the Inland and Seaward Kaikoura Ranges [Figure 1.1]. The crests of the two ranges are about 15 km apart and trend approximately northeast-southwest. Separating the Ranges is the Clarence Valley. The Clarence River flows parallel to the Ranges until south of The Pikes where it has cut a narrow gorge through the northern end of the Seaward Kaikoura Ranges, then flows south before reaching the sea. The Inland Kaikoura Range, commonly with peaks in excess of 2000 m high, terminates where it intersects the Blue Mountain Range in the vicinity of the headwaters of the Waima River. The Seaward Kaikoura Range, which rises to about 2000 m within 10-15 km of the coastline, ends just south of Kekerengu. Due to the ruggedness of the terrain, access in the Clarence Valley is by 4-wheel drive tracks and on foot. Compared to the topography just described, the area north from the Waima River to Cape Campbell is of moderate relief. Coastal plains are limited to the area around Kaikoura Peninsula.

1.3. PROCEDURE

Field data were obtained from a series of measured (tape and compass survey) sections throughout the area. The locations of these sections, plus other localities mentioned in the text, are given in Figure 1.2.

Analytical work comprised petrographic and mineralogical determinations which utilized thin section petrography, scanning electron microscopy, x-ray diffraction, and cathodoluminescence. Geochemical analyses were performed on carbonate and silica phases separately, so that data did not have to be recalculated on a carbonate or silica free basis. The bulk of geochemical data is from chert or carbonate whole rock analyses, x-ray fluorescence (cherts) and atomic absorption spectroscopy (carbonates). Mass spectrometry was used for isotope determinations. Dolomites, such as those encountered in this study ideally should be analyzed by point analyzers, that is microprobes. However, such equipment often lacks the necessary sensitivity, particularly for Sr, Na, K, Mn, and Fe (Veizer *et al.* 1978). The size of the electron beam also imposes analytical limitations. Crystals analyzed must be of a size that the beam covers only a single crystal at a time, to avoid contamination by other crystals or minerals. Thus, whole rock carbonate data is supplemented with single

Figure 1.2 Location of measured sections and other sample sites. An '*' indicates a sample locality that is not part of a measured section. The shading denotes the distribution of the Amuri Limestone. References in the text to coastal sections include those associated with the Puhi Puhi syncline.

1* Haumuri Bluffs
2* Oaro, beach platform
3 South Bay, Kaikoura Peninsula
4 Lab Rocks, Kaikoura Peninsula
5 Puhi Puhi River - adjacent to bridge
6* Clinton Stream
7 Jordan Stream-Puhi Puhi River Confluence (Jordan Stream)
8 Mt Alexander (informal name; section adjacent to but not at Mt Alexander)
9 Wharekiri Stream
10 Waipapa Bay - Railway cutting (Mororimu Stream)
11 Waipapa Bay-beach platform
12 Upper Gorge, Woodside Creek
13 Lower Gorge, Woodside Creek
14 South Wharanui Point (informal name)
15 Wharanui Point
16 Needles Point
17 Flaxbourne River Mouth
18 Chancet Rocks
19* Thomson's Gully (informal name)
20 Isolation Creek
21 Waima River
22* Whernside Spur
23 Swale Stream
24 Main channel and middle tributary, Mead Stream
25 Southern tributary, Mead Stream
26 Limburn Stream
27 Dee Stream
28 Middle tributary, Branch Stream
29 Southern tributary, Branch Stream
30 Northern tributary, Dart Stream
31 Southern tributary, Dart Stream
32 Northern tributary, Muzzle Stream
33 Southern tributary, Muzzle Stream
34 Dead Horse Gully
35 Upper Bluff Stream
36 Lower Bluff Stream
37 Bluff River

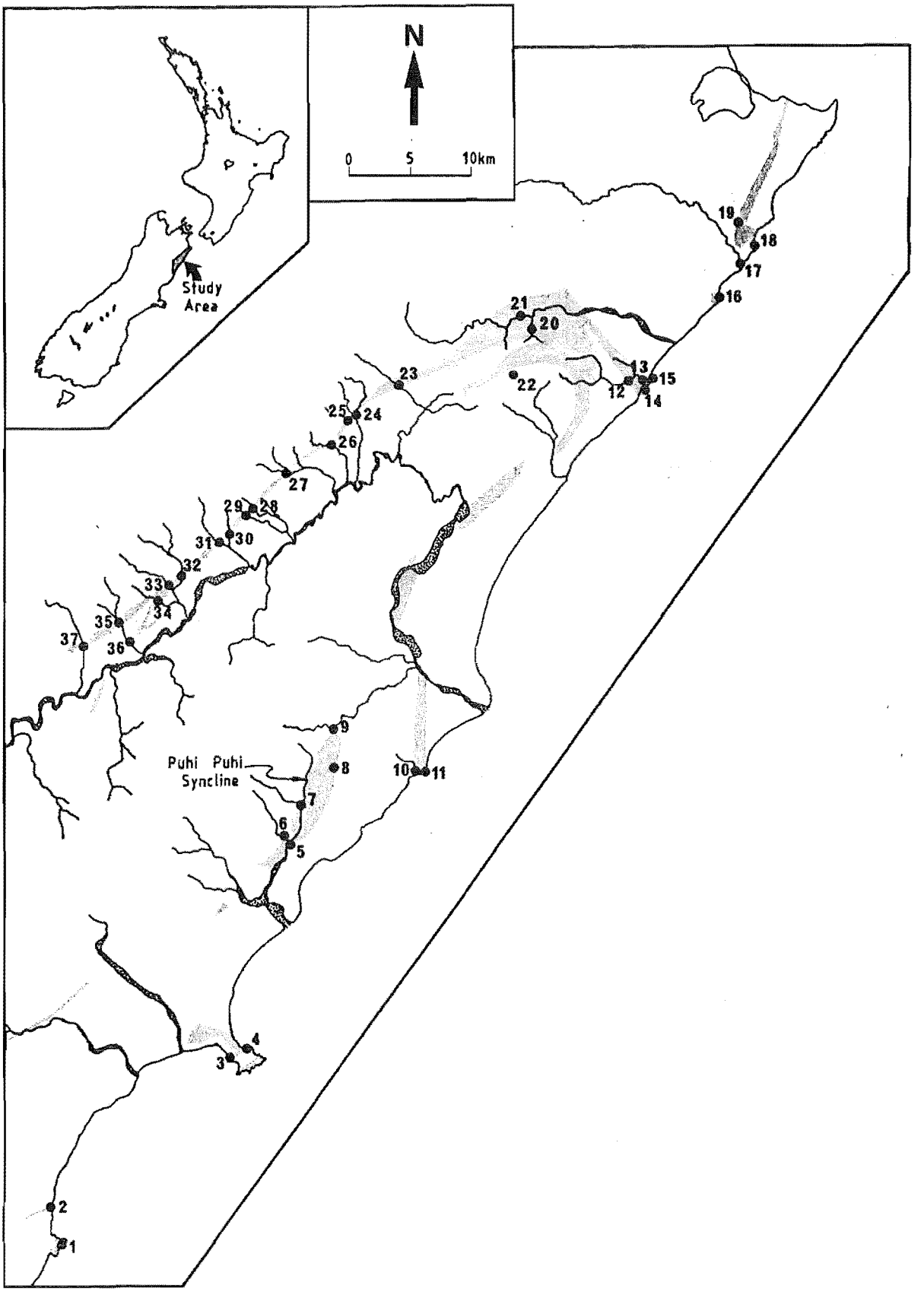
N
0
5
10km
Study Area
Puhi Puhi Syncline
1
2
3
4
5
6
7
8
9
10
11
12
13
14
15
16
17
18
19
20
21
22
23
24
25
26
27
28
29
30
31
32
33
34
35
36
37

crystal analyses only where practicable.

Sodium and K in carbonate phases were analyzed because they have been suggested as potential salinity indicators (Fritz and Katz 1972, Land and Hoops 1973). Strontium, which is known to substitute for Ca^{2+} in the carbonate lattice, was analyzed because, as suggested by Baum *et al.* (1985), it has the greatest potential of retaining a 'memory' of early stage diagenesis. Iron and Mn were analyzed to obtain information about redox conditions during deposition and diagenesis (e.g. Calderoni *et al.* 1988). Stable carbon and oxygen isotopes provide information about carbon sources ($\delta^{13}C$) and fluid temperatures and compositions ($\delta^{18}O$).

There is virtually no background information on the composition of Amuri Limestone siliceous phases. In addition, with the exception of SiO_2, most elements are in phases associated with cherts, rather than in the chert itself. For these reasons a much wider range of elements were analyzed than in the carbonates.

All methods are detailed in Appendix 1. Detailed stratigraphic columns and descriptions of lithologies are in Appendix 2. Appendices 3-6 contain descriptive petrography, mineralogy and geochemistry. Figure or section numbers prefixed by the letter 'A' cited in the main body of the thesis refer to Appendix figures or sections. Locality numbers from Figure 1.2 are included with sample localities mentioned in the text. References cited in the text and appendices are listed together in the reference section following Chapter 6.

1.4. DEFINITIONS AND USAGE

Micrite is a purely calcareous sediment with crystals <4 μm (Folk 1959). The term *marl* is used to describe clay-rich (smectitic; Fergusson 1985, Morris 1987), poorly cemented, calcareous mudstones commonly found throughout the Amuri Limestone Group sequence. As used by Pettijohn (1975) and in this thesis, *dolomite* is used as both a mineral name and a rock term. Micrites that contain abundant silica, commonly indicated by a high degree of induration and a conchoidal fracture, are termed *siliceous micrites*. *Stylobedding* describes bedding structures due to stylolitic partings, which may be parallel to, or at various angles to, the original sedimentary layering (Flügel 1982).

Chert is a dense, hard, vitreous rock, with a conchoidal fracture, which consists of one or several forms of microcrystalline or cryptocrystalline authigenic silica (Lancelot 1973, Pettijohn 1975, Hein *et al.* 1983). *Flint* is a term widely used as a synonym for chert and as a variety of usually dark or black chert. However, because of varied usage in the past this term should be restricted to siliceous artifacts, in line with the suggestion of Tarr (1938). A *bedded chert* shows a specific rhythmic interlayering with shale (or mudstone) partings (Iijima and Utada 1983). The shales are composed of detrital material. Chert *nodules* are three dimensional bodies of chert which are less than 1-2 m long, rounded or lensoid, and contained in carbonate or detrital sediments. Cherts, which are more elongated and/or planar and less rounded or lensoid than nodules, but still contained within limestone beds, and traceable for 2 m or more, are referred to as *chert bands*. Lithologies which have the outward appearance of micrite (e.g. colour, texture), but have been completely replaced by authigenic silica, are described as *silicified micrites*. *Silica* is used as a general term for silicon dioxide in all its forms. *Chertification* and *silicification* are essentially synonymous, and refer to the complete replacement of the host rock (Bates and Jackson 1984).

The bulk of cherts are varying shades of grey and also black. For descriptive purposes 'pale grey' cherts are those with colours ranging from medium light grey to medium dark grey (N6-N4, Goddard *et al.* 1970), and dark cherts are those which are dark grey to black (N3-N1).

Authigenic silica has been further subdivided on the basis of x-ray diffraction patterns (i.e. crystal ordering). The definitions used in this thesis are summarized from Jones and Segnit (1971), Berger and von Rad (1972), and Wise *et al.* (1972). *Opal-A* is a naturally occurring, highly disordered amorphous silica. X-ray diffraction patterns display a prominent diffuse band at 4.1Å. Opal-A is the main constituent of biogenic siliceous tests. Crystalline, natural hydrous, unidimensionally highly disordered α-cristobalite, or α-tridymite, is called *opal-CT*. It can occur as a cryptocrystalline spherulitic variety, referred to as lepispheres (e.g. Wise and Weaver 1974). X-ray diffraction patterns of opal-CT show broadened but well defined α-cristobalite peaks. The well ordered, natural hydrous α-cristobalite with α-cristobalite x-ray diffraction patterns is termed *opal-C*. *Cristobalite* is a chemically precipitated authigenic mineral and denotes an early phase in the

diagenesis of carbonate sediments and chert formation. It commonly forms spherules or lepispheres. *Chalcedony* is disordered, fibrous quartz with quartz x-ray diffraction peaks. Some authors have used the term chalcedony for all cryptocrystalline quartz, because both chalcedony and cryptocrystalline quartz have the same x-ray diffraction peaks. In this thesis chalcedony is restricted to fibrous quartz. *Quartz* can be cryptocrystalline, unoriented, or microcrystalline all of which show sharp quartz x-ray diffraction peaks.

1.5. REGIONAL GEOLOGY

The regional geology is summarized in Figure 1.3. A timescale with New Zealand stages is provided in Figure 1.4. Detailed discussions of Marlborough stratigraphy can be found in Hall (1964), Lensen (1962, 1978a,b), Prebble (1976, 1980), Warren (1978), Reay (1980), Ritchie (1986) and Morris (1987).

1.5.1. SUMMARY OF REGIONAL STRATIGRAPHY

The basement rocks of Marlborough consist of Torlesse Supergroup: flysch-like greywackes and argillites, with minor chert and lava (Warren 1978). Ages range from Late Triassic to Early Cretaceous (Lensen 1962, Warren 1978). The youngest Torlesse rocks in the area comprise the Sawtooth Group, which ranges in age from Korangan to Motuan (Ritchie 1986). The Sawtooth Group is interpreted as a submarine fan deposit.

Unconformably overlying the Sawtooth Group are non-Torlesse Coverham Group rocks. These rocks are generally Motuan in age but some Teratan ages have also been found (Lensen 1978a, Ritchie 1986). Lithologies consist of flysch-like alternating mudstones and sandstones, inferred to have been deposited below wave base in restricted basins (Ritchie 1986).

The Iwitahi Group unconformably overlies Motuan and older rocks. Lithologies consist of shallow marine and nonmarine sandstones, mudstone, coal measures and some volcanics (Lensen 1978a). Nonmarine deposits of central Marlborough grade into the marine lithologies of the Coverham area (Morris 1987). The Iwitahi Group ranges in age from Ngaterian to Late Haumurian (Lensen 1978a, Reay 1980). Upper and lower units of the Iwitahi Group are separated by a major hiatus. The hiatus is marked by an

Figure 1.3 General geology of field area.

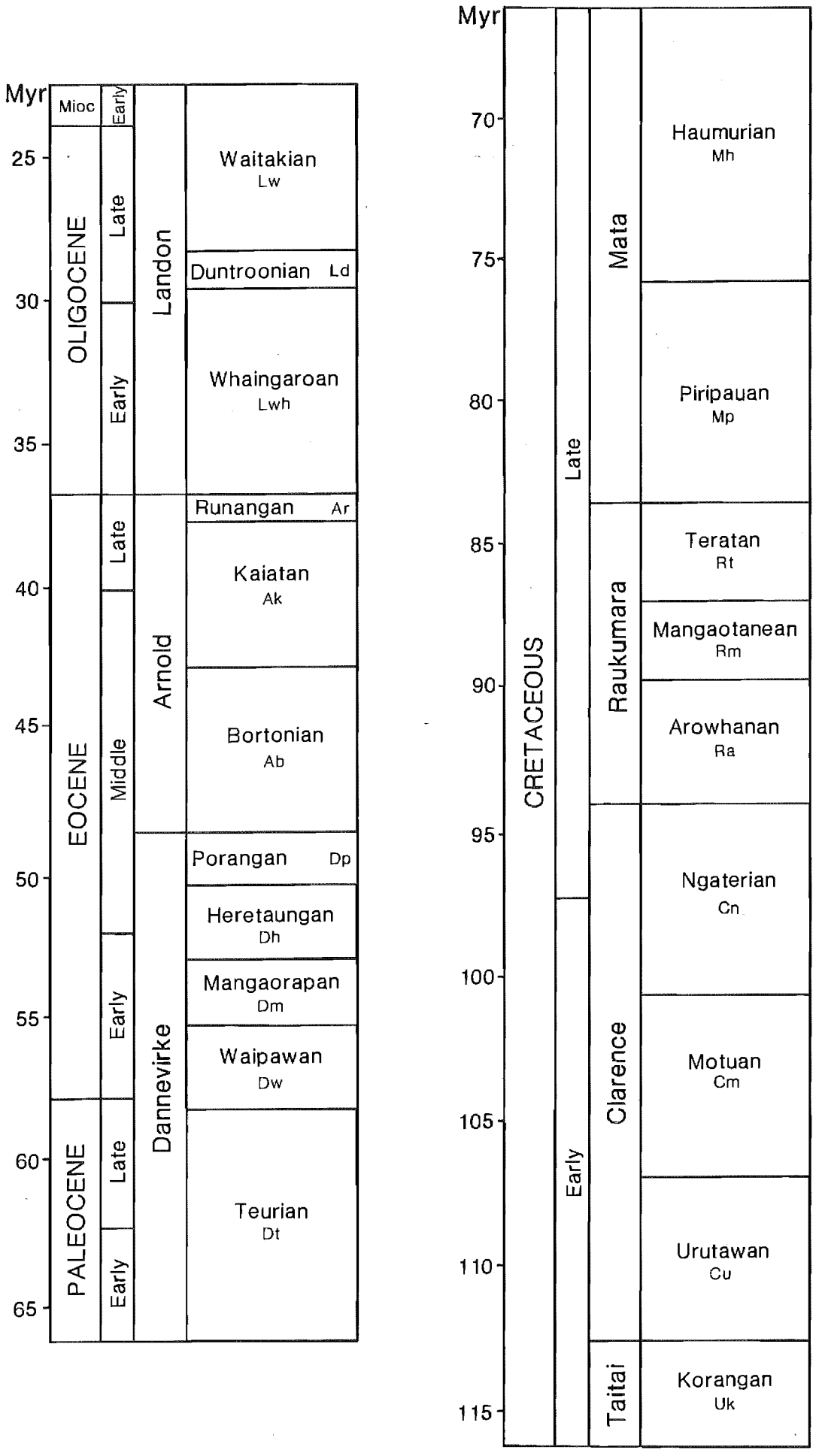
Myr
Mioc
Early
Late
Early
OLIGOCENE
Landon
Waitakian
Lw
Duntroonian Ld
Whaingaroan
Lwh
25
30
35
Late
Middle
Early
EOCENE
Arnold
Runangan Ar
Kaiatan
Ak
Bortonian
Ab
40
45
50
55
Late
Early
PALEOCENE
Dannevirke
Porangan Dp
Heretaungan
Dh
Mangaorapan
Dm
Waipawan
Dw
Teurian
Dt
60
65
Myr
70
75
80
85
90
95
100
105
110
115
CRETACEOUS
Late
Early
Mata
Haumurian
Mh
Piripauan
Mp
Raukumara
Teratan
Rt
Mangaotanean
Rm
Arowhanan
Ra
Clarence
Ngaterian
Cn
Motuan
Cm
Urutawan
Cu
Taitai
Korangan
Uk

unconformity south of Coverham, and a widespread glauconitic sandstone to the north (Morris 1987). The upper Iwitahi Group (of which the Claverley Sandstone and the Woolshed Formation are the major constituents) are Piripauan to Haumurian in age (Reay 1980, Morris 1987).

The Iwitahi Group is overlain by the Amuri Limestone Group [Section 2.1.]. According to Morris (1987), the Limestone of Late Haumurian Age to the north of Branch Stream conformably overlies the upper Iwitahi Group. To the south, where the base of the Amuri Limestone Group is of Early Eocene Age, it rests unconformably on either the Claverley Sandstone or the Woolshed Formation. The age of the Amuri Limestone Group ranges from Haumurian to Runangan.

Overlying the Amuri Limestone Group with angular unconformity are the Cookson Volcanic and Motunau Groups (the latter includes the Weka Pass Stone Formation). The Motunau and Cookson Groups are of Whaingaroan to Waitakian or possibly younger Age. The Weka Pass Stone commonly overlies the Amuri Limestone Group, and grades up into the Waima Siltstone (Waitakian or younger in age, Morris 1987). Within the Waima Siltstone are found lenses of Great Marlborough Conglomerate (Early Miocene) containing clasts from all the lithologies discussed above.

1.5.2. SUMMARY OF REGIONAL STRUCTURE

The study area is at the southern end of a tectonic zone called the East Coast Deformed Belt (Spörli 1980). Structures in the Belt reflect northeast trending subduction related deformation. In the Marlborough area, styles of deformation are inferred to reflect the transition from subduction to transform plate margins. Northeast-trending transcurrent faults are the dominant structure in basement rocks of the study area. Deformation of the cover rocks consists of northwest thrusting, folding along northeast trending axes, and dextral faulting (Prebble 1980).

The amount of movement across faults in the area must be considered in paleoenvironmental interpretations of the Amuri Limestone Group. The work by Morris (1987) inferred 5-10 km of movement on the Hope Fault north of the junction with the Kekerengu Fault [Figure 1.3], with 10-15 km of dextral movement on the Kekerengu Fault itself. Cumulative movement south of the fault junction is estimated to be 15-25 km. Similar offsets were

Figure 1.4 Relevant New Zealand stages and absolute ages (from Raine 1987, Morris 1987).

calculated by Freund (1971).

1.6. PREVIOUS WORK ON CHERT AND DOLOMITE IN THE AMURI LIMESTONE GROUP AND WOOLSHED FORMATION

The presence of "flints" was noted in limestone at Kaikoura Peninsula by Buchanan (1868), and at Haumuri Bluffs by Haast (1871). Chalk beds containing flints at Haumuri Bluffs were later described as cherty limestone by Hector (1874). The cherty nature of the beds was also recognized by McKay (1877), during geological investigation of the Haumuri Bluffs and Kaikoura areas. The origin of the flints was not considered by any of these authors.

The first detailed description of chert lithology and distribution was by McKay (1886), following visits to a number of localities in the Clarence Valley-Coverham area. The flints were described as nodular bedded, and commonly branched with *"grey to white coatings"*. Although dolomite was not recognized, it is likely that it at least in part formed the grey to white coatings. The branched nature of the flint lead McKay to suggest the chert resulted from silicification of fucoid stems.

In a review of New Zealand Tertiary Limestones, Marshall (1916) noted the *"highly siliceous and flinty"* nature of the Amuri Limestone. He also remarked upon the absence of siliceous organisms in these deposits, and suggested that they may have been dissolved. No further assessment of the origin of the chert was made.

Detailed descriptions of the flint, including petrographic examinations were made by Thomson (1916, 1919). This included, with the aid of chemical analysis, the first recognition of the presence of dolomite. Also documented was the fact that the chert is best developed where the Amuri Limestone is thickest. In both papers there is much discussion as to the origin of the flint beds. The flint was considered to be *"chemically deposited along with the dolomite, or that it is of extraneous origin"* (Thomson 1916, p56). The silica was derived from siliceous organisms (Thomson 1919). The flint formed in a low-oxygen, organic-rich sediment, where there was a paucity of bottom dwelling organisms. The decomposition of organic matter by *"sulphur bacteria"* caused sulphide precipitation and an increase in alkalinity. The carbonate produced *"acts*

on the calcium and magnesium salts in solution in the sea, precipitating calcium and magnesium carbonate in the sea, and probably also on dissolved colloidal silica, which is precipitated as flint or chert" (Thomson 1916, p56). In addition the flints were believed to be concretionary, and that formation of both flint and dolomite occurred soon after deposition (Thomson 1919).

Speight and Wild (1918) described the flint associated with the Amuri Limestone-Weka Pass contact, and suggested that the flint formation was later than burrowing. Their evidence is glauconite filled burrows in chert, which the authors doubted could be produced by organisms boring into cherts.

Wellman (1945) made a very brief description of the Waipapa Bay chert locality, apparently to assess the economic value of the chert. Since publication of the Wellman article, a number of stratigraphic studies have included the chert and dolomite, but not investigated their significance further (e.g. MacPherson 1952, Suggate 1958, Lensen 1962, 1978a,b, Webb 1966, Price 1974, Prebble 1976, Osborne 1981). Curiously, Lensen (1962, 1978a,b) and Webb (1966) appear to have misidentified the dolomite in the chert as greensand, despite its correct identification by Thomson (1916, 1919).

The occurrence of chert and dolomite in the Amuri Limestone at coastal sections was discussed by Armstrong (1972). He concluded that both the chert and dolomite are of early diagenetic origin. He believed that chert formation followed dolomitization, and that the bulk of the chert has replaced the host sediment. However, he also suggested that some of the chert, particularly at the base of the sequence, has a primary origin.

In an outline of chert-bearing formations in New Zealand, Moore (1983) discussed the origin and occurrence of the Amuri Limestone chert. A replacement origin was recognized. He suggested that the silica may have been derived from the dissolution of radiolaria, devitrification of acidic tuff, and possibly from intrastratal solution of quartz-rich sediments.

The concretions in the Woolshed Formation have been noted in a number of the stratigraphic studies cited above, but little specific attention has been paid to their origin and genesis. The early diagenetic history of

the dolomite concretions at Kaikoura Peninsula has been briefly discussed by Browne (1985).

The most recent work to include the chert and dolomite of the Amuri Limestone Group is that of Morris (1987). He described in detail the stratigraphy of the Amuri Limestone Group, and its relationship to overlying and underlying units. The early diagenetic nature of both the chert and dolomite was recognized.

CHAPTER 2

DEPOSITIONAL AND DIAGENETIC STRATIGRAPHY

2.1. DEPOSITIONAL LITHOSTRATIGRAPHY

The stratigraphy of the Amuri Limestone Group, and its relationship to overlying and underlying units is detailed in Morris (1987). The depositional stratigraphy is summarized from this source, and from personal observation. A diagrammatic summary is given in Figure 2.1.

2.1.1. UPPER IWITAHI GROUP

Woolshed Formation

The Woolshed Formation is the oldest unit studied in this thesis. It is regionally extensive, attaining thicknesses of the order of 200 m in the southern half of the field area. Thicknesses of about 650 m are found in the Woodside Creek (12,13)-Waima River (21) area (Prebble 1976). The lithology is dominantly a very poorly sorted, finely skewed, very fine sandy mudstone. Clay comprises 25-30% of the sediment. Large carbonate concretions are confined to the upper parts of the Formation.

Sedimentation in a deep water, possibly an outer shelf environment is inferred for the Woolshed Formation in the northern part of the field area (Morris 1987). Shallow water facies are inferred for Woolshed Formation sediments to the southwest. The age of the Formation is confined to within the Haumurian stage (Morris 1987).

Claverley Sandstone (Formation)

The Claverley Sandstone unconformably overlies the Woolshed Formation, and has an average thickness of about 10 m. The Formation does not occur north of Branch Stream (28,29) inland, and Waipapa Bay (10,11) on the coast. The lithology is a moderately indurated, commonly massive, fine to medium noncalcareous sandstone. The age of the Formation is Late Haumurian, and it is thought to have been deposited in a high energy, shallow water, inner shelf environment (Morris 1987).

2.1.2. AMURI LIMESTONE GROUP

The Amuri Limestone Group is divided into six main regionally extensive units [Figure 2.1.]: Mead Hill Formation, Teredo Limestone Formation,

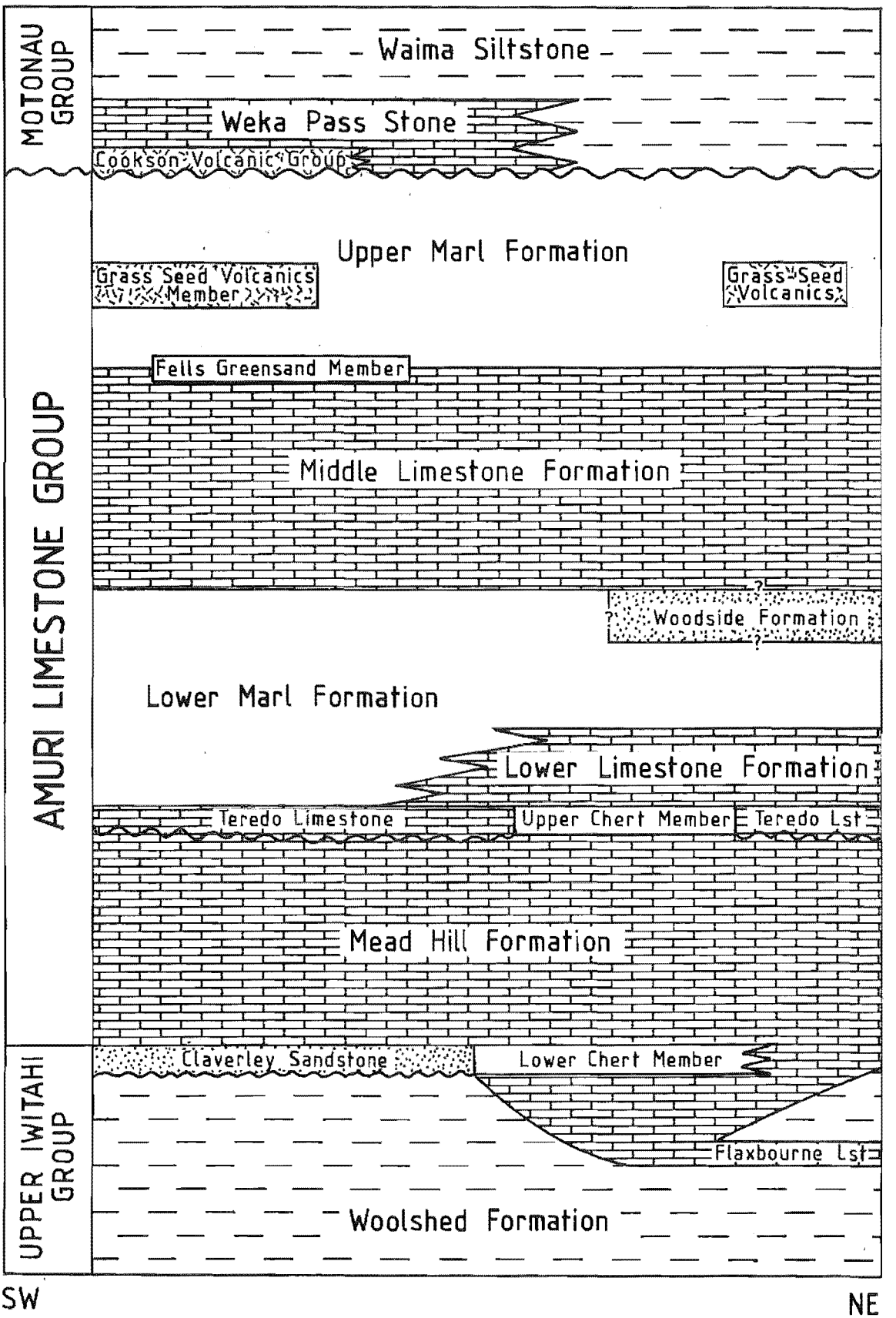

Figure 2.1 Summary of the Amuri Limestone Group stratigraphy in Marlborough (Morris 1987, Figure 2.3).

Lower Limestone Formation, Lower Marl Formation, Middle Limestone Formation, and Upper Marl Formation (Morris 1987). The Mead Hill Formation is of greatest significance to the chert and dolomite studied in this thesis. In addition to the above, there are three other less extensive units: Woodside Formation, Fells Greensand, and the Grass Seed Volcanics, which are of limited importance to this study.

Mead Hill Formation

The Lower Chert Member and the Flaxbourne Limestone are members of the Mead Hill Formation. The Mead Hill Formation is defined by Morris (1987, p72) as *"decimetre thick, greenish grey, very well indurated, muddy, foraminiferal, micritic limestone, interbedded with millimetre to centimetre thick, medium dark grey, poorly indurated, calcareous, smectitic mudstones or marls."* It is by far the major dolomite and chert bearing formation however, occurrences thereof are not intrinsic to the definition of the unit (Morris 1987).

The Mead Hill Formation attains its maximum thickness in the vicinity of Mead Stream (24,25). Isopachs [Figure 2.2.] indicate an approximately northwest trending trough with a depocentre near Swale Stream (23). It is diachronous and conformable over the Upper Iwitahi Group, overlying the Woolshed Formation north of Branch Stream (28,29), and the Claverley Sandstone further south. At its thickest, the Mead Hill Formation probably represents most of the Haumurian, but its base youngs away from the depocentre. The top of the Formation is probably restricted to the earliest Waipawan. Within the Mead Hill Formation are well documented occurrences of the Cretaceous-Tertiary (K-T) boundary (Strong 1977, Strong *et al.* 1987, 1988, Brooks *et al.* 1984, 1985, 1986, Morris 1987). The Lower Chert Member is probably of uppermost Haumurian age.

An outer shelf to mid to upper bathyal depositional environment is inferred for the Mead Hill Formation (Morris 1987). Water depths appear to have increased in a northeasterly direction. A gentle trough may have existed near the depocentre, which gradually subsided during deposition.

Teredo Limestone (Formation)

The Teredo Limestone unconformably overlies the Mead Hill Formation, and

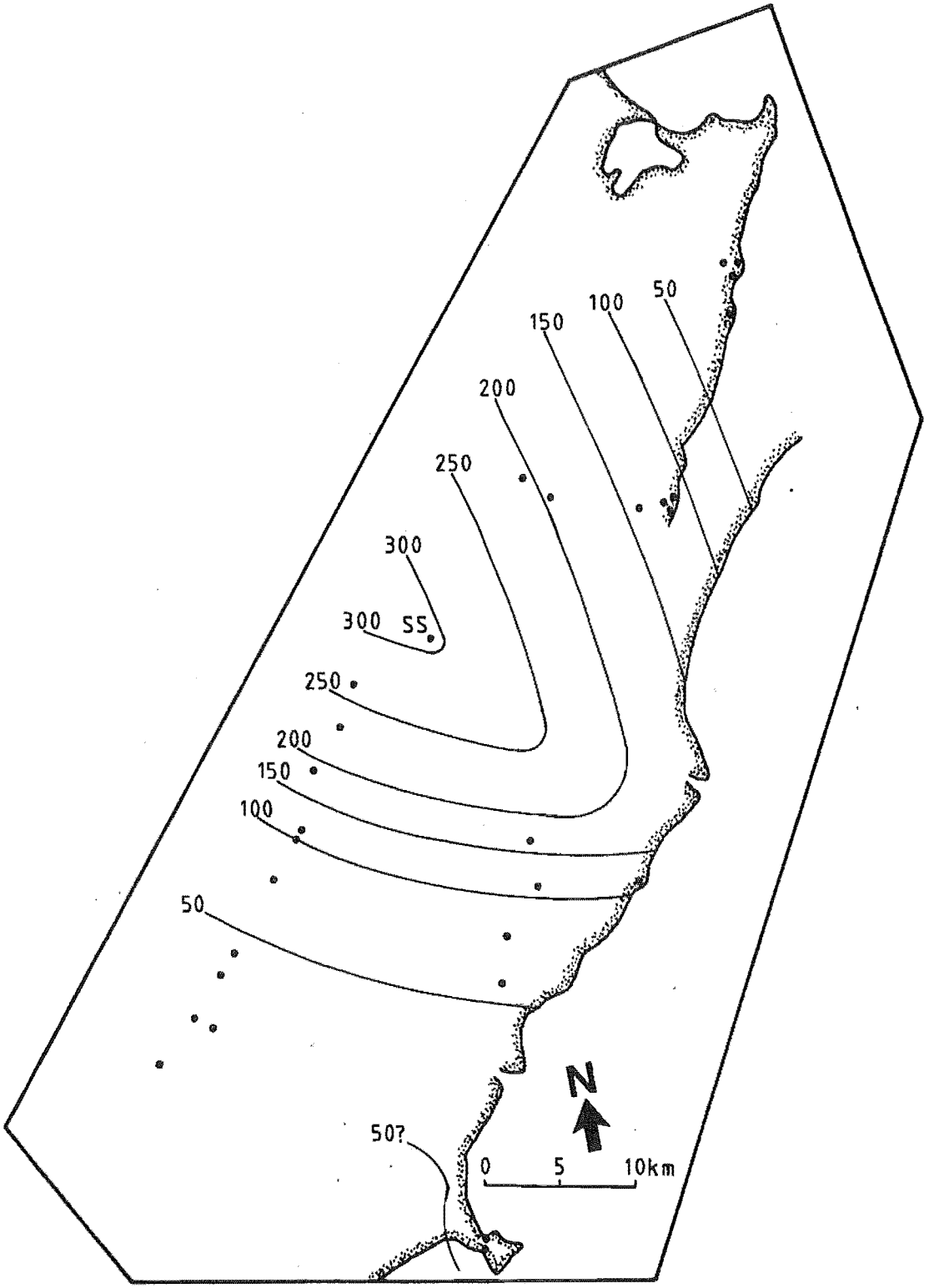

Figure 2.2 Paleoisopach map of Mead Hill formation, after restoration of movement along the Hope and Kekerengu faults (modified from Figure 4.1.1, Morris 1987).

is a bioturbated, sandy, glauconitic, foraminiferal, micritic limestone (Morris 1987). The unit youngs to the south from Branch Stream (28,29) with ages ranging from Waipawan to mid Mangaorapan, and possibly as young as Heretaungan. Paleontological determinations north of Branch Stream are poor, and only Waipawan ages are indicated. Deep marine, possibly bathyal, deposition is suggested (Morris 1987).

Lower Limestone (Formation)

The Lower Limestone is a minor chert bearing unit. Limestone lithologies are similar to those of the Mead Hill Formation. The Upper Chert Member is included in the Lower Limestone Formation (Morris 1987). The base of the Lower Limestone youngs southwards (and possibly northwards) from the depocentre, and conformably overlies the Teredo Limestone. An outer slope to bathyal depositional environment is inferred, with ages ranging from Waipawan to Mangaorapan. Subsidence of the Amuri depocentre appears to have continued during Lower Limestone deposition.

Lower Marl (Formation)

This unit consists of poorly indurated, smectitic mudstones which are interbedded with 1-10 cm thick, indurated, micritic limestones.

As with the Lower Limestone, which it conformably overlies north of Bluff River, an outer shelf to bathyal depositional environment is indicated (Morris 1987). South of Bluff River (37) and Kaikoura Peninsula (3,4) the Lower Marl conformably overlies the Teredo Limestone. Deposition of the Lower Marl was initiated in the vicinity of Muzzle Stream (32,33) and Woodside Creek (12,13). The base of the Formation youngs from these localities towards the Mead Stream (24,25) depocentre. South of Muzzle Stream the base also becomes younger. Ages range from Late Waipawan to Early Heretaungan (Morris 1987). The Lower Marl is devoid of any chert or dolomite.

The Woodside Formation is in part coeval with parts of the Lower Limestone however, its exact relationship is still uncertain (Morris 1987).

Middle Limestone (Formation)

The Middle Limestone consists of 1-10 cm thick, commonly stylobedded, micritic limestone, and contains localized intercalations of Fells Greensand and Grass Seed Volcanics, and minor quantities of chert. The Limestone conformably overlies the Lower Marl. The Middle Limestone Formation is possibly of bathyal origin, and ranges in age from Mangaorapan to Bortonian.

Upper Marl (Formation)

The Upper Marl Formation is similar to the Lower Marl both lithologically and in terms of depositional environment. Conformably overlying the Middle Limestone, the Upper Marl ranges in age from Porangan to Runangan. It contains intercalations of Fells Greensand and Grass Seed Volcanics, but no chert or dolomite.

2.1.3. MOTUNAU GROUP

At the base of the Motunau Group is a phosphatized conglomeratic bed, which unconformably overlies the Upper Marl Formation. Of the Motunau Group, only the Weka Pass Stone will be mentioned further in this thesis. The Weka Pass Stone is essentially a centimetre-bedded to decimetre-bedded sandy biomicrite, of latest Whaingaroan to Waitakian age.

2.2. PROPOSED DIAGENETIC STRATIGRAPHY

Diagenetic features are not necessarily confined within the boundaries of lithostratigraphic units. Therefore separate discussion and interpretation of diagenetic lithologies is thought preferable. To this end a stratigraphy based on post-depositional features is proposed.

2.2.1. DEFINITION OF DIAGENETIC ZONES

The relationship between the depositional and diagenetic stratigraphies is shown in Figure 2.3. Diagenetic zones are defined primarily on the basis of the relative abundance of chert, dolomite and limestone, and the presence of concretions.

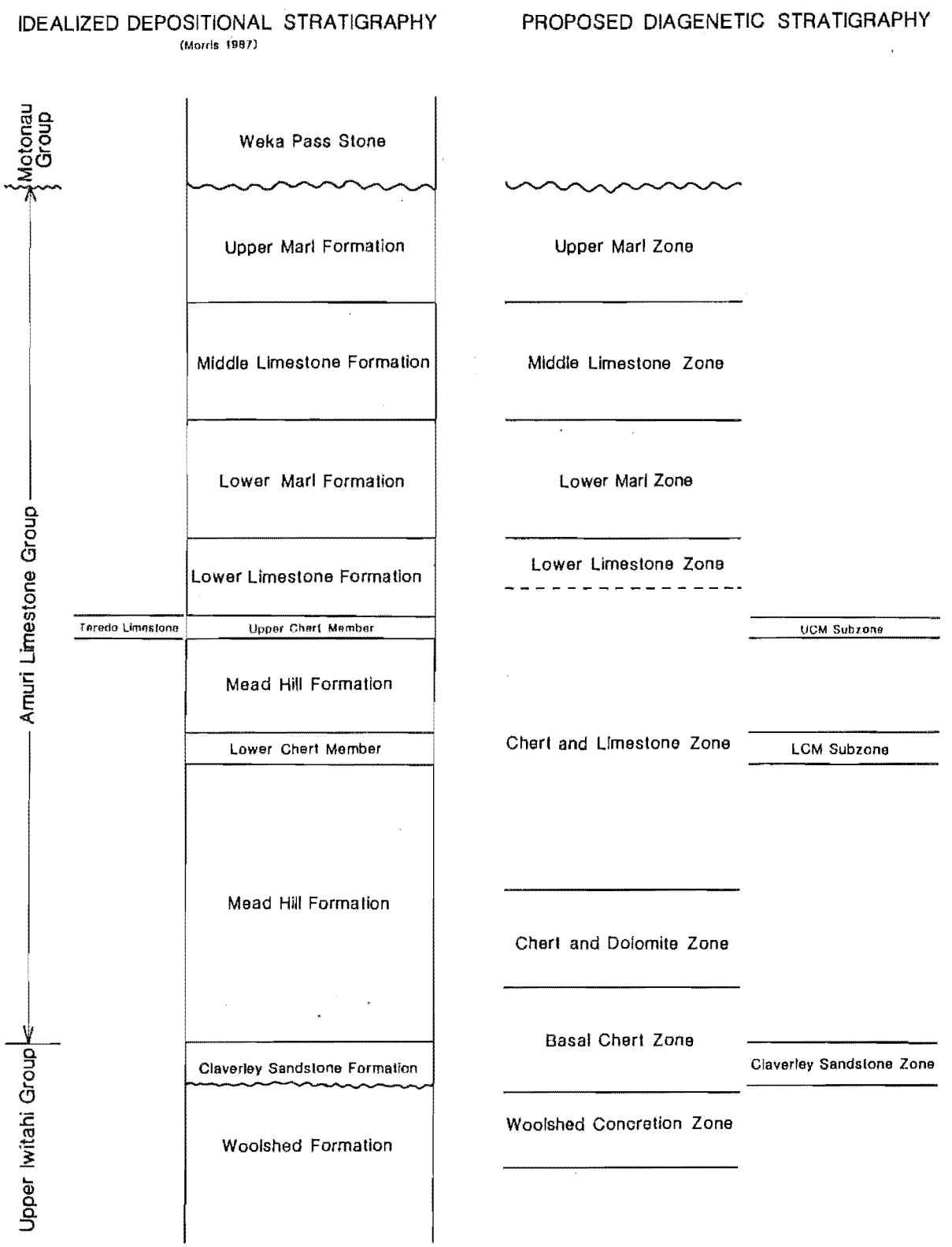

Figure 2.3 Schematic summary of the relationship between depositional stratigraphy and the proposed diagenetic stratigraphy.

See also Figure 2.3a [Map Pocket].

The base of the *Woolshed Concretion Zone (WC Zone)* at any given location is set at the lowermost occurrence of concretions in the Woolshed Formation. The Zone is restricted to the upper Woolshed Formation and consists of centimetre-bedded, medium grey, mudstones and very fine sandstones, which contains variably sized spheroidal or elongate carbonate concretions.

The *Claverley Sandstone Zone (CS Zone)* is confined within the Claverley Sandstone Formation. The lithology is commonly a noncalcareous sandstone containing less than about 25% chert and/or dolomite by volume.

The *Basal Chert Zone (BC Zone)* consists of rocks containing in excess of 75% chert, less than approximately 10% dolomite, and a variable abundance of detrital material. This Zone is stratigraphically above the WC and CS Zones, but may extend down into the Woolshed or Claverley Sandstone Formations. The upper boundary is within the lowermost Mead Hill Formation.

Stratigraphically above the BC Zone is the *Chert and Dolomite Zone (CD Zone)*. This Zone is confined to the lower Mead Hill Formation, and contains chert and dolomite as the dominant lithologies. Limestone generally comprises <10% of the rock.

Rocks which consist mostly of chert and limestone belong to the *Chert and Limestone Zone (CL Zone)*. Dolomite constitutes less than 10% of the rock. In the Mead Hill Formation depocentre the CL Zone overlies the CD Zone. North of Isolation (20) and Woodside Creeks (12,13), and south from Branch Stream (28,29) the CL Zone overlies Upper Iwitahi Group sediments. The upper boundary of the CL Zone is placed at the uppermost occurrence of chert in either the Mead Hill or Lower Limestone Formations. In some places, such as Kaikoura Peninsula (3,4), the upper boundary is placed at the sub-Teredo unconformity. Two subzones within the CL Zone are also defined. Both the Lower and Upper Chert Members (Morris 1987) form distinct lithostratigraphic units. The Upper Chert Member is designated the *UCM Subzone*, with upper and lower boundaries conforming to the lithostratigraphic boundaries of Morris (1987). The Lower Chert Member is designated the *LCM Subzone*. At localities where a dolomite bed occurs below the Lower Chert Member, the lower boundary of the LCM Subzone is placed immediately below this dolomite occurrence. The upper boundary is

placed immediately above any dolomite occurring above the Lower Chert Member. These dolomite occurrences are included within the LCM Subzone because of their petrographic and geochemical similarity to dolomite from within the Lower Chert Member itself. Where there is no dolomite above and/or below the Lower Chert Member, LCM Subzone boundaries correspond to the Lower Chert Member lithostratigraphic boundaries of Morris (1987).

The *Lower Limestone Zone (LL Zone)* extends from the top of the CL Zone to the upper boundary of the Lower Limestone Formation. This Zone is devoid of chert and dolomite.

All other zonal boundaries conform to the lithostratigraphic boundaries of Morris (1987). The Middle Limestone Formation is designated the *Middle Limestone Zone (ML Zone)*. The Upper and Lower Marls are called the *Upper Marl Zone (UM Zone)* and *Lower Marl Zone (LM Zone)* respectively. Since both the LM and UM Zones do not contain chert or dolomite, they will not be detailed further in following sections.

2.2.2. SUMMARY CORRELATION OF ZONES

Figure 2.4 [Map pocket] summarizes the distribution and correlation of the diagenetic zones throughout the field area (and includes a reduced version of Figure 1.2 showing the locations of measured sections). Correlations are discussed in more detail in following sections. Detailed descriptions of lithologies are in Appendix 2 along with detailed measured sections.

2.2.3. WOOLSHED CONCRETION (WC) ZONE

The WC Zone occurs in the Clarence Valley at Branch Stream (28,29) and sections further south [Figure 2.4]. At sections from Dee Stream (27) to Swale Stream (23) the Woolshed Formation has apparently been removed by faulting. The best exposures of WC Zone concretions are found at Kaikoura Peninsula (3,4), where they are most numerous. Although the WC Zone is exposed at Woodside Creek (12,13), concretions are only found as float in the creek bed. Woolshed Formation outcrops in sections through the Puhi Puhi Syncline, but concretions are only found at Wharekiri Stream (9). Only a thin exposure of Woolshed Formation with no concretions is found at Waipapa Bay (11).

WC Zone thicknesses are variable. At Isolation Creek (20) and Kaikoura Peninsula the Zone is about 80 m thick. About twice this thickness is found at Branch (28,29) and Bluff Streams (35,36). There are 60 m of WC Zone at Dart stream (30), and about 20 m at the Muzzle Stream (32,33) and Mt Alexander sections (8). The geographic spread of data points and the high variability of thicknesses precludes construction of a sensible paleoisopach map. The variability of WC Zone thicknesses results from faulting (i.e. complete removal from Swale to Dee Streams) and erosion of the upper surface further south, prior to deposition of the overlying Claverley Sandstone. No unconformity is detected at Isolation Creek (20). The WC Zone generally comprises thinly bedded (<5 cm thick), pyritic very fine sandstones to mudstones. At Dart Stream (30) some 1 cm thick pyrite cemented beds are associated with concretions. The WC Zone is chertified at Kaikoura Peninsula (3,4), Isolation Creek (20), and Whernside Spur (22), but only immediately below the Amuri Limestone Group. Chertification is not observed at other localities.

Concretions vary from a few centimetres to a few metres in diameter, and are commonly elongated in the plane of bedding [Figure A2.2]. Some relatively spherical examples are also found [Figure A2.4]. Differential compaction around concretions is observed at all localities [e.g. Figure A2.2]. Two concretions contain internal bedding 5-6 times the thickness of beds in the surrounding sediment [e.g. Figure A2.3]. The thickness of beds in concretions is constant throughout the concretion. At Lab Rocks (4) some concretions have been exhumed and subsequently phosphatized and bored [Figure A2.6], and are inferred to have been reworked (Morris 1987).

2.2.4. CLAVERLEY SANDSTONE (CS) ZONE

The CS Zone is found as far north as Branch Stream (28,29) inland and Waipapa Bay (10,11) on the coast. At Waipapa Bay (10) the CS Zone is intercalated within the BC Zone [Figures 2.4, A2.9]. Faulting has removed the basal Amuri Limestone Group and Upper Iwitahi Group from Dee (27) to Swale Streams (23). At Isolation Creek (20) the Amuri Limestone Group conformably overlies the Woolshed Formation, implying the CS Zone pinches out somewhere in the Branch-Swale (28-23) Stream area. Some thin, (<5 cm thick) sandstone beds at the base of the Swale Stream (23) section are possibly from the CS Zone. No CS Zone is identified north of Waipapa Bay (10,11) on the coast, or inland from Isolation Creek (20). The CS Zone as

such is not recognized at Mt Alexander (8), but is found nearby at Wharekiri Stream (9) [Figure A2.7]. The CS Zone is found at Lab Rocks (4), but not at South Bay (3). The Zone's absence from South Bay (3) is due to removal through injection as clastic dikes into overlying sediments (Morris 1987). At Branch Stream (28) the Zone is 5 m thick, and 10-20 m thick at the Waipapa Bay (10,11) sections. The average thickness of the CS Zone at other localities is about 10 metres. It has no distinctive isopach pattern.

The lithology is generally a massive, locally calcareous, fine to medium sandstone. Chertification is restricted to a few chertified (*?Thalassinoides*) burrows and small, centimetre-scale lenticular chert nodules [e.g. Figure A2.8].

2.2.5. BASAL CHERT (BC) ZONE

The BC Zone is found at Isolation Creek (20), Waipapa Bay (10,11), Jordan Stream (7), Swale Stream (23), and Mt Alexander (8). The BC Zone may occur at the Puhi Puhi River bridge section (5), but cannot be verified for lack of exposure. The sequence at Wharekiri Stream (9) appears to be conformable, but no unit comparable to the BC Zone is recognized. Faulting has complicated the lower part of the Swale Stream (23) section [Section A2.9], probably repeating some of the sequence. The fault-bounded dolomitic chert below what is interpreted to be the BC Zone is thought to have been displaced, so correlations in Figure 2.4 are drawn accordingly. The base of the BC Zone at Swale Stream is placed immediately above the thin intercalated sandstone beds.

The hypothesized geographical extent of the BC Zone, along with thicknesses at specific localities is shown in Figure 2.5. The BC Zone is thickest at Isolation Creek (20, 70 metres), and is 50 m thick at Mt Alexander (8). At the Swale (23) and Jordan Stream (7) sections the Zone is only about 10 m thick. However, faulting may be responsible for attenuation of the sequence at Swale Stream. The beach platform section at Waipapa Bay (11) has 5 m of BC Zone with possibly a further 5-10 m unexposed. Nearby, there is 15 m of BC Zone in the Mororimu Stream section (10); however, the lowermost 5 m is separated from the upper 10 m by 13 m of CS Zone [Figure 2.4].

Construction of a paleoisopach map of the BC Zone is difficult because of the lack of data between inland and coastal sections, and because of large thickness variations between sections. The same lack of data between inland and coastal sections applies to all other isopach maps, including Figure 2.2. No reasonable contours could be drawn for the BC Zone. Therefore only the geographic distribution, based on the Mead Hill Formation isopachs [Figure 2.2], is shown in Figure 2.5. If this interpretation is correct, it shows that the BC Zone was only in part confined to the thickest development of the Mead Hill Formation. At Isolation Creek (20) and Swale Stream (23) the BC Zone occurs where the Mead Hill Formation is in excess of 150 m thick, whereas at the Puhi Puhi Syncline and Waipapa Bay localities the Mead Hill Formation is less than 150 metres.

Two types of BC Zone chert are recognized in the field; a detrital-rich and a detrital-poor chert. Detrital-rich cherts are essentially chertified Claverley Sandstone or Woolshed Formation sediments consisting of dark, centimetre-bedded to decimetre-bedded, nodular or relatively planar beds of chertified fine sandstone or mudstone with interbeds of unchertified fine sandstone or mudstone less than 1 cm thick [Figures A2.9 to A2.12]. The interbeds are less abundant, and pyrite is more common in chertified Woolshed Formation sediments than in chertified Claverley Sandstone. In the Mororimu Stream section (10) are laminated cherts consisting of millimetre-scale alternations of chertified and unchertified sandstone [Figure A2.11]. Chert commonly comprises in excess of 75% of the rock.

Relatively detrital-poor cherts are dark, commonly lustrous nodular beds of chert with rare unchertified interbeds [Figure A2.13]. Discrete nodules within beds are virtually undetectable. Detrital-poor cherts commonly constitute more than 90% of the rock.

2.2.6. CHERT AND DOLOMITE (CD) ZONE

The CD Zone occurs at Limburn (26), Mead (24), Swale (23), and Wharekiri Streams (9), Isolation Creek (20), Waipapa Bay (10) and possibly Wharanui Point (15) [Figure 2.4]. The complete thickness of the Zone cannot be ascertained in Clarence Valley sections since faulting has removed the lower part of the Amuri Limestone Group. The only 'complete' section is

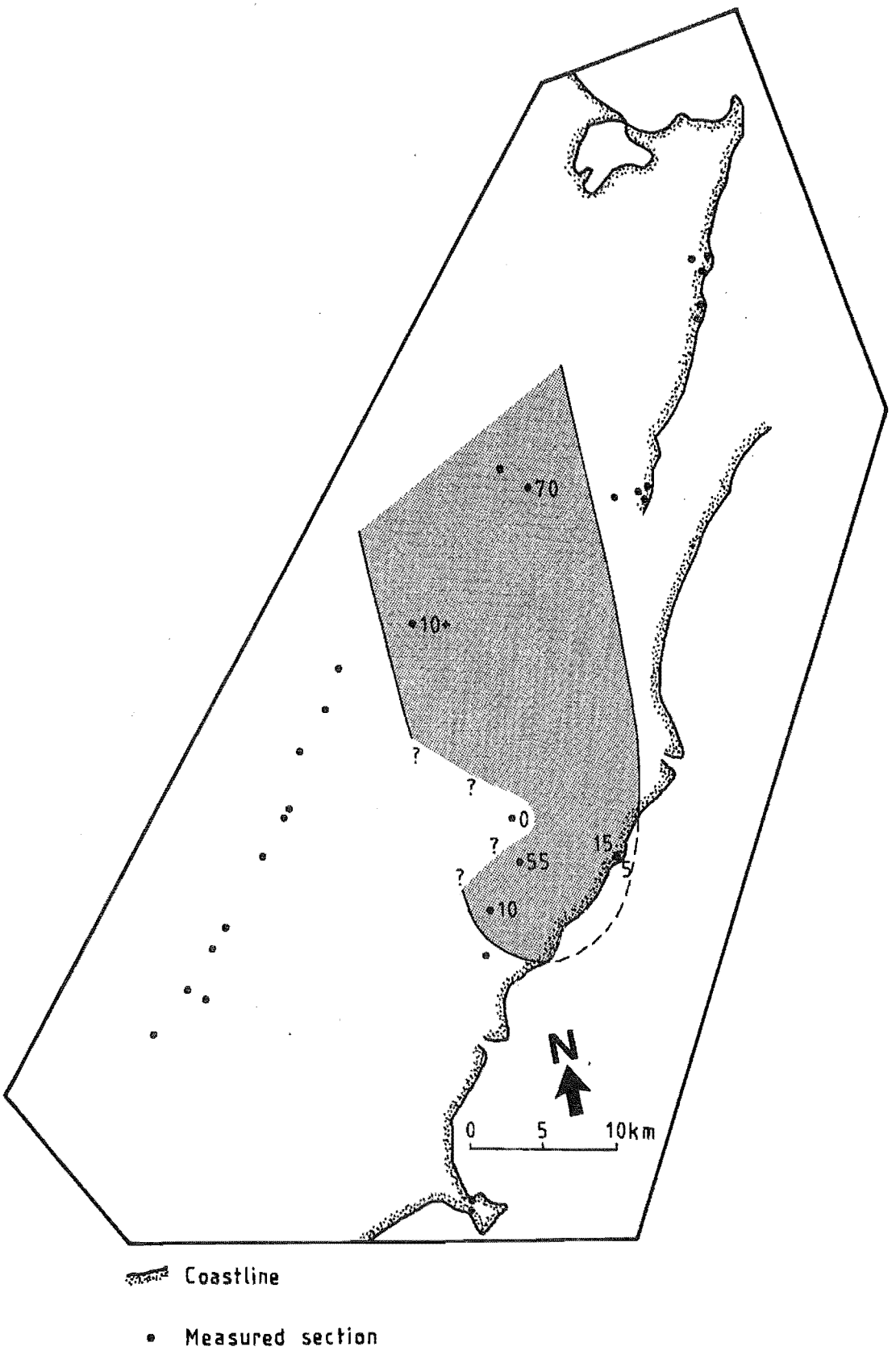

Figure 2.5 Inferred paleodistribution of BC Zone (shaded) with thicknesses (in metres) for specific localities.

at Isolation Creek (20) where the CD Zone is 244 m thick. At Mead Stream (24) only 90 m of the CD Zone is exposed. In addition 20 m from the base of the Mead Stream section (24) is a 0.5 m thick shear zone [Section A2.9]. Fault-caused shortening or lengthening of the sequence is difficult to assess, but is assumed to be minimal. The CD Zone is 110 m thick at Limburn Stream (26), with the upper contact at the base of the LCM Subzone. Sixty-seven metres of CD Zone is found at Swale Stream (23). There is no CD Zone or equivalent south of Limburn Stream. The upper contact with the CL Zone is inaccessible at Wharekiri Stream (9). Although it could not be precisely located in the cliff face, it is probably no more than about 20 m stratigraphically above the end of the measured section. Therefore at Wharekiri Stream (9) the CD Zone is inferred to be about 40 m in Figure 2.4. The upper contact is not exposed at Waipapa Bay (10,11) either, and only 20 m of CD Zone is found. At Wharekiri Stream (9), the CD Zone overlies the CS Zone in the absence of the BC Zone.

As with the BC Zone, there appears to be no consistent or recognizable isopach pattern. The geographic distribution [Figures 2.4, 2.6] shows the CD Zone to occur where the Mead Hill Formation is at least 150 m thick [Figure 2.2]. However, the CD Zone at Wharekiri Stream (9) and Waipapa Bay (10) occurs where the Mead Hill Formation is less than 150 m thick.

Although CD Zone cherts are outwardly similar to detrital-poor BC Zone chert, they are laterally discontinuous and discrete elongated nodules predominate. Dolomite consists of beds and/or lenses of chert cemented, <1 mm diameter, apparently euhedral rhombic crystals [Figures A2.14 to A2.18]. The bulk of the dolomite occurs outside chert nodule margins, with dolomite beds commonly pinching out around nodules [Figures A2.15 to A2.17]. Slightly nodular and continuous beds of dolomite alternating with beds of chert are also found [Figure A2.18]. Dolomite crystals are commonly disseminated through chert beds and nodules [Figure A2.16]. The volume of dolomite may be as high as 50% of the rock with chert comprising the remainder. Sulphide nodules, usually $\leq$1 cm in diameter, are distributed sporadically throughout the Zone.

Evidence of soft sediment deformation occurs in the form of contorted beds [Figure A2.18], flame structures [Figure A2.19], and chert nodules that appear to disrupt adjacent beds [Figure A2.17].

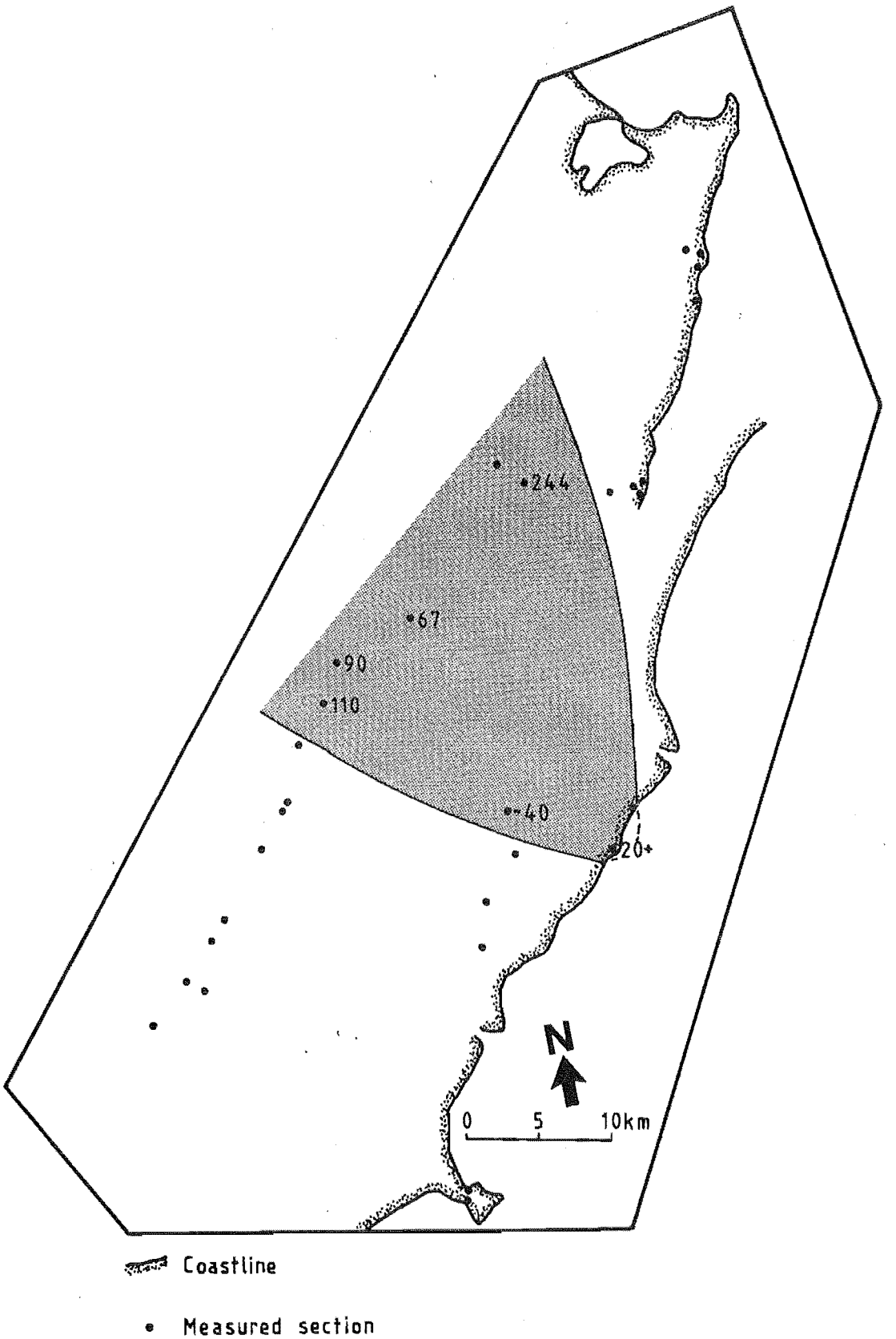

Figure 2.6 Inferred paleodistribution of the CD Zone chert (shaded). Thickness (in metres) is shown for specific localities.

2.2.7. CHERT AND LIMESTONE (CL) ZONE

The CL Zone is regionally the most extensive diagenetic unit studied, and contains the greatest lithologic variation. The LCM and UCM Subzones are dealt with separately in Section 2.2.8 however, total thicknesses mentioned in the following discussion include the LCM and UCM Subzones.

The thickest CL Zone exposures are at Mead (24,25) and Dee Streams (27). At Mead Stream (24,25) the Zone comprises a continuous 257 m thick sequence, whereas at Dee Stream (27), faulting has removed the base and only 250 m is exposed. Upper parts of the CL Zone have been removed by faulting at Isolation Creek (20), Branch Stream (28,29), and possibly Woodside Creek (13), where 60 m, 180 m, and 120 m (respectively) of the Zone are measured. A maximum of 26 m of CL Zone is found at Muzzle Stream (32,33); faulting may have affected the sequence here as well. Eighty-seven metres are recognized at Limburn Stream (26). Only minimum thicknesses are obtained at Swale (23) and Wharekiri Streams (9), Waipapa Bay (11), and Chancet Rocks (18), because of incomplete exposure or inaccessibility. An erosional unconformity truncates the CL Zone at Jordan Stream (7) where the Zone is only 7.5 m thick, and at Kaikoura Peninsula (3,4). Fifty metres of CL Zone are found at Lab Rocks (4) and 2.3 m at South Bay (3). Although only containing very siliceous nodular micrites, the Kaikoura localities are retained within the CL Zone, and not placed within the LL Zone. This is because the nodular micrites underlie the Teredo Limestone, and elsewhere (e.g. Muzzle Stream) contain minor quantities of chert nodules. The low chert volumes at the top of the Waipapa Bay (11, where 100 m of section was measured) and Woodside Creek section (13) suggests that neither exceeded more than about 150 m thick. Similarly, the chert volume at the top of the Branch Stream section (29) suggests that the CL Zone at this locality may not have exceeded 200 metres. Interpretations from Mead Hill Formation thickness [Figure 2.2], air photographs and maps, suggests that there are about 250 m of CL Zone at Swale Stream (23), and there may have been 100-150 m at Isolation Creek (20). At South Wharanui Point (14) and Chancet Rocks (18), 60 m and 45 m respectively of CL Zone are exposed, whereas the Puhi Puhi River (5) and Mt Alexander (8) sections contain 33 m and 45 m respectively. In the Clarence Valley, the Zone thins southwards from Dart Stream (30,31, 57 m) to Bluff River (37, 15 m).

From the above measured and inferred thicknesses an isopach map has been constructed [Figure 2.7]. The thickest development of the CL Zone is associated with the thickest part of the Mead Hill Formation [Figure 2.2]. However, the CL Zone attains a maximum thickness near Mead Stream (24,25), whereas the Mead Hill Formation depocentre is in the vicinity of Swale Stream (23).

The CL Zone overlies the CS Zone at Kaikoura Peninsula (3,4), and at Clarence Valley sections south of Dee Stream (27) [Figure 2.4]. At Puhi Puhi Syncline sections (except Wharekiri Stream 9), the CL overlies the BC Zone, and at Isolation Creek (20), Waipapa Bay (10,11), Mead (24), Wharekiri (9), and Swale (23) Streams it rests on the CD Zone. The Zone probably (as the contact is not always exposed) overlies the WC Zone (or Woolshed Formation) at coastal localities north from Woodside Creek (12,13). The relationship of the CL Zone to underlying rocks at Dee Stream (27) is uncertain. At Limburn Stream (26) the LCM Subzone forms the base of the CL Zone, and overlies the CD Zone [Figure 2.4].

Micrite beds are usually 10-20 cm thick, nodular or planar bedded, siliceous and fossiliferous and commonly interbedded with approximately 1 cm thick marls. The majority of the micrites are grey to white, but at coastal localities north from Woodside Creek (12,13), pink to red micrites are common. Dolomite is rare and restricted to localized occurrences. Sulphide nodules, usually $\leq$1 cm in diameter, and their associated Fe-oxide weathering stain are distributed throughout the Zone.

Chert morphology is variable [Section A2.5], ranging from very small millimetre-scale nodules to bands [Figure A2.24] a few metres long. Chert-micrite boundaries may be smooth or very irregular, sharp or diffuse. Chert nodules may be dark and noncalcareous (as in the BC and CD Zones) or micrite-rich and light grey in colour. The bulk of chert nodules are lenticular or lensoid [Figures A2.21a, A2.22] however, at Needles Point (16) and Chancet Rocks (18) cylindrical chert nodules [Figures A2.33, A2.34], or 'halos' occur. Large nodules which disrupt adjacent beds [Figure A2.25] may be found scattered throughout the sequence. Some nodules consist of a series of silicification fronts resembling growth-rings [Figure A2.20]. In the Waima River section (21) are found some chert nodules oriented approximately perpendicular to bedding [Figure A2.29]. These nodules are approximately 1-2 m long and

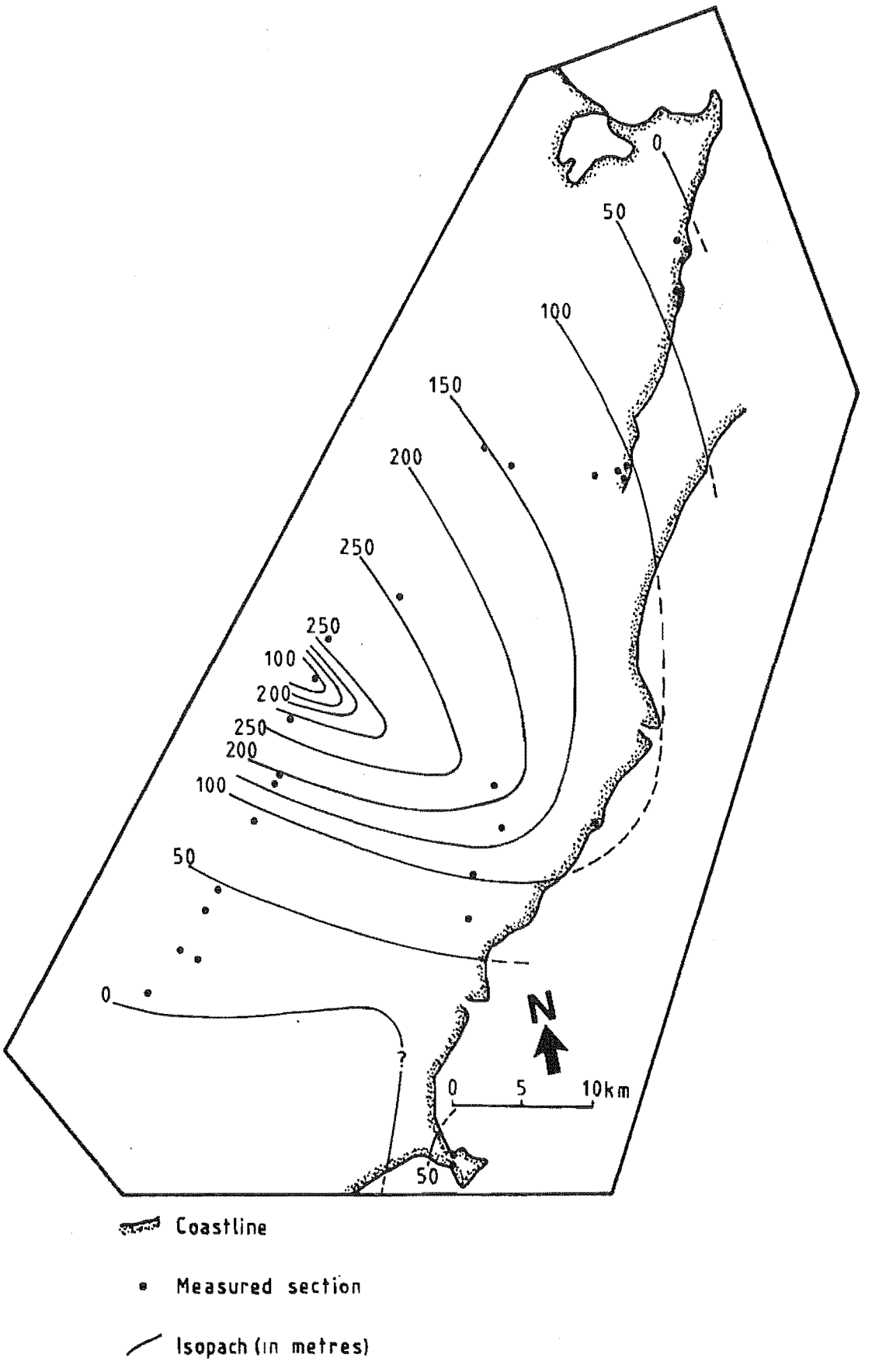

Figure 2.7 Inferred isopachs (in metres) for the CL zone.

only occur at this locality.

Planar-bedded micrites usually contain either chert bands or elongated chert nodules [Figures A2.23, A2.24], or are relatively chert free. Nodular beds contain lenticular chert nodules [Figures A2.21a, A2.35], and have a distinctive pinch-and-swell morphology.

Chert volumes are usually less than about 50% of the rock. In general chert abundance decreases stratigraphically upwards, and away from the Mead Hill Formation depocentre. This pattern of overall decreasing chert abundance is paralleled by an increase in the relative abundance of micrite-rich and micrite-centred chert nodules.

2.2.8. LOWER CHERT MEMBER (LCM) AND UPPER CHERT MEMBER (UCM) SUBZONES

LCM Subzone

The LCM Subzone [Figure A2.37a,b] is 26 m thick at Mead Stream (25). Further north, poor access prevented correlation at Swale Stream (23) however, a 14 m thick LCM Subzone is recognized in the Waima River (21). Faulting (Prebble 1976, 1980) may explain the absence of the LCM Subzone nearby at Isolation Creek (20). No LCM Subzone is found at Woodside Creek (12,13) and localities to the north, or at coastal localities to the south. At Branch Stream (29) the LCM Subzone is 16.5 m thick, and 38.3 m thick at Dee Stream (27). At Limburn Stream (26) it is only 17.3 m thick and at Dart Stream (31) 4.3 m of the Subzone is recognized. In contrast, Morris (1987) does not recognize the Lower Chert Member south of Branch Stream (28,29). From Figure 2.4 it can be seen that the LCM Subzone is confined to the Clarence Valley area, with its greatest development near Dee Stream (27) [Figure 2.8]. The LCM Subzone is therefore at its thickest further south of the maximum development of the CL Zone as a whole [Figure 2.7], but still within the Mead Hill Formation 100 m contour [Figure 2.2].

Morris (1987) infers the base of the Lower Chert Member to be laterally equivalent to the unconformity immediately below the Claverley Sandstone [Figure 2.1]. At Branch (29), Dee (27), and Limburn (26) Streams the basal dolomite in the LCM Subzone occurs immediately below the base of the Lower Chert Member. No basal dolomite occurs at Dart Stream (31) or Waima

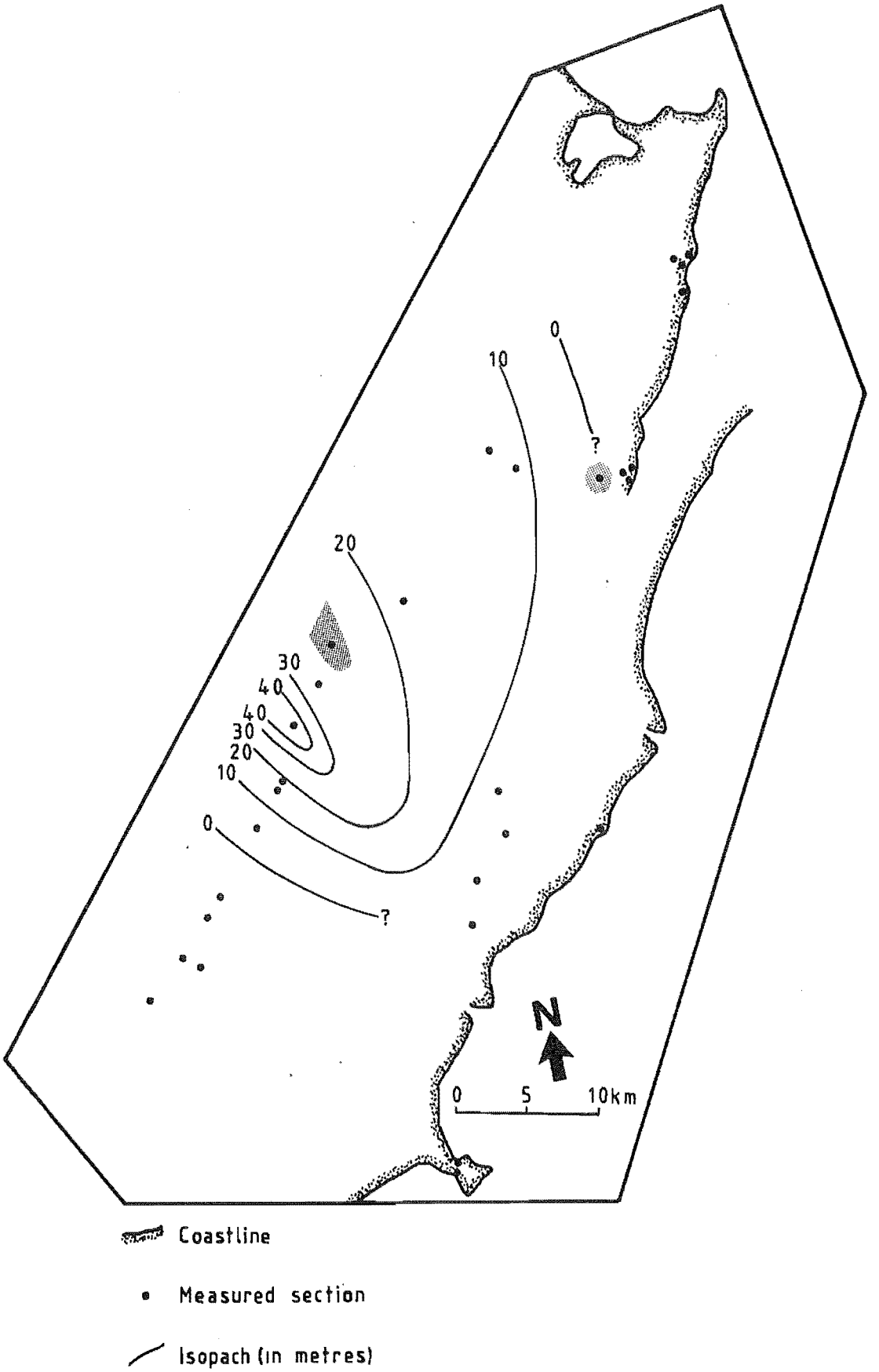

Figure 2.8 Isopach map (in metres) of the LCM Subzone. The shading indicates the distribution of the UCM Subzone lithologies.

River (21), and at Mead Stream (25) only a 0.5 m thick lens of dolomite occurs 20 m below the Lower Chert Member [Figure A2.25]. The basal dolomite unit is up to 13 m thick and consists of decimetre thick beds of silica cemented, ≤1 mm in diameter rhombic dolomite crystals. A few very small lenticular chert nodules also occur.

Above the base of the Lower Chert Member the LCM Subzone contains mainly chert and dolomite along with micrite and/or silicified micrite. Micrite-rich cherts are rare. The volume of chert is much greater than in the CL Zone above or below, and is usually in excess of 50% of the rock but decreases upwards. In the lower half of the unit are beds of dark chert up to 0.5 m thick, interbedded with noncalcareous, commonly fissile mudstones. In the upper parts of the Subzone beds of chert become increasingly discontinuous and nodular with dolomite and micrite or silicified micrite commonly surrounding discrete nodules. The dolomite occurs as beds or lenses of chert cemented rhombs similar to those found in the CD Zone. Some dolomite crystals are disseminated through chert nodules or beds. Interbeds are increasingly calcareous.

UCM Subzone

The UCM Subzone conforms to the lithostratigraphic boundaries of the Upper Chert Member (Morris 1987). The Subzone is found at Mead Stream (25) [Figure A2.37a,c] where it is 2.8 m thick. A similar, poorly exposed unit occurs in the upper gorge of Woodside Creek (12). Unfortunately, the poor exposure, and structural complications make determination of the precise stratigraphic position of the Woodside Creek unit difficult. UCM Subzone occurrences are shown in Figure 2.8.

Morris (1987) suggested that the Upper Chert Member at Mead Stream (25) extends to what here is identified as the LCM Subzone at Limburn Stream (26). He also correlates the Member as far south as Dee Stream (27). The correlation by Morris is thought to be incorrect because the 'Chert Member' at Limburn Stream (26) and the Upper Chert Member at Mead Stream (25) are lithologically different [see Section A2.6.1]. The Upper Chert Member comprises centimetre-thick planar beds of black, pyritic chertified fine sandstone to mudstone with interbedded unchertified fissile mudstones. No other detrital-rich units have been found that occupy a similar stratigraphic position. The base of the UCM Subzone overlies the

inferred lateral equivalent of the unconformity below the Teredo Limestone (Morris 1987).

2.2.9. MIDDLE LIMESTONE (ML) ZONE

The distribution and thickness of the ML Zone is as for the Middle Limestone Formation (see also Morris 1987). Maximum thicknesses are found at Kaikoura Peninsula (3,4), Isolation Creek (20), and near Dart Stream (30,31). Although chert is found in most ML Zones, it is of limited extent and small in volume. Only at Kaikoura Peninsula (3,4) has there been significant chert development. At Waipapa Bay (11), limited exposure at critical places makes precise identification of the ML Zone difficult.

At localities except those south of Kaikoura Peninsula, ML Zone micrites are centimetre-thick and stylobedded. Chert consists of dark, commonly irregularly shaped nodules ranging from a few centimetres up to 20 cm long. Beds or parts of beds that contain chert are not generally stylolitized and are thicker than surrounding beds devoid of chert [Figure A2.39].

South of Kaikoura Peninsula (3,4) where stylobedding is absent, there are networks of chert nodules [Figure A2.40] interpreted as silicified *Thalassinoides* burrows.

2.3. DISCUSSION AND SUMMARY

Conclusions as to the genesis of the chert and dolomite in the units described requires discussion of petrographic and geochemical data (provided in subsequent chapters). Nevertheless, some salient observations may be made from the data presented thus far.

1) A series of distinct diagenetic zones are recognized: the WC Zone, BC Zone, CD Zone, ML Zone and the CL Zone with the LCM and UCM Subzones. In addition, three further zones are recognized where chert and dolomite are limited or absent: the CS Zone and the LM and UM Zones. The boundaries of the latter two zones coincide with lithostratigraphic boundaries defined by Morris (1987), but they do not necessarily coincide in the other zones. Chert morphology is highly variable, ranging from bedded cherts to very small discrete nodules, and siliceous micrite is very common. Aphanitic

dolomite occurs in WC Zone concretions, and phaneritic, rhombic dolomite crystals are found in beds or lenses in overlying zones. With a few exceptions, pyrite is common in all zones.

2) Broadly the extent of chert and dolomite development in the Amuri Limestone Group is related to the distribution and thickness of the Mead Hill Formation (this does not include the ML Zone, where the relationship between chert development and host lithology is equivocal). Although controls on the construction of isopach maps [Figures 2.2, 2.5, 2.6, 2.7, 2.8] are less than ideal, the BC, CD, and CL Zones are best developed where the Mead Hill Formation is thickest. However, the maximum thicknesses of the CL Zone and LCM Subzone are further south than the inferred Mead Hill Formation depocentre. In general, the bulk of the chert and dolomite development occurs within the Mead Hill Formation 100 m isopach. The sensitivity of chert development to host lithology thickness has been noted in other studies. For example Mortimore (1986) showed that Upper Cretaceous cherts in the South Downs of England also formed in thicker parts of the sequence.

3) The base of the Teredo Limestone (and by inference the Upper Chert Member) overlies an unconformity at the top of the Mead Hill Formation [Figure 2.1]. Also Morris (1987) interprets the base of the Lower Chert Member to overly an offshore manifestation of the sub-Claverley Sandstone unconformity. Where the Mead Hill Formation is thickest, there are major developments of chert above both unconformities. In addition, at some localities the basal dolomite bed of the LCM Subzone occurs immediately below the unconformity at the base of the Lower Chert Member. In sediments below the two Subzones, chert volumes tend to decrease upwards towards the unconformities. At Jordan Stream, the chert sequence is abruptly terminated by an unconformity [Figure A2.36]. Therefore unconformities appear to exert some influence on the extent of chert and dolomite formation in the Amuri Limestone Group. The concentration of concretions in the upper Woolshed Formation at first suggests some association with the unconformity at the top of the Formation. However, it is thought unlikely that the unconformity development influenced concretion formation because:

i) No evidence of an unconformity is found in the Woolshed Formation-Amuri Limestone Group sequence at Isolation Creek, and concretions are present at this locality.

ii) Concretions appear to have formed soon after deposition of the sediment and are found up to 100 m below the unconformity, implying formation occurred before development of the unconformity.
iii) Reworking of concretions at Lab Rocks indicates concretion formation prior to unconformity development.

4) The vertical cherts [Figure A2.29] are interpreted to be chert dikes, similar to those described by Steinitz (1970). They were probably intruded into overlying beds before complete lithification of the sediment had occurred. Large bulbous cherts which disrupt bedding [e.g. Figures A2.25, A2.35a] may also result from some form of soft sediment deformation before complete lithification. Smaller nodules such as in Figure A2.17 may have been similarly emplaced. For both the vertical and bed-disrupting cherts it is envisaged that initial silicification of the original sediment had occurred, prior to emplacement. The intruding material was probably poorly lithified and was emplaced as a plastic flow (Steinitz 1970). Complete chertification and lithification did not occur until after emplacement.

5) A number of features indicate that the bulk of the chert and dolomite is of early diagenetic origin. The features are:
i) Differential compaction around dolomite concretions [Figure A2.2], and large differences between the thickness of beds within and surrounding concretions [Figure A2.3].
ii) Differential compaction of micrite [Figure A2.35b] and dolomite [Figure A2.15] beds around chert.
iii) Soft sediment deformation structures [Figure A2.19] and contorted bedding [Figures A2.18, A2.25].
iv) The presence of what are interpreted as chert dikes [Figure A2.29].
v) The absence of stylolites from chert bearing beds in the ML Zone indicates chert formation prior to compaction and pressure solution which is abundant in limestone beds devoid of chert.

In contrast, the lack of differential compaction, and the planar bedded nature of the thin chert bands shown in Figure A2.24, suggest that at least some chert formed slightly later during diagenesis, possibly after compaction of the host sediment.

6) Some chert beds and bands may result from the coalescence of nodules. Incomplete chertification may result in highly irregular nodules,

micrite-centred and micrite-rich forms.

7) Some authors note an intimate association of burrowing with silicification (e.g. Kelts 1976, Hein *et al*. 1981, 1983, Bromley and Ekdale 1984, 1986). Hein *et al* (1983) report that in 90% of their thin sections (DSDP Leg 69), silicification was initiated in burrows. In the current study the burrow chert association is much less consistent. The influence of burrowing in the BC and CD Zones, and the LCM and UCM Subzones cannot be adequately determined. In other Zones there are some examples of chert formation associated with burrows or parts of burrows [e.g. Figure A2.32, A2.40]. Trace fossils such as *Zoophycos*, *Planolites*, and *Teichichnus* (Morris 1987) are found preserved in chert [Figure A2.22], but are seldom preferentially silicified. *Thalassinoides* may be preferentially chertified [Figure A2.40], but not always. In some instances the *Thalassinoides* burrows may be only partly chertified. However, the cylindrical cherts at Chancet Rocks are an interesting case. Previously they were described as fossilized sponges (McCulloch 1976, Lensen 1978b, Lewis and Laird 1980). Another possibility is that they may be cylindrical chert halos around a trace similar to *Bathichnus paramoudrae*, (Bromley and Ekdale 1984, 1986, Clayton 1986). The lack of a canal within the central rod of the structures (Bromley *et al*. 1975) argue against them being *Bathicnus paramoudrae*, although the central rod implies some form of burrow origin. Morris (1987) suggested that the cylindrical chert halos formed around the vertical shafts of *Thalassinoides* burrows. However, many of the cylindrical cherts are contained within a single bed and are commonly separated from beds containing *Thalassinoides* burrow networks. Where both cylindrical and *Thalassinoides* burrow cherts occur in the same bed, connections between the two are indistinct. Cigar-shaped chert nodules [Section A2.5] cannot be easily explained in terms of burrows either. Whether cylindrical cherts are burrow or sponge related is as yet undetermined. Burrow-dolomite associations are limited to a solitary occurrence [Figure A2.26].

CHAPTER 3

LIMESTONE AND LIMESTONE DIAGENESIS

3.1. ORIGIN OF PRIMARY CARBONATE GRAINS

Although considerable recrystallization has occurred, the Amuri Limestone Group depositional sequence resembles chalk sequences of Europe (such as described by Wolfe 1968, Håkansson *et al.* 1974, Scholle 1974, Hancock 1975, Scholle *et al.* 1983, Johnsson and Reynolds 1986, Mount and Ward 1986), and North America (e.g. Scholle *et al.* 1983, ROCC 1986, Laferrier *et al.* 1987). Chalks such as these consist mostly of coccoliths (defined as the calcareous plates that constitute the outer skeleton of coccolithophorids, Bates and Jackson 1984) and coccolithophorids (Scholle 1977). The Oxford Chalk of Canterbury, which along with the Amuri Limestone Group is considered part of the same time transgressive lithological unit (van der Lingen *et al.* 1978), is also composed of nannofossils. The scanning electron microscope (SEM) and petrographic analyses, plus the similarity to the examples mentioned above, suggest that the Amuri Limestone was originally a nannofossil ooze, with subordinate microfossils comprising mainly planktonic foraminifera. With the exception of the Upper and Lower Marls, the oozes were probably detrital poor. Like other nannofossil chalks (e.g. Hancock 1975), Amuri Limestone micrites have high $CaCO_3$ contents (excluding authigenic insoluble residue). Analogous foraminifera-bearing, nannofossil oozes, poor in detrital and biogenic siliceous material have been found in DSDP cores in the vicinity of New Zealand (e.g. Nelson 1985). The primary carbonate mineralogy of foraminifera bearing nannofossil oozes is low-Mg calcite (Garrison 1981, Scholle *et al.* 1983). It therefore seems reasonable to assume an initial low-Mg calcite mineralogy for Amuri Limestone Group sediments.

No evidence of a significant siliceous microfossil component is found. However, this does not preclude the possibility of accumulations of siliceous organisms in units currently completely chertified (e.g. BC Zone, LCM Subzone).

3.2. MARL-MICRITE ALTERNATIONS

Marl-micrite alternations are absent from the BC Zone, rare to absent in the CD Zone, volumetrically minor in the CL Zone, and relatively abundant in the LL and ML Zones. The alternations are best developed in the LM and UM Zones. The main distinguishing feature between the micrites and

interbedded marls is the carbonate content. The two reasons for this difference which are debated in the literature are discussed below.

3.2.1. DIAGENETIC CONTROL

A number of authors favour a primarily diagenetic control for the genesis of marl-micrite alternations (e.g. Hallam 1964, 1986, Eder 1982, Ricken and Hemleben 1982, Gluyas 1984, Ricken 1985, 1986, 1987). Local dissolution and reprecipitation in oozes to form limestones and chalks may occur during early burial (Matter 1974). The extent of this process depends on the "diagenetic potential" the sediment possessed on burial (Schlanger and Douglas 1974). Differentiation into marls and micrites results from the early diagenetic redistribution of carbonate due to migration of pore waters (Eder 1982). Redistribution of major and trace elements may also occur (Ricken 1986). The fluids may be meteoric in origin (Steinen 1978), hydrothermal (Scholle 1974), or marine. Probably bacterially initiated, the carbonate redistribution may enhance differences in carbonate/clastic composition of an originally marly sediment (Eder 1982).

A bacterial influence in carbonate precipitation has been advanced by a number of authors (e.g. Lippman 1973, Jeans 1980, Hesse 1986, Raiswell 1987, 1988a). It is proposed that thin zones of methane oxidation produce confined zones of carbonate precipitation in the upper one metre of the sediment (Raiswell 1987, 1988a). The primary control, which also governs the final bed thickness, is a break in sedimentation (see also Jeans 1980). Contributions of carbonate from anaerobic methane oxidation are recognized by the occurrence of pyrite that is isotopically heavier than pyrite in the host sediment (Raiswell 1988a).

Earlier analyses of diagenetic bedding (Ricken 1986) were generally qualitative. More recently, Ricken (1986, 1987) has provided a quantitative assessment of this type of bedding. According to his model the diagenetic alternations are formed in bioturbated calcareous oozes, with small to moderate variations in carbonate content. The resulting marl-micrite alternations are produced parallel to bedding under an overburden of 100 metres or more. Initial differences in the primary carbonate content of layers later to become dissolution (marl) and cementation (micrite) zones range from 2-17 percent. Following mechanical

compaction, cementation of micrite layers occurs. It is thought that differences in lithostatic stress arises at the contacts between grains in cemented and grains in uncemented layers, leading to a self perpetuating carbonate dissolution-reprecipitation process. However, large diagenetic carbonate oscillations are not generated until pore space is reduced to less than 30 percent. At the overburden pressures indicated (i.e. >100 m) in this model, the carbonate is apparently redistributed in a closed system. Trace elements in the marls behave like insoluble particles, and become relatively enriched therein. Any elements that do get mobilized from the marls will be reprecipitated in adjacent micrites. Early lithification with little reduction in pore volume, means that the micrite beds could receive large volumes of carbonate from marls, and that the marls would later undergo a high degree of compaction.

Ricken (1986) recognizes three types of alternation which depend on the degree of compaction (the compaction is related to the primary carbonate content). Primary sediments with 60-80% carbonate undergo relatively high degrees of compaction and relatively little carbonate redistribution. The result is moderate to poor rhythmicity of alternations. A carbonate content of 75-90 percent and moderate compaction produce marl beds approximately half the thickness of micrite beds. When the carbonate content of the sediment is in excess of 85% and there is little compaction, the result is highly rhythmic marl-micrite alternations. In this latter case marls are thin and the micrite beds are much thicker. Alternations may be produced in this manner irrespective of whether the original sediment possessed primary stratification or not (Ricken 1986).

For massive beds in argillaceous platform limestones, Bathurst (1987) suggested a similar mechanism, whereby the micrites are cemented before the completion of mechanical compaction. Thereafter, mechanical compaction and pressure solution are concentrated in the less cemented layers to produce the marls. These processes follow hydrodynamic reworking and bioturbation of the sediments, with pressure solution acting late in the diagenetic history.

3.2.2. DEPOSITIONAL CONTROL

The second view is that marl-micrite alternations are a response to a primary depositional trigger (e.g. Einsele 1982, Mount and Ward 1986).

The primary mechanisms invoked are Milankovitch-type climate controls (Schwarzacher and Fischer 1982, Laferriere *et al.* 1987, ROCC 1986) which may govern carbonate productivity (e.g. Johnsson and Reynolds 1986), and processes supplying detrital material to the pelagic realm (ROCC 1986).

The result of primary depositional control is a rhythmic dilution of carbonate by detrital material (Mount and Ward 1986). Later modification by diagenesis may enhance the primary depositional differences (Einsele 1982, ROCC 1986). Sediment fluxes are governed by weathering regimes, rainfall, and runoff on adjacent landmasses, whereas carbonate productivity depends upon nutrient supply which in turn is governed by oceanographic factors such as upwelling. Whether detrital fluxes or fluctuations in productivity are more important depends on the depositional setting. Where sediment fluxes are minimal, productivity becomes more important and vice versa. Authors commonly suggest a combination of productivity variations and dilution by clastic material (e.g. Johnsson and Reynolds 1986, ROCC 1986). Cycles in the middle and upper chalks of the Late Cretaceous of southeast England consist of chalk alternations, omission surfaces, winnowed horizons, nodular chalks and hardgrounds (Kennedy and Garrison 1975). All these features are related by these authors to fluctuations in the energy of bottom currents which in turn are induced by the earth's orbital cycles (e.g. Robinson 1986). In addition, tectonic effects such as uplift on adjacent landmasses will affect sediment supplies, and may mask Milankovitch-type cyclicity (Laferriere *et al.* 1987).

Interestingly, although the mechanism proposed by Bathurst (1987) is essentially diagenetically controlled, he suggested that the selective cementation was controlled by some depositional signal that was widespread. However, he could not discern what the signal was, nor could he explain how it might have survived bioturbation and hydrodynamic reworking.

3.2.3. ORIGIN OF MARL-MICRITE ALTERNATIONS IN THE AMURI LIMESTONE GROUP

Detailed sedimentological and geochemical investigation, plus detailed stratigraphic correlation between sections of differing thicknesses, is required to adequately determine the origin of the alternations in the Amuri Limestone Group. However, the alternations are thought to result

primarily from the diagenetic enhancement of minor carbonate variations in the sediment, as described by Ricken (1986). Although the data in this study is limited, the following observations support the diagenetic control hypothesis:

1) Higher concentrations of most elements in the carbonate fraction of marls than in micrites. It seems reasonable to assume that the composition of the original carbonate in both marls and micrites was initially similar. Therefore the observed geochemical differences could only have come about after deposition. Differences cannot be explained in terms of analytical uncertainty or from leaching of insoluble residues.

2) Limited development of marl-micrite alternations where there are extensive chert and dolomite occurrences. If alternations were dominantly controlled by depositional mechanisms, evidence of primary lithologic variation in the units such as the upper BC Zone and the CD Zone would be expected. In the field such evidence is limited to only rare mudstones and marls. In thin section, samples of dolomite marginal to chert nodules tend to contain more detrital material than cherts from bed centres [see Sections A5.2.4 and A6.2.3]. This implies that although primary lithologic variations may have existed, alternations did not develop. Only where early silica cementation did not occur could alternations form.

3) The presence of diagenetic pyrite suggests a bacterial influence [see also Chapters 4 and 5], implying organically controlled carbonate precipitation. Unfortunately $\delta^{34}S$ data is unavailable for verification.

3.3. NODULAR BEDDING

3.3.1. CAUSES OF NODULAR BEDDING

Examples of very early diagenetic origins for nodular beds are described from the Upper Cretaceous Chalk of southern England (Kennedy and Garrison 1975), and from Jurassic pelagic deposits in the Alpine Mediterranean region (Jenkyns 1974). In these cases the nodular chalks are thought to be associated with periods of little or no sedimentation, and result from early cementation. Proximity to the sediment-water interface is thought to be a prerequisite. Nodules grow from isolated centres and may later coalesce to form continuous to semi-continuous lithified layers. The source of the cementing carbonate is seawater (Kennedy and Garrison 1975).

Diagenetic unmixing may also produce nodular beds (Hallam 1986). In northwest European shales, the nodular beds are also of early diagenetic origin, with the carbonate generated from bacterial catabolysis of organic matter (Gluyas 1984). Submarine dissolution at or near the sea floor, which may postdate some early cementation (Bjørklykke 1973), can produce nodular carbonates.

Examples of later diagenetic origins include sedimentary boudinage (McCrossan 1958), or pressure solution (Wanless 1979, 1983). Sedimentary boudinage is caused by the unconfined compaction of oozes containing varying proportions of clay near the depositional surface (McCrossan 1958). Unconfined compaction causes lateral extension of beds, during which the more carbonate-rich beds thin and eventually pinch out to form carbonate lenses. Continued burial compaction and increased hydrostatic pressure due to overburden cause the lenses to become more rounded, and carbonate-poor material to be squeezed between them. Finally a complete random scattering of carbonate lenses throughout the sediment may be achieved (McCrossan 1958). The genesis of nodular bedding by pressure solution occurs along non-sutured seams under overburden pressure (Wanless 1979, 1983). The seam acts as a pathway for the dissolved carbonate, which may precipitate elsewhere in the bed. The thinning of beds between nodules occurs from solution in "microstylolite swarms" (Wanless 1979, 1983). Nodular bedding produced in this manner may or may not be defined by precursor sediment characteristics (Wanless 1983).

Möller and Kvingan (1988) present an integrated model for the genesis of nodular limestones in Ordovician and Silurian rocks of the Oslo region. Essentially the nodular beds were formed by early diagenetic concretionary cementation close to the sediment-water interface. The final shape of the beds is due to deep burial–induced pressure solution and cleavage. The carbonate for early cementation was derived from seawater in coarse grained permeable beds, and in finer grained clay-rich sediments the carbonate is redistributed from relatively clay-rich layers to clay-poor layers (Möller and Kvingan 1988). As a cautionary note, these authors add that no single mechanism, or sequence of mechanisms, exist that explain the formation of all nodular limestones (Möller and Kvingan 1988).

Another interesting hypothesis for the formation of nodular beds is nodule expansion due to growth of cement crystals (McBride and Folk 1979). The

idea is based on volume increases during crystallization (as in the formation of ice from water) however, there is no evidence for expansive crystal growth of silica (McBride and Folk 1979).

3.3.2. NODULAR BEDDING IN THE AMURI LIMESTONE GROUP

Unlike the situations discussed above, nodular bedding in the Amuri Limestone Group is associated with chert and siliceous limestone, and also with dolomite. Therefore any explanation of nodular bedding must take these occurrences into account.

In Chapter 2 it is concluded that chert and dolomite formation was an early diagenetic process. Therefore, it is suggested that early silica cementation occurred in an analogous fashion to concretionary carbonate cementation. Some centres of cementation may have coalesced to form elongated nodules and bands. The common 'pinch and swell' morphology [such as shown in Figures A2.14. A2.15, A2.21, A2.35b] is then produced by differential compaction of poorly cemented beds, or parts of beds, around nodules as suggested by McBride and Folk (1979). Localized dissolution may aid the process.

Early and relatively homogeneous cementation of beds prior to compaction may result in more planar bedding, whereas differential cementation may be reflected by nodular beds. Support for the early formation of nodular beds comes from soft sediment deformation features [e.g. Figures A2.18, A2.19] and that individual beds are thinnest where they contain little or no chert. The highly nodular and contorted beds such as in Figures A2.25 and A2.35a, are thought to result from soft sediment deformation of partially silica cemented sediments which are subsequently completely chertified [Section 2.3]. Formation of all forms of nodular bedding is envisaged to occur in the upper ten's of metres of the sediment column. Stylolitic development of nodular bedding is thought unlikely, primarily because of the paucity of stylolites. In addition, stylolitization is inferred to be a later diagenetic process. To develop the microstylolites associated with the thinning of beds apparently requires insoluble residue contents in excess of 10% (Wanless 1979). Unchertified micrites are very pure, suggesting that insoluble residues were below 10 percent. Therefore, it is thought unlikely that microstylolites could develop prior to dolomitization and silica cementation.

3.4. COMPACTION

3.4.1. GENERAL CONSIDERATIONS

There are essentially two types of compaction: mechanical and chemical (Scholle 1977). Mechanical compaction moves grains closer together by breakage or repacking. Chemical compaction involves pressure solution which causes stylolites and solution seams, and reduction in volume by solution transfer and reprecipitation (Scholle 1977).

It was at one time generally accepted that carbonate muds underwent little early mechanical compaction (Friedman and Sanders 1978, see also discussions in Shinn *et al.* 1977, Bhattacharyya and Friedman 1984). The reasons commonly advanced for little compaction are the resistance to compression of limestones due to early cementation (e.g. Steinen 1978), and the unfragmented nature of fossils in some limestones (e.g. Zankl 1969, Blatt *et al.* 1980). There is now increasing evidence for compaction in marls and micrites. For example Shinn *et al.* (1977), and Bhattacharyya and Friedman (1984), showed that microfossils in marls commonly remain relatively unfragmented despite high compaction. Experiments have shown that under as little as 100 metres of overburden, carbonate sediments can compact to one-half their original thickness, with accompanying porosity losses of 50-60% (Choquette and James 1987). Deformation of burrows has been used as evidence of compaction (Ricken 1985, 1986, 1987). In addition there is some evidence that the mechanical breakage of fossils may result from compaction (Matter 1974, Schlanger and Douglas 1974). There is considerable evidence for the differential compaction between carbonate-rich (cemented) and argillaceous-rich (uncemented) layers [see Section 3.2 and references therein]. The argillaceous layers generally undergo greater compaction than the cemented layers.

Unlike mechanical compaction, pressure solution has for some time been recognized as significant in limestones (see review by Choquette and James 1987). The products of pressure solution, stylolites and other solution seams, and their significance have been studied by numerous workers (e.g. Bathurst 1975, 1987, Wanless 1979, 1983, Flügel 1982, Choquette and James 1987, and others). Chemical compaction is inferred to be a later diagenetic process than mechanical compaction (Bathurst 1987), probably occurring at depths of 100 metres or more (Scholle 1977, Choquette and

James 1987, Möller and Kvingan 1988). However, in contrast to the conclusions of Wanless (1979), porosity reduction by pressure solution is now thought to be subordinate to porosity reduction due to mechanical compaction (Choquette and James 1987, Bathurst 1987).

Ricken (1986, 1987) has attempted to quantify compaction effects in micrites and marl alternations. Compaction can be measured directly by analysis of deformation of circular bioturbation traces. The measure of deformation is obtained from the ratio of major and minor axes of the burrow ellipses. A critical factor in these calculations is that burrows are compacted to the same extent as the surrounding sediment. If early cementation occurs in burrows, they will compact to a lesser extent than the surrounding sediment, giving erroneous compaction measurements. In addition, the relative timing of burrowing and compaction must be ascertained. Trace fossil assemblages are usually produced by successive communities reworking the same sediment (Bromley and Ekdale 1986). Assemblages consist of a mixture of deformed and relatively undeformed burrows (see illustrations in Ekdale and Bromley 1984a,b, Bromley and Ekdale 1986). The best preserved traces most commonly represent the deepest burrows, and therefore are less indicative of conditions at the sea floor than poorly preserved shallow traces (Bromley and Ekdale 1986). In addition, well preserved and relatively undeformed traces may result from burrowing into already partially lithified sediments. On selectively cemented burrow structures an indirect method of determining compaction may be employed. This technique uses the "carbonate compaction law" (Ricken 1986, 1987) and requires measurement of the carbonate and clay contents in both the burrow and surrounding sediment. The insoluble residue content in both the burrow and surrounding sediment are assumed to be constant (Ricken 1986, 1987). The compaction is then obtained from the ratio of the standardized insoluble (i.e. standardized to the primary decompacted sediment volume) and the relative insoluble content (i.e. the insoluble residue content expressed as 100 - weight% measured carbonate).

3.4.2. COMPACTION IN THE AMURI LIMESTONE GROUP

Early cementation in the BC, CD, and CL Zones [Section 3.2] may imply that compaction thereafter was limited to rare marl beds, and to differential compaction of uncemented micrite beds around nodules. If so, then overall compaction in the BC to CL Zones was probably limited. Compaction in the

LM and UM Zones, as a result of their primary argillaceous nature, was probably much more pronounced than in underlying zones. Compaction in the ML Zone may have been greater than in Zones in the Mead Hill Formation. The few LM and UM Zone samples analyzed, and literature on similar lithologies suggests that the marls underwent significant mechanical compaction and pressure solution (probably non-sutured seam solution, Wanless 1979). The ML Zone on the other hand underwent considerable stylolitization; the stylolites probably reflect a lower original detrital content than in the UM and LM Zones. The absence of stylolites from chert bearing beds in the ML Zone [Figure A2.39], and the thickness of such beds suggests that stylolite formation in nonchert bearing beds post-dated chert formation (this conclusion also applies to the Zones in the Mead Hill Formation). Mechanical compaction effects in the ML Zone are difficult to ascertain.

Quantitative determinations of compaction using the methods of Ricken (1986, 1987) are difficult. In the BC to CL Zones, suitable burrows for direct measurement are rare, and those present are silicified to greater or lesser extent. The silicification means the constancy of insoluble residue contents cannot be assumed, and such rocks are specifically excluded by Ricken (1986). The relative timing of burrowing and compaction may be equivocal, as suggested in the discussion in Section 3.4.1. However, it is clear that the extent of compaction throughout the Amuri Limestone Group is variable. Sediments of similar original composition to the Amuri Limestone Group have porosities of the order of 80% (Garrison 1981 and references therein). Figure A3.4b for example, shows Amuri Limestone sediments to have low porosities. Discussions in Sections 3.2 and 3.3 indicate the importance of early cementation to porosity reduction. Without detailed study, quantitative assessment of compaction in the Amuri Limestone Group is at best rudimentary. Measurement of the thickness of beds containing chert nodules, and beds that thin around nodules (in the BC, CD, and CL Zones), yields differences of approximately 30 percent. In some instances thickness differences are extreme [e.g. Figure A2.35b]. Compaction of 20-30% has been measured in micrite beds in other studies (Ricken 1985). As suggested earlier, the bulk of compaction probably occurred in the marls. In other studies, compaction of marls of up to 80% have been recorded (Ricken 1985), and similar compaction is conceivable for Amuri Limestone Group marls. The ML Zone is a very pure limestone, indicating that little compaction could

have occurred in any original marly layers. Stylolitization may account for thickness reductions of about 20-35% in ML Zone type lithologies (Choquette and James 1987).

In contrast, there is direct measurable evidence of compaction in the WC Zone. This is indicated by the difference in bed thickness between concretions and the surrounding sediment. At Kaikoura Peninsula (3) beds are 16-20 cm thick in concretions and 3-5 cm thick in the sediment. At Branch Stream (28) beds in concretions are 12-13 cm thick and <2 cm thick in surrounding mudstones. Both represent compaction of 75-80 percent, which is similar to values suggested for marls.

3.5. ASPECTS OF LIMESTONE GEOCHEMISTRY

3.5.1. ORIGIN OF RED MICRITES

Pyrite in white to light grey micrites which comprise the bulk of the Amuri Limestone implies reducing conditions, whereas Fe-oxides and rare pyrite in red to pink micrites indicates oxidizing conditions. Similar associations of red colours with oxidized sediments and grey to white colours with pyrite and reducing conditions are found in DSDP cores (e.g Nelson 1985).

Channel *et al.* (1982) interpreted haematite in red limestones from Gubbio (Italy) to be of diagenetic origin because colours varied both within and between beds. Similar variations may be seen at Chancet Rocks and Needles Point, and thin sections of rare pyrite from these localities are commonly surrounded by Fe-oxide. Thus Fe-oxides in red Amuri Limestone Group micrites are inferred to be of diagenetic origin.

Diagenetic Fe-oxides such as haematite in pelagic limestones may be produced in a number of ways including by alteration of Fe-Mg silicates or Fe-bearing clay minerals, or the dehydration of goethite (Channell *et al.* 1982). The paucity of detrital grains in the pink limestones suggests that goethite dehydration is most likely, although clay mineral-derived Fe may still be an important contributor. Goethite is inferred to be the first form of hydrous Fe-oxide to be deposited, which then converts to haematite (Murray 1979). In limestones similar to the Amuri, haematite production is thought to depend upon the

organic matter content and the relative sedimentation rate (Channel *et al.* 1982). Low sedimentation rates cause organic matter to be continually oxidized, thereby favouring goethite precipitation and subsequent dehydration to hematite. Higher sedimentation rates favour pyrite formation due to goethite reduction (Channell *et al.* 1982). Morris (1987) suggested that sedimentation rates were lower in the Amuri Limestone basin margins than in the depocentre. His evidence for sedimentation rate variations was differences in bed thickness between depocentre and basin margin micrites (the latter includes the red micrites). However, such variations in sedimentation rate remain equivocal because:

i) Individual beds were not traced from locality to locality.
ii) If micrite beds are primarily diagenetic (as suggested in Section 3.2.3) then measured bed thicknesses may not represent depositional bed thicknesses.
iii) Only a few basin margin localities contain red micrites.
iv) There is no evidence for variations in sedimentation rate between red and white micrite beds at individual localities.

The oxidation zone in DSDP oozes is usually only a few centimetres thick, but some are found to extend to depths of 7 m below the sediment-water interface (e.g. Nelson 1985). The oxidation zone at localities north from Woodside Creek may also have been relatively thick and/or pervasive, resulting in greater oxidation of organic matter than occurred elsewhere. The relatively greater permeability in burrows probably aided the distribution of oxic water into the sediment. Thus, the distribution of Fe-oxides was probably influenced by variations in organic matter content and the extent of oxic water penetration into the sediment. Oxidation was not homogeneous as indicated by variations in colour both between and within beds [e.g. Figure A2.31]. Not all the Fe in red micrites was oxidized as many cherts contain pyrite, indicating that reducing conditions could still prevail on a microscopic scale.

3.5.2. OXYGEN ISOTOPE GEOCHEMISTRY

The range of Amuri Limestone Group micrite compositions is -1.32·/..$_{PDB}$ to -6.90·/..$_{PDB}$ with a mean of -4.36·/..$_{PDB}$ [Table A5.1]. Paleotemperatures are obtained using the now well established calcite-water fractionation (O'Neil *et al.* 1969, Friedman and O'Neil 1977):

$$1000 \times \ln\alpha_{Calcite\text{-}Water} = 2.78 \times 10^6 \times (T^{-2}) - 2.89$$

where:

T = Temperature (°K)

α = The fractionation factor

$= \{(O^{18}/O^{16})_{Calcite}/(O^{18}/O^{16})_{Water}\}$

$= (1000 + \delta^{18}O)_{Calcite}/(1000 + \delta^{18}O)_{Water}$

Calcite temperatures are calculated from the O'Neil *et al.* equation in the form derived by Epstein *et al.* (1953) which is as follows (Shackleton and Kennett 1975):

$$T\ (°C) = 16.9 - 4.38(\delta_{Calcite} - \delta_{Water}) + 0.10(\delta_{Calcite} - \delta_{Water})^2$$

Results are summarized in Table 3.1.

The ^{18}O composition of calcite in micrites depends on the temperature and isotopic composition of the fluids of crystallization. The isotopic composition of Late Cretaceous to Early Tertiary ocean water (Shackleton and Kennett 1975), combined with evidence of pore water ^{18}O depletions, suggests that Amuri Limestone Group micrites formed and/or recrystallized in fluids of -1.2·/.. to possibly -2.0 per mil. These values and that of modern seawater (0·/..) are used for δ_{Water}.

Bottom water temperatures estimated for the Cretaceous to Paleocene were approximately 10°C, whereas surface water temperatures of 20-25°C (Savin *et al.* 1975, Savin 1977, Savin and Yeh 1981). Therefore lower temperatures (i.e. $\delta^{18}O$ in the approximate range of 0·/.. to -2.0·/..) may represent temperatures associated with primary carbonate formation (cf. curves for coccolithophorids and foraminifera constructed by Savin *et al.* 1975). Some calcite temperatures are in excess of 20°C. These higher temperatures, and depletion in ^{18}O to less than -2·/.., may arise through interaction with meteoric water depleted in ^{18}O compared to seawater (Land 1980, 1983a), or recrystallization at elevated temperatures (Land 1980, Jørgensen 1987). Unfortunately both processes may produce carbonates of similar composition.

Magnesium, Sr^{2+}, Fe^{2+}, K^+, Na^+ and Mn^{2+} concentrations do not appear to reflect meteoric water interaction [see also discussions in Sections 4.3]. Land (1980, 1983a) presents an example of basinward increases in trace element concentrations and $\delta^{18}O$ due to meteoric induced recrystallization.

Table 3.1 Paleotemperatures for the range of micrite $\delta^{18}O$ values.

$\delta^{18}O$	T_1°C δ Water = 0	T_2°C δ Water = -1.2	T_3°C δ Water = -2.0
Minimum = -6.90	23	17	14
Maximum = -1.32	52	45	41
Mean = -4.36	38	32	2

The lack of any similar regional pattern in this study also argues against regional meteoric influences.

Recrystallization is inferred to account for Sr^{2+} concentrations [Section 4.3.2]. Solid calcite in sediments has been found to be depleted in ^{18}O, and the surrounding pore water enriched (Land 1980, Jørgensen 1987), as a result of early calcite recrystallization. SEM micrographs [Figure A3.4] plus stylolitization show that recrystallization has occurred in Amuri Limestone Group micrites. Comparison of marl-micrite pairs [Table A3.1] show an overall depletion in ^{18}O with age, suggesting the effect was greatest near the base of the sequence. In addition, many of the calcites analyzed are closely associated with chert. The ^{18}O composition of the calcite may have been altered through enhancement of calcite dissolution and reprecipitation by chertification, resulting in secondary calcite forming at shallower depth than indicated by their paleotemperature.

Therefore the range of ^{18}O compositions in micrites are interpreted to represent relative degrees of recrystallization in each sample. Less recrystallization has occurred in samples approximating seawater temperatures and more in relatively ^{18}O depleted samples. A much more detailed analysis of ^{18}O is required to assess accurately the relative importance of burial and chertification in recrystallization. However, it is thought that early chert formation would have a significant effect in the Mead Hill Formation, with burial diagenetic recrystallization (e.g. stylolitization in the ML Zone) predominating stratigraphically above.

3.6. SUMMARY

Despite limited data, the following observations may be made:

1) The original Amuri Limestone sediment was probably a foraminiferal nannofossil ooze. Comparison with literature data suggests low-Mg calcite was the primary mineralogy.

2) Nodular bedding probably results from concretionary style cementation, followed by differential compaction.

3) Marl-micrite alternations are probably primarily diagenetically controlled. Primary depositional signals may or may not have exerted some

influence on the final distribution of marl and micrite layers. The alternations result from carbonate redistribution, which was probably bacterially mediated. Subsequent compaction enhanced the difference between marls and micrites. The absence of alternations from units containing extensive chert and dolomite suggests that the development of marls and micrites post-dates chert and dolomite formation.

4) The amount of compaction in the Amuri Limestone Group is variable, with different Zones compacting to differing extents, depending upon factors such as the abundance of marls, and the extent of early cementation. The bulk of compaction probably post-dated early cementation (i.e. chert and dolomite formation) in the BC, CD, CL Zones, and LCM Subzone.

5) The isotopic composition of the micrites appears to primarily reflect the degree of calcite recrystallization. Red micrites result from the presence of oxidized Fe, whereas white to light grey micrites contain reduced Fe in the form of sulphides.

CHAPTER 4

DOLOMITE PETROLOGY AND GEOCHEMISTRY

4.1. DOLOMITE TEXTURES AND FABRIC

4.1.1. DOLOMITE FABRIC

Detailed petrographic descriptions are in Sections A5.2 to A5.4. A summary of carbonate recrystallization fabrics and terminology is given in Section A7.2.4.

In general Amuri Limestone Group dolomites are idiotopic according to the scheme of Gregg and Sibley (1984). However, in the CD Zone, a number of samples have the crystal shape associated with idiotopic-S, but the crystal-matrix relationship of idiotopic-P. This is also the case for the LCM Subzone dolomites from within the CL Zone at Mead Stream. Porphyrotopic dolomite in both the LCM Subzone and CD Zone range from idiotopic-P to xenotopic-P. Thin sections from a single concretion from Lab Rocks [Figure A5.2a,b], have xenotopic-A textures at the centre of the concretion and idiotopic-S at the margins.

Idiotopic dolomite is thought to form at a temperature below which dolomite crystals with irregular margins form. The temperature is referred to as the critical roughening temperature or CRT (Gregg and Sibley 1984, Sibley and Gregg 1987). If such a temperature dependence of fabric is valid, then much of the dolomite in this study formed below the (CRT) inferred by these authors to be approximately 50°C (however, Shukla (1986) contends the CRT may be as low as 35°C). Whatever the value of the CRT, the petrographic evidence suggests a low temperature or early diagenetic origin, which is supported by $\delta^{18}O$ data [Section 4.4.2]. Thin section petrography also indicates that Amuri Limestone Group dolomite result from heterogeneous dolomitization [see Section A7.2.4] initiated by nucleation of isolated dolomite rhombs in a usually calcite mud matrix. According to the model of Randazzo and Zachos (1983/1984), porphyrotopic to almost mosaic fabrics (as observed in the Amuri Limestone Group), suggest that dolomitization may have proceeded over a relatively long period of time (i.e. of the order of 1000 years or more). Replacement by dolomite tends to be affected by grainsize of the precursor mineral with smaller grains being replaced preferentially (Bullen and Sibley 1984). The high surface area of crystals in micrites means more possible nucleation sites (see discussions in Murray and Lucia 1967, Sibley 1982, Bullen & Sibley 1984). Thus allochems are replaced progressively after

micrite; hence the lack of attack of foraminifera in porphyrotopic samples [e.g. Figure A5.9].

Although generally applicable, observations from this study indicate shortcomings in the fabric classification schemes [see Section A7.2.4]. All the schemes consider recrystallization of carbonate alone and ignore competing reactions such as chertification. Contemporaneous chertification may effect crystal growth by the physical presence of nucleated silica, or through alteration of physio-chemical conditions due to silica deposition. The Gregg and Sibley scheme claims temperature to be the dominant control over fabric, but there are other controls on crystal morphology in addition to temperature (Gregg and Sibley 1984, Sibley and Gregg 1986, Shukla 1986). Sibley (1982, p1097) states that textures are controlled by; *"1) the mineralogy of the material being replaced, 2) whether or not the dolomitizing solution is saturated with respect to the mineral being replaced, and 3) the availability of nucleation sites."* Controls other than temperature are indicated by the variation in crystal morphology across concretions (as in this study), or even within a single thin section (Shukla 1986). The presence of non-carbonate material is likely to be important. Detrital grains are commonly seen in intercrystalline matrix, and samples from the lower BC, and CD Zones are more xenotopic where detrital material is more abundant. Thus the presence of detrital grains may govern crystal morphology by inhibiting the development of crystal faces. Factors such as ion availability, nucleation competition (Gregg and Sibley 1984), and possibly crystal growth rates will also have effects.

4.1.2. CRYSTAL TEXTURES

Origin of Inclusion Patterns

Cloudy-centre clear-rim (CCCR) dolomites are commonly reported in the literature (e.g. Murray 1964, Sibley 1980, 1982,). They result from the concentration of inclusions, commonly calcite (Sibley 1982) or fluid, at crystal centres. The Amuri Limestone Group fluid inclusions appear to be primary and as such probably contain remnants of the dolomitizing brines. Previously, the local source theory has been used to explain the origin of CCCR dolomites (Murray 1960, 1964, Weyl 1960, Blatt *et al.* 1980). In this theory Mg^{2+} replaces Ca^{2+} with CO_3^{2-} being derived from the site of

formation and essentially remaining conservative. As the dolomite grows, it creates porosity around the growing margin which results in clear rims due to lack of material to include. Remaining porosity is either subsequently destroyed by compaction or remains resulting in sucrosic dolomites. Sibley (1980, 1982) found from examination of low-Mg calcite inclusions in dolomites that this theory may be incorrect, and suggested that CCCR dolomites may be associated with freshwater diagenesis. Initially, dolomitizing waters were near saturation with respect to calcite, hence their incorporation as fluid inclusions. Later, undersaturated fluids meant that rims were inclusion free. Neither the local source theory, nor the meteoric water hypothesis, explain the inclusion patterns associated with the LCM Subzone. To be adequate, any model for the incorporation of inclusions must explain both CCCR and planar patterns.

Work by Kastner (1970) on hourglass inclusion patterns in gypsum provides a possible mechanism for variations in inclusion patterns. Inclusions are either pushed aside or included depending on crystal growth rates. At relatively low growth rates, particles are pushed aside, whereas at progressively higher rates proportionally more particles are included.

If slow growing crystals push aside prospective inclusions then inclusion domes or 'halos' may be expected around CCCR dolomite crystals. Even in detrital-rich samples no such halos are observed. However, silt size detrital grains are usually at crystal margins indicating that they may have been excluded during crystallization. Unfortunately since the inclusions are primarily fluid, halos are unlikely to have been preserved particularly following chertification. It is thought however, that growth rates may be important in forming CCCR dolomites.

Planar inclusion patterns in LCM Subzone dolomites [Figure 4.1a,b,c] resemble sector zones or hour glass structures such as in gypsum (Kastner 1970), or igneous minerals like kaersutite (Mokhtari and Velde 1987, Figure 1). The latter example is a compositional effect. The sector-like association combined with observed inclusion patterns [Figure 4.1a,b,c] suggest two possible inclusion distributions [Figure 4.1d,e]. If correct then inclusions are concentrated along growth sector boundaries. Explanation purely in terms of growths rates is thus difficult to rationalize, implying other kinetic factors may be involved [see following

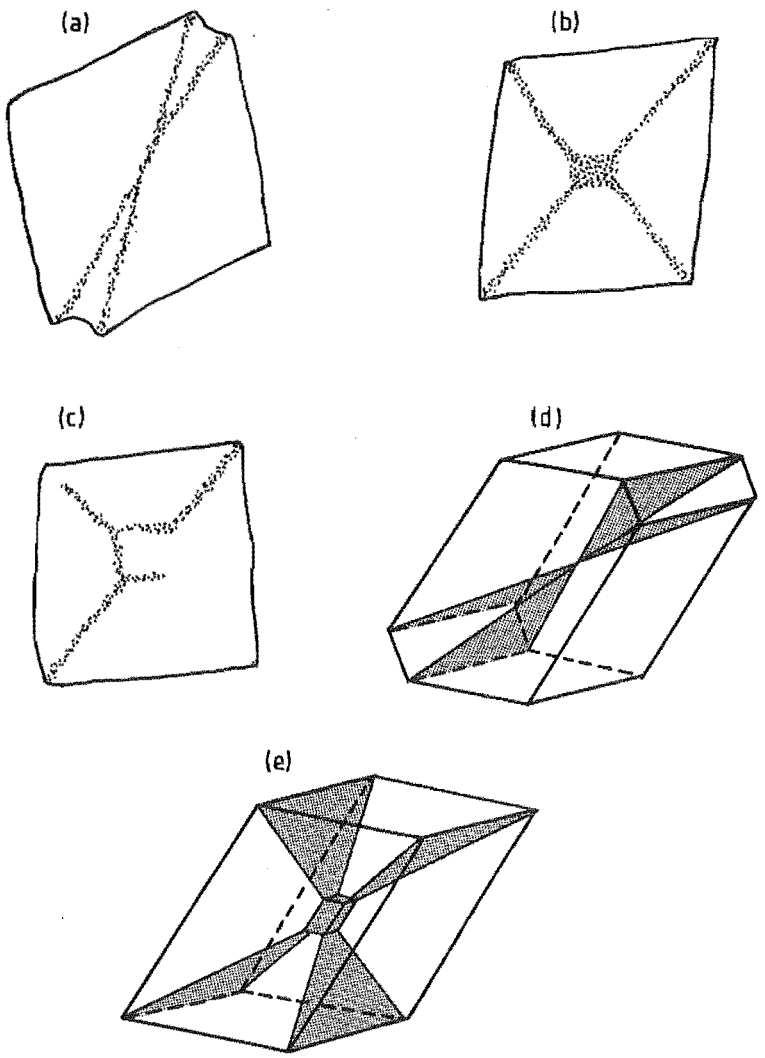

Figure 4.1 Inclusion patterns.
(a,b,c) Inclusion patterns commonly encountered in LCM Subzone dolomites. Inclusion patterns such as (c) indicate that although crystal centres where nucleation commenced may be inclusion free they may be surrounded by inclusions incorporated during later growth.
(d) Inferred three dimensional view of inclusion pattern shown in (a).
(e) Pattern based on (b) and (c).

discussion of extinction patterns].

Possible causes of Sector-like Extinction Patterns

Sector zones usually imply a compositional difference between zones, as has been documented for silicate minerals (e.g. Hollister 1970, Hollister and Garcanz 1970, Dowty 1976, Mokhtari and Velde 1987, and others). Relatively little has been documented in carbonates. The only work found by the author of this thesis is by Frondel *et al.* (1942), Walkden and Berry (1984), Reeder and Prosky (1986), Reeder and Grans (1987).

Differing compositional sectors in carbonates arise from variations in Fe and Mn in particular, and differences in the relative proportions of Ca and Mg (Reeder & Prosky 1986). Invoking the protosite model of Nakamura (1973), these authors state that sector zoning indicates metastable crystallization and may be influenced by differing growth rates on different faces. Thus different crystal faces are likely to have different compositions, and if more than one crystallographic form is present in a crystal, compositional sector zoning may result. If the same form (e.g. 1014) is present throughout, then all faces may theoretically incorporate trace elements to the same extent, and no differences will be observed. Both the planar inclusion and sector-like extinction patterns suggest there is compositional sector zoning in Amuri Limestone Group dolomites. However, the scanning electron microscope (SEM)-EDAX and microprobe analyses did not reveal any significant differences between sectors [Section A5.5.3]. Observed differences between core and rim compositions, and the cathodoluminescence zoning suggests that later homogenization of intracrystal composition to be unlikely. It is suspected that the instruments used lacked the required sensitivity [analyses plus detection limits are discussed in more detail in Section A5.5.3]; thus compositional differences between sectors may be too small to detect. Nothing approximating sector zones was seen by cathodoluminescence either. Therefore, compositional zoning in Amuri Limestone Group dolomite crystals remains unproven.

As well as variations in kinetic factors such as growth rates between crystal forms, there may also be variations along individual faces. Variations may be particularly marked between the crystal face itself and the crystal apex where growth sector boundaries meet. Such variations

along faces may also result in preferential incorporation or exclusion of trace elements. It is conceivable that concentrations of fluid inclusions may be similarly controlled, giving rise to the observed planar patterns along growth sector boundaries. Some supporting evidence for such a control comes from Transmission Electron Microscope observations of other dolomites which show a slight curvature of growth bands (Reeder and Prosky 1986). The curvature was inferred to result from growth rate variation.

Reeder & Prosky (1986) point out that the form of sector zoning they studied is unlikely to be unique, although such sectors may not necessarily be found in all euhedral dolomites. LCM Subzone dolomites display apparent sector zoning as defined by the inclusion patterns. If the extinction patterns also represent sector zones, then they would be expected to completely coincide with planar inclusion patterns. Since they do not, it is likely that the extinction patterns are due to some other effect, and their partial coincidence with the inclusions may be fortuitous. One possible explanation, though not tested, is that trace element incorporation may produce distortions in the crystal lattice. The distortion manifests itself optically in the irregular extinction pattern.

While investigating the extinction patterns an additional feature was observed in a few crystals. Parts of dolomite crystals adjacent to pores have a very undulatory outline and associated radial extinction pattern. The latter may result from a fibrous crystal habit, normal to the plane of the crystal face, such as has been described on diamonds (Machado *et al.* 1985). It may represent growth into voids.

Whether the extinction patterns are produced by a form of sector zoning or lattice distortions remains unresolved. A much more detailed crystallographic analysis is required. It is likely that both the inclusion and extinction patterns are kinetically (possibly growth rate) controlled, but factors such as crystal habit and fluid chemistry are also important. Another possibility, though requiring much more rigorous analysis than can be undertaken here, is that episodes of fibrous growth may also have an effect in some cases.

4.1.3. GROWTH HISTORY

Concentric cathodoluminescence banding provides a record of the growth

history of the crystal, which is not detected in ordinary transmitted light. Some crystals [e.g. Figure A5.12b] appear to have maintained a more or less euhedral shape since nucleation. In others [e.g. Figure A5.13] there is evidence of changes in the orientation of one, or more, crystal faces during growth. In no crystals where concentric zonation can be traced back to early stages of growth is there evidence of termination of zones from dissolution, such as described by Gregg and Hagni (1987) from late dolomite cements. However, other crystals (and detrital grains) may obstruct crystal growth [Figure A5.11b]. Crystal intergrowth is common in idiotopic samples. Beyond the limits of the obstruction the overall luminescence banding is not affected. Correlation of 'growth events', as delineated by concentric banding, from one sample to another, and ultimately stratigraphically (e.g. Ebers and Kopp 1979), is not possible in Amuri Limestone Group samples. Despite intrasample uniformity, too much variability in cathodoluminescence zonation exists within and between diagenetic units.

The core of crystals such as in Figure A5.12a, are different to the final shape of margins. Walkden and Berry (1984) described how an irregular crystal substrate can produce euhedral crystal overgrowths [Figure 4.2]. Growth around irregular cores as in Figure A5.12a may have occurred as shown in Figure 4.2. It is evident however, that dislocations in the crystal structure do not always progress to planar growth surfaces. Dislocations and re-entrant angles in some crystals have been either retained throughout crystal growth, or were initiated later during growth [Figure A5.13]. These features may result from inhibiting (probably kinetic) factors, which affect the crystallographic control of non-facial growth surfaces [Figure 4.2]. The result is the development of irregular or curved crystal margins (Walkden and Berry 1984).

Elucidation of early growth history of CD Zone samples is precluded by the presence of inclusions. Microprobe analyses provide no further information. Clearly, the presence of inclusions in crystals affects the cathodoluminescence zonation. The greater the abundance of inclusions the greater the effect on luminescence. Such an effect is seen in luminescence patterns produced by other authors (e.g. Gregg and Hagni 1987). Cathodoluminescence bands may also be related to physical features in crystals such as surface distortions and cracks (Nickel 1978). Cracks and distortions may be seen in Figure A5.12a where surface irregularities

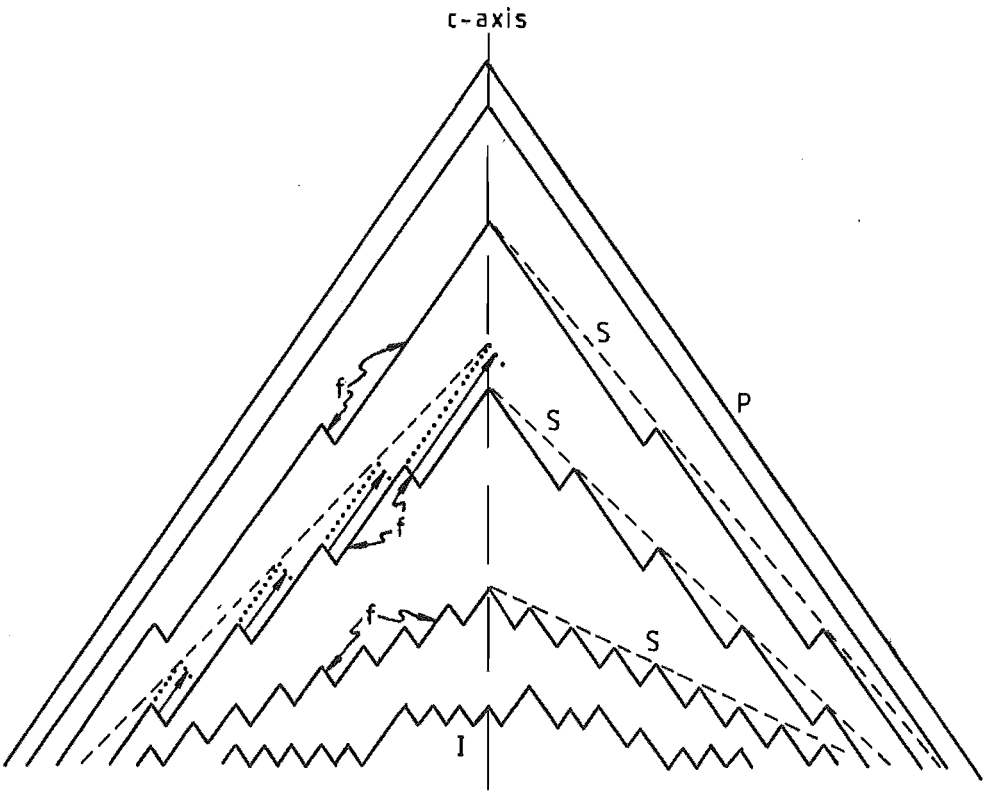

Figure 4.2 Growth of crystal faces from an irregular crystal substrate (I). Unidirectional and independent growth of small facets (F), which define a series of planar non-facial growth surfaces (S - dashed lines), increase in rate and extent towards the crystal apex (arrows and dotted lines). The growth of facets progressively alters the attitude of non-facial growth surfaces until normal crystal-face parallel (P) growth takes over, (From Walken and Berry 1984, Figure 4).

are well marked. Inclusions appear to luminesce in a similar fashion to surface distortions, with both commonly having higher luminescence intensity than the rest of the crystal. The masking of concentric cathodoluminescence zonation by preferential replacement of crystal interiors (e.g. Banner *et al.* 1988) is not observed.

4.2. INSOLUBLE RESIDUE CONTENTS

4.2.1. WC ZONE CONCRETIONS

A single concretion can be considered a zone of carbonate cementation. Concretionary cementation is therefore related to the host sediment porosity (Raiswell 1971). It has been argued that cement precipitation does not enlarge these pore spaces (Raiswell 1971, 1976, Oertel and Curtis 1972). The densities of surrounding sediments (i.e. quartz, feldspar and clay minerals are about 2.6-2.9 gm/cm^3) and dolomite (about 2.8 gm/cm^3) are similar, therefore the weight percent calcite is almost entirely equivalent to the volume percent pore space of the host sediment. The weight% insoluble residue contours in the Lab Rocks concretion [Figure A5.29b] indicate a decrease in porosity from 89% at the nucleation centre to about 80% at the margin. Thus very high porosities prevailed throughout the growth of the concretion. Most of the concretions in this study have porosities in excess of about 70% or more.

The proportion of insoluble residue may be used to estimate burial depths, when it is assumed that carbonate is the only cement precipitated. No replacement or dissolution of the host sediment is also assumed. Theoretically, a mudstone becomes more compacted with burial, enabling burial depth estimates to be made using the following equation (Baldwin and Butler 1985):

$$\text{Burial depth (km)} = 6.02 \times S^{6.35}$$

where:

S = 'solidity' or volume percent of solid grains or insoluble residue (1 - porosity)

Porosity values in excess of 60% indicate burial depths of less than 18 metres, and porosities greater than 80% indicate burial to less than 1

metre. Therefore the weight% insoluble residue in the concretion in Figure A5.29b [Map pocket] indicates an increase in burial depth during formation. While it is realized that there is considerable uncertainty in such estimates, these results are consistent an early diagenetic origin for all concretions.

4.2.2. AMURI LIMESTONE GROUP CARBONATES

There is no systematic variation in insoluble residue content with the presence or absence of dolomite [Section A5.5.2]. Poor relationships between insoluble residue and dolomite or limestone facies have been described by other authors (e.g. Hatfield and Rohrbacher 1966, Lumsden 1974). The bulk of the matrix around Amuri Limestone Group dolomite crystals is authigenic quartz. Silica is also abundant in micrites. Precipitation of authigenic quartz has resulted in the higher insoluble residues in Amuri Limestone Group samples than in WC Zone concretions. In addition, the amount of insoluble residue depends on the proximity to chert nodules; for example micrite samples adjacent to cherts contain more insoluble residue than those further from nodules. Therefore the abundance of insoluble residue in Amuri Limestone Group carbonates reflects the degree of chert development in each sample. The effect of primary deposited insoluble residue is subordinate in the limestone beds, but is more important in marl beds where the extent of silicification is relatively less.

Dolomite insoluble residue compositions are intermediate between marl insoluble residues and Woolshed Formation mudstones, and micrite insoluble residues. Dolomite beds tend to be around or near chert bed margins [Figures A2.14 to A2.19]. If the original sediment was composed of alternating relatively detrital-rich, and relatively detrital-poor layers [see also discussion in Section 3.2.1] then the dolomite may have formed at or near the boundary of the two lithologies. The result would be dolomite insoluble residue compositions reflecting both marl and micrite insoluble residue characteristics. The SiO_2 contents in dolomite insoluble residues are primarily from authigenic silica with the addition of some from detrital sources. Al_2O_3, K_2O and TiO_2 are probably due to the presence of micas and clay minerals [Section 5.2.3].

4.3. MAJOR AND TRACE ELEMENT GEOCHEMISTRY

Geochemical data is described in Section A5.5 and raw data is given in Appendices 9 and 10. Statistical correlations (Pearsons-*r*) quoted in the text were calculated on the data at the 90% significance level. Statistical significance is determined from tables to test Pearsons correlation coefficient, using N-2 degrees of freedom (where N = the number of samples). Verification of correlations is from examination of scatter plots. The correlations are classified as follows: good or high correlations are in the range -1.0 to -0.8 and +0.8 to +1.0; moderate correlations are -0.8 to -0.5 and +0.5 to +0.8. All other values represent poor or low correlations. All correlations mentioned in the text indicate a linear relationship, unless otherwise stated.

4.3.1. MAGNESIUM AND CALCIUM

A number of dolomite formation stoichiometries have been postulated [Table 4.1]. All are essentially mass transfer reactions where only the mass balance of the initial reactants and final products is considered (Machel and Mountjoy 1986). Weyl (1960) suggested that porosity generation by dolomitization of limestone may follow reaction (4.1). A number of authors have since reported that most dolomitized rocks do not appear to have undergone volume changes and display good fabric preservation, suggesting volume-for-volume replacement (Morrow 1982a, Halley and Schmoker 1983, Machel and Mountjoy 1986). Halley and Schmoker (1983) showed that the porosity in dolomites could be inherited from the pre-existing carbonate. Equation (4.1) is thus unsatisfactory as other transfer reactions may be operating (Machel and Mountjoy 1986). These authors suggest that reaction (4.4) and (4.5) which is similar, best represent dolomitization under a variety of conditions because most of the other reactions are derivatives of equation (4.4), and equation (4.4) allows for adjustment for the preservation, loss, or gain of porosity.

For the reasons outlined above it is thought that equation (4.4) is applicable to the dolomitization of the Amuri Limestone Group, and that volume changes may have been limited. Dolomitization of carbonate implies that calcite is dissolved in the molar ratio to dolomite of 2:1, resulting in a volume reduction unless there are additional supplies of Ca^{2+} (Maliva

Table 4.1 Selection of dolomitization reaction stoichiometries (from Machel and Mountjoy 1986, Table 1). Reaction (4.1) is for the general dolomitization of carbonate (Weyl 1960). Reactions (4.2) and (4.3) may represent the formation of dolomite cements. Reaction (4.4) is intermediate between (4.2) and (4.3). Reaction (4.5) is essentially reaction (4.4) but with carbonate in the form of HCO_3^- and includes the pH. Reactions (4.6)-(4.9) are derivations of reaction (4.5) with different values of x. Reactions (4.10)-(4.12) attempt to account for other ions in solution.

$$2CaCO_3 + Mg^{2+} \rightarrow CaMg(CO_3)_2 + Ca^{2+} \quad (4.1)$$

$$Ca^{2+} + Mg^{2+} + 2CO_3^{2-} \rightarrow CaMg(CO_3)_2 \quad (4.2)$$

$$CaCO_3 + Mg^{2+}\ CO_3^{2-} \rightarrow CaMg(CO_3)_2 \quad (4.3)$$

$$(2-x)CaCO_3 + Mg^{2+} + xCO_3^{2-} \rightarrow CaMg(CO_3)_2 + (1-x)Ca^{2+} \quad (4.4)$$

$$(2-x)CaCO_3 + Mg^{2+} + xHCO_3^- \rightarrow CaMg(CO_3)_2 + (1-x)Ca^{2+} + xH^+ \quad (4.5)$$

$$Ca^{2+} + Mg^{2+} + 2HCO_3^- \rightarrow CaMg(CO_3)_2 + 2H^+ \quad (4.6)$$

$$Ca^{2+} + Mg^{2+} + 4HCO_3^- \rightarrow CaMg(CO_3)_2 + 2H_2CO_3^0 \quad (4.7)$$

$$Ca^{2+} + Mg^{2+} + 2HCO_3^- + 2OH^- \rightarrow CaMg(CO_3)_2 + 2H_2O \quad (4.8)$$

$$Ca^{2+} + Mg^{2+} + 4HCO_3^- \rightarrow CaMg(CO_3)_2 + 2H_2O + CO_2 \quad (4.9)$$

$$2CaCO_3 + Mg^{2+} + eSO_4^{2-} + 2dCl^- \rightarrow CaMg(CO_3)_2 + eCaSO_4 + d(Ca^{2+} + 2Cl^-) \quad (4.10)$$

$$2CaCO_3 + Mg^{2+} + SO_4^{2-}(+2H_2O) \rightarrow CaMg(CO_3)_2 + CaSO_4(2H_2O) \quad (4.11)$$

$$aCaCO_3 + bCa^{2+} + cMg^{2+} + dCO_3^{2-} + eSO_4^{2-} + fCl_2^{2-} \rightarrow gCaMg(CO_3)_2 + (a+b-g)Ca^{2+} + (c-g)Mg^{2+} + (a+d-2g)CO_3^{2-} + eSO_4^{2-} + fCl_2^{2-} \quad (4.12)$$

---

and Siever 1988). However, the generation of Ca^{2+} due to replacement by chert (e.g. van der Lingen and Packham 1975) suggests that the dolomitization process in the Amuri Limestone Group can be regarded as essentially a volume-for-volume replacement. In contrast, the carbonate content of the Woolshed Formation was probably limited (see Webb 1966, Morris 1987) which implies stoichiometries such as equations (4.2), (4.3), and (4.6) to (4.9) may be more appropriate.

Source of Magnesium

The Mg/Ca ratio of a dolomite reflects conditions at the time of formation, conditions involved in later stabilization reactions during burial, or a combination of both [see discussions in Section A7.2.2]. The relative importance of these conditions in the dolomites of this study must be assessed. Amuri Limestone Group dolomite crystal compositions become increasingly stoichiometric towards their margins [Figure A5.27], and dolomite at the margins of the Lab Rocks concretion is more stoichiometric than dolomite from the concretion centre [Figure A5.29c,d]. Both cases may be interpreted as resulting from later stabilization reactions. Increases in Fe and Mn concentrations towards concretion margins [Figure A5.29f,g] supports such a contention for WC Zone dolomites. However, Fe and Mn concentrations in single dolomite crystals from the Amuri Limestone Group decrease towards crystal margins [Figure A5.27], whereas the reverse might be expected during deep burial. The bulk of evidence presented in Chapter 2 and later in this Chapter indicates an early diagenetic origin for both Amuri Limestone Group and WC Zone dolomites, which implies the extent of subsequent stabilization reactions may have been limited. In the Amuri Limestone Group the early formation of the associated chert [Chapter 5] would have occluded the sediment porosity precluding interaction of dolomite with pore fluids during deep burial. Thus Mg and Ca contents are interpreted as reflecting conditions at the time of dolomite formation.

Reaction stoichiometries in Table 4.1 indicate the availability of Mg^{2+} to be a limiting factor in the dolomitization of carbonate sediments. In noncarbonate sediments such as the Woolshed Formation, dolomitization may be limited by any one or combination of Ca^{2+}, Mg^{2+}, or HCO_3^-. In both cases the supply of Mg^{2+} is critical [see Section A7.2.3]. High-Mg can be ruled out as a source because the primary mineralogy of the Amuri

Limestone Group was probably low-Mg calcite [Section 3.1] and there was little carbonate originally in the Woolshed Formation. It is unlikely the adsorbed Mg^{2+} contributed significantly to the dolomite in this study [see discussion in Section A7.2.3]. Clay mineral transformations (e.g. smectite to illite) can generate significant volumes of Mg^{2+} at temperatures above approximately 100°C [Section A7.2.3]. Although smectites and illites are present in both the Amuri Limestone Group [Section A3.1] and the Woolshed Formation [Section A4.1], the field evidence for early dolomite formation [Chapter 2] plus isotopic [Section 4.4.2] and petrographic [Section 4.1.1] evidence that all dolomites formed at temperatures less than about 60°C indicates that little Mg^{2+} was derived from clay mineral transformations. The most likely source is seawater and seawater derived pore waters.

Compton and Siever (1986) used the average of the maximum and minimum values of porosity, grain density, weight% dolomite in the rock, and mole% Mg in the dolomite to calculate a dolomite Mg mass balance for the Monterey Formation of California. They showed that the average dolostone contained 8050 moles Mg^{2+}/m^3, such that a noncompacted section containing 1 volume% dolostone required the transport of 80.5 moles of Mg^{2+}/m^3 of sediment. The composition of seawater in the upper sediment column is similar to that of the overlying seawater (e.g. Mottl *et al.* 1983). Seawater contains 55 moles/m^3 of Mg^{2+} [Section A7.2.3]. Total porosities (including intraparticle porosity) in the upper 50-60 m of DSDP oozes are usually 60-80 percent, though some may be as low as 50% (Bathurst 1975, Scholle 1977). At DSDP site 288 porosities in calcareous sediments of about 70% were measured at the surface and about 60% at 210 m depth (van der Lingen and Packham 1975). Thus the pore waters in 1 m^3 of uncompacted sediment with a porosity ranging from 60-80% will contain 33-44 moles of Mg^{2+}. If all this pore water Mg is used, which is unlikely, then only a few volume percent dolomite will be produced (see also discussion in Compton and Siever 1986). To produce significant volumes of dolomite (such as found in the CD Zone for example) additional Mg^{2+} to that supplied at the site of formation is required. The concentration gradient caused by the removal of Mg^{2+} by dolomite formation will facilitate diffusion of adjacent pore water Mg^{2+}, and ultimately from overlying seawater (Chilingar *et al.* 1979, Irwin 1980, Compton and Siever 1986), towards the site of reaction. To investigate the possibility further mass balance calculations are performed.

Theoretical Magnesium Mass Balance Calculation

The mass balance calculation is similar to that of Compton and Siever (1986). However, as extensive silicification in a unit such as the CD Zone precludes direct measurement of porosity and grain density, a theoretical estimate is first tested before applying the calculation to analytical data. It is assumed that the original sediment was a carbonate ooze with the bulk of the dolomite having formed in the upper few metres of the sediment column. Both assumptions seem reasonable in terms of the field and petrographic evidence. Porosities of 60-80% (Bathurst 1975, Scholle 1977) are used as the maximum and minimum values in the calculation.

Uncompacted sediment would contain pore waters with a density (ρ) of approximately 1.02 gm/cm^3. The density of the primary ooze mineral, calcite, is 2.71 gm/cm^3. Assuming an initial porosity of 60 percent:

40% of the volume is sediment (calcite) where $\rho = 2.71$
60% of the volume is seawater where $\rho = 1.03$

Then the uncompacted sediment $\rho = 1.702$ gm/cm^3. Assuming complete dolomitization, the weight of dolomite in such a sediment would be 1.702×10^6 gms. Assuming an ideal dolomite, the weight of the Mg would be:

$$24.31/184 \times 1.702 \times 10^6 = 224868 \text{ gm Mg/m}^3$$
$$= 9250 \text{ moles Mg/m}^3$$

where 184 = molecular weight of dolomite
and 24.31 = atomic weight of Mg.

Using an initial porosity of 80 percent, (overall density of 1.35 gm/cm^3) and applying the same treatment yields 7424 moles Mg/m^3. The calculated sediment densities above are close to those found at the top of oceanic cores consisting of argillaceous sediments (1.25-1.35 gm/cm^3; Rieke and Chillingarian 1974), or calcareous sediments (1.6-1.7 gm/cm^3 van der Lingen and Packham 1975). The calculations indicate that theoretically an average dolomite would contain between 7424 and 9250 moles Mg/m^3. The average of 8337 moles Mg/m^3 is of the same order as calculated by Compton

and Siever (1986).

Magnesium Mass Balance for Amuri Limestone Group and WC Zone Dolomite

Having determined that the theoretical values are consistent with the literature, analyzed values are now used. The maximum concentration of Mg in an Amuri Limestone Group whole rock dolomite sample is about 137000 ppm with a mean of 114000 ppm [Table A5.1]. These values are also used for WC Zone concretions.

The weight of Mg/m^3 of sediment is calculated by multiplying the above measured concentration of Mg in the carbonate by the theoretically calculated densities. The results [Table 4.2] assume complete dolomitization of the initial Amuri Limestone Group sediment. The median for the mean values is 7212 moles Mg^{2+}/m^3 and for maximum values is 8649 moles Mg^{2+}/m^3; both of which are comparable to the theoretical values calculated previously and to that of Compton and Siever (1986). An Amuri Limestone Group sediment with 1 volume% dolomite requires 72.1-86.5 moles Mg^{2+}/m^3.

To determine the Mg required to form the dolomite observed in the sediments, the uncompacted volume percent dolomite must be evaluated. According to Compton and Siever (1986) the ratio of total dolomite thickness to the sediment thickness gives the present volume of dolomite. The present volume of dolomite divided by the degree of compaction gives the noncompacted volume percent dolomite. The uncompacted volume percent dolomite is then multiplied by the moles Mg^{2+}/m^3 required to dolomitize 1 volume percent of the sediment (for this study obtained from Table 4.2) to obtain the moles of Mg required to produce the observed volumes of dolomite for the units in this study [Table 4.3]. Measurement of dolomite bed thicknesses in the Amuri Limestone Group is difficult because beds are frequently discontinuous and highly irregular in shape [e.g. Figure A2.15]. Therefore the visual estimates of volume percent dolomite [Sections A2.4, A2.6] are used. The present volume percent dolomite in WC Zone concretions is 70-90 percent, with the volume of concretions probably amounting to less than 2% of the total sediment. The degree of compaction is assessed from differential compaction [Section 3.4.2]. Beds in WC Zone concretions are five to six times thicker than in the surrounding sediment. Differential compaction around chert nodules in the Amuri

Table 4.2 Calculated Mg/m^3 required for 100% dolomitization of a carbonate sediment. Values are calculated using densities derived from assumed maximum and minimum porosities.

	60% Porosity (= 1.70 gm/cm^3)		80% Porosity (= 1.35 gm/cm^3)	
	gm Mg/m^3	moles Mg/m^3	gm Mg/m^3	moles Mg/m^3
Mean	194510	8001	156111	6422
Maximum	233285	9596	127231	7702

Table 4.3 Estimated moles of Mg/m^3 required to produce the observed volumes of dolomite in the WC and CD Zones, and in the LCM Subzone. It has been estimated that the total volume% dolomite throughout the WC Zone would not exceed 2%, but individual concretions contain between 70% and 90% dolomite.

	Present Volume% Dolomite	Degree of Compaction	Uncompacted Volume% Dolomite	Moles Mg/m^3 required - uncompacted sed. Porosity = 60% Mean	Porosity = 60% Maximum	Porosity = 80% Mean	Porosity = 80% Maximum
LCM	40	2	20.0	1600	1919	1284	1540
Subzone		3	13.3	1064	1276	854	1024
		5	8.0	640	768	513	616
	90	2	45.0	3600	4318	2890	3466
		3	30.0	2400	2879	1927	2311
		5	18.0	1440	1727	1156	1386
CD	30	2	15.0	1200	1439	963	1155
Zone		3	10.0	800	960	642	770
		5	6.0	480	578	385	462
	50	2	25.0	2000	2399	1606	1926
		3	16.7	1336	1603	1072	1286
		5	10.0	800	960	642	770
WC	<2	5	<0.3	<24	<29	<19	<23
Zone		6	<0.4	<32	<38	<26	<30
	70	5	14.0	1120	1343	899	1078
		6	11.7	936	1123	751	901
	90	5	18.0	1440	1727	1156	1386
		6	15.0	1200	1439	963	1155

Limestone Group suggests degrees of compaction of about three and up to five (measured from beds thicknesses such as shown in Figure A2.15]. Therefore a range of degrees of compaction is used.

Table 4.3 gives a range of required volumes of Mg^{2+} that might be expected, depending upon the estimated percent dolomite and degrees of compaction. It must be stressed however, that such calculations are only crude estimates due to the nature of the assumptions involved, and probably represent maximum volumes of Mg^{2+}. Actual volumes may have been lower. Volumes of Mg^{2+} required by the Amuri Limestone Group are higher than those required by the Monterey Formation or DSDP dolomites. The Monterey range from 31-692 moles Mg^{2+}/m^3 and DSDP sites range from 32-169 moles Mg^{2+}/m^3 (Compton and Siever 1986), whereas in this study the overall range is from 19-4318 moles Mg^{2+}/m^3. The greater range may well represent the greater degree of dolomitization particularly in the Amuri Limestone Group. The maximum volume of dolomite in the Monterey Formation is 21% and there is only about 4% in the DSDP cores (Compton and Siever 1986).

Low dolomite volumes ($\leq$2 percent, e.g. Compton and Siever 1986) could possibly be formed by pore waters alone. Seawater is the only source that could supply the large volumes of Mg^{2+} required for the early dolomitization of the sediments in this study. An estimate of the diffusive seawater fluxes of Mg^{2+} into some DSDP sediments produced values as high as 885 moles/m^3 of uncompacted sediment where accumulation rates are 50 m/myr (Compton and Siever 1986). Fluxes of this magnitude could adequately provide enough Mg^{2+} to produce the observed volumes of dolomite in the Amuri Limestone Group, and would be more than adequate to account for WC Zone concretions. The extent of dolomitization resulting from seawater diffusion is controlled by the rate of dolomite precipitation and residence time in the upper sediment column (Compton and Siever 1986). Reaction rates depend upon pore water chemistry, sediment composition and temperature [Section A7.2.1]. For extensive dolomitization, nucleation must be within what is here referred to as the 'zone of effective seawater diffusion'. The longer the sediment remains within this zone the greater will be the volume of dolomite produced. Sedimentation rate and compaction will govern the residence time (Compton and Siever 1986). High sedimentation rates mean that the downward velocity of a packet of sediment with respect to the sediment/water interface increases, thereby reducing residence time. The downward velocity will be reduced by

increasing the amount of compaction during early stages of burial. Dolomitization is optimized during periods of low sedimentation rate and/or high compaction. The corollary of this argument is that dolomite in the Amuri Limestone Group may indicate periods of low sedimentation. A lack of dolomite may indicate increases in sedimentation rate. During a hiatus the lack of sedimentation causes a prolonged residence in the zone of diffusion. Thus the inferred unconformity at the base of the Lower Chert Member [Figure 2.1] is thought to have enabled the development of the basal dolomite bed found in the LCM Subzone at some localities.

Source of Calcium

The calcium required for dolomitization of Amuri Limestone Group sediments can be obtained from precursor calcite.

In the WC Zone Ca^{2+} as well as Mg^{2+} was supplied to the site of dolomitization. The moles of Ca^{2+} in the pore water of 1 m^3 of sediment with a porosity of 80% is significantly less than the moles in a 1 m^3 concretion. Therefore Ca^{2+} diffusion from adjacent pore waters and ultimately from overlying seawater is likely. Under such circumstances dolomitization was Ca^{2+} limited, as Ca^{2+} is only one fifth the concentration of Mg^{2+} in seawater (Compton 1988) and in pore waters (e.g. Mottl *et al.* 1983). Thus dolomitization in the WC Zone would be localized to sites where the sediment contained minor accumulations of calcareous fossils and/or organic matter, and where porosity and permeability allowed adequate diffusion of reactants. The metabolism of organic matter by bacteria can cause the required increases in alkalinity for the precipitation of carbonate [see Section 3.2.1 and references therein].

4.3.2. STRONTIUM

Controls on Strontium Partitioning

Partition Coefficients

Incorporation of trace elements into a carbonate mineral is governed by the distribution coefficient (D) according to the following relationship (McIntyre 1963):

$$(Tr/Cr)_{Solid} = D \times (Tr/Cr)_{Aqueous}$$

where: Tr = the concentration of the trace component in moles
Cr = the concentration of the carrier component in moles

In the case of Sr, it can be written for carbonates as follows (Kinsman 1969):

$$(Sr^{2+}/Ca^{2+}) = D^{Sr}_{Carbonate} \times (Sr^{2+}/Ca^{2+})$$

This relationship is valid when a system is at equilibrium, and when the liquid and solid phases show no concentration gradients in the trace component during precipitation (Veizer 1983).

The partitioning of Sr between calcite, dolomite, and liquids is independent of temperature (Jacobsen and Usdowski 1976, Katz and Mathews 1977). In addition if the final liquid is near equilibrium then reaction rate is not a factor. It is assumed that Sr substitutes for Ca in the lattice because the ionic radius of Sr^{2+} (112×10^{-12} m) is closer to that of Ca^{2+} (99×10^{-12} m) than Mg^{2+} (66×10^{-12} m). Calcite has twice as many Ca-sites as ordered dolomite for Sr substitution. Therefore, the formation of calcite and dolomite together under equilibrium conditions results in Sr incorporation into both minerals in the ratio of 2:1 respectively. Early diagenetic, commonly disordered dolomites may contain higher Sr contents than later diagenetic ordered dolomites (Veizer and Demovic 1974, Jacobsen and Usdowski 1976). Baker and Burns (1985) and Burns and Baker (1987) suggested that reaction stoichiometries effect Sr incorporation depending upon whether pre-existing carbonate is dolomitized (e.g. equation 4.3), or whether all reactants must be obtained from fluids at the site of formation (e.g. equation 4.6). In the case of equation (4.3) Sr^{2+} in excess of that in pore waters is derived from the primary carbonate.

Values of $D^{Sr2+}_{Dolomite}$

The value of $D^{Sr2+}_{Dolomite}$ is very important in any Sr compositional interpretations. There is considerable debate in the literature as to the value of $D^{Sr2+}_{Dolomite}$. Much of the debate arises from a paucity of successful dolomite syntheses at earth surface conditions. Kinsman (1969) proposed a value $D^{Sr2+}_{Calcite} = 0.14$, determined on the basis of the molar ratio of seawater (Sr/Ca = 0.0086) and analyses of modern marine

carbonate. This hypothesis has problems (Land 1980), in that high Mg-calcite contains about twice as much Sr as low Mg-calcite (Land and Hoops 1973). Therefore a direct comparison of calcite with dolomite cannot be made. Aragonite $D^{Sr2+}_{Aragonite}$ values of 1.17 (at 16°C) to 0.88 (at 80°C) were determined by Kinsman and Holland (1969).

Since a simple extrapolation of values from one carbonate to the other is invalid, $D^{Sr2+}_{Dolomite}$ values for dolomite must be determined by other means. Behrens and Land (1972) suggested that the Ca planes in dolomite act like calcite and therefore the D value for dolomite should be half that of calcite (i.e. using $D^{Sr2+}_{Calcite}$ = 0.14 means $D^{Sr2+}_{Dolomite}$ = 0.07). Supratidal Persian Gulf dolomites contained the expected Sr using this reasoning. However, Baffin Bay supratidal samples contained 30% more Sr, which lead Behrens and Land (1972) to postulate a $D^{Sr2+}_{Dolomite}$ of 0.08 to 0.11. The latter values are supported by Jacobsen and Usdowski (1976) who experimentally determined $D^{Sr2+}_{Calcite}$ = 0.096 and $D^{Sr2+}_{Dolomite}$ = 0.048. Katz and Mathews (1977) experimentally determined coefficients of 0.0231 to 0.0278 for temperatures of 252-295°C. The D^{Sr2+} value was thus thought to be temperature independent. Baker and Burns (1985) used pore water and associated dolomite analyses to determine a $D^{Sr2+}_{Dolomite}$ = 0.060. Advancing the argument that dolomite should contain approximately half the Sr of a coexisting calcite in equilibrium, Baker and Burns (1985) then argued that the dolomite and calcite D^{Sr2+} values should be similar. This is because the Sr would substitute for the Ca and not the Mg. Supporting this contention is a value of $D^{Sr2+}_{Calcite}$ = 0.043-0.058 determined by Baker *et al.* (1982), which equates with lower $D^{Sr2+}_{Dolomite}$ values.

Land (1980) proposed the recrystallization of chalk as an analogue for dolomitization. He suggested that $D^{Sr2+}_{Calcite}$ = 0.14 and $D^{Sr2+}_{Dolomite}$ = 0.07 are too high. Such high D^{Sr2+} values require extremely large pore volumes of meteoric water to reduce Sr concentrations to levels predicted by the original D^{Sr2+} value (Morrow and Mayers 1978, Land 1980). The requirement for low D^{Sr2+} values is alleviated to some extent if seawater, with its higher initial Sr/Ca ratios, is the source. Nevertheless, lower D^{Sr2+} values are supported by the experimental work of Pingitore and Eastman (1986) who determined a $D^{Sr2+}_{Calcite}$ = 0.06 for solutions with Sr/Ca ratios greater than 10^{-3} molar.

Many D^{Sr2+} values as discussed above have been determined empirically, hence the broad range of values. They have not considered constraints on Sr^{2+} distribution other than the Sr/Ca ratio. The kinetics involved in substitution are not yet fully understood (Hardie 1987). For example, any divalent cations smaller than calcium (e.g. Mn^{2+}) may affect the partition between calcite and solution by increasing D^{Sr2+} (Ichikuni 1973). Competition for lattice sites from cations such as Na^{+} and Ba^{2+} may also suppress $D^{Sr2+}_{Calcite}$ and fast growth crystal growth rates may lead to higher $D^{Sr2+}_{Calcite}$ (Pingitore and Eastman 1986). Values of $D^{Sr2+}_{Aragonite}$ appear to be temperature independent (Kinsman and Holland 1969), and some authors claim that $D^{Sr2+}_{Dolomite}$ is temperature dependent. The temperature dependence may however, be a function of extrapolation of higher temperature data to the lower temperatures experienced in diagenesis. Although not yet proved or disproved there is the possibility that temperature may effect values of D^{Sr2+}. Therefore, D^{Sr2+} for both calcite and dolomite may vary depending on the conditions. Since precise determinations of $D^{Sr2+}_{Dolomite}$ cannot be made, quantitative interpretations in terms of Sr depletion may not be totally valid (Land 1980). However, useful qualitative information may still be obtained.

In the light of the preceding discussion there are two probable causes for dolomite to contain less Sr than associated calcites:

i) If high distribution coefficients are assumed (e.g. $D \geq 0.1$), the Sr/Ca ratio of the solution is less than in seawater, or whatever solution precipitated the original carbonate. Meteoric water interaction is usually the interpreted dolomitization process.

ii) If low distribution coefficients are assumed, (e.g. $D \leq 0.06$), the requirement for such 'special waters' is removed. In this case the reduced Sr/Ca ratio in the solid phase can be produced in seawater.

In terms of the Amuri Limestone Group and WC Zone dolomites low D^{Sr2+} values are favoured because:

i) All dolomites in this study contain measurable amounts of other trace elements, notably Fe and Mn. These cations would have caused distortions in the crystal lattice (Ichikuni 1973) and competed for lattice sites thereby reducing D^{Sr2+}. As suggested by Land (1980), large volumes of meteoric water would be needed to reduce Sr concentrations in the Amuri Limestone Group dolomites and micrites [Section A5.5.2 and Figure A5.20].

ii) Although meteoric waters have been recorded in progradational

sand-rich wedges at distances of the order of 20 km from shore (e.g. Galloway 1984, Gieskes 1981 and references therein) it is thought unlikely that they have affected the sediments in this study. The bulk of the Amuri Limestone dolomite is in the deepest part of the basin and consists of such fine sediments that they could not have acted as a good aquifer at any time. As shown in the following discussion, the Sr concentrations found in this study can be explained without invoking complex hydrological conditions.

Strontium in Amuri Limestone Group Dolomites

Baker and Burns (1985) presented Sr^{2+} incorporation models for calcite-rich and calcite-poor sediments. Assuming a reaction stoichiometry similar to equation (4.5) for a calcite-rich sediment the model is as follows:

Two moles of pelagic calcite would yield 4×10^{-3} moles Sr (Baker *et al.* 1982). If the initial Sr/Ca ratio of the pore waters = 0.0086, then the Sr/Ca ratio of the first dolomite precipitated = 0.06×0.0086

$= 5.1 \times 10^{-4}$

~ 245 ppm

where $D^{Sr2+}_{Dolomite} = 0.06$

The result of forming this dolomite is that the pore waters are altered by $4 \times 10^{-3} - 5.1 \times 10^{-4}$ moles Sr^{2+}/mole Ca^{2+}. The next dolomite to form will thus contain proportionally less Sr. Therefore progressive dolomitization results in progressive Sr depletion of pore waters and lower concentrations of Sr in dolomites. Such a mechanism explains the low Sr concentrations in Paleozoic shelf carbonates (about 187 ppm, Weber 1964a), and in dolomite in parts of the Monterey Formation (Baker and Burns 1985).

The estimated value above is the calculated mean for CD Zone dolomites and can explain the bulk of Sr concentrations therein. Sr enrichment in the LCM Subzone compared with the CD Zone suggests that some modification of the theory is necessary. Enrichment implies either an increase in $D^{Sr2+}_{Dolomite}$ or a continual supply of Sr resulting in less depletion in pore waters. Although higher D^{Sr2+} values cannot be totally discounted, a form of pore water replenishment is more likely. Seawater diffusion

appears capable of supplying the Mg^{2+} for dolomitization and may also supply some Sr^{2+}. This source of additional Sr^{2+} may only be minor however, as the concentration of Sr^{2+} in seawater is about 8 ppm (Brownlow 1979). A more likely source is from precursor carbonate dissolved as a result of chertification. Such a source could easily supply Sr^{2+}, particularly to packets of the sediment to which dolomitization has been restricted. Samples containing less than about 245 ppm Sr may contain relatively more dolomite formed prior to chertification, whereas those with higher Sr contents may reflect comparatively greater amounts of dolomite formed during chert formation. With Sr^{2+} from pre-existing carbonate the requirement for meteoric water, and variations in $D^{Sr2+}_{Dolomite}$ is removed. Chertification may cause additional calcite precipitation arising from the dissolution of primary carbonate (see van der Lingen and Packham 1975). The reprecipitated calcite may in turn be dolomitized.

Strontium in WC Zone Concretions

For WC Zone concretions, a reaction stoichiometry such as equation (4.7) is likely. Where these sediments contain organic matter, sulphate reduction, and reactions such as ammonification and nitrate reduction (e.g. Jeans 1980, Hesse 1986) may produce adequate HCO_3^- to precipitate calcite [Sections 3.2 and 4.3.1]. The presence of a few calcite-rich concretions supports this possibility. Subsequent dolomitization of the precipitated calcite follows a reaction stoichiometry such as equation (4.5) (Baker and Burns 1985). Calcite precipitation depletes pore waters in Ca^{2+} and slightly in Sr^{2+}. Dolomitization of the calcite causes the pore water Sr^{2+} concentration and the Sr^{2+}/Ca^{2+} ratio to increase. DSDP pore waters at sub-bottom depths (5-70 m) below the zone of depleted Ca^{2+}, are found to have Sr^{2+}/Ca^{2+} ranges of 0.017 to 0.045 (Baker and Burns 1985). With $D^{Sr2+}_{Dolomite} = 0.06$ the expected Sr concentration ranges in dolomites would 480-1290 ppm. A higher Sr^{2+}/Ca^{2+} ratio than in the calcite-rich sediments means that proportionally more Sr can be incorporated into the dolomite. Where there is primary carbonate available, pore water depletion of the Sr/Ca ratio may result in lower Sr concentrations in the dolomite.

The majority of concretions contain in excess of the 245 ppm Sr calculated for dolomite derived from primary calcite. Therefore, the Sr

concentrations indicate that in general the concretions formed by dolomitization of very early diagenetic calcite in pore waters of relatively high Sr^{2+}/Ca^{2+} ratio. However, dolomitization must have closely followed calcite precipitation. Adequate porosity is required to enable Mg^{2+} to get to the site of dolomitization. Prolonged calcite precipitation prior to dolomitization will result in only outer parts of concretions being dolomitized. Therefore, it is envisaged that concretion growth commenced at sites of early calcite precipitation disseminated throughout the sediment. Dolomitization of the calcite occurred as further calcite was precipitated at sites adjacent to, and/or around the site of dolomitization. In addition, once the dolomitization of calcite had commenced, the direct precipitation of dolomite without a calcite precursor may also have occurred depending upon the Mg/Ca ratio at the site of precipitation. Concretion growth would have occurred by the accretion of dolomitized calcite and possibly some directly precipitated dolomite. The relatively complex Sr contours [Figure A5.29e] compared to analyses such as insoluble residue [Figure A5.29b] in the Lab Rocks (4) concretion (KP3), may result from localized variations in dolomite reaction stoichiometry.

The broad range of Sr concentrations in WC Zone samples probably reflects the sporadic distribution of concretions. Pore water Sr^{2+}/Ca^{2+} ratios may not necessarily have been uniform throughout the sediment, and probably varied on a very localized scale. They would depend on the rate and extent of the initial calcite precipitation, reactant flux, diffusion rates, and fluid migration if any. In a single concretion, the resultant Sr^{2+} concentration of a given piece of carbonate, would depend upon the extent of modification of pore water Sr^{2+}/Ca^{2+} ratios by carbonate precipitation at adjacent sites. Each concretion may therefore be a separate diagenetic system not necessarily related to others.

4.3.3. IRON AND MANGANESE

Partitioning of Iron and Manganese into Carbonates

As is the case for Sr^{2+}, partition coefficients for Mn^{2+} and Fe^{2+} are important in interpretation of Fe and Mn contents in carbonates. Unfortunately, D^{Mn2+} and D^{Fe2+} are poorly known (Mattes and Mountjoy 1980). Partition coefficients can affect inter-element relationships.

Churnet and Misra (1981) believe that $D^{Mn2+}_{Dolomite}$ may not be constant under natural conditions. Although such a concept is disputed by McIntyre (1963), variable $D^{Mn2+}_{Dolomite}$ may be caused by the presence of other ions (e.g. the effect of Mn^{2+} on Sr partitioning). Ion complexing may also be important in controlling $D^{Mn2+}_{Dolomite}$. Partitioning is effected by competition between cations for lattice sites. Inclusion of small cations may distort the crystal lattice to the extent that larger cations are excluded. Variation in growth rates as suggested in Section 4.1.2 may also control incorporation of trace components.

McKee and Gutschick (1969) suggested that both Fe and Mn can substitute in any amount in the dolomite lattice (but not in calcite). However, such a suggestion seems unlikely. Sommer (1972a,b) postulated that Mn^{2+}, and presumably Fe^{2+}, can populate both Ca and Mg sites in the dolomite lattice, which implies that there should be good correlations of Fe and Mn with Ca and Mg. More recently Kretz (1982) showed that Mn tended to populate Mg^{2+} sites to a greater extent than Ca^{2+} sites. However, preliminary work by Lumsden and Lloyd (1984) provided evidence that these ions may substitute for either Ca or Mg differently in different dolomites, depending on the range of Ca and Mg concentrations in the solid. Stoichiometric dolomites were found to contain a wide range of Mn concentrations whereas non-stoichiometric dolomites had more uniform Mn concentrations. The authors suggested that narrow ranges of Mn contents reflect an equilibrium distribution of Mn, whereas a wide distribution reflects nonequilibrium conditions. Ion availability in pore fluids also governs the amount of Fe^{2+} and Mn^{2+} that is incorporated into a dolomite. The solution which dolomitized one bed may not necessarily be chemically identical to that which dolomitized others. Pore water concentrations may vary from site to site, resulting in a range of concentrations within a particular unit.

Elemental Interrelationships

When Fe and Mn whole rock data are plotted against Mg [Figure 4.3] or Ca, only vague trends are observed, with only WC Zone concretions displaying a statistically significant correlation. Similarly, the Fe and Mn linear covariance for whole rock data from the different units is generally poor [Figure 4.4]. Only the concretions and the CD Zone show statistically significant correlations; both low, negative and positive respectively.

Figure 4.3 Scatter plots of Mg versus Mn (a) and Mg versus Fe (b). Three plots are required for each because the spread of values could not be shown adequately on single graphs. Ca displays a similar scatter when plotted against Fe and Mn.

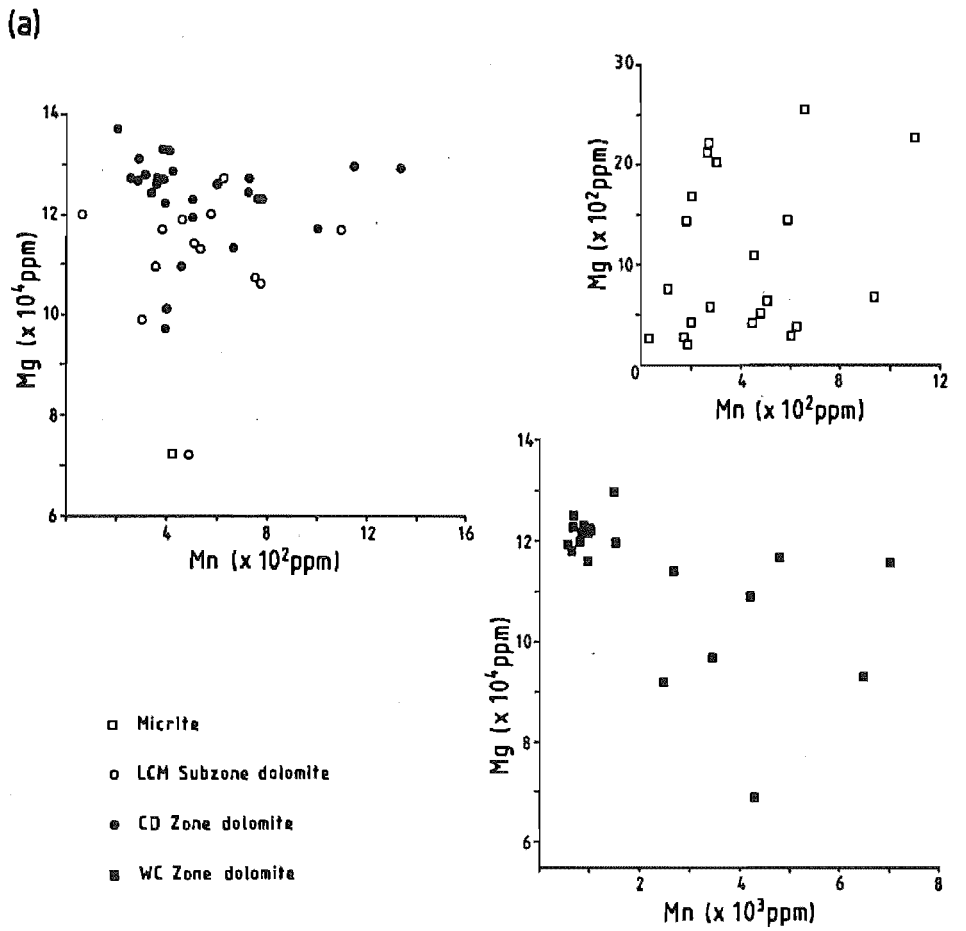
(a)
Mg (x 10⁴ppm)
Mn (x 10²ppm)
Mg (x 10²ppm)
Mn (x 10²ppm)
Mg (x 10⁴ppm)
Mn (x 10³ppm)
Micrite
LCM Subzone dolomite
CD Zone dolomite
WC Zone dolomite

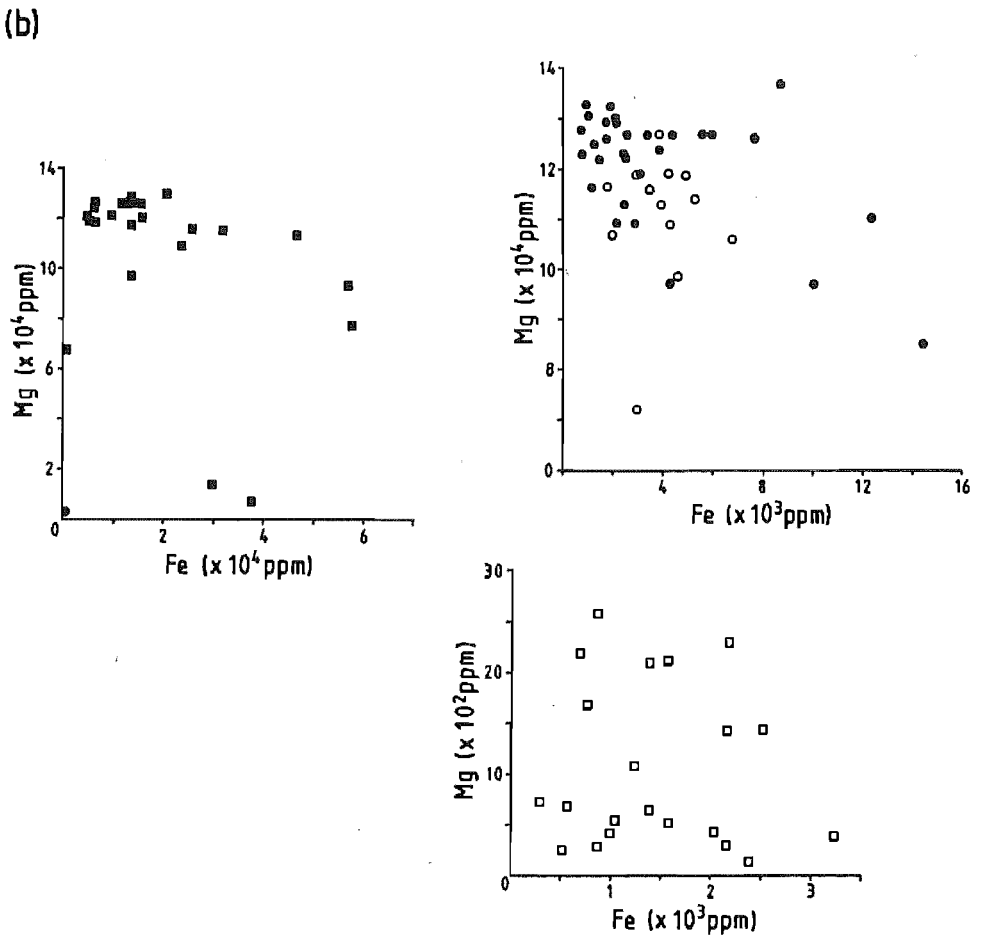
(b)
Mg (x 10⁴ppm)
Fe (x 10⁴ppm)
Mg (x 10⁴ppm)
Fe (x 10³ppm)
Mg (x 10²ppm)
Fe (x 10³ppm)

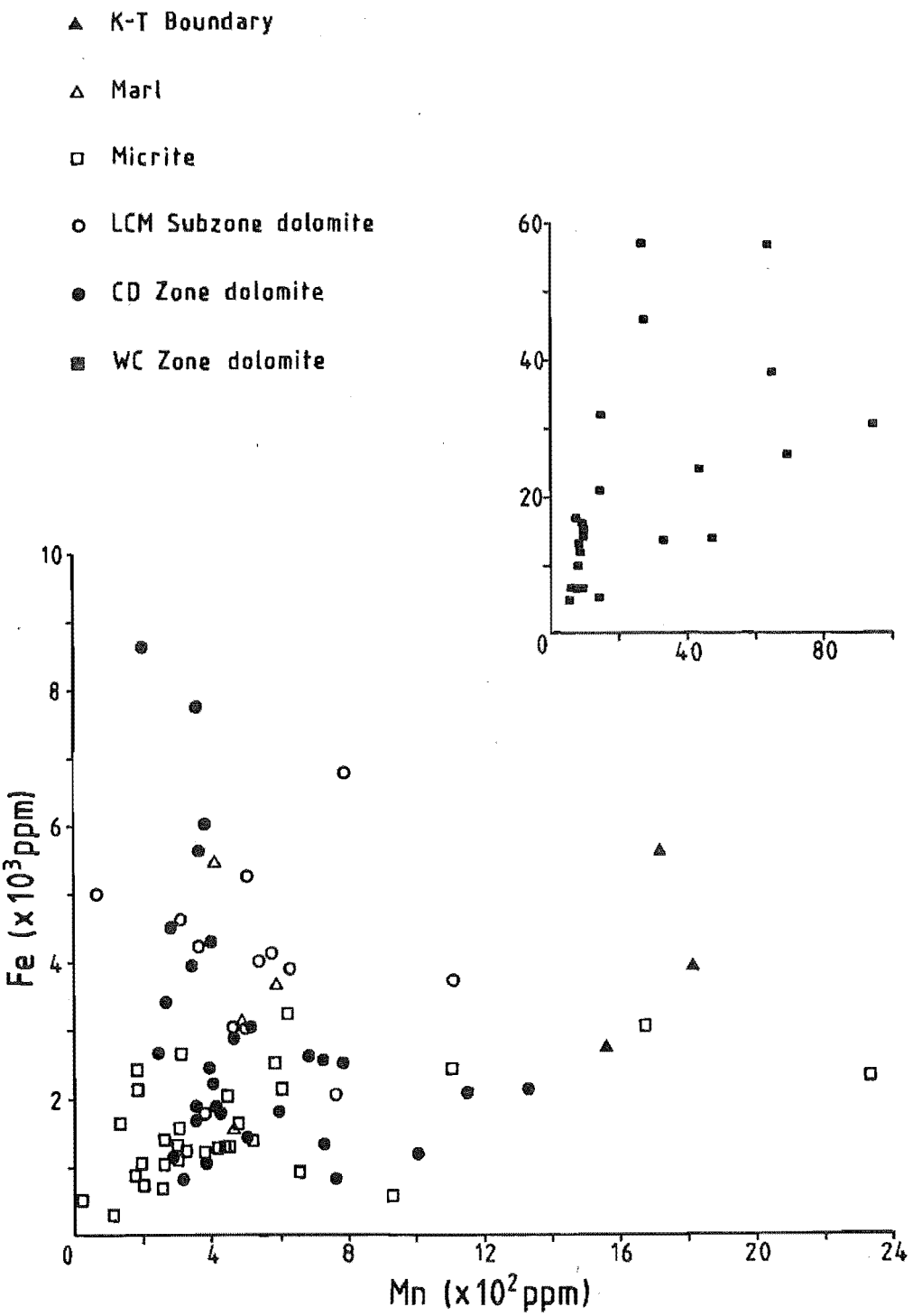

Figure 4.4 Scatter plot of Fe versus Mn. The higher Fe concentrations in concretions necessitate a separate plot. The scale on the separate graph is the same as that of the main graph.

The LCM Subzone and CD Zone dolomites show some suggestion of a non-linear relationship. The correlations for the other two units are about zero. Despite such generally poor correlations, samples with high concentrations of Fe also contain high concentrations of Mn. These correlations are contrary to results found by Burns and Baker (1987) for Monterey Formation dolomites. From the similarity in chemical properties of these two elements, similar behaviour in terms of incorporation into carbonates might have been expected. However, in the literature poor correlations of Mn with Fe and other elements are moderately common, and nonsystematic relationships between Mn and other trace elements have been found by a number of authors (e.g. Weber 1964a, Veizer and Demovic 1974, Pingitore 1978, Churnet and Misra 1981). The latter two authors interpret poor correlations as indicating different sources of water for the respective elements. However, such multiple fluid sources would imply a complicated hydrological regime.

One reason for the scatter of Amuri Limestone Group samples [Figure 4.4] may be the generally low Fe concentrations observed. Associated micrites and dolomites in this study contain less than 2 mole% $FeCO_3$, whereas published data with good correlations have Fe concentrations ranging from 2-10 mole% $FeCO_3$ (e.g. Burns and Baker 1987). It is noticeable in the present study that WC Zone concretions have higher Fe concentrations than Amuri Limestone Group dolomite, and show the best correlations.

Where both Fe and Mn were detected by microprobe, a good Fe/Mn correlation is obtained, implying that non-lattice Mn and/or Fe is included in whole rock analyses. Inclusion of non-lattice Fe^{2+} is also indicated by moderate to good, positive correlations of whole rock Fe data with insoluble residues in Amuri Limestone Group carbonates. Strangely there is no parallel relationship between Mn^{2+} and insoluble residues. Although Table A5.2 shows insoluble residues contain little Fe or Mn, and sample chips for powdering were carefully selected to avoid sulphide nodules or Fe-oxide stains, input from leaching of finely disseminated sulphides contained in micrites and dolomites during HCl digestion is unavoidable. Leaching of Fe from disseminated Fe-oxide in pink micrites is also likely, as is some leaching from clay minerals in the marls. A somewhat greater input from leaching can be expected from WC Zone concretions due to the detrital and clay mineral content. Therefore, some non-carbonate Fe^{2+} and Mn^{2+} has unavoidably contributed to analyses, more so in the concretions

perhaps.

A negative correlation between Mn and Sr is exhibited by micrite and WC Zone concretion samples [Figure 4.5]. Both the LCM Subzone and CD Zone dolomites display low positive correlations but only the LCM Subzone correlation is statistically significant. Correlations between Fe and Sr are similarly unsystematic.

Sources of Iron and Manganese

The pre-existing carbonate will include some Fe and Mn that can be incorporated into subsequently formed dolomite. The amount incorporated into the dolomite will depend on Fe and Mn concentrations in the precursor carbonate, the composition of equilibrating fluids, and whether or not dolomitization occurs in a closed system (see discussions in Pingitore 1978, Brand and Veizer 1980).

Smectite to illite transformations can release Fe^{2+} (Perry and Hower 1970, Boles and Franks 1979, Lahann 1980, McHargue and Price 1982). The Fe^{2+} is released at temperatures in excess of 100°C (Boles and Franks 1979), and occurs during the later stages of diagenesis (Choquette 1971). The most likely lithologies where clay mineral transformations may occur are the Woolshed Formation and marl interbeds in the Amuri Limestone Group. Any late stage dolomitization may have derived Fe^{2+} and Mn^{2+} from clay minerals.

Since the Mg^{2+} for dolomitization is seawater derived, then a possible source for some of the Fe and Mn may also be seawater. Concentrations of both Fe^{2+} and Mn^{2+} in seawater are very low; Mn ~8 ppb (Crerar and Barnes 1974), Fe ~3 ppb (Brownlow 1979). Much of this is tied up as complexes (e.g. approximately 72% of the Mn^{2+} is complexed; Crerar and Barnes 1974) reducing potential incorporation. However, mixing with freshwater is one mechanism that can reduce complexing (Churnet and Misra 1981), but as indicated in Section 4.3.2. mixing of meteoric water is unlikely for the dolomitization of sediments in this study. If either Mn^{2+} or Fe^{2+} had been incorporated from seawater then much lower concentrations in micrites would be expected than are observed. A large $D^{Mn2+}_{Dolomite}$ (possibly in excess of 15, e.g. Pingitore 1978) would be necessary to produce the Mn^{2+} concentrations commonly observed in these carbonates. Such a value is

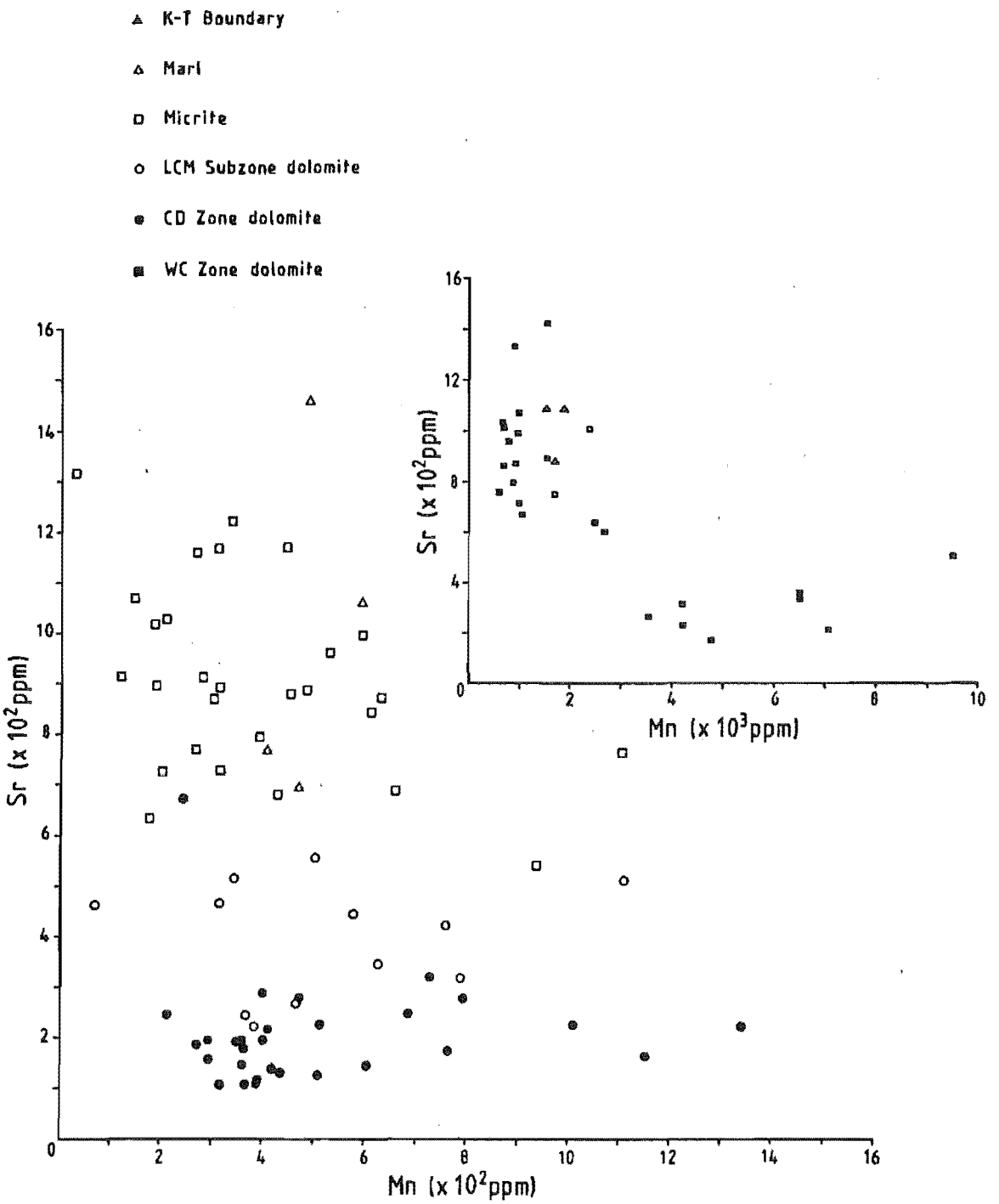

Figure 4.5 Scatter plot of Sr versus Mn.

unlikely which implies that other sources are more important.

Oxides and organic matter are likely to be significant Fe and Mn sources. Commonly Fe^{2+} is transported as Fe-oxides coating detrital mineral grains, in particular clay minerals (Carroll 1958, Curtis 1967, Berner 1978). Manganese tends to be transported as dissolved Mn^{2+} because it has a greater solubility than Fe^{2+} (Hem 1972, Crerar and Barnes 1974), although as stated earlier much of this is complexed with other ions. However, like Fe, most of the deposited Mn occurs in the form of oxides (Matsumoto 1983). Some of the oxides may form in the ocean basins at the time of sedimentation (Calderoni *et al.* 1988). Organic matter, which is an important reducing agent, may also contain complexed Fe and Mn oxides. Iron and Mn are then mobilized by the reduction of oxides (Carroll 1958, Berner 1978, Taylor and Sibley 1986), which may follow a biogenic pathway (Gieskes 1981). Bacterial oxidation of organic matter may release Fe^{2+} complexed therein. Of note is that both Mn-reducing and Mn-oxidizing bacteria have been isolated from manganese nodules (Crerar and Barnes 1974). Mobilized Fe^{2+} is then taken up by sulphide precipitation as a result of H_2S produced from sulphate reduction. In some circumstances MnS may be precipitated instead of Fe-sulphides (Suess 1979). The sulphate reduction process can itself produce sulphide directly (Irwin 1980, Berner 1985):

$$6(CH_2O) + 3SO_4^{2-} + 2FeOOH \rightarrow FeS + FeS_2 + 6HCO_3^- + 4H_2O \quad (4.13)$$

Any excess Fe with respect to sulphide production may be available for incorporation into carbonates (Suess 1979, Burdige and Gieskes 1983). In addition, Fe in excess of that required for sulphide precipitation may cause the observed enrichment in Fe in pore water over seawater (Michard 1971, Mottl *et al.* 1983). The precipitation of MnS in association with sulphate reduction may similarly govern Mn^{2+} availability for incorporation into carbonates (see Suess 1979, Burdige and Gieskes 1983), although the chemistry of Mn^{2+} below the sulphate reduction zone is poorly understood (Seuss 1979, Burns and Baker 1987). This is where Mn-sulphide precipitation may be important. Oxidation of solid or dissolved Fe-sulphides may occur when brought into close contact with Mn-oxides by reworking (Aller and Rude 1988). Although variable in organic rich sediments, the reaction could possibly be important particularly where bioturbation has occurred. The reaction results in a rise in pH,

oxidation of Fe, an increase in SO_4^{2-} which may inhibit the formation of dolomite, and depletion in alkalinity through Mn and Ca carbonate precipitation. The reaction is probably biologically mediated (Myers and Nealson 1988); for which the general equation is (Aller and Rude 1988):

$$4.5MnO_2 + FeS + 7CO_2 + 4H_2O \rightarrow 4.5Mn^{2+} + SO_4^{2-} + 7HCO_3^- + FeOOH \quad (4.14)$$

Evidence for a similar effect by Fe-oxides is only slight.

Iron and Manganese in Amuri Limestone Group Dolomites

The Fe in carbonate sediments reflects the Fe delivered to that sediment at the time of deposition and during early diagenesis (Land *et al.* 1975). Murata *et al.* (1972) claim that high Fe and Mn contents are caused by introducing oxygenated freshwater to the system. In contrast, Land (1980) suggests that the bulk of high Fe dolomite forms in saline water, but not as the early phases often associated with oxidizing conditions. Gluyas (1984) found low Fe in early diagenetic carbonates and higher Fe concentrations in later diagenetic carbonates. It would seem therefore that differing environmental conditions can produce similar Fe and Mn contents. Low Fe and Mn concentrations, and the inferred origin of Sr concentrations [Section 4.3.2] argue against an oxygenated freshwater origin for Amuri Limestone Group dolomites. The Fe (and Mn) concentrations are consistent with early dolomite formation (e.g. Gluyas 1984), where the bulk of the Fe (and probably Mn) is included in other minerals such as sulphides.

All the Fe and Mn in Amuri Limestone Group dolomites was derived from sediment pore waters. The ultimate sources of Fe^{2+} and Mn^{2+} in the pore water was most likely mainly derived from oxides complexed with organic matter, formed at the time of deposition, or coating clastic grains including clay minerals. Minor quantities of Fe^{2+} and Mn^{2+} may have been derived from the precursor carbonate and diffusing seawater. Bender (1971) suggested that the upward diffusion of Mn^{2+} in pelagic sediments is minor. Such diffusion in Amuri Limestone Group sediments may have been similarly limited. The derivation of Fe^{2+} and Mn^{2+} from smectite to illite transformations can be discounted. Despite the presence of both these clay minerals in the Amuri Limestone Group and the Woolshed Formation there are no systematic trends in Mn or Fe concentrations to

suggest that either the Woolshed Formation or the marls are the source for these elements. The early diagenetic origin, and relatively low carbonate formation temperatures (≤50°C, Table 4.4) in Amuri Limestone Group dolomites argue against smectite-illite reactions occurring at the site of carbonate diagenesis.

The Fe^{2+} and Mn^{2+} available for incorporation into dolomites from pore waters may to some extent result from the balance between sulphide reduction [e.g. equation 4.13] and oxidation reactions [e.g. equation 4.14]. A link between dolomite precipitation and the production of pyrite has already been suggested for the genesis of marl-micrite alternations. A similar link between dolomite precipitation, sulphate reduction, and pyrite precipitation appears to explain the Fe and Mn concentrations in dolomite crystals. Support for such a conclusion comes from the intimate association of sulphides with dolomite [e.g. Figures A5.4, A5.8], which in other dolomites have commonly been interpreted to indicate contemporaneous origins (e.g. Curtis *et al.* 1986).

The decrease in Fe and Mn concentrations towards crystal margins [Figure A5.27] may reflect a decrease in the available Fe^{2+} and Mn^{2+} in pore waters at the site of dolomite crystal formation, due to sulphide precipitation. Superimposed on the overall decrease in Fe and Mn are minor fluctuations in the proportions of Fe^{2+} and Mn^{2+} concentrations in crystals, which in turn are reflected in the cathodoluminescence banding. Abrupt boundaries indicate sharp changes and poorly defined boundaries indicate slower changes (Frank *et al.* 1982). In the LCM Subzone these criteria suggest that rates of change differed from sample to sample [cf. Figures A5.11a and A5.13]. It thus appears that variations in pore water chemistry were not constant during dolomitization, and that chemical variations were of a very localized nature. Similarity in colour and colour intensity of adjacent bands may result from more subtle changes in conditions than occurred in crystals with marked differences in colour and colour intensity. The thickness and number of luminescence bands reflects the maintenance of a particular set of environmental conditions. Thick bands may indicate a longer period of conditions or faster growth rates [e.g. Figure A5.13]. The reverse would be the case for more numerous thinner bands [Figure A5.12b].

Historically, concentric luminescence bands were attributed to variations

in the Mn^{2+} and Fe^{2+} supply, and hence the redox potential of the dolomitizing environment (Machel 1985 and authors cited therein). Precipitation of pyrite results in the formation of Fe-poor dolomite which luminesces brightly. Thin section evidence indicates that both bright and dull luminescent Amuri dolomites are associated with pyrite, implying that SO_4^{2-} reduction via pyrite precipitation may influence the banding in addition to Eh/pH effects. The incorporation of Fe and Mn is governed by kinetic factors implying that banding records variations in crystallization kinetics. Variable dolomite luminescence could also be caused by a combination of different substitution sites, or the presence of the activator in different oxidation states, even with constant activator concentrations (Machel 1985).

Iron and Manganese in WC Zone Concretions

As in Amuri Limestone Group dolomites, incorporation of Fe and Mn into WC Zone concretions linked to sulphate reduction is indicated by the association of pyrite and dolomite. Support for this conclusion comes from $\delta^{13}C$ data [Section 4.4.3].

The increase in Fe^{2+} and Mn^{2+} away from concretion nucleation centres, such as observed in the Lab Rocks concretion, is indicative of the progressively greater availability of these two cations in pore waters (Kushnir and Kastner 1984). The increase in Fe^{2+} and Mn^{2+} uptake may reflect the depletion in SO_4^{2-} in pore waters during concretion growth; increasing amounts of Fe^{2+} and Mn^{2+} were available for incorporation into carbonates because progressively less was removed by sulphide precipitation. A variation in sedimentation rate may also cause increases in Fe and Mn concentrations. A packet of sediment is buried more quickly to depths below the sulphate reduction zone during periods of rapid sedimentation than when slow sedimentation rates prevail. More Fe^{2+} (and by inference Mn^{2+}) is available because quicker burial reduces the amount of Fe^{2+} removed from the system by sulphide precipitation (Berner 1984). The Fe/Mn ratio also increases towards the concretion margins. Divalent manganese ions are more stable in oxidizing conditions than Fe^{2+}. Therefore, the increase in Fe/Mn ratio may result from a reduction in oxidation potential (Boles *et al.* 1985), caused by progressive burial during formation.

The difference in concentrations of Fe and Mn between the concretions and the Amuri Limestone Group dolomites may in part reflect the abundance of oxides and/or organic matter in the original sediments. The considerably higher detrital and clay mineral content of the Woolshed Formation provides a greater source of Mn and Fe.

4.3.4. SODIUM AND POTASSIUM

Elemental Interrelationships

Since both Na and K are Group I elements with similar chemistries, it might be expected that they would be reasonably well correlated. Instead, only the micrites display a good correlation [Figure 4.6], although this may be in part due to one sample with a very high Na^+ concentration. The abundances of Na and K in dolomites may thus be differently controlled.

Correlations of Na and K with insoluble residue content in the Amuri Limestone Group are generally moderate to good, but correlations are poor in concretions. The best correlation is between Na and insoluble residue in micrites [Figure 4.7a]. All Amuri Limestone Group dolomites tend to show a moderately wide spread [Figure 4.7]. The numerically good CD Zone correlation may relate to a few unusually high insoluble residue contents. All samples show reasonable numerical and graphical K correlations with insoluble residue [Figure 4.7b]. However, extreme values may again control correlations, particularly in concretions and possibly in the CD Zone. Graphically [Figure 4.7], K shows an overall better correlation with insoluble residue than Na. This suggests that insoluble residue exerts greater control over K abundances than Na abundances. Relatively greater insoluble residue control over K may cause the poor Na-K interrelationship.

Sodium is positively correlated with Ca and Sr, and negatively correlated with Mg in the LCM Subzone. Potassium has a low negative correlation with Ca in concretions and a low positive correlation with Sr in micrites. No other correlations are statistically significant. Generally poor correlations between Na (and possibly by inference K) with Mg and Ca may in part be due to coprecipitation being independent of the Mg concentration in carbonates.

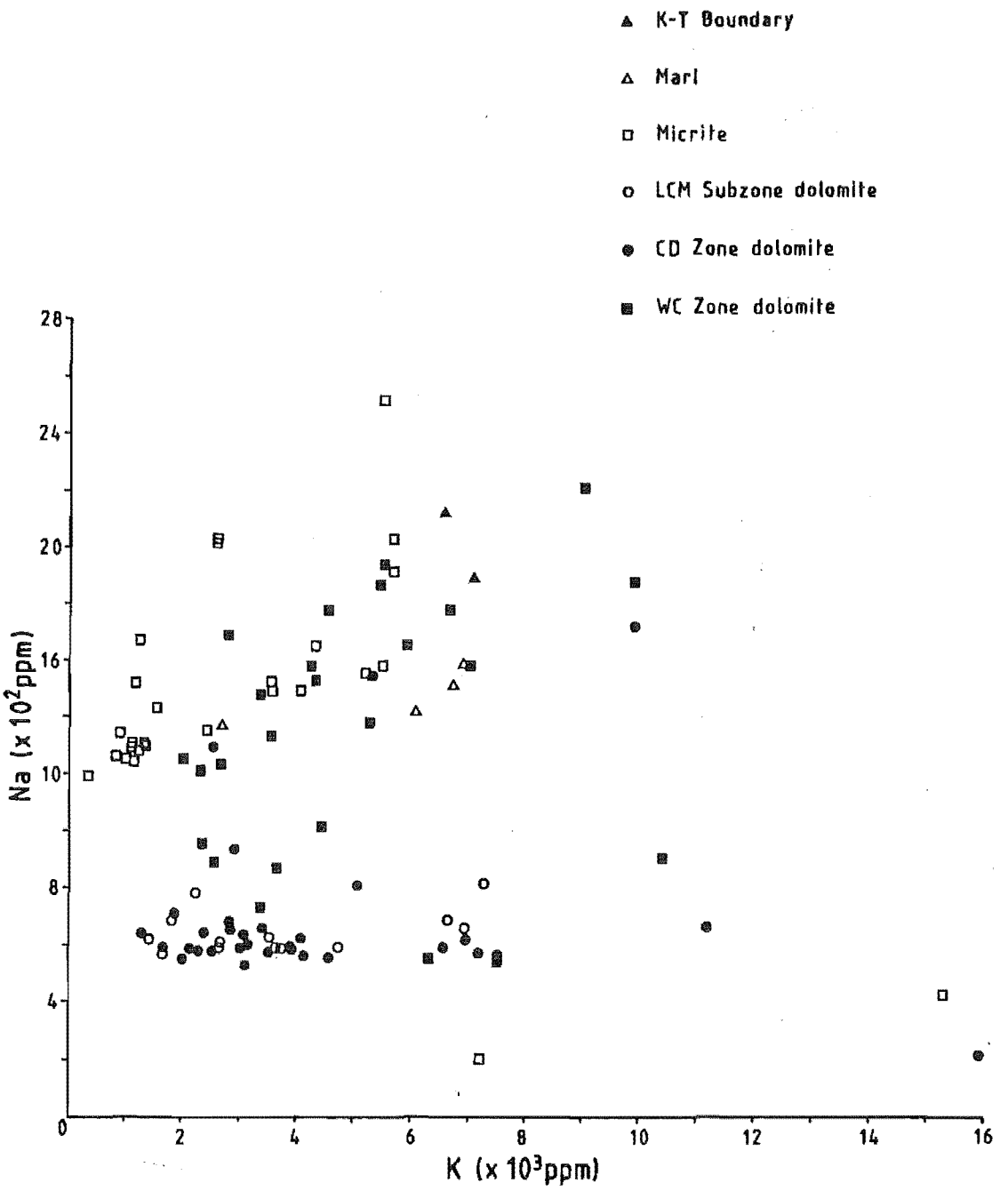

Figure 4.6 Scatter plot of Na versus K.

Figure 4.7 Scatter plots of Na (a) and K (b) versus insoluble residue.

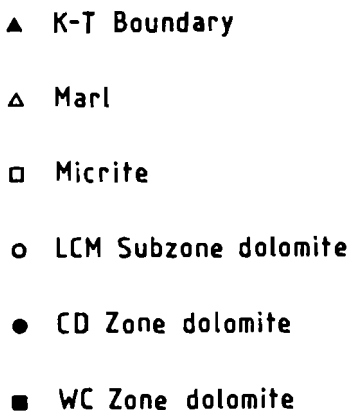

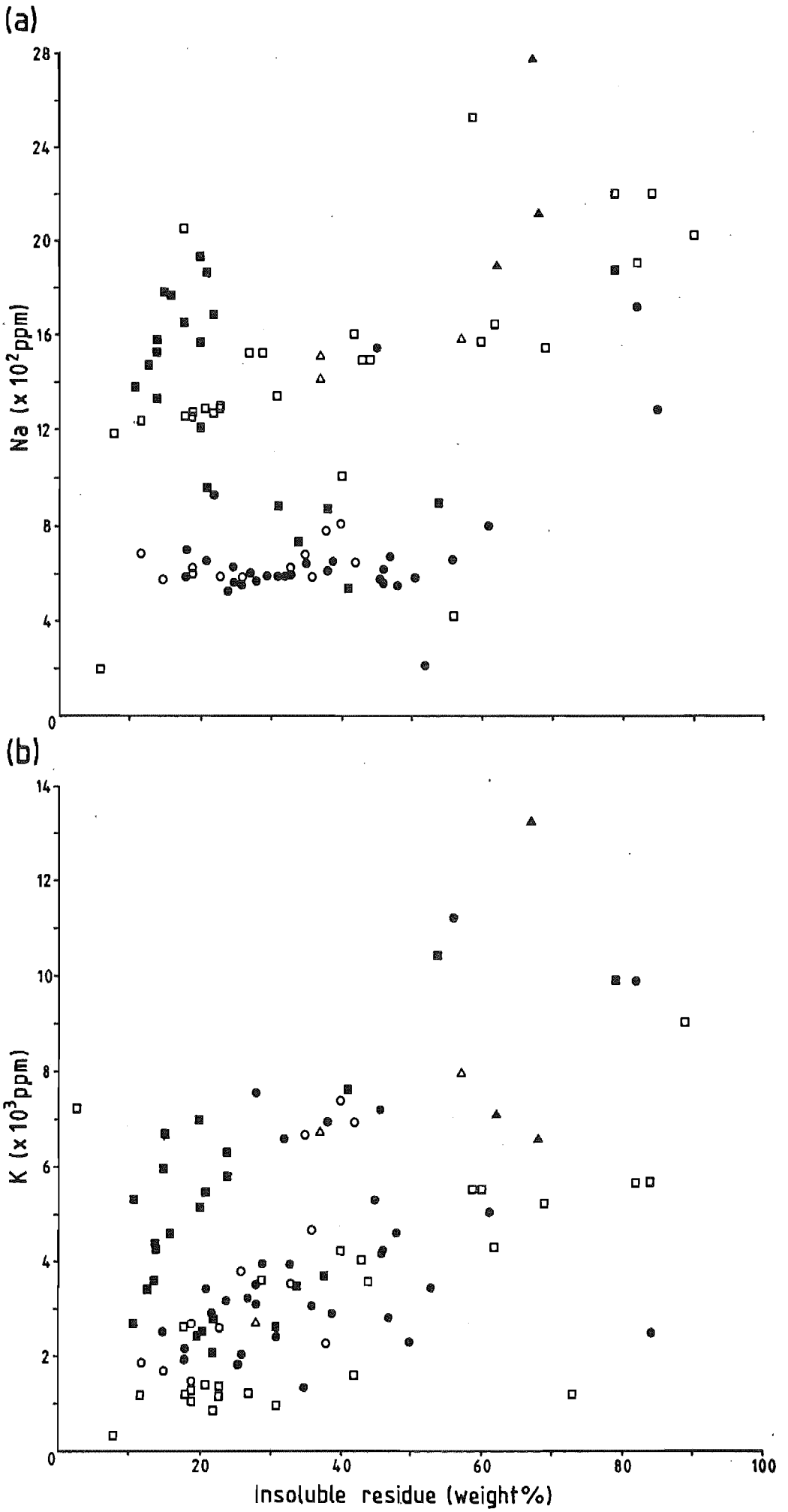
(a)
Na (x 10²ppm)
0
4
8
12
16
20
24
28
(b)
K (x 10³ppm)
0
2
4
6
8
10
12
14
20
40
60
80
100
Insoluble residue (weight%)

Both Na and K display good positive correlations with Fe. However, despite the good numerical correlation, the interelement plots show much scatter [Figure 4.8]. A few extreme values probably govern the correlation. Mn^{2+} shows an almost universally poor correlation with both Na^+ and K^+. Since Na, K, and Fe all display some correlation with insoluble residue, the scatter in Figure 4.8 implies different noncarbonate lattice associations between Transition and Group I metals.

Paleosalinity and Origin of Sodium and Potassium Concentrations in Dolomites

The use by a number of authors of Na and K in carbonates as paleosalinity indicators has met with varying degrees of success (e.g. Veizer *et al* 1977, 1978, Sibley 1980, Baum *et al*. 1985). Following the suggestion of Veizer *et al* (1978), analyses for each dolomite type are grouped together [Figure A5.22] rather than using individual samples. The boundary between seawater and hypersaline environments [Figure A5.22a] is about 230 ppm Na^+ in the carbonate (Veizer *et al* 1977); carbonates with >230 ppm Na^+ indicate hypersaline environments, and those with less normal seawater. They add that depending on the facies variability and post-depostional effects, the boundary will be diffuse and thereby approximate a zone.

According to Figure A5.22a all Amuri Limestone Group carbonates would be classified as hypersaline. Sodium concentrations in the CD Zone and LCM Subzone dolomites equate with values for supratidal dolomites (Fritz and Katz 1972). Potassium values from this study exceed those for either seawater or hypersaline dolomites presented by Veizer *et al*. (1977). A hypersaline origin contradicts evidence presented thus far that dolomites in this study are of early diagenetic marine origin. The differences between observed and expected concentrations in carbonates can be explained by determining the manner in which Na^+ and K^+ are incorporated into crystals. Given a seawater diffusion source for the Mg^{2+}, the most likely source of Na^+ and K^+ is ultimately also seawater.

The analytical accuracy of Na^+ and K^+ is the poorest of all the carbonate analyses [Section A1.3.2]. However, taking the worst precision (±30%), and assuming that the results are an overestimate, K^+ concentrations will still be in excess of 1000-2000 ppm. Sodium concentrations will still plot in the hypersaline field. Therefore, poor accuracy does not explain

Figure 4.8 Scatter plots of Fe versus Na (a) and Fe versus K (b). Separate plots for micrites and marls (a) and WC Zone dolomite (b) are required to adequately illustrate trends.

▲ K-T Boundary

△ Marl

□ Micrite

○ LCM Subzone dolomite

● CD Zone dolomite

■ WC Zone dolomite

(a)

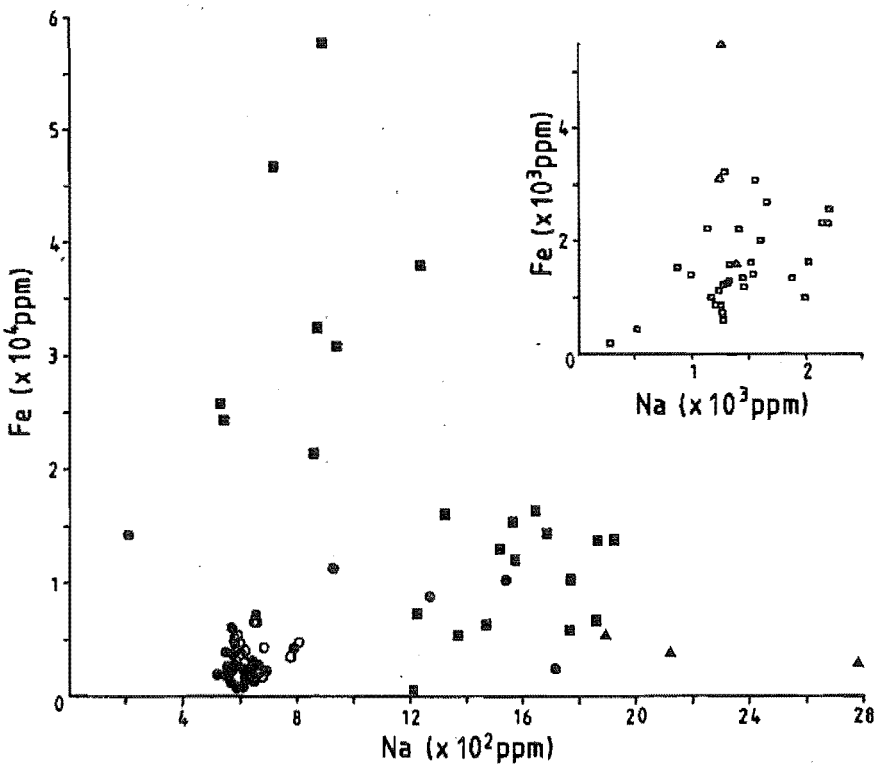
Fe (x 10⁴ppm)
Na (x 10²ppm)
Fe (x 10³ppm)
Na (x 10³ppm)

(b)

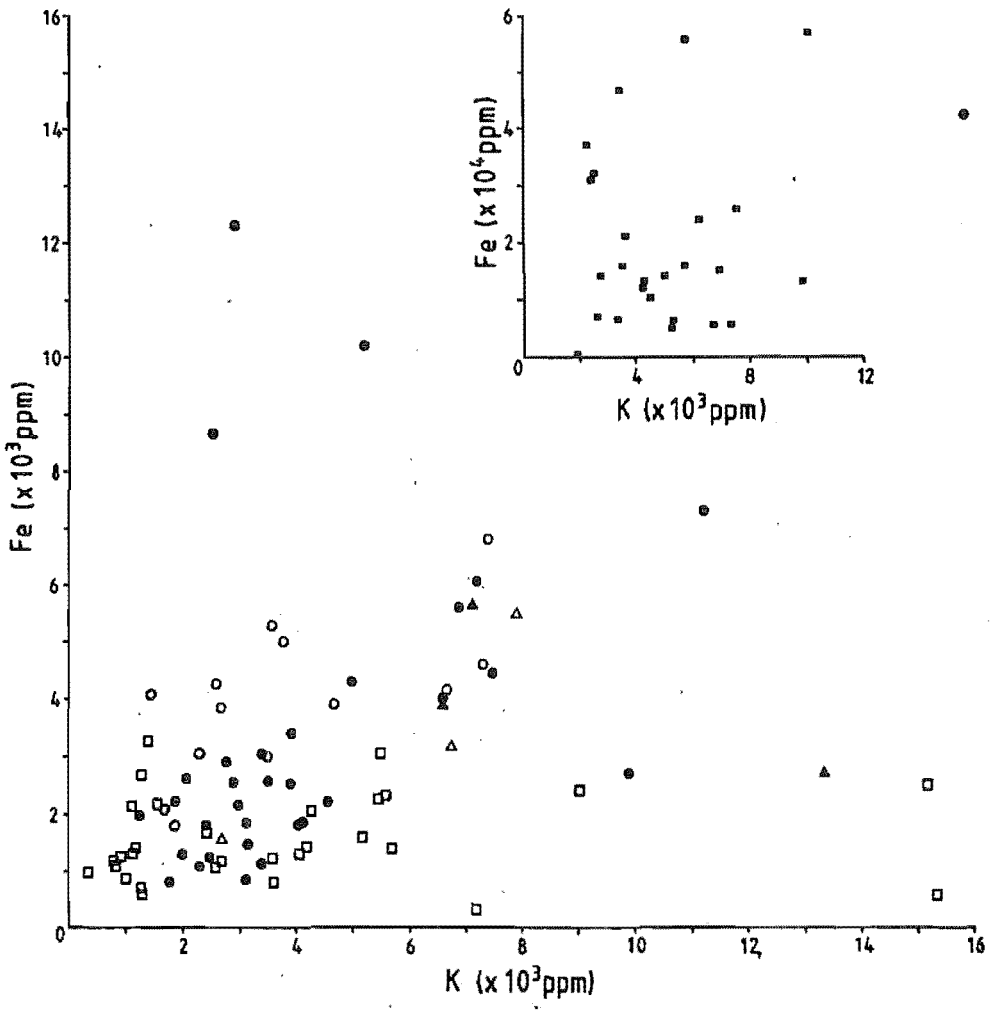
Fe (x 10³ppm)
K (x 10³ppm)
Fe (x 10⁴ppm)
K (x 10³ppm)

all the differences.

Veizer (1983) suggested that Na^+ and K^+ in the lattice is likely to be swamped by Na^+ and K^+ leached from the insoluble residue during acid digestion. Since the matrix around Amuri Limestone Group dolomite crystals is primarily chert, only limited leaching is expected. The scatter in plots of Na^+-insoluble residue, and to a lesser extent K^+-insoluble residue, supports this contention.

Badiozamani (1973) showed that interaction with meteoric waters lowered Na^+ concentrations in dolomites. This was also implied by Land and Hoops (1973), and the hypothesis was used to explain the lower than expected Na^+ concentrations in Bonaire dolomites (Sibley 1980). Thus varying amounts of meteoric water interaction can cause differences in Na^+ concentrations between different carbonates. The higher concentrations of Na^+ and K^+ in this study than predicted by comparison with data in Veizer *et al.* (1977, 1978) indicate meteoric interaction can be discounted. Such a conclusion is also consistent with Sr, Fe and Mn data.

Thin sections show fluid inclusions to be common in Amuri Limestone Group dolomites, and present in WC Zone concretions. Inclusions can contain considerable and often unknown quantities of Na^+ (Fritz and Katz 1972, Veizer 1983) and probably K^+. No analyses of fluids in inclusions were made for dolomites in the present study; however, as suggested by Veizer (1983), a significant proportion of the Na^+ and K^+ in whole rock analyses may be found in these inclusions. Significant quantities of Na^+ and K^+ in inclusions may account for the poor correlation of K and Na with Ca, Mg, Fe, and Mn.

White (1978) found that Na^+ coprecipitation in calcites and dolomites increases in the presence of aqueous citrate and then suggested that organic substances in invertebrate body fluids may account for high Na^+ concentrations in Recent relative to older carbonates. Disseminated organic matter may be an additional cause of higher than expected Na^+ concentrations in dolomites in this study. In addition it has been documented by Suess (1968; cited in White 1978) that calcite surfaces may adsorb organic components which may modify the inorganic equilibrium in the precipitating solution. Any complexed Na^+ would thus increase the amount of Na^+ incorporated into the crystal structure.

Discussion of Sodium and Potassium Contents

Whole rock Na and K analyses of both WC Zone concretions and Amuri Limestone Group dolomites do not reflect salinities at the time of dolomite formation. The bulk of the Na and K analyzed was probably contained in fluid inclusions with some associated with organic matter. Whole rock Na and K analyses are therefore inconclusive.

4.4. STABLE ISOTOPE GEOCHEMISTRY

4.4.1. ELEMENTAL AND ISOTOPIC INTERRELATIONSHIPS

Relationship to Major and Trace Elements

The $\delta^{13}C$ of Amuri Limestone Group carbonates display moderate to good negative numerical correlations with weight% insoluble residue and Fe. The WC Zone concretions exhibit a low positive correlation with Fe and a low negative correlation with insoluble residue. Besides the examples described above, all other element-isotope correlations, although high in a given unit, are not necessarily similarly related in other units. Correlations between elemental and isotopic composition are not systematic throughout the sequence.

$\delta^{13}C$ and $\delta^{18}O$

Statistically significant, moderately good positive correlations between $\delta^{18}O$ and $\delta^{13}C$ are found in WC Zone concretion and LCM Subzone samples. The correlations are low and negative in micrites, and not statistically significant in the CD Zone. Plots of $\delta^{18}O$ versus $\delta^{13}C$ define three distinct fields [Figure 4.9a]:

i) A field with $\delta^{18}O$ in the range -2·/.. to -7·/.., and $\delta^{13}C$ ~0·/.. which contains the Amuri Limestone Group micrites and dolomites [Figure 4.9b]. This group will henceforth be referred to as 'the Amuri Dolomite and Micrite (ADM) group'.

ii) A field containing concretions with $\delta^{18}O$ >-4·/.., and $\delta^{13}C$ >-9·/.., henceforth referred to as 'the heavy carbon group'.

iii) A second field of concretions with $\delta^{18}O$ $\leq$-6·/.. and $\delta^{13}C$ $\leq$-6·/.. mil, called 'the light carbon group'.

Figure 4.9 Scatter plots of $\delta^{13}C$ versus $\delta^{18}O$.
(a) Plot for all data. 1 = the ADM group, 2 = the heavy carbon group, and 3 = the light carbon group.
(b) Expanded scale plot of the ADM group, which also includes marls from Table A3.1.

▲ K-T Boundary

△ Marl

□ Micrite

○ LCM Subzone dolomite

● CD Zone dolomite

■ WC Zone dolomite

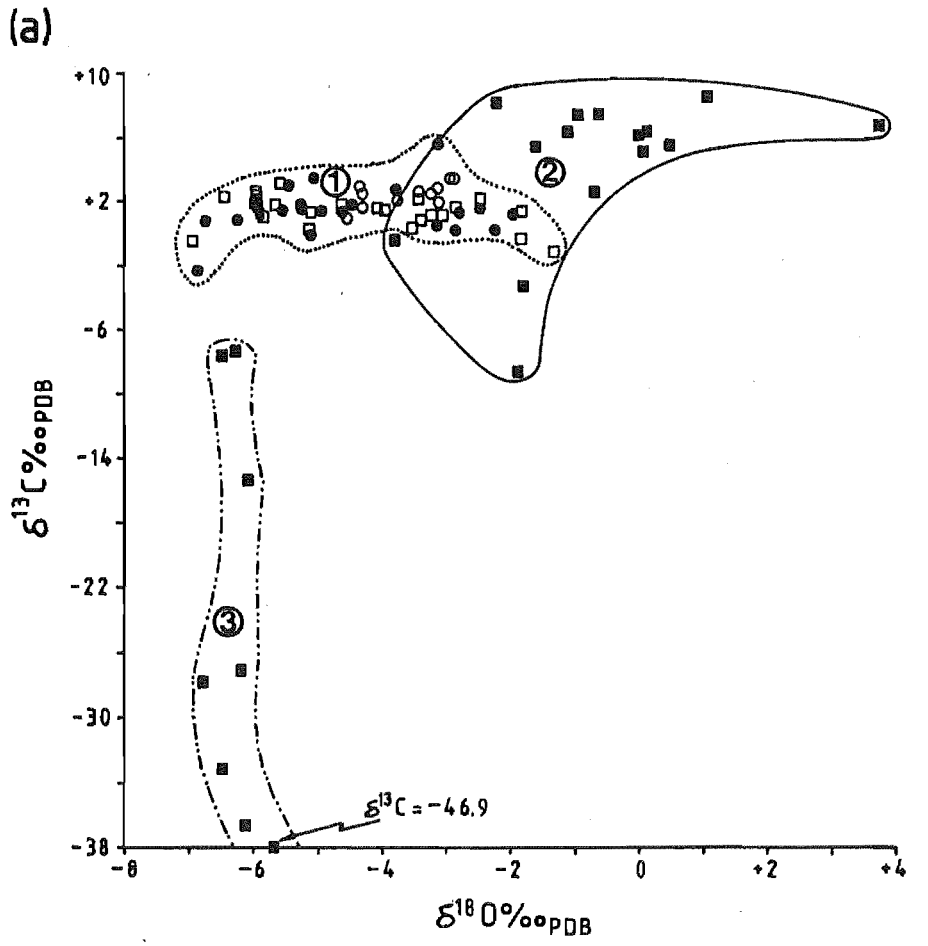
(a)
+10
+2
-6
-14
-22
-30
-38
-8
-6
-4
-2
0
+2
+4
δ13C‰PDB
δ18O‰PDB
①
②
③
δ13C = -46.9

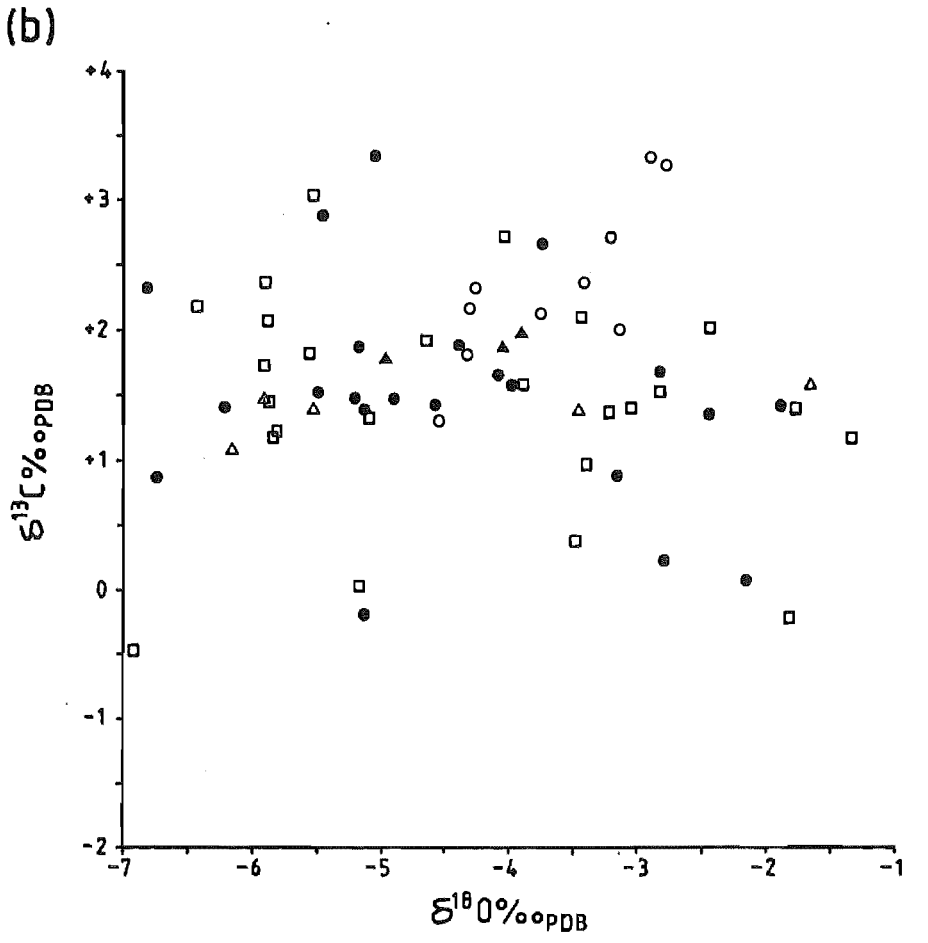
(b)
+4
+3
+2
+1
0
-1
-2
-7
-6
-5
-4
-3
-2
-1
δ13C‰PDB
δ18O‰PDB

Both concretion groups display a geographical separation. The light carbon group consists of samples from Dee Stream (27), Branch Stream (28) and Isolation Creek (20), all in the deeper parts of the basin. Heavy carbon group concretions are found further from the basin depocentre. Unfortunately none of the Woolshed Formation sequence is present at Mead (24,25), Limburn (26), or Swale (23) Streams. Had concretions been found at these localities they might also have been included in the light carbon group.

The relative insolubility of CO_2 makes alteration of the $\delta^{13}C$ of an original carbonate sediment difficult (Land 1980). Unlike $\delta^{18}O$, measured carbon isotope variations record the original carbon reservoir at the time of formation (Magaritz 1985). Therefore dolomite formed from primary or recrystallized carbonate should have the same ^{13}C signature as its precursor, hence the similarity between Amuri Limestone Group dolomites and micrites.

Micrites and CD Zone dolomites display a very crude non-linear trend of increasing $\delta^{18}O$ with decreasing $\delta^{13}C$ [Figure 4.9b]. LCM Subzone samples show the opposite trend.

The ADM group lies within the field of marine limestones [Figure 4.10], and partly within the organically derived dolomite field (organically derived dolomites are produced as a result of the bacterial metabolism of organic matter). ADM Group values agree well with the range of values for Upper Cretaceous chalks of the Danish sub-basin and North Sea central graben (Jørgensen 1987). At this stage a marine but organically influenced genesis is therefore implied.

The light carbon group tend to be more ^{18}O depleted than the organic dolomite field. Light carbon group values are close to the field of early diagenetic concretions (Hudson 1977, Figure 1), and are similar to diagenetic carbonates, including other New Zealand concretions analyzed by Hodgson (1966). The heavy carbon group lie above the marine limestone field, and just inside (with a few exceptions) the organic dolomite field. Again an organic carbon influence may be inferred.

Figure 4.10 $\delta^{18}O$ and $\delta^{13}C$ compositional fields for carbonates of various origin (From Pisciotto and Mahoney 1981).

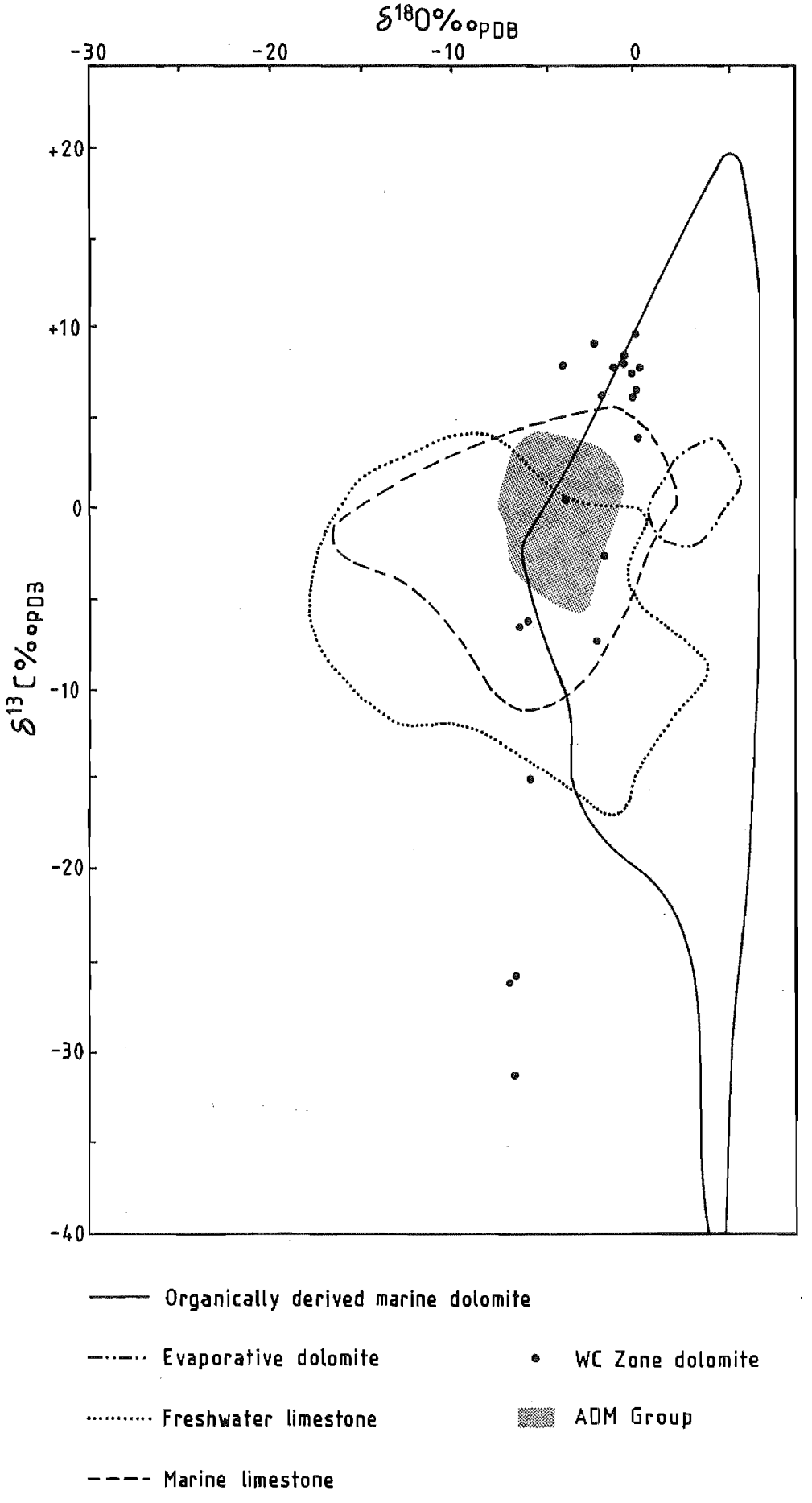
δ18O‰PDB
-30
-20
-10
0
+20
+10
0
-10
-20
-30
-40
δ13C‰PDB
Organically derived marine dolomite
Evaporative dolomite
Freshwater limestone
Marine limestone
WC Zone dolomite
ADM Group

4.4.2. OXYGEN ISOTOPE GEOTHERMOMETRY

The $\delta^{18}O$ composition of the carbonate is dependent upon the temperature and the isotopic composition of the fluids of formation. The bulk of Amuri Limestone carbonates have ^{18}O compositions less than about -2·/..$_{PDB}$. According to Land (1983a) such dolomites must have formed from water depleted in ^{18}O with respect to seawater (even if the seawater is as light as -4·/..), or at elevated temperatures. Dolomites with ^{18}O in excess of -2·/.. may therefore have formed at lower temperature, or in water slightly enriched in ^{18}O with respect to seawater. Therefore the significance of calculated paleotemperatures must be interpreted with caution (see discussion by Land 1980, Hardie 1987).

Temperature and the Fractionation Factor

Dolomite-water fractionations are much less certain than calcite-water fractionations [Section 3.5.2] at low temperatures (Land 1980, Pisciotto and Mahoney 1981). The main problem is the lack of experimental data on dolomites at temperatures less than 100°C. Land (1980) suggested that the fractionation should be somewhere between +1 and +7 per mil, and is possibly not constant. Holocene dolomites indicate a value between +2 and +4 per mil. The implication of this uncertainty is that calculated paleotemperatures are best interpreted in relative terms (i.e. warmer or cooler) rather than as absolute temperatures.

Naturally occurring dolomites may be similar, although usually somewhat enriched in $\delta^{18}O$, compared with coexisting calcite, as suggested by theoretical predictions and experimental observations (Degens and Epstein 1964, Epstein *et al.* 1964, Weber 1964b, Clayton *et al.* 1968, Hoefs 1980 and others). Small observed fractionations result from Mg substitution (Tarutani *et al.* 1969) in the calcite lattice during dolomite formation. Fractionations occur because dolomitization is a dissolution-precipitation process (Mathews and Katz 1977).

As a result of the uncertainty in the fractionation factors, there appear to be two ways of calculating paleotemperatures (from Pisciotto and Mahoney 1981): i) Subtract +0.06·/.. per mole% $MgCO_3$ from the measured $\delta^{18}O$ and then use the calcite-water fractionation (The value of +0.06·/.. is derived from the results of Tarutani *et al.* 1969); and, ii) Use the

protodolomite-water or experimental dolomite-water fractionation expressions, which involve extrapolation from data relating to temperatures in excess of 100°C.

The validity of extrapolation of high temperature experimental curves (e.g. Mathews and Katz 1977) is suggested by Land (1980) to be preferable to the use of protodolomite fractionations. In support, Land (1980 p91) states that Holocene dolomites are; *'more nearly in accord with conclusions reached by extrapolation of high temperature data ($\Delta^{18}O$ = +4 to +7·/..) than the oft-cited conclusions of Degens and Epstein (1964)'.* Land also supports the Clayton *et al.* (1968) contention that coexisting calcites and dolomites have differing $\delta^{18}O$ ratios resulting from exchange during a solution-precipitation dolomitization mechanism. A solid-state diffusion mechanism is likely to be too slow to cause the observed fractionations (Land 1980 and references therein).

The protodolomite expressions are based upon a near zero protodolomite-calcite fractionation (Degens and Epstein 1964). The later formed sedimentary dolomite inherits the protodolomite isotopic signature. Land (1980 p91) argues that; *'There is absolutely no reason to suppose that the replacement of protodolomite by dolomite even if such a process occurs, would be closed to O^{18}.'* It is difficult to understand how a system may be closed to ^{18}O but open to cations such as Mg^{2+} or Sr^{2+}, as appears to be the case for sediments in this study. For a near zero fractionation during a solution-precipitation process Mathews and Katz (1977) suggest that the reaction occurs in restricted solution zones around dissolving grains. The composition of these zones differ from the bulk solution, and have only minor interaction with it. Much of the debate as to the validity of the zero calcite-dolomite fractionation centres on work on calcite-dolomite pairs. As Land (1980) points out, there is no undisputed primary coprecipitated calcite-dolomite pair. Most dolomites form from precursor carbonate in the sediment, which means that the ^{18}O is not necessarily cogenetic. It seems there is little evidence for dolomite replacement of calcite without any isotopic exchange (Land 1983b). In contrast Pisciotto and Mahoney (1981) claim the protodolomite expression to be more accurate between 25°C and 79°C than curves extrapolated from higher temperatures. They also believe that the protodolomite expressions agree with theoretical dolomite-water fractionation computed from dolomite-calcite fractionations, and with the

+0.06·/.. per mole% $MgCO_3$ correction.

The outcome of this still unresolved debate is that there are a series of equations for the dolomite-water fractionation obtained by a variety of investigators [Figure 4.11], and there is no consensus concerning the most reliable expression. Whichever equation is used, the result may be an 'average' of possibly more than one dolomitizing event. Dolomites are commonly inhomogeneous at a single crystal scale (Land *et al.* 1975). Cathodoluminescence petrography in Amuri Limestone Group dolomites [Section A5.3] shows compositional variations during crystal growth, and these variations although constant in a particular sample, vary between samples. Therefore, what is needed is a technique accurate to the per mil level on a micron scale (Land 1983a).

The choice of a dolomite equation is difficult. When the fractionation curves are plotted against temperature, there are differences over a range of about 15°C (Pisciotto and Mahoney 1981, Land 1983a). It was decided to use the equation of Fritz and Smith (1970) because it has been used on data obtained by other authors (e.g. Irwin *et al.* 1977, Irwin 1980, Pisciotto and Mahoney 1981) with which comparisons are to be made.

Paleotemperature Calculation

Paleotemperatures are calculated from the Fritz and Smith (1970) equation in the form derived by Irwin (1980):

$$T\ (°C) = 31.9 - 5.55(\delta_{Dolomite} - \delta_{Water}) + 0.17(\delta_{Dolomite} - \delta_{Water})^2$$

In addition to the fractionation problems outlined there is debate as to what isotopic composition should be assigned to the fluids (δ_{Water}) involved in calcite formation/recrystallization and dolomitization. A range of values is used in this study: 0·/.., -1.2·/.., -4.2·/.., and -4.9 per mil, and are chosen for a number of reasons. The isotopic composition of present seawater is 0 per mil. The isotopic composition of oceans prior to the formation of the present Antarctic ice sheet has been estimated as -1.2·/..$_{PDB}$ (Shackleton and Kennett 1975; -1.2·/..$_{PDB}$ is equivalent to -1.0·/..$_{SMOW}$; the difference between the two values is negligible, therefore $\delta^{18}O_{Water}$ for modern seawater is assumed to be zero with respect to PDB). In addition, depletions in ^{18}O of 1-3·/.. in pore

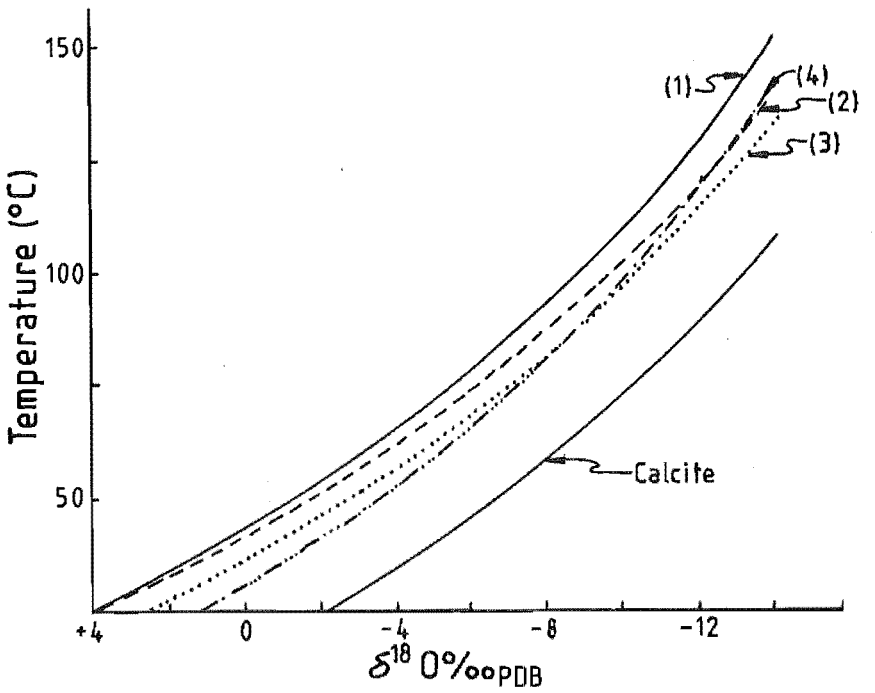

Figure 4.11 Plots of dolomite-water fractionation for $\delta^{18}O_{Water}$ = 0‰ PDB (from Pisciotto and Mahoney 1981, Land 1983a). The equations are listed below. An '*' indicates equations from Pisciotto and Mahoney (1981). Other equations are from Land (1983) and have been corrected to be consistent with Friedman and O'Neil (1977). The calcite-water fractionation is included for comparison.

(1) Northrup and Clayton (1966)

$$1000\ln\alpha_{Dolomite\text{-}Water} = 3.20 \times 10^6.T^{-2} - 1.50$$

(2) O'Neil and Epstein (1966)

$$1000\ln\alpha_{Dolomite\text{-}Water} = 3.34 \times 10^6.T^{-2} - 3.34$$

(3) Sheppard and Schwarz (1970)

$$1000\ln\alpha_{Dolomite\text{-}Water} = 3.23 \times 10^6.T^{-2} - 3.29$$

Fritz and Smith (1970)*

$$1000\ln\alpha_{Dolomite\text{-}Water} = 2.78 \times 10^6.T^{-2} + 0.21$$

(4) Fritz and Smith (1970)

$$1000\ln\alpha_{Dolomite\text{-}Water} = 2.78 \times 10^6.T^{-2} + 0.11$$

Mathews and Katz (1977) (not plotted)

$$1000\ln\alpha_{Dolomite\text{-}Water} = 3.06 \times 10^6.T^{-2} - 3.24$$

O'Neil *et al.* (1969)

$$1000\ln\alpha_{Calcite\text{-}Water} = 2.78 \times 10^6.T^{-2} - 2.89$$

waters have been reported (Lawrence *et al.* 1975, 1976). The greatest depletions are at greatest depth. Irwin *et al.* (1977) suggested that some dolomite that had formed immediately below the sulphate reduction zone was in equilibrium with pore waters of -4.9 per mil.

The results [Table 4.4] show that temperatures may differ by 25-30°C depending on the assumed seawater composition. Ranges of temperatures calculated for the Amuri Limestone Group dolomites are similar to those for the micrites, although dolomites have higher mean temperatures. The poor down-profile trends in $\delta^{18}O$ [Figure A5.23a] indicate only a slight increase in temperature with burial depth. The only geographic trend is an approximately 10°C increase in LCM Subzone dolomites from Branch (28,29) to Mead (24,25) Streams. All but one of the concretions have $\delta^{18}O$ compositions of less than +0.51 per mil. Ignoring the one value of +3.75·/.., all concretions have formation temperatures similar to, and in some cases slightly lower than, Amuri Limestone Group dolomites and micrites.

Significance of Paleotemperatures

Variations in temperature ranges such as shown in Table 4.4, plus the problems with fractionation factors and the assumptions therein have generated skepticism as to the validity of paleotemperature measurements. Absolute accuracy is probably at best 3-4°C for a given δ_{Water} (Savin 1977). However, as long as the limitations of the technique are kept in mind, useful interpretations may be made.

Depletion of ^{18}O in ancient dolomites can be attributed to stabilization of an earlier phase during burial. The isotopic composition of the dolomite is thought to be controlled by the latest recrystallization event and by the chemistry of the precursor carbonate (Land 1983b), although it must be remembered that the $^{18}O/^{16}O$ ratio of dolomite is less susceptible to diagenetic re-equilibration with surrounding fluids than calcite (Epstein *et al.* 1964). More recently the relative abundances of opal-A and opal-CT have been used to show that the $\delta^{18}O$ of dolomite is primarily temperature dependent (Hennessy and Knauth 1985). Temperature dependence and early formation would mean precipitation at temperatures similar to ocean bottom waters, that is $\leq$10°C. However, all the Amuri Limestone Group dolomites indicate temperatures in excess of 10°C even with

Table 4.4 Dolomite paleotemperatures calculated using various $\delta^{18}O_{Water}$ compositions. Two maximum values for WC Zone concretions are used as all but one sample have $\delta^{18}O$ compositions of less than 0.51‰ $_{PDB}$. Values for micrites are included for comparison.

	O-18 Range	T1°C	T2°C	T3°C	T4°C	T5°C
	δ Water =	0	-1.2	-2.0	-4.2	-4.9
Micrites	Maximum = -1.33	23	17	14	5	3
	Minimum = -6.90	52	45	41	29	26
	Mean = -4.36	38	32	28	18	15
LCM	Maximum = -2.75	48	41	36	24	21
Subzone	Minimum = -4.25	59	50	45	32	28
Dolomite	Mean = -3.65	54	47	42	29	25
CD Zone	Maximum = -1.89	43	36	31	20	17
Dolomite	Minimum = -6.82	78	68	63	35	43
	Mean = -4.01	57	49	44	31	27
WC Zone	Maximum = +3.75	14	9	7	-1	-3
Dolomite	+0.51	29	23	19	10	7
	Minimum = -6.79	77	68	62	47	43
	Mean = -2.16	45	37	32	21	18

$\delta^{18}O_{Water}$ = -4.9 per mil. Only a few WC Zone concretions have temperatures of less than 10°C. The implication is that dolomites, like some of the calcites [Section 3.5.2], record diagenetic temperatures.

Isotopic variations across individual beds or concretions have been investigated by other workers (e.g. Kelts and McKenzie 1982, 1984, Kushnir and Kastner 1984, Mertz 1984). From such work it was inferred that dolomites precipitate in isotopic equilibrium with burial temperatures (Kelts and McKenzie 1982). Changes across an individual bed may indicate a range of burial depths, implying that dolomites continue to grow for periods of time as they are buried to higher temperatures (Burns and Baker 1987). Therefore one sample from a single concretion or bed may record only part of the thermal or burial history.

It is realized that recrystallization effects on pore water composition may control ^{18}O in solid phases, to some extent invalidating calculated paleotemperatures. However, the discussion in the preceding paragraph indicates that the temperature dependence of the ^{18}O in dolomites may still provide some useful information. Dolomite paleotemperature can be used to estimate the depth of burial at which precipitation occurred (e.g. Irwin *et al.* 1977, Irwin 1980, Hennessy and Knauth 1985). An estimate of geothermal gradients are required. For this study a range of geothermal gradients of 25°C/km to 35°C/km is used, measured from wells in the Taranaki Basin (Suggate 1974). The latter gradient is a maximum whereas gradients of about 25°C/km are normal for the New Zealand situation (J R Pettinga *pers. comm.* 1988, see also Moore 1988a). In performing calculations of burial depth, it is implicitly assumed that a lower temperature dolomite crystallized before a higher temperature dolomite; that is at shallower burial depth, and/or in earlier diagenetic pore waters. Dolomites with the lowest temperatures (17°C in Amuri Limestone Group dolomites and 7°C in WC Zone concretions, both with $\delta^{18}O_{Water}$ = -4.9·/..) are assumed to have precipitated just below the sulphate reduction zone, at about 10 m depth. Results are listed in Table 4.5. The lowest Amuri Limestone Group temperature is similar to the 15.6°C used by Irwin *et al.* (1977) and Irwin (1980).

Amuri Limestone Group Dolomites

The results [Table 4.5] show that Amuri Limestone Group dolomites formed

Table 4.5 Estimated depths of dolomite precipitation calculated from paleotemperatures given in Table 4.4 using a range of geothermal gradients. It is assumed that δ_{Water} = -4.9‰ and the first dolomite formed at 10 m depth in the sediment column.

		Temperature (°C)	Burial Depth (m) 25°C/km	35°C/km
LCM Subzone dolomite	Maximum	28	450	324
	Minimum	21	170	153
	Mean	25	330	239
CD Zone dolomite	Maximum	43	1050	753
	Minimum	17	10	10
	Mean	27	410	296
WC Zone dolomite	Maximum	43	1450	1029
	Minimum	7	10	10
	Mean	18	450	324

at burial depths of less than 1 km. With a geothermal gradient of 35°C/km, 30% of the CD Zone and 40% of the LCM Subzone dolomites formed at burial depths of less than 200 m. All LCM Subzone and 88% of the CD Zone samples formed at less than 500 m.

Evidence for early diagenetic origins [Sections 2.2.6, 2.3] implies that depths less than 100 m might be expected. Deeper than expected burial depths may be caused by a number of factors. There may have been fluctuations in temperatures in the sedimentary basin, and that they were higher in the past. A higher geothermal gradient means shallower burial depths (c.f. Kelts and McKenzie 1982, geothermal gradient 95.9°C/km; Hennessy and Knauth 1985, geothermal gradient 90°C/km). Although the validity of different geothermal gradients cannot be assessed, there is no available evidence to suggest any difference between current gradients and those during the Late Cretaceous and Early Tertiary. Discrepancies between dolomite isotope temperatures and measured subsurface temperatures may indicate non-equilibrium fractionation during precipitation, which can result in an uncertainty in calculated burial depths of about 100 m (Pisciotto and Mahoney 1981). Variations in ocean bottom water temperatures may also introduce uncertainty into calculated depths (Friedman and Murata 1979). The presence and assimilation of primary carbonate can distort the calculated burial depth downwards (Irwin 1980). Assimilation of primary carbonate is probably a major factor in Amuri Limestone Group dolomites, and would imply that pore water composition may be more important in governing the isotopic composition of these carbonates than temperature. Nevertheless the dolomite appears to have formed in the upper few hundred metres of the sediment pile. This is well within the range of burial depths at which dolomites are found in DSDP cores (e.g. Matsumoto 1983), and effectively discounts deep burial dolomitization.

Graphical relationships between estimated burial depth and elemental concentrations are inconsistent between CD Zone and LCM Subzone dolomites. LCM Subzone samples display slight increases in Fe and Mn concentrations and slight decreases in Mg, Na, and Sr concentrations with increasing calculated burial depth. Such trends are less clear in CD Zone dolomites. Increasing Fe and Mn concentrations imply increasing Fe^{2+} and Mn^{2+} with depth, whereas decreases in Mg and Na may reflect burial below the zone of effective seawater diffusion. The overall poor definition of burial

depth/composition relationships (c.f. Irwin 1980, Figures 7-10), and their virtual non-existence in the CD Zone, probably result from uncertainty in burial depth estimates. However, despite the quality of the relationships they lend some credence to the sources for cations such as Mg^{2+} (seawater), Fe^{2+} and Mn^{2+} (oxides, hydroxides, and organic matter) outlined in earlier Sections.

Plots of calculated dolomite burial depth against $\delta^{13}C$ display a positive non-linear relationship [Figure 4.12]. Samples tend to become more negative in $\delta^{13}C$ with increasing depth. A good relationship is displayed by the LCM Subzone. Greater spread is seen in the CD Zone data, with some shallow depth samples more depleted in ^{13}C than might be expected. Inaccuracy in burial depth estimation is probably the source of the spread of data.

WC Zone Concretions

A few concretions apparently formed deeper than 1 km, but most samples (55%) indicate burial depths in excess of 200 m, only 35% are in excess of 500 m. Fewer samples form at depths less than 200 m if the geothermal gradient was 25°C/km. The field evidence for early diagenetic origin [Sections 2.2.3, 2.3] suggest burial depths of no more than 150 m, and probably less than 50 m are expected. However, as indicated for Amuri Limestone Group dolomites, concretions formed in the upper sediment column and deep burial dolomitization can be discounted. There is also a suggestion that WC Zone concretions may have formed at shallower depth than Amuri Limestone Group dolomites.

With the exception of significant ^{18}O contributions from assimilated primary carbonate, reasons for greater than expected burial depths in Amuri Limestone Group dolomites may also be applied to WC Zone concretions. In addition, because generally only the exteriors of concretions could be sampled, analyses reflect later dolomitization events, rather than the initiation of dolomite formation. The $\delta^{18}O$ contours from the Lab Rocks concretion [Figure A5.29h] may be explained in terms of dissolution and reprecipitation processes (e.g. Land 1980). Hennessy and Knauth (1985) suggest that the original ^{18}O patterns of concretions are usually approximately concentric. The original ^{18}O signature is then altered during the protodolomite to dolomite conversion

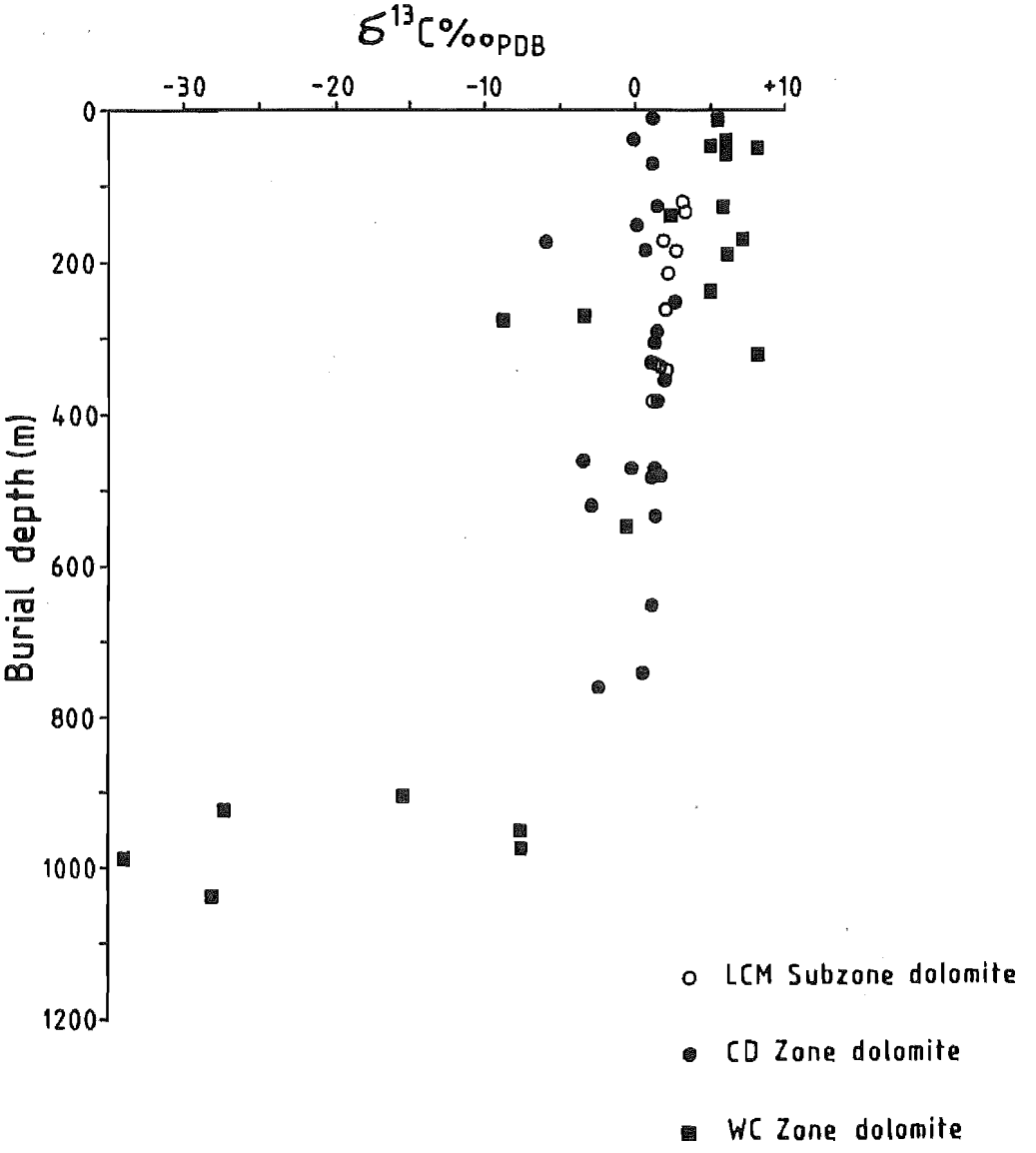

Figure 4.12 Plot of $\delta^{13}C$ versus burial depth calculated from ^{18}O data.

(Hennessy and Knauth 1985, Burns and Baker 1987). The validity of 'protodolomite' arguments is debated (e.g. Land 1980). However, an analogous mechanism may be invoked. The Sr^{2+} concentrations are explained by initial precipitation of calcite, with subsequent replacement by dolomite [Section 4.3.2]. The original ^{18}O signature may have been lost during this process. Large variations between closely spaced concretions suggest that local source factors may control the isotopic properties of pore waters (Coleman and Raiswell 1981). Perhaps growth is initiated along sites of greatest porosity (Hennessy and Knauth 1985), which may be quite variable locally. Variations in porosity would locally govern the diffusion of fluids to the site of nucleation, hence the $\delta^{18}O$ variations from site to site. Thus, as is the case for Amuri Limestone Group dolomites, the $\delta^{18}O$ of WC Zone concretions dominantly reflects variations in the pore fluid composition during growth, rather than temperature.

As in Amuri Limestone Group dolomites the relationships between calculated burial depth and chemical composition in WC Zone concretions is inconsistent. Fe^{2+} and Mn^{2+} concentrations display a slight increase, Mg^{2+} and Na^{+} decrease slightly, and ^{13}C becomes more depleted with increasing burial depth in concretions. As suggested for Amuri dolomites, these trends support the inferred origins for cations.

Burial depths derived from the rate of concretion formation may be used as a comparison with ^{18}O derived depths. The rate of concretion formation is estimated from a combination of pore water composition and fluid migration. Concretions formed in zones of moving fluid are usually elongated in the direction of flow, whereas spherical concretions suggest ionic diffusion (Boles *et al.* 1985). The Lab Rocks (4) concretion (KP3, see Section A5.5.4) is used, which as well as others tend to be elongated or at least elliptical. Concretion elongation parallel to bedding indicates pore waters migrated parallel to bedding planes. Berner (1968) derived two equations for estimating the rate of concretion growth. For growth by ionic diffusion the equation is as follows:

$$t = R^2/(2\ D(C_i - C_R))$$

For precipitation from moving fluids the equation is as follows:

$$t = \{(R - U/(0.715U))(1 + RU/D)^{0.715} + (D/0.715U)\}/1.715U \times (C_1 - C_R)$$

where:

t = time (seconds)

C_i = concentration at distance from the concretion

C_R = concentration at the surface of the concretion assumed to represent the saturation concentration at solubility, and hence (C_i - C_R) = the degree of supersaturation (moles/cm^3).

R = concretion radius (cm)

U = Groundwater flow velocity (cm/sec)

= molar volume of the cementing mineral (cm^3/mole)

D = diffusion coefficient (cm^2/sec)

The following values were used; (C_i - C_R) = 10^{-7} mole/cm = 10 ppm supersaturation (Berner 1968). D = 10^{-5} cm^2/sec is used because of the sediment lengthening and restricting the diffusion path due to tortuosity of channels, the rates of diffusion are 1/2 to 1/20 those of the free solution (Manheim 1970). Both these end member factors were used giving values of D = $5x10^{-5}$ cm^2/sec and D = $5x10^{-6}$ cm^2/sec. The radius of the long axis of the concretion (KP3) was used, that is 250 cm. Calculations were made assuming U = 0 m/yr and U = 0.3 m/yr. The latter figure was thought reasonable considering the grain size and clay mineral content of the Woolshed Formation. Growth by diffusion only took from 0.46-4.6 myr, but where some fluid migration was involved concretion growth took from just over 0.3 myr to 1.9 myr. The concretion shape suggests that the latter estimate is more likely. These figures are at best crude estimates because of the assumptions made; for example, constant saturation, value of supersaturation, diffusion coefficients and so on. In addition, Raiswell (1988b) suggested that the growth rate of concretions may also be (crystal) surface-reaction controlled (i.e. kinetic effects may inhibit growth on freshly precipitated crystal surfaces). Therefore, the reliability of the above growth rate estimates cannot be ascertained. However, assuming the slowest growth rate (4.6 myr), and a sedimentation rate of 43 m/myr, the burial depth was a little over 120 m by the end of the concretion formation, compared to the deepest burial depth estimate from $\delta^{18}O$ data which is 185 m. Using a growth rate of 1.9 myr gives a burial depth of 82 m by the end of concretion formation. Since the concretion shape suggests that fluid migration occurred, the latter estimate of burial depth is probably more reasonable.

4.4.3. ORGANIC MATTER AND $\delta^{13}C$

Land (1980) stated that few authors interpreted the significance of ^{13}C in dolomites. More recently, $\delta^{13}C$ has been used to determine organic matter reactions within the sediment, and hence the site and time of carbonate precipitation (Curtis *et al.* 1972, Irwin *et al.* 1977, Irwin 1980, Jeans 1980, Baker and Burns 1985, Jenkyns and Clayton 1986, Raiswell 1976, 1987, Ritger *et al.* 1987 and many others).

Effect of Organic Matter on $\delta^{13}C$

The type of organic matter reaction can be related to the relative depth of burial [Figure 4.13], although the actual depth and thickness of each reaction 'horizon' may vary from site to site. In the upper zone of bacterial oxidation there is no carbonate precipitation. Soluble reaction products will tend to be lost back to reaction waters (Curtis 1978). In the zone of anaerobic sulphate reduction light carbon CO_2 is produced in the form of dissolved HCO_3^-. Incorporation of this carbon produces $\delta^{13}C$ in carbonates in the range 0·/.. to -25·/.. (Claypool and Kaplan 1974, Irwin *et al.* 1977, Irwin 1980, Curtis 1978). Authigenic pyrite and carbonate associations related to sulphate reduction are commonly described in the literature (Coleman and Raiswell 1981, Coleman 1985, Curtis *et al* 1986). The sulphate reduction zone usually extends to about 10 m depth in the sediments. Below the sulphate reduction zone is the zone of methanogenesis, or bacterial fermentation, which may extend to depths of the order of 1 km. Carbonate precipitated in this zone has ^{13}C in the range -10 to -15 per mil. Discrimination against ^{13}C by micro-organisms involved in methane production results in ^{13}C enriched residual HCO_3^- in interstitial waters (Claypool and Kaplan 1974). Decarboxylation at greater burial depths will generate more ^{13}C depleted carbon, which will result in carbonates precipitated with ^{13}C of the order of -20·/.. (Curtis 1978). More negative ^{13}C values may also be found in carbonates near the bottom of the methanogenic zone. The ^{13}C signature recorded in a dolomite is caused by the interplay of the above organic carbon sources plus the primary sedimentary carbonate (Irwin 1980). The latter has a ^{13}C of about 0 per mil.

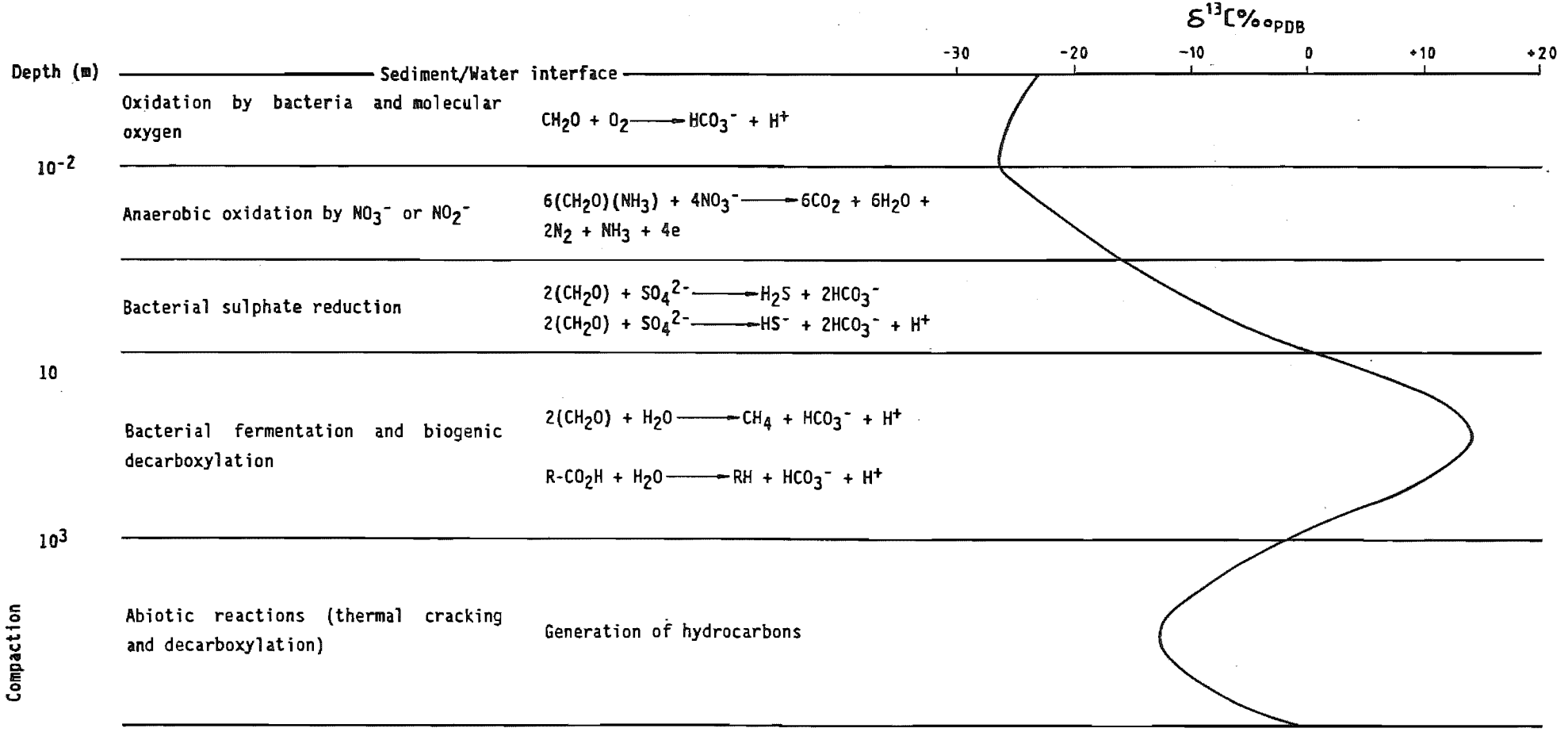

Figure 4.13 Schematic representation of the relationship between microbial metabolic reactions, burial depth, and expected ^{13}C in authigenic carbonates. (Drawn from Irwin 1980, Pisciotto and Mahoney 1981).

Carbon Sources

Amuri Limestone Group Dolomites

Most Amuri Limestone Group dolomites are confined to the range 0·/.. to +3.5 per mil. The expected $\delta^{13}C$ curve for authigenic carbonates [Figure 4.13] suggests that $\delta^{13}C$ values in this range may be expected about the sulphate reduction/methanogenesis zone interface. A similar $\delta^{13}C$ value may be expected near the base of the zone of methanogenesis. Zero values may be obtained by the mixing carbon extremely enriched and extremely depleted in ^{13}C. Abiotic extremely negative CO_2 has been detected in near surface sediments (Claypool and Threkeld 1983). Finally, values of about 0·/.. will be obtained if primary carbonate is the predominant carbon source (e.g. Hoefs 1980).

The $\delta^{13}C$ of Amuri Limestone Group dolomites appears to be dominantly derived from the original carbonate sediment. Since both micrites and dolomites have very similar $\delta^{13}C$ ranges, the effect of organic reactions on $\delta^{13}C$ is subordinate. Sass and Kolodny (1972) used the following equation to estimate the relative proportions of carbon derived from organic and primary carbonate sources, for samples which fall between the two end member compositions, that is organically derived carbon $\delta^{13}C$ = -25·/.. and primary carbonate $\delta^{13}C$ = 0 per mil:

$$\text{Organic matter (\%)} = \text{Total carbonate (\%)} \times \delta^{13}C/-25$$

Calculations for Amuri Limestone Group dolomites assume $\delta^{13}C$ = +15·/.. for methanogenic carbonate. A maximum of only about 16% organic carbon is thus calculated. Since the bulk of samples are slightly positive there may be minor input from bacterial fermentation, particularly in those samples between +2·/.. and +3 per mil. The LCM Subzone tends to be approximately 1·/.. enriched in ^{13}C compared to the CD Zone, possibly reflecting a slightly greater methanogenic carbon input. The three slightly more negative samples may have been associated with sulphate reduction. Other evidence for the early diagenetic origins of the dolomite favour an association with the sulphate reduction zone, rather than deeper burial into the zone of methanogenesis. Unfortunately, estimates of the position in the sediment column of the Amuri Limestone Group dolomite precipitation are obscured by the effect of primary

carbonate of the host sediment. It is thought that these samples are likely to have precipitated in the vicinity of the sulphate reduction zone or at the top of the bacterial fermentation zone. Support comes from the pyrite associated, and sometimes enclosed in dolomite crystals [e.g. Figures A5.4, A5.8].

WC Zone Concretions

WC Zone concretions appear to be derived from a mixture of ^{13}C sources. A number are enriched in ^{13}C and some are drastically depleted. Few samples are in the same range as the Amuri Limestone dolomites [Figure 4.9a]. Primary carbonate was probably minimal in this sediment, hence little carbon could have been contributed from this source. The range of $\delta^{13}C$ values indicates that the heavy carbon group contains carbon derived from bacterial fermentation. The $\delta^{18}O$ of these concretions indicates a shallower burial origin than for the light carbon group. Field evidence for an early diagenetic origin [Sections 2.2.3 and 2.3], plus the presence of pyrite suggests formation after, or, in conjunction with sulphate reduction. Therefore the heavy carbon group probably formed at or near the boundary between the bacterial fermentation and sulphate reduction zones. The peneconcentric increase of $\delta^{13}C$ in the Lab Rocks concretion [Figure A5.29i] suggests an increase in carbon from fermentation sources during progressive growth, and may imply progressive burial through the fermentation zone. These results are the reverse of those reported by Ritger *et al.* (1987), whose concretions are increasingly ^{13}C depleted concentrically due to a greater volume of deep source ^{13}C-depleted CH_4-derived carbonate.

With the exception of samples highly ^{13}C depleted, the light carbon group probably were associated with sulphate reduction. Again, the presence of pyrite and field evidence support this conclusion. The more ^{13}C depleted samples require a different explanation. Deuser (1970) described dolomites from oceanic canyon walls with $\delta^{13}C$ as low as -64·/.. and $\delta^{18}O$ between +5·/.. and +7 per mil. Other workers such as Nelson and Lawrence (1984), and Ritger *et al.* (1987) also found similarly depleted authigenic carbonates. Claypool and Threkeld (1983) measured values of $\delta^{13}C$ in dissolved HCO_3^- as low as -31 per mil. Anaerobic methane oxidation has been found to be coupled with sulphate reduction (Reeburgh 1980, Devol and Ahmed 1981, Devol *et al* 1984, Berner 1985) in accord with the following

equation:

$$CH_4 + SO_4^{2-} \rightarrow HS^- + HCO_3^- + H_2O \qquad (4.15)$$

Approximately 10% of the HCO_3^- in this reaction is thought to come from the oxidation of methane, which has diffused up into the sulphate reduction zone. Extreme negative values are generated either through methane oxidation resulting from methane diffusion (e.g. Nelson and Lawrence 1984, Ritger *et al*. 1987), or from erosion and exposure to oxic conditions (Deuser 1970). Thus the light carbon group were probably precipitated in the zone of sulphate reduction, with $\delta^{13}C$ reflecting the relative mixing of HCO_3^- derived from anaerobic oxidation of methane, rare primary calcite in some cases, and HCO_3^- derived from sulphate reduction. It appears from the distribution of light carbon concretions that methane diffusion was concentrated in the basin depocentre.

Light carbon group concretions are also the most depleted in ^{18}O. Even when the problems involved in temperature calculations and estimates of burial depth are considered, the association is difficult to explain. Deep burial implies more positive $\delta^{13}C$ values (i.e. $\geq$-10 per mil, cf. Figures 4.12 and 4.13), than measured for these samples. $\delta^{13}C$ indicates a sulphate reduction zone origin implying that the dolomite did not precipitate in equilibrium with respect to $\delta^{18}O$, or precipitation occurred in ^{18}O depleted pore waters. Such depletion may have resulted from some low temperature alteration reactions in the sediments as suggested by Hesse *et al* (1985). Reactions of this sort include the alteration of volcanic glass (Hesse *et al* 1985), or the precipitation of various diagenetic minerals (Coleman and Raiswell 1981). Meteoric water interaction, or even meteoric-derived burial waters (Hudson 1978), would deplete the ^{18}O reservoir. In WC Zone concretions elemental concentrations can be explained without a requirement for meteoric waters and there is no independent evidence of volcanic material in the Woolshed Formation. Localized factors may also control the ^{18}O of the pore waters. Large differences in $\delta^{18}O$ from closely spaced concretions are explained in this manner (Coleman and Raiswell 1981). Replenishment of pore waters by diffusing seawater will decrease with increasing burial. Restrictions on water diffusion in the vicinity of the concretion will result in progressive ^{18}O depletion with growth. The depletion may also be enhanced by supplies of light oxygen from organic matter and sulphate (Coleman and

Raiswell 1981).

Using the Sass and Kolodny (1972) equation, the light carbon group contains 24-46% organically derived carbon. Samples of $\delta^{13}C$ <-25·/.. could be derived entirely from organic carbon. For the heavy carbon concretions, an estimated maximum of about 48% organic carbon is calculated.

Sulphate Reduction and Sedimentation Rate

The $\delta^{13}C$ data discussed above indicates that sulphate reduction was important in the precipitation of dolomite within the sediments in this study. Fe reduction is also important within the zone. Fe reduction and the precipitation of pyrite can be associated with carbonate dissolution followed by reprecipitation, resulting in the presence of both minerals. The product of SO_4^{2-} is H_2S which is removed from the system by Fe as pyrite, so Fe reduction may to some extent control sulphate reduction (Coleman 1985). If Fe reduction accompanies methanogenesis in sediments below the SO_4^{2-} reduction zone, carbonates that precipitate will tend to accommodate Fe (Coleman 1985). Thus some of the more Fe enriched WC Zone concretions may have precipitated during combined methanogenesis and Fe reduction.

A number of authors have suggested that sedimentation rates are important in the formation of authigenic carbonates (Pisciotto and Mahoney 1981, Kablanow *et al.* 1984, Baker and Burns 1985, Burns and Baker 1987). The effects are summarized from Pisciotto and Mahoney (1981), and Kablanow *et al.* (1984) as follows:

i) Low sedimentation rates result in more complete oxidation of organic matter through aerobic pathways or anaerobic sulphate reduction. The consequence is light carbon carbonates. Low to medium sedimentation rates will also enable greater Mg^{2+} diffusion from the overlying water, as a given packet of sediment would remain in the zone of effective seawater diffusion longer. Therefore during a hiatus, dolomitization would proceed to a greater extent for any given set of conditions (i.e. diffusion and sulphate reduction rates and so on). Dolomites are commonly found immediately below unconformities (e.g. Morrow 1982b, Compton and Siever 1986).

ii) High sedimentation rates inhibit oxygen and sulphate diffusion into

the sediment, thereby promoting methanogenesis. The result is heavier carbon carbonates than found at shallower depths.

iii) Very high sedimentation rates could result in dolomitization occurring in the zone of thermocatalytic decarboxylation. The result would be the reversal of the increasingly heavy carbon trend.

The relationship between $\delta^{13}C$ and sedimentation rate is shown in Figure 4.14. For comparative purposes Woolshed Formation and Amuri Limestone Group samples are also plotted. Morris (1987) determined a compacted sedimentation rate of 24 m/myr for the upper part of the Woolshed Formation. Rates of about 26 m/myr were calculated for the Amuri Limestone Group lithologies. Preserved bedding in concretions suggests that the Woolshed Formation may have been compacted by up to 80 percent, with the original porosity in excess of 80 percent, whereas Amuri Limestone Group samples may only have compacted to about 30 percent [Section 3.4.2]. Assuming 80% compaction in the WC Zone and 30% in the Amuri, implies uncompacted sedimentation rates of the order of 43 m/myr for the WC Zone and 33 m/myr for the Amuri Limestone Group.

The bulk of samples in this study are more ^{13}C enriched than predicted by trends indicated by Pisciotto and Mahoney (1981) in Figure 4.14, but still lie within the range of values for some DSDP sites. There are a number of differences between dolomites from this study and DSDP examples. Differences may arise because the estimation of sedimentation rates in this study are crude. There is very little direct evidence for changes in sediment accumulation, and there is poor chronostratigraphic control in both the Woolshed Formation and the Amuri Limestone Group. WC Zone concretion samples fit the trend better if it is assumed that the light carbon group were associated with lower sedimentation rates than the heavy carbon group. This implies decreasing sedimentation rates towards the basin centre. A lower sedimentation rate implies that the light carbon group should contain less Fe^{2+} and Mn^{2+} than the heavy carbon group. This is not supported by the Fe^{2+} and Mn^{2+} data. Possibly the sedimentation rate differences were enough to cause variations in $\delta^{13}C$, but not in Fe^{2+} or Mn^{2+}, implying that sedimentation rate variations cannot be totally discounted. Alternatively, a wider $\delta^{13}C$ range may be expected for a given sedimentation rate [Figure 4.14]. Where deposition is slow, localized factors may be more important, such as diffusion and subsequent oxidation of methane, erosion causing oxidation of sediments, and the influence of primary carbonate. These effects may diminish at progressively higher

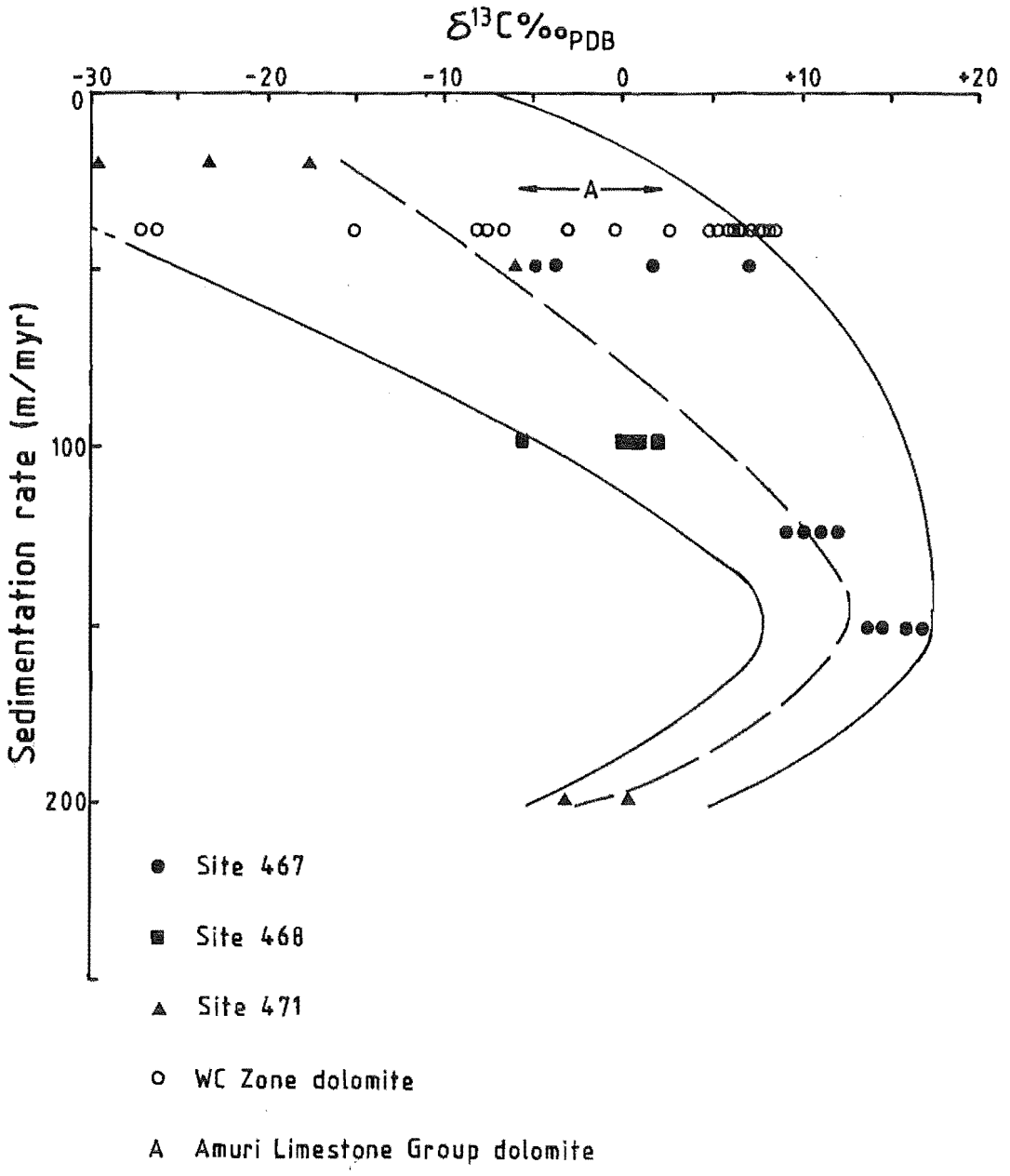

Figure 4.14 Plot of $\delta^{13}C$ versus sedimentation rate for DSDP Leg 63 carbonates (Pisciotto and Mahoney 1981, Figure 12) and dolomites from this study. The dashed line is the trend indicated by Pisciotto and Mahoney (1981). The solid lines indicate the range of possible values.

sedimentation rates.

4.5. SUMMARY

1) All dolomites are Ca-rich and moderately well ordered.

2) There is no evidence for further subdivision of diagenetic units on the grounds of dolomite petrology or mineralogy. Differences in dolomite geochemistry and crystal textures between diagenetic units reflect variations in the geochemical environment of dolomite formation, which may be influenced by primary depositional lithology. Compositional variations between samples, or within a single concretion, indicate the localized nature of geochemical variations.

3) The causes of inclusion and extinction patterns in crystals appears complex and cannot be equivocally determined. Both types of pattern are likely to be kinetically controlled, but factors such as crystal habit and fluid chemistry are also important. The relationship between trace element distributions in crystals and extinction patterns could not be established.

4) Despite both the WC Zone concretion and Amuri Limestone Group dolomites being compositionally different and representing separate dolomitizing events, both occurrences can be explained in terms of early dolomitization in the upper sediment column under normal marine conditions. Deep burial and meteoric mixing zone dolomitization can be discounted.

5) The association of pyrite with dolomite plus Fe and $\delta^{13}C$ data are interpreted as indicating dolomite formation in association with sulphate reduction, and in some instances with bacterial fermentation of organic matter. Fabric interpretations and $\delta^{18}O$ data indicate dolomite formation occurred at temperatures less than 60°C

6) The source of Mg^{2+} is seawater which has diffused into the sediment. The ultimate source of Na^{+} and K^{+} was probably also seawater, but their concentration in dolomites appears to depend on the abundance of fluid inclusions. Insoluble residues also exert some control over Na^{+} and K^{+} concentrations. Iron and Mn^{2+} are derived from oxides and hydroxides and organic matter associated with the host sediment. The availability of

Fe^{2+} and Mn^{2+} for incorporation into dolomites depends upon sulphate reduction, and the balance between oxidation and reduction processes. Strontium in Amuri Limestone Group dolomites was probably derived from the primary carbonate sediment, whereas Sr in WC Zone concretion dolomite came from sediment pore waters.

7) Dolomite formation in the Amuri Limestone Group results from the dolomitization of a primary sedimentary carbonate. WC Zone concretions are inferred to have formed via the dolomitization of very early diagenetic calcite.

CHAPTER 5

CHERT PETROLOGY AND GEOCHEMISTRY

5.1. CHERT TEXTURES

5.1.1. SKELETAL MATERIAL

Calcareous Fossils

Foraminiferal chambers in dark, dense chert contain coarser quartz than the surrounding matrix. Exceptions arise where the chamber was originally micrite filled. Replacement of micrite results in fine grained quartz whereas precipitation as cement produces coarse quartz. Precipitation as cement or replacement produces size variations within the micrite itself. Hein *et al.* (1981, 1983), reported that silica can completely pseudomorph nannofossils in porcelanite. Coarse quartz also results from pseudomorphic replacement of foraminiferal tests [Figure A6.8a].

Chertification textures in foraminifera vary from sample to sample, and in some instances within a single sample. No distinct stratigraphic or geographic pattern is detected. The most common is filling of chambers by spar or quartz [Figure A6.6]. The latter in some cases may have replaced earlier precipitated spar. Foraminiferal walls may or may not be replaced [c.f. Figures A6.8b and A6.8d], implying that chambers may be filled first followed by replacement of the test.

Few of the more complicated skeletal replacement and chamber fills [e.g. Figure A6.7] are observed. Chalcedony is a much less common chamber fill than microquartz or megaquartz. In DSDP cores it has been found as a void fill associated with geopetal sediments in foraminiferal chambers (Lancelot 1973). Since length-fast chalcedony [as in Figure A6.7] never pseudomorphs skeletal grains, carbonate mud, or geopetal fillings, and never contains undigested carbonate inclusions, it is thought to be a void-filling cement and not a replacement (c.f. Meyers 1977). Microquartz in the foraminiferal chamber in Figure A6.7, appears to be replacing sparry calcite. From the above information the following sequence of events in Figure A6.7 is deduced:

i) Partial filling of foraminiferal chamber with sparry calcite.
ii) Replacement of microspar by microquartz at the same time as filling of remaining pore space with chalcedony.
iii) Continuation of ii) and replacement of test walls by length-slow chalcedony.

Folk and Pittman (1971) claim that length-slow chalcedony indicates an evaporitic origin. Such an origin is unlikely in the Amuri Limestone Group. Meyers (1977) describes length-slow chalcedony that has replaced fossil fragments. It is likely that the chalcedony is length-slow through having replaced the original calcite.

Siliceous Fossils

Siliceous nannofossils are abundant in many DSDP chert sequences (e.g. Berger and von Rad 1972, Keene 1975, Riech 1979, Hein *et al.* 1981, 1983), and are commonly cited as the silica source (Lancelot 1973, Keene 1975 and others). In comparison they are rarely identified using the scanning electron microscope (SEM) or thin sections from this study. They are also scarce in the upper Woolshed Formation. The bulk of replaced skeletal material appears to be foraminiferal. Comparatively abundant radiolaria are seen only in the UCM Subzone [Figure A6.16], where they are reasonably well preserved. Radiolaria have been extracted in varying states of preservation and abundance from marls, micrites and cherts from some Amuri Limestone localities (Y. Aita, C. Hollis *pers. comm.* 1988), so their apparent absence in this study is puzzling. It is possible that some chertified bodies thought to have been foraminifera in thin section are in fact radiolaria. Sponge spicules have been extracted from micrites containing cylindrical chert nodules at Chancet Rocks (McCulloch 1976).

5.1.2. NONSKELETAL MATERIAL

Trace Fossils

Field evidence indicates an association of burrowing with silicification and suggests that they may in some instances act as a site for the initiation of the process, as noted in studies by Kelts (1976), Hein *et al.* (1981, 1983). Hein *et al.* (1983) claim that in 90% of the thin sections they studied that silicification was initiated in burrows, and the rest nucleated in organic-rich or iron-rich parts of the sediment. Authors such as Heath (1973), Garrison *et al.* (1975), and Keene (1975) also mention chert-burrow associations in deep sea sediments. The conditions described below may be applied equally well to chertified Woolshed Formation wherein authigenic quartz crystals are best developed in pores, burrows and skeletal fragments.

Inferences as to chert-burrow relationships are difficult in the BC Zone, and to some extent in the CD Zone, due to the advanced stage of silicification. In the CL Zone it is noticeable that some burrows seem to have a greater predisposition to chertification [Section A2.5]. *Thalassinoides* burrows display the type of silicification described in the literature, that is coarser quartz than in the surrounding matrix. *Zoophycos* burrows show no preferential silicification in thin section [Figure A6.12] although they contain more Fe-oxide and/or pyrite. As in the European chalks (Bromley and Ekdale 1984), *Zoophycos* burrows are silicified only where they intersect chert nodules. Higher organic content and a high porosity and permeability of burrow fill may predispose *Thalassinoides* to chertification, and also result in coarser quartz than in the less porous burrows such as *Zoophycos*. The original burrow porosity probably relates to the burrow function, for example dwelling or feeding. Longer occupancy, such as in dwelling burrows, results in greater porosity and organic matter deposition than non-dwelling burrows (Bromley and Ekdale 1984). Thus burrows such as *Zoophycos*, which represent feeding burrows, remain similar in texture and composition, and are chertified in the same manner as the surrounding micrite [Figure A6.12].

The difference in quartz crystal sizes between foraminiferal chambers and the surrounding micrite appears to depend on porosity differences and the size of replaced or pseudomorphed grains. Foraminiferal chambers permit greater unimpeded growth of crystals if initially empty. Large crystals in chambers may also result from replacement of original void filling sparry calcite cement. The smaller size of both pores and grains and impedance of crystal growth by competing crystals in the micrite matrix promotes smaller authigenic quartz crystal sizes. Abundant and highly disseminated organic material, (probably at sites now occupied by finely disseminated pyrite), could cause similarly abundant and disseminated nucleation sites in micrite. Differential growth rates between biogenic structures and matrix may also be a factor in determining authigenic crystal size.

Crystal Size and Fabric

Quartz crystallinity determinations (XRD) show poor quartz crystallinity throughout the studied lithologies [Section A6.1.1]. SEM evidence shows

that allegedly poorly crystalline chert may contain euhedral quartz [e.g. Figures A6.19a,b]. Poor crystallinity may in part be due to mixtures of massive and euhedral quartz [Figure A6.19d,e,f]. More probably it is due to crystal size effects whereby small crystals produce an apparently low crystallinity. The crystal size of the XRD standard should be similar to that of the samples. For very small crystals, such as in this study, a technique based on SEM would perhaps be more appropriate.

Differences in authigenic quartz crystal sizes are common throughout chert matrix samples. Some differences result from the orientation of the fragment with respect to the plane of the thin section [Figure 5.1a], or the orientation of the fracture surface in SEM. Although not proven, bedding parallel sections appear to show coarser crystals, whereas bedding normal sections show smaller crystal sizes. Fluids which preferentially migrate along bedding planes may result in authigenic crystal growth dominantly parallel to the plane of bedding. Variations within single chert fragments reflect microscale differences in porosity and permeability within the sediment. The recrystallization of lime mud resulted in distinctly bimodal distributions of crystal sizes (Steinen 1978). Coarser crystals tended to be in clusters and were inferred to have grown into open pore space. By analogy, clusters of quartz crystals such as in Figure A6.19b, may also reflect growth into pores.

Many authors (e.g. Lancelot 1973, Keene 1975, Riech and von Rad 1979a, Hein *et al* 1981 and others) provide evidence for quartz replacement of host carbonate. Volume-for-volume replacement can occur (Hein *et al.* 1981). The size and shape of host sediment crystals can control the size and shape of their replacement. Rhombic or tabular shapes are probably pseudomorphs of recrystallized or skeletal calcite. Hein *et al.* (1981) reports that silica can pseudomorph minerals other than carbonate as well. The hexagonal forms [Figure A6.19b] may result from precipitation of silica as pore filling cement where there are fewer restraints on crystal growth.

Chertification probably occurred in conjunction with calcite recrystallization [see Section 5.3.1]. Replacement of calcite by silica results in enrichment of $CaCO_3$ adjacent to nodules, which is thus available for reprecipitation (van der Lingen and Packham 1975). As the chert nodule grows, this reprecipitated carbonate may again be replaced by

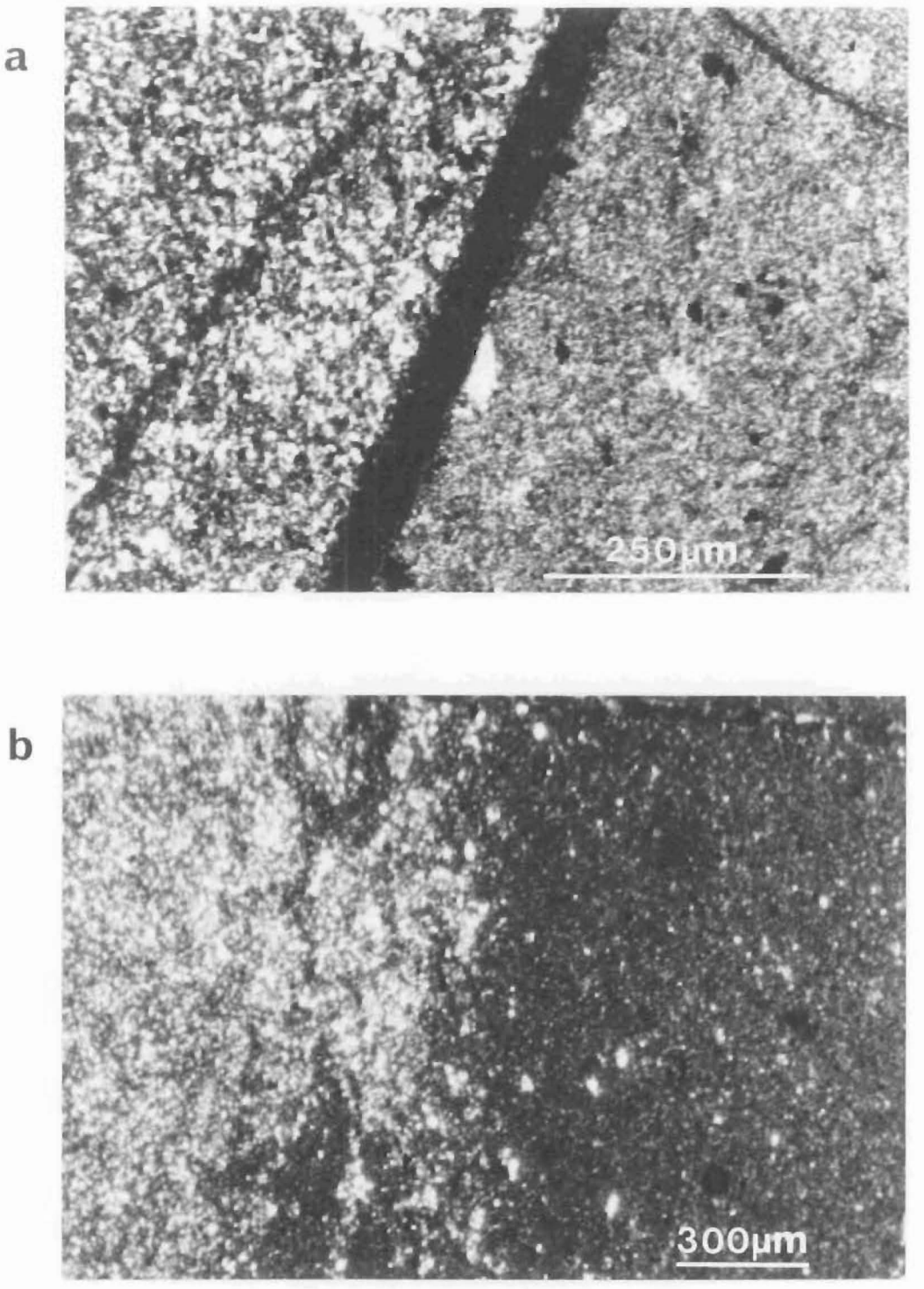

Figure 5.1 Thin section micrographs showing variation in quartz crystal size. (a) Crystal size differences in an epoxy mount of two differently oriented chert fragments from a single sample (CPL, sample BS9), and (b) within a single chert fragment (CPL, sample MS25).

silica, migrate and be reprecipitated. The pseudomorphic replacement of carbonate implies direct quartz precipitation. Therefore the bimodality of quartz textures may also result from pseudomorphic replacement of bimodal calcite. In fact, Lancelot (1973) believes that in carbonates direct quartz precipitation is the primary mechanism of chertification. The silica mineralogy, but micritic appearance of concretion bore fillings [Figure A2.6.] has also resulted from pseudomorphic replacement.

In addition to obviously crystalline textures, there are massive and/or porous varieties of chert. Porous or spongy cherts have been ascribed to chalcedonic quartz (Folk and Weaver 1952, Monroe 1964, Oldershaw 1968). The fibrous nature of the chalcedony will not necessarily be evident in SEM, although fluid inclusions should be commonly observed (Monroe 1964). Spongy or chalcedony dominated chert may result from either an increase in impurities or increase in the rate of silica precipitation. Madsen (1974) suggested that spongy cherts were initially deposited as cristobalitic porcelanites. However, in the Amuri Limestone Group only the sample in Figure A6.21f bears any resemblance to the spongy cherts as described by the above authors. The pores are larger than expected if the material were to be chalcedony. Rather it is thought that the pores represent original sediment porosity and that a large proportion of the chert has replaced calcite. Thus spongy cherts may also be formed by the preservation of some original porosity. The other irregular pits and cavities [Figure A6.21e] may also represent remnant original porosity.

Many Amuri Limestone Group cherts consist of massive textures mixed with euhedral crystals [e.g. Figure A6.19e,f]. Under high magnifications, massive textures in some DSDP studies are due to fibrous chalcedony (e.g. van der Lingen and Packham 1975). This is not the case in the present study. Cristobalitic samples such as in Figures A6.22a,b have a very platy appearance which at high magnification also appears massive. Coalescence of opal-CT lepispheres can result in massive opal-CT (Riech and von Rad 1979a). Recrystallization of opal-CT to quartz could conceivably retain the same massive SEM textures. Mixed euhedral and massive textures imply that both opal-CT and quartz precipitation occurred on a microenvironmental scale in Amuri Limestone Group sediments. Indeed, XRD evidence shows the coexistence of both opal-CT and authigenic quartz in micrites at Kaikoura Peninsula (3,4). An alternative but unlikely hypothesis for the origin of massive textures is submicroscopic quartz

with crystals below the resolution of the SEM.

Preferred orientation textures probably arise from primary sedimentary characteristics, as is almost certainly the case for the laminated chert [Figure A6.20e]. In these, the strial fabric has governed crystal growth directions. The lower abundance of detrital material in the LCM Subzone means preferred orientation effects are not as pronounced as in the lower BC Zone. The process of injection of dike material may also produce a similar preferred orientation due to flow. In addition, the presence of phyllosilicates in detrital-rich sediments (e.g. BC Zone, UCM and LCM Subzones) can physically restrict the growth of euhedral quartz (Blatt 1987), thereby governing both crystal size and shape.

From the preceding discussion it is apparent that chert textures at SEM scale result from a combination of the following sediment characteristics: fossil content, porosity, permeability, and depositional structures such as primary bedding and detrital sediment content; and from varied precipitation sites and mechanisms such as cement versus replacement, and opal-CT versus direct quartz nucleation. Features such as the rounded crystals [Figure A6.22d] are not as easy to explain. Their similarity to the detrital quartz in the Woolshed Formation [Figure A4.5] suggests they may result from silica overgrowths on detrital grains, or possibly replacement of carbonate overgrowths.

Presence of Cristobalite

The presence of an opal-CT horizon bounded above and below by dominantly crystalline authigenic quartz at Chancet Rocks (18) and Thomson's Gully (19) is rather puzzling. A number of authors (e.g. Keene 1975, Riech 1980 and others) have noted the predominance of opal-CT in clay-rich sediments. In such sediments opal-CT precipitation is favoured and the subsequent conversion to quartz is much slower [Section A7.3.3], which may account for the presence of opal-CT in the Woolshed Formation. However, the Chancet Rocks (18) and Thomson's Gully (19) samples are predominantly carbonate lithologies. It is possible that this horizon may have contained a greater abundance of detrital and clay mineral material than above or below, thereby enabling opal-CT preservation.

5.1.3. SITE AND RELATIVE TIMING OF SILICA NUCLEATION

The relative timing of chertification between foraminifera and/or burrows and the surrounding micrite is difficult to determine unequivocally. In the BC Zone, and to a lesser extent the CD Zone, everything has been converted to quartz so there is no way of telling what was first chertified. In some CL Zone samples, micrite is replaced first [e.g. Figure A6.6a] and in others foraminiferal chambers appear to be silicified first [as possibly in Figure A6.6b]. Keene (1975) has also described a replacement sequence for a foraminiferal/nannofossil ooze (93-95% $CaCO_3$) without siliceous microfossils from DSDP Leg 32. Primary Amuri Limestone sediments were probably of similar composition. The sequence is broadly modelled on that of Heath and Moberly (1971). A very similar sequence was also outlined by Garrison *et al.* (1975). Opal-CT precipitates in sediment interstices and foraminiferal chambers. With continued growth of opal-CT, the carbonate matrix dissolves or is replaced by silica. Some nannofossils, often with calcitic overgrowths, resist silicification. The opal-CT does not usually entirely fill foraminiferal chambers. Opal-CT is then converted to chalcedony. The initiation of silicification cannot be ascribed to any specific site, be it in matrix, burrows or skeletal material. It may be initiated at any site, or sites, within the sediment, and at differing times.

Lancelot (1973) and Greenwood (1973) suggested that quartz can precipitate directly if conditions prevent opal-CT formation [see Section A7.3.3]. Primary precipitation of quartz is found in foraminiferal tests [e.g. Figure A6.7], veins, and cavities (Keene 1975). In carbonate sediments, a high foraminifera/nannofossil ratio (Keene 1975), a high permeability and a lack of Al and metallic cations other than Ca^{2+} and Na^{+}, favour direct precipitation of quartz (Lancelot 1973). Keene (1975) found that only Cenozoic and clay associated cherts in DSDP Leg 32 cores contained opal-CT. Kastner *et al.* (1977) noted that opal-CT predominates in Mesozoic clayey sediments, whereas quartz is most common in carbonate sediments. The presence of carbonate appears to aid the opal-A to quartz transformation. The rate of transformation of opal-A to opal-CT is also higher in carbonates than in clay-rich sediments (Kastner *et al.* 1977, Kastner and Gieskes 1983). The presence of dolomite in some sediments, such as the CD Zone, may have favoured opal-CT nucleation (Riech 1979). In the Mead Hill Formation, as in most terrestrial and pre-Cenozoic

cherts, diagenetic processes have destroyed most of the early diagenetic textural evidence (cf. DSDP cherts where ongoing diagenetic processes are observed in their original depositional environment, Kastner *et al.* 1977). Thus the relative significance of different nucleating reactions can only be inferred. No evidence of opal-CT precursors is detected in Amuri Limestone Group thin sections. Cristobalite at localities such as Kaikoura, plus indications of excess Mg^{2+} in the form of dolomite, suggest that opal-CT may have nucleated initially in sediment interstices. The likely greater abundance of metallic cations and the relative paucity of calcareous microfossils, has resulted in the dominance of opal-CT at localities such as Kaikoura Peninsula.

The so called patchy silicification (Baltuck 1986) observed in a number of CL Zone samples [e.g. Figure A6.6b], probably results from dissemination of nucleation sites throughout the sediment, followed by a non-uniform spread of the process. The host sediment porosity and distance between nucleation centres probably governs the 'patchiness' of silicification.

5.1.4. POST-DIAGENETIC FEATURES

Chert brecciation has been recorded in DSDP cores (Lancelot 1973, Kelts 1976), and in units such as the Monterey Formation which contain both dolomite and authigenic silica minerals (Roehl 1981, Redwine 1981). Lancelot (1973) claimed that brecciation and fracture filling in DSDP cores occurred subsequent to initial lithification. In Amuri Limestone Group samples lithification must have occurred prior to brecciation in order to explain the angularity of the micrite fragments, as well as the fact that no sediment infilling occurs in any of the fractures. The large sparry calcite crystals both in the zebra-beds [Figure A6.14], and in breccias [Figure A6.15] may result from later refracturing of an original vein, followed by precipitation of calcite. Similar structures are described by Lancelot (1973). Kelts (1976) suggested a mechanism where pressure solution due to compaction could expel materials such as clay minerals, thereby producing pure quartz zones, hence tectonism may not be necessary to produce these features. The veins described by Kelts consist of fibrous chalcedony with fibres generally perpendicular to fracture surfaces, like those in Figure A6.13, and around micrite fragments [Figure A6.15].

The breccias and zebra-beds are commonly associated in outcrop. Zebra-beds are essentially veins [Figure A6.14], commonly alternating with millimetre-thick layers of host rock [Figure A2.27]. The pressure solution hypothesis of Kelts (1976) may, with modification, explain both zebra-bedding and brecciation. To form zebra-bed structures, beds may have been compacted causing cracks to form. Silica then precipitated in stress formed cracks. Later refracturing enabled further precipitation, which in zebra-beds [Figure A6.14] resulted in precipitation of large crystals of sparry calcite. A similar mechanism is envisaged for the breccias, but with a more random vein orientation. Micrite fragments in the breccia are surrounded by two layers of chalcedony [Figure A6.15]. In this case a second refracturing event resulted in further chalcedony precipitation, followed by calcite precipitating during final refracturing. It appears imperative that the limestone was silicified prior to brecciation and zebra-bed formation, as in the examples of Roehl (1981). Obviously not all veins were refractured and so not all show multiple precipitation events.

Veins [e.g. Figure A6.13] are commonly observed throughout the sequence. They intersect all other diagenetic features and are associated with later tectonic activity.

5.2. GEOCHEMISTRY OF CHERT

All numerical correlations are determined using Pearsons-*r* [see Section 4.3 for details].

5.2.1 ELEMENTAL DISTRIBUTION IN DETRITAL SEDIMENTS

The limited stratigraphic control and quantity of data limits interpretations of detrital sediment composition. In addition, detrital sediments have been analyzed primarily for comparative purposes, so detailed interpretations are not pursued. The chemical composition of mudstone and sandstone is dependent upon factors such as the grain size and mineralogical maturity of the sediment (Pettijohn 1975). Ideally, analysis of separate grain size fractions and a more rigorous determination of mineralogy is required.

In general the coarse fraction of the sediments are often richer in

silica, whereas the fine grain sizes contain more Al_2O_3, Na_2O, K_2O, Fe_2O_3 and water (Pettijohn 1975). Quartz controls silica abundance. The main control on other major elements is the clay mineralogy (Hirst 1962). The high SiO_2 in the Claverley Sandstone results from the dominance of detrital quartz. The Woolshed Formation with its finer grain size and greater clay abundance contains proportionally less SiO_2 and more of the other major elements.

Mean values for the Woolshed Formation include both cemented and uncemented samples. Opal-CT forms the cement. No opal-CT is detected in uncemented samples. Nevertheless the SiO_2 concentrations of uncemented samples are similar to those of cemented samples. The same relationship applies to trace and other major elements. This similarity in SiO_2 between cemented and uncemented samples suggests that the SiO_2 for cementation was derived internally.

5.2.2. WATER CONTENT OF CHERTS

The loss on ignition equals the sum of the volatiles (e.g. $H_2O + CO_2$), minus the weight gain resulting from the transformation of iron from the Fe^{2+} to the Fe^{3+} state. The weight gain factor in this transformation is 1.1113. The maximum total Fe_2O_3 in chert analyses is about 1 percent. If all the iron is assumed to be initially in the Fe^{2+} state, then the maximum weight gain on transfer to the Fe^{3+} state is 0.11 percent. Since the bulk of cherts contain much less than 1% total Fe_2O_3, weight gains are considered negligible. In addition, carbonate phases are removed during sample pretreatment [Section A1.2.1]. Therefore, the loss on ignition in Amuri Limestone Group cherts can be interpreted as comprising dominantly water. Other volatiles may be given off but these are probably subordinate.

Knauth and Epstein (1976) showed that there is no systematic variation in water content for cherts of Precambrian to Tertiary age. A similar lack of correlation between loss on ignition and age is noted in Amuri Limestone Group cherts. The range of water contents listed by the above authors is 0-1.2 percent. The bulk of Amuri Limestone Group cherts are in the range 0.7-1.6% with the majority containing about 1.0% which is at, and somewhat above the range described by Knauth and Epstein (1976).

The variability in water content of non-detrital cherts may result from the water being non-stoichiometric and located in point defects, lattice faults, and dislocations (Micheelsen 1966). Poor correlations with other analyses support this hypothesis. Higher water contents (about 2%) in detrital bearing units are probably associated with the presence of hydrous minerals such as micas and clays.

5.2.3. SOURCE AND SIGNIFICANCE OF TRACE COMPONENTS IN CHERTS

Source of Trace Components

Essentially, SiO_2 is the major component of chert and all other components occur at trace concentrations. In terms of crystal structure, the substitution of tetravalent silicon in quartz by transition and rare earth elements is possible to a limited extent only. Such substitution has been observed for Al^{3+}, Fe^{3+}, Ti^{4+} and Ge^{4+}, with other cations in interstitial sites (Lehmann and Bambauer 1973). Trace elements in quartz rarely exceed 0.1% with Al^{3+} being the commonest impurity (see data in Lehmann and Bambauer 1973). Therefore only minor quantities of trace components are lattice bound. The remainder must be associated with other phases in the rock such as organic matter, fluid inclusions, clay and authigenic minerals, or with crystal defects and at grain boundaries.

Besides SiO_2, Al_2O_3 is the most abundant component of clay minerals. Irrespective of chertification, elements whose abundance is controlled by clay minerals should all show similar abundance patterns (Brueckner and Snyder 1985). TiO_2 displays a very good correlation with Al_2O_3 [Figure 5.2a]. K_2O shows a similarly good correlation. Moderately good correlations with some scatter are displayed by Fe_2O_3 [Figure 5.2b] and Rb. Zirconium, Ba [Figure 5.2c], and Sr are very poorly correlated with Al_2O_3, K_2O, and TiO_2. Nickel, Zn, Cr, and V are moderately interrelated and display moderate correlations with Al_2O_3, Fe_2O_3, and TiO_2. Losses on ignition display poor correlations with all other analyses. Plots of MgO against Al_2O_3, Fe_2O_3, and TiO_2 show that its high correlation is controlled by extreme values. Also the proximity of analyses to detection limits, particularly MnO, MgO, and in some instances Na_2O, affect correlations and complicate interpretations.

The good correlations between Al_2O_3, K_2O, and TiO_2 suggest their abundance

(a)

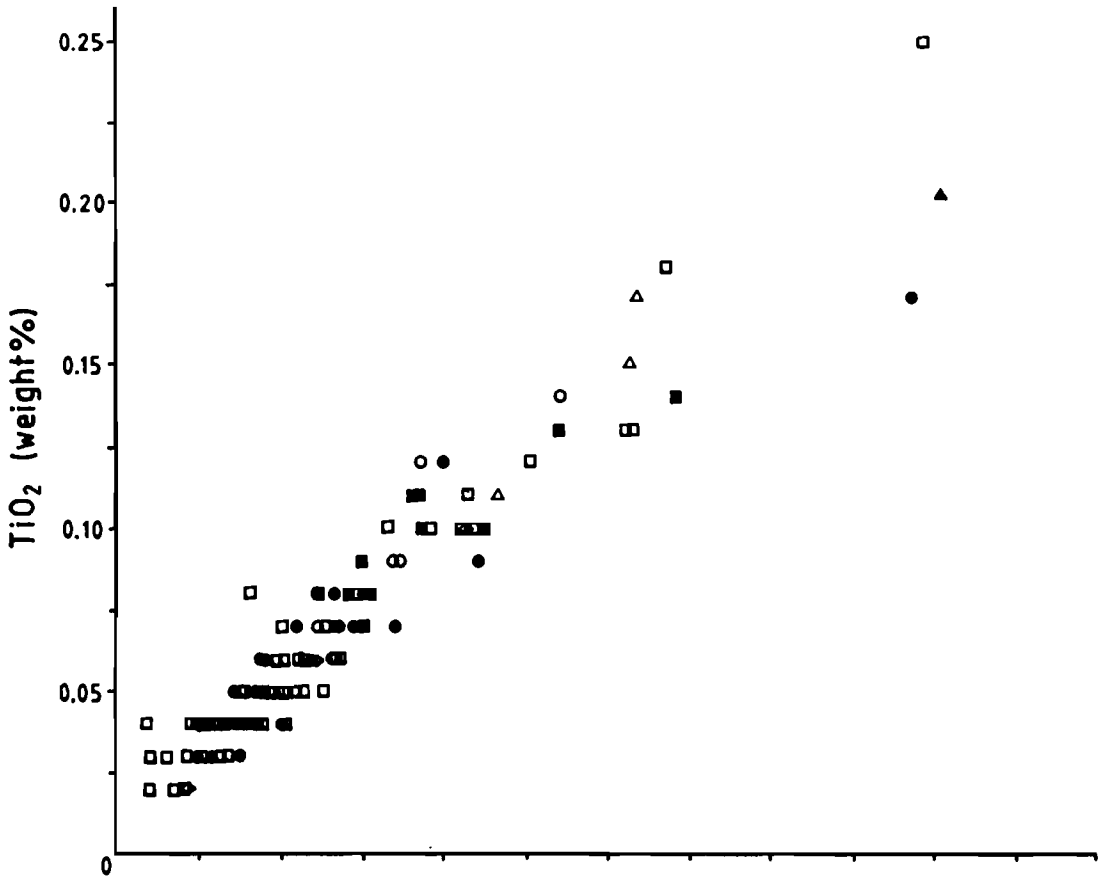
0.25
0.20
0.15
0.10
0.05
0
TiO2 (weight%)

(b)

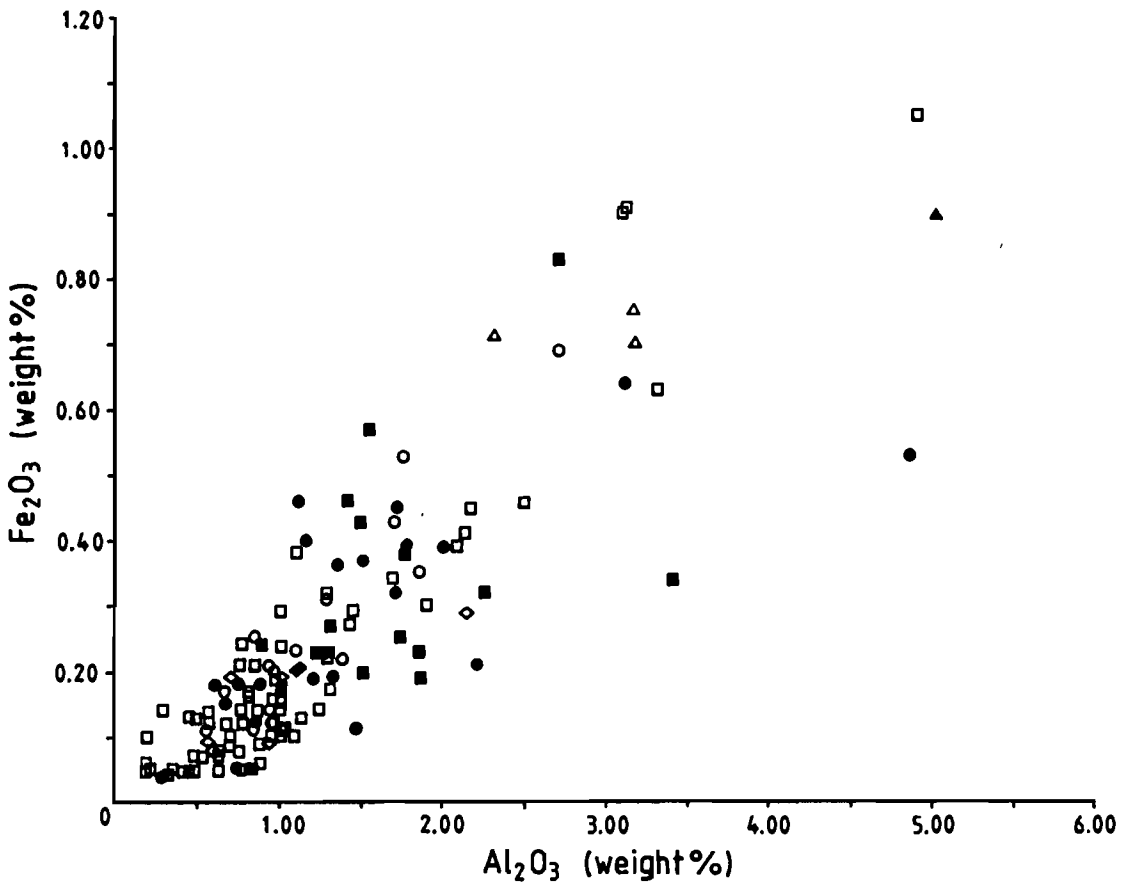
1.20
1.00
0.80
0.60
0.40
0.20
0
Fe2O3 (weight%)
1.00
2.00
3.00
4.00
5.00
6.00
Al2O3 (weight%)

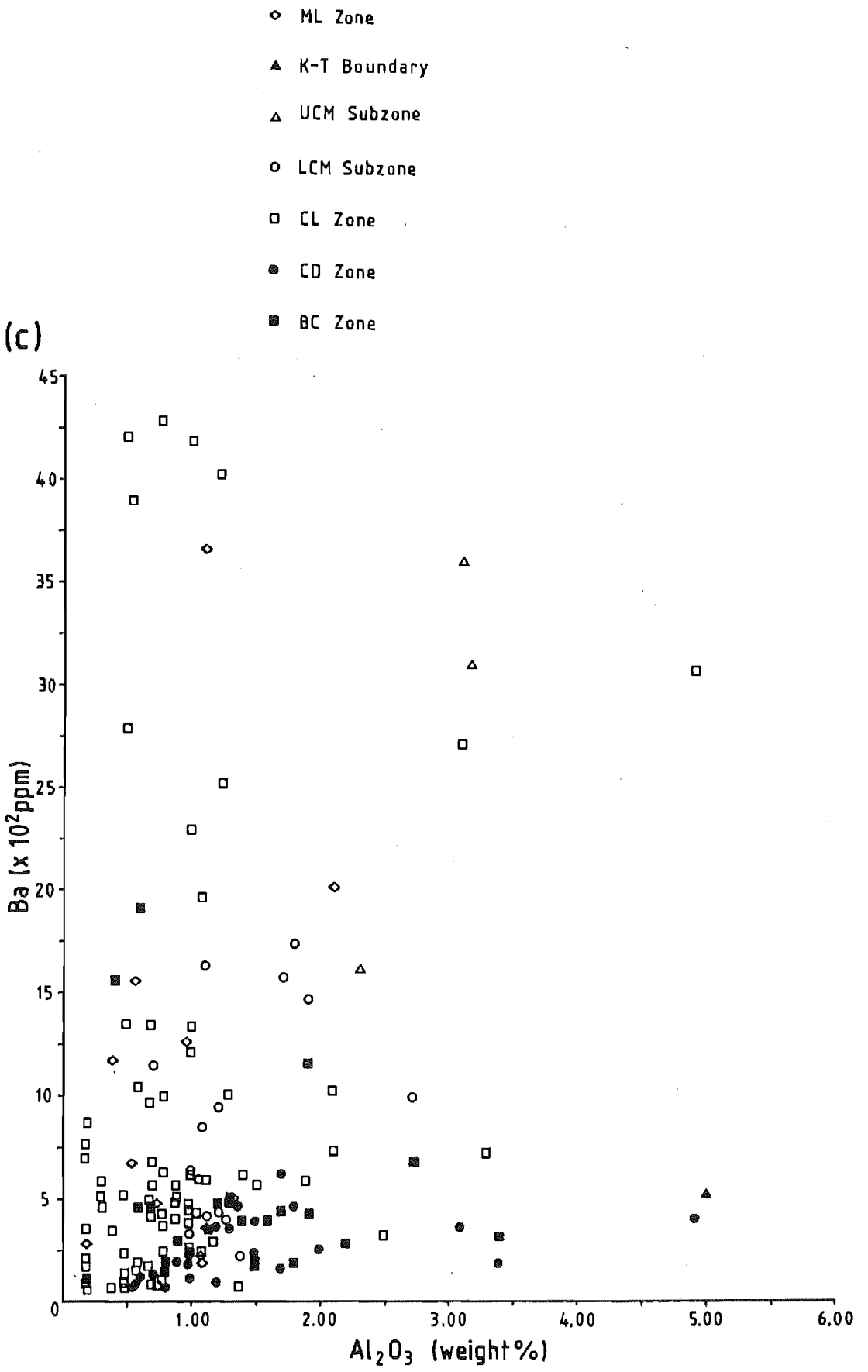

Figure 5.2 Scatter plots of TiO_2 (a), Fe_2O_3 (b), and Ba (c) versus Al_2O_3 displaying examples of good, moderately good, and poor correlations respectively.

to be clay mineral controlled. Fe_2O_3 and Rb also display clay mineral control. The scatter in the Fe_2O_3-Al_2O_3 plot probably results from inclusion of sulphide-bound Fe, leached from pyrite. The ultimate sources of Fe (and Mn) are oxides and hydroxides as described in Section 4.3.3. As discussed, Fe may also be associated with organic matter and sulphate reduction. Enrichment in Fe and Mn may be explained through hydrothermal activity and/or association with volcanic rocks (e.g. Barrett 1981, Dymond 1981, Hein *et al.* 1983, Yamamoto 1987). However, the generally low Fe and Mn concentrations, as well as the field evidence, indicate that such sources can be discounted. Traces of Rb and Sr have been found in quartz, but the bulk of concentrations are not found in the crystal structure but in other phases in crystals such as fluid inclusions (Rossman *et al.* 1987). The minor lattice-bound Rb may account for some of the scatter in Al_2O_3-Rb plots. However, minor quartz lattice-bound Sr cannot explain the poor Sr-Al_2O_3 relationship. Weis and Wasserburg (1987) report a correlation between Al and Sr and interpret it to indicate silica nucleation around Sr-bearing clay. Certainly some of the Sr in chert from the present study is lattice-bound and some is associated with clay minerals. However, further Sr (and Rb) may be in fluid inclusions (Rossman *et al.* 1987). Dissolution of the host carbonate will liberate Sr^{2+} into pore waters, which may subsequently be trapped in fluid inclusions. Some Na^+ may be similarly trapped. Minor amounts of Sr from celestite in radiolarian skeletons has also been reported (Audley-Charles 1965), although its significance in this case is indeterminate. In the detrital-rich samples, Sr bound in feldspar lattices has probably also been included.

Correlations indicate some clay mineral control over the abundances of V, Cr, Ni, and Zn. These elements may also be associated with trapped organic matter (Brueckner and Snyder 1985), implying that not all the organic matter is removed from the sediments before chertification.

Barium and Zr do not appear to be associated with either clay minerals or with the transition elements discussed in the preceding paragraph. There is some correspondence of Ba with Sr. The overall poor correlation of Ba with K_2O is somewhat surprising, because Ba (and K_2O) is commonly associated with clay minerals and feldspars in other rocks. The higher content of Ba in mudstones compared to adjacent micrites implies there is some detrital mineral control. However, some detrital-free cherts have

very high Ba contents (e.g. MA18 from the ML Zone contains 7237 ppm Ba). Thus Ba behaviour appears rather complex. A number of sources for Ba and Zr may be suggested. Zircons are often found in the insoluble residues of sediments (Goldschmidt 1954). Zircons are found in the heavy mineral fraction of a number of mid Cretaceous sediments of Marlborough (Smale 1985), which reworked, may be the source for some of the detrital material in the cherts. Some Zr may be adsorbed to other mineral phases such as clays (Goldschmidt 1954). Barite is found in Amuri Limestone Group sediments (Morris 1987). Other possible sources are organic matter (Dymond 1981, Brueckner and Snyder 1985), apatite (Brueckner and Snyder 1985), or biogenic sources (Audley-Charles 1965, Dymond 1981).

Implications of Chert-Mudstone Elemental Partitioning

Differences in composition between mudstone partings and cherts in Japan are explained by a 'double accumulation' model (Iijima and Utada 1983). In this model deposition of siliceous sediments was essentially slow and constant, punctuated by rapid and intermittent episodes of clay deposition. High concentrations of clay associated elements will occur in these clay-rich layers. Low clay volumes in chert beds means low abundances of clay associated elements. Therefore differences in composition result from differences in the amount of each element deposited with the original sediments, and not from migration of elements due to diagenesis. Data from detrital-bearing cherts in this thesis is consistent with this type of model. The concept may also be applied with minor modification to sediments where carbonate rather than siliceous material was the primary depositional sediment. In the LCM Subzone (sample WUR3), carbonate replaced by chertification was reprecipitated as calcite or dolomite in the pore spaces, or was removed entirely, possibly to another bed. Precipitating chert essentially diluted the original insoluble materials left behind by the dissolved carbonate. Only limited redistribution of elements into mudstone partings may have occurred. However, wholesale redistribution of elements into mudstones is unlikely.

Using this primary deposition model, crude estimates of sedimentation rates may be determined for the mudstones and chert beds. There is an inversely proportional relationship between the MnO/Al_2O_3 ratio and the sedimentation rate [Figure 5.3] in marine sediments (Matsumoto and Iijima 1983, Iijima *et al.* 1985). Plotting Amuri Limestone Group data on Figure

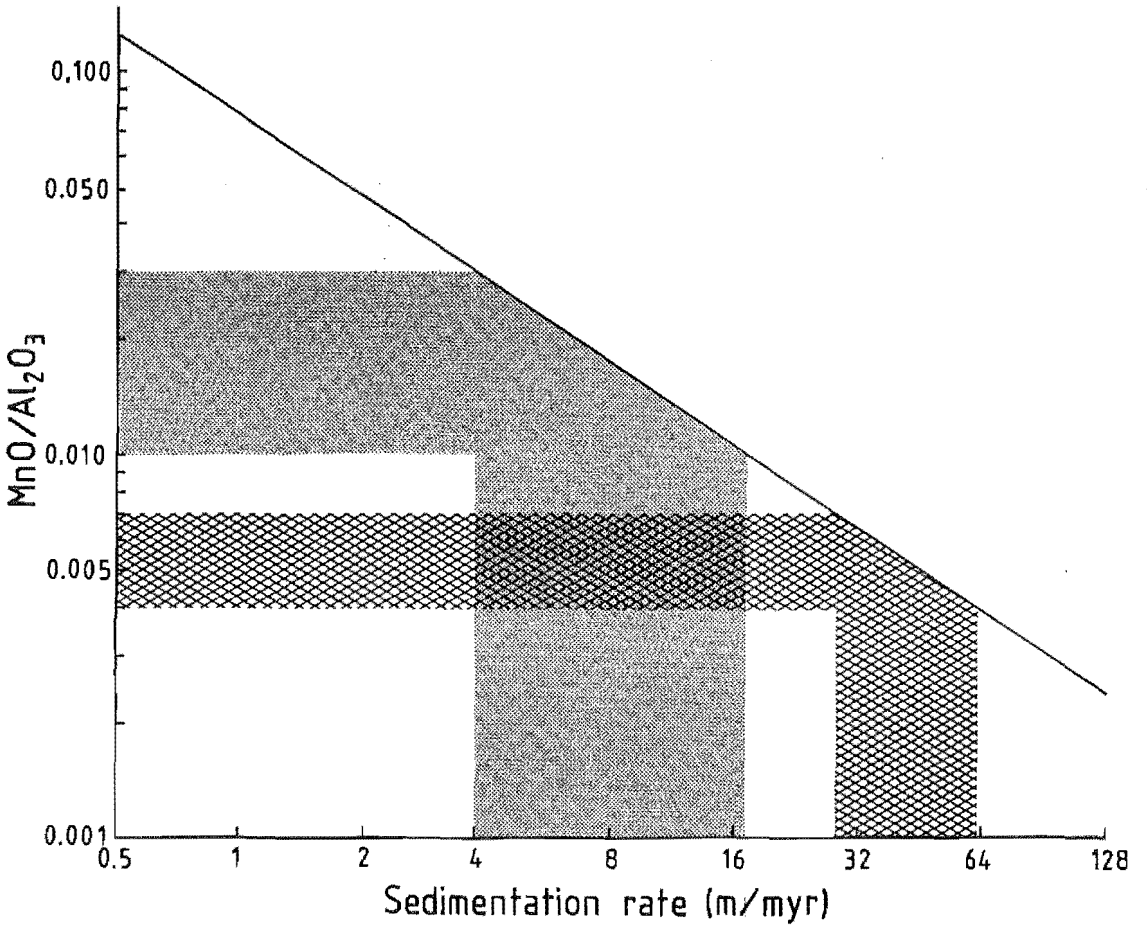

Figure 5.3 Plot of MnO/Al_2O_3 ratio versus sedimentation rate (from Matsumoto and Iijima 1983, Iijima *et al.* 1985) showing inferred sedimentation rates for Amuri Limestone Group cherts (shaded), and mudstone partings (hatched).

5.3 provides estimates of sedimentation rates for cherts of 3.8-19 m/myr (MS10, WUR3, LS2) and in excess of 100 m/myr (MS41). All shales including those associated with MS41, indicated sedimentation rates of 30-60 m/myr. These estimates are comparable with rates estimated for the Woolshed Formation and Amuri Limestone Group by Morris (1987), who suggested a range of about 24-70 m/myr. Generally sedimentation rates for shales are higher than for the cherts.

5.2.4. OXYGEN ISOTOPE GEOTHERMOMETRY

Factors Controlling the $\delta^{18}O$ of Cherts

The ^{18}O composition of a chert depends on the temperature of formation and the isotopic composition of equilibrating fluids (Pisciotto 1981a, Kolodny 1986). These parameters depend in turn upon the rates of sedimentation and diagenesis, burial, geothermal gradients, and the presence or absence of fresh water intrusions (Kolodny 1986). $\delta^{18}O$ decreases in the transformation from biogenic opal to opal-CT, and again in the opal-CT to quartz transformation (Murata *et al.* 1977). Quartz may be up to 2‰ depleted compared to coexisting opal-CT, irrespective of burial (Knauth and Epstein 1975, Kolodny and Epstein 1976, Pisciotto 1981a). Alteration of $\delta^{18}O$ only occurs during a phase transformation. Increasing burial depth does not alter the $\delta^{18}O$ of a specific phase (Murata *et al.* 1977), thus phase transformations reflect solution precipitation-reactions (Stein and Kirkpatrick 1976, Williams *et al.* 1985, Williams and Crerar 1985).

There is debate as to whether the $\delta^{18}O$ of marine cherts reflect paleoclimates, that is ocean bottom water temperatures (Degens and Epstein 1962, Knauth and Epstein 1975, 1976, Kolodny and Epstein 1976), or diagenetic environments (Kastner 1981, Pisciotto 1981a, Hein and Yeh 1981, 1983, Kolodny 1986). The paleotemperature interpretation relies on:

i) The correlation of ^{18}O silica and ^{18}O foraminifera based temperatures.
ii) The assumption that silica transformations, particularly opal-A to cristobalite, occur at shallow burial depths and low temperatures which are equivalent to ocean bottom water temperatures (Pisciotto 1981a).

Problems with paleotemperature interpretations include inconsistency between benthic foraminifera and chert temperature curves, the much wider range of temperatures indicated by cherts when compared to carbonates, and

differences between on-land and deep-sea cherts (Kolodny and Epstein 1976). Kastner (1981) thinks it questionable that the ^{18}O of cherts record paleotemperatures of any geologic age. However, since interstitial water composition is inherited from ocean bottom waters, the paleoclimate hypothesis may still be applicable but in a very limited way (Pisciotto 1981a).

Diagenetic environmental interpretations do not totally exclude climate factors (Pisciotto 1981a), but enable explanation of isotopic temperatures higher or lower than those of the ocean subsurface. Such temperature differences may result from burial to greater depth (e.g. Murata *et al.* 1977), or interaction with ^{18}O enriched/depleted waters (Pisciotto 1981a).

Kolodny and Epstein (1976) and Kolodny (1986) found that cherts exposed on land, and of probable continental margin origin, appear to be depleted in ^{18}O compared to deep sea cherts [see later]. This is interpreted as reflecting the lower temperatures in the deep sea compared to continental margin deposits (Kolodny and Epstein 1976, Hein and Yeh 1981, 1983). Lower temperatures cause a much slower transformation of opal-A to opal-CT (see Williams and Crerar 1985). In addition, it has been suggested that continental margin cherts are more likely to exchange with ^{18}O depleted meteoric waters (Knauth and Epstein 1976, Kolodny 1986).

Finally, when comparing isotopic compositions it must be remembered that diagenetic histories can vary between sites. Therefore caution must be exercised in all interpretations (Pisciotto 1981a).

Temperature and the Fractionation Factor

Selection of a silica-water fractionation factor is fraught with similar problems to the dolomite-water fractionation. Neither are as well constrained as the calcite-water fractionation. There are essentially two types of silica-water fractionation expressions; a quartz-water fractionation and a biogenic silica-water fractionation (see Pisciotto 1981b for a full list). The opal-CT fractionation is virtually unknown (Friedman and O'Neil 1977), so quartz-water expressions are used for all cherts. However, it is not known whether this single fractionation is valid for all cherts (Knauth and Epstein 1975).

The two expressions most often used are as follows:

i) Clayton *et al.* (1972):

$$1000\ln\alpha_{Quartz\text{-}Water} = 3.38 \times 10^6(T^{-2}) - 3.40$$

ii) Knauth and Epstein (1976):

$$1000\ln\alpha_{Quartz\text{-}Water} = 3.09 \times 10^6(T^{-2}) - 3.29$$

where:

$$\alpha_{Quartz\text{-}Water} = (^{18}O/^{16}O_{Quartz})/(^{18}O/^{16}O_{Water})$$

Of the available fractionation expressions, the above equations yield the highest and lowest results respectively (Friedman and O'Neil 1977, Pisciotto 1981b). From data in this thesis, the difference is about 13°C [Table 5.1]. The Knauth and Epstein equation may have greater validity because of the correspondence of calculated temperatures with some measured sub-bottom temperatures (Hein and Yeh 1983).

Paleotemperature Calculation

As is the case for carbonates the ^{18}O of cherts is determined by the temperature and by the isotopic composition of the precipitating fluids (Kolodny 1986). Hein and Yeh (1983) suggest that the oxygen isotopic composition of waters from which DSDP Leg 69 cherts were formed was between 0·/.. and -4.2·/..$_{SMOW}$. The latter is derived from the composition of DSDP core pore waters (Mottl *et al.* 1983). For comparison with calcites and dolomites the same isotopic compositions are used as in Table 4.4. Calculated paleotemperatures for Amuri Limestone Group cherts are listed in Table 5.1. There is a range of about 23°C between water with ^{18}O of 0·/.. and -4.9 per mil. The temperature range for any given water composition is about 9°C. Virtually all temperatures are less than 60°C, and most are below 50°C.

$\delta^{18}O$ of Amuri Limestone Group Cherts

Amuri Limestone Group cherts are similar to other Late Cretaceous-Early Tertiary cherts [Figure 5.4]. They are in the same range as cherts of

Table 5.1 Paleotemperatures calculated from the equations of Knauth and Epstein (1976) and Clayton *et al.* (1972). The figures in brackets are calcite paleotemperatures calculated from the equation of Friedman and O'Neil (1969).

	T1°C	T2°C	T3°C	T4°C	T5°C
δ Water =	0	-1.2	-2.0	-4.2	-4.9
MS45	39-53	33-47	29-43	20-33	17-30
	(32)	(26)	(22)	(13)	(10)
MS42	41-55	35-49	32-45	22-36	19-32
DS5	38-52	33-46	29-42	20-33	17-30
MS32	36-50	31-44	27-40	18-31	15-28
	(40)	(34)	(30)	(20)	(16)
MS29	44-58	38-51	34-48	24-37	21-34
DS12	37-51	31-45	28-41	19-32	16-29
MS12a	42-56	36-49	32-46	22-36	20-33
	(49)	(42)	(38)	(27)	(23)
DS16	40-53	34-47	30-43	21-34	18-31
MS2	47-62	41-55	37-51	27-40	24-37

Figure 5.4 Compilation of chert ^{18}O with respect to age. Data sources are as follows:

(1) Perry and Tan (1972)
(2) Knauth and Lowe (1978)
(3) Knauth and Epstein (1976)
(4) Degens and Epstein (1979)
(5) Jones and Knauth (1979)
(6) Knauth and Epstein (1975)
(7) Amuri Limestone Group
(8) Hein and Yeh (1981)
(9) Pisciotto (1981b)
(10) Murata *et al.* (1977)
(11) Hein and Yeh (1983)

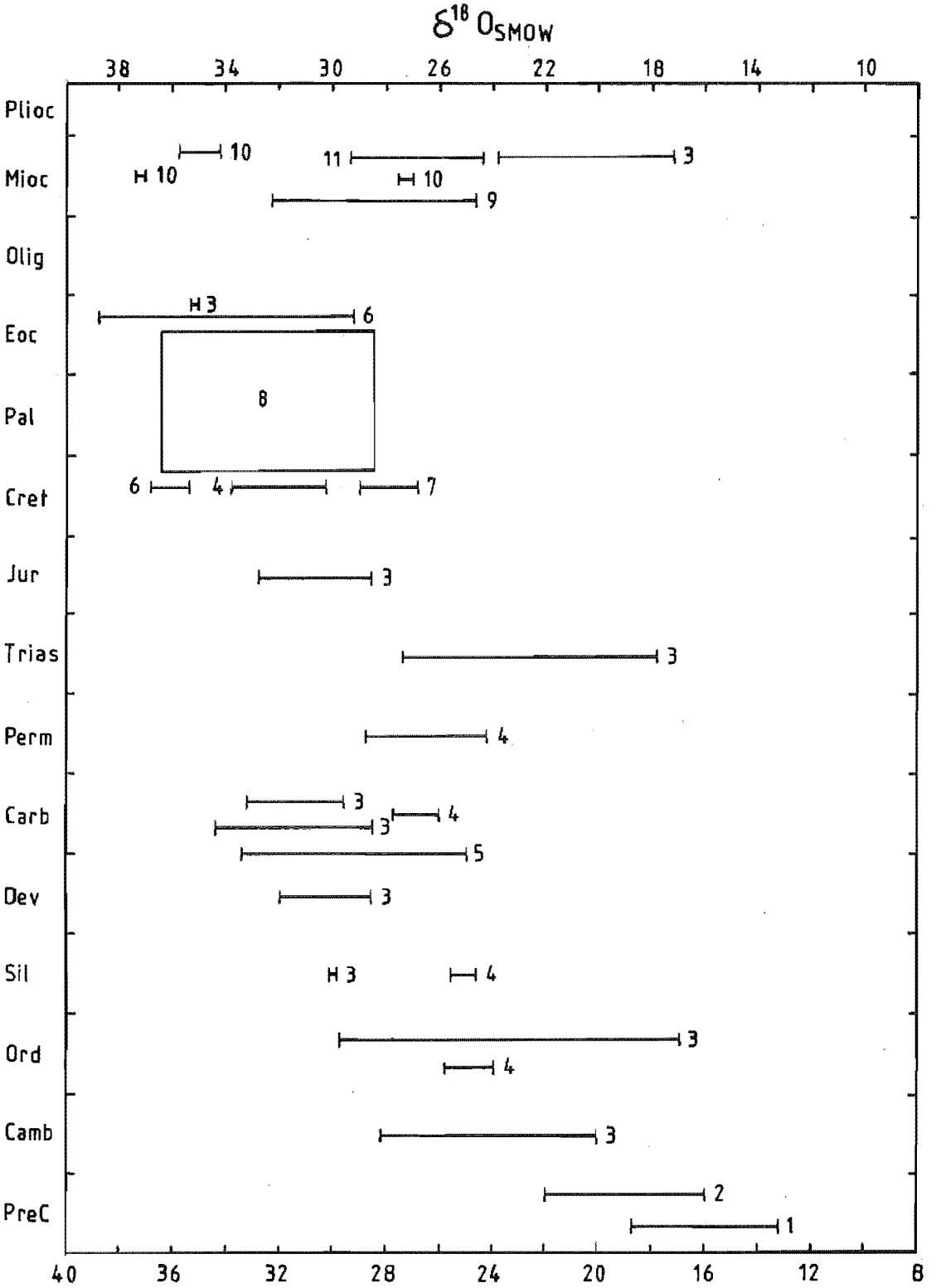
δ18 OSMOW
38
34
30
26
22
18
14
10
Plioc
Mioc
Olig
Eoc
Pal
Cret
Jur
Trias
Perm
Carb
Dev
Sil
Ord
Camb
PreC
H 10
10
11
3
10
9
H 3
6
8
6
4
7
3
3
4
3
4
5
3
H 3
4
3
4
3
2
1
40
36
32
28
24
20
16
12
8

Cambrian to Miocene age. There appears to be a general increase in ^{18}O until the Eocene followed by a decrease in the Miocene. However, the ^{18}O increase with time is not as pronounced as that described by Degens and Epstein (1962) and Perry and Tan (1972). There are some wide fluctuations. Perry and Tan (1972) ascribed the increase since the Precambrian to a 15‰ increase in the composition of the oceans. The effects of sedimentation of ^{18}O rich hydrous minerals, isotopic exchange with submarine basalts, input of mantle water to the oceans, and glaciation, all cannot fully account for the variations in cherts since the Precambrian (Knauth and Epstein 1976). They therefore discount change in ocean composition and interpret the variations in terms of changes in climatic temperature. The relative importance of temperature and composition on the long term ^{18}O secular variations is still debated.

The ^{18}O data are consistent with Amuri Limestone Group cherts being of continental margin type [Figure 5.5], thereby supporting conclusions from basin analysis (Morris 1987).

The opal-A to opal-CT transformation normally occurs at about 50°C (Kastner *et al.* 1977, Murata *et al.* 1977, Hein and Yeh 1983, Pisciotto 1981b). However, the reaction may also occur at temperatures between 18°C and 56°C (Pisciotto 1981b). The conversion of opal-CT to quartz occurs between 31°C and 165°C (Murata *et al* 1977, Mizutani 1977, Pisciotto 1981b, Hein and Yeh 1983). All these temperatures were calculated assuming $\delta^{18}O_{Water}$ = 0 per mil. Temperatures for Amuri Limestone Group samples (assuming $^{18}O_{Water}$ = 0 per mil, Table 5.1) are in the upper temperature range for the opal-A to opal-CT transformation, and in the lower part of the temperature range for the opal-CT to quartz transformation. Temperatures calculated using the Clayton *et al.* (1972) equation are within the upper part of the dolomite temperature range [Table 4.4], whereas those calculated from the Knauth and Epstein (1976) equation are in the lower part of the dolomite range. All the $\delta^{18}O$ analyses in this study are from quartz cherts, hence two situations are considered below; the direct precipitation of quartz and the precipitation of opal-CT followed by transformation to quartz (in the latter situation the ^{18}O may reflect the isotopic composition at advanced stages of chert genesis):

i) If quartz is the primary precipitate, then the calculated temperatures represent conditions at the time of silica nucleation and/or deposition, and by inference during dolomitization. In this

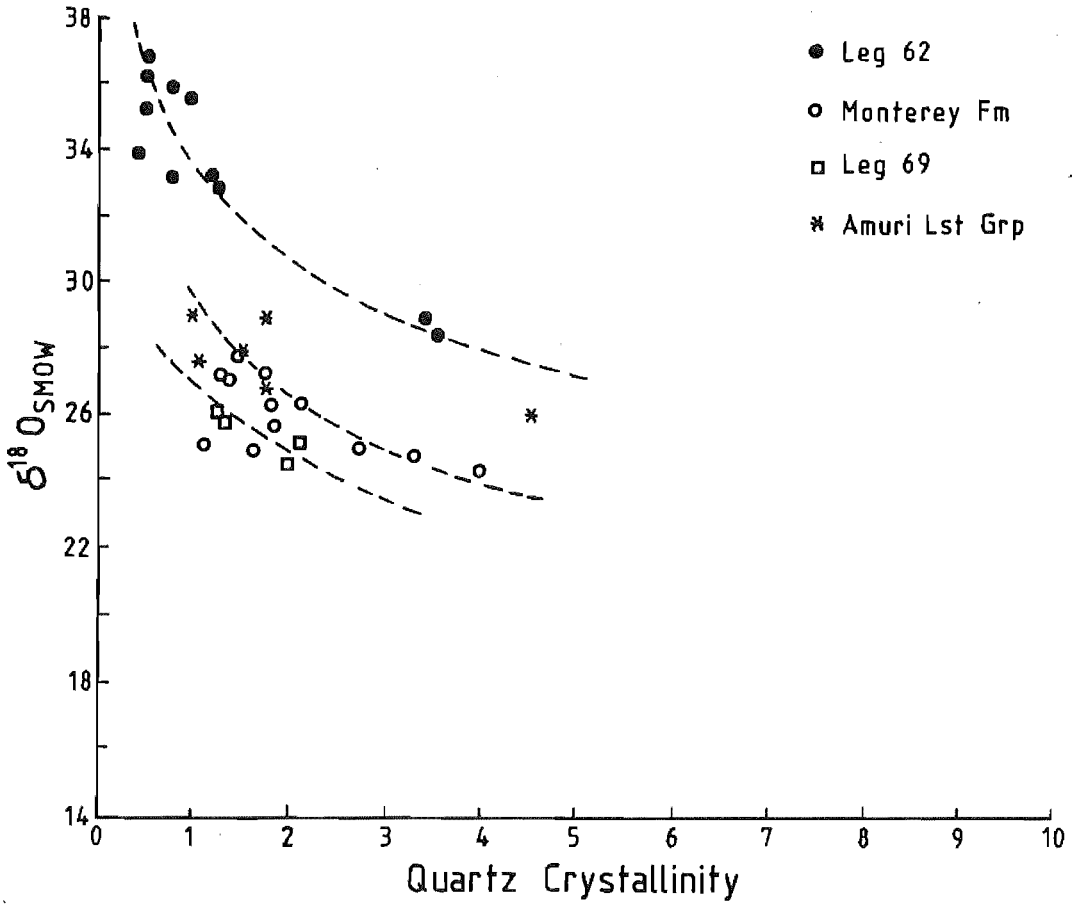

Figure 5.5 Plot of $\delta^{18}O$ versus quartz crystallinity for cherts of continental margin (Monterey Formation and DSDP Leg 69) and deep sea (DSDP Leg 62) affinity. Amuri Limestone Group samples generally plot near cherts of continental affinity. This figure is modified from Hein and Yeh (1983, Figure 4).

situation the carbonate and chert analyses indicate formation at similar temperatures, and hence burial depths, within the limits of uncertainty in temperature calculations for both chert and dolomite. Quartz is usually 0.5‰ to 2.0‰ (Knauth and Epstein 1975, 1976, Kolodny and Epstein 1976), and as high as 5.0‰ (Murata *et al.* 1977) depleted in ^{18}O compared to cristobalite. Using these values, estimated paleotemperatures for precursor opal-CT in Amuri Limestone Group cherts, range from 10°C (2‰ depletion) to 25°C (5‰ depletion) cooler than the later formed quartz (for a given $\delta^{18}O_{Water}$ and irrespective of the fractionation expression).

ii) Assuming the Clayton *et al* fractionation then opal-CT temperatures would be within the range of micrite temperatures but lower than Amuri Limestone Group dolomite temperatures. This suggestion raises the possibility of chert nucleation preceding dolomitization. Knauth and Epstein opal-CT temperatures are lower than both micrite and dolomite formation temperatures.

iii) If opal-CT is the primary silica phase three considerations, or combinations thereof, are required to explain the isotopic composition of Amuri Limestone Group cherts: a) inherent problems in the fractionation expressions; b) the possibility that chert and carbonates precipitated from different fluids; and c) the possibility that the fractionation between opal-CT and quartz was small.

The fractionation expressions are extrapolations of high temperature data and as such their validity at low temperatures may be questioned [see also discussion of dolomite fractionations, Section 4.4.2]. The validity of applying a single fractionation to all forms of silica is similarly questionable. Fractionation expressions always assume isotopic equilibrium, whereas results may in fact reflect isotopic non-equilibrium during precipitation. Therefore problems with the chert (and dolomite) fractionation factor may well cause differences in temperatures between coexisting phases. If the assumption of more or less contemporaneous chert and dolomite formation is correct, then the similarity in the isotopic range of chert and dolomite would substantiate this assertion.

The preceding discussion has assumed that temperature is the primary control on the ^{18}O composition of the chert. Depletions in ^{18}O during recrystallization can result from interaction with ^{18}O depleted fluids. Degens and Epstein (1962) argued that Cretaceous cherts with ^{18}O less

than 30·/.. to 34·/.. (their assumed reasonable range for marine chert of this age) had interacted with meteoric waters depleted in ^{18}O compared to seawater. Using both $\delta^{18}O$ and δD data, Knauth and Epstein (1976) concluded that meteoric water was involved in the formation of many cherts. However, Kolodny and Epstein (1976) stated that the interaction with freshwater is unnecessary for most post-Jurassic cherts. Discussion of the carbonate data in this thesis indicates that ^{18}O depletions arose without the influence of meteoric fresh water. Therefore if there was a fractionation between opal-CT and quartz, it would have to be explained in terms of pore water depletion without any external input.

A relatively ^{18}O enriched opal-CT implies formation in positively shifted pore waters. Retaining the isotopic composition of the dolomite, necessitates precipitation from fluids of different isotopic composition to the dolomitizing fluids. There is no problem with this type of situation if the dolomitization is a much later event however, there is more evidence for contemporaneous chert and dolomite formation. The similarity of chert ^{18}O compositions to both micrites and dolomites cannot be explained by separate fluids of formation. It is more logical to suggest that both the cherts and diagenetic carbonates formed from pore waters that were at least similar in composition. A small depletion in ^{18}O between quartz and opal-CT (e.g. <1·/..) removes the necessity for separate fluids. The situation would essentially be the same as for direct quartz precipitation. Support for this contention comes from the relatively faster transformation of opal-CT to quartz in carbonate sediments (Lancelot 1973, Calvert 1974, Keene 1975, Kastner *et al.* 1977, Williams *et al.* 1985). A shorter time between initial deposition and transformation means there is less chance of pore water modification. The isotopic evolution of the pore water at the time of opal-CT transformation to quartz and/or direct quartz precipitation is recorded by the chert. By analogy, the fractionation between silica phases is dependent upon the stage of pore water evolution at the time of formation.

The isotopic evolution as described above does not discount temperature effects. Rather the isotopic composition of the pore fluids may have been relatively more important than temperature effects in Amuri Limestone Group sediments. As is the case for dolomite analyses, chert analyses record an average composition. However, different parts of chert nodules may nucleate at different times, either as quartz or as opal-CT.

Conversion of opal-CT does not necessarily occur homogeneously throughout the nodule. Certainly these silica reactions do not occur at the same rate as dolomitization or calcite recrystallization. On a localized scale, faster diagenetic reactions will alter the isotopic composition of the fluid before completion of the slower adjacent or competing process. The result is small shifts in isotopic composition such as seen between adjacent chert and calcite [Table A6.3]. Overall the isotopic composition of the cherts remains within a specific range as determined by factors such as sedimentation rate and burial depth.

5.3. GEOCHEMISTRY OF SILICA DEPOSITION

5.3.1. SILICA DEPOSITION IN THE AMURI LIMESTONE GROUP AND WOOLSHED FORMATION

Field and geochemical evidence indicate progressive silicification and carbonate replacement, during which elements contained in carbonate phases were expelled from the site of chert formation. Similar explanations are given for chert-bearing carbonates in DSDP sediments (e.g. Hein *et al.* 1981, 1983). In detritus-bearing units, such as the WC and BC Zones, and the UCM and LCM Subzones, the authigenic silica effectively dilutes the non-carbonate residue.

Temperature has often been cited as the main control on silica diagenesis. However, its primary effect seems to be one of increasing reaction rates (Williams *et al.* 1985). Other factors such as pH, host sediment composition, competing diagenetic reactions, and sulphate reduction are also significant [see Section A7.3.3]. The $\delta^{18}O$ data suggest that the cherts formed from fluids comparable in composition and temperature to the dolomites. Comparable early diagenetic origins are indicated by field evidence. The association of dolomitization with sulphate reduction indicates that sulphate reduction may also be related to chert formation.

Clayton (1986) presented a model for the association of chert formation and sulphate reduction in the Upper Cretaceous western European chalks. The evidence for the model consists of changes in concentrations of major elements across a *paramoudra* and a chert band. The *paramoudrae* consist of chalk cemented cores surrounded by chert. Near the centre of each core, pyrite and some glauconite are concentrated. A chert band had pyrite

concentrated near its base. As described in Chapter 4 of this study, pyrite is related to sulphate reduction in the simplified reaction below (Coleman 1985):

$$2CH_2O + SO_4^{2-} \rightarrow H_2S + 2HCO_3^- \qquad (5.1)$$

The equilibrium between the sulphide and carbon species determines the extent of sulphide and carbonate precipitation (Clayton 1986) thus:

$$S^{2-} + CO_2 + H_2O \rightarrow HS^- + HCO_3^- \rightarrow H_2S + CO_3^{2-} \qquad (5.2)$$

Where Fe^{2+} is available, FeS_2 is precipitated and CO_2 is lost. In carbonate sediments such as the Amuri Limestone Group, the reaction is likely to be Fe limited, but less so in the Woolshed Formation. Therefore the CO_3^{2-} can initiate carbonate precipitation and the H_2S is lost. If the liberated H_2S reaches more oxidizing conditions, it may be reconverted to SO_4^{2-} and S^0 by oxidizing bacteria (Coleman 1985, Clayton 1986):

$$H_2S + 2O_2 \rightarrow SO_4^{2-} + 2H^+ \qquad (5.3)$$

Such reactions occur near the boundary between oxic and sulphate reducing pore waters. Released H^+ cause localized carbonate dissolution, with the dissolved carbonate ions initiating the seeding of silica from saturated solutions (Clayton 1986). Some debate exists as to the effectiveness of carbonate in precipitating colloidal silica (Kastner *et al.* 1977). However, the decrease in pH and the presence of $Mg(OH)_2$ nuclei in this environment will certainly enhance silica deposition. The morphology of the chert is thus governed by the geometry of the H_2S-O_2 mixing zone. Mixing may be confined to well defined burrows (due to factors such as increased permeability, see Section 5.1.2), or distributed in an even layer in relatively homogeneous intervals. The latter situation in particular, requires periods of non-deposition associated with a more or less stationary redox stratification. In the European chalks episodic cementation has resulted in regular chert bands at 0.5-2 m intervals (Clayton 1986).

A genetic relationship between chert formation and sulphate reduction in the Amuri Limestone Group and Woolshed Formation is consistent with the association of chert, dolomite and pyrite, and with chert geochemistry

(i.e. the expulsion of the bulk of the cations from the host sediment other than those in insoluble residues). Calcite dissolution and silica deposition can thus occur concurrently on a localized scale in sediments. The dissolved carbonate may reprecipitate nearby as calcite, dolomite, or calcite that is subsequently dolomitized subject to Mg^{2+} availability. The result is authigenic silica and carbonate minerals with similar isotopic compositions, with no requirement for separate or exotic fluids of formation.

Concentration of chert around burrows is only locally important in Amuri Limestone Group samples. Chertification directly associated with burrows (Clayton 1986) only occurs to limited extent in the Amuri Limestone Group [Sections 2.2.7, A2.5, A6.2.4]. Unlike the European chalks most are associated with Fe-oxide dominated micrites [see Section 3.5.1]. However, on a microscopic scale pyrite is still found in most of these cherts. No pronounced association of burrows with the majority of the chert is noted in this study [Section A6.2.4]. The dissemination of pyrite throughout cherts, the lack of regularly chertified intervals as in the European chalks, and the pervasiveness of chertification particularly in the BC and CD Zones, and LCM Subzone, suggests that stable redox stratification may not have been established. In addition the chert of the LCM Subzone is best developed above, rather than below an unconformity. Although sedimentation rates have bearing on the extent of sulphate reduction [Section 4.4.3], the distribution of organic matter may be more significant.

Conceivably the extent of chertification may depend upon the abundance of organic matter (e.g. Namy 1974), as well as sedimentation rates, and the availability of silica. The organic matter distribution in a sediment is a function of primary supply and depositional processes and post-depositional redistribution resulting from bioturbation. The latter process ensures a high organic matter content (Bromley and Ekdale 1984) and enhances the porosity and permeability of the sediment. The extent of chert development in the BC and CD Zones, and LCM Subzone makes assessment of burrowing impossible. In parts of the CL Zone burrows coincide with chert development indicating that burrows may have some influence on chert development, albeit indirect. In contrast, significant volumes of chert are developed in the CL Zone where there is little evidence of burrowing. In these sediments the distribution of organic matter was probably a

function of primary depositional processes. Sulphate reduction would only have occurred at sites where organic matter existed, now reflected in the distribution of pyrite. However, equation (5.3) indicates that oxidation of H_2S and the consequent reduction in pH is required to initiate silica deposition. In this study where reducing conditions dominated in the sediments, only residual or localized quantities of O_2 would have been available for the oxidation of H_2S. Minor amounts of O_2 from seawater diffusion may have been similarly used, and Moses *et al.* (1987) showed that pyrite oxidation can be accomplished in anaerobic conditions with the release of H^+ as follows:

$$FeS_2 + 14Fe^{3+} + 8H_2O \rightarrow 15Fe^{2+} + 2SO_4^{2-} + 16H^+ \qquad (5.4)$$

If reaction (5.4) occurred in the sediments of this study, the Fe^{3+} could have been derived from residual Fe-oxides, particularly in detrital-rich units such as the WC or BC Zones. Decreases in pH at the sites of H_2S oxidation would enable the dissolution of carbonate and the deposition of silica. Initially deposited silica then acted as nucleation centres for further silica deposition. Assuming silica saturation in pore fluids and an adequate supply of dissolved SiO_2, the dispersed nuclei may eventually grow and coalesce. Thus, initial nucleation of silica may occur in association with sulphate reduction, but can continue after the sediment has been buried below the sulphate reduction zone and during later compaction. For example, chert bands such as in Figure A2.24 may be explained in this manner. The extent of further chert development would therefore be dependent upon the supply of dissolved silica. The levels of silica saturation at nucleation sites will determine whether quartz or opal-CT precipitate.

The scheme for silica deposition described in the preceding paragraph is essentially the reverse of the Clayton (1986) model for *paramoudrae*. The Clayton model describes localized sulphate reduction under reducing conditions in an otherwise dominantly oxic environment. For the bulk of the Amuri Limestone Group localized oxidation in a dominantly reducing environment appears to have occurred. In the volumetrically minor occurrences of burrow related chert, such as at Chancet Rocks (18) and Woodside Creek (13), chertification most likely occurred in similar fashion to that described by Clayton (1986) for *paramoudrae*.

5.3.2. SOURCES OF SILICA

The volumes of silica in the sediments of this study are large. The volume of authigenic silica required to form chert may be estimated as follows:

The average SiO_2 analysis for cherts in this study = 96 weight% SiO_2 and ρ_{Quartz} = 2.65 gm/cm^3

Therefore the mass of SiO_2/m^3 of sediment = $2.65 \times 0.96 \times 10^6$

$= 2.544 \times 10^6$ gm SiO_2

which is equivalent to 42,336 moles SiO_2

Therefore 1 volume% chert = 423 moles SiO_2/m^3.

The BC Zone, and parts of the LCM Subzone, would therefore require about 42,000 moles of SiO_2/m^3, whereas a siliceous micrite (e.g. from the Lower Limestone which contains about 20% insoluble residue dominated by authigenic quartz) would require 8460 moles SiO_2/m^3. Chert in the CD Zone constitutes about 50% of the rock volume, with chert nodules accounting for about 25% to 50% of the volume in the CL Zone. The insoluble residues of the carbonate fractions account for an additional 20% to 40% [Table A5.1]. Therefore the approximate range of chert volumes for incompletely chertified sediments is of the order of 24% to 70%, requiring 10,152 to 29,610 moles SiO_2/m^3.

Volcanic and hydrothermal sources for SiO_2 from within the Amuri Limestone Group and Woolshed Formation can be discounted on the basis of field relationships. In addition, the low Fe and Mn contents, and the lack of volcanogenic material in thin section argue against both internal and external volcanogenic inputs. Isotopic analyses constrain chert formation to temperatures $\leq$60°C, which preclude direct precipitation from volcanic or geothermal emanations. The three other silica sources that must be evaluated are:

i) Seawater.
ii) Dissolution of biogenic siliceous skeletons.
iii) Inorganic sources.

Seawater

Two-thirds of the silica supplied to the oceans comes from rivers

(DeMaster 1981, DeMaster *et al.* 1983). Other sources include volcanic emanations (Calvert 1974, DeMaster 1981, Kastner 1981), glacial weathering (DeMaster 1981), and diffusive loss of silica from sediments into the overlying seawater as a result of dissolution of volcanic glass, basalt (Calvert 1974, DeMaster 1981, Kastner 1981), or siliceous organisms (DeMaster 1981, Wakefield 1982). Silica concentrations in the oceans depend upon locality and depth. Concentrations are usually less than 170 µmoles/litre (Calvert 1974), which is about 10 ppm SiO_2 (cf. 129,000 ppm Mg^{2+}). The much lower levels of dissolved silica in the oceans compared to rivers results from biogenic uptake of SiO_2 (Calvert 1974, DeMaster *et al.* 1983). Hydroxide bound silica (see later) has also been suggested as a significant mechanism for SiO_2 removal from ocean waters (Buurman 1976).

To chertify the sediments in this study with seawater as the dominant source would require prohibitively large volumes of water flushing through the system, and/or a large time span within the zone of effective seawater diffusion. Concentrations of SiO_2 in pore waters are usually greater than in overlying seawater (Calvert 1974), and range from about 100-1250 µmoles/litre (e.g. Mottl *et al.* 1983, Baker 1985). Sharp concentration gradients across the sediment/water interface and in the upper sediment column, indicate a net flux into the overlying seawater (Calvert 1974, Wakefield 1982). Therefore the possibility of contributions from seawater would appear to be essentially nil.

Biogenic Silica

The paucity of siliceous organisms in WC Zone and Amuri Limestone Group sediments may be a function of sampling and search procedures, or reflect the complete dissolution of biogenic silica. Relatively abundant siliceous microfaunas have been extracted from parts of the sequence at Kaikoura Peninsula, Waipapa Bay, Benmore Stream, Isolation and Woodside Creeks (C. Hollis *pers. comm.* 1988), supporting the latter alternative. Fossil preservation is best in the purer limestones, with poorer preservation in chert bearing beds. Cherts show the poorest fossil preservation. In addition, radiolaria are moderately abundant in the Whangai Shale of the eastern North Island (Moore 1988a). Both the Whangai Shale and the Woolshed Formation are inferred to be part of the same facies (Morris 1987), which implies a similar radiolaria content to the

Whangai Shale may be present in the Woolshed Formation.

Silica is extracted from ocean waters by diatoms, radiolaria, sponges, and silicoflagellates (Kastner 1981). The bulk of cherts are commonly considered to form from the alteration of biogenic silica (Heath and Moberly 1971, von Rad and Rösch 1972, Lancelot 1973, Heath 1974, Wise and Weaver 1974, Funk 1975, Keene 1975, Kastner *et al.* 1977, Riech and von Rad 1979a,b, Kastner 1981, Karpoff *et al.* 1981, Pisciotto 1981a,b and many others). The development of biogenic chert depends on the distribution and rate of accumulation of biogenic silica. Biogenic silica distributions in oceans are dependent upon biological productivity (Ramsey 1971, Leinen 1979, Wakefield 1982), which in turn depends upon physical oceanographic factors such as circulation patterns and nutrient upwelling (Ramsey 1971, Calvert 1974, Heath 1974, Leinen 1979). There is a crude correlation between the productivity in the oceans and the abundance of silica in the upper sediment column (Wakefield 1982). Currently the Antarctic region as a whole is thought to accumulate as much as 75% of the silica supplied to the world oceans (Ledford-Hoffman *et al.* 1986).

Modern silica accumulation rates vary from 5-6 gm/cm^2/myr for the central Pacific (65-146 myr B.P.) to 28-30 gm/cm^2/myr for the northwest Pacific (103-124 myr B.P.). The only estimate for the southwest Pacific is 22 gm/cm^2/myr (Pisciotto 1981a). An accumulation rate of 40 gm/cm^2/myr has been determined for the Late Oligocene (23-30 myr B.P.). The effective range of accumulation rates is assumed to be 22-40 gm/cm^2/myr. In other words, each square metre of ocean floor could accumulate 3661 to 6657 moles SiO_2/myr. Although these figures are comparable to estimated volumes of silica in siliceous micrites in the Amuri Limestone Group (<8500 moles SiO_2), they are lower than required for rocks containing more than 24% silica by volume (>10,100 moles SiO_2). It would require at least 2 million years to accumulate 10,152 moles of SiO_2, and about 6-12 million years to accumulate the 42,336 moles/m^3 in the BC Zone. Twelve million years is almost one-third of the inferred age of the whole Mead Hill Formation (Morris 1987). Increased deposition rates could reduce the time required for requisite accumulation.

The problem may also be looked at from the point of view of how much silica may be supplied by 1 m^3 of biogenic siliceous sediment. The following calculation assumes the sediment consists entirely of biogenic

silica undiluted by other material such as carbonate or clay minerals. Reasoning similar to that involved in the dolomite Mg^{2+} mass balance calculation [Section 4.3.1] is used:

The density range of biogenic silica is about 1.9-2.2 gm/cm^3 (Hurd and Theyer 1977, Iler 1979), and porosities of diatomaceous sediments of about 71% are found at up to 500 m burial depth (Hamilton 1976, Isaacs 1981).
With $\rho_{Seawater}$ = 1.03 gm/cm^3

71% of the sediment = water with ρ = 1.03 gm/cm^3
29% of the sediment = silica with ρ = 1.9-2.2 gm/cm^3
giving a total sediment density of ρ = 1.28 to 1.37 gm/cm^3
Therefore 1 m^3 of uncompacted biogenic silica contains:
1.28×10^6 to 1.37×10^6 gm SiO_2
= 21,301 to 22,799 moles SiO_2

As such, biogenic silica alone could provide enough SiO_2 to produce chert volumes of less than 54%, assuming complete fossil dissolution.
These volumes of silica alone are insufficient for chertification of units such as the BC Zone, accounting for little over 50% of the silica therein. Less chertified parts of the Amuri Limestone Group contain dominantly micrite and calcareous microfossils and nannofossils. Common foraminiferal 'ghosts' in basal sequences indicate a similar calcareous component. Therefore biogenic siliceous skeletal material was probably a secondary component in the sediments. As such, potentially much less chert could have been formed. The preceding analysis therefore shows that biogenic silica can account for a proportion of the chert in these sediments, but it cannot account for it all.

Inorganic Sources

Except in hydrothermal systems, direct precipitation of silica, from supersaturated solution by inorganic means, is thought to be unlikely since the Cambrian because of the removal of SiO_2 by siliceous organisms (Heath 1974). However, SiO_2 may be concentrated inorganically by hydroxide adsorption and clay mineral transformations.

Adsorption of SiO_2 by Fe^{3+}, Mn^{2+}, and Al^{3+} hydroxides may be important during estuarine mixing (Buurman 1976). The hydroxides may either be in suspension, in solution, or coating suspended material, all of which are

subsequently deposited in the open ocean (Buurman 1976). Variable deposition of hydroxide bound silica may result in variable amounts of silica in the sediments. Parts of a sediment containing relatively greater abundances of silica may be where chert nucleation takes place. The resulting concentration gradient causes migration to, and precipitation in, these layers. In addition hydroxide bound silica apparently forms quartz directly (Buurman 1976). Buurman suggests that silica adsorbed in this manner can explain features such as rapid chert formation, chert morphology, and chert in chalks which contain few siliceous organisms. Any hydroxide bound silica may be released into pore waters during reduction of Fe and Mn.

Heath (1974) stated that about 10% of the total river influx of dissolved SiO_2 may be removed by inorganic adsorption. However, the relative importance of various inorganic mechanisms in estuarine silica removal is uncertain (DeMaster *et al.* 1983). Therefore the significance of inorganically bound silica in chert formation remains equivocal until satisfactory estimates of silica removal and deposition can be made. Nevertheless it is possible that although silica from such a source may not be major, it may be important at a localized scale.

The presence of smectite clays in the Amuri Limestone Group and the Woolshed Formation suggests that clay minerals may be a source of silica. Towe (1962) was one of the first to suggest the importance of clay mineral diagenesis as a source of silica for secondary cementation. Supergene weathering of Fe-rich montmorillonite to kaolinite was shown to result in the formation of goethite and secondary chert (Altschuler *et al.* 1963). Keene and Kastner (1974) recognized clay derived silica as an important chert source. They concluded that silica was derived from smectite (montmorillonite) transformation to hydrous mica or illite. The general reaction as expressed by Hower *et al.* (1976) is:

$$\text{Smectite} + Al^{3+} + K^{+} \rightarrow \text{Illite} + Si^{4+} \qquad (5.5)$$

From data in Hower *et al.* (1976) the above equation was expanded by Boles and Franks (1979), and follows two possible reaction stoichiometries:

$$4.5K^{+} + 8Al^{3+} + KNaCa_2Mg_4Fe_4Al_{14}Si_{38}O_{100}(OH)_{20}.10H_2O \rightarrow Na^{+} + 2Ca^{2+} + 2.5Fe^{3+} + 2Mg^{2+} + 3Si^{4+} + K_{5.5}Mg_2Fe_{1.5}Al_{22}Si_{35}O_{100}(OH)_{20} + 10H_2O \qquad (5.6)$$

$$3.93K^{+} + 1.57KNaCa_2Mg_4Fe_4Al_{14}Si_{38}O_{100}(OH)_{20}.10H_2O \rightarrow 1.57Na^{+} + 3.14Ca^{2+} + 4.28Mg^{2+} + 4.78Fe^{2+} + 24.66Si^{4+} + K_{5.5}Mg_2Fe_{1.5}Al_{22}Si_{35}O_{100}(OH)_{20} + 57O^{2-} + 11.40OH^{-} + 15.7H_2O \quad (5.7)$$

Although the ions released by both reactions are the same the quantities differ significantly. Three moles of silica are produced in reaction 5.6, compared to nearly 25 moles from reaction 5.7. Lahann (1980) calculated that from reaction 5.6, one litre of sediment containing 500 gm of montmorillonite would produce 45 gm (0.7 moles) of SiO_2, assuming the reaction proceeds to completion. Since reaction 5.7 produces about eight times as many moles of SiO_2, the same quantities of montmorillonite and sediment would produce about 361 gm (6 moles) of SiO_2. According to Boles and Franks (1979) the illitization process in shales best approximates reaction 5.7. It should also be noted that both reactions generate significant quantities of water.

An important reactant in the process is K^{+}, which is probably supplied by seawater (Keene and Kastner 1974). If the smectite is rich in iron, Fe-oxides or Fe-hydroxides may be concentrated in the surrounding sediment (Keene and Kastner 1974). Oxides so formed may then oxidize pyrite and promote silica deposition according to equation (5.4).

Illitization is initiated at about 50°C (Perry and Hower 1970), with the bulk of silica being generated between 50°C and 100°C (Boles and Franks 1979). The isotopic paleotemperatures for Amuri Limestone Group cherts are however maximum formation temperatures with much of the silica precipitated at lower temperatures [Section 5.2.4]. However, some chert paleotemperatures [Table 5.1] are just below or within the lower part of the illitization temperature range. Marl and micrite paleotemperatures indicate that in general the Amuri Limestone Group did not attain temperatures higher than 50°C [Table 3.1]. Therefore it is unlikely that significant silica generation occurred from smectites in marls. In addition, most would be expected from detrital-rich units such as the WC Zone, the BC Zone, the UCM Subzone, and to a lesser extent the lower LCM Subzone. However, this does not preclude a scenario where early stages of precipitation involved biogenic silica with clay mineral silica becoming more important later (see also Keene 1975).

Another possible source of clay mineral derived silica is the Woolshed Formation. It contains a 20-30% clay size fraction, consisting of smectites and illite-muscovite. No direct measurements of the proportions of smectite in the sediments were made. However, a crude estimate of the SiO_2 potentially released by 1 m^3 of Woolshed Formation sediments may be made by assuming: i) a maximum of approximately half (i.e. about 15% of the total sediment) of the clay size fraction consisted of smectitic clay, ii) a sediment porosity of about 30% at the time of clay mineral transformation, iii) an average sediment density of approximately 2.5 gm/cm^3, and iv) that reactions go to completion. The total weight of 1 m^3 of sediment is thus 2.06×10^6 gm, and the smectite contained therein weighs 3.08×10^5 gm. Using the ratios of smectite to SiO_2 produced, determined by Lahann (1980), indicates that 1 m^3 of Woolshed Formation sediment could potentially produce 461 moles of SiO_2 according to reaction (5.6), and 37,009 moles according to reaction (5.7). In units such as the UCM Subzone, or WC and BC Zones, some of the SiO_2 thus produced may have precipitated at or near the site of reaction. In the WC Zone, the presence of smectite indicates that not all was converted to illite. However, further quantities of SiO_2 may have been derived from clay mineral reactions much deeper within the Woolshed Formation. Houseknecht (1988) speculates that the upward migration and deposition of silica may occur in shallowly buried sandstone. Pressure solution of sand or silt grains (Houseknecht 1988), or feldspar and mica dissolution (Hurst and Irwin 1982) may also have contributed SiO_2. The movement of SiO_2 thus generated may be accomplished by diffusion in pore waters, the upward migration of SiO_2-rich pore waters, or by the sinking of the upper Woolshed Formation and Amuri Limestone Group into SiO_2-rich solutions as Woolshed Formation sediments compact.

The most important agent of primary fluid migration is compaction (Magara 1980). Water expelled from compacting interbedded sandstone/shale sequences travels along dip from the basin centre to the margins. In continuous shale sequences vertical migration dominates (Magara 1976). Where both continuous shale, and alternating sandstone/shale sequences are combined migration will occur in both horizontal and vertical directions (Magara 1976). Other factors which aid fluid migration include aquathermal effects (water expansion by geothermal heating), generation of water from clay mineral transformations, and osmosis (Magara 1980). Aquathermal effects are more important at depth (Magara 1980), whereas

clay mineral reactions and osmosis may be more applicable further up the sediment column. Osmosis arises from salinity gradients through ion filtration by clays and shales (Magara 1980 and references therein). Precipitation of authigenic phases may cause similar effects. The rate and extent of fluid migration is dependent upon a large number of factors which include porosity, permeability, tortuosity of diffusion path, fractures, pressure-temperature-salinity gradients and so on. The characteristic diffusion distance for silica is about 30 m (Lahann 1980). The diffusion distance is temperature dependent. Increases in temperature decrease diffusion distances by accelerating precipitation. Therefore the lower the temperature at which the silica is released, the greater will be the distance to which it may potentially diffuse. Slow sedimentation rates, and hence lower burial rates, mean the rate of temperature increase due to geothermal heating will be low, thereby enhancing migration (Lahann 1980).

The general view of compaction expelled pore water migrating towards a depositional surface is not always correct (Bonham 1980). During early diagenesis a considerable proportion of the fluid flux is downward, as is the diffusive seawater supply of Mg^{2+} for dolomitization. As deposition and burial progress the sediments are essentially compacted down through an essentially fixed water column (Bonham 1980). Therefore relative to a stratigraphic marker the fluids move upwards, but not necessarily reaching the depositional surface. It is inferred that compaction through SiO_2-rich porewaters derived from the Woolshed Formation was the main source of SiO_2 in the basin centre where the greatest chert volumes occur. Also found in the basin centre are the greatest volumes of sediment (see Morris 1987) which may increase the rate of compaction through the water column, and provide the largest potential source of inorganically derived silica. It is further suggested that elements such as Fe and Mg (also produced by reactions such as 5.6 and 5.7) may have been depleted from pore waters by other diagenetic reactions. The SiO_2 remained in pore waters until it was deposited as chert in the Amuri Limestone Group.

5.4. SUMMARY

1) No further subdivision of chert units in terms of mineralogy, petrography, or geochemistry is considered possible. No 'marker' horizons, other than those already recognized in the field, have been

detected.

2) There is a general uniformity of chert mineralogy throughout the sequence. The bulk of the chert is composed of quartz. Opal-CT is rare in Amuri Limestone Group chert but locally important in the Woolshed Formation. Disseminated pyrite is common to all cherts.

3) Paralleling the mineralogical trends, there is a general uniformity of chemical composition in the majority of cherts. Variations arise from the presence of detrital material in the UCM and lower LCM Subzones, and the BC Zone in particular. Chert colour, morphology, and geographic location do not correlate with chemical composition. There are no chemical differences between dike or 'redeposited' cherts, and the rest of the chert sequence. Silica is the major component with all other elements forming trace components. The abundance of trace components is controlled by clay and detrital minerals, and organic matter. Progressive chertification is inferred to have resulted in the expulsion of carbonate bound elements from the site of chert formation and the effective dilution of non-carbonate bound insoluble residues.

4) The bulk of the chert appears to have formed at burial temperatures of less than about 60°C, which combined with the field evidence [Chapter 2, Appendix 2], indicates an early diagenetic origin within the upper sediment column. Cogenesis of chert and dolomite is indicated by their similarity in paleotemperatures, along with petrographic and other geochemical considerations indicating initial nucleation of silica in association with sulphate reduction. However, notwithstanding early nucleation, chert formation in some instances continued during and possibly after host-sediment compaction.

5) SEM and petrographic analyses indicate that both opal-CT and quartz were primary silica precipitates in the Amuri Limestone Group. The relative proportions of each initially precipitated in the sediment was a function of the abundance of clays and foreign cations, the distribution and abundance of microfossils, and levels of silica saturation. These conditions probably varied on a microenvironmental scale to produce mixed euhedral and massive textures. A sequence of chert formation is inferred for Amuri Limestone Group carbonates, which is similar to that proposed by Keene (1975) for carbonate sediments, and is as follows:

i) Nucleation of opal-CT and/or quartz in sediment interstices and foraminiferal chambers.
ii) Coalescence of opal-CT lepispheres to form massive textures; concomitant and continued direct precipitation of quartz.
iii) Chalcedony, microquartz and megaquartz fills remaining foraminiferal chambers and pores. Opal-CT rarely completely fills a foraminiferal chamber.
iv) Replacement of foraminiferal tests, and other large carbonate grains by chalcedony, or sometimes microquartz. Opal-CT is never a replacement.
v) Conversion of opal-CT to quartz.

The relatively faster conversion of opal-CT to quartz in carbonate sediments than in detrital sediments has resulted in the extremely limited preservation of opal-CT in the Amuri Limestone Group. In contrast, the abundance of clay and detrital minerals in the Woolshed Formation has resulted in limited conversion to quartz, and a predominance of opal-CT. In addition, the paucity of calcareous microfossils and the likely prevalence of metallic cations in pore waters probably precluded significant direct quartz precipitation in the WC Zone.

6) Chert crystal size and morphology depends on initial porosity and permeability, mineralogy of the primary precipitate, and whether the silica is precipitated as a cement or a replacement. Silica precipitated in burrows or fossil cavities is often coarser than in the surrounding matrix. Hein *et al.* (1981) suggested that silica phase transformations in such structures is one step ahead of the host rock. It may also result from either the replacement of coarse material, such as sparry calcite cement, or the filling of large pores.

7) Patterns of chertification are governed by the interplay between sediment texture, permeability, porosity, organic matter, and skeletal and trace fossil content. All these characteristics amount to the sediment 'chertification potential' which is analogous to the diagenetic potential of Schlanger and Douglas (1974), and which may vary on both a microscale and a macroscale.

8) Volcanic or geothermal emanations, volcanic glass and seawater can be discounted as significant silica sources in the WC Zone and Amuri Limestone Group. Few siliceous microfossils were observed in this study.

However, the extraction of relatively abundant siliceous microfaunas from the Amuri Limestone Group by other workers, indicates that siliceous organisms are a source of silica for the chert. However, mass balance estimates suggest that biogenic sources may not be able to supply all the silica in some units. An additional input from low temperature clay mineral reactions is suggested. These reactions were probably of greatest significance in detrital bearing units which are completely chertified (e.g. the BC Zone, UCM Subzone), and which occur in the Amuri Limestone Group depocentre. Some of the clay mineral derived silica may have been produced near the site of chert nucleation. In addition, silica derived from the Woolshed Formation may have been precipitated after relative upward migration in pore waters. Hydroxide-bound silica may also have contributed to varying extents in all cherts. Unfortunately the chertification process has changed totally the original sediment, particularly in the LCM Subzone, and BC and CD Zones.

9) Veining and brecciation post-date chertification, and are probably related to later tectonic events. Some zebra-beds may have formed in association with compaction.

CHAPTER 6

MODELS FOR THE GENESIS OF CHERT AND DOLOMITE

6.1. INTRODUCTION

In general, models for chert development described in the literature suggest that early chert formation occurs a few metres below the seafloor (e.g. Namy 1974, Buurman 1976, Kelts 1976, Geeslin and Chafetz 1982, Clayton 1986, and others). Data from DSDP literature (see Kastner 1981) indicate that under relatively low to moderate sedimentation rates and low to moderate temperatures the opal-A to opal-CT transformation may take 40-90 myr (see von Rad and Rösch 1974, Keene 1975). The time required for these transformations may be reduced by increases in temperature caused by burial or by high geothermal gradients. The rate of transformation will depend upon how quickly the initially deposited silica (usually but not always biogenic) dissolves. Some authors suggest that dissolution occurs very soon after deposition (e.g. Williams *et al.* 1985, Clayton 1986), facilitating the early formation of chert. From experimental evidence Ernst and Calvert (1969) inferred the opal-CT to quartz transformation to take 180 myr at 20°C, 4-5 myr at 50°C, and about 36,000 years at 100°C. Although such estimates are by no means accurate, they indicate that diagenetic silica reactions not only occur very early in the sediment history, but can continue for considerable periods after nucleation.

As is the case for chert, models suggesting early dolomite formation in the upper few metres of the sediment column are common (e.g. Baker and Burns 1985, Compton and Siever 1986, Compton 1988, and others). The formation of dolomite generally appears to be a faster process than chert formation. For example, dolomite may form at earth surface temperatures and pressures in only a few months (Mansfield 1980).

Preceding chapters of this study indicate that the bulk of chert and dolomite in the Woolshed Formation and Amuri Limestone Group formed during the early diagenetic history of the sediments. Some evidence also exists for the later genesis of chert in the Amuri Limestone Group, and chertification of the WC Zone mainly after compaction of the sediments. The diagenetic models presented in the following sections address the following topics:

i) Paragenesis of chert and dolomite.
ii) Variations in the stratigraphic and geographic distribution of chert and dolomite in the Amuri Limestone Group.
iii) The relationship of concretion formation in the WC Zone to chert and

dolomite genesis in the Amuri Limestone Group.

iv) The limited extent of dolomitization in the Amuri Limestone Group.

v) The dissemination of dolomite crystals in chert.

6.2. POSSIBLE CAUSES OF DIAGENETIC VARIATIONS

Changes in overall sedimentation patterns appear to have promoted the deposition of chert and dolomite in Amuri Limestone Group sediments. There was a progressive change from siliciclastic Woolshed Formation sedimentation to Amuri Limestone Group carbonate sedimentation, probably in response to increasing carbonate productivity in overlying waters. Biogenic silica productivity could also have increased. Increased carbonate deposition combined with dissolution and precipitation of biogenic silica may have enabled the precipitation of silica derived from the Woolshed Formation. Without the initial 'seeding' of sediments with silica from biogenic sources, silica derived from the Woolshed Formation may otherwise not have precipitated. The result was significant chertification occurring only in the Amuri Limestone Group and Woolshed Formation sediments adjacent to the Mead Hill Formation. Chert deposition appears to have occurred to greater or lesser extent throughout the Mead Hill Formation. The ultimate controls on chertification were the supply of silica and the reduction of sulphate.

Dolomite formation is more restricted than chert formation. The relatively abrupt appearance of significant volumes of dolomite, which characterize the CD Zone and LCM Subzone, indicate that some variation in environmental conditions occurred that enabled precipitation of dolomite to a considerably greater extent than in the CL or BC Zones.

Baker and Kastner (1981) found that even very low levels of SO_4^{2-} may inhibit dolomitization. Concentrations of SO_4^{2-} above which dolomite can not precipitate may result from low levels of organic matter and low populations of SO_4^{2-} reducing bacteria. Baker (1985) found that sulphate reduction in hemipelagic DSDP cores (in the New Zealand region) was greater than in carbonate rich sediments. Thus, the slightly higher detrital content of the CD Zone may have predisposed it to dolomitization. Alternatively, sedimentation rates in the CL Zone may have been such that burial of sediments to below the sulphate reduction zone occurred before significant reduction in SO_4^{2-} concentrations. Relatively high

sedimentation rates have the additional effect of limiting the flux of Mg^{2+} by burying sediments relatively quickly to depths below the zone of effective seawater diffusion. Excluding the LCM and UCM Subzones, there is little direct evidence for differences in sedimentation rate within the CL Zone, although it is unlikely that sedimentation rates remained constant throughout CL Zone deposition. The precise reason for the absence of dolomite in the CL Zone is difficult to deduce from the available evidence. However, it is thought that although sulphate reduction occurred (as it does in carbonate oozes to varying degrees), SO_4^{2-} concentrations remained high enough to inhibit dolomitization. The underlying cause may have been insufficient levels of organic matter in the sediments. Decreases in organic matter in sediments may also have contributed to the lower levels of silica precipitation in the CL Zone compared to the CD and BC Zones. Dolomitization in the CL Zone was thus limited to rare isolated accumulations of organic matter [e.g. the dolomitized *Zoophycos* in Figure A2.26] where SO_4^{2-} concentrations were sufficiently low. An increase in carbonate productivity may have increased sedimentation rates but this remains unproven.

The relationship of unconformities to dolomite genesis has been noted by a number of authors (e.g. Morrow 1982b, Compton and Siever 1986). Similarly, Berggren and Hollister (1974) suggested that the dissolution of siliceous organisms and the genesis of porcelanite was associated with periods of erosion and nondeposition. In contrast, studies by Meyers (1977) and Riech and von Rad (1979b) did not establish causal relationships between unconformities and chert development. Indeed Riech and von Rad (1979b) suggested that dissolution of siliceous organisms and the formation of chert was favoured under increased sedimentation rates. In the Mead Hill Formation, significant changes in sedimentation patterns can only be inferred with certainty to have occurred at the base of the Upper and Lower Chert Members. Sedimentation patterns immediately following the unconformity in both cases were different from those above and below the Chert Members. Sediments deposited on the unconformities at the base of both Chert Members contain a greater abundance of detrital material and are more intensively chertified than CL Zone sediments. Immediately below the unconformity at the base of the Lower Chert Member is the basal dolomite bed of the LCM Subzone [Section 2.2.8]. In this study unconformities and associated changes in sedimentation have influenced chert and dolomite formation in parts of the sequence.

6.3. GENESIS OF WC ZONE CONCRETIONS

Deposition of the Woolshed Formation began in the northern part of the field area and spread rapidly southwards (Morris 1987). Concretion development probably first occurred at depocentre localities such as at Isolation Creek (20). The development of concretions soon after sediment deposition, the occurrence of concretions up to 100 m below the Amuri Limestone Group, plus separation of Amuri Limestone Group and Woolshed Formation sediments by an unconformity that post-dates concretion formation [see discussions in Chapters 2 and 4] all indicate that concretion development occurred independently of chertification and dolomitization of the Amuri Limestone Group.

Concretion formation is summarized diagrammatically in Figure 6.1 [Map pocket].

The Sr and ^{13}C data are interpreted as indicating that concretions formed by early dolomitization of very early diagenetic calcite, which was precipitated in the upper sediment column in the zone of sulphate reduction. Dolomitization of early diagenetic calcite also resulted in relatively complex ^{18}O contours (compared to ^{13}C which is more stable) in the Lab Rocks (4) concretion [sample KP3, Sections 4.4.2 and 4.4.3].

One of the most important factors in the generation of early diagenetic calcite is the abundance and distribution of organic matter in the sediment. The distribution and abundance of organic matter resulted from a combination of primary depositional processes and sediment reworking due primarily to bioturbation. Biogenic metabolism of organic matter, which occurred during bacterial sulphate reduction, generated HCO_3^- which is inferred to have contributed to precipitation of calcite [Figure 4.13]. In addition, reactions such as ammonification and nitrate reduction (both of which are bacterially mediated and also occurred in the sulphate reduction zone) may also have contributed to carbonate precipitation [see Sections 4.4.3 and 3.2.1, Figure 4.13]. Some of the H_2S produced from the reduction of SO_4^{2-} was removed by precipitation as Fe (or Mn) sulphides, but the bulk was probably lost by diffusion.

Calcite precipitation was probably also governed by the availability of Ca^{2+}. Pore waters at the site of HCO_3^- generation would have been the

initial source of Ca^{2+}. Depletion of this source by calcite precipitation would result in a Ca^{2+} concentration gradient. Diffusion of Ca^{2+} from adjacent pore waters and ultimately from overlying seawater could then occur. The extent of diffusion (or fluid migration if it occurred) was governed by the porosity and permeability of the sediment. Poor permeability and/or porosity limited Ca^{2+} diffusion, and hence the extent of calcite precipitation. In addition to providing Ca^{2+}, diffusion and/or fluid migration must have supplied the necessary Mg^{2+} for dolomitization.

The precipitated calcite was then dolomitized. Any primary carbonate present may also have been dolomitized, although it is important to note that fossils were commonly preserved [e.g. Figure A5.14e,f] rather than being destroyed. Dolomitization occurred soon after precipitation of diagenetic calcite. Complete occlusion of porosity (as would have occurred from formation of a complete concretion) was unlikely as only concretion exteriors would have been dolomitized. However, dolomitization could not commence until SO_4^{2-} concentrations at the site of calcite precipitation were reduced to levels that did not inhibit the precipitation of dolomite. The exact concentrations of sulphate below which dolomite will precipitate have not been accurately determined. Baker and Kastner (1981) claim that SO_4^{2-} levels of less than 5% of normal seawater (approximately 1400 ppm) inhibit dolomite formation. Other workers have found dolomite forming in environments where relatively high levels of SO_4^{2-} are present. For example, De Dekker and Last (1988) investigated dolomite formation in lakes where mean SO_4^{2-} concentrations were up to approximately 8000 ppm. It is possible that under some circumstances other factors, such as very high alkalinity, may override the inhibitory effects of SO_4^{2-}.

The inhibitory effect of SO_4^{2-} on dolomite precipitation may have been the underlying cause for the initial precipitation of calcite rather than dolomite. Once SO_4^{2-} concentrations had been adequately reduced dolomitization of calcite occurred, very probably contemporaneously with calcite precipitation. The Ca^{2+} liberated by dolomitization [see equation 4.4] would have been available for further calcite precipitation, as shown below (from Jeans 1980, Machel and Mountjoy 1986):

$$Ca^{2+} + SO_4^{2-} + C + 4H \rightarrow CaCO_3 + H_2S + H_2O$$

$$\uparrow \qquad\qquad\qquad\qquad \downarrow$$

$$(1\text{-}x)Ca^{2+} + CaMg(CO_3)_2 \leftarrow (2\text{-}x)CaCO_3 + Mg^{2+} + xCO_3^{2-}$$

where C and H represent organically-bound food for bacteria (Jeans 1980). Analysis of Fe, Mn, and ^{13}C in the Lab Rocks (4) concretion (sample KP3) indicate progressive burial through the sulphate reduction zone, and probably into the bacterial fermentation zone during concretion growth [Section 4.4.3]. Similar histories are inferred for other concretions which could not be as comprehensively sampled. As organic matter is buried, ^{12}C is preferentially metabolized by bacteria, resulting in a relative increase in ^{13}C in remaining organic matter. Thus with depth, progressively more ^{13}C is incorporated in precipitated carbonate, producing the concentric increase in ^{13}C seen in KP3. Concentric increases in Fe and Mn concentrations probably reflect a relative decrease in the amount of H_2S produced. With lower H_2S production, less Fe and Mn were removed by sulphide precipitation and potentially more could be incorporated into the carbonate.

Since only the exteriors of many concretions could be sampled, their $\delta^{13}C$ signatures reflect the most recent carbon sources. In heavy carbon group concretions [Figure 4.9a], the most recent carbon was derived from the vicinity of the boundary between the zones of sulphate reduction and bacterial fermentation. This boundary is usually about 10-20 m below the sediment-water interface [Figure 4.13]. By inference, concretion formation must have been initiated at shallower depth. Light carbon group samples contain carbon derived from the oxidation of methane [Section 4.4.3]. Incorporation of this methane-derived carbon appears confined to the basin depocentre. Relatively greater accumulation rates for basin centre sediments compared to basin margin sediments were inferred by Morris (1987). A relatively greater amount of unmetabolized organic matter may have been buried into the bacterial fermentation zone than in basin margin areas. This resulted in a relatively higher production of methane than occurred in basin margin sediments. The incorporation of methane-derived carbon into concretions probably became more significant with burial into the bacterial fermentation zone during the latter stages of concretion growth.

Cessation of concretion growth occurred when concentrations of SO_4^{2-} and/or organic matter became insufficient to support suitable levels of sulphate reducing bacteria. Without sulphate reduction the production of HCO_3^- decreased. Limited quantities of organic matter in sediments below the sulphate reduction zone also restricted the amount of anaerobically produced HCO_3^-. Exhaustion of available Ca^{2+} and Mg^{2+} because of burial to depths below which these ions can diffuse from seawater also halted dolomite precipitation. After concretion formation, progressive burial caused the compaction of surrounding sediments. Later erosion of Woolshed Formation sediments from basin margin localities exhumed some concretions which were subsequently phosphatized and bored.

Although concretions are currently found at the top of the Woolshed Formation in basin margin localities, they may not necessarily have formed in the uppermost sediments prior to erosion. However, because concretions are found only near the top of the Woolshed Formation in the depocentre where there appears to have been no erosion, it is likely that concretion formation may have been restricted to the upper Woolshed Formation at other localities. The amount of material removed by erosion is (as yet) unknown.

6.4. GENESIS OF CHERT AND DOLOMITE IN THE AMURI LIMESTONE GROUP

6.4.1. DERIVATION OF SILICA

Silica from Biogenic Sources

Abundant radiolaria have been found in CL and ML Zone micrites (C. Hollis *pers. comm.* 1988). Although their abundance in heavily chertified units is unknown, it is possible that similar siliceous components existed in all units. Thus, in all units, siliceous tests were probably the earliest source of SiO_2 because biogenic silica dissolves relatively quickly, particularly in carbonate-rich sediments [Section 5.3.1]. The importance of biogenic silica as a source increased stratigraphically upwards and towards basin margins, as the relative upward movement of clay mineral derived silica from the Woolshed Formation decreased.

The LCM Subzone, although containing a slightly greater amount of detrital material is essentially a heavily chertified version of the CL Zone. The

question is whether adequate silica can be derived from biogenic sources alone to extensively chertify this interval. Morris (1987) infers that the Claverley Sandstone and the Lower Chert Member were in part coeval. Conceivably, SiO_2 derived from the Woolshed Formation may have migrated up-dip along the Claverley Sandstone. However, at localities such as Branch Stream (28,29), the Lower Chert Member and Claverley Sandstone are separated by approximately 100 m of CL Zone. Lateral removal of SiO_2-rich pore waters from the depocentre would have reduced the extent of chertification in the BC and CD Zones. In addition, more extensive chertification of the CL Zone overlying the Claverley Sandstone might also be expected. A supply of SiO_2 via the Claverley Sandstone is therefore discounted. Although the LCM Subzone contains more detrital material than is found in the CL Zone, quantities are considerably less than in the BC Zone. Thus SiO_2 derived from *in situ* clay mineral reactions would have been limited. Volcanic and hyrdrothermal inputs are discounted [Section 5.3.2]. Either there was a significant increase in the amount of biogenic silica deposited compared to the CL Zone, or some post-depositional concentration of the siliceous material occurred.

An increase in biogenic silica productivity is a simple means of obtaining an enlarged silica supply. Indeed, Morris (1987) inferred that the Lower Chert Member was deposited as a siliceous ooze. However, in the field, the Lower Chert Member appears to consist of highly chertified micrites [Section 2.2.8]. Other than the presence of the chert itself, there is no direct evidence for increased silica production. However, an increase in biogenic silica supply cannot be totally discounted.

Nelson (1985) interpreted increases in the abundance of foraminifera in DSDP carbonates to be caused by periods of enhanced winnowing of fine particles by bottom currents. Sediment accumulation rates on the unconformity at the base of the Lower Chert Member could also have been slow due to winnowing of fine material. Siliceous tests and precipitated authigenic silica may have been left concentrated in the coarse fraction. The upward decrease in chert in the LCM Subzone would thus reflect the decreasing influence of winnowing and the resumption of 'normal' Mead Hill Formation sedimentation. However, the LCM Subzone occurs within the Mead Hill Formation basin on what is envisaged as an even pelagic surface. Such a scenario places restrictions on the direction of movement of winnowed sediments, and where and how such sediments could accumulate.

The only plausible movement direction would have been along the axis of the basin in what is now a northwesterly direction [see Figure 2.2]. Possibly chert formed at basin margin localities (e.g. Chancet Rocks 18) may have in part been influenced by the post-depositional concentration of siliceous material by winnowing. Winnowed sediments from basin margins would have been deposited downslope in the basin. However, arguments that invoke sediment winnowing also require a reason for the cessation of production of larger foramininfera, as they too should be concentrated as a lag. No evidence of such lags have been found and there is no obvious reason for the discontinuation of production of large foraminifera. An alternative to winnowing is the selective dissolution of $CaCO_3$. Like winnowing, carbonate dissolution would also have resulted in slow overall sediment accumulation rates, a relative increase (compared to $CaCO_3$) of siliceous tests or precipitated silica, and could explain the greater abundance of detrital material in LCM Subzone chert than in CL Zone chert. In addition, the problems of removal and redeposition of sediment and foraminifera production are alleviated. The cause of selective carbonate dissolution would have been an influx of cold ocean water into the basin. Although there is no direct evidence for such an influx, selective carbonate dissolution is possibly a more plausible cause of LCM Subzone chertification than winnowing. Carbonate dissolution may also have been a contributory factor in the chertification of other Zones.

Silica from Inorganic Sources

Mass balance estimates suggest that biogenic silica alone could not supply the quantities of SiO_2 required to chertify units in the basin centre such as the BC Zone. Silica adsorbed onto oxides and hydroxides, and derived from clay mineral transformations represent the only plausible additional sources [Section 5.3.2].

Silica adsorbed onto oxides and hydroxides of Fe and Mn in particular, could have been made available for early silica deposition. The reduction of Fe^{3+} and Mn^{3+} and subsequent precipitation as sulphides would liberate any adsorbed SiO_2. This silica source may have been of most significance in detrital-rich units such as the BC Zone and the UCM Subzone.

Clay mineral derived silica came from either the Woolshed Formation, or from clay mineral transformations that occurred at or near the site of

chert deposition. Silica derived from clay mineral transformations deeper within the Woolshed Formation was deposited after Amuri Limestone Group sediments were displaced downward through SiO_2-rich pore waters as a result of compaction. The pore waters essentially remained static but the nett effect was relative upward migration with respect to the sediment. Deposition of such silica is likely to post-date silica from very early biogenic sources since such pore waters do not necessarily reach depositional surfaces (see Bonham 1980). The amount of relative upward migration of dissolved SiO_2 would be dependent upon the physical properties of the sediment (such as porosity and permeability) through which the pore waters travelled. Simplistically one could envisage fluids being progressively depleted in SiO_2 as sediments were compacted down through the pore waters. Thus, a given volume of water precipitated progressively less silica as it passed up through overlying sediments. The result is the overall upward stratigraphic decrease in chert abundance, which with the exception of the LCM and UCM Subzones, is observed in the Mead Hill Formation. Lower chert volumes at basin margins may reflect the restriction of these limited SiO_2-rich fluids to the basin centre.

The derivation of silica from clay mineral reactions at or near the site of chertification would not have occurred until the sediments were buried to depths where temperatures were of the order of 50°C. It is therefore suggested that such clay mineral transformations provided silica for the latest stages of diagenesis, particularly in sediments containing detrital material (e.g. BC Zone, UCM Subzone). Dolomite beds also appear to have formed in slightly more detrital-rich parts of the sediment than the chert [Section 4.2.2]. Clay minerals therein may have provided some of the silica for chertification of the matrix between dolomite crystals, and possibly Mg^{2+} for any late stage dolomite that may be present.

6.4.2. MECHANISMS FOR CHERT AND DOLOMITE FORMATION

Chert and dolomite formation in the Amuri Limestone Group can be divided into three categories:

i) Precipitation of predominantly opal-CT in relatively detrital-rich units; the upper WC Zone, BC Zone, and UCM Subzone.

ii) Precipitation in micritic sediments of silica as opal-CT or quartz, and the precipitation of dolomite; the CD Zone and LCM Subzone.

iii) Precipitation in micritic sediments of silica as either opal-CT or quartz, with no dolomite precipitation; the CL Zone, and ML Zone.

Chert in Detrital-Rich Sediments - BC and upper WC Zone, UCM Subzone

The initiation of silica deposition in the BC Zone resulted from the oxidation of H_2S produced by sulphate reduction [Section 5.3.1, Figure 6.2]. Sulphate reduction commenced very soon after deposition of the sediment causing an increase in alkalinity, generation of H_2S [Equation 5.1], and a decrease in SO_4^{2-} concentrations. Increases in alkalinity (hence pH) aided the dissolution of biogenic silica in the sediment. As for WC Zone concretions, dissemination of organic matter throughout the sediment was important in determining the extent and site of sulphate reduction. Oxidation of H_2S occurs from contact with molecular O_2 and from contact with unreduced Fe^{3+}. The relatively high abundance of Fe-oxides in BC Zone sediments implies that the latter process may have been relatively more significant than in detrital-poor Zones, particularly during the early stages of diagenesis. Reduced pH due to oxidation of H_2S promoted silica precipitation and carbonate dissolution. The very early precipitated silica acted as 'seed' crystals for continued deposition of silica. Seed crystals were continuously produced as sulphate reduction proceeded. Unlike the CD Zone, dolomite precipitation was severely limited. Despite sulphate reduction, SO_4^{2-} concentrations were such that dolomite formation was inhibited, or the rate of H_2S oxidation and extent of silica deposition was such that pH conditions prevented carbonate precipitation. A combination of both factors probably occurred. The extent of BC Zone chertification implies high levels of SiO_2 in pore waters, which would have removed large quantities of Mg^{2+} during precipitation. In addition, abundant oxides and hydroxides compared to sediments such as in the CD or CL Zones, may have facilitated high rates of H_2S oxidation and maintained relatively high levels of SO_4^{2-}, allowing calcite but not dolomite to precipitate.

With progressive burial, compaction and/or pressure solution of less cemented beds or parts of beds around centres of early cementation produced nodular bedding. Where cementation was relatively homogeneous only limited differential compaction occurred.

In time, virtually all the BC Zone sediment was chertified, probably

because of its stratigraphic proximity to the Woolshed Formation silica source. Silica could have been derived from clay mineral transformations within the BC Zone during later stages of diagenesis. Silica deposited in the sulphate reduction zone provided nucleation sites for later precipitation during burial and following compaction.

Eventually opal-CT converted to quartz via a solution-precipitation process [Sections 5.2.4 and A7.3.3]. The silica conversion probably commenced at localized sites throughout the sediment. By this stage the sediment porosity was likely to be so low that major exchanges with bulk fluids were unlikely. Only very small ^{18}O fractionations between opal-CT and quartz resulted [Section 5.2.4].

The thinly bedded cherts of the UCM Subzone, the thin cemented beds of the WC Zone at Kaikoura Peninsula (3,4), and the relatively thin chertified beds of the upper WC Zone and lowermost BC Zone at Isolation Creek (20) are volumetrically minor compared to BC Zone chert. Chertification in these thin beds is inferred to have occurred after compaction. However, direct evidence of post-compaction chertification is only found at South Bay (3) where the thickness of beds within a concretion exceeds that of the surrounding sediment. The UCM Subzone contains the most conspicuous evidence of siliceous organisms found in this study [Figure A6.16]. However, they are well preserved implying only limited mobilization of biogenic silica. The most likely silica source in this unit was from clay mineral transformations within the sediments. The same is suggested for Woolshed Formation sediments at Kaikoura Peninsula, but possibly with a minor biogenic silica input. Thin chertified beds at Isolation Creek could have derived silica from either *in situ* clay mineral reactions and biogenic sources, or were silicified during later diagenesis after compaction through SiO_2-rich fluids.

Chert and Dolomite in Micritic Sediments - CD Zone, LCM Subzone

Deposition of authigenic silica in the CL Zone and LCM Subzone was as indicated for the BC Zone. However, if oxidation of H_2S by unreduced Fe^{3+} occurred, it was probably much less common than in the BC Zone because of the lower detrital content. The inferred higher primary calcite content of the CD Zone implies that significant direct quartz precipitation occurred [Sections 5.1.3 and A7.3.3], as well as opal-CT deposition. The

most significant difference from the BC Zone was the production of abundant dolomite. The diagenetic sequence is shown diagrammatically in Figure 6.2 [Map pocket].

It is inferred that both dolomite and silica initially nucleated contemporaneously at disseminated sites in the upper sediment column. Dolomite nucleated at localized sites of very low SO_4^{2-} concentration, and silica precipitated at localized sites of reduced pH. At sites of high alkalinity and high SO_4^{2-}, calcite recrystallized until SO_4^{2-} concentrations decreased to levels where dolomite could precipitate. With the rate of dolomite crystallization being faster than the rate of silica precipitation, the abundance of dolomite crystals disseminated through parts of the sediment during early stages of diagenesis was probably greater than the abundance of nucleated opal-CT or quartz. Some beds or parts of beds were rapidly dolomitized in response to higher organic matter levels which enabled significant sulphate reduction to occur. At such sites of relatively greater dolomite precipitation, silica nucleation was limited because of high alkalinity, and possibly by removal of Mg^{2+} by dolomitization [the role of Mg^{2+} in silica precipitation is discussed in Sections 5.3.1 and A7.3.3]. Additional supplies of Ca^{2+} and HCO_3^- for dolomitization were derived from the dissolution of calcite by adjacent chertification. Exhaustion of Mg^{2+} supplies caused the cessation of dolomite formation, although calcite recrystallization could have continued. Any recrystallized calcite could later be chertified. Diffusion of Mg^{2+} decreased due to burial to depths below the zone of effective seawater diffusion, and occlusion of porosity (by either chertification or dolomitization) which prevented the movement of Mg^{2+} to the site of dolomite nucleation. Dolomitization would have also ceased if the supplies of organic food were such that populations of sulphate reducing bacteria could not be adequately supported, thereby causing a build up in SO_4^{2-} concentrations.

The basal dolomite bed of the LCM Subzone was formed by a modification of the process described above. The Lower Chert Member overlies an unconformity, the nature of which has not been definitely identified. There is no direct evidence for significant erosion, although it certainly represents a period of non-deposition (see also Morris 1987). It is inferred that the hiatus enabled the sediments immediately below the unconformity to remain within the zone of sulphate reduction long enough

for SO_4^{2-} concentrations to be reduced to levels below which dolomite precipitated. In addition, these sediments remained within the zone of effective seawater diffusion long enough to enable almost complete dolomitization.

During rapid dolomitization of parts of the sediment, progressive silicification continued elsewhere. Reductions in pH and removal of Mg^{2+} by silica nucleation would have slowed dolomite genesis. Progressively, disseminated dolomite crystals and areas of major dolomitization were isolated by chertification, resulting in dolomite crystals (and also pyrite) enclosed in silica. The greater resistance of dolomite to dissolution compared to calcite resulted in the surrounding primary or recrystallized calcite being replaced and the dolomite being left 'floating' in the chert.

Chertification continued as sediments were buried to depths below the SO_4^{2-} reduction zone, and as dolomitization decreased. Compaction effects increased with increasing burial. As in the BC Zone, less cemented parts of beds were compacted around relatively cemented sediments. Contorted beds and features such as flame structures or chert dikes were formed. It is envisaged that at this stage the sediments were in a 'plastic' state and significant fluid filled porosity still existed. Complete chertification of contorted or compacted beds, and the intercrystalline matrix in dolomite beds occurred during later stages of diagenesis.

Chert in Micritic Sediments - CL and ML Zones

The bulk of silica was deposited as described in the BC and CD Zones. However, in the BC and CD Zones, the influence of burrowing could only be inferred. At the bulk of CL Zone localities, visible burrows are preserved in chert but have not been preferentially silicified, indicating an indirect influence on chertification. Bioturbation influenced the organic matter distribution, sediment porosity and permeability, which in turn influenced the sites of silica nucleation.

More direct influences of burrowing on chertification are found in CL Zone cherts at Woodside Creek (12) and localities further north, and a number of ML Zone cherts. Chert halos probably formed according to the mechanism outlined by Clayton (1986). Sulphate reduction within the centre of the

structure produced H_2S which diffused outwards. Oxidation of the H_2S caused the precipitation of silica, with calcite being precipitated in the centre. The restriction of chertification to within the margins of preferentially silicified burrows (which generally appear to be *Thalassinoides*, Section A2.5) suggests that H_2S did not diffuse beyond burrow margins. Perhaps such burrows penetrated partially lithified (calcite cemented) sediments. The higher porosity and permeability of the burrows compared to surrounding sediments may have resulted in restriction of H_2S generation to the burrows at the critical time in diagenesis during which SiO_2 was available for precipitation.

The genesis of nodular and/or contorted chert beds was similar to that of underlying Zones. However, chert generally becomes less nodular stratigraphically upwards. As in underlying sediments, nucleation of silica in chert bands, nodules, or planar beds was probably initiated during early diagenesis. Despite early nucleation, the lower availability of SiO_2 compared with that in underlying sediments resulted in generally slow chertification. In some instances a greater amount of compaction occurred prior to complete chertification, with only a few sites in the sediments where significant early nodule development occurred. Early calcite recrystallization may have been limited and would have further predisposed beds to compaction. This resulted in relatively thinner beds containing chert bands and mixtures of nodules and chert bands such as shown in Figures A2.23 and A2.24. Relatively thick planar beds indicate resistance to early compaction. Such beds are usually siliceous throughout and commonly contain pale grey or diffuse chert nodules [e.g. Figure A2.22]. Significant differential compaction was prevented by widespread early calcite recrystallization and silica cementation. However, the reduced supply of SiO_2 compared to underlying Zones resulted in limited chertification, and produced diffuse rather than dark intensively chertified nodules.

6.5. SEQUENCE OF DIAGENETIC EVENTS

The diagenetic sequence of events in the Amuri Limestone Group and Woolshed Formation parallel the depositional sequence described by Morris (1987), and is described below as well as shown diagrammatically in Figure 6.3 [Map pocket]. Deposition occurred in a progressively subsiding trough (Morris 1987).

1) Woolshed Formation sediments are deposited in the central basin and progressively further south. Concretion formation occurs in the upper Woolshed Formation (WC Zone) in the vicinity of the depocentre.

2) Woolshed Formation sedimentation continues. Concretion formation continues in the basin centre and progresses southwards. The generation of SiO_2 from clay mineral transformations in sediments buried in the basin centre may have commenced. The compaction of the very earliest Woolshed Formation sediments in the basin centre may have been initiated.

3) Deposition of Woolshed Formation sediments progresses to basin margins as does WC Zone concretion formation. WC Zone concretion formation ceases in the depocentre. Sedimentation patterns in the basin centre change with increasing deposition of pelagic (?siliceous) carbonate. Significant compaction of Woolshed Formation sediments occurs. Amuri Limestone Group sediments are compacted down through SiO_2-rich pore waters derived from the Woolshed Formation. Silicification of pelagic carbonate commences (BC Zone).

4) All WC Zone concretion formation ceases. Woolshed Formation sediments in the southern margin of the basin are eroded and exhumation of some concretions occurs. Claverley Sandstone deposition is initiated, some of which interrupts BC Zone sedimentation and chertification. Deposition of BC Zone sediments and chertification thereof continues.

5) Continued deposition of (possibly siliceous) micrite occurs in the basin centre. Chertification diminishes, probably due to the reduced supply of Woolshed Formation-derived silica. Dolomite formation becomes significant in the basin centre (CD Zone), but little or no dolomite formation occurs in micrites (CL Zone) immediately to the north and south of the depocentre. Claverley Sandstone deposition probably occurs in the southern margin of the basin. Late stage BC Zone chertification occurs.

6) Deposition of micrite ooze continues and extends further to the north and south of the depocentre than previously. Dolomitization in the depocentre ceases, but chert formation continues (CL Zone) as does late stage chertification of the CD Zone. Supplies of Woolshed Formation derived SiO_2 further diminish.

7) A hiatus in micrite deposition enables the development of the LCM Subzone basal dolomite bed in the basin centre, followed by development of LCM Subzone chert and dolomite.

8) Micrite deposition as in 6) recommences throughout the field area with continued formation of CL Zone cherts until development of the sub-Teredo unconformity. Late stage chertification probably occurs in the lower CL Zone.

9) The Teredo Limestone and equivalent sediments are deposited. Chertification of the UCM Subzone is initiated.

10) Micrite deposition occurs as in 8), but becomes progressively more detrital rich (marls). Late stage chertification of underlying sediments continues.

11) Deposition and diagenesis of the remaining Amuri Limestone Group with only minor chertification.

6.6. GENERAL IMPLICATIONS OF THE STUDY

The results and interpretations of this study give rise to a number of implications for generalized models of dolomitization and chertification.

1) The deposition of both chert and dolomite as a result of sulphate reduction is another example of how early diagenesis is influenced by biological processes in sediments. Diagenetic reactions are commonly treated purely as inorganic processes and biological factors are ignored. Biological interaction probably overcomes many of the kinetic or thermodynamic barriers to early diagenetic reactions which, from purely inorganic considerations, appear not to be feasible.

2) Processes which result in wholesale alteration of sediments, such as the chertification and dolomitization of Amuri Limestone Group sediments, can be initiated at a very localized scale in the sediment. The implication is that dolomitization or chertification may commence without products equilibrating with the bulk solution (see also Maliva and Siever 1988). Thus, as suggested in this study, data such as $\delta^{18}O$ may reflect highly localized variations in composition rather that the bulk fluid

composition.

3) Dolomite formation does not necessarily require the presence of pre-existing depositional carbonate (see also Baker and Burns 1985).

4) The concept of sediments compacting through a water column has been noted by some authors (e.g. Bonham 1980). However, to the knowledge of the author of this thesis such a mechanism is seldom invoked for the delivery of diagenetic fluids. More consideration of this mechanism should be given in other diagenetic environments, particularly in chertification where in many cases siliceous microfossils are simply assumed to be the primary silica source. Mass balance estimates suggest that even radiolarites may require additional SiO_2 for complete sediment chertification. Relative upward migration seems a most suitable delivery mechanism.

6.7. SUGGESTIONS FOR FUTURE WORK

1) A study of the diagenetic modifications to the Woolshed Formation particularly in the basin centre should be carried out. Clay mineralogy needs to be investigated with a view to finding evidence for clay mineral transformations, and possibly quantifying the amount of silica that could be produced therefrom. Evidence for dissolution of sand and silt grains should also be investigated and possibly quantified. Finally, the feasibility and direction of transport of silica so produced needs to be accurately evaluated.

2) Chapter 3 of this thesis proposed an origin for marl-micrite alternations in the Amuri Limestone Group. However, the data presented is limited and an integrated study of marl-micrite geochemistry and sedimentology is required to determine their origin with more certainty. In addition, it may be worth studying the stable isotope stratigraphy of unchertified micrites, for comparison with the DSDP record.

3) A more rigorous study of zonation patterns in Amuri Limestone Group dolomite crystals is required than presented in this thesis.

4) Radiolaria and diatoms of both the Woolshed Formation and Amuri Limestone Group need to be studied in some detail. Such studies would

provide greater insight as to the significance of biogenic silica in Amuri Limestone chertification, and may help improve the chronostratigraphy.

5) The cysts of dinoflagellates consist of tough, acid resistant organic polymer. Studies of dinoflagellates may provide a relatively reliable biostratigraphy of intensively chertified units.

6) A detailed study of the sulphide minerals is required to verify their inferred origins. Work should include sulphur isotope studies to determine the relative timing of pyrite genesis and whether it occurred in an open or closed system. Such a study should also be done in association with studies of organic matter in the sediments.

7) On a more speculative note, there may have been some regional control on factors involved in WC Zone concretion genesis. Other sediments in New Zealand of similar age and type to the Woolshed Formation also contain concretions. These other sediments include the Mangakahia Group in Kaipara (Hodgson 1968), the Moeraki Formation of North Otago (Boles *et al.* 1985), and the Whangai Formation of northern Wairarapa (Moore 1988b). A comparative study of the depositional setting and concretion formation would be required to verify any regional control.

ACKNOWLEDGEMENTS

I wish to thank my supervisors: Dr D.W. Lewis who suggested the topic and critically reviewed drafts of the manuscript; Dr S.D. Weaver for assistance with geochemical analyses, review and discussion of the manuscript, and transport to one day cricket internationals. Dr J.C. Morris is thanked for his considerable assistance in the field. The advice and discussion of some crystallographic and mineralogic aspects of this thesis by Dr D. Shelley is also gratefully acknowledged. I also acknowledge the financial assistance of DSIR Research Contract No. UV/2/43.

The efforts of technical staff are much appreciated. Thanks go to: A. Alloway (Geol. Dept.) for running XRF analyses and assisting with sample preparation; K. Holder (Geol. Dept.) for producing many of the thin sections; B. Reid (Chem. Dept.) for making the AA spectrophotometer available; K. Swanson (Geol. Dept.), K. Card and N. Andrews (Plant and Microbial Sciences) for SEM work; T. Robinson (Zool. Dept) for the laser printing, A. Downing (Geol. Dept.) for photographic work; C. Wiltshire, D. Jones, A. Nicholas (Geol. Dept.) and J. Smith (NZGS) for putting up with continual harassment for various bits of equipment.

The assistance provided by members at establishments other than the University of Canterbury are also thanked: Dr C. Hendy (Chem. Dept., University of Waikato) for allowing use of the stable C and O isotope evolution line, A. Cuthbertson (Chem. Dept., University of Waikato) for the refresher course in mass spectrometry, Dr Y. Kawachi (Geol. Dept., University of Otago) for use of the microprobe, Dr P. Blattner and C. Houston (INS, Lower Hutt) for chert ^{18}O analyses, and B.D. Field (NZGS, Christchurch) for providing assistance with, and use of the Survey cathodoluminescence microscope.

Farmers of coastal Marlborough are thanked, in particular those who provided accommodation as well as access to their properties: D. and M. Parsons (Benmore), R. Murray (Bluff Station), D. and L. Buick (Blue Mountain Station), and C. Nimmo (Muzzle Station). Access to properties owned by the Cameron brothers (Kaikoura), and B. Thomson (Ward) is also appreciated.

Finally, and in many ways most importantly, I wish to thank my wife Penny for her support, encouragement, and understanding.

REFERENCES

Adams, J.E., Rhodes, M.L. (1960): Dolomitization by seepage refluxion. *American Association of Petroleum Geologists Bulletin* 44(12): 1912-1920.

Aller, R.C., Rude, P.D. (1988): Complete oxidation of solid phase sulfides by manganese and bacteria in anoxic marine sediments. *Geochimica et Cosmochimica Acta* 52(3): 751-765.

Altschuler, Z.S., Dwornik, E.J., Kramer, H. (1963): Transformation of montmorillonite to kaolinite during weathering. *Science* 141(3576): 148-152.

American Public Health Association (APHA) (1975): Standard Methods for the Analysis of Water and Wastewater. 14th Edition. New York. 1193pp.

Amiel, A., Friedman, G.M., Miller, D.S. (1973): Distribution and nature of incorporation of trace elements in modern aragonitic corals. *Sedimentology* 20(1): 47-64.

Andrews, P.B. (1982): Revised Guide to Recording Field Observations in Sedimentary Sequences. New Zealand Geological Survey 102. 74pp.

Armstrong, W.J. (1972): The Amuri Limestone. Unpublished B.Sc. Honours Thesis. University of Canterbury. Christchurch. 72pp.

Astin. T.R. (1987): Petrology (including fluorescence microscopy) of cherts from the Portlandian of Wiltshire, UK - evidence of an episode of meteoric water circulation. *In* Marshall, J.D. (Ed) Diagenesis of Sedimentary Sequences. Geological Society Special Publication No. 36: 73-85.

Audley-Charles, M.G. (1965): Some aspects of the chemistry of Cretaceous siliceous sedimentary rocks from eastern Timor. *Geochimica et Cosmochimica Acta* 29(11): 1175-1192.

Badiozamani, K. (1973): The Dorag dolomitization model - application to the Middle Ordovician of Wisconsin. *Journal of Sedimentary Petrology* 43(4): 965-984.

Baker, P.A. (1985): Pore-water chemistry of carbonate-rich sediments, Lord

Howe Rise, Southwest Pacific Ocean. *In* Kennett, J.J., von der Borch, C.C., *et al.* Initial Reports of the Deep Sea Drilling Project 90: 1249-1256.

Baker, P.A., Burns, S.J. (1985): Occurrence and formation of dolomite in organic-rich continental margin sediments. *American Association of Petroleum Geologists Bulletin* 69(11): 1917-1930.

Baker, P.A., Gieskes, J.M., Elderfield, H. (1982): Diagenesis of carbonates in deep-sea sediments - Evidence from Sr/Ca ratios and interstitial dissolved Sr^{2+} data. *Journal of Sedimentary Petrology* 52(1): 71-82.

Baker, P.A., Kastner, M. (1981): Constraints on the formation of sedimentary dolomite. *Science* 213(4504): 214-216.

Baldwin, B., Butler, C.O. (1985): Compaction curves. *American Association of Petroleum Geologists Bulletin* 69(4): 622-626.

Baltuck, M. (1986): Authigenic silica in Tertiary and upper Cretaceous sediments of the East Mariana Basin, Deep Sea Drilling Project Site 585. *In* Moberly, R., Schlanger, S.D., *et al.* Initial Reports of the Deep Sea Drilling Project 89: 389-398.

Banner, J.L., Hanson, G.N., Meyers, W.J. (1988): Rare earth element and Nd isotopic variations in regionally extensive dolomites from the Burlington-Koekuk Formation (Mississippian): Implications for REE mobility during carbonate diagenesis. *Journal of Sedimentary Petrology* 58(3): 415-432.

Barrett, T.J. (1981): Chemistry and mineralogy of Jurassic bedded chert overlying ophiolites in the north Apennines, Italy. *Chemical Geology* 34(3/4): 289-317.

Barton, D.C. (1918): Notes on the Mississippian chert of the St Louis area. *Journal of Geology* 26(4): 361-374.

Bates, R.L., Jackson, J.A. (Eds) (1984): Dictionary of Geological Terms. 3rd Ed. American Geological Institute. Anchor Press, New York. 571pp.

Bathurst, R.G.C. (1975): Carbonate Sediments and their Diagenesis. 2nd Ed: Developments in Sedimentology 12. Elsevier Scientific Publishing Company, Amsterdam. 658pp.

Bathurst, R.G.C. (1987): Diagenetically enhanced bedding in argillaceous platform limestones: stratified cementation and selective compaction. *Sedimentology* 34(5): 749-778.

Baum, G.R., Harris, W.B., Drez, P.E. (1985): Origin of dolomite in the Eocene Castle Hayne Limestone, North Carolina. *Journal of Sedimentary Petrology* 55(4): 506-517.

Behrens, E.W., Land, L.S. (1972): Subtidal Holocene dolomite, Baffin Bay, Texas. *Journal of Sedimentary Petrology* 42(1): 155-161.

Bender, M.L. (1971): Does upward diffusion supply the excess manganese to pelagic sediments. *Journal of Geophysical Research* 76(16): 4212-4215.

Berger, W.H., von Rad, U. (1972): Cretaceous and Cenozoic sediments from the Atlantic Ocean. *In* Hayes, D.E., Pimm, A.C., *et al*. Initial Reports of the Deep Sea Drilling Project 14: 787-954.

Berggren, W.A., Hollister, C.D. (1974): Paleogeography, paleobiology and the history of circulation in the Atlantic Ocean. *In* Hay, W.W. (Ed) Studies in Paleo-oceanography. Society of Economic Paleontologists and Mineralogists Special Publication No.20: 126-186.

Berner, R.A. (1968): Rate of concretion growth. *Geochimica et Cosmochimica Acta* 32(5): 477-483.

Berner, R.A. (1978): Iron. Behaviour during weathering, sedimentation and diagenesis. *In* Wedepohl, K.H. (Ed) Handbook of Geochemistry Volume II/3. 26/6/1-26/6/8.

Berner, R.A. (1980): Early Diagenesis: A Theoretical Approach. Princeton University Press. Princeton, New Jersey. 241pp.

Berner, R.A. (1984): Sedimentary pyrite formation: An update. *Geochimica et Cosmochimica Acta* 48(4): 605-615.

Berner, R.A. (1985): Sulphate reduction, organic matter decomposition, and pyrite formation. *Philosophical Transactions of the Royal Society of London* A315: 25-38.

Bhattacharyya, A., Friedman, G.M. (1984): Experimental compaction of ooids under deep-burial diagenetic temperatures and pressures. *Journal of Sedimentary Petrology* 54(2): 362-372.

Bjørlykke, K. (1973): Origin of limestone nodules in the Lower Paleozoic of the Oslo region. *Norsk Geologisk Tidsskrift* 53(4): 419-431.

Blatt, H. (1987): Oxygen isotopes and the origin of quartz. *Journal of Sedimentary Petrology* 57(2): 373-377.

Blatt, H., Middleton, G., Murray, R. (1980): Origin of Sedimentary Rocks. 2nd Edition. Prentice-Hall. Englewood Cliffs, New Jersey. 782pp.

Boles, J.R., Franks, S.G. (1979): Clay diagenesis in Wilcox sandstones of southwest Texas: implications of smectite diagenesis on sandstone cementation. *Journal of Sedimentary Petrology* 49(1): 55-70.

Boles, J.R., Landis, C.A., Dale, P. (1985): The Moeraki Boulders - anatomy of some septarian concretions. *Journal of Sedimentary Petrology* 55(3): 398-406.

Bonham, L.C. (1980): Migration of hydrocarbons in compacting basins. *In* Roberts, W.H., Cordell, R.J. (Eds) Problems of Petroleum Migration. American Association of Petroleum Geologists Studies in Geology No. 10: 69-88.

Bramlette, M.N. (1946): Monterey Formation of California and origin of its siliceous rocks. United States Geological Survey Professional Paper 212.

Brand, U., Veizer, J. (1980): Chemical diagenesis of multicomponent carbonate system - 1: Trace elements. *Journal of Sedimentary Petrology* 50(4): 1219-1236.

Bromley, R.G., Ekdale, A.A. (1984): Trace fossil preservation in flint in the European Chalk. *Journal of Paleontology* 58(2): 298-311.

34(6): 1079-1092.

Bromley, R.G., Ekdale, A.A. (1986): Flint and fabric in the European Chalk. *In* Sieveking, G.de G., Hart, M.B. (Eds) The Scientific Study of Flint and Chert. Proceedings of the Fourth International Flint Symposium held at Brighton Polytechnic, 10-15 April 1983: 71-82.

Bromley, R.G., Schulze, M.G., Peake, N.B. (1975): Paramoudras: giant flints, long burrows and early diagenesis of chalks. *Biologiske Skrifter Danske Videnskabernes Selskab* 20(10): 1-31.

Brooks, R.R., Hoek, P.L., Reeves, R.D., Strong, G.P. (1986): Geochemical delineation of the Cretaceous/Tertiary boundary in some New Zealand sequences. *New Zealand Journal of Geology and Geophysics* 29(1): 1-8.

Brooks. R.R., Hoek, P.L., Reeves, R.D., Wallace. R.C., Johnston, J.H., Ryan, D.E., Holzbecher, J., Collen, J.D. (1985): Weathered spheroids in a Cretaceous/Tertiary boundary shale at Woodside Creek, New Zealand. *Geology* 13(10): 738-740.

Brooks, R.R., Reeves, R.D., Yang, X-H., Ryan, D.E., Holzbecher, J., Collen, J.D., Neal, V.E., Lee, J. (1984): Elemental anomalies at the Cretaceous/Tertiary boundary, Woodside Creek, New Zealand. *Science* 226(4674): 539-542.

Browne, G.H. (1985): Dolomite concretions in Late Cretaceous sediments at Kaikoura Peninsula, Marlborough. *New Zealand Geological Survey Record* 8: 120-127.

Brownlow, A.H. (1979): Geochemistry. Prentice-Hall. New Jersey. 498pp.

Brueckner, H.K., Snyder, W.S. (1985): Chemical and Sr-isotope variations during diagenesis of Miocene siliceous sediments of the Monterey Formation, California. *Journal of Sedimentary Petrology* 55(4): 553-568.

Buchanan, J. (1868): Kaikoura District. New Zealand Geological Survey. Report of Geological Explorations No.4: 34-41.

Bullen, S.B., Sibley, D.F. (1984): Dolomite selectivity and mimic

replacement. *Geology* 12(11): 655-658.

Burdige, D.J., Gieskes, J.M. (1983): A pore water/solid phase diagenetic model for manganese in marine sediments. *American Journal of Science* 283(1): 29-47.

Burns, D.A. (1980): Aspects of the Oxygen Isotope Geochemistry of some New Zealand Cenozoic Calcareous Sediments. Unpublished M.Sc. Thesis. University of Waikato. Hamilton. 141pp.

Burns, S.J., Baker, P.A. (1987): A geochemical study of dolomite in the Monterey Formation, California. *Journal of Sedimentary Petrology* 57(1): 128-139.

Buurman, P. (1976): Biogenic and inorganic cherts *Staringia* 3: 23-25.

Calderoni, G., Ferrini, V., Masi, U. (1988): Geological significance of trace-element abundances in the "Red Scaglia" limestones from Gubbio (central Italy). *Chemical Geology* 67(1-2): 63-74.

Calvert, S.E. (1968): Silica balance in the oceans and diagenesis. *Nature* 219(5157): 919-920.

Calvert, S.E. (1971): Composition and origin of North Atlantic deep-sea cherts. *Contributions to Mineralogy and Petrology* 33(4): 273-288.

Calvert, S.E. (1974): Deposition and diagenesis of silica in marine sediments. *In* Hsü, K.J., Jenkyns, H.C. (Eds) Pelagic Sediments: on Land and Under the Sea. International Association of Sedimentologists Special Publication No.1: 273-299.

Calvert, S.E. (1977): Mineralogy of silica phases in deep-sea cherts and porcelanites. *Philosophical Transactions of the Royal Society of London* A286: 239-252.

Carballo, J.D., Land, L.S., Miser, D.E. (1987): Holocene dolomitization of supratidal sediments by active tidal pumping, Sugarloaf Key, Florida. *Journal of Sedimentary Petrology* 57(1): 153-165.

Carroll, D. (1958): Role of clay minerals in the transportation of iron.

Geochimica et Cosmochimica Acta 14(1-2): 21-26.

Channell, J.E.T., Freeman, R., Heller, F., Lowrie, W. (1982): Timing of diagenetic haematite growth in red pelagic limestones from Gubbio (Italy). *Earth and Planetary Science Letters* 58(2): 189-201.

Chave, K.E., (1952): A solid solution between calcite and dolomite. *Journal of Geology* 60(2): 190-192.

Chilingar, G.V. (1956): Relationship between Ca/Mg ratio and geologic age. *American Association of Petroleum Geologists Bulletin* 40(9): 2256-2266.

Chilingar, G.V., Zenger, D.H., Bissel, H.J., Wolf, K.H. (1979): Dolomites and dolomitization. *In* Larsen, G., Chilingar, G.V. (Eds) Diagenesis in Sediments and Sedimentary Rocks. Developments in Sedimentology 25A: 423-536.

Choquette, P.W. (1971): Late ferroan dolomite cement, Mississippian carbonates, Illinois Basin, USA. *In* Bricker, O.P. (Ed) Carbonate Cements. 339-346.

Choquette, P.W., James, N.P. (1987): Diagenesis #12. Diagenesis in limestones - 3. The deep burial environment. *Geoscience Canada* 14(1): 3-35.

Choquette, P.W., Steinen, R.P. (1980): Mississippian non-supratidal dolomite, Ste. Genevieve Limestone, Illinois Basin: evidence for mixed-water dolomitization. *In* Zenger, D.H., *et al.* (Eds) Concepts and Models of Dolomitization. Society of Economic Paleontologists and Mineralogists Special Publication No.28: 163-197.

Churnet, H.G., Misra, K.C. (1981): Genetic implications of the trace element distribution patterns in the Upper Knox carbonate rocks, Copper Ridge district, East Tennessee. *Sedimentary Geology* 30(3): 173-194.

Claypool, G.E., Kaplan, I.R. (1974): The origin and distribution of methane in marine sediments. *In* Kaplan, I.R. (Ed) Natural Gases in Marine Sediments. Marine Science Volume 3: 99-139.

Claypool, G.E., Threlkeld, C.N. (1983): Anoxic diagenesis and methane generation in sediments of the Blake Outer Ridge, Deep Sea Drilling Project site 533, Leg 76. *In* Sheridan, R.E., Gradstein, F.M., *et al.* Initial Reports of the Deep Sea Drilling Project 76: 391-402.

Clayton, C.J. (1986): The chemical environment of flint formation in Upper Cretaceous chalks. *In* Sieveking G.de G., Hart, M.B. (Eds) The Scientific Study of Flint and Chert. Proceedings of the Fourth International Flint Symposium held at Brighton Polytechnic, 10-15 April 1983: 43-54.

Clayton, R.N., Jones, B.F., Berner, R.A. (1968): Isotope studies of dolomite formation under sedimentary conditions. *Geochimica et Cosmochimica Acta* 32(4): 415-432.

Clayton, R.N., O'Neil, J.R., Mayeda, T.K. (1972): Oxygen isotope exchange between quartz and water. *Journal of Geophysical Research* 77(17): 3057-3067.

Coleman, M.L. (1985): Geochemistry of diagenetic non-silicate minerals: kinetic considerations. *Philosophical Transactions of the Royal Society of London* A315: 39-56.

Coleman, M.L., Raiswell, R. (1981): Carbon, oxygen and sulphur isotope variations in concretions from the Upper Lias of NE England. *Geochimica et Cosmochimica Acta* 45(3): 329-340.

Compton, J.S. (1988): Degree of supersaturation and precipitation of organogenic dolomite. *Geology* 16(4): 318-321.

Compton. J.S., Siever, R. (1986): Diffusion and mass balance of Mg during early dolomite formation, Monterey Formation. *Geochimica et Cosmochimica Acta* 50(1): 125-135.

Coniglio, M. (1987): Biogenic chert in the Cow Head Group (Cambro-Ordovician), western Newfoundland. *Sedimentology* 34(5): 813-823.

Coplen, T.B., Kendall, C., Hopple, J. (1983): Comparison of stable isotope reference samples. *Nature* 302(5905): 236-238.

Crerar, D.A., Barnes, H.L. (1974): Deposition of deep-sea manganese nodules. *Geochimica et Cosmochimica Acta* 38(2): 279-300.

Curtis, C.D. (1967): Diagenetic iron minerals in some British Carboniferous sediments. *Geochimica et Cosmochimica Acta* 31(11): 2109-2123.

Curtis, C.D. (1978): Possible links between sandstone diagenesis and depth-related geochemical reactions occurring in enclosing mudstones. *Journal of the Geological Society of London* 135(1): 107-117.

Curtis, C.D., Coleman, M.L., Love, L.G. (1986): Pore water evolution during sediment burial from isotopic and mineral chemistry of calcite, dolomite and siderite concretions *Geochimica et Cosmochimica Acta* 50(10): 2321-2334.

Curtis, C.D., Petrowski, C., Oertel, G. (1972): Stable C isotope ratios within carbonate concretions: a clue to place and time of formation. *Nature* 235(5333): 98-100.

Cuthbertson. A.M. (1985): Stable Isotope Studies of Deep Sea Cores. Unpublished M.Sc. Thesis. University of Waikato. Hamilton.

Dapples, E.C. (1959): The behaviour of silica in diagenesis. *In* Ireland, H.A. (Ed) Silica In Sediments. A Symposium with Discussion. Society of Economic Paleontologists and Mineralogists Special Publication No.7: 36-54.

Dapples, E.C. (1979): Silica as an agent in diagenesis. *In* Larsen, G., Chilingar, G.V. (Eds) Diagenesis in Sediments and Sedimentary Rocks. Developments in Sedimentology 25A: 99-141.

Davies, P.J., Ferguson, J., Bubula, B. (1975): Dolomite and organic material. *Nature* 255(5508): 472-474.

Davies, T.A., Supko, P.R. (1973): Oceanic sediments and their diagenesis: some examples from deep sea drilling. *Journal of Sedimentary Petrology* 43(2): 381-390.

De Deckker, P., Last, W.M. (1988): Modern dolomite deposition in

continental, saline lakes, western Victoria, Australia. *Geology* 16(1): 29-32.

Deelman, J.C. (1975): Dolomite synthesis and crystal growth. *Geology* 3(8): 471-472.

Deelman, J.C. (1978): Discussion: Protodolomite redefined. *Journal of Sedimentary Petrology* 48(3): 1004-1007.

Deffeyes, K.S., Lucia, F.J., Weyl, P.K. (1964): Dolomitization: observations on the island of Bonaire, Netherlands Antilles. *Science* 143: 678-679.

Deffeyes, K.S., Lucia, F.J., Weyl, P.K. (1965): Dolomitization of recent and Plio-Pleistocene sediments by marine evaporite waters on Bonaire, Netherlands Antilles. *In* Pray, L.G., Murray, R.C. (Eds) Dolomitization and Limestone Diagenesis. SEPM Special Publication No.13: 71-88.

Degens, E.T., Epstein, S. (1962): Relationship between $^{18}O/^{16}O$ ratio in coexisting carbonates, cherts and diatomites. *American Association of Petroleum Geologists Bulletin* 46(4): 534-542.

Degens, E.T., Epstein, S. (1964): Oxygen and carbon isotope ratios in coexisting calcites and dolomites from recent and ancient sediments. *Geochimica et Cosmochimica Acta* 28: 23-44.

Demaster, D.J. (1981): The supply and accumulation of silica in the marine environment. *Geochimica et Cosmochimica Acta* 45(10): 1715-1732.

Demaster, D.J., Knapp, G.B., Nittrouer, C.A. (1983): Biological uptake and accumulation of silica on the Amazon continental shelf. *Geochimica et Cosmochimica Acta* 47(10): 1713-1723.

Deuser, W.G. (1970): Extreme $^{13}C/^{12}C$ variations in Quaternary dolomites from the continental shelf. *Earth and Planetary Science Letters* 8(2): 118-124.

Devol, A.H., Ahmed, S.I. (1981): Are high rates of sulphate reduction associated with anaerobic oxidation of methane? *Nature* 291(5814):

407-408.

Devol, A.H., Anderson, J.J., Kuivila, K., Murray, J.W. (1984): A model for coupled sulfate reduction and methane oxidation in the sediments of Saanich Inlet. *Geochimica et Cosmochimica Acta* 48(5): 993-1004.

Dietrich, R.V. Hobbs, C.R.B., Lowry, W.D. (1963): Dolomitization interrupted by silicification. *Journal of Sedimentary Petrology* 33(3): 646-663.

Donnelly, Th.W., Merrill, L. (1977): The scavenging of magnesium and other chemical species by biogenic opal in deep sea sediments. *Chemical Geology* 19(3): 167-186.

Dowty, E. (1976): Crystal structure and crystal growth: II Sector zoning in minerals. *The American Mineralogist* 61(5-6): 460-469.

Dymond, J. (1981): Geochemistry of Nazca Plate surface sediments: An evaluation of hydrothermal, biogenic, detrital, and hydrogenous sources. *In* Kulm, L.D., *et al.* (Eds) Nazca Plate: Crustal formation and Andean Convergence. Geological Society of America Memoir 154: 133-173.

Ebers, M.L., Kopp, O.C. (1979): Cathodoluminescent microstratigraphy in gangue dolomite, the Mascot - Jefferson City district, Tennessee. *Economic Geology* 74(4): 908-113.

Eder, W. (1982): Diagenetic redistribution of carbonate, a process in forming limestone - Marl alternations (Devonian and Carboniferous, Rheinisches Schiefergebirge, W. Germany) *In* Einsele, G., Seilacher, A. (Eds) Cyclic and Event Stratification: 98-112.

Einsele, G. (1982): Limestone-marl cycles (Periodites): Diagnosis, significance, causes - a review. *In* Einsele, G., Seilacher, A. (Eds) Cyclic and Event Stratification: 8-53.

Ekdale, A.A., Bromley, R.G. (1984a): Comparative ichnology of shelf-sea and deep-sea chalk. *Journal of Paleontology* 58(2): 322-332.

Ekdale, A.A., Bromley, R.G. (1984b): Sedimentology and ichnology of the

Cretaceous-Tertiary boundary in Denmark: implications for the causes of the terminal Cretaceous extinction. *Journal of Sedimentary Petrology* 54(3): 681-703.

Epstein, S., Buchsbaum, R., Lowenstam, H.A., Urey, H.C. (1953): Revised carbonate-water isotopic temperature scale. *Geological Society of America Bulletin* 64(11): 1315-1326.

Epstein, S., Graf, D.L., Degens, E.T. (1964): Oxygen isotope studies on the origin of dolomites. *In* Craig, H., Miller, S.L., Wasserburg, G.J. (Eds) Isotopic and Cosmic Chemistry. 169-180.

Ernst, W.G., Calvert, S.E. (1969): An experimental study of the recrystallization of porcellanite and its bearing on the origin of some bedded cherts. *American Journal of Science* 267-A: 114-133.

Eugster, H.P. (1969): Inorganic bedded cherts from the Magadi area, Kenya. *Contributions to Mineralogy and Petrology* 22(1): 1-31.

Fairbridge, R.W. (1957): The dolomite question. *In* Le Blanc, R.J., Breeding, J.G. (Eds) Regional Aspects of Carbonate Deposition. Society of Economic Paleontologists and Mineralogists Special Publication No. 5: 125-178.

Fairchild, I.J. (1983): Chemical controls of cathodoluminescence of natural dolomites and calcites: new data and review. *Sedimentology* 30(4): 579-583.

Fergusson, L. (1985): The Mineralogy, Geochemistry and Origin of Lower Tertiary Smectite-Mudstones, East Coast Deformed Belt, New Zealand. Unpublished M.Sc. Thesis. University of Canterbury. 180pp.

Flügel, E. (1982): Microfacies Analysis of Limestones. Springer-Verlag, Berlin. 633pp.

Folk, R.L. (1959): Practical petrographic classification of limestones. *American Association of Petroleum Geologists Bulletin* 43(1): 1-38.

Folk, R.L., Land, L.S. (1975): Mg/Ca ratio and salinity: two controls over crystallization of dolomite. *American Association of Petroleum*

Geologists Bulletin 59(1): 60-68.

Folk, R.L., Pittman, L.S. (1971): Length slow chalcedony: a new testament for vanished evaporites. *Journal of Sedimentary Petrology* 41(4): 1045-1058.

Folk, R.L., Weaver, C.E. (1952): A study of the texture and composition of chert. *American Journal of Science* 250(7): 498-510.

Fournier, R.O., Marshall, W.L. (1983): Calculation of amorphous silica solubilities at 25°C and 300°C and apparent cation hydration numbers in aqueous salt solution using the concept of effective density of water. *Geochimica et Cosmochimica Acta* 47(3): 587-596.

Frank. J.R., Carpenter, A.B., Oglesby, T.W. (1982): Cathodoluminescence and composition of calcite cement in the Taum Sauk Limestone (Upper Cambrian), southeast Missouri. *Journal of Sedimentary Petrology* 52(2): 631-638.

Freund, R. (1971): The Hope Fault, a strike-slip fault in New Zealand. *New Zealand Geological Survey Bulletin* 86: 49pp.

Friedman, G.M. (1965): Terminology of crystallization textures and fabrics in sedimentary rocks *Journal of Sedimentary Petrology* 35(3): 643-655.

Friedman, G.M., Sanders, J.E. (1978): Principles of Sedimentology. John Wiley and Sons. New York. 792pp.

Friedman, I., Murata, K.J. (1979): Origin of dolomite in Miocene Monterey Shale and related formations in the Temblor Range, California. *Geochimica et Cosmochimica Acta* 43(8): 1357-1365.

Friedman, I., O'Neil, J.R. (1977): Compilation of stable isotope fractionation factors of geochemical interest. Data of Geochemistry 6th Edition. United States Geological Survey Professional Paper 440-KK.

Fritz, P., Smith, D.G.W. (1970): The isotopic composition of secondary dolomites. *Geochimica et Cosmochimica Acta* 34(11): 1161-1173.

Fritz, P., Katz, A. (1972): The sodium distribution of dolomite crystals. *Chemical Geology* 10(3): 237-244.

Frondel, C., Newhouse, W.H., Jarrell, R.F. (1942): Spatial distribution of minor elements in single crystals. *The American Mineralogist* 27(11): 726-745.

Funk, H. (1975): The origin of authigenic quartz in the Helvetic siliceous limestone (Helvetischer Kieselkalke), Switzerland. *Sedimentology* 22(2): 299-306.

Gaines, A.M. (1974): Protodolomite synthesis at 100°C and atmospheric pressure. *Science* 183(4124): 518-520.

Gaines, A.M. (1977): Protodolomite redefined. *Journal of Sedimentary Petrology* 47(2): 543-546.

Gaines, A.M. (1980): Dolomitization kinetics: recent experimental studies. *In* Zenger, D.H., *et al.* (Eds) Concepts and Models of Dolomitization. Society of Economic Paleontologists and Mineralogists Special Publication No.28: 81-86.

Galloway, W.E. (1984): Hydrogeological regimes of sandstone diagenesis. *In* McDonald, D.A., Surdam, R.C. (Eds) Clastic Diagenesis. American Association of Petroleum Geologists Memoir 37: 3-13.

Garrison, R.E. (1981): Diagenesis of oceanic carbonate sediments: A review of the DSDP perspective. *In* Warme, J.E., Douglas, R.G., Winterer, E.L. (Eds) The Deep Sea Drilling Project: A Decade of Progress. Society of Economic Paleontologists and Mineralogists Special Publication No.32: 181-207.

Garrison, R.E., Douglas, R.G., Pisciotto, K.E., Isaacs, C.M., Ingle, J.C. (Eds) (1981): The Monterey Formation and Related Siliceous Rocks of California. Society of Economic Paleontologists and Mineralogists Pacific Section Special Publication No. 15. 327pp.

Garrison, R.E., Rowland, S.M., Horan, L.J., Moore, J.C. (1975): Petrology of siliceous rocks recovered from marginal seas of the western Pacific, Leg 31. *In* Karig, D.E., Ingle, J.C., *et al.* Initial Reports

of the Deep Sea Drilling Project 31: 519-529.

Gebelein, C.D., Hoffman, P. (1973): Algal origin of dolomite laminations in stromatalitic limestone. *Journal of Sedimentary Petrology* 43(3): 603-613.

Geeslin, J.H., Chafetz, H.S. (1982): Ordovician Aleman ribbon cherts: an example of silicification prior to carbonate lithification. *Journal of Sedimentary Petrology* 52(4): 1283-1293.

Gidman, J. (1978): Discussion: Protodolomite redefined. *Journal of Sedimentary Petrology* 48(3): 1007-1008.

Gieskes, J.M. (1981): Deep sea drilling interstitial water studies: Implications for chemical alteration of the oceanic crust, Layers I and II. *In* Warme, J.E., Douglas, R.G., Winterer E.L. (Eds) The Deep Sea Drilling Project: A Decade of Progress. Society of Economic Paleontologists and Mineralogists Special Publication No.32: 149-167.

Gluyas, J.G. (1984): Early carbonate diagenesis within the Phanerozoic shales and sandstones of the NW European Shelf. *Clay Minerals* 19(3): 309-321.

Goddard, E.N., Trask, P.D., De Ford, R.K., Rove, O.N., Singewald, J.F., Overbeck, R.M. (1970): Rock Colour chart. Geological Society of America. Boulder Colorado.

Goldschmidt, V.M. (1954): Geochemistry. Oxford Univeristy Press. London. 730pp.

Goldsmith, J.R., Graf, D.L. (1958): Structural and compositional variations in some natural dolomites. *Journal of Geology* 66(6): 678-693.

Goldsmith, J.R., Graf, D.L., Heard, H.C. (1961): Lattice constants of the calcium-magnesium carbonates. *American Mineralogist* 46(3&4): 453-457.

Goodell, H.G., Garman, R.K. (1969): Carbonate geochemistry of superior deep test well, Andros Island, Bahamas. *American Association of Petroleum Geologists Bulletin* 53(3): 513-536.

Grabowski, R.J., Unice, R.C. (1958): Quantitative spectrochemical determination of barium and strontium. *Analytical Chemistry* 30(8): 1374-1379.

Graf, D.L., Goldsmith, J.R. (1956): Some hydrothermal syntheses of dolomite and protodolomite. *Journal of Geology* 64(2): 173-186.

Greenwood, R. (1973): Cristobalite: Its relationship to chert formation in selected samples from the Deep Sea Drilling Project. *Journal of Sedimentary Petrology* 43(3): 700-708.

Gregg, J.M. (1985): Regional epigenetic dolomitization in the Bonne-terre Dolomite (Cambrian), southeastern Missouri. *Geology* 13(7): 503-506.

Gregg, J.M., Hagni, R.D. (1987): Irregular cathodoluminescent banding in late dolomite cement: evidence for complex faceting and metalliferous brines. *Geological Society of America Bulletin* 98(1): 86-91.

Gregg, J.M., Sibley, D.F. (1984): Epigenetic dolomitization and the origin of xenotopic dolomite texture. *Journal of Sedimentary Petrology* 54(3): 908-931.

Grinsted, M.J. (1977): A Study of the Relationships Between Climate and Stable Isotopes in Tree Rings. Unpublished D.Phil. Thesis. University of Waikato. Hamilton. 237pp.

Gunatilaka, A. (1987): The dolomite problem in the light of recent studies. *Modern Geology* 11(4): 311-324.

Haast, J. (1871): On the geology of the Amuri District, in the provinces of Nelson and Marlborough. Geological Survey of New Zealand Reports of Geological Explorations No. 6: 25-46.

Håkansson, E., Bromley, R.G., Perch-Nielsen, K. (1974): Maastrichtian Chalk of north-west Europe - a pelagic shelf sediment. *In* Hsü, K.J., Jenkyns, H.C. (Eds) Pelagic Sediments: On Land And Under The Sea. International Association of Sedimentologists Special Publication No. 1: 211-233.

Hall, W.D.M. (1964): The Geology of Coverham and the upper Waima Valley,

Marlborough. Unpublished M.Sc. Thesis. University of Victoria. Wellington.

Hallam, A. (1964): Origin of the limestone-shale rhythms in the Blue Lias of England: A composite theory. *Journal of Geology* 72(2): 157-168.

Hallam, A. (1986): Origin of minor limestone-shale cycles: climatically induced or diagenetic. *Geology* 14(7): 609-612.

Halley, R.B., Schmoker, J.W. (1983): High-porosity Cenozoic carbonate rocks of south Florida: progressive loss of porosity with depth. *American Association of Petroleum Geologists* 67(2): 191-200.

Hamilton, E.L. (1976): Variations of density and porosity with depth in deep-sea sediments. *Journal of Sedimentary Petrology* 46(2): 280-300.

Hancock, J.M. (1975): The petrology of the chalk. *Proceedings of the Geologists Association* 86(4): 499-535.

Hanshaw, B.B., Back, W., Dieke, R.G. (1971): A geochemical hypothesis for dolomitization by ground water. *Economic Geology* 66(5): 710-724.

Hardie, L.A. (1987): Dolomitization: a critical view of some current views. *Journal of Sedimentary Petrology* 57(1): 166-183.

Hatfield, C.B., Rohrbacher, T.J. (1966): Dolomite-insoluble residue relationships in the Ten Mile Creek Dolomite (Middle Devonian) near Toledo, Ohio. *Journal of Sedimentary Petrology* 36(3): 828-831.

Heath, G.R. (1973): Cherts from the eastern Pacific, Leg 16, Deep Sea Drilling Project. *In* van Andel, Tj.H., Heath, G.R., *et al.* Initial Reports of the Deep Sea Drilling Project 16: 609-613.

Heath, G.R. (1974): Dissolved Silica and deep-sea sediments. *In* Hay, W.W., (Eds) Studies in Paleooceanography. Society of Economic Paleontologists and Mineralogists Special Publication No.20: 77-93.

Heath, G.R., Moberly, R. (1971): Cherts from the western Pacific , Leg 7, Deep Sea Drilling Project. *In* Winterer, E.L., *et al.* Initial Reports of the Deep Sea Drilling Project 7 (Part 2): 991-1007.

Hector, J. (1874): On the fossil reptilia of New Zealand. *Transactions and Proceedings of the New Zealand Institute* 6: 333-358.

Hein, J.R., Sancetta, C., Morgenson, L.A. (1983): Petrology and geochemistry of silicified Upper Miocene chalk, Costa Rica Rift, Deep Sea Drilling Project, Leg 69. *In* Cann, J.R., Langseth, M.G., *et al.* Initial Reports of the Deep Sea Drilling Project 69: 395-422.

Hein, J.R., Vallier, T.L., Allan, M.A. (1981): Chert petrology and geochemistry, mid-Pacific Mountains and Hess Rise, Deep Sea Drilling Project, Leg 62. *In* Vallier, T.L., Thiede, J., *et al.* Initial Reports of the Deep Sea Drilling Project 62: 711-748.

Hein, J.R., Yeh, H-W. (1981): Oxygen-isotope composition of chert from the mid-Pacific Mountains and Hess Rise, Deep Sea Drilling Project, Leg 62. *In* Vallier, T.L., Thiede, J., *et al.* Initial Reports of the Deep Sea Drilling Project 62: 749-758.

Hein, J.R., Yeh, H-W. (1983): Oxygen-isotope composition of secondary silica phases Costa Rica Rift, Deep Sea Drilling Project, Leg 69. *In* Cann, J.R., Langseth, M.G., *et al.* Initial Reports of the Deep Sea Drilling Project 69: 423-429.

Hem, J.D. (1972): Chemical factors that influence the availability of iron and manganese in aqueous systems. *Geological Society of America Bulletin* 83(2): 443-450.

Hennessy, J., Knauth, L.P. (1985): Isotopic variations in dolomite concretions from the Monterey Formation, California. *Journal of Sedimentary Petrology* 55(1): 120-130.

Hesse, R. (1986): Diagenesis #11. Early diagenetic pore water/sediment interaction: Modern offshore basins. *Geoscience Canada* 13(3): 165-196.

Hesse, R., Lebel, J., Gieskes, J.M. (1985): Interstitial water chemistry of gas hydrate bearing sections on the Middle-America Trench Slope, Deep Sea Drilling Project Leg 84. *In* von Huene, R., Aubouin, R., *et al.* Initial Reports of the Deep Sea Drilling Project 84: 727-737.

Hirst, D.M. (1962): The geochemistry of modern sediments from the Gulf of Paria - I. The relationship between the mineralogy and the distribution of major elements. *Geochimica et Cosmochimica Acta* 26(2): 309-334.

Hodgson, W.A. (1966): Carbon and oxygen isotope ratios in diagenetic carbonates from marine sediments. *Geochimica et Cosmochimica Acta* 30(12): 1223-1233.

Hodgson, W.A. (1968): The diagenesis of spherulitic carbonate concretions and other rocks from Mangakahia Group sediments, Kaipara Harbour, New Zealand. *Journal of Sedimentary Petrology* 38(4): 1254-1263.

Hoefs, J. (1980): Stable Isotope Geochemistry. 2nd Edition. Springer-Verlag. Berlin. 208pp.

Hollister, L.S. (1970): Origin, mechanism, and consequences of compositional sector-zoning in staurolite. *The American Mineralogist* 55(5-6): 742-766.

Hollister, L.S., Gancarz, A.J. (1971): Compositional sector-zoning in clinopyroxene from the Narce area, Italy. *The American Mineralogist* 56(5-6): 959-979.

Houseknecht, D.W. (1988): Intergranular pressure solution in four quartzose sandstones. *Journal of Sedimentary Petrology* 58(2): 228-246.

Hower, J., Eslinger, E.V., Hower, M.E., Perry, E.A. (1976): Mechanism of burial and metamorphism of argillaceous sediment: 1 Mineralogical and chemical evidence. *Geological Society of America Bulletin* 87(5): 735-737.

Hudson, J.D. (1977): Stable isotopes and limestone lithification. *Journal of the Geological Society* 133(6): 637-660.

Hudson, J.D. (1978): Concretions, isotopes and diagenetic history of the Oxford Clay (Jurassic) of central England. *Sedimentology* 25: 339-370.

Hurd, D.C., Birdwhistell, S. (1983): On producing a more general model for

biogenic silica dissolution. *American Journal of Science* 283(1): 1-28.

Hurd, D.C., Theyer, F. (1975): Changes in the physical and chemical properties of biogenic silica from the central Equatorial Pacific: Part I. Solubility, specific surface area and solution rate constants of acid cleaned samples. *In* Gibb, T.T.R.P. (Ed) Analytical Methods in Chemical Oceanography. American Chemical Society Advances in Chemistry Series No.147: 211-230.

Hurd, D.C., Theyer, F. (1977): Changes in the physical and chemical properties of biogenic silica from the central Equatorial Pacific: II refractive index, density, and water content of acid-cleaned samples. *American Journal of Science* 277(9): 1168-1202.

Hurst, A., Irwin, H. (1982): Geological modelling of clay diagenesis in sandstones. *Clay Minerals* 17(1): 5-22.

Ichikuni, M. (1973): Partition of strontium between calcite and solution: effect of substitution by manganese. *Chemical Geology* 11(4): 315-319.

Iijima, A., Hein, J.R., Siever, R. (Eds) (1983): Siliceous Deposits in the Pacific Region. Developments in Sedimentology 36: 472pp.

Iijima, A., Matsumoto, R., Tada, R. (1985): Mechanism of sedimentation of rhythmically bedded chert. *Sedimentary Geology* 41(2/4): 221-233.

Iijima, A., Utada, M. (1983): Recent developments in the sedimentology of siliceous deposits in Japan. *In* Iijima, A., *et al.* (Eds) Siliceous Deposits in the Pacific Region. Developments in Sedimentology 36: 45-64.

Iler, R.K. (1979): The Chemistry of Silica: Solubility, Polymerization, Colloid and Surface Properties, and Biochemistry. John Wiley and Sons. New York. 787pp.

Illing, L.V., Wells, A.J., Taylor, J.C.M. (1965): Penecontemporary dolomite in the Persian Gulf. *In* Pray, L.C., Murray, R.C. (Eds) Dolomitization and Limestone Diagenesis. Society of Economic

Paleontologists and Mineralogists Special Publication 13: 89-111.

Ireland, H.A. (Ed) (1959): Silica in Sediments. A symposium with discussions. Society of Economic Paleontologists and Mineralogists Special Publication No.7: 185pp.

Irwin, H. (1980): Early diagenetic carbonate precipitation and pore fluid migration in the Kimmeridge Clay of Dorset, England. *Sedimentology* 27(5): 577-591.

Irwin, H., Curtis, C., Coleman, M. (1977): Isotopic evidence for source of diagenetic carbonates formed during burial of organic-rich sediments. *Nature* 269(5625): 209-213.

Isaacs, C.M. (1981): Porosity reduction during diagenesis of the Monterey Formation, Santa Barbara coastal area, California. *In* Garrison R.E., *et al.* (Eds) The Monterey Formation and Related Siliceous Rocks of California. Society of Economic Paleontologists and Mineralogists Pacific Section Book 15: 257-271.

Isaacs, C.M. (1982): Influence of rock composition on kinetics of silica phase changes in the Monterey Formation, Santa Barbara area, California. *Geology* 10(6): 304-308.

Jacka, A.D. (1974): Replacement of fossils by length-slow chalcedony and associated dolomitization. *Journal of Sedimentary Petrology* 44(2): 421-427.

Jacobsen, R.L., Usdowski, H.E. (1976): Partitioning of strontium between calcite, dolomite, and liquids: An experimental study under higher temperature diagenetic conditions and the model for the prediction of mineral pairs for geothermometry. *Contributions to Mineralogy and Petrology* 59(2): 171-185.

Jeans, C.V. (1980): Early submarine lithification in the Red Chalk and Lower Chalk of eastern England: a bacterial control model and its implications. *Proceedings of the Yorkshire Geological Society* 43 pt2 No.6: 81-157.

Jenkyns, H.C. (1974): Origin of red nodular limestones (Ammonitico Rosso,

Knollenkalke) in the Mediterranean Jurassic: a diagenetic model. *In* Hsü, K.J., Jenkyns, H.C. (Eds) Pelagic Sediments: On Land And Under The Sea. International Association of Sedimentologists Special Publication No.1: 249-271.

Jenkyns, H.C., Clayton, C.J. (1986): Black shales and carbon isotopes in pelagic sediments from the Tethyan Lower Jurassic. *Sedimentology* 33(1): 87-106.

Johnsson, M.J., Reynolds, R.C. (1986): Clay mineralogy of shale-limestone rhythmites in the Scaglia Rossa (Turonian-Eocene), Italian Apennines. *Journal of Sedimentary Petrology* 56(4): 501-509.

Jodry, R.L. (1969): Growth and dolomitization of Silurian reefs, St Clair County, Michigan. *American Association of Petroleum Geologists Bulletin* 53(4): 957-981.

Jones, D.L., Knauth, L.P. (1979): Oxygen isotopic and petrographic evidence relevant to the origin of the Arkansas Novaculite. *Journal of Sedimentary Petrology* 49(2): 581-598.

Jones, J.B., Segnit, E.R. (1971): The nature of opal. 1. Nomenclature and constituent phases. *Journal of the Geological Society of Australia* 18(1): 56-68.

Jørgensen, N.O. (1987): Oxygen and carbon isotope compositions of Upper Cretaceous chalk from the Danish sub-basin and the north sea Central Graben. *Sedimentology* 34(4): 559-570.

Kablonow, R.I., Surdam, R.C., Prezbindowski, D. (1984): Origin of dolomites in the Monterey Formation: Pismo and Huasna Basins, California. *In* Garrison, R.E., *et al.* (Eds) Dolomites of the Monterey Formation and Other Organic-Rich Units. Society of Economic Paleontologists and Mineralogists Pacific Section 41: 103-117.

Kahle, C.F. (1965): Possible roles of clay minerals in the formation of dolomite. *Journal of Sedimentary Petrology* 35(2): 448-453.

Karpoff, A-M., Hoffert, M., Clauer, N. (1981): Sedimentary sequences at Deep Sea Drilling Project site 464: Silicification processes and

transition between siliceous biogenic oozes and brown clays. *In* Vallier, T.L., Thiede, J., *et al.* Initial Reports of the Deep Sea Drilling Project 62: 759-771.

Kastner, M. (1970): An inclusion hourglass pattern in synthetic gypsum. *The American Mineralogist* 55(11-12): 2128-2130.

Kastner, M. (1981): Authigenic silicates in deep-sea sediments: Formation and diagenesis. *In* Emiliani, C. (Ed) The Oceanic Lithosphere. The Sea Volume 7: 915-980.

Kastner, M., Gieskes, J.M. (1983): Opal-A to opal-CT transformation: A kinetic study. *In* Iijima, A., *et al.* (Eds) Siliceous Deposits in the Pacific Region. Developments in Sedimentology 36: 211-227.

Kastner, M., Keene, J.B., Gieskes, J.M. (1977): Diagenesis of siliceous oozes. I. Chemical controls on the rate of opal-A to opal-CT transformation - and experimental study. *Geochimica et Cosmochimica Acta 41(8):1041-1059.*

Kastner, M., Mertz, K., Hollander, D., Garrison, R. (1984): The association of dolomite-phosphorite-chert: causes and possible diagenetic sequences. *In* Garrison, R.E., *et al.* (Eds) Dolomites of the Monterey Formation and Other Organic-Rich Units. Society of Economic Paleontologists and Mineralogists Pacific Section 41: 75-86.

Katz, A., Mathews, A. (1977): The dolomitization of $CaCO_3$: an experimental study at 252-295°C. *Geochimica et Cosmochimica Acta* 41(2): 297-308.

Keene, J.B. (1975): Cherts and porcellanites from the North Pacific, Deep Sea Drilling Project Leg 32. *In* Larson, R.L., Moberly, R.J., *et al.* Initial Reports of the Deep Sea Drilling Project 32: 429-507.

Keene, J.B., Kastner, M. (1974): Clays and formation of deep-sea chert. *Nature* 249(5459): 754-755.

Keller, W.D. (1941): Petrography and origin of the Rex Chert. *Geological Society of America Bulletin* 52(8): 1279-1298.

Kelts, K. (1976): Summary of chert occurrences from Line Islands sites,

314, 315, 316 Deep Sea Drilling Project Leg 33. *In* Schlanger, S.O., Jackson, E.D., *et al.* Initial Reports of the Deep Sea Drilling Project 33: 855-865.

Kelts, K., McKenzie, J.A. (1982): Diagenetic dolomite formation in Quaternary anoxic diatomaceous muds of Deep Sea Drilling Project Leg 64, Gulf of California. *In* Carray, J., Moore, D., *et al.* Initial Reports of the Deep Sea Drilling Project Leg 64. 553-570.

Kelts, K., McKenzie, J.A. (1984): A comparison of anoxic dolomite from deep-sea sediments: Quaternary Gulf of California and Messinian Tripoli Formation of Sicily. *In* Garrison, R.E., *et al.* (Eds) Dolomites of the Monterey Formation and Other Organic-Rich Units. Society of Economic Paleontologists and Mineralogists Pacific Section 41: 19-28.

Kendall, A.C. (1977): Origin of dolomite mottling in Ordovician limestones from Saskatchewan and Manitoba. *Bulletin of Canadian Petroleum Geology* 25(3): 480-504.

Kennedy, W.J., Garrison, R.E. (1975): Morphology and genesis of nodular chalks and hardgrounds in the Upper Cretaceous of southern England. *Sedimentology* 22(3): 311-386.

Kent, D.B., Kastner, M. (1985): Mg^{2+} removal in the system Mg^{2+}-amorphous SiO_2-H_2O by adsorption and Mg-hydroxysilicate precipitation. *Geochimica et Cosmochimica Acta* 49(5): 1123-1136.

Kharaka, Y.K., Law, L.M., Carothers, W.W., Goerlitz, D.F. (1986): Role of organic species dissolved in formation waters from sedimentary basins in mineral diagenesis. *In* Gautier, D.L. (Ed) Roles of Organic Matter in Sediment Diagenesis. Society of Economic Paleontologists and Mineralogists Special Publication No.38: 111-122.

Kinsman, D.J.J. (1969): Interpretation of Sr^{2+} concentrations in carbonate minerals and rocks. *Journal of Sedimentary Petrology* 39(2): 486-508.

Kinsman, D.J.J., Holland, H.D. (1969): The coprecipitation of cations with calcium carbonate - IV. The coprecipitation of Sr with aragonite between 16 and 96°C. *Geochimica et Cosmochimica Acta* 33(1): 1-17.

Knauth, L.P. (1979): A model for the origin of chert in limestone. *Geology* 7(6): 274-277.

Knauth, L.P., Epstein, S. (1975): Hydrogen and oxygen isotope ratios in silica from the JOIDES Deep Sea Drilling Project. *Earth and Planetary Science Letters* 25(1): 1-10.

Knauth, L.P., Epstein, S. (1976): Hydrogen and oxygen isotope ratios in nodular and bedded cherts. *Geochimica et Cosmochimica Acta.* 40(9): 1095-1108.

Knauth, L.P., Lowe, D.R. (1978): Oxygen isotope geochemistry of cherts from the Onverwacht Group (3.4 billion years), Transvaal, South Africa, with implications for secular variations in the isotopic composition of cherts. *Earth and Planetary Science Letters* 41(2): 209-222.

Kolodny, Y. (1986): The origin of cherts as members of high productivity sequences: isotopic evidence. *In* Sieveking, G. de G., Hart, M.B., (Eds) The Scientific Study of Flint and Chert. Proceedings of the Fourth International Flint Symposium held at Brighton Polytechnic, 10-15 April 1983: 55-62.

Kolodny, Y., Epstein, S. (1976): Stable isotope geochemistry of deep sea cherts. *Geochimica et Cosmochimica Acta* 40(10): 1195-1209.

Kretz, R. (1982): A model for the distribution of trace elements between calcite and dolomite. *Geochimica et Cosmochimica Acta* 46(10): 1979-1981.

Kushnir, J., Kastner, M. (1984): Two forms of dolomite occurrences in the Monterey Formation, California: concretions and layers - a comparative mineralogical, geochemical and isotopic study. *In* Garrison, R.E., *et al.* (Eds) Dolomites of the Monterey Formation and other Organic-Rich Units. Society of Economic Paleontologists and Mineralogists Pacific Section 41: 171-183.

Laferriere, A.P., Hattin, D.E., Archer, A.W. (1987): Effects of climate, tectonics, and sea-level changes on rhythmic bedding patterns in the Niobrara Formation (Upper Cretaceous), U.S. Western Interior.

Geology 15(3): 233-236.

Lahann, R.W. (1980): Smectite diagenesis and sandstone cement: the effect of reaction temperature. *Journal of Sedimentary Petrology* 50(3): 755-760.

Lancelot, Y. (1973): Chert and silica diagenesis in sediments from the central Pacific. *In* Winterer, E.L., *et al.* Initial Reports of the Deep Sea Drilling Project 17: 377-405.

Land, L.S. (1973): Holocene meteoric dolomitization of Pleistocene limestones, North Jamaica. *Sedimentology* 20(3): 411-424.

Land, L.S. (1980): The isotopic and trace element geochemistry of dolomite: the state of the art. *In* Zenger, D.H., *et al.* (Eds) Concepts and Models of Dolomitization. Society of Economic Paleontologists and Mineralogist Special Publication No. 28: 87-110.

Land, L.S. (1983a): The application of stable isotopes to studies of the origin of dolomite and to problems of diagenesis of clastic sediments. Society of Economic Paleontologists and Mineralogists Short Course No.10: 4.1-4.22.

Land, L.S. (1983b): Dolomitization. American Association of Petroleum Geologists Education Course Note Series No.24.

Land, L.S. (1985): The origin of massive dolomite. *Journal of Geological Education* 33(2): 112-125.

Land, L.S., Hoops, G.K. (1973): Sodium in carbonate sediments and rocks: a possible index to the salinity of diagenetic solutions. *Journal of Sedimentary Petrology* 43(3): 614-617.

Land, L.S., Salem, M.R.I., Morrow, D.W. (1975): Palaeohydrology of ancient dolomites: geochemical evidence. *American Association of Petroleum Geologists Bulletin* 59(9): 1602-1625.

Lawrence, J.R., Gieskes, J.M., Anderson, T.F. (1976): Oxygen isotope material balance calculations, Leg 35. *In* Hollister, C.D., Craddock, C., *et al.* Initial Reports of the Deep Sea Drilling Project

35: 507-512.

Lawrence, J.R., Gieskes, J.M., Broecker, W.S. (1975): Oxygen isotope and cation composition of DSDP pore waters and alteration of Layer II basalts. *Earth and Planetary Science Letters* 27(1): 1-10.

Ledford-Hoffman, P.A., Demaster, D.J., Nittrouer, C.A. (1986): Biogenic-silica accumulation in the Ross Sea and the importance of Antarctic continental-shelf deposits in the marine silica budget. *Geochimica et Cosmochimica Acta*. 50(9): 2099-2110.

Lee, Y.I., Friedman, G.M. (1987): Deep-burial dolomitization in the Ordovician Ellenburger Group Carbonates, West Texas and southeastern New Mexico. *Journal of Sedimentary Petrology* 57(3): 544-557.

Lehmann, G., Bambauer, H.U. (1973): Quartz crystals and their colours. *Angewandte Chemie International. Edition in English* 12(4): 283-291.

Leinen, M.S. (1979): Biogenic silica accumulation in the central equatorial Pacific and its implication for Cenozoic paleooceanography: Summary *Geological Society of America Bulletin* Part 1 90: 801-803.

Lensen, G.J. (1962): Sheet 16 - Kaikoura. Geological Map of New Zealand 1:250000. Department of Scientific and Industrial Research.

Lensen, G.J. (1978a): The late mobile phase: Cretaceous - Marlborough. *In* Suggate, R.P., *et al.* (Eds) The Geology of New Zealand Volume II: 383-390.

Lensen, G.J. (1978b): The late mobile phase: Tertiary - Marlborough. *In* Suggate R.P., *et al.* (Eds) The Geology of New Zealand Volume II: 482-488.

Lewis, D.W. (1984): Practical Sedimentology. Hutchinson Ross. Stroudsburg Pennsylvania. 227pp.

Lewis, D.L., Laird, M.G. (1980): Marlborough Excursion. *In* Weaver, S.D., Lewis, D.W. (Eds) Field Excursions Guide Book. Geological Society of New Zealand 1980 Conference: B1-B17.

Lippmann, F. (1973): Sedimentary Carbonate Minerals. Springer-Verlag. Berlin. 228pp.

Lumsden, D.N. (1974): Relationships among insoluble residue, dolostone and limestone facies. *Journal of Sedimentary Petrology* 44(2): 450-455.

Lumsden, D.N., Chimahusky, J.S. (1980): Relationship between dolomite nonstoichiometry and carbonate facies parameters. *In* Zenger, D.H., *et al.* (Eds) Concepts and Models of Dolomitization. Society of Economic Paleontologists and Mineralogists Special Publication No.28: 123-137.

Lumsden, D.N., Lloyd, R.V. (1984): Mn (II) partitioning between calcium and magnesium sites in studies of dolomite origin. *Geochimica et Cosmochimica Acta* 48(9): 1861-1865.

Machado, W.G., Moore, M., Woods, G.S. (1985): On the dodecahedral growth of coated diamonds. *Journal of Crystal Growth* 71(3): 718-727.

Machel, H.G. (1985): Cathodoluminescence in calcite and dolomite and its chemical interpretation. *Geoscience Canada* 12(4): 139-147.

Machel, H.G., Mountjoy, E.W. (1986): Chemistry and environments of dolomitization - a reappraisal. *Earth Science Reviews* 23(3): 175-222.

Macpherson, E.O. (1952): The stratigraphy and bentonitic shale deposits of Kekerengu and Blue Slip, Marlborough. *New Zealand Journal of Science and Technology* B33(4): 258-286.

Madsen, B.M. (1974): Origin of spongy cherts. *Journal of Research of the United States Geological Survey* 2(6): 685-687.

Magara, K. (1976): Water expulsion from clastic sediments during compaction-directions and volumes. *American Association of Petroleum Geologists Bulletin* 60(4): 543-553.

Magara, K. (1980): Agents for primary hydrocarbon migration: a review. *In* Roberts, W.H., Cordell, R.J. (Eds) Problems of Petroleum Migration. American Association of Petroleum Geologists Studies in Geology No.10: 33-45.

Magaritz, M. (1985): The carbon isotope record of dolostones as a stratigraphic tool: a case study from the upper Cretaceous shelf sequence, Israel. *Sedimentary Geology* 45(1-2): 115-123.

Malivia, R.G., Siever, R. (1988): Diagenetic replacement controlled by force of crystallization. *Geology* 16(8): 688-691.

Manheim, F.T. (1970): The diffusion of ions in unconsolidated sediments. *Earth and Planetary Science Letters* 9(4): 307-309.

Mansfield, C.G. (1980): A urolith of biogenic dolomite - another clue in the dolomite mystery. *Geochimica et Cosmochimica Acta* 44(6): 829-840.

Marshall, P. (1916): The younger limestones of New Zealand. *Transactions and Proceedings of the New Zealand Institute* 48: 87-99.

Mathews, A., Katz, A. (1977): Oxygen isotope fractionation during the dolomitization of calcium carbonate. *Geochimica et Cosmochimica Acta* 41(10): 1431-1438.

Matsumoto, R. (1983): Mineralogy and geochemistry of carbonate diagenesis of the Pliocene and Pleistocene hemipelagic mud on the Blake Outer Ridge, site 533, Leg 76. *In* Sheridan, R.E., Gradstein, F.M., *et al.* Initial Reports of the Deep Sea Drilling Project 76: 411-427.

Matsumoto, R., Iijima, A. (1980): Carbonate diagenesis in cores from sites 438 and 439 off Northeast Honshu, Northwest Pacific, Leg 57, Deep Sea Drilling Project. *In* Lee, M., Stout, L.N., (Eds) Initial Reports of the Deep Sea Drilling Project 56,57 Part 2: 1117-1127.

Matsumoto, R., Iijima, A. (1983): Chemical sedimentology of some Permo-Jurassic and Tertiary bedded cherts in central Honshu, Japan. *In* Iijima, A., *et al.* (Eds) Siliceous Deposits in the Pacific Region. Developments in Sedimentology 36: 175-191.

Matter, A. (1974): Burial diagenesis of pelitic and carbonate deep-sea sediments in the Arabian Sea. *In* Whitmarsh, R.B., Weser, O.E., *et al.* Initial Reports of the Deep Sea Drilling Project 23: 421-470.

Mattes, B.W., Mountjoy, E.W. (1980): Burial dolomitization of the upper

Devonian Miette Buildup, Jasper National Park, Alberta. *In* Zenger, D.H., *et al.* (Eds) Concepts and Models of Dolomitization. Society of Economic Paleontologists and Mineralogists Special Publication No.28: 259-297.

McBride, E.F. (Ed) (1979): Silica in sediments: Nodular and bedded cherts. Society of Economic Paleontologists and Mineralogists Reprint Series No.8: 184pp.

McBride, E.F., Folk, R.L. (1979): Features and origin of Italian Jurassic radiolarites deposited on continental crust. *Journal of Sedimentary Petrology* 49(3): 837-868.

McCrea. J.M. (1950): On the isotopic chemistry of carbonates and a paleotemperature scale. *Journal of Chemical Physics* 18(6): 849-857.

McCrossan, R.G. (1958): Sedimentary "boudinage" structures in the Upper Devonian Ireton Formation of Alberta. *Journal of Sedimentary Petrology* 28(3): 316-320.

McCulloch, B. (1976): The Paleoecology of Some Fossil Sponges from Ward, Marlborough. Unpublished 3rd Year Report. Geology Department, University of Canterbury. Christchurch. 38pp.

McHargue, T.R., Price, R.X. (1982): Dolomite from clay in argillaceous or shale - associated marine carbonates. *Journal of Sedimentary Petrology* 52(3): 873-886.

McIntyre, W.L. (1963): Trace element partition coefficients - a review of theory and applications to geology. *Geochimica et Cosmochimica Acta* 27(12): 1209-1264.

McKay, A. (1877): Report on Kaikoura Peninsula and Amuri Bluff. Geological Survey of New Zealand Reports of Geological Explorations No.9: 172-184.

McKay, A. (1886): On the Geology of the eastern part of Marlborough provincial district. Geological Survey of New Zealand. Reports of Geological Explorations No.17: 27-136.

McKee, E.D., Gutschick, R.E. (1969): History of the Redwall Limestone of Northern Arizona. Geological Society of America Memoir 114. 726pp.

McKenzie, J.A., Hsü, K.J., Schneider, J.F. (1980): Movements of subsurface waters under the sabkha, Abu Dhabi, UAE, and its relation to evaporite dolomite genesis. *In* Zenger, D.H., *et al.* (Eds) Concepts and Models of Dolomitization. Society of Economic Paleontologists and Mineralogists Special Publication No.28: 11-30.

Mertz, K.A. (1984): Diagenetic aspects, Sandholdt Member, Miocene Monterey Formation, Santa Lucia Mountains, California: implications for depositional and burial environments. *In* Garrison, R.E., *et al.* (Eds) Dolomites of the Monterey Formation and Other Organic-Rich Units. Society of Economic Paleontologists and Mineralogists Pacific Section 41: 49-73.

Meyers, W.J. (1977): Chertification in the Mississippian Lake Valley Formation, Sacramento Mountains, New Mexico. *Sedimentology* 24(1): 75-105.

Meyers, W.J., James, A.T. (1978): Stable isotopes of cherts and carbonate cements in the Lake Valley Formation (Mississippian), Sacramento Mountains, New Mexico. *Sedimentology* 25(1): 105-124.

Michard, G. (1971): Theoretical model for manganese distribution in calcareous sediment cores. *Journal of Geophysical Research* 76(9): 2179-2186.

Micheelsen, H. (1966): The structure of dark flint from Stevns, Denmark. *Meddelelser Dansk Geologisk Forening* 16(3): 285-368.

Mitsui, K., Taguchi, K. (1977): Silica mineral diagenesis in Neogene Tertiary shales in the Tempoku district, Hokkaido, Japan. *Journal of Sedimentary Petrology* 47(1): 158-167.

Mizutani, S. (1966): Transformation of silica under hydro-thermal conditions. *The Journal of Earth Sciences, Nagoya University* 14(1): 56-88.

Mizutani, S. (1967): Kinetic aspects of diagenesis of silica in sediments.

The Journal of Earth Sciences, Nagoya University 15(2): 99-111.

Mizutani, S. (1970): Silica minerals in the early stage of diagenesis. *Sedimentology* 15(3/4): 419-436.

Mizutani, S. (1977): Progressive ordering of cristobalitic silica in the early stage of diagenesis. *Contributions to Mineralogy and Petrology* 61(2): 129-140.

Molnia, B.F. (1974): A rapid and accurate method for the analysis of calcium carbonate in small samples. *Journal of Sedimentary Petrology* 44(2): 589-590.

Mokhtari, A., Velde, D. (1987): Sector zoned kaersutite in camptonites from Morocco. *Mineralogical Magazine* 51(1): 151-156.

Möller, N.K., Kvingan, K. (1988): The genesis of nodular limestones in the Ordovician and Silurian of the Oslo Region (Norway) *Sedimentology* 35(3): 405-420.

Monroe, E.A. (1964): Electron optical observation of fine ground silica minerals. *American Mineralogist* 49(3+4): 339-347.

Mook, W.G. (1968): Geochemistry of the Stable Carbon and Oxygen Isotopes of Natural Waters in the Netherlands. Unpublished Thesis. University of Groningen. 157pp.

Moore, P.R. (1983): Chert bearing formations of New Zealand. *In* Iijima, A., *et al.* (Eds) Siliceous Deposits in the Pacific Region. Developments in Sedimentology 36: 93-108.

Moore, P.R. (1988a): Stratigraphy, composition and environment of deposition of the Whangai Formation and associated Late Cretaceous-Paleocene rocks, North Island, New Zealand. New Zealand Geological Survey Bulletin 100. 82pp.

Moore, P.R. (1988b): Dolomite concretions in the Whangai Formation (Late Cretaceous-Paleocene) at Mara Quarry, northern Wairarapa. *New Zealand Geological Survey Record* 35: 52-54.

Morris, J.C. (1987): The Stratigraphy of the Amuri Limestone Group, East Marlborough, New Zealand. Unpublished Ph.D. Thesis. University of Canterbury. Christchurch. 388pp.

Morrow, D.W. (1978a): Dolomitization of lower Paleozoic burrow-fillings. *Journal of Sedimentary Petrology* 48(1): 295-306.

Morrow, D.W. (1978b): The influence of the Mg/Ca ratio and salinity on dolomitization in evaporite basins. *Bulletin of Canadian Petroleum Geology* 26(3): 389-392.

Morrow, D.W. (1982a): Diagenesis 1. Dolomite - Part 1: the chemistry of dolomitization and dolomite precipitation. *Geoscience Canada* 9(1): 5-13.

Morrow, D.W. (1982b): Diagenesis 2. Dolomite - Part 2: dolomitization models and ancient dolostones. *Geoscience Canada* 9(2): 95-107.

Morrow, D.W., Mayers, I.R. (1978): Simulation of limestone diagenesis: a model based on strontium depletion. *Canadian Journal of Earth Sciences* 15(3): 376-396.

Morrow, D.W., Ricketts, B.D. (1986): Chemical controls on the precipitation of mineral analogues of dolomite: the sulfate enigma. *Geology* 14(5): 408-410.

Mortimore, R.N. (1986): Controls on Upper Cretaceous sedimentation in the South Downs, with particular reference to flint distribution. *In* Sieveking, G. de G., Hart, M.B. (Eds) The Scientific Study of Flint and Chert. Proceedings of the Fourth International Flint Symposium held at Brighton Polytechnic, 10-15 April 1983: 21-42.

Moses, C.O., Nordstrom, D.K., Herman, J.S., Mills, A.L. (1987): Aqueous pyrite oxidation by dissolved oxygen and ferric iron. *Geochimica et Cosmochimica Acta* 51(6): 1561-1571.

Mottl, M.J., Lawrence, J.R., Keigwin, L.D. (1983): Elemental and stable-isotope composition of porewater and carbonate sediments from Deep Sea Drilling Project sites 501/504 and 505. *In* Cann, J.R., Langseth, M.G., *et al.* Initial Reports of the Deep Sea Drilling

Project 69: 461-473.

Mount, J.F., Ward, P. (1986): Origin of limestone/marl alternations in the Upper Maastrichtian of Zumaya, Spain. *Journal of Sedimentary Petrology* 56(2): 228-236.

Muir, M., Lock, D., von der Borch, C. (1980): The Coorong model for penecontemporaneous dolomite formation in the Middle Proterozoic McArthur Group, Northern Territory, Australia. *In* Zenger, D.H., *et al.* (Eds) Concepts and Models of Dolomitization. Society of Economic Paleontologists and Mineralogists Special Publication No.28: 51-67.

Müller, Irion, G., Förstner, U. (1972): Formation and diagenesis of inorganic Ca-Mg carbonates in the lacustrine environment. *Naturewissenschaften* 59(4): 158-164.

Murata, K.J., Friedman, I., Cremer, M. (1972): Geochemistry of diagenetic dolomites in Miocene marine formations of California and Oregon. United States Geological Survey Professional Paper 724-C. 12pp.

Murata, K.J., Friedman, I., Gleason, J.D. (1977): Oxygen isotope relations between diagenetic silica minerals in Monterey Shale, Temblor Range, California. *American Journal of Science* 277(3): 259-272.

Murata, K.J., Nakata, J.K. (1974): Cristobalitic stage in the diagenesis of diatomaceous shale. *Science* 184(4136): 567-568.

Murata, K.J., Norman, M.B. (1976): An index of crystallinity for quartz. *American Journal of Science* 276(9): 1120-1130.

Murray, J.W. (1979): Iron oxides. *In* Burns, R.G. (1979): Marine Minerals Reviews in Mineralogy Volume 6: 47-98.

Murray, R.C. (1960): Origin of porosity in carbonate rocks. *Journal of Sedimentary Petrology* 30(1): 59-84.

Murray, R.C. (1964): Preservation of primary structures and fabrics in dolomite. *In* Imbrie, J., Newell, N. (Eds) Approaches to Paleoecology: 388-403.

Murray, R.C. (1969): Hydrology of South Bonaire, N.A. - A rock selective dolomitization model. *Journal of Sedimentary Petrology* 39(3): 1007-1013.

Murray, R.C., Lucia, F.J. (1967): Cause and control of dolomite distribution by rock selectivity. *Geological Society of America Bulletin* 78(1): 21-35.

Myers, C.R., Nealson, K.H. (1988): Microbial reduction of manganese oxides: Interactions with iron and sulphur. *Geochimica et Cosmochimica Acta* 52(11): 2727-2732.

Nakamura, Y. (1973): Origin of sector-zoning in igneous clinopyroxenes. *The American Mineralogist* 58(11-12): 986-990.

Namy, J.N. (1974): Early diagenetic chert in the Marble Falls Group (Pennsylvanian) of central Texas. *Journal of Sedimentary Petrology* 44(4): 1262-1268.

Nelson, C.S. (1985): Lithostratigraphy of deep sea drilling project leg 90 drill sites in the southwest Pacific: an overview. *In* Kennett, J.P., von der Borch, C.C., *et al.* Initial Reports of the Deep Sea Drilling Project 90: 1471-1491.

Nelson, C.S., Lawrence, M.J.F. (1984): Methane derived high-Mg calcite submarine cement in Holocene nodules from the Fraser Delta, British Columbia, Canada. *Sedimentology* 31(5): 645-654.

Nickel, E. (1978): The present status of cathodoluminescence as a tool in sedimentology. *Minerals Science and Engineering* 10(2): 73-100.

Norrish, K., Hutton, J.T. (1969): An accurate spectrographic method for the analysis of a wide range of geological samples. *Geochimica et Cosmochimica Acta* 33(4): 431-453.

Northrop, D.A., Clayton, R.N. (1966): Oxygen isotope fractionation in systems containing dolomite. *Journal of Geology* 74(2): 174-196.

Oehler, J.H. (1975): Origin and distribution of silica lepispheres in porcelanite from the Monterey Formation of California. *Journal of*

Sedimentary Petrology 45(1): 252-257.

Oehler, J.H. (1976): Hydrothermal crystallization of silica gel. *Geological Society of America Bulletin* 87(8): 1143-1152.

Oertel. G., Curtis, C.D. (1972): Clay-ironstone concretion preserving fabrics due to progressive compaction. *Geological Society of America Bulletin* 83(9): 2597-2606.

Officers of the New Zealand Geological Survey (1985): New Zealand Geological Survey Annual Report 1984. New Zealand Geological Survey Report G106. 64pp.

Oldershaw, A.E. (1968): Electron-microscope examination of Namurial bedded cherts, north Wales (Great Britain). *Sedimentology* 10(4): 255-272.

O'Neil, J.R., Epstein, S. (1966): Oxygen isotope fractionation in the system dolomite-calcite-carbon dioxide. *Science* 152(3719): 198-201.

O'Neil, J.R., Clayton, R.N., Mayeda, T.K. (1969): Oxygen-isotope fractionations in divalent metal carbonates. *Journal of Chemical Physics* 51(12): 5547-5558.

Osborne, M.I. (1981): The Stratigraphy and Structure of the Clarence-Kekerengu Sector, Marlborough. Unpublished M.Sc. Thesis. University of Canterbury. Christchurch. 141pp.

Patterson, R.J., Kinsman, D.J.J. (1982): Formation of diagenetic dolomite in coastal sabkha along Arabian (Persian) Gulf. *American Association of Petroleum Geologists Bulletin* 66(1): 28-43.

Perry, E.A., Hower, J. (1970): Burial diagenesis in Gulf Coast pelitic sediments. *Clays and Clay Minerals* 18(3): 165-177.

Perry, E.C., Tan, F.C. (1972): Significance of oxygen and carbon isotope determinations in early PreCambrian cherts and carbonate rocks of southern Africa. *Geological Society of America Bulletin* 83(3): 647-664.

Peterson, M.N.A. (1962): The mineralogy and petrology of Upper

Mississippian carbonate rocks of the Cumberland Plateau in Tennessee. *Journal of Geology* 70: 1-31.

Pettijohn, F.J. (1975): Sedimentary Rocks. 3rd Edition. Harper and Row. New York. 628pp.

Pierre, C., Ortlieb, L., Person, A. (1984): Supratidal evaporitic dolomite at Ojo de Liebre Lagoon: mineralogical and isotopic arguments for primary crystallization. *Journal of Sedimentary Petrology* 54(4): 1049-1061.

Pierson, B.J. (1981): The control of cathodoluminescence in dolomite by iron and manganese. *Sedimentology* 28(5): 601-610.

Pingitore, N.E. (1978): The behaviour of Zn^{2+} and Mn^{2+} during carbonate diagenesis: theory and applications. *Journal of Sedimentary Petrology* 48: 799-814.

Pingitore, N.E., Eastman, M.P. (1986): The co-precipitation of Sr^{2+} with calcite at 25°C and 1 atmosphere. *Geochimica et Cosmochimica Acta* 50(10): 2195-2203.

Pisciotto, K.A. (1981a): Distribution, thermal histories, isotopic compositions and reflection characteristics of siliceous rocks recovered by the Deep Sea Drilling Project. *In* Warme, J.E., *et al.* The Deep Sea Drilling Project: A Decade of Progress. Society of Economic Paleontologists and Mineralogists Special Publication No.32: 129-147.

Pisciotto, K.A. (1981b): Diagenetic trends in the siliceous facies of the Monterey Shale in the Santa Maria region, California. *Sedimentology* 28(4): 547-571.

Pisciotto, K.A., Mahoney, J.J. (1981): Isotopic survey of diagenetic carbonates, Deep Sea Drilling Project, Leg 63. *In* Yeats, R.S., Haq, B.U., *et al.* Initial Reports of the Deep Sea Drilling Project 63: 595-610.

Pollock, S.G. (1987): Chert formation in an Ordovician volcanic arc. *Journal of Sedimentary Petrology* 57(1): 75-87.

Prebble, W.M. (1976): The Geology of the Kekerengu-Waima River District, Northeast Marlborough. Unpublished M.Sc. Thesis. Victoria University. Wellington.

Prebble, W.M. (1980): Late Cenozoic sedimentation and tectonics of the East Coast Deformed Belt, in Marlborough, New Zealand. *In* Ballance, P.F., Reading, H.G. (Eds) Sedimentation in Oblique-Slip Mobile Zones. International Association of Sedimentologists Special Publication No.4: 217-228.

Price, G.P., (1974): Structural Geology of the Coastal Hills of Ward. Unpublished B.Sc. Honours Thesis. University of Canterbury. Christchurch. 53pp.

Raine, J.I. (1987): Geological Time Scale (Cretaceous). New Zealand Geological Survey Record 20.

Raiswell, R. (1971): The growth of Cambrian and Liassic concretions. *Sedimentology* 17(3-4): 147-171.

Raiswell, R. (1976): The microbiological formation of carbonate concretions in the Upper Lias of north east England. *Chemical Geology* 18(3): 227-244.

Raiswell, R. (1987): Non-steady state microbiological diagenesis and the origin of concretions and nodular limestones. *In* Marshall, J.D. (Ed) Diagenesis of Sedimentary Sequences. Geological Society Special Publication No.36: 41-54.

Raiswell, R. (1988a): Chemical model for the origin of minor limestone-shale cycles by anaerobic methane oxidation. *Geology* 16(7): 641-644.

Raiswell, R. (1988b): Evidence for surface reaction-controlled growth of carbonate concretions in shales. *Sedimentology* 35(4): 571-575.

Ramsay, A.T.S. (1971): Occurrence of biogenic siliceous sediment in the Atlantic Ocean. *Nature* 233(5315): 115-117.

Ramsay, A.T.S. (1973): A history of organic siliceous sediments in oceans *In* Hughes, N.F. (Eds) Organisms and Continents through Time. Special

Paper in Paleontology No.12: 199-234.

Randazzo, A.F., Zachos, L.G. (1983/1984): Classification and description of dolomite fabrics of rocks from the Floridan aquifer, U.S.A. *Sedimentary Geology* 37(3): 151-162.

Reay. M.B. (1980): Cretaceous and Tertiary Stratigraphy of Part of the middle Clarence Valley, Marlborough. Unpublished M.Sc. Thesis. University of Canterbury. 236pp.

Redwine, L.E. (1981): Hypothesis combining dilation, natural hydraulic fracturing, and dolomitization to explain petroleum reservoirs, in Monterey Shale, Santa Maria Area, California. *In* Garrison, R.E., *et al* (Eds) The Monterey Formation and Related Siliceous Rocks of California. Society of Economic Paleontologists and Mineralogists Pacific Section Book 15: 221-248.

Reeburgh, W.S. (1980): Anaerobic methane oxidation: Rate depth distribution in Skan Bay sediments. *Earth and Planetary Science Letters* 47(3): 345-352.

Reeder, R.J., Grams, J.C. (1987): Sector zoning in calcite cement crystals: Implications for trace element distribution in carbonates. *Geochimica et Cosmochimica Acta* 51(2): 187-194.

Reeder, R.J., Prosky, J.L. (1986): Compositional sector zoning in dolomite. *Journal of Sedimentary Petrology* 56(2): 237-247.

Research on Cretaceous Cycles (ROCC) Group (1986): Rhythmic bedding in Upper Cretaceous pelagic carbonate sequences: varying sedimentary response to climatic forcing. *Geology* 14(2): 153-156.

Ricken, W. (1985): Epicontinental marl-limestone alternations: event deposition and diagenetic bedding (Upper Jurassic southwest Germany) *In* Bayer, U., Seilacher, A. (Eds) Sedimentary and Evolutionary Cycles: 127-162.

Ricken, W. (1986): Diagenetic Bedding. A Model for Marl-Limestone Alternations. Lecture Notes in Earth Sciences 6. Springer-Verlag Berlin. 210pp.

Ricken, W. (1987): The carbonate compaction law: a new tool. *Sedimentology* 34(4): 571-584.

Ricken, W., Hemleben, C. (1982): Origin of marl-limestone alternation (Oxford 2) in southwest Germany. *In* Einsele, G., Seilacher, A. (Eds): Cyclic and Event Stratification: 63-71.

Riech, V. (1979): Diagenesis of silica, zeolites, and phyllosilicates at sites 397 and 398. *In* von Rad, V., Ryan, W.B.F., *et al.* Initial Reports of the Deep Sea Drilling Project 47 Part 1: 741-759.

Riech, V. (1980): Diagenesis of siliceous sediments, porcellanites, and cherts of the Moroccan Basin, Deep Sea Drilling Project sites 370, 415, 416. *In* Lancelot, Y., Winter, E.L. *et al.* Initial Reports of the Deep Sea Drilling Project 50: 725-729.

Riech, V., von Rad, U. (1979a): Silica diagenesis in the Atlantic Ocean: diagenetic potential and transformations *In* Talwani, M., Hay, W., Ryan, W.B.F. (Eds) Deep Drilling Results in the Atlantic Ocean: Continental Margins and Paleoenvironment. 315-340.

Riech, V., von Rad, U. (1979b): Eocene porcellanites and early Cretaceous cherts from western North Atlantic Basin. *In* Tucholke, B.E., Vogt, P.R., *et al.* Initial Reports of the Deep Sea Drilling Project 43: 437-456.

Rieke, H.H., Chilingarian, G.V. (1974): Compaction of Argillaceous Sediments: Developments in Sedimentology 16. Elsevier. Amsterdam. 424pp.

Ritchie, D.D. (1986): Stratigraphy, Structure and Geological History of Mid-Cretaceous Sedimentary Rocks Across the Torlesse-like/non-Torlesse Boundary in the Sawtooth Range-Coverham Area, Marlborough. Unpublished M.Sc. Thesis. University of Canterbury. Christchurch. 173pp.

Ritger, S., Carson, B., Suess, E. (1987): Methane-derived authigenic carbonates formed by subduction induced pore-water expulsion along the Oregon/Washington Margin. *Geological Society of America Bulletin* 98(2): 147-156.

Robinson, N.D. (1986): Fining-upward microrhythms with basal scows in the chalk of Kent and Surrey, England and their stratigraphic importance. *Newsletters on Stratigraphy* 17(1): 21-28.

Roehl, P.O. (1981): Dilation brecciation - A proposal mechanism of fracturing, petroleum expulsion and dolomitization in the Monterey Formation, California. *In* Garrison, R.E., *et al* (Eds) The Monterey Formation and Related Siliceous Rocks of California. Society of Economic Paleontologists and Mineralogists Pacific Section Book 15: 285-315.

Rosen, M.R., Miser, D.E., Starcher, M.A., Warren, J.K. (1989): Formation of dolomite in the Coorong region. South Australia. *Geochimica et Cosmochimica Acta* 53(3): 661-669.

Rossman, G.R., Weis, D., Wasserburg, G.J. (1987): Rb, Sr, Nd, and Sm concentrations in quartz. *Geochimica et Cosmochimica Acta* 51(9): 2325-2329.

Saller, A.H. (1984): Petrologic and geochemical constraints on the origin of subsurface dolomite, Enewetok Atoll: An example of dolomitizing by normal seawater. *Geology* 12(4): 217-220.

Sass, E. (1965): Dolomite-calcite relationships in sea water: theoretical considerations and preliminary experimental results. *Journal of Sedimentary Petrology* 35(2): 339-347.

Sass, E., Kolodny, Y. (1972): Stable isotopes, chemistry and petrology of carbonate concretions (Mishash Formation, Israel). *Chemical Geology* 10(4): 261-286.

Savin, S.M. (1977): The history of the earth's surface temperature during the past 100 million years. *Annual Review of Earth and Planetary Sciences* 5: 319-355.

Savin, S.M., Douglas, R.G., Stehli, F.G. (1975): Tertiary marine paleotemperatures. *Geological Society of America Bulletin* 86(11): 1499-1510.

Savin, S.M., Yeh, H-W. (1981): Stable isotopes in ocean sediments. *In*

Emiliani, C. (Ed) The Oceanic Lithosphere: The Sea Volume 7. 1521-1554.

Schlanger, S.O., Douglas, R.G. (1974): The pelagic ooze-chalk-limestone transition and its implications for marine stratigraphy. *In* Hsü, K.J., Jenkyns, H.C. (Eds) Pelagic Sediments: On Land And Under The Sea. International Association of Sedimentologists Special Publication No.1: 117-148.

Scholle, P.A. (1974): Diagenesis of Upper Cretaceous chalks from England, Northern Ireland, and the North Sea. *In* Hsü, K.J., Jenkyns, H.C. (Eds) Pelagic Sediments On Land And Under The Sea. International Association of Sedimentologists Special Publication No.1: 177-210.

Scholle, P.A. (1977): Chalk diagenesis and its relation to petroleum exploration: oil from chalks, a modern miracle? *American Association of Petroleum Geologists Bulletin* 61(7): 982-1009.

Scholle, P.A., Arthur, M.A., Ekdale, A.A. (1983): Pelagic environment *In* Scholle, P.A., Bebout, D.G., Moore, G.H. Carbonate Depositional Environments. American Association of Petroleum Geologists Memoir 33: 620-691.

Schwarzacher, W., Fischer, A.G. (1982): Limestone-shale Bedding and Perturbations of the Earths orbit. *In* Einsele, G., Seilacher, A. (Eds) Cyclic and Event Stratification: 72-95.

Shackleton, N.J., Kennett, J.P. (1975): Paleotemperature history of the Cenozoic and the initiation of Antarctic Glaciation: Oxygen and carbon isotope analyses in DSDP sites 277, 279, and 281. *In* Kennett, J.P., Houtz, R.E., *et al.* Initial Reports of the Deep Sea Drilling Project 29: 743-755.

Sheppard, S.M.F., Schwarcz, H.P. (1970): Fractionation of carbon and oxygen isotopes and magnesium between metamorphic calcite and dolomite. *Contributions to Mineralogy and Petrology* 26(3): 161-198.

Shinn, E.A., Halley, R.B., Hudson, J.H., Lidz, B.H. (1977): Limestone compaction: an enigma. *Geology* 5(1): 21-24.

Shukla, V. (1986): Epigenetic dolomitization and the origin of xenotopic dolomite texture - Discussion. *Journal of Sedimentary Petrology* 56(5): 733-734.

Sibley, D.F. (1980): Climatic control of dolomitization, Seroe Domi Formation (Pliocene), Bonaire, N.A. *In* Zenger, D.H., *et al.* (Eds) Concepts and Models of Dolomitization. Society of Economic Paleontologists and Mineralogists Special Publication No.28: 247-258.

Sibley, D.F. (1982): The origin of common dolomite fabrics: clues from the Pliocene. *Journal of Sedimentary Petrology* 52: 1087-1100.

Sibley, D.F., Dedoes, R.E., Bartlett, T.R. (1987): Kinetics of dolomitization. *Geology* 15(12): 1112-1114.

Sibley, D.F., Gregg, J.M. (1987): Classification of dolomite rock textures. *Journal of Sedimentary Petrology* 57(6): 967-975.

Siever, R. (1962): Silica solubility, 0-200°C, and the diagenesis of siliceous sediments. *Journal of Geology* 70(2): 127-150.

Siever, R., Woodford, N. (1973): Sorption of silica by clay minerals. *Geochimica et Cosmochimica Acta* 37(8): 1851-1880

Smale, D. (1985): Heavy Minerals in Cretaceous Sandstones in Marlborough. New Zealand Geological Survey Report SL14. 29pp.

Sommer, S.E. (1972a): Cathodoluminescence of carbonates, 1. Characterization of cathodoluminescence from carbonate solid solutions. *Chemical Geology* 9(4): 257-273.

Sommer, S.E. (1972b): Cathodoluminescence of carbonates, 2. Geological applications. *Chemical Geology* 9(4): 275-284.

Speight, R., Wild, L.J. (1918): The stratigraphical relationship of the Weka Pass Stone and the Amuri Limestone. *Transactions of the New Zealand Institute* 50: 65-93.

Sperber, C.M., Wilkinson, B.H., Peacor, D.R. (1984): Rock composition, dolomite stoichiometry, and rock/water reactions in dolomite

carbonate rocks. *Journal of Geology* 92(6): 609-622.

Spörli, K. B. (1980): New Zealand and oblique-slip margins: tectonic development up to and during the Cainozoic. *In* Ballance, P.F., Reading, H.G. (Eds) Sedimentation in Oblique-Slip Mobile Zones. International Association of Sedimentologists Special Publication No.4: 147-170.

Stein, C.L., Kirkpatrick, R.J. (1976): Experimental porcelanite recrystallization kinetics: A nucleation and growth model. *Journal of Sedimentary Petrology* 46(2): 430-435.

Steinen, R.P. (1978): On the diagenesis of lime mud: scanning electron microscope observations of subsurface material from Barbados, W.I. *Journal of Sedimentary Petrology* 48(4): 1139-1148.

Steinitz, G. (1970): Chert "dike" structures in Senonian chert beds, Southern Negev, Israel. *Journal of Sedimentary Petrology* 40(4): 1241-1254.

Strong, C.P. (1977): Cretaceous-Tertiary boundary at Woodside Creek, north-eastern Marlborough. *New Zealand Journal of Geology and Geophysics* 20(4): 687-696.

Strong, C.P., Brooks, R.R., Orth, C.J., Mao, X-Y. (1988): An iridium-rich calcareous claystone (Cretaceous-Tertiary boundary) from Wharanui, Marlborough, New Zealand. *New Zealand Journal of Geology and Geophysics* 31(2): 191-195.

Strong, C.P., Brooks, R.R., Wilson, S.M. Reeves, R.D., Orth, C.J., Mao, X-Y., Quintania, L.R., Anders, E. (1987): A new Cretaceous-Tertiary boundary site at Flaxbourne River, New Zealand: Biostratigraphy and geochemistry. *Geochimica et Cosmochimica Acta* 51(10): 2769-2777.

Suess, E. (1979): Mineral phases formed in anoxic sediments by microbial decomposition of organic matter. *Geochimica et Cosmochimica Acta* 43(3): 339-352.

Suggate, R.P. (1958): The geology of the Clarence Valley from Gore Stream to Bluff Hill. *Transactions of the Royal Society of New Zealand*

85(3): 397-408.

Suggate, R.P. (1974): Coal ranks in relation to depth and temperature in Australian and New Zealand oil and gas wells. *New Zealand Journal of Geology and Geophysics* 17(1): 149-167.

Swett, K. (1965): Dolomitization, silicification and calcitization in Cambro-Ordovician oolites from northwest Scotland. *Journal of Sedimentary Petrology* 35(4): 928-938.

Taberner, C., Santisteban, C. (1987): Mixed-water dolomitization in a transgressive beach-ridge system, Eocene Catalan Basin, NE Spain. *In* Marshall, J.D. (Ed) Diagenesis of Sedimentary Sequences. Geological Society Special Publication No 36: 123-139.

Tada, R., Iijima, A. (1983): Identification of mixtures of opaline silica phases and its implication for silica diagenesis. *In* Iijima, A., *et al.* (Eds) Siliceous Deposits in the Pacific Region. Developments in Sedimentology 36: 229-245.

Taliaferro, N.L. (1934): Contraction phenomenon in cherts. *Geological Society of America Bulletin* 45(2): 189-232.

Tarr, W.A. (1917): Origin of chert in the Burlington Limestone. *American Journal of Science* Series 4 44(264): 409-452.

Tarr, W.A. (1938): Terminology of the chemical siliceous sediments. Report of the Commission on Sedimentology, 1937-1938. National Research Council. 8-27.

Tarutani, T., Clayton, R.N., Mayeda, T.K. (1969): The effect of polymorphism and magnesium substitution on oxygen isotope fractionation between calcium carbonate and water. *Geochimica et Cosmochimica Acta* 33(8): 987-996.

Taylor, T.R., Sibley, D.F. (1986): Petrographic and geochemical characteristics of dolomite types and the origin of ferroan dolomite in the Trenton Formation, Ordovician Michigan Basin, U.S.A. *Sedimentology* 33(1): 61-86.

Thomson. J.A. (1916): The flint-beds associated with the Amuri Limestone of Marlborough. *Transactions of the New Zealand Institute* 48: 48-58.

Thomson J.A. (1919): The geology of the middle Clarence and Ure Valleys, east Marlborough, New Zealand. *Transactions and Proceedings of the New Zealand Institute* 51: 289-349.

Towe, K.M. (1962): Clay mineral diagenesis as a possible source of silica cement in sedimentary rocks. *Journal of Sedimentary Petrology* 32(1): 26-28.

Usdowski, H.E. (1968): The formation of dolomite in sediments. *In* Müller, G., Friedman, G.M. (Eds) Recent Developments in Carbonate Sedimentology in Central Europe: 21-32.

van der Lingen, G.J., Packham, G.H. (1975): Relationships between diagenesis and physical properties of biogenic sediments of the Ontong-Java Plateau sites 288 and 289, Deep Sea Drilling Project. *In* Andrews, J.E., Packham, G.H., *et al.* Initial Reports of the Deep Sea Drilling Project 30: 443-481.

van der Lingen, Smale, G.J., Lewis, D.W. (1978): Alteration of a pelagic chalk below a paleokarst surface, Oxford, South Island, New Zealand. *Sedimentary Geology* 21(1): 45-66.

van Tuyl, F.M. (1918): The origin of chert. *American Journal of Science* 45(270): 449-456.

Veizer, J. (1983): Chemical diagenesis of carbonates: theory and application of trace element technique. *In* Arthur, M.A., *et al.* (Eds) Stable Isotopes in Sedimentary Geology. Society of Economic Paleontologists and Mineralogists Short Course Notes 10.

Veizer, J., Demovic, R. (1974): Strontium as a tool in facies analysis. *Journal of Sedimentary Petrology* 44(1): 93-115.

Veizer, J., Lemieux, J., Jones, B., Gibling, M.R., Savelle, J. (1977): Sodium: paleosalinity indicator in ancient carbonate rocks. *Geology* 5(3): 177-179.

Veizer, J., Lemieux, J., Jones, B., Gibling, M.R., Savelle, J. (1978): Paleosalinity and dolomitization of a Lower Paleozoic carbonate sequence, Somerset and Prince of Wales Islands, Arctic Canada. *Canadian Journal of Earth Sciences* 15(9): 1448-1461.

von der Borch, C.C. (1976): Stratigraphy and formation of Holocene dolomite, carbonate deposits of the Coorong area, South Australia. *Journal of Sedimentary Petrology* 46(4): 952-966.

von der Borch, C.C., Jones, J.B. (1976): Spherular modern dolomite from the Coorong area, South Australia. *Sedimentology* 23(4): 587-591.

von der Borch, C.C., Lock, D.E. (1979): Geological significance of Coorong dolomites. *Sedimentology* 26(6): 813-824.

von der Borch, C.C., Lock, D.E., Schwebel, D.J. (1975): Ground - water formation of dolomite in the Coorong region of South Australia. *Geology* 3(5): 283-285.

von Rad, U., Rösch, H. (1972): Mineralogy and origin of clay mineral, silica and authigenic silicates in Leg 14 sediments. *In* Hayes, D.E., Pimm, A.C., *et al.* Initial Reports of the Deep Sea Drilling Project 14: 727-751.

von Rad, U., Rösch, H. (1974): Petrography and diagenesis of deep-sea cherts from the central Atlantic. *In* Hsü, K.J., Jenkyns, H.C. (Eds) Pelagic Sediments: on Land and Under the Sea. International Association of Sedimentologists Special Publication No.1: 327-347.

von Rad, U., Riech, V., Rösch, H. (1978): Silica diagenesis in continental margin sediments off NW Africa. *In* Gardner, J., Herring, J., *et al.* Initial Reports of the Deep Sea Drilling Project 41: 879-897.

Wakefield, S.J. (1982): Silica distribution in interstitial waters and sediments from the southeastern Pacific. *Sedimentary Geology* 31(1): 13-31.

Walkden, G.M., Berry, J.R. (1984): Natural calcite in cathodoluminescence: crystal growth during diagenesis. *Nature* 308(5959): 525-527.

Wanless, H.R. (1979): Limestone response to stress: pressure-solution and dolomitization. *Journal of Sedimentary Petrology* 49(2): 437-462.

Wanless, H.R. (1983): Burial diagenesis in limestones. *In* Parker, A., Sellwood, B.W. (Eds) Sediment Diagenesis. Proceedings of the NATO Advanced Study Institute on Sediment Diagenesis 1981. Series C. Mathematical and Physical Sciences Volume 115: 379-417.

Ward, W.C., Halley, R.B. (1985): Dolomitization in a mixing zone of near-seawater composition, Late Pleistocene, northeastern Yucatan Peninsula. *Journal of Sedimentary Petrology* 55(3): 407-420.

Warren. G. (1978): Torlesse Supergroup - Eastern South Island. *In* Suggate, R.P., *et al*.. (Eds) The Geology of New Zealand Volume I: 271-277.

Weaver, F.M., Wise, S.W. (1972): Ultramorphology of deep-sea cristobalitic chert *Nature Physical Science* 237(73): 56-57.

Weaver, F.M., Wise, S.W. (1974): Opaline sediments of the south eastern Coastal Plain and Horizon A: biogenic origin. *Science* 184(4139): 899-901.

Webb, P.N. (1966): New Zealand Late Cretaceous Foraminifera and Stratigraphy. Unpublished Ph.D. Thesis. University of Utrecht. Utrecht.

Weber, J.N. (1964a): Trace element composition of dolostones and dolomites and its bearing on the dolomite problem. *Geochimica et Cosmochimica Acta* 28(11): 1817-1868.

Weber, J.N. (1964b): Oxygen isotope fractionation between coexisting calcite and dolomite. *Science* 145(3638): 1303-1305.

Weis, D., Wasserburg, G.J. (1987): Rb-Sr and Sm-Nd systematics of cherts and other siliceous deposits. *Geochimica et Cosmochimica Acta* 51(4): 959-972.

Wellman, H.W. (1945): Flint, Kaikoura. *New Zealand Journal of Science and Technology* B27(2): 156-157.

Weyl, P.K. (1960): Porosity through dolomitization: conservation of mass requirements. *Journal of Sedimentary Petrology* 30(1): 85-90.

White, A.F. (1978): Sodium coprecipitation in calcite and dolomite. *Chemical Geology* 23(1): 65-72.

Williams, L.A., Crerar, D.A. (1985): Silica diagenesis, II. General mechanisms. *Journal of Sedimentary Petrology* 55(3): 312-321.

Williams, L.A., Parks, G.A., Crerar, D.A. (1985): Silica diagenesis, I. Solubility controls. *Journal of Sedimentary Petrology* 55(3): 301-311.

Wise, S.W., Buie, B.F., Weaver, F.M. (1972): Chemically precipitated sedimentary cristobalite and the origin of chert. *Eclogae Geologie Helvetiae* 65(1): 157-163.

Wise, S.W., Weaver, F.M. (1974): Chertification of oceanic sediments *In* Hsü, K.J., Jenkyns, H.C. (Eds) Pelagic sediments: On Land and Under the Sea. International Association of Sedimentologists Special Publication No.1: 301-326.

Wolfe, M.J., (1968): Lithification of carbonate mud: Cenomanian chalk in Northern Ireland. *Sedimentary Geology* 2(4): 263-290.

Xun, Z., Fairchild, I.J. (1987): Mixing zone dolomitization of Devonian carbonates, Guangxi, South China. *In* Marshall, J.D. (Ed) Diagenesis of Sedimentary Sequences. Geological Society Special Publication No.36: 157-170.

Yamamoto, K. (1987): Geochemical characteristics and depositional environments of cherts and associated rocks in the Franciscan and Shimanto Terranes. *Sedimentary Geology* 52(1/2): 65-108.

Yamamoto, S. (1981): Metallic trace elements in some chert nodules of Pacific Seamounts: a comparative study. *In* Vallier, T.L., Thiede, J., *et al* Initial Reports of the Deep Sea Drilling Project 62: 773-777.

Zankl, H., (1969): Structural and textural evidence of early lithification in fine-grained carbonate rocks. *Sedimentology* 12(3/4): 241-256.

Zen, E-A., (1959): Clay mineral-carbonate relations in sedimentary rocks. *American Journal of Science* 257(1): 29-43.

Zenger, D.H., Dunham, J.B., Ethington, R.L., (Eds) (1980): Concepts and Models of Dolomitization. Society of Economic Paleontologists and Mineralogists Special Publication No.28. 320pp.

Zenger, D.H. (1983): Burial dolomitization in the Lost Burro Formation (Devonian), east-central California, and the significance of late diagenetic dolomitization. *Geology* 11(9): 519-522.

APPENDIX 1

METHODOLOGY

A1.1. GENERAL TECHNIQUES

A summary of the techniques is shown in Figure A1.1.

A1.1.1. FIELDWORK

Sections were measured by tape and compass survey, and sampled at intervals to give a representative coverage of observed lithological variations. Visual estimates were made of the proportions of chert, dolomite and micrite. Chert colour was determined using Goddard *et al.* (1970).

A1.1.2. THIN SECTIONS

Thin sections were made using standard techniques (see Lewis 1984 and others) with the following modifications:

(i) Chert samples: the rock slice was glued with epoxy resin to prevent it from being plucked from the slide during grinding.

(ii) Shattered samples: fragments were poured into moulds containing epoxy resin and allowed to harden. The 'reconstituted' sample was then glued to a glass slide with epoxy, and thin sectioned as per normal.

Estimates of the proportions of detrital constituents in thin sections were made using the comparator chart in Figure A1.2.

A1.1.3. POLISHED SECTIONS AND ELECTRON MICROPROBE ANALYSIS

Polished Sections

Polished sections were made by gluing rock slices to glass slides using epoxy resin. The samples were ground to thin section thickness (0.03 mm) using progressively finer grade carborundum grit and carborundum paper. Once at the correct thickness samples were then polished with an Al_2O_3 paste on an automatic polishing machine to remove all surface scratches and pits. The quality of the polish was checked using a reflecting light microscope.

Microprobe Analysis

Analyses were performed at the Geology Department, University of Otago,

Non-carbonate

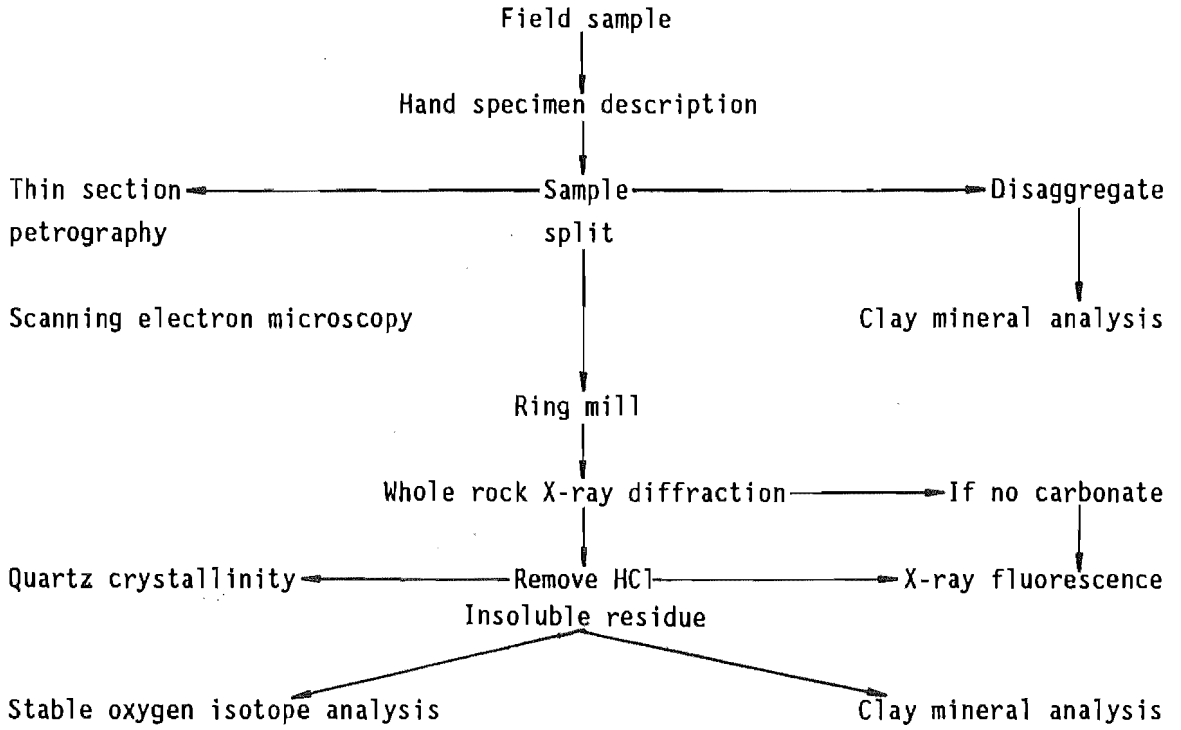

Carbonate

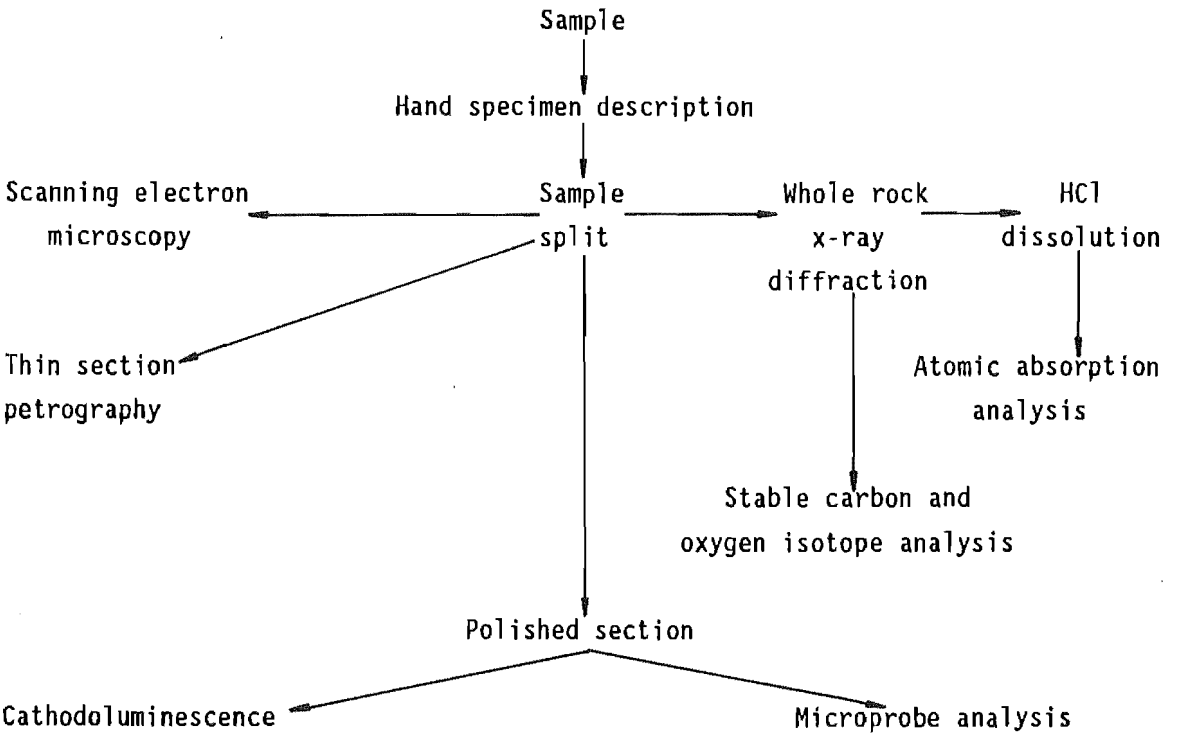

Figure A1.1 Flow diagram of sample analyses. It should be noted that carbonate and chert analyses could be performed on a single sample however, not all analyses were performed on every sample.

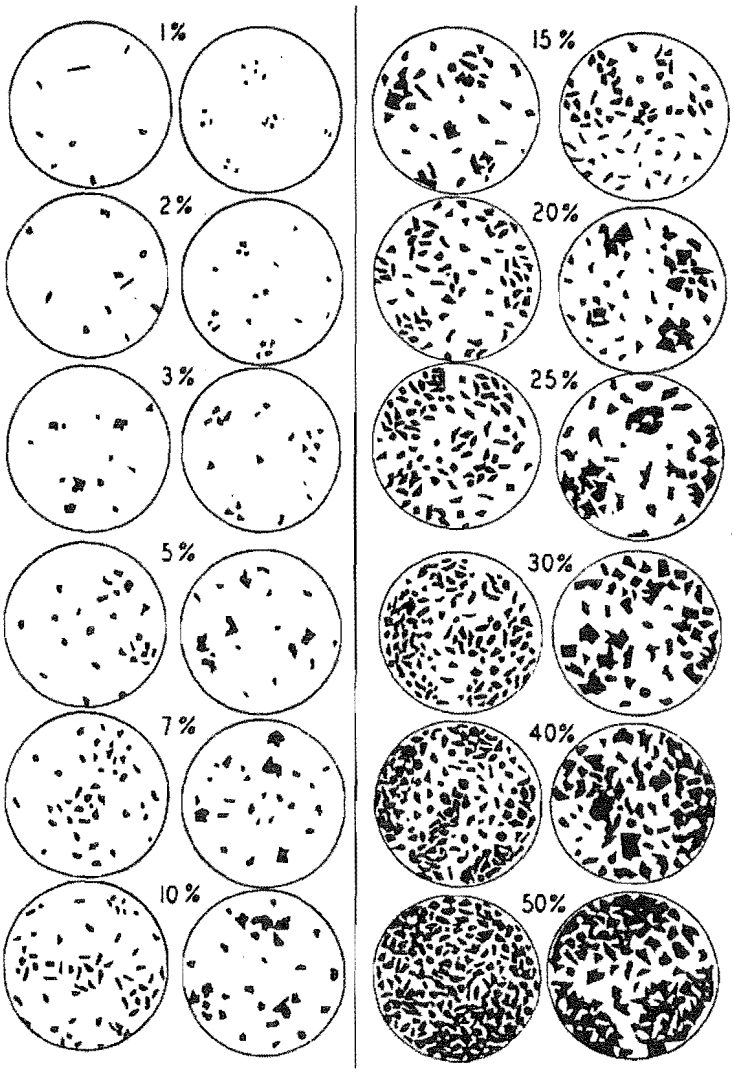

Figure A1.2 Comparator for estimation of percentages of constituents (reproduced after R.D. Terry and G.V. Chilingar, 1955: *Journal of Sedimentary Petrology* 25: 229-334 and American Geological Institute Data Sheet 6).

under the guidance of Dr Y. Kawachi. Polished sections were initially cleaned with ethanol, amyl acetate, and acetone to remove all traces of organic contamination. They were then carbon coated using a JEOL JEE Carbon Coater. The carbon coat provides a conducting surface on the sample for the electron beam. A JEOL JXA-5A Electron Probe X-Ray Micro-analyser with an attached EDS system was used for analyses.

The instrument was calibrated on a "standard" feldspar crystal. Unlike silicate analyses where all cations can be assumed to be bonded to oxygen, cations in carbonates are bonded to a CO_3^{2-} radicle. To compensate for this difference, co-ordination with 6 oxygen ions was assumed. If the total cations in the analysis did not add up to 6 then the result was discarded [Figure A1.3].

Estimated sensitivities for elements (in weight%) are as follows (Dr Y. Kawachi *pers. comm.* 1987): MgO = 0.3, CaO = 0.15, FeO and MnO = 0.1. All microprobe analyses were recalculated to mole% carbonate.

A1.1.4. SCANNING ELECTRON MICROSCOPY (SEM)

SEM Images of Fresh Fracture Surfaces

Samples were broken and fragments with suitable fracture surfaces were selected for analysis. Sample fragments and stubs were cleaned and then soaked in ethanol briefly and dried. The stubs were made of aluminium, about 12 mm in diameter. After drying, neither samples nor stubs were touched by hand. Sample fragments, preferably with flat upper surfaces were glued to the stub using a quick-bonding adhesive, to ensure there was no gap between stub and sample. A copper suspension was then painted onto the glue to ensure a complete conducting surface between sample and stub [Figure A1.4]. Samples were then Au coated for high quality photographs. Instrumentation consisted of a Cambridge Stereoscan 250 Mark II.

SEM Electron Maps

In addition to the high resolution imaging described above, an attempt was made to detect compositional differences within single crystals using the SEM-EDAX system. A polished section was etched in 10% HCl for about 30 seconds to create a surface relief enabling differentiation of carbonate

(a)

MINERAL & SPOT # : WPT3 XTAL 3 POINT 8
NO. OF OXYGEN : 6.0

	WT %	CATIONS
FEO	.59	.048
MNO	.56	.046
MGO	17.71	2.546
CAO	32.54	3.361
TOTAL	51.40	6.000

(b)

MINERAL & SPOT # : WC2 XTAL 4 POINT 3
NO. OF OXYGEN : 6.0

	WT %	CATIONS
AL2O3	1.78	.197
MGO	17.53	2.457
CAO	32.23	3.247
TOTAL	51.54	5.901

Figure A1.3 Example of microprobe printout. (a) is a good analysis whereas in (b) the total cations do not add up to the number of oxygens specified. This suggests that some non-carbonate contaminant has been included in the analysis and the result should therefore be discarded. The limit of acceptability for total cations is 6.000 ± 0.002.

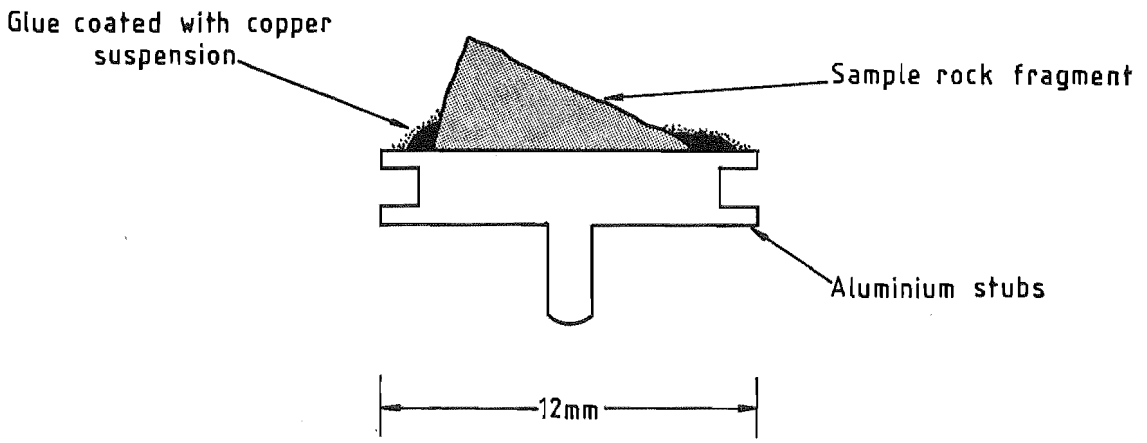

Figure A1.4 Cross-section of an SEM sample mount.

and noncarbonate. Although the resultant maps were of good quality the sensitivity of the detector was such that no differences within dolomite crystals were detected. Therefore the analysis was not continued beyond preliminary investigation.

A1.1.5. CLAY MINERAL ANALYSIS

Clay mineral analyses were performed on the <4ϕ fraction from the upper Woolshed Formation. Samples were first disaggregated, sometimes with the aid of calgon, and the desired size fraction obtained by pipette analysis (Lewis 1984). To obtain enough material, sample concentration was employed in some cases. Mineral phases were identified using X-ray diffraction (XRD). An attempt was made to identify clay minerals in cherts using ring-milled powders, but was singularly unsuccessful.

A1.2. CHERT/INSOLUBLE RESIDUE TECHNIQUES

A1.2.1. SAMPLE PRETREATMENT

Cherts were analyzed on a $CaCO_3$-free basis, so a pre-treatment technique was devised as follows:

(i) Selected samples were crushed to small fragments, then hand-picked for powdering. As little calcareous material as possible was included.

(ii) Fragments were powdered in a tungsten-carbide ring-mill. Milling times of three to five minutes were common, although some samples required longer. Powders were stored in small sealed plastic bags.

(iii) Before further processing, whole rock mineralogy was determined by XRD of subsamples. The presence or absence of carbonates determined the next pre-treatment step. Additional checks were performed on some samples with HCl. Non-calcareous samples were prepared for X-ray Fluorescence (XRF) analysis directly.

(iv) Samples containing carbonate were weighed into pyrex or polyethylene beakers. A solution of approximately 20% v/v HCl was added to digest the carbonate. The solutions were stirred periodically and more acid was added until all visible reaction ceased. To aid dissolution, dolomite samples were heated to about 60°C over a steam bath. Insoluble residues were allowed to sink to the bottom of the beaker on completion of the reaction. The supernatant was siphoned

off and distilled water added and thoroughly mixed. After the residue had settled the liquid was again siphoned. This rinsing process was repeated 6 times. The insoluble residues were then dried under a heat lamp or in a 110°C oven, weighed (to estimate carbonate/insoluble residue proportions), and sealed in plastic bags, ready for major and trace element analysis.

Although the first two rinses could be completed in under 12 hours, the whole rinsing process took two to three weeks. This was because with progressive H^+ removal, the pH increased resulting in less flocculation, which meant residues took progressively longer to settle from suspension. All treated residues were re-tested for carbonate using XRD and dilute HCl. The presence of carbonates lead to a repetition of the procedure.

A1.2.2. MAJOR AND TRACE ELEMENTS

Trace elements were analyzed from pressed powder pellets and major elements from fusion beads using a Phillips PW 1400 Wavelength Dispersive X-ray Fluorescence Spectrometer. For major elements a Cr x-ray tube was used; Au and Mo tubes were used for trace element analysis. Full mass absorption corrections were applied to raw count data.

Fusion Beads

Fusion beads were prepared from powdered samples according to the method of Norrish and Hutton (1969).

Pressed Powder Pellets

Seventeen grams of sample was mixed with 35-40 drops of 7% 'Mowiol' solution and pressed into discs. 'Mowiol' is a polyvinyl alcohol and is prepared as a mixture of ethyl alcohol and distilled water. It does not affect analytical sensitivity in geological samples. Sample pretreatment often caused the formation of aggregates which had to be removed by lightly hand grinding with an agate mortar and pestle prior to mixing. If there was insufficient sample smaller 7 gm pellets were prepared using 12-15 drops of 'Mowiol'.

Precision and Accuracy

Major Elements

Table A1.1 lists major element analyses and recommended values for international standards respectively. The standards were prepared by Mr A. Alloway, and used for calibration of the instrument. In addition, NBS97a was prepared by the author and analyzed as an unknown to check the accuracy and quality of sample preparation [Table A1.2].

There is good agreement between recommended and analyzed values. To check precision four samples were replicated [Table A1.3].

Relatively high errors arise from the proximity of analyses to detection limits. Minor changes in calibration can lead to wide variations in relative error. These high errors do not affect conclusions derived from elements of low concentration. The error in loss on ignition (LOI) was higher than expected, particularly for MS32. However, if the first LOI determination (-0.63%, which is probably due to a weighing error) is ignored the error for all samples reduces to 17.67 percent.

Trace Elements

Comparison of analyzed and recommended trace values for standards are listed in Table A1.4. Replicates produced identical results. Variation in grainsize of powders in pellets (up to coarse silt) did not affect precision.

A1.2.3. STABLE OXYGEN ISOTOPE ANALYSIS

The initial proposal was that chert samples would be analyzed using the facilities at the Institute of Nuclear Sciences (INS), Lower Hutt. Dr P. Blattner and C. Houston (both INS) performed some preliminary analyses to see if a major analytical programme was warranted. Nine samples were submitted from a variety of chert morphologies, representing the complete chert stratigraphy. As minimal variation was observed it was deemed not worth proceeding further.

Table A1.1 Recommended (Rec) and analyzed (Anal) major element analyses (weight% oxide) for international standards.

	AGV		G2		GA		GSP	
	Rec	Anal	Rec	Anal	Rec	Anal	Rec	Anal
SiO_2	59.72	60.23	69.19	68.22	69.96	69.72	67.31	67.67
TiO_2	1.05	1.07	0.50	0.49	0.38	0.37	0.66	0.67
Al_2O_3	17.22	17.65	15.35	15.40	14.51	14.88	15.19	15.20
Fe_2O_3	6.88	6.76	2.62	2.62	2.83	2.71	4.34	4.21
MnO	0.10	0.09	0.04	0.04	0.09	0.07	0.04	0.04
MgO	1.55	1.61	0.77	0.78	0.95	0.94	0.96	1.04
CaO	5.00	4.99	1.98	1.89	2.45	2.43	2.02	2.02
Na_2O	4.31	4.28	4.06	4.05	3.55	3.63	2.80	2.72
K_2O	2.93	2.94	4.52	4.36	4.03	3.98	5.53	5.33
LOI		0.65		0.51		0.68		0.54
P_2O_5	0.50	0.50	0.14	0.14	0.12	0.13	0.28	0.29
Total		100.81		98.51		99.55		99.71

	MRG		GH		SY-2		SiO2	
	Rec	Anal	Rec	Anal	Rec	Anal	Rec	Anal
SiO_2	39.24	38.85	75.85	75.03	60.09	60.28	100.00	99.48
TiO_2	3.75	3.76	0.08	0.09	0.15	0.15		<0.20
Al_2O_3	8.56	8.56	12.51	12.47	12.15	12.17		<0.05
Fe_2O_3	17.79	17.80	1.34	1.31	6.29	6.29		<0.05
MnO	0.17	0.16	0.05	0.03	0.32	0.29		<0.01
MgO	13.51	13.50	<0.10	<0.10	2.69	2.71		0.12
CaO	14.72	14.73	0.69	0.70	8.00	8.02		<0.01
Na_2O	0.71	0.86	3.85	3.72	4.35	4.38		0.20
K_2O	0.18	0.18	4.76	4.62	4.51	4.43		0.02
LOI		1.03		1.49		0.39		0.33
P_2O_5	0.07	0.07	<0.05	<0.05	0.44	0.44		<0.05
Total		99.50		99.57		99.54		100.22

Table A1.2 Analyzed and recommended values for NBS97a (wt%) and relative % error. The mean error is used where applicable. BDL = Below detection limits.

OXIDE	VALUE	ANALYZED	VALUE	ERROR
SiO_2	43.67	43.41	44.38	0.5
TiO_2	1.90	1.88	1.90	0.5
Al_2O_3	38.79	40.09	40.84	4.3
Fe_2O_3	0.45	0.44	0.44	2.2
MnO	-	0.02	<0.01	?
MgO	0.15	0.20	0.18	26.0
CaO	0.11	0.10	0.10	10.0
Na_2O	0.037	0.16	<0.10	BDL
K_2O	0.50	0.53	0.54	7.0
LOI	13.32	13.73	13.34	1.6
P_2O_5	0.36	0.36	0.38	2.8

Sample Pretreatment

The powdered samples used were pretreated as outlined in A1.2.1. HCl treatment to remove carbonate does not affect the $^{18}O/^{16}O$ ratio of cherts (Degens and Epstein 1962). In addition selected untreated, rock fragments of the samples were also used for comparative purposes.

Precision and Accuracy

Precision was estimated at -1·/..$_{SMOW}$ (P. Blattner *pers. comm.* 1986).

A1.2.4. QUARTZ CRYSTALLINITY

Crystallinity determinations were made on powdered, carbonate free (HCL insoluble) samples. After removal of carbonate (where necessary), powders were sieved to obtain the <45 μm (350 mesh) fraction. The experiments were performed using the techniques outlined in Murata and Norman (1976). Powdered euhedral igneous quartz was used as an internal standard.

Precision and accuracy

The precision of the method is estimated to be approximately 5 percent. Accuracy is estimated to be about 10 percent.

A1.3. CARBONATE PHASES

A1.3.1. ANALYSIS OF CARBONATE

Two methods were available for analysis of the carbonate fraction: (i) analyze as an aqueous phase using atomic absorption (AAS) or atomic emission (AAE) spectroscopy, or, (ii) analyze as a solid phase using XRF. To obtain XRF data free from contamination by insoluble residue, a whole rock and an insoluble residue fraction must be analyzed for each sample. The difference between the two being the composition of the carbonate. The volume of sample required for a pressed disc and a fusion bead is roughly 17 gm [Section A1.2.2]. The separation method would be that described already. Since the insoluble residue has to settle out through the acid after reaction there would probably be leaching of cations from clay minerals and sulphides. For some samples very large amounts of

Table A1.3 Replicate analyses and detection limits (DL). The percent error is calculated from (100 x standard deviation)/mean. A different calibration was used for samples MS37vi-MS37ix and DS3vi-DS3ix, implying that DS3 and MS37 errors may be overestimates. Percent errors were not calculated from samples with a mean below detection limits.

SAMPLE	SiO_2	TiO_2	Al_2O_3	Fe_2O3	MnO	MgO	CaO	Na_2O	K_2O	LOI	P_2O_5	TOTAL
DS3	96.67	0.05	1.25	0.13	0.02	0.11	0.11	0.22	0.21	1.21	<0.05	100.00
DS3i	96.64	0.05	1.27	0.15	0.04	0.12	0.11	0.15	0.21	1.54	<0.05	100.30
DS3ii	96.43	0.05	1.27	0.15	0.02	<0.10	0.11	0.18	0.21	1.63	<0.05	100.13
DS3iii	96.40	0.05	1.27	0.15	0.04	<0.10	0.12	0.13	0.21	1.34	<0.05	99.81
DS3iv	96.68	0.05	1.27	0.15	0.04	<0.10	0.12	<0.10	0.21	1.61	<0.05	100.32
DS3v	96.71	0.05	1.25	0.15	0.05	<0.10	0.21	0.19	0.21	1.37	<0.05	100.15
DS3vi	95.84	0.06	1.20	0.15	<0.10	<0.10	0.11	0.15	0.21	1.10	<0.05	98.93
DS3vii	95.76	0.06	1.26	0.17	<0.10	<0.10	0.11	0.10	0.21	1.42	<0.05	99.18
DS3viii	93.73	0.06	1.20	0.16	<0.10	<0.10	0.10	0.18	0.21	1.09	<0.05	96.84
DS3ix	95.11	0.06	1.25	0.16	<0.10	0.11	0.10	0.17	0.22	1.24	<0.05	98.46
Mean	96.00	0.05	1.25	0.15	0.03	<0.10	0.12	0.16	0.21	1.36	<0.05	99.41
S.Dev	.95	0.01	0.03	0.01	0.02		0.03	0.04	0.00	0.20		1.10
%Error	.99	20.00	2.40	6.67	66.67		25.00	25.00	0.00	14.71		1.11
DS9i	97.95	0.03	0.68	0.05	0.04	<0.10	0.12	<0.10	0.13	0.87	<0.05	100.01
DS9ii	97.58	0.03	0.67	0.06	0.03	<0.10	0.11	0.14	0.13	1.00	<0.05	99.81
DS9iii	96.87	0.03	0.65	<0.05	0.02	<0.10	0.09	<0.10	0.13	0.87	<0.05	98.78
DS9iv	97.70	0.03	0.64	<0.05	0.04	<0.10	0.09	<0.10	0.13	0.93	<0.05	99.65
DS9v	98.29	0.03	0.67	0.05	0.05	<0.10	0.10	<0.10	0.13	0.94	<0.05	100.41
Mean	97.68	0.03	0.66	0.05	0.04	<0.10	0.10	<0.10	0.13	0.92	<0.05	99.73
S.Dev	.53	0.00	0.02	0.00	0.01		0.01		0.00	0.05		.60
%Error	.54	0.00	3.03	0.00	25.00		10.00		0.00	5.43		.60
MS32	98.23	0.02	0.35	<0.05	<0.10	<0.10	0.04	<0.10	0.06	-0.63	<0.05	99.23
MS32i	99.08	0.02	0.34	<0.05	<0.10	<0.10	0.04	0.13	0.06	0.90	<0.05	100.63
MS32ii	98.36	0.02	0.34	<0.05	<0.10	<0.10	0.04	<0.10	0.06	0.80	<0.05	99.74
MS32iii	98.37	0.02	0.33	<0.05	<0.10	<0.10	0.04	<0.10	0.06	1.27	<0.05	100.17
MS32iv	98.47	0.02	0.35	<0.05	<0.10	<0.10	0.04	<0.10	0.07	1.00	<0.05	100.10
MS32v	98.58	0.02	0.34	<0.05	<0.10	<0.10	0.04	<0.10	0.06	0.83	<0.05	100.05
Mean	98.52	0.02	0.34	<0.05	<0.10	<0.10	0.04	<0.10	0.06	0.70	<0.05	99.99
S.dev	.30	0.00	0.01				0.00		0.00	0.67		.47
%Error	.30	0.00	2.94				0.00		0.00	95.71		.47

SAMPLE	SiO_2	TiO_2	Al_2O_3	Fe_2O3	MnO	MgO	CaO	Na_2O	K_2O	LOI	P_2O_5	TOTAL
MS37i	99.09	0.02	0.37	0.13	0.01	<0.10	0.03	0.13	0.08	0.63	<0.05	100.53
MS37ii	98.61	0.02	0.38	0.14	0.02	<0.10	0.03	<0.10	0.07	1.07	<0.05	100.42
MS37iii	98.57	0.02	0.37	0.14	0.05	<0.10	0.03	<0.10	0.07	0.87	<0.05	100.26
MS37iv	98.48	0.02	0.34	0.14	0.04	<0.10	0.03	0.14	0.07	1.06	<0.05	100.38
MS37v	98.63	0.02	0.37	0.14	0.03	<0.10	0.03	<0.10	0.07	0.82	<0.05	100.16
MS37vi	98.34	0.03	<0.20	0.14	<0.10	<0.10	0.02	0.12	0.07	0.56	<0.05	99.66
MS37vii	98.05	0.03	<0.20	0.14	<0.10	<0.10	0.02	<0.10	0.07	0.84	<0.05	99.54
MS37viii	98.16	0.03	<0.20	0.13	<0.10	<0.10	0.02	<0.10	0.07	0.52	<0.05	99.30
MS37ix	98.65	0.03	<0.20	0.13	<0.10	<0.10	0.02	<0.10	0.07	0.47	<0.05	99.72
Mean	98.49	0.02	0.30	0.14	0.02	<0.10	0.03	<0.10	0.07	0.76	<0.05	99.98
S.dev	.29	0.01	0.09	0.01	0.01		0.01		0.00	0.21		.42
%Error	.29	50.00	30.00	7.14	50.00		33.33		0.00	27.63		.42
DL	<0.20	<0.01	<0.20	<0.05	<0.01	<0.10	<0.01	<0.10	<0.01		<0.05	

Table A1.4 Recommended (Rec) and analyzed (Anal) trace element analyses (in ppm) for international standards.

	AGV		G2		GA		GSP		MRG	
	Rec	Anal	Rec	Anal	Rec	Anal	Rec	Anal	Rec	Anal
V	125	111	36	32	38	41	54	43	520	559
Cr	10	13	8	8	12	8	12	10	450	522
Ni	15	16	4	4	7	6	9	9	195	188
Zn	86	81	84	83	80	71	105	92	190	188
Ga	21	20	23	22	16	15	23	21	18	19
Rb	67	66	170	173	175	175	254	252	8	7
Sr	660	664	480	484	310	309	240	232	260	260
Y	19	20	11	10	21	21	29	25	16	14
Zr	230	235	300	314	150	135	500	504	105	72
Nb	16	17	13	13	10	14	23	27	20	20
Ba	1200	1220	1900	1951	850	837	1300	1328	-	-
Ce	71	73	160	180	70	60	360	324	25	19
Nd	37	29	58	59	25	37	190	145	19	23
La	36	41	92	101	38	31	195	136	-	10
Pb	33	35	30	33	30	30	54	48	10	8
Th	6	5	25	24	17	16	105	98	1	3

material would be required to obtain adequate insoluble residue. Production of two fusion beads in addition to the pretreatment would have been considerably time consuming. However, the technique has the advantage that it analyzed a greater range of elements. A pilot study for this technique showed that for some elements, Na in particular, concentrations were near XRF detection limits. When the insoluble residue values were subtracted from whole rock values, negative results were obtained. It was decided to opt for analysis of the carbonate in the aqueous phase as the simpler and more accurate method. This meant fewer elements could be analyzed overall however, all the key elements in carbonate diagenesis were covered; that is Ca, Mg, Mn, Fe, Sr, Na, and K.

Experimental Carbonate Determinations

The weight percent carbonate dissolved from each sample must be accurately determined. Two techniques are currently available: (i) NaOH titration, and, (ii) weight by difference. An experiment was designed to determine the most efficient method. For an AAS/AAE analysis of carbonate about one gram of sample was dissolved, filtered and made up to 250 ml. The experiment utilized a 'synthetic' rock powder consisting of AR $CaCO_3$ and acid cleaned rhyolitic quartz. All glassware was acid washed and all solutions were made with glass distilled, de-ionized water. The procedure is listed below:

i) Accurately weighed proportions of AR $CaCO_3$ and quartz, totalling about one gram were weighed into a 250 ml conical flask.

ii) 25 ml of ~1N (10% v/v) AR HCl was pipetted onto the sample, and allowed to react. This quantity of HCl is in excess of that required to dissolve one gram of $CaCO_3$. Dissolution was deemed complete once all visible reaction had ceased.

iii) The solution and insoluble residue was filtered through pre-weighed Millipore Type HA (or similar) 0.45 µm filter papers. The conical flask was rinsed thoroughly with distilled water as was the filter to ensure all reacted solution was collected.

iv) The filter papers were stored on petrie dishes and the filter holder was rinsed so all the insoluble residue was collected. The filter papers were dried at 60°C then re-weighed. The amount of carbonate dissolved is the difference between the filter paper plus residue and the initial weight of the filter paper. It was found that there was variability in weight due to atmospheric moisture, so filters were

stored in a desiccator prior to initial weighing, and after drying the sample while cooling. Desiccation was found to reduced the variability between weighings over a 48 hour period [Table A1.5].

v) The filtered solution (from iv) is then made up accurately to 250 ml.

vi) A 25 ml aliquot of this solution was titrated with 1N NaOH and a phenolpthalein indicator to determine the quantity of HCl left after dissolution of the carbonate. The end point is when the first permanent pink colour was observed. Titrations were repeated until reproducibility was ±0.02 ml. The following calculation was then used to determine the weight of carbonate dissolved:

$$CaCO_3 \text{ (gm)} = [(A \times B \times C)-((D \times E) - F)] \times G/C \times 0.5 \times 100.08$$

where:

A = HCl molarity/1000
B = Volume of HCl used/total volume of the sample (in this case usually 250 ml)
C = Volume of sample titrated (usually 25 ml)
D = NaOH molarity/1000
E = Volume of NaOH used
F = Concentration of the blank
G = Total volume of the sample (250 ml)
0.5 = From reaction stoichiometry
100.08 = Molecular weight of $CaCO_3$

Figure A1.5 shows the percentage error in titrated and weight by difference methods. Both methods are increasingly accurate with higher carbonate concentrations however, the weight by difference technique appears the most accurate overall and was used for all analyses. Therefore the method adopted for analyses was as follows:

i) Weigh accurately into a 250 ml conical flask approximately one gram of sample.

ii) Add approximately 25 ml of ~10% v/v HCl, allow to react until all visible reaction has ceased. Dolomitic samples were heated to 60°C over a steam bath to aid reaction.

iii) Once all visible reaction had ceased, samples were filtered as described earlier. Filter papers were stored in a desiccator prior to initial weighing and during cooling of samples before re-weighing.

iv) Filtrates were made up to 250 ml and stored in acid cleaned

Table A1.5 Variation between desiccated and undesiccated filters plus residues over 48 hours.

Sample	Weight	% Variation
KP14b	0.8702	0.54
KP3/9	0.7788	0.72
KP3/6	0.8594	0.48
KP3/3	0.8765	0.23 (desiccated)
KP3/10	0.8639	0.52
KP3/7	0.8185	0.59
KP3/4	0.8401	0.24 (desiccated)
KP3/2	0.8555	0.29 (desiccated)
KP3/8	0.8363	0.38 (desiccated)
NBS88a(iii)	0.9752	0.41 (desiccated)
NBS1c(iii)	0.9066	0.47 (desiccated)
LS3	0.5412	0.87

Figure A1.5 Plot of percent error versus weight of carbonate analyzed displaying the accuracy of weight% carbonate determination methods. Open circles = carbonate determinations by titration and closed circles = carbonate determinations by weight difference.

$$\text{The percent error} = ((W_i - W_a)/W_i) \times 100$$

where:

W_i = the initial weight of carbonate in the sample.

W_a = the analyzed weight of carbonate in the sample.

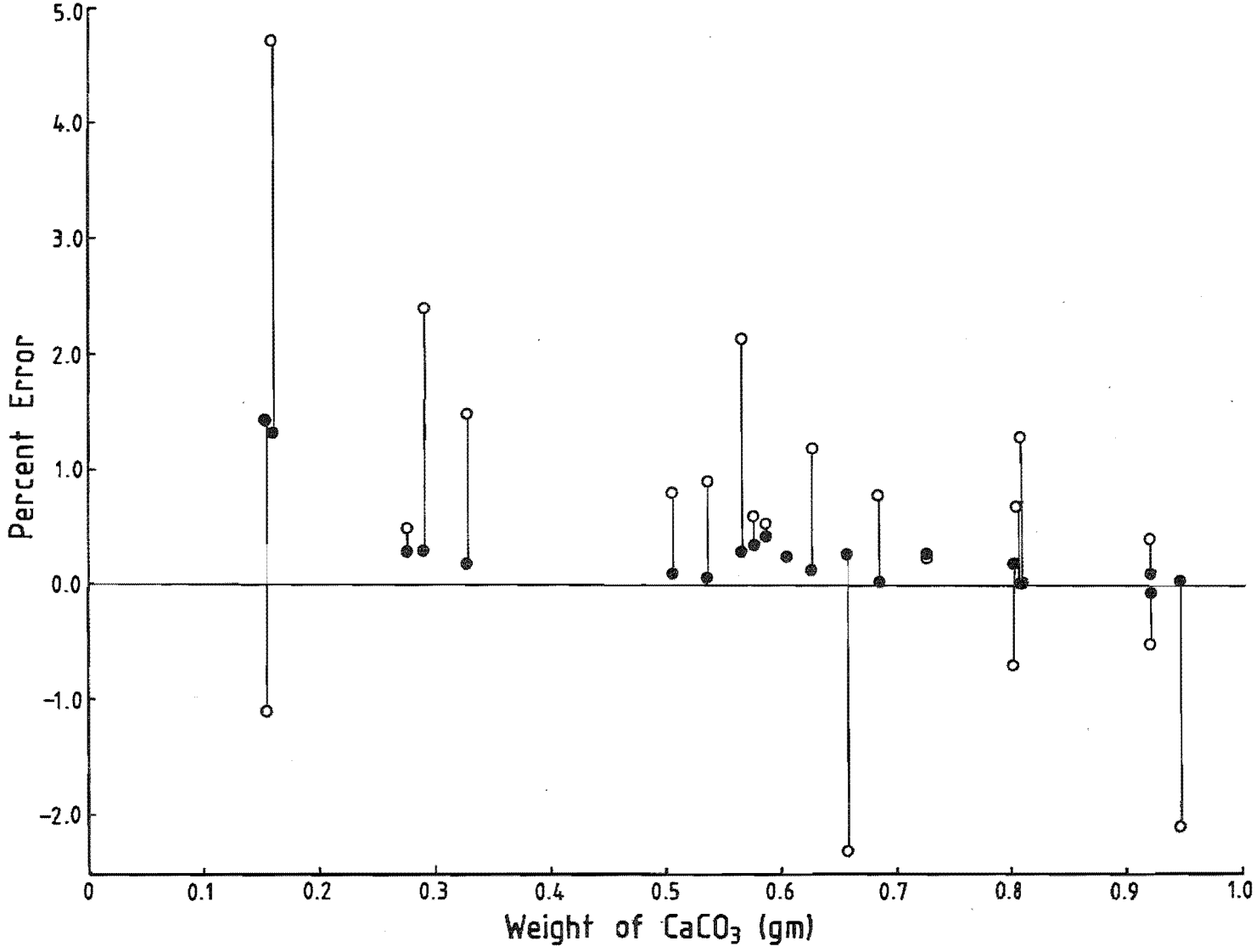
5.0
4.0
3.0
2.0
1.0
0.0
-1.0
-2.0
Percent Error
0
0.1
0.2
0.3
0.4
0.5
0.6
0.7
0.8
0.9
1.0
Weight of $CaCO_3$ (gm)

polyethylene or polypropylene bottles at 4°C, ready for analysis. It was later discovered that this is a modified version of the method designed by Molnia (1974).

A1.3.2. ELEMENTAL ANALYSIS

Table A1.6 lists the instrumentation used. Analytical stock standard solutions were made up from the AR grade reagents listed in Table A1.7.

Production of analytical standards was according to APHA (1975) and the Varian Techtron Manual. Samples were analyzed in the concentration ranges specified in the Varian Techtron Manual. Analytical standards had a matrix added which approximated the composition of the dissolved samples. A releasing agent (about 2000 ppm K^+) was added to all standards and blanks for Ca, Mg, and Sr analyses.

Ca Enhancement

All elements with the exception of Sr were analyzed without problem. Establishing calibration curves for Sr proved difficult. Emission lines for Sr are near low intensity Ca emission lines. Although these lines are minor they apparently interfere because of high concentrations of Ca in solutions. An experiment was designed to quantify the effect. Known concentrations of Ca (0-1000 ppm) were added to Sr standards [Figure A1.6]. About 1000 ppm Ca^{2+} will artificially increase the concentration of Sr^{2+} by approximately 1 ppm. The Ca^{2+} did not affect Mg^{2+} concentrations. It was subsequently found that similar experiments had been performed by Grabowski and Unice (1958) where similar effects were observed.

From these curves corrections for analyzed results could be obtained. Analysis of standards NBS88a and NBS1c showed corrected data to be less accurate than uncorrected data. Investigation of the literature dealing with AA analyses of carbonates does not mention this problem (this excludes papers where standard addition techniques were used). There is commonly no implicit statement that corrections were or were not made on primary analyses, for example see Amiel *et al.* (1973). Brand and Veizer (1980) do not appear to add matrices to solutions. They state that Ca^{2+} was added only to Na^+ calibration solutions and standard rock solutions.

Table A1.6 Analytical instrumentation for analysis of carbonate phases. AAS = Atomic absorption spectroscopy, AES = Atomic emission spectroscopy, FP = Flame photometry.

ANALYTE	METHOD	INSTRUMENTATION
Ca, Mg, Fe, Mn, Zn	AAS-air acetylene flame	Varian Techtron
Sr, Ba	AES-nitrous oxide/ acetylene flame	as above
Na, K	FP-air propane flame	Eel Flame Photometer

Table A1.7 Reagents used to make standard solutions. (H^+) indicates the solution was acidified.

ELEMENT	COMPOUND
Ca	$CaCO_3$ + AR HCl
Mg	$MgCl_2.6H_2O$ (H^+)
Mn	$MnSO_4.4H_2O$ (H^+)
Fe	$(NH_4)_2SO_4.FeSO_4.6H_2O$ (H^+)
Sr	$SrCl_2.6H_2O$ (H^+)
K	KCl (H^+)
Na	NaCl (H^+)

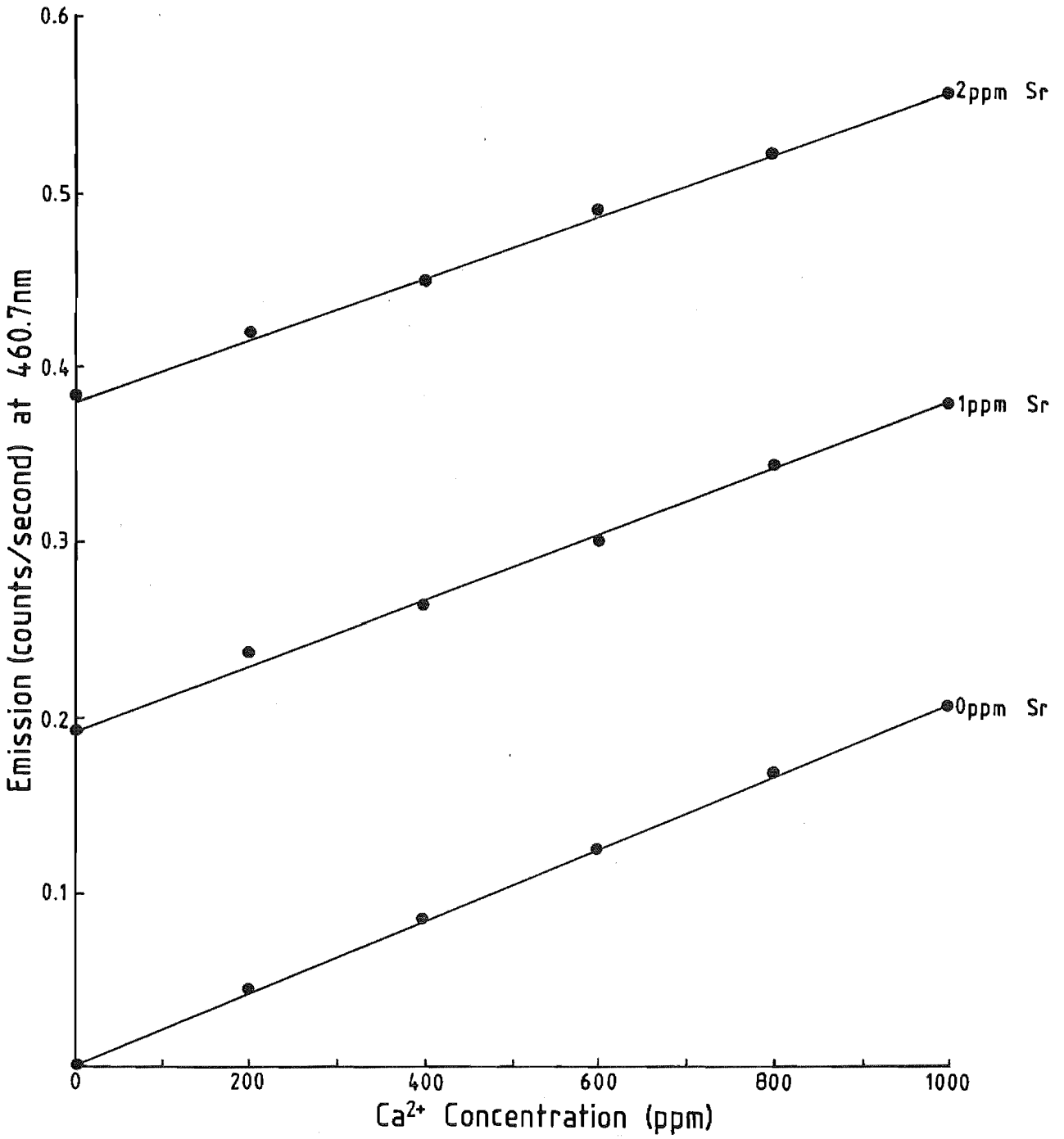

Figure A1.6 Graph showing the effect of Ca^{2+} concentration on Sr^{2+} emission.

Therefore in both cases it appears that Ca enhancement of Sr was either not considered or possibly deemed insignificant.

Analysis of Sr in this thesis was performed using calibration standards without the addition of a matrix. Results tended to be lower compared to known standards. Higher values due to enhancement were expected instead. In addition variations in Ca did not consistently parallel Sr variations within chemically grouped samples. In hindsight the standard addition technique may have been preferable despite being considerably more time consuming.

Precision and Accuracy

Precision and accuracy for elemental analyses of carbonates is summarized in Table A1.8. Good analytical precision is obtained, usually being <11 percent. The relatively high error in accuracy is noted.

The highest accuracy errors are associated with lowest concentrations (as observed for XRF analyses, Section A1.2.2), usually those less than 0.03 weight percent, for example Sr and to some extent Mn. As concentrations increase the error decreases. Sr, Na, and Mn are in much higher concentrations in samples than in the analyzed standards, implying better accuracy for samples.

Ideally a number of standards covering a range of concentrations should be analyzed (e.g. Veizer *et al.* 1978, Brand and Veizer 1980). These authors obtained mean accuracy errors of up to 11% for 7 and 9 sets of standards respectively. For this thesis, expense precluded obtaining more than two standards.

As an additional check, some whole rock XRF analyses were performed on NBS1c and NBS88a. Analysis included the HCl insoluble component. These results were nearer the recommended values for elements with low concentrations, such as Sr. This suggested that some of the error in AAS/AES accuracy may be accounted for by the exclusion of the insoluble residue fraction, particularly as AAS results underestimated concentrations.

Despite analytical accuracy not being as good as hoped, it is felt that

Table A1.8 Summary of precision and accuracy (relative percent), and published concentrations (weight% oxide) for analyzed standards.

	NBS1c			NBS88a		
	Concn	Accuracy	Precision	Concn	Accuracy	Precision
Ca	50.3	8.0	1.0	30.1	8.8	2.1
Fe	0.55	11.2	5.2	0.28	10.9	3.4
K	0.28	10.7	11.6	0.12	16.7	11.5
Mg	0.42	23.6	0.7	21.3	0.3	1.7
Mn	0.025	29.5	3.3	0.03	18.1	3.4
Na	0.02	20.3	1.0	0.01	29.8	2.3
Sr	0.03	18.3	2.1	0.01	21.2	10.2

interpretations of the carbonate geochemistry in this thesis will not be affected greatly. This is because elements with higher accuracy errors are present in greater concentrations in the samples, with an implied improved accuracy. Exclusion of insoluble residues may account for some inaccuracy. Finally, to a large extent it is the differences between samples that is more important than the absolute value, hence the significance of the good reproducibility.

As an additional note, published literature often only mentions analytical precision with no mention of accuracy. No mention of either is made in some cases. One wonders whether this is good practice.

A1.3.3. STABLE CARBON AND OXYGEN ISOTOPES ANALYSIS

Analyses were performed using orthophosphoric acid decomposition in a 25°C reaction line (Burns 1980) based on the system designed by McCrea (1950). Instrumentation consisted of a Micromass 602c Mass Spectrometer which is a 90° magnetic deflection instrument with a six centimetre radius. The 602c was modified by replacement of the amplifiers and the addition of an Epson HX-20 control unit to bring it up to 602e specifications. Both the line and mass spectrometer are housed in the Chemistry Department, University of Waikato.

Sample Preparation

Samples were selected that consisted solely of either dolomite or calcite as verified by XRD. This meant that no separation of CO_2 from different carbonate phases had to be performed. The few samples of mixed mineralogy usually had less than 10% of another carbonate phase.

Prior to analysis samples were roasted at 400°C to remove organic carbon. Initially this was done under vacuum but the samples were invariably sucked out of the roasting vials and dispersed throughout the roasting tube. Roasting was henceforth done without vacuum.

Preparation of Phosphoric Acid

The acid preparation method is from Cuthbertson (1985). One hundred to two hundred ml of 80% H_3PO_4 were placed in the bowl of a rotary

evaporator. The system was evacuated, and a liquid N_2 trap was positioned between the pump and the evaporator to aid pumping by removing H_2O as it was driven off. The acid was heated at 200°C for 6 hours and then left overnight at room temperature. This was repeated the next day and allowed to cool ready for use.

Procedure

The vacuum line is shown in Figure A1.7, and the method is as follows:

i) Some powdered sample (10-30 mgm) was placed in the bottom of the reaction vessel; a few ml of 100% H_3PO_4 was pipetted into the side arm.

ii) The vessels were outgassed, with the aid of heating, for 30 minutes and after sealing placed in a 25°C constant temperature water bath to thermally equilibrate.

iii) The acid was then tipped onto the carbonate and left to react overnight.

iv) Following reaction the reaction vessels were put back on the reaction line and the system evacuated. The pumps were then isolated.

v) CO_2 from the sample was frozen into 'U_1' using liquid N_2. The reaction vessel was isolated, and an ethanol slush trap (approximately -95°C) replaced the liquid N_2; the N_2 was placed on 'U_2'. The CO_2 was thus transferred to 'U_2' leaving water frozen in 'U_1'.

vi) 'U_1' was isolated and non-condensible gases were pumped off the CO_2 in 'U_2'.

vii) The slush bath replaced the liquid N_2 on 'U_2' and the CO_2 sample was frozen into the sample vial which was flamed off for mass spectrometry. Gas volume could be measured using the Hg-manometer if necessary.

Both the $\delta^{13}C$ and $\delta^{18}O$ analyses were obtained from the one gas sample.

Standard Gas

The reference gas used in the mass spectrometer was Waitomo Limestone (Burns 1980), which was compared to PDB.

Figure A1.7 Stable isotope reaction line.

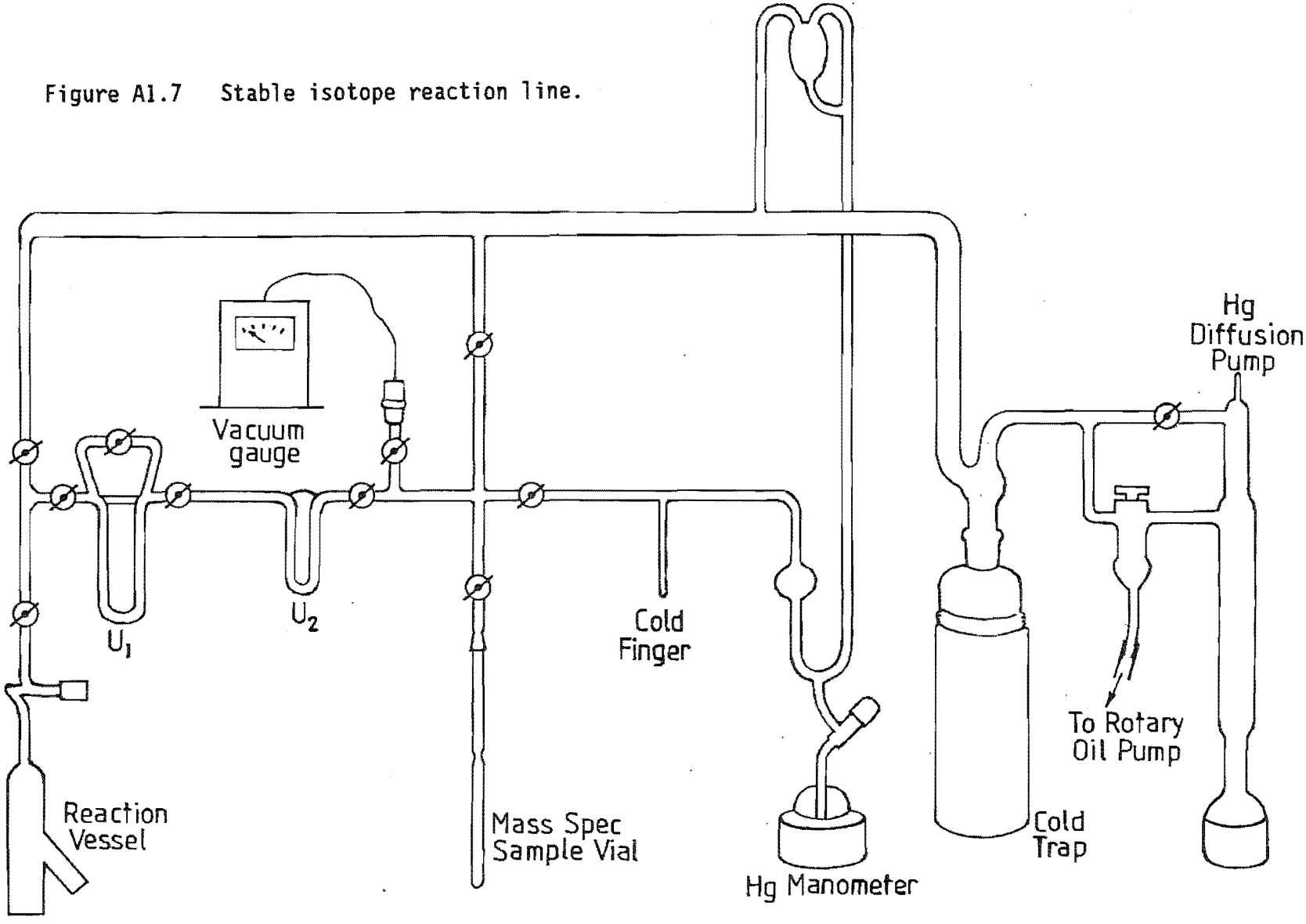

Calculations

The mass spectrometer obtains the $^{13}C/^{12}C$ and $^{18}O/^{16}O$ ratios by comparing the ion beams of mass 45/44 and mass 46/45+44 respectively between sample and standard. The difference between isotopic ratios of the sample and the standard in per mil (δ‰) is defined by :

$$\delta \text{ ‰} = (R_{sample} - R_{standard})/R_{standard} \times 100$$

where R = isotope ratio (Hoefs 1980).

The $\delta^{18}O$ and $\delta^{13}C$ values are obtained from the comparison of the δ^{45} and δ^{46} ratios. Equations for calculating the isotopic compositions of samples (below) are derived from Burns (1980) which in turn is based on the work of Mook (1968) and Grinsted (1977).

$$\delta^{18}O_{PDB} = 0.999\delta^{46} + 0.0098\delta^{45} - 1.06$$

$$\delta^{13}C_{PDB} = 1.063\delta^{45} - 0.0034\delta^{46} - 3.6277$$

Precision and Accuracy

Owing to a limited number of reaction vessels, samples were processed in batches of 17. With each batch a standard (The USGS Toilet Seat Standard - TSS, which is equivalent to NBS19) was run to check accuracy and precision. Replicate analyses of sample KP3/3 were run as an additional check for precision. Standard deviations for replicates are listed in Table A1.9.

The δ^{46} of TSS differed by 0.91‰ to that quoted on the label on the bottle containing the standard. All samples were adjusted appropriately before calculation of $\delta^{18}O$ and $\delta^{13}C$. The reason for the difference was that the temperature for the quoted value was 50°C. As these samples were reacted at 25°C the difference probably represents a temperature fractionation. The resulting $\delta^{18}O$ and $\delta^{13}C$ values differ from those quoted by Coplen *et al.* (1983). There is a difference in $\delta^{18}O$ of -0.16‰, which is approximately equal to one standard deviation for replicate analyses. It may result from some exchange effects during storage and is not considered significant. The $\delta^{13}C$ values differ by

Table A1.9 Standard deviations for replicate stable isotope analyses (‰ PDB).

	$\delta^{18}O$	$\delta^{13}C$
TSS	0.14	0.16
KP3/3	0.13	0.17

+0.93 per mil. No suitable explanation for this exists, other than to suggest that the quoted δ^{45} on the standard was wrong. For consistency all $\delta^{13}C$ analyses were modified accordingly.

No corrections have been made for H_3PO_4 fractionation, in line with arguments presented by Land (1980, p107).

A1.3.4. CATHODOLUMINESCENCE

Cathodoluminescence petrography utilized the same polished sections as for microprobe analysis, minus the carbon coat. The instrumentation was a Nuclide Corporation Luminoscope-Model Elm-2E 2EX, belonging to the NZ Geological Survey, Christchurch. It was operated at 15kV and 0.4-0.6 mA. Photomicrographs were taken using 1600 ASA colour print film, exposed as 200 ASA, but printed as 1600 ASA. By experiment this processing was found to give the best results (B.D. Field *pers. comm.* 1987).

APPENDIX 2

DESCRIPTION OF LITHOLOGIES

A2.1. WOOLSHED CONCRETION (WC) ZONE

A2.1.1. MUDSTONES/SANDSTONES

Generally the lithology is medium grey, commonly with a weathered rusty brown, Fe-oxide stained outer surface, poorly indurated, usually centimetre-bedded but laminated in places (<1 cm thick), siltstone or very fine sandstone. Disseminated pyrite is common and some sulphur efflorescence (jarosite?) is observed.

Some coarse sandstone clastic dikes occur 20-30 m from the base of the WC Zone at Isolation Creek (20). These are seen at other localities such as Branch Stream (29), but below the WC Zone.

At Isolation Creek (20) the upper 30 m of the WC Zone becomes increasingly cemented and indurated. The cementation is manifested in increasing numbers of weathering resistant, 'step-like' layers [Figure A2.1]. The main cementing agent appears to be silica, but layers are also dolomitic between 12 m and 20 m from the top of the Zone. The uppermost 10 m are primarily silica cemented with negligible dolomite. The top of the WC Zone consists of a 1 m thick bed of cherty, dolomitic, very fine sandstone. The dolomite forms 'pod-like' aggregates of large (up to 3 mm diameter) crystals which comprise about 25% of the rock. Outwardly this bed is the same as below (with the exception of the dolomite) but more indurated.

Silica cementation of the WC Zone is also found at Whernside Spur (22) and Kaikoura Peninsula (3,4). At both localities different beds are preferentially cemented [Figure A2.2]. Browne (1985) described the Kaikoura Peninsula lithology as alternating centimetre-bedded to decimetre-bedded sandstones and mudstones. In this study only alternations in induration are observed, with little apparent grain size variation.

Pyrite cementation of individual beds is seen at Dart Stream (30). The cemented beds are a few centimetres thick and irregularly spaced. In one instance a pyrite cemented bed could be seen intersecting a concretion. Unfortunately this particular occurrence was inaccessible.

Figure A2.1 WC and BC Zones, Isolation Creek (Grid Ref. NZMS 260 P29 916229). View looking southwest. The arrows indicate resistant, cemented layers.

Figure A2.2 Flattened spheroidal dolomite concretion in the WC Zone, South Bay, Kaikoura Peninsula (Grid Ref. NZMS 260 031 661647). Pair of legs for scale. Alternating centimetre-bedded relatively cemented and uncemented beds are differentially compacted around the concretion. Polygonal cracks (arrow) can be seen on the upper surface of the concretion.

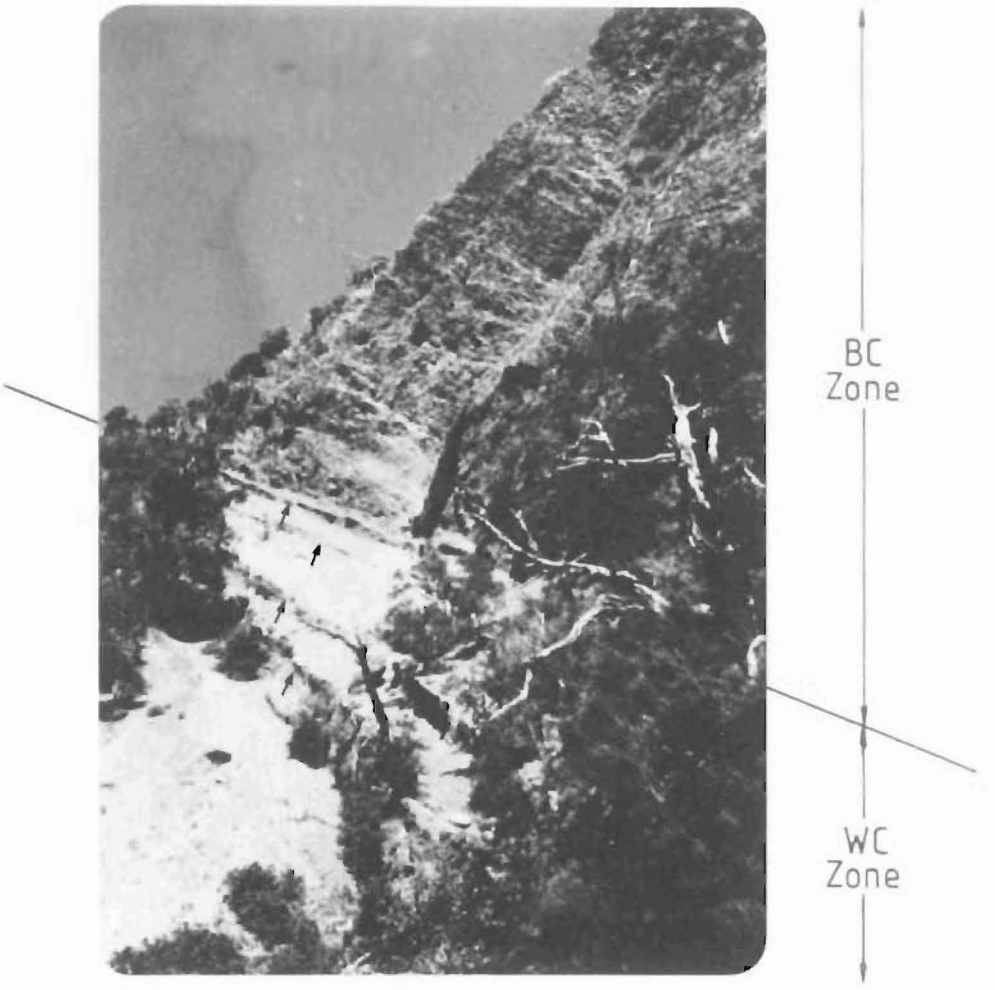

A2.1

A2.2

A2.1.2. CONCRETIONS

Most concretions are spheroidal or flattened spheroids and consist of dolomite cemented mudstone or fine sandstone [Section A5.2.1.]. The flattened spheroids have the plane of their longest axes parallel to bedding. These axes tend to be approximately equal in length, and locally measure up to 5 m (e.g. South Bay, 3). The axis perpendicular to bedding can be up to 1 m or more in some examples. Unfortunately, accurate measurement of all three axes could not be performed because one axis is invariably incompletely exposed, or the concretion broken. Spheroidal varieties tend to have a shorter long axis than flattened spheroids. Generally well indurated, the concretions usually have a weathered brown to buff outer surface, commonly with "septarian-like" cracks [Figure A2.2]. Small concretions show either no such cracks or very few. Fresh broken surfaces are medium grey and fine grained. Differential compaction around concretions [Figure A2.2] is observed at all sections.

By far the largest concretions are to be found at South Bay (3). In one broken example, the original bedding (16-20 cm thick) is observed, although only faintly. A broken concretion in Branch Stream (28) also shows the original bedding [Figure A2.3] which is about 13 cm thick. Between the indurated dolomitic beds are less indurated shaley layers. In both the South Bay (3) and Branch Stream (28) concretions, beds thicknesses remain constant and do not thin at concretion margins. Unfortunately, primary bedding was observed in only these two examples.

Septarian structures, similar to those described by Raiswell (1971) in sections cut through Cambrian and Liassic concretions from south Wales, and in the Moeraki Boulders (Boles *et al.* 1985), are found in a concretion from Muzzle Stream (32). The structures are calcite filled. Generally too large to be removed whole, the concretions could not be sectioned completely to investigate further such internal features. Despite the lack of means for verification for internal bedding and septarian cracks, it is thought likely that other concretions contain these features. When sampled, most concretions broke away in concentric layers, analogous to a peeled onion, rather than parallel to any expected bedding direction. Similar concentric banding is described by Browne (1985).

Twenty-five metres from the top of the WC Zone at Isolation Creek (20),

Figure A2.3 Dolomite concretion in millimetre-bedded to centimetre-bedded very fine sand to siltstone, WC Zone, Branch Stream (Grid Ref. NZMS 260 O30 694093).

Figure A2.4 Small concretion, WC Zone, Isolation Creek (Grid Ref. NZMS 260 P29 916229). The core (C) contains microcrystalline cement and is surrounded by a coarsely crystalline exterior (E). The concretion is associated with a dolomite cemented mudstone bed (M). The potatoe peeler is 15 cm long.

Figure A2.5 Small concretion elongated parallel to bedding, WC Zone, Branch Stream (Grid Ref. NZMS 260 O30 694094). As well as an uncemented core, the concretion contains shell fragments (circled).

A2.3

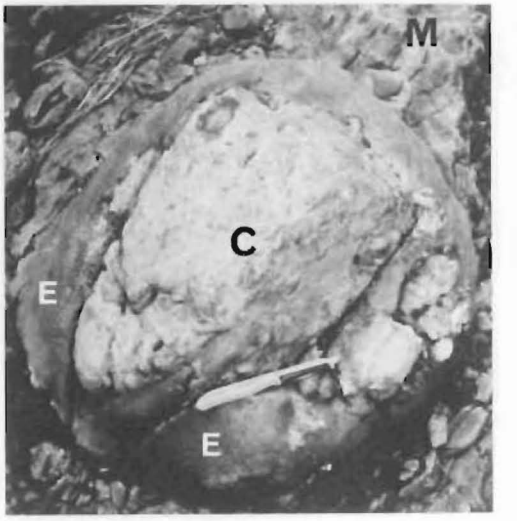

A2.4

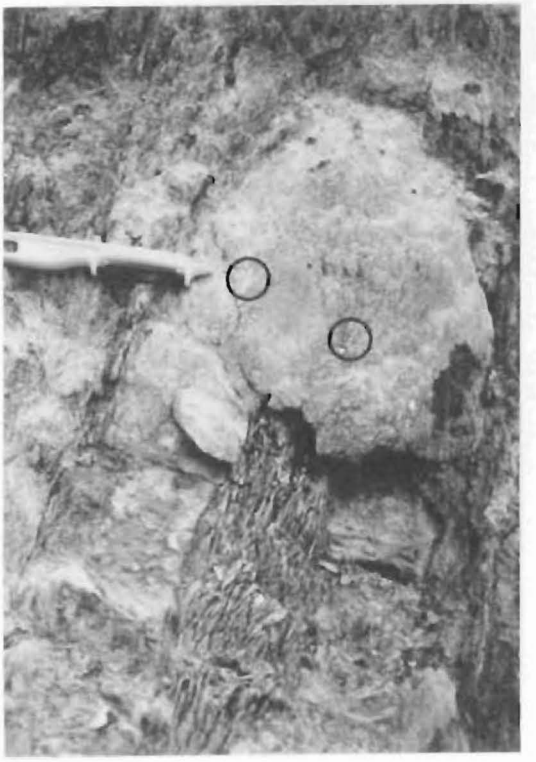

A2.5

concretions appear markedly different. Smaller (<0.5 m in diameter), with an irregular and rough exterior, they occur in dolomite cemented layers [Figure A2.4]. The moderately indurated core is surrounded by a less indurated, coarsely dolomitic outer layer. The outer layer may represent a separate phase of concretion growth around an already formed core.

At Branch Stream (28), about 20 m below the top of the WC Zone [Figure A2.5], is a concretion with an uncemented core. Although the outer layer is dolomite cemented, it is poorly indurated compared to the concretions in Figures A2.2 to A2.4. Shell fragments, possibly *Inoceramus*, parallel to bedding, can be seen. These are the only example of macrofossils found in WC Zone concretions. Browne (1985) however, reports foraminiferal fauna from concretions at South Bay (3).

Some unusual examples of concretions are found at Lab Rocks (4), Kaikoura Peninsula [Figure A2.6a,b]. Outer surfaces are phosphatized and pitted. Borings, approximately 1 cm in diameter, extend up to 5 cm into the concretions and are filled with silicified micrite, glauconitic or phosphatic material [Figure A2.6b]. A subsequent analysis of the boring fill showed it to consist of microcrystalline quartz with some glauconite. There is no carbonate. Borings cross the phosphatized outer layer [Figure A2.6a], indicating that phosphatization preceded the boring. These concretions are contained in a highly chaotic part of the sequence which consists mainly of sandstone and coarser fragments, inferred to represent reworking of the underlying sediments (Morris 1987). Morris places this part of the sequence within the Claverley Sandstone Formation, but it is included in this discussion as it was originally from the Woolshed Formation.

Also at Lab Rocks (4) is one dolomite concretion which contains a chert nodule at its centre (see also Browne 1985). The example was observed by the author during a preliminary investigation but has not been found since. It has probably been buried by storm deposits.

A2.2. CLAVERLEY SANDSTONE (CS) ZONE

The CS Zone consists of a generally massive, fine to medium, light-grey, non-calcareous sandstone (see also Morris 1987). In general, authigenic minerals occur as (minor) detrital clasts, or as pyrite and glauconite

Figure A2.6 Bored and phosphatized concretion, Lab Rocks, Kaikoura Peninsula (Grid Ref. NZMS 260 031 676657).
(a) Bored exterior.
(b) Cross section through a boring (circled) containing silicified micrite infill.

Figure A2.7 CS-CD Zone contact, Wharekiri Stream (Grid Ref. NZMS 260 P30 752914). The sandstone is generally massive (lower left of photograph) with little grain size variation. The bedded appearance towards the top of the CS Zone results from increasing silica cementation. Near the contact with the CD Zone beds are moderately nodular.

Figure A2.8 Small chert nodule, CS Zone, beach platform, Waipapa Bay (Grid Ref. NZMS 260 P31 816874). The apparent bedding results from differential silica cementation.

a

b

A2.6

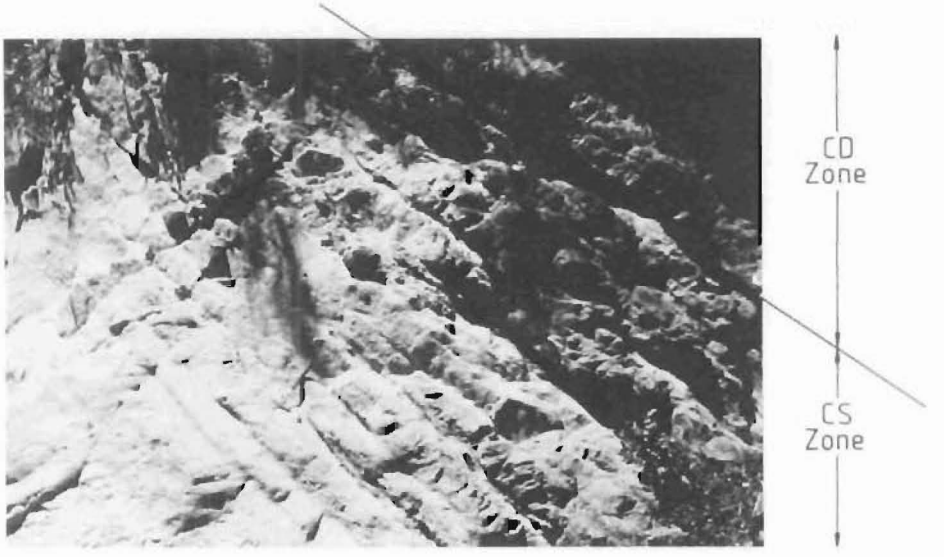

A2.7

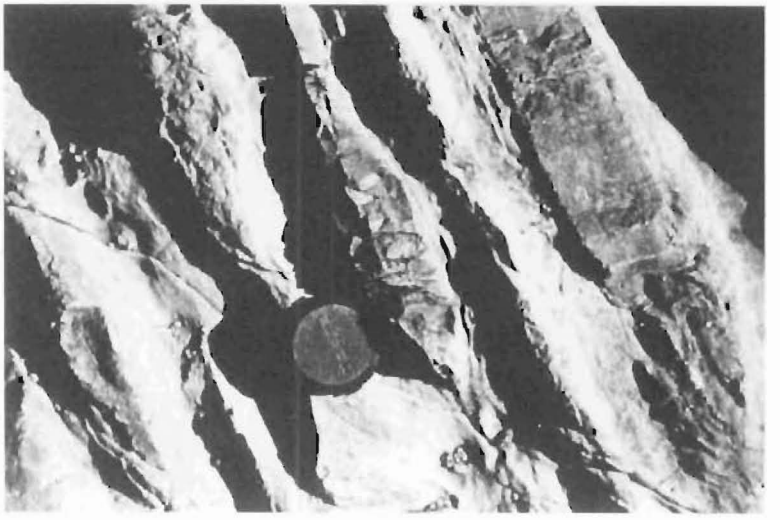

A2.8

(Morris 1987). At Bluff River (37), Branch (28) and Dart (30) Streams, the CS Zone is free of chert and dolomite. At Dead Horse Gully (34), are a few small (about 10 mm diameter) chertified burrows. Most notably at Waipapa Bay (11), and Wharekiri Stream (9) [Figure A2.7], the sandstone becomes progressively cherty towards the top. Minor discrete nodules [Figure A2.8] are also found. The Waipapa Bay locality also contains some disseminated dolomite rhombs.

A2.3. BASAL CHERT (BC) ZONE

In the field two chert types are recognized in the BC Zone. The lowermost of the two consists of chertified fine sandstone or mudstone, and is referred to as detrital-rich. Overlying the detrital-rich cherts are what appear to be nondetrital bearing cherts. However, thin section evidence [Section A6.2.2] shows these nondetrital cherts (for discussion purposes referred to as detrital-poor) also contain detrital material, but much less than in detrital-rich cherts.

A2.3.1. DETRITAL-RICH CHERT

The lowermost 3 metres of the BC Zone at Jordan Stream (7), consists of large decimetre-thick nodules, some up to 1 m long, with pronounced light coloured, silicified outer rims. The rims are usually 3-5 mm thick, and always less than 1 cm thick. Interbedded with the cherts are muddy, commonly fissile, very fine sandstones, 1-2 cm thick. Between the large chert nodules are small and partially chertified sandy nodules. Above the basal 3 m, the cherts become more elongate and thinner but retain the nodular bedding. The still obvious nodule rims are calcareous, as are the interbeds.

The BC Zone below the CS Zone at Waipapa Bay (10) [Figure 2.4, map pocket], consists of relatively planar, decimetre-thick, chertified sandstone beds, with up to 2 cm thick silicified, pale grey rims [Figure A2.9]. Some beds are slightly nodular and thickness variations between and within beds are observed. A 1 m thick unchertified sandstone bed is also present. Above the CS Zone interval, the BC Zone lithologies become increasingly nodular stratigraphically upwards. Interbedded mudstones are common [Figure A2.10], and in general this part of the sequence is similar to that at Jordan Stream (7). A number of the chertified sandstone beds

Figure A2.9 Detrital-rich BC Zone chert, railway Cutting, Waipapa Bay (Grid Ref. NZMS 260 P31 816876). The hammer (0.5 m long) rests against a lens of unchertified quartz sandstone. Note the light coloured rims of the chert beds. The younging direction is from right to left.

Figure A2.10 Nodular, detrital-rich BC Zone chert, stratigraphically above the CS Zone interval, railway cutting, Waipapa Bay (Grid Ref. NZMS 260 P31 816876). The younging direction is from right to left.

Figure A2.11 Laminated, chertified sandstone, BC Zone, railway cutting, Waipapa Bay (Grid Ref. NZMS 260 P31 816876).

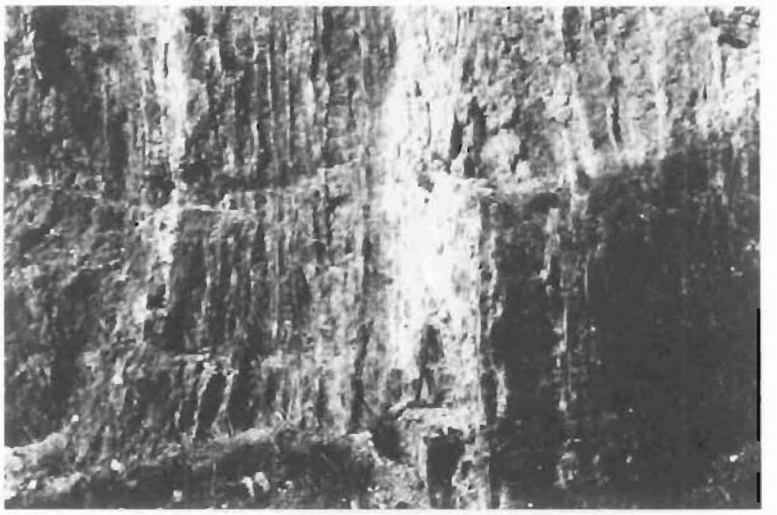

A2.9

A2.10

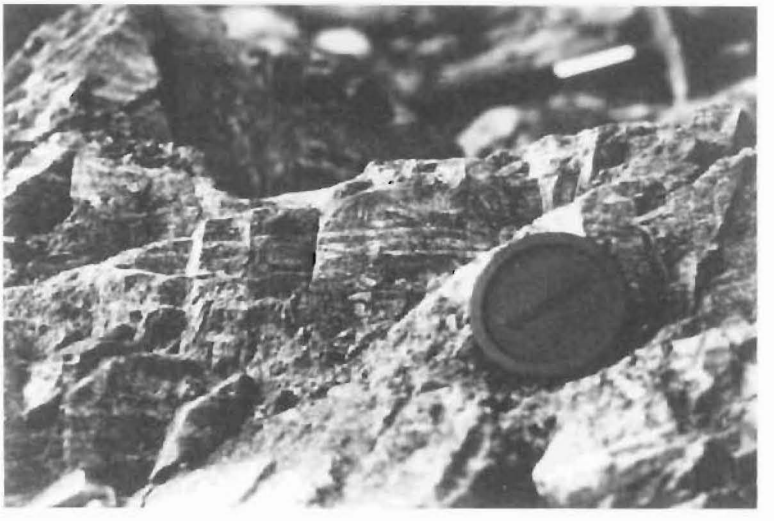

A2.11

at Waipapa Bay (10) have a laminated appearance [Figure A2.11]. The laminations are caused by alternation of relatively chertified and unchertified layers, a few millimetres thick. These laminations are not found in nodules.

BC Zone chert at Mt Alexander (8) is similar to BC Zone chert above the CS Zone at Waipapa Bay (10). However, the Mt Alexander (8) section contains a slightly greater abundance of silicified rims than at Waipapa Bay, and in addition contains some dolomite. Dolomite is in the form of rhombs (<1 mm) concentrated in small discontinuous and lenticular beds which are silica-cemented. There are no laminated sandy cherts. The uppermost 10 m consists of dolomite free, planar bedded cherts interbedded with thin sandy mudstones.

The detrital-rich cherts described thus far are essentially chertified Claverley Sandstone. In contrast, at Isolation Creek (20) the BC Zone appears to conformably overly the WC Zone [Figure A2.12]. The lowermost 11.6 m of BC Zone is essentially chertified mudstones or very fine sandstones from the Woolshed Formation. The lithology consists of increasingly chertified very fine sandstone beds up to 10 cm thick, interbedded with millimetre-scale thick sandy mudstones, both of which are pyritic. Coarsely crystalline dolomite in 'pod-like' aggregates, similar to those in the upper WC Zone, constitute less than 5% of the rock. Bedding becomes increasingly nodular stratigraphically upwards, and chert nodules become darker (olive black to black in colour), more vitreous, and show more distinct interbed boundaries. The detrital content decreases upwards.

A2.3.2. DETRITAL-POOR CHERT

Unlike detrital-rich cherts which have a dull lustre, BC Zone rocks containing limited detrital material have a more vitreous lustre. The 59 m thick monotonous sequence of detrital-poor BC Zone chert at Isolation Creek (20) consists of about 10 cm thick (with some beds up to 20 cm thick), very well indurated, heavily fractured, beds of chert [Figure A2.13], which comprise more than 95% of the rock. The remaining 5% consists of minor interbedded shales and sulphide nodules. The boundaries between nodules in different beds are sharp. Inter-nodule boundaries within individual beds are at best vague, and it is suggested that some

Figure A2.12 Contact between WC Zone (below) and BC Zone (above), Isolation Creek (Grid Ref. NZMS 260 P29 916229). The hammer rests on the contact.

Figure A2.13 Detrital-poor BC Zone chert, Isolation Creek (Grid Ref. NZMS 260 P29 916229). Interbed boundaries are discernable, and some pinching out of beds is apparent (arrowed). Potatoe peeler = 15 cm long.

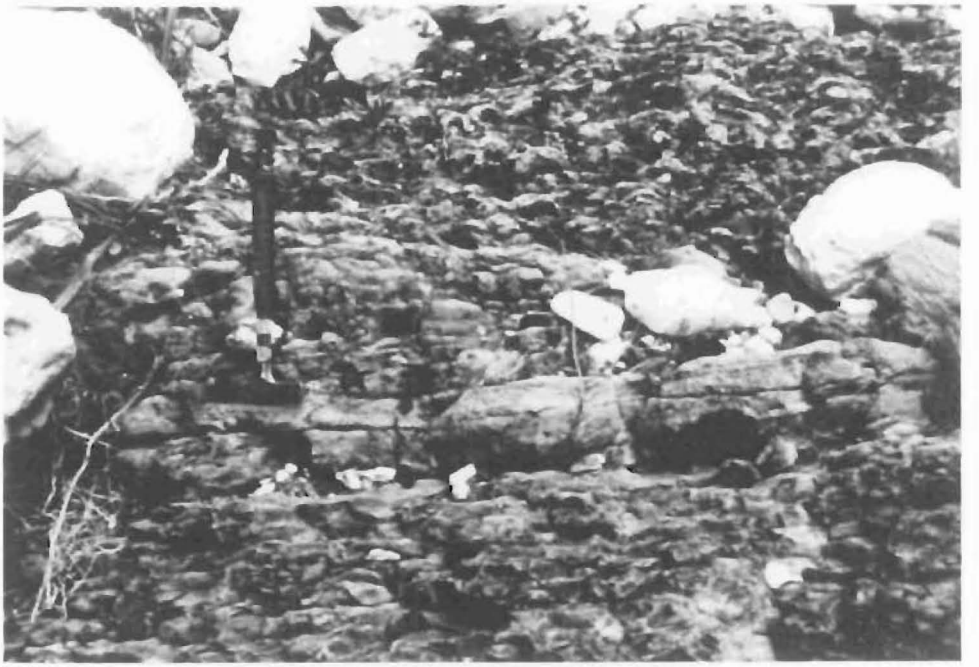

A2.12

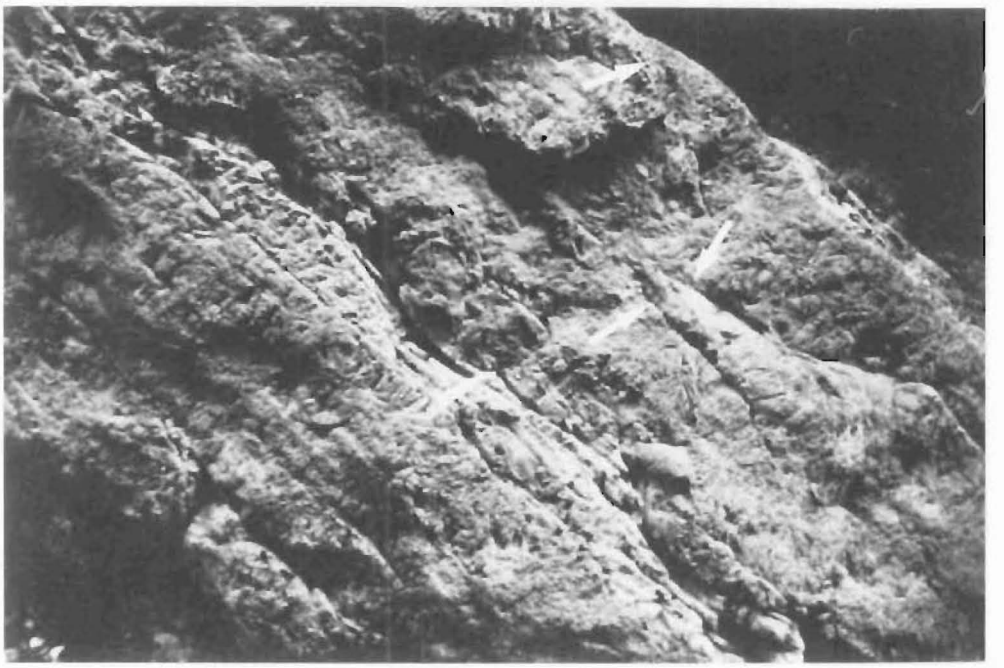

A2.13

beds formed from coalescence of nodules.

The Swale Stream (23) chert is similar to the Isolation Creek (20) examples, although some beds are up to 80 cm thick. There are also a few centimetre-scale shaley interbeds, and minor volumes of silicified micrite in some chert beds.

A2.4. CHERT AND DOLOMITE (CD) ZONE

The only continuous exposure of the CD Zone is at Isolation Creek (20). Here the base of the CD Zone is marked by the appearance of dolomite. Unfortunately, the actual contact is poorly exposed. The chert beds are the same as in the underlying BC Zone, but the interbedded fissile mudstones become increasingly rare throughout the lower 40 metres. Dolomite appears initially as lenses of 2-3 cm thick, and about 50 cm long, containing discernibly rhombic, euhedral dolomite crystals less than 1 mm in diameter, set in chert [Figure A2.14]. The number of dolomite lenses gradually increase to 25-30% of the rock. Dolomite lenses are both contained within and between chert beds. In the lower part of this Zone, the beds of chert, although nodular, are relatively continuous and uniform in thickness. No definite inter-nodule boundaries are apparent within beds. Approximately 70 m from the base of the CD Zone the cherts become increasingly discontinuous, and include some 'bulbous' nodules (good examples of bulbous nodules are found in the CD Zone, Mead Stream 24). Interbed boundaries are as sharp as in the lower part of the Zone however, individual nodules within beds become more apparent. In addition to the change in chert morphology, the dolomite lenses increase in size, commonly averaging 1 m long, and about 10 cm thick. Some are up to 15 cm thick. Dolomite rhombs are also disseminated within chert nodules.

The CD Zone at Mead Stream (24) is similar to the upper part of the CD Zone at Isolation Creek (20). At Mead Stream the Zone consists of centimetre-bedded to decimetre-bedded, indurated beds of medium to dark grey nodular chert, with lenses and discontinuous beds of light grey centimetre-bedded dolomite [Figure A2.15]. The beds have a nodular appearance. Interbedded marls are rare. Chert nodules are generally less than 10 cm thick however, some examples are up to 20 cm thick. Although nodules are usually less than 0.5 m long, some are traceable for a few metres (these commonly appear to be coalesced nodules). The dolomite

Figure A2.14 Chert containing lenses of dolomite (d), approximately 40 m above the base of the CD Zone, Isolation Creek (Grid Ref. NZMS 260 P29 917230).

Figure A2.15 Chert and dolomite, CD Zone, main channel, Mead Stream (Grid Ref. NZMS 260 P30 765163). The arrow indicates the nodule detailed in Figure A2.17.

Figure A2.16 Detail of CD Zone chert and dolomite, main channel, Mead Stream (Grid Ref. NZMS 260 P30 765163). Note the moderately sharp boundary between the chert (c) and dolomite lens (d). The sucrosic appearance of the chert is due to disseminated dolomite crystals.

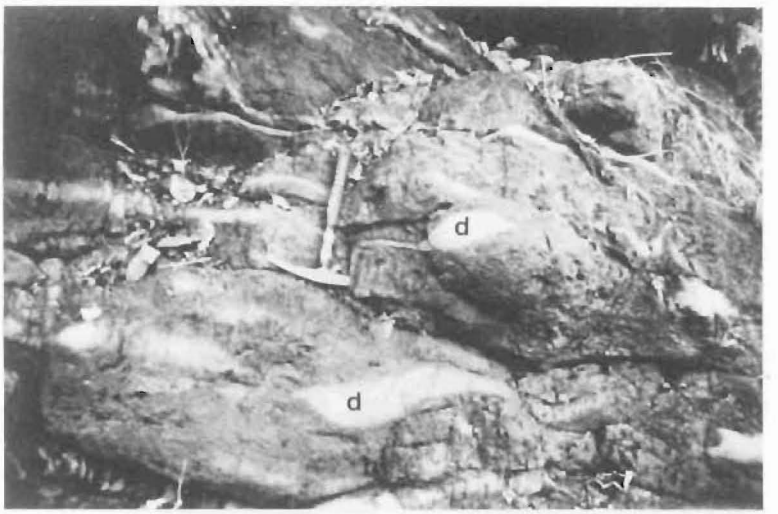

A2.14

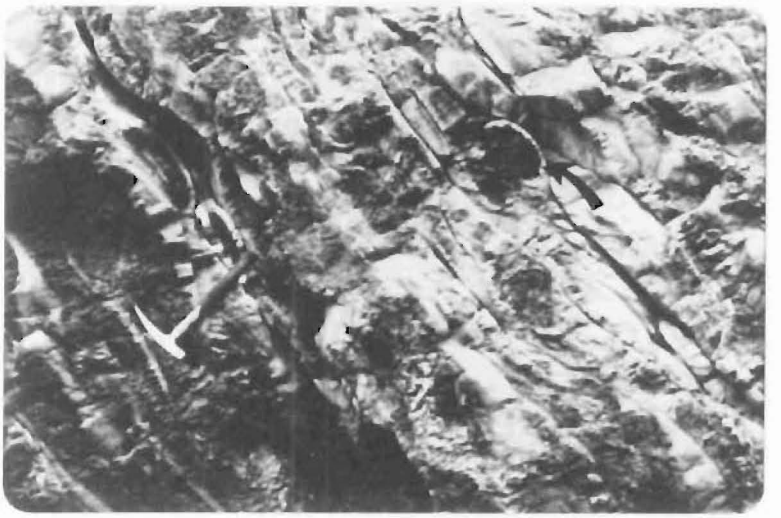

A2.15

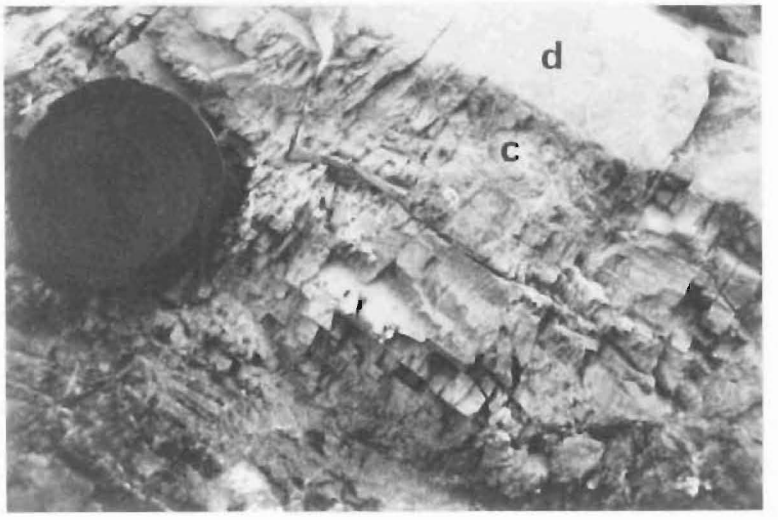

A2.16

consists of aggregates of rhombic crystals, each less than 1 mm in diameter, in a chert matrix. Dolomite lenses pinch in and out around chert nodules [Figure A2.15]. Although dolomite is predominantly outside chert nodule margins, rhombs dispersed within the cherts give nodules a sucrose appearance [Figure A2.16]. The proportions of chert and dolomite are approximately 1:1 for the lower half of the CD Zone, whereas above the proportions are about 3:2. In the upper half of the Zone, chert nodules become increasingly elongated and rims of silicified micrite become more common. The less dolomitic, more calcite-rich cherts at the top of the Zone tend to be paler grey than those near the base of the sequence. Also in the upper half of the CD Zone occur a number of bulbous chert nodules. These nodules are dolomite-free, have silicified micrite rims, and are darker in colour than adjacent dolomitic chert nodules [Figure A2.17]. They appear to 'disrupt' bedding by severely restricting the thickness of surrounding chert and dolomite beds. The nodule shown in Figure A2.17 was the only accessible example; others seen higher in the cliff face commonly affect bedding to a greater extent.

The CD Zone at Waipapa Bay (10) is similar to that at Mead Stream but is sandier.

Cherts at Wharanui Point (15) are predominantly dark to occasionally olive grey bands, $\leq$10 cm thick, in slightly nodular $\leq$10 cm thick beds of siliceous micrite. Interbeds are 5-10 cm thick beds of dolomite rhombs, similar to those at Mead Stream (24) and Isolation Creek (20). The dolomite disappears abruptly near the top of the exposure. CD Zone lithologies at Wharekiri (9) and Limburn (26) Streams resemble those at Mead Stream, and include bulbous cherts. The only differences being variations in the proportions of chert and dolomite. In addition, at Wharekiri Stream (9) the dolomite beds are relatively continuous, giving rise to chert-dolomite alternations [Figure A2.18]. There is evidence of soft sediment deformation of beds [Figure A2.18], and a feature resembling a flame structure is observed [Figure A2.19]. Considerable disruption of the bedding adjacent to the flame structure has occurred.

Fe-sulphide nodules, with associated Fe-oxide weathering products, are seen throughout the CD Zone at all localities.

Figure A2.17 Dolomite-free chert nodule with silicified micrite rim (sm), CD Zone, main channel, Mead Stream (Grid Ref. NZMS 260 30 765163). No dolomite is found in the rim despite adjacent dolomite beds (d). Note the sharp boundary between the chert and silicified micrite rim, and the variation in thickness of dolomite beds.

Figure A2.18 Alternating beds of chert and dolomite, CD Zone, Wharekiri Stream (Grid Ref. NZMS 260 P30 751913). Here dolomite beds are more continuous than at Mead Stream. In the upper part of the photograph beds are contorted, probably as a result of soft sediment deformation.

Figure A2.19 Flame structure in a dolomite bed, CD Zone, Wharekiri Stream (Grid Ref. NZMS 260 P30 751913). The chert nodule at bottom left truncates the dolomite bed, and chert above the flame structure appears chaotic. This example is approximately 10 m stratigraphically above rocks in Figure A2.18.

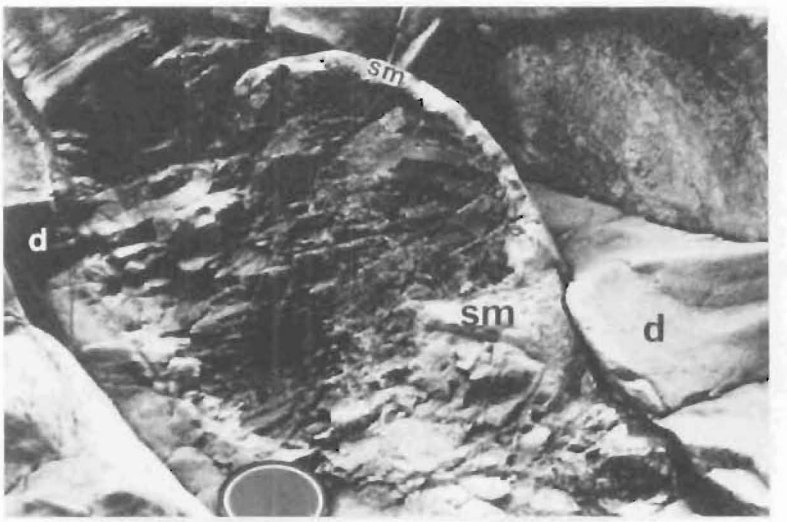

A2.17

A2.18

A2.19

A2.5. CHERT AND LIMESTONE (CL) ZONE

Limestone lithologies in the CL Zone throughout the field area, are generally 10-20 cm thick, indurated, nodular or planar-bedded, siliceous fossiliferous micrites with varying numbers of about 1 cm thick marl interbeds. Chert morphologies are diverse, consisting of bands or nodules of varying shape. Small sulphide nodules (of about 1-2 cm diameter, and commonly smaller), and their red-brown Fe-oxide weathering products are common throughout the CL Zone at all except coastal localities north from Woodside Creek (9). Dolomite is generally rare.

At Isolation Creek (20) the contact between the CL Zone and the underlying CD Zone shows up as an eroded 'step' in the stream gorge walls. Examination of this contact produced no evidence of faulting. The lithology consists of decimetre-bedded, indurated, siliceous, nodular micrite containing centimetre-thick to decimetre-thick (depending on micrite bed thickness) dark grey to black, fractured chert nodules. Nodular chert bands are common in the lowermost 4.3 m of the Zone, but become rare upwards. Chert accounts for about 50% of the volume of the rock, with micrite constituting the remainder. Chert/micrite boundaries tend to be sharp near the base of the CL Zone, but diffuse boundaries are more prevalent further up the sequence. Dolomite occurs over the lowermost 4.3 metres of the Zone (constituting less than 5% of the rock), and consists of crystals, <1 mm across, dispersed in both micrite and chert, or as rare (usually decimetre-thick and up to approximately 1 m long) lenses of dolomite rhombs.

Near the top of the Isolation Creek (20) section is a nodule with a 'growth-ring like' morphology. Close examination shows the 'rings' to consist of silicification fronts which intersect each other, to produce a series of semi-prismatic segments [Figure A2.20].

At Mead Stream (24,25) the CL Zone is essentially split into three by the LCM and UCM Subzones [Figure 2.4] Purely for descriptive purposes, the CL Zone at this locality will be divided into the lower (below the LCM Subzone), middle (between the Subzones), and upper (above the UCM Subzone) CL Zone.

The base of the (lower) CL Zone shows the same marked lithological break

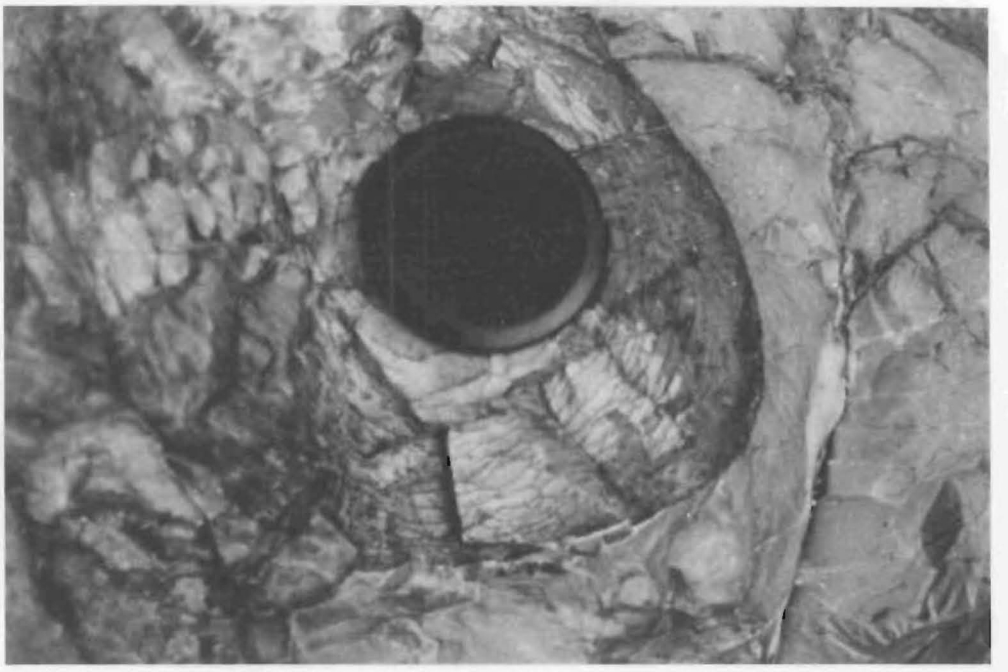

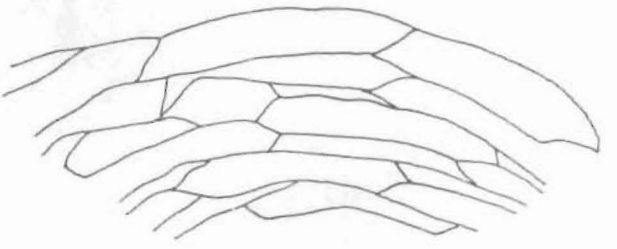

Figure A2.20 Chert 'growth-ring' morphology (with lens cap for scale), CL Zone, Isolation Creek (Grid Ref. NZMS 260 P29 918232). The sketch beneath shows how the silicification fronts form segments (scale is approximate).

as observed at Isolation Creek (20). A 20 cm thick dolomitic marl occurs 10 m above the base. With the exception of this marl layer (which comprises about 50% dolomite), the dolomite, which occurs as dispersed rhombs in both chert and micrite, gradually disappears over the lowermost 25 metres. Maximum dolomite concentrations of about 15% occur locally near the base of the Zone. Chert and micrite occur in approximately equal proportions below the dolomitic marl. Above the marl, micrite constitutes a little over 50% of the rock, chert about 40 percent, and marl interbeds up to 2 cm thick amount to about 10 percent. Cherts consist of discrete nodules which may be up to 2 metres long and 20 cm thick [Figure A2.21a], with an average thickness of about 10 cm, and an average length of about 1.5 metres. Numerous smaller cherts also occur. Above the marl bed, nodules do not exceed 10 cm thick, but lengths remain the same. In plan view, nodule centres appear distributed in semi-regular fashion [Figure A2.21b], with oval, circular and even branched morphologies. Although cross-sectional chert morphologies show little change stratigraphically upwards, there are an increasing number of pale grey cherts and the number of darker nodules decreases. The light coloured nodules are increasingly calcareous towards their centres compared to the dark cherts. A few-pale grey specimens have a growth-ring like morphology similar to that shown in Figure A2.20. Some very irregularly shaped nodules are also observed. The upper 45 m of the lower CL Zone has a chert volume of about 30% of the rock, increasing occurrences of large, dark, bulbous, bed-disrupting cherts morphologically similar to those in the CD Zone, and a predominance of pale grey or diffuse margined cherts (diffuse margined cherts are those where the boundary between the chert of the nodule and the surrounding micrite is transitional and often indistinct, in contrast to nodules with sharp margins such as shown in Figure A2.17). The outer margins of these become darker and sharper towards the base of the LCM Subzone. Seven metres below the LCM Subzone the chert volume decreases sharply, then increases again over the upper 3 m of the lower CL Zone. Dolomite reappears over the upper 2.1 m in the form of dispersed rhombs around chert margins. The dolomite constitutes about 20% of the rock.

Planar and centimetre-bedded to decimetre-bedded micrite is the predominant lithology in the middle CL Zone of Mead Stream (25). In the upper part of the Zone burrowing [e.g. Figure A2.22] becomes more prevalent (see Morris 1987). Interbedded marls are present in the lower 27 m of the Zone, but are much less common above. Cherts tend to be

Figure A2.21 CL Zone chert and limestone, main channel, Mead Stream (Grid Ref. NZMS 260 P30 764163).
(a) Cross section through chert and limestone beds displaying nodular bedding. Parts of beds which lack chert tend to be thinner than those parts containing chert.
(b) Large exposed bedding plane approximately 50 m along strike from rocks in Figure A2.21a. Such exposed surfaces are rare.

Figure A2.22 Micrite-rich (pale grey) chert nodule in burrowed micrite, CL Zone, southern tributary, Mead Stream (Grid Ref. NZMS 260 P30 760161). Note how the burrows intersect chert margins (arrow).

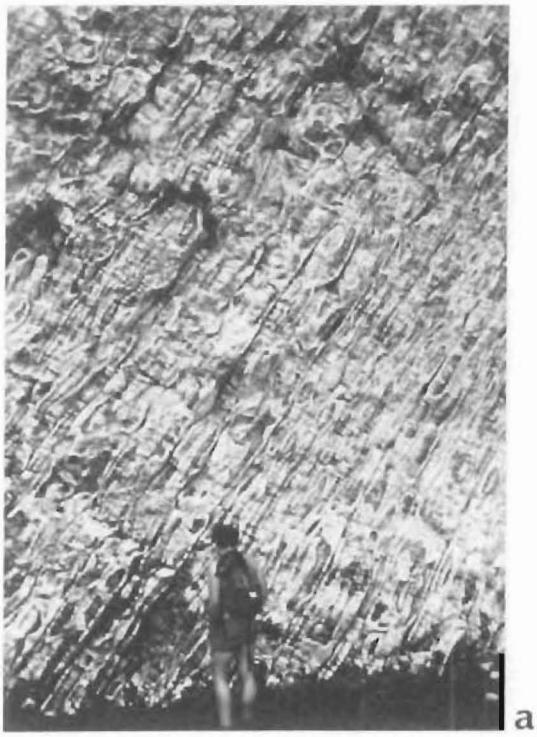

a

A2.21

b

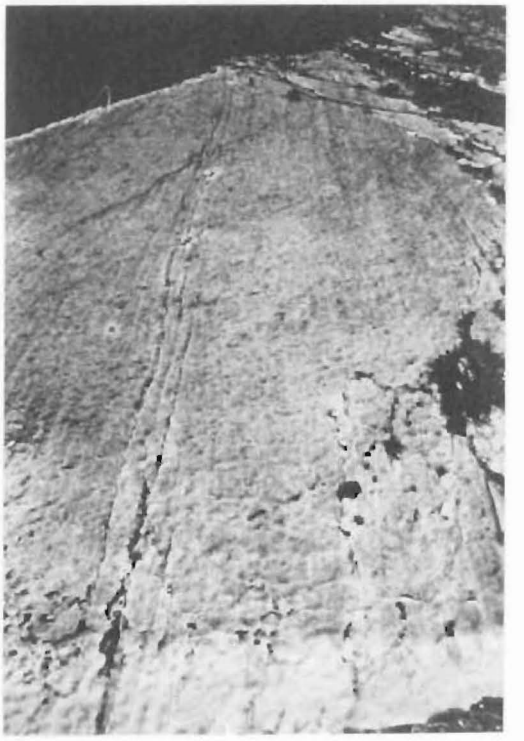

A2.22

longer and thinner than in the lower CL Zone, with a mixture of pale grey and darker coloured varieties. The cherts in the lower 30 m of the middle CL Zone are generally ≤10 cm thick, and commonly form bands 5-10 m long. The chert bands often have highly irregular margins similar to those in Figure A2.23]. Some bands only 1 cm thick can be 0.5 m long. Very small, centimetre-scale chert nodules are common; some may result from incomplete exposure of larger chert bands. A few micrite centred chert nodules are also found. About 30 m above the LCM Subzone some large, bed disrupting cherts are present. All these cherts are generally dark in colour. Thirteen metres above the LCM Subzone are some nodules which have the appearance of chertified *Thalassinoides* burrows, similar to those described from Woodside Creek (13, see later). The chert is dark with an outer rim of silicified micrite. From 30-60 m above the LCM Subzone, micrites average about 10 cm thick and marls are absent. There is evidence of minor stylolitization. The cherts are mostly pale grey, commonly micrite-rich [Figure A2.22], and a few metres long. Some bands are nodular, and there are a few large bulbous cherts which constrict surrounding beds. Highly irregular chert margins are not common, and there are few of the very small cherts. The middle CL Zone from 60 m above the LCM Subzone to the base of the UCM Subzone contains micrites which are generally centimetre-bedded (<10 cm thick) and stylobedded in places. In the interval 60-65 m above the LCM Subzone, cherts are highly irregular in shape and size. The nodules vary in length from a few centimetres to 0.5 metres. Above this interval and up to the base of the UCM Subzone, chert bands increase in number and ultimately predominate. Six metres below the UCM Subzone, the bands decrease in length [Figure A2.23], giving rise to discrete nodules which are highly irregular in outline, 10-20 cm thick, and sub-parallel to bedding. These may in fact be incompletely exposed or formed chert bands. Some large bulbous chert nodules are also apparent. Chert volume in the middle CL Zone is about 25% of the rock. Chert proportions differ only in an interval of 5 m (where volume is about 30%) 22 m below the top, and in the uppermost 5 m (where chert volume is about 50%).

In the 54 m thick upper CL Zone chert, distribution is sporadic, with the overall chert abundance progressively decreasing stratigraphically upwards. Micrites are usually 10-20 cm thick, indurated and siliceous, and interbedded with approximately 1 cm thick marls. These marls increase in number progressively up the sequence. Burrowing is common. Chert

Figure A2.23 Irregularly shaped chert bands and discrete chert nodules in the CL Zone, 5 m below the UCM Subzone, southern tributary, Mead Stream (Grid Ref. NZMS 260 P30 759161). Beds are 10-20 cm thick.

Figure A2.24 Chert bands in the CL Zone above the UCM Subzone, southern tributary, Mead Stream (Grid Ref. NZMS 260 P30 759161). Most beds are continuous throughout the 10 m thick exposure.

A2.23

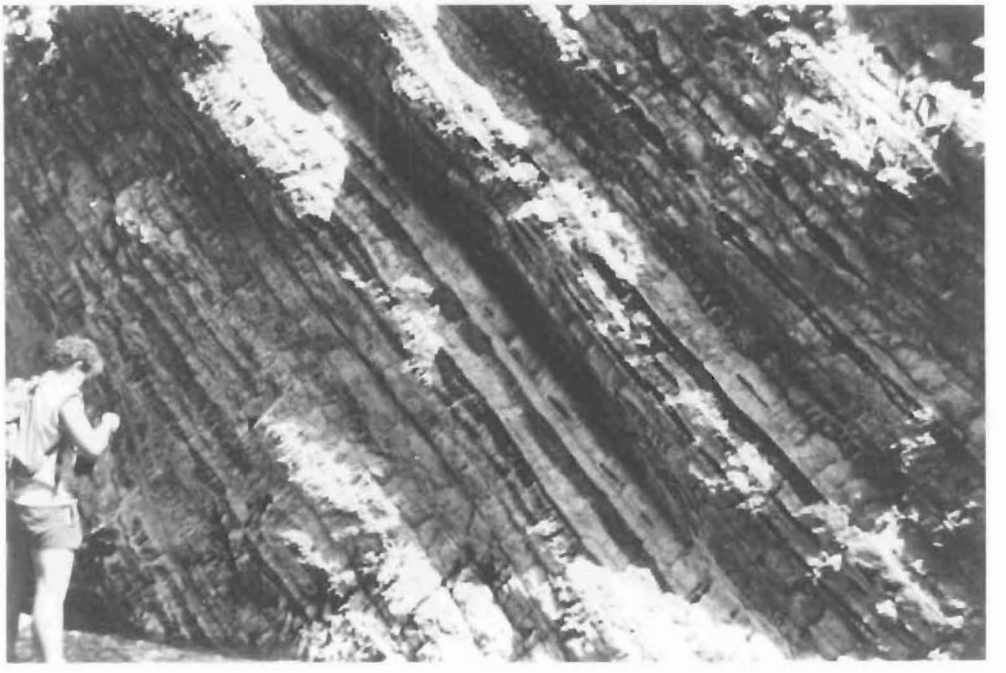

A2.24

volume never exceeds 20 percent. For 3 m above the UCM Subzone cherts are similar to those immediately below the Subzone. These then disappear with the next 6 m consisting of micrite with a few millimetre-scale chert nodules. The overlying 18.6 m contains about 20% chert, which consists of a mixture of slightly irregular and regular margined, centimetre-scale nodules, and thin centimetre-thick chert bands, all in approximately equal proportions. An 8.2 m thick interval of limestone devoid of chert is overlain by 18.3 m of limestone which contains the last major chert occurrence. Chert occurs initially as rare small nodules in a stylobedded micrite in the lowermost part of this 18.3 m, and then increases in volume to about 15% of the rock, comprising nodules and bands in roughly equal proportions. The uppermost 10 m of the CL Zone contains an interval of dark grey to black, usually 10 cm thick chert bands which comprise about 20% of the rock [Figure A2.24]. Most bands extend beyond the limits of the outcrop. Associated small, thin chert nodules appear to be pinched-out bands. Above this interval of bands, chert abundance dramatically decreases.

Although the presence of minor dolomite in the CL Zone at Mead Stream has been mentioned, there are two occurrences in the southern tributary of Mead Stream (25) which warrant special mention. The first is a dolomite interval, 20-28 m below the LCM Subzone. Approximately 25 m below the LCM Subzone, the dolomite occurs in beds similar to those in the CD Zone, gradually increasing in number upwards, apparently at the expense of interbedded marls. Dolomite accounts for about 25% of the rock. Five metres from the base of the interval is a 0.5 m thick, contorted, dolomite lens associated with a bulbous irregularly shaped chert [Figure A2.25]. The bedding is severely disrupted. In the opposite bank of the stream (about 50 m north), only a very thin lens of dolomite is seen. This dolomite appears to be an isolated occurrence in the CL Zone and of is limited extent. Beyond this 8 m thick interval there is no dolomite. Petrographically and geochemically this dolomite has more affinity with LCM Subzone dolomite than with CD Zone dolomite [Appendix 5]. The other occurrence is in the same tributary, 28 m above the LCM Subzone, where there are some dispersed dolomite crystals (about 10% of the rock) in the chert and micrite. A few metres below these dispersed crystals is a dolomitized *Zoophycos* burrow [Figure A2.26] exposed in plan view. The spreite have been enhanced by the dolomite.

Figure A2.25 Contorted lens of dolomite (d) and associated bulbous chert in the CL Zone, southern tributary, Mead Stream (Grid Ref. NZMS 260 P30 761160). Beds above and below are 10-15 cm thick.

Figure A2.26 Dolomitized *Zoophycos*, CL Zone, southern tributary, Mead Stream (Grid Ref. NZMS 260 P30 760161). Note the pyrite nodules and associated Fe-oxide staining. The spreite (s) are enhanced by dolomite crystals.

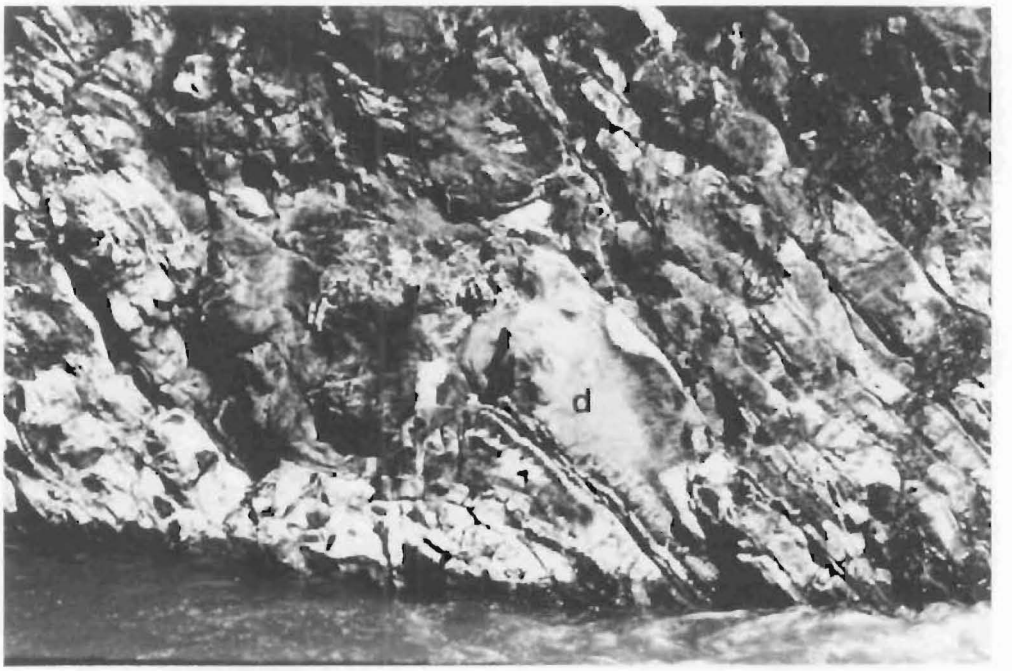

A2.25

A2.26

At Limburn Stream (26) chert comprises about 30% of the rock outcrop over a 15 m interval. The enclosing micrite is planar bedded, and contains generally pale grey, 10-20 cm thick chert nodules, which may be up to 1 m long. Above the 15 m interval chert abundance decreases rapidly to <5 percent, however rare pale grey nodules are seen almost to the base of the LM Zone.

Chert nodules in the CL Zone, below the LCM Subzone at Dee Stream (27), are pale-grey lenticular to ovoid, usually 10-20 cm thick, and <40 cm long. They constitute about 20% of the rock. Minor speckling of disseminated dolomite rhombs is common below the LCM Subzone. For 47 m above the LCM Subzone, micrites are moderately nodular. Chert nodules generally have the same morphology as below the Subzone. Disseminated dolomite rhombs are common. Occasional large bulbous cherts as described at Mead Stream (24,25) are found just above the LCM Subzone. The overall chert volume is about 35 percent. Above and to the top of the CL Zone, micrites are planar bedded. Sixty-five metres above the LCM Subzone, burrowing is more evident and there is no dolomite. Forty metres above the bottom of this burrowed interval, is a 7 m thick horizon of flat, elongated, chert nodules and bands. The chert volume in this horizon is about 50 percent. Overlying the chert bands is a 35 cm thick, heavily bioturbated, siliceous micrite, devoid of chert. Above the micrite chert volume never exceeds 20 percent. Both chert bands and pale-grey nodules occur. The boundaries between chert and micrite in beds are sharp irrespective of chert morphology.

Cherts at Branch Stream (28,29) are similar in size and shape to those in lowermost Dee Stream (27), but are micrite-centred. The chert comprises about 35% of the rock, occurring in decimetre-bedded nodular micrites, totalling about 55 m. Above and up to the LCM Subzone, the micrites are planar bedded, with chert volume decreasing to about 10 percent. Both pale grey and dark cherts occur, as do some large bulbous nodules. The cherts become darker towards the base of the LCM Subzone. Above the LCM Subzone cherts are increasingly elongated, forming bands.

The CL Zone below the LCM Subzone at Dart Stream (31) contains similar micrite-centred cherts to those found at the base of the Dee Stream section. Nodular bedding extends seven metres above the LCM Subzone, and chert nodules become increasingly pale-grey in colour. Chert below, and

immediately above the LCM Subzone constitute about 35% of the rock. Dark chert bands and nodules constitute about 25% of the rock for the next 20 m, up to a 2 m thick bioturbated micrite (Teredo Limestone - Morris 1987). At the top of this micrite is a 5 cm thick glauconitic sandstone. Above the Teredo Limestone, cherts are limited to rare nodules and thin centimetre-bedded bands, 4.5 m above the Teredo Limestone. The top of the CL Zone is 8 m above the Teredo Limestone.

At Dead Horse Gully (34) the CL Zone resembles a condensed version of the Branch and Dart Stream sections, except that the LCM Subzone is absent. In addition, millimetre-scale alternating layers of micrite and vein calcite or chert, or so-called 'zebra-beds' [Figure A2.27], are commonly found near the base of the nodular micrites. Zebra-beds are common at Kaikoura Peninsula (3,4) also, where the thin alternating layers are commonly more arcuate than shown in Figure A2.27. The uppermost cherts at Dead Horse Gully (34) are dark or pale coloured, flattened, 1-2 cm thick, 30-40 cm long, slightly irregular nodules, with pronounced outer rims. They are confined to irregularly-spaced micrite beds.

At Bluff Stream (35) the top of the chert sequence is at the base of the Teredo Limestone. The bulk of the chert is found in a 10 m interval, 5 m above the base of the section. The chert comprises about 10% of the rock, forming dark ovoid nodules about 10 cm in diameter. The chert interval is terminated by a fault, above which cherts are restricted to a few large dark nodules. In contrast, the CL Zone in the Lower Limestone only rare millimetre-scale chert flecks are found. The lower Bluff Stream section (36) contains nodular bedded micrites with common zebra-bedding but no chert nodules.

In the southern tributary of Muzzle Stream (33), chert nodules are dark or pale grey and micrite centred. Micrites are very nodular up to the Teredo Limestone, but are planar bedded above. The chert comprises about 10% of the rock. In the northern tributary cherts are 20-30 cm thick, mostly irregularly shaped, dark nodules which constrict surrounding beds. They are contained within nodular, decimetre-bedded micrites.

Only rare, small, pale grey chert nodules occur at Bluff River (37). A thin brecciated chert layer is found at the base of the sequence. Rare brecciated cherts [Figure A2.28] are also found at Kaikoura Peninsula.

Figure A2.27 Example of zebra-beds, in places cut by very small veins (arrows). This sample comes from Kaikoura Peninsula and was supplied by Dr D.W. Lewis.

Figure A2.28 Brecciated chert (sample KP1), beach platform near Lyell Creek, Kaikoura Peninsula (Grid Ref. NZMS 260 031 664668).

Figure A2.29 Vertical chert nodules (arrows), Waima River (Grid Ref. NZMS 260 P29 909244). Tops of nodules are spread out and flattened in the plane of bedding. Hammer for scale is circled.

Figure A2.30 Burrowing on the base of an overhanging bedding plane near the top of the CL Zone, Woodside Creek (Grid Ref. NZMS 260 P30 990194). The bulk of burrows appear to be *Thalassinoides*. Scale bar is approximately 0.5 m.

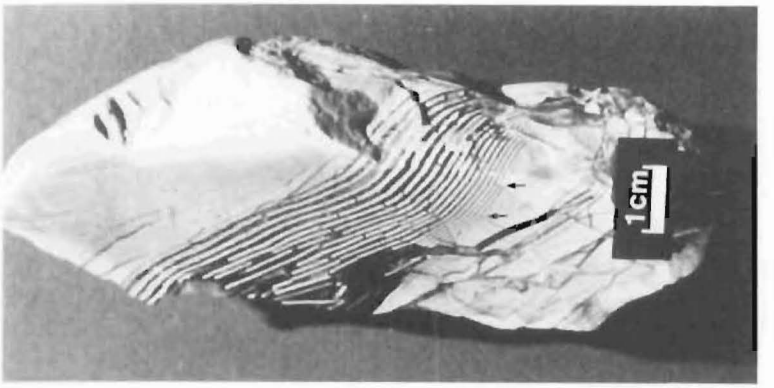

A2.27

A2.28

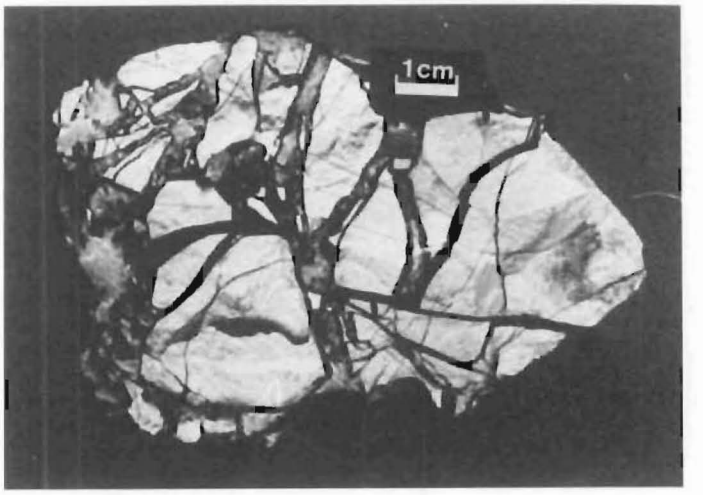

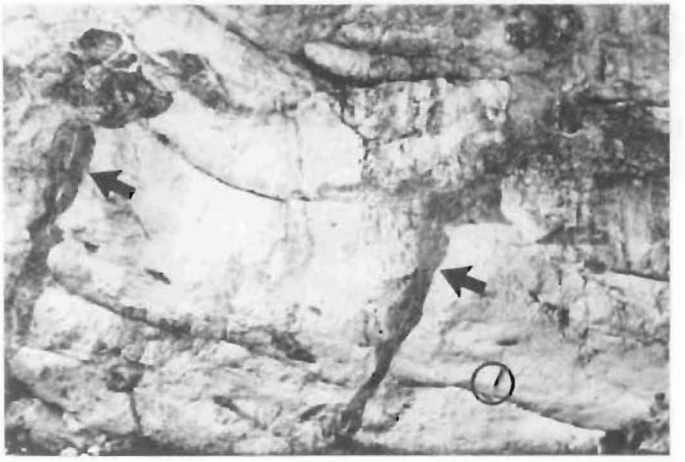

A2.29

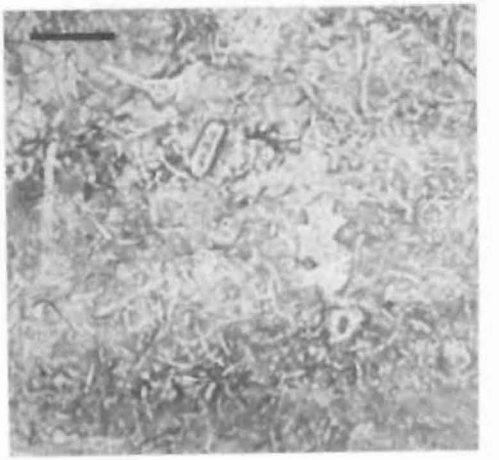

A2.30

The Waima River (21) provided only a limited amount of measurable section. The chert below the LCM Subzone is similar to that described at Mead Stream (24,25). Above the LCM Subzone are approximately 1 m long cherts, oriented perpendicular to bedding [Figure A2.29]. Close inspection reveals what appear to be thin fractures up the centre of each nodule. In some cases these are minor faults with small offsets. Sometimes aligned along the fractures are numbers of small nodules, or more commonly silicified micrite. The tops of the nodules are frequently irregular in shape and coincide with a bedding plane. No contact between these vertical cherts and the underlying LCM Subzone is exposed.

In the poorly exposed lower 20 m of the CL Zone at Woodside Creek (13), cherts are a mixture of dark and pale grey micrite-centred nodules, in slightly nodular decimetre-bedded micrites. A 10 cm thick layer of dolomite rhombs occurs near the top of this part of the sequence. The lowermost 2.4 m contains disseminated dolomite crystals. The next 20 m also contains disseminated dolomite rhombs. Micrites are 10-20 cm thick, planar to slightly nodular, interbedded with marls a few millimetres to 1-2 cm thick. Cherts are primarily pale grey with some reddish-brown, $\leq$20 cm thick, micrite centred bands. The 40 m thus described constitutes the bulk of the chert development at Woodside Creek. Chert volume never exceeds 35 percent. For approximately the next 23 m, chert abundance decreases to less than 5 percent. Cherts, although predominantly bands a few metres long, tend to be more nodular. Above, up to the K-T boundary (described in detail in Strong 1977, Morris 1987), chert is absent and micrite bed thickness is much greater, with some beds up to 60 cm thick. Chert reappears about half a metre above the K-T boundary. Nodular and band morphologies predominate, with mainly pale grey colours. Eight metres above the K-T boundary is a 0.5 m thick bed of pale grey nodules constituting about 80% of the rock. Aside from this layer, the nodules are similar to those below the K-T boundary. Fourteen metres above the boundary, chert is absent. Over the last 20 m of section, siliceous nodules predominate. Micrites are thicker, some up to 1 m, in places, and commonly pink to red in colour. Interbedded marls are rare, although a few sandy lenses are found in some micrites. The upper part of the section is intensely burrowed [Figure A2.30]. Many of the burrows have been preferentially chertified. The chertified burrows form flattened ovoid and irregular nodules, about 1 cm across, some are up to 15 cm long. Around the chert centre is a silicified micrite rim a few millimetres

thick. In some instances, silicified micrite may occupy the entire burrow.

Cherts at Wharanui Point (15) are predominantly dark to occasionally olive grey bands, ≤10 cm thick, in slightly nodular approximately 10 cm thick siliceous micrite beds. Interbeds are composed of 5-10 cm thick beds of dolomite crystals, which disappear abruptly near the top of the section. Nearby at South Wharanui Point (14), the micrites are approximately the same thickness, but are planar bedded in places and pink to pale reddish brown in colour. The pink colouration is not uniformly distributed within individual beds. Stylolitization is also evident in places. The sporadically distributed chert nodules are usually small, centimetre-scale, and pale-greenish grey in colour. One very large, approximately 1 m diameter, bulbous, chert nodule occurs near the top of the exposure. Five metres from the base of the exposure is a 90 cm thick laminated, siliceous, shaley micrite, in which lies the K-T boundary (see also Strong *et al.* 1988).

The CL Zone at Chancet Rocks (18) has features similar to the Woodside Creek CL Zone, including the K-T boundary. Immediately above the boundary are three approximately 10 cm thick, black, slightly laminated chert beds, each separated by about 0.5 m of siliceous micrite. These are traceable for about 100 m along strike from the section to the northwest, which is as far as exposure permits. Within 5 m to the immediate east of the measured section, these beds lens out and are replaced by cherty laminations in the micrite. About 12 m from the base of the section, pink micrites [Figure A2.31] similar to those at Woodside Creek are prevalent. There are numerous chert nodules [Figure A2.32] which resemble networks of chertified *?Thalassinoides* burrows. The cherts are frequently elongated along strike. In some cases they are composed of siliceous micrite, but more commonly of silicified micrite, with varying amounts of chert. The chert is recognized by its darker colour [Figure A2.32]. There are numerous nodules which are more or less cylindrical [Figure A2.33], oriented perpendicular to bedding, and in some instances are associated with thin chert layers that are parallel to bedding [Figure A2.33b]. Although commonly contained within a single bed, a few cross more than one bed. The cylindrical cherts are commonly about 10 cm in diameter [Figure A2.34]. The central body of the nodule consists of siliceous micrite and in some cases contains a central rod structure [Figure A2.34]. The chert

Figure A2.31 Pink micrites, CL Zone, beach platform, Chancet Rocks (Grid Ref. NZMS P29 092298).

Figure A2.32 Cherts, CL Zone, beach platform, Chancet Rocks (Grid Ref. NZMS P29 092298). Some nodules appear to be chertified *Thalassinoides* burrows.

A2.31

A2.32

a

b

Figure A2.33 Cylindrical chert nodules, CL Zone, beach platform, Chancet Rocks (Grid Ref. NZMS 260 P29 092298).
(a) Large example from near the top of the section. The nodule is longer than the average limestone bed thickness at Chancet Rocks.
(b) Small nodule with associated thin bedding-parallel chert (arrows). This cylindrical nodule cannot be traced completely through the bed.

with marginal silicified micrite, forms a 'halo' around the body of the 'structure'. The third type of chert nodule at this locality is usually ≥10 cm long and more or less cigar shaped. Outer margins consist of chert or silicified micrite. Centres, which were probably calcite, are commonly weathered out in outcrop. Both chert halos and chertified *?Thalassinoides* burrows occur in the same bed in some instances, but there is no definite connection between them. Stylolites are found in varying abundance, particularly towards the top of the sequence, and are compacted around all cherts.

CL Zone cherts at Flaxbourne River Mouth (17) are micrite-centred chert nodules, similar to those described elsewhere, and constitute about 25% of the rock.

The lowermost 15 m of the exposed CL Zone at Waipapa Bay (11), consists of nodular, centimetre-bedded to decimetre-bedded micrites containing lenticular to ovoid, dark, pale grey, and micrite centred chert nodules described from elsewhere. Large bulbous chert nodules, up to 1 m across are common [Figure A2.35]. Towards the top of the 15 m interval, micrite centred cherts predominate. Above, bedding becomes planar and cherts more elongated, forming bands which comprise less than 25% of the rock. Only minor occurrences of bulbous chert nodules are found, as well as a few cylindrical nodules. The chert bands are ≤10 cm thick and some tens of metres long. However, unlike the bands described at other localities, they occur between the micrite beds. In addition, they can vary along strike from siliceous marl to silicified marl or micrite, to chert. Not all partings between micrite beds contain bands and there is no rhythmicity to occurrences.

At Mt Alexander (8), Jordan Stream (7), and the Puhi Puhi River bridge (5) sections, cherts are dark, ovoid to lenticular nodules in nodular micrites, similar to those described elsewhere. Glauconite filled *Thalassinoides* burrows extending downwards from the Teredo Limestone into underlying chert nodules [Figure A2.36], are seen at Jordan Stream (7).

A2.6. LOWER CHERT MEMBER (LCM) AND UPPER CHERT MEMBER (UCM) SUBZONES

Both the LCM and UCM Subzones are shown in Figure A2.37.

Figure A2.34 Cross section through a cylindrical chert from the beach platform, Chancet Rocks (sample from McCulloch 1976). The remains of a central rod is seen at the right hand end of the nodule. Arrows indicate silicified micrite.

Figure A2.35 Large, bulbous nodules, CL Zone, beach platform, Waipapa Bay (Grid Ref. NZMS 260 P31 819875).
(a) Bedding is almost completely obscured (arrow) by large nodule development in some cases.
(b) Unchertified limestone beds are commonly compacted around nodules.

Figure A2.36 Chert nodule containing a glauconite filled *Thalassinoides* burrow, CL Zone, Puhi Puhi River (Grid Ref. NZMS 260 P31 723848). At this locality the sequence is overturned, so the younging direction is towards the bottom right hand corner of the photograph.

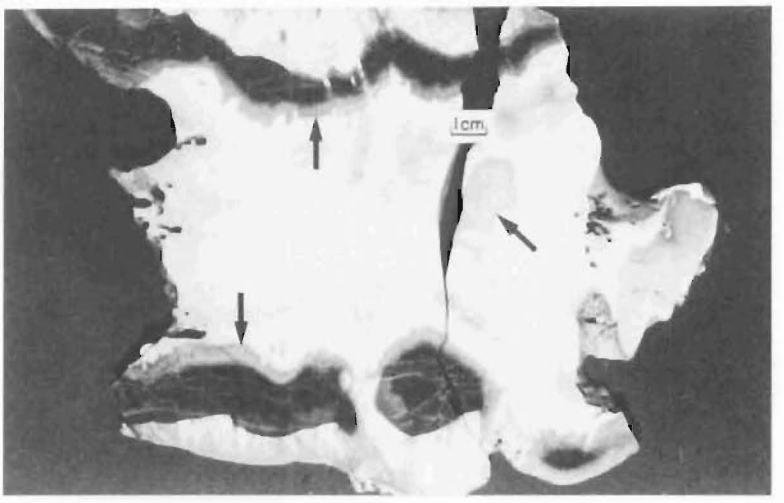

A2.34

a

A2.35

b

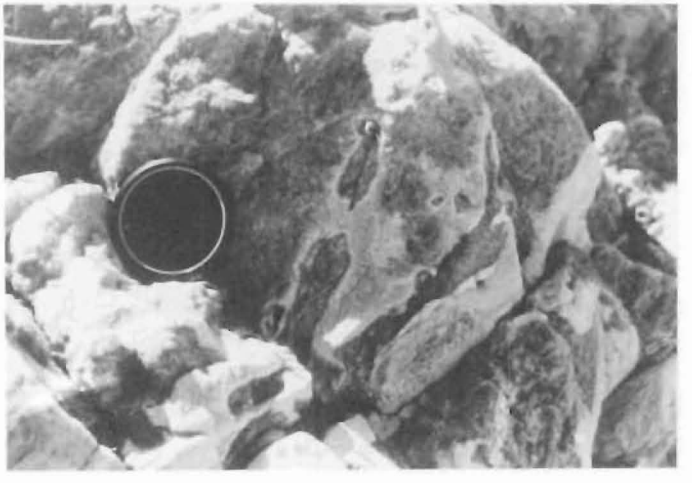

A2.36

A2.6.1. LCM SUBZONE

All LCM Subzone rocks contain sulphide nodules. No basal dolomite unit occurs at Mead Stream (24,25). The basal 8.2 m consists of dark grey to black, 10-50 cm thick planar bedded cherts with silicified micrite rims. Silicified micrite may also occur within chert beds. Lenses of dolomite rhombs, similar to those in the CD Zone, are common both within and around cherts. Chert comprises 70-80% of the rock and dolomite about 20 percent. The remainder consists of siliceous micrite rims, and interbedded dark grey to black, commonly noncalcareous, approximately 1 cm thick, commonly fissile, sandy mudstones. The thickness of the chert beds means that surrounding silicified micrites and the interbedded shales are few in number. In some instances dolomite layers are very thin and appear 'compressed' between silicified micrites [Figure A2.38]. Above the lowermost 8.2 m there is a decrease in chert volume and a concomitant increase in abundance of silicified micrite, and a greater abundance of interbedded mudstone. Cherts are more nodular. The amount of dolomite is only slightly less than in the lowermost 8.2 m. The chert volume gradually decreases to about 40% at the top of the Subzone, but the range of bed thicknesses are the same as below. As beds become more nodular upwards, discrete nodules (up to 1 m long) become more common. Where chert nodules are thin, the remainder of the bed is composed of silicified micrite. Mudstone interbeds are more prevalent than in the lowermost 8.2 m and are white to grey, fissile, about 1 cm thick, and slightly calcareous. The greater mudstone abundance may be at the expense of the dolomite.

The basal part of the LCM Subzone at Limburn Stream (26) consists of a 13 m thick decimetre-bedded dolomite unit, in which the lowermost 5.8 m is chert free. Above the lowermost 5.8 m occurs increasing proportions of dark, <10 cm thick chert nodules, with the overall volume of chert gradually increasing to about 60% of the rock. The dolomite is similar to that in the CD Zone, consisting of rhombic crystals <1 mm across, set in chert. Overlying the dolomite unit is 4.3 m of centimetre-bedded to decimetre-bedded chert, commonly with outer margins of silicified micrite. The silicified micrite constitutes about 5-10% of the rock, with chert comprising the rest. Dolomite is absent. The upper 7.2 m of the LCM Subzone consists of decimetre-bedded siliceous micrite with 10-15% dolomite, and 10-15% dark chert. The chert and dolomite form <10 cm thick

Figure A2.37 LCM and UCM Subzones, southern tributary, Mead Stream.
(a) View of both Subzones looking approximately southwest along the Chalk Range structure. The LCM Subzone can be traced throughout the exposure (lines). Note the fault offsets. The arrow indicates the position of the UCM Subzone which cannot be traced with certainty more than a few tens of metres above the stream bed.
(b) Stream bed exposure of the LCM Subzone (lines) (Grid Ref. NZMS 260 P30 760161).
(c) Stream bed exposure of the UCM Subzone (between the arrows) (Grid Ref. NZMS 260 P30 759161).

Figure A2.38 Field sketch of dolomite layers in silicified micrite between chert nodules, LCM Subzone, southern tributary, Mead Stream (Grid Ref. NZMS 260 P30 759161).

a

A2.37

b

c

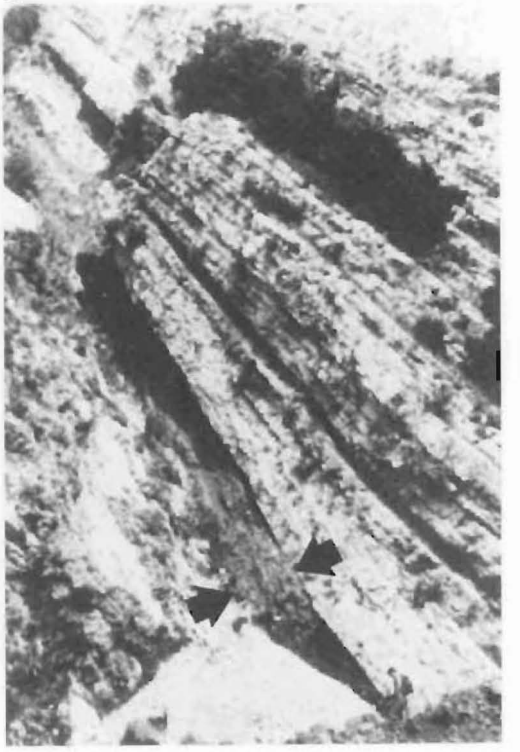

A2.38

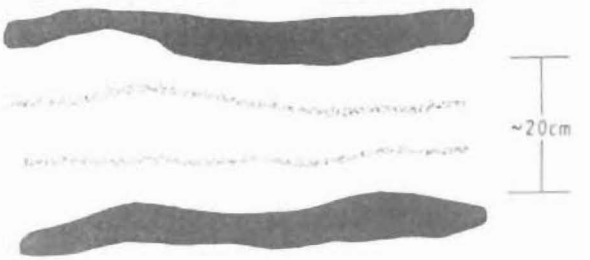

nodules and lenses respectively.

The base of the LCM Subzone at Dee Stream (27) consists of a 1.4 m thick unit of ≤10 cm thick beds of dolomite rhombs, surrounded by siliceous micrite. There are also a few small, pale grey chert nodules. The next 10.7 m consists of ≤30 cm thick nodular beds of dark chert, micrite and silicified micrite containing disseminated dolomite crystals. The proportion of micrite and chert varies somewhat, although chert volume tends to increase stratigraphically upwards, reaching a maximum of about 75 percent. Micrites become increasingly silicified upwards. Above this interval is 10.8 m containing chert nodules up to 40 cm thick, with lenses of dolomite rhombs both in and outside the nodules. Both are surrounded by silicified micrite. Interbeds consist of centimetre-bedded noncalcareous mudstones. Chert volumes are about 75 percent, with dolomite <20% and silicified micrite comprising the rest. The uppermost 15.4 m of the Subzone comprises decimetre-bedded, slightly nodular micrite, with dark centimetre-thick chert nodules, surrounded by centimetre-thick lenses of dolomite. There are also some large bulbous cherts. Chert and dolomite constitute 30% and 25% of the rock respectively, with micrite accounting for the rest.

The southernmost occurrence of the basal dolomite bed is at Branch Stream (29) where it is 7.2 m thick. The lowermost 2.7 m thereof is a centimetre-bedded to decimetre-bedded dolomite (as at Limburn Stream), with minor silicified micrite and chert. The rest is a decimetre-bedded dolomitic micrite (about 40% dolomite) with about 15% chert nodules. The overlying 9 m consists mainly of beds of coalesced or nodular cherts, averaging about 10 cm thick (with some up to 30 cm thick), constituting about 80% of the rock. Lenses or beds of rhombic dolomite crystals occur (≤5%), but tend to decrease in volume upwards, with a concomitant increase in the volume of silicified micrite.

At Dart Stream (31) the 4.3 m thick LCM Subzone contains about 50% chert (c.f. 25-30% for the CL Zone), comprising nodules averaging 10 cm thick, with common large (approximately 30 cm thick) bulbous cherts, particularly near the base. This interval is identified as the LCM Subzone on the basis of its stratigraphic position and the higher chert volume compared to the rest of the CL Zone above and below.

In the Waima River section (21) the LCM Subzone contains a greater proportion of silicified micrite at the base than at the top. Cherts form 30-40 cm thick beds, with centimetre thick interbedded mudstones. The lithologies are otherwise similar to those at Mead or Limburn Streams, except for the absence of dolomite.

A2.6.2. UCM SUBZONE

The Subzone at Mead Stream (25) consists of 5-10 cm thick, black, Fe-oxide stained, planar-bedded, chertified very fine sandstone to siltstone, interbedded with 1-3 cm thick, black, Fe-oxide stained, fissile mudstone. Both lithologies contain abundant disseminated pyrite, the mudstone more so. The interbeds are not as abundant, and chert beds are slightly thicker in the lowermost 0.3 m than in the rest of the unit. No nodular morphologies are observed at all. The upper and lower boundaries of the Subzone are sharp. The lithology in the upper gorge of Woodside Creek (12) is otherwise similar to that described from Mead Stream (25).

A2.7. MIDDLE LIMESTONE (ML) ZONE

At localities from Kaikoura Peninsula (3,4) north, micrite beds are centimetre to decimetre thick, indurated, and stylobedded.

Fourteen metres from the top of the ML Zone at Mead Stream (25) is a 5 m thick interval containing <20% chert. The chert occurs as nodules up to 20 cm long, but $\leq$5 cm thick, irregular and flattened, with silicified micrite rims a few millimetres thick. Small chert nodules a few millimetres in diameter are also common. At Mt Alexander (8) there are small flattened nodules similar to those shown in Figure A2.32. With the exception of Kaikoura Peninsula (3,4) and Waipapa Bay (11), the ML Zone cherts elsewhere are similar to those described at Mead Stream (25), and quantitatively minor.

Waipapa Bay (11) cherts tend to be micrite centred nodules with some cylindrical forms. In general the cherts at this locality have a greater similarity to those in the CL Zone than to ML Zone cherts from elsewhere.

Chert in the ML Zone at Kaikoura Peninsula (3,4) is more abundant than in other ML Zones, and constitutes the bulk of chert development at this

locality. The nodules are dark coloured, up to 30 cm long and ≤10 cm thick, and commonly micrite centred [Figure A2.39]. For beds that do not contain chert the average micrite bed thickness is 2-4 centimetres. Beds, or parts of beds containing chert nodules are usually about 10 cm thick. Micrites devoid of chert compact around chert bearing beds [Figure A2.39].

South of Kaikoura Peninsula, the ubiquitous stylobedding is absent, and micrites are ≤10 cm thick and planar bedded. On a beach platform at Oaro (2), branched networks of flattened, decimetre-thick, grey chert nodules are found [Figure A2.40]. Individual nodules may be up to 5 m, and nodules intersecting at about 120° are common. They are interpreted as silicified *Thalassinoides* burrows, similar to those described by Bromley and Ekdale (1984).

A2.8. OTHER CHERT OCCURRENCES

Found in the Weka Pass Stone, only at South Bay (3), is a single bed containing chert nodules [Figure A2.41]. The chert consists of pale grey, irregular, decimetre-thick nodules, in a 10-15 cm thick bed of sandy biomicrite. The limestone is centimetre-bedded immediately above and below the chert bearing bed. Twenty centimetres below the chert is a phosphatized conglomerate bed. The base of the conglomerate bed unconformably overlies the UM Zone.

Figure A2.39 Chert nodules, ML Zone, Lab Rocks, Kaikoura Peninsula (Grid Ref. NZMS 260 031 681658). Stylolitized beds are devoid of chert, and are much thinner than chert bearing beds.

Figure A2.40 Silicified *Thalassinoides* burrows, beach platform, Oaro (Grid Ref. NZMS 260 032 516536). The burrows are about 5 cm thick.

Figure A2.41 Chert nodules in Weka Pass Stone (W), South Bay, Kaikoura Peninsula (Grid Ref. NZMS 260 031 665644). The Phosphatized Conglomerate Bed (Morris 1987) is indicated by the arrow.

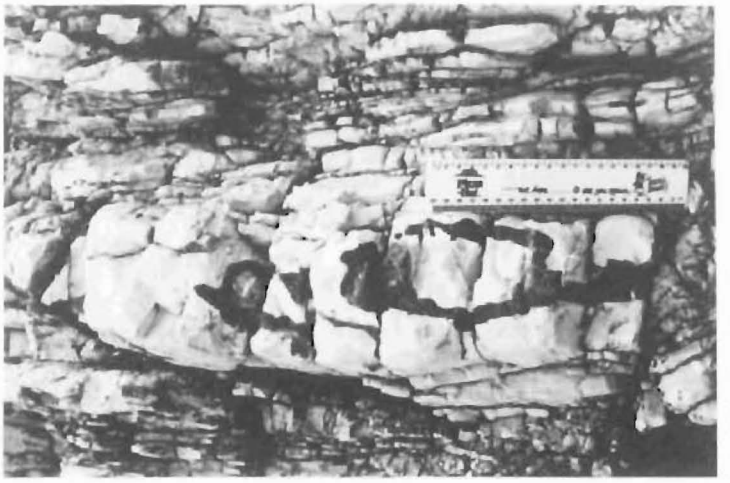

A2.39

A2.40

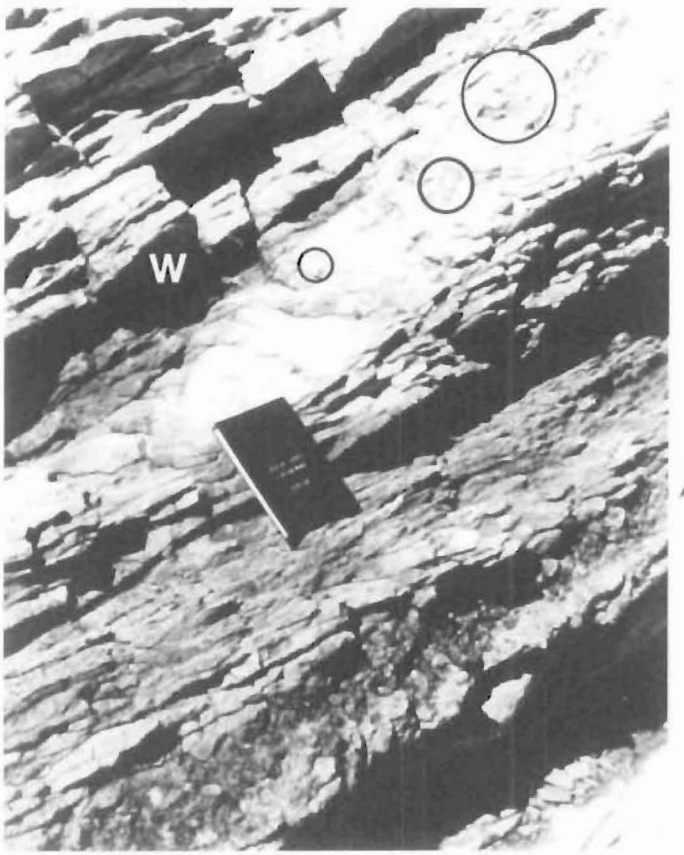

A2.41

A2.9. DETAILED STRATIGRAPHIC COLUMNS

Stratigraphic columns are presented according to location number. Grid references are quoted from the NZMS 260 1:50,000 series topographic maps [see also Appendix 8]. Abbreviations and graphic symbols are modified from Andrews (1982) and are listed below.

ABBREVIATIONS

A	a/a	as above	a/b	as below
	abund	abundant, abundance	adj	adjacent
	assoc	associated	av	average
	Ad Gr	Additional Graphic		
B	bdd	bedded	bdies	boundaries
	bddg	bedding	bdy	boundary
	biotd	bioturbated	bl	blue
	blk	black	bor	bored
	brec	brecciated	brn	brown
	Bur	burrow		
C	ca	about, approximately	Calc	calcite
	calc	calcareous	carb	carbonaceous
	cem	cemented	Cht	chert
	cht	cherty	cm	centimetre
	com	common, commonly	concr	concretion
	cont	contains, containing	crs	coarse
	crys	crystal, crystals		
D	decr	decrease(s), decreasing	diam	diameter
	diff	diffuse	dissem	disseminated
	dk	dark	dm	decimetre
	dol	dolomitic	Dol	dolomite
E	effl	efflorescence	ellip	elliptical
	elong	elongated	euh	euhedral
F	f	fine, finely	fis	fissile
	Flt	fault	fract	fractured

	frag	fragment, fragments
G	gen	generally
	glc	glauconitic
	Gwke	greywacke
I	ibdd	interbedded
	incl	includes
	ind	indurated
K	K-T	Cretaceous-Tertiary
L	lam	laminated
	loc	local, locally
	Lst	limestone
M	m	metre
	med	medium
	mic	micritic
	mod	moderately
	Mrl	marl
	Mst	mudstone
N	ncalc	noncalcareous
	Nod	nodule
P	pa	pale
	phosph	phosphatic, phosphatized
	Pyr	pyrite
R	reg	regular
S	s	sandy
	silic	siliceous
	sl	slightly
	stybdd	stylobedded
	Sul	sulphide
	surr	surrounded

Glc	glauconite
grn	green
gy	grey
ibds	interbeds
incr	increase, increases
irreg	irregular
lge	large
lt	light
mass	massive
Mic	micrite
mm	millimetre
morph	morphology
mrl	marly
ndol	nondolomitic
nod	nodular
Pbl	pebble
ppn	proportion(s)
pyr	pyritic
sh	shaley
silicif	silicified
Sst	sandstone
stybdg	stylobedding
Sulph	sulphur
Su	sulphur efflorescence

T	tk	thick	tn	thin
U	u	unconformity	uncem	uncemented
	unwthd	unweathered		
V	v	very	var	variable, variation
	vn	veined		
W	w	with	wh	white
	wthd	weathered	wthg	weathering
X	xbdd	crossbedded		
Y	yell	yellow		
Z	Zeb-bdg	zebra-bedding	Zst	siltstone

GRAPHIC SYMBOLS


Fault


No exposure

Sample


Sample (unanalyzed)

Carbonate


Dolomite


Dolomite concretions

Limestone (micrite)


Dolomitic limestone

Sandy Limestone


Marl

Chert


Lensoidal/lenticular nodules


Irregular nodules


Micrite centred or diffuse nodules


Bulbous nodules


Chert bands


Irregular bands


Micrite centred or diffuse bands


Chert beds or bedded cherts


Very small nodules

Detrital


Mudstone


Sandstone


Siltstone

Zones


WC Zone


CS Zone


BC Zone


CD Zone


CL Zone


LCM Subzone


UCM Subzone


LL Zone


LM and UM Zones


ML Zone

Additional Symbols


Massive


Well bedded

Gradational contact


Nodular bedded


Faintly bedded

Sharp contact


Foraminfera


Bioturbated


Burrows


Dolomitic

Stylolites


Contorted beds


Fossil

SM Silicified Micrite


Dike

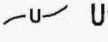
Unconformity


Disconformity

Su Sulphur efflorescence

Brackets qualify adjectives as 'slightly'.

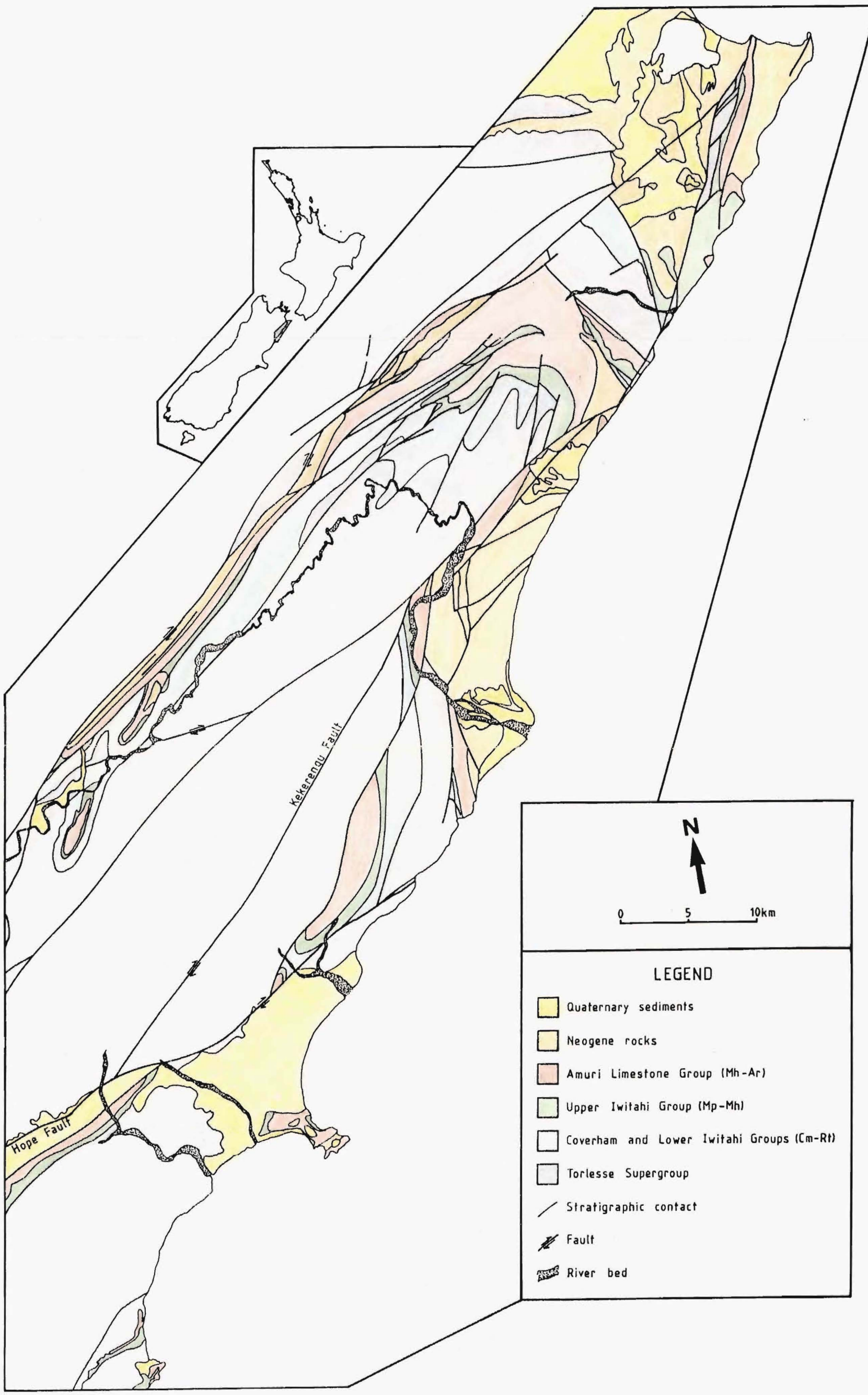
Kekerengu Fault
Hope Fault
N
0
5
10km
LEGEND
Quaternary sediments
Neogene rocks
Amuri Limestone Group (Mh-Ar)
Upper Iwitahi Group (Mp-Mh)
Coverham and Lower Iwitahi Groups (Cm-Rt)
Torlesse Supergroup
Stratigraphic contact
Fault
River bed

LOCALITY: Bluff River (37), Clarence Valley.

GRID REFERENCES

Sheet Number: 030

Base of Section: 541972

Top of Section: 541972

DATE: 30/11/84

METHOD OF MEASUREMENT: Visual estimate.

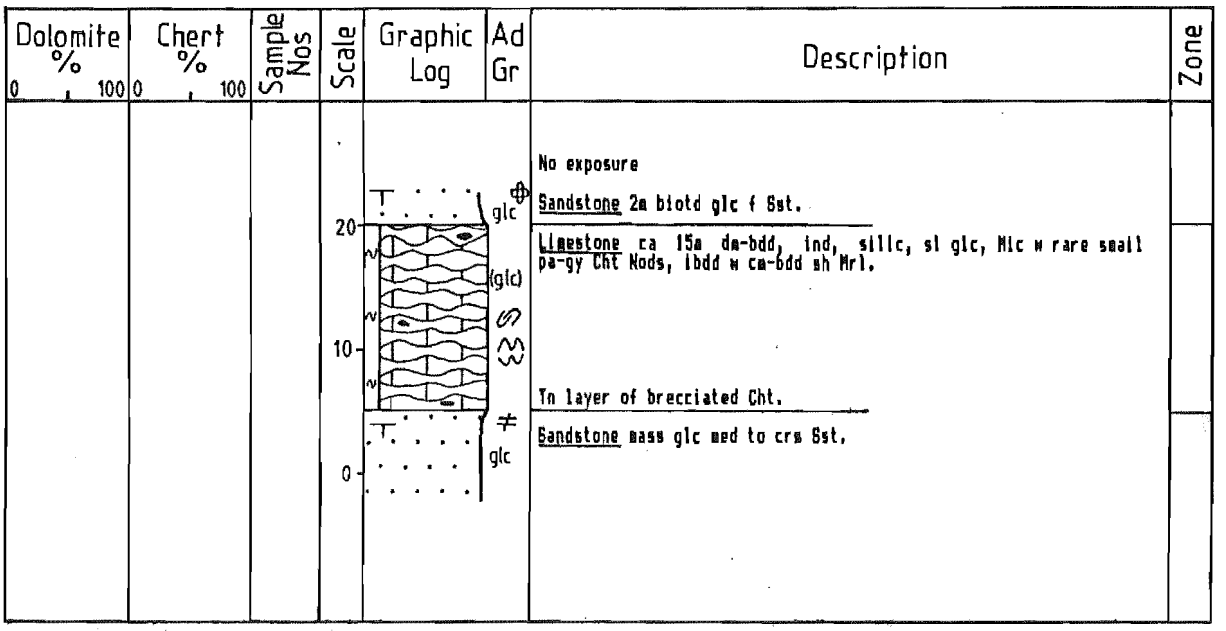

LOCALITY: Bluff Stream - Composite section of the upper gorge in the Chalk Range (35), Clarence Valley.

GRID REFERENCES

Sheet Number: 030

Base of Section: 576999

Top of Section: 576003

DATE: 28-29/11/84

METHOD OF MEASUREMENT: Tape and compass survey.

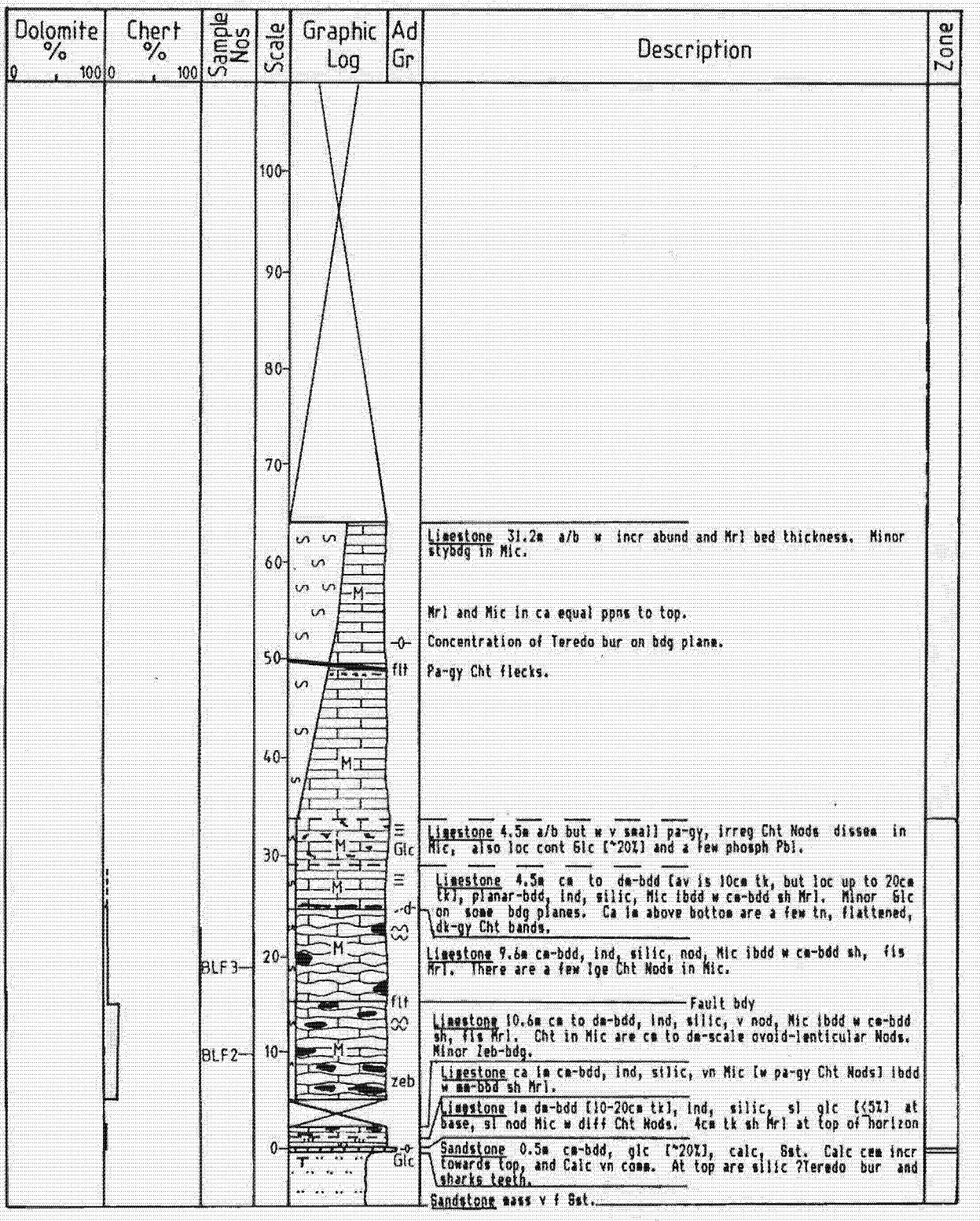

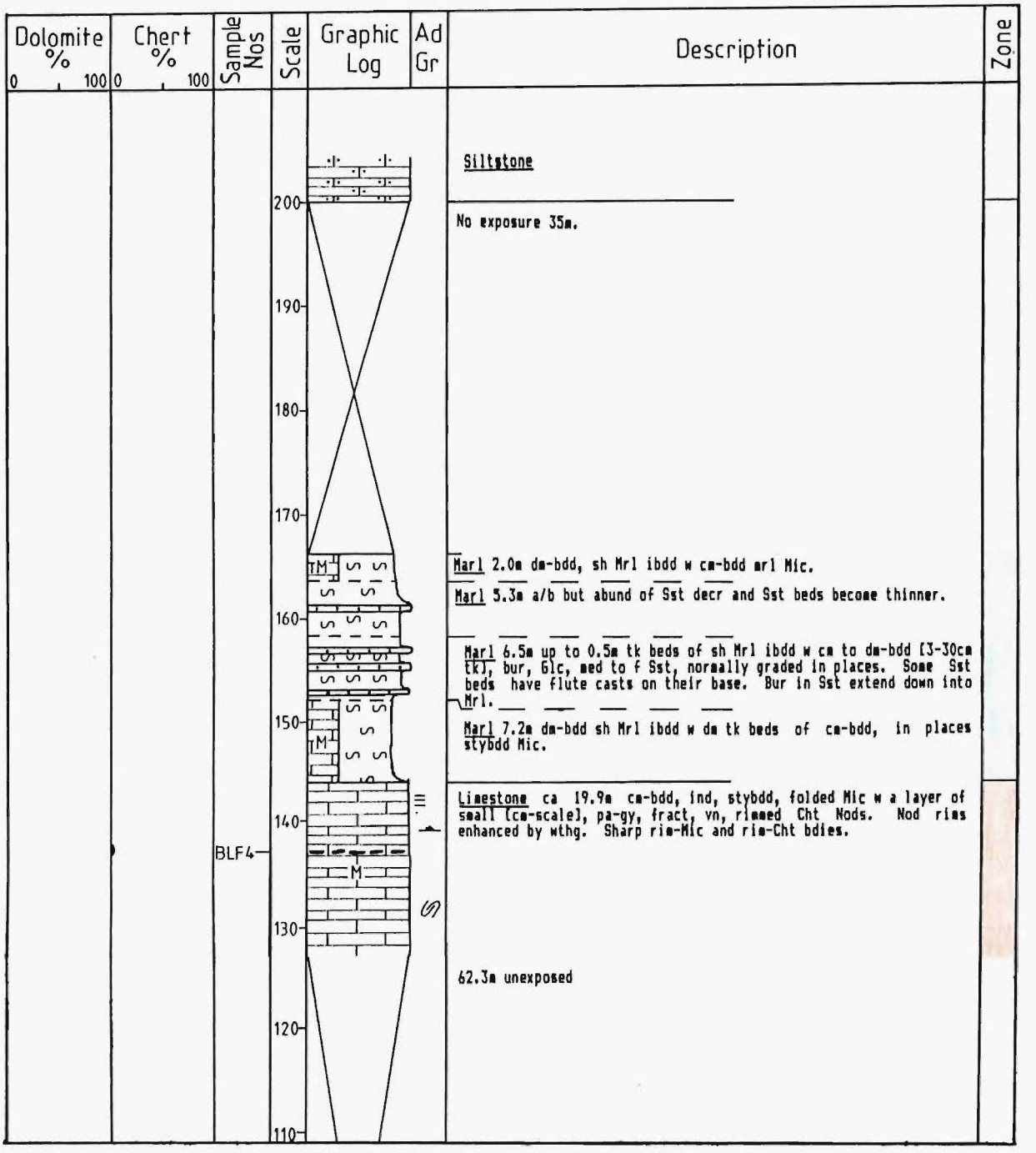
Dolomite %
0 100
Chert %
0 100
Sample Nos
Scale
Graphic Log
Ad Gr
Description
Zone
Siltstone
No exposure 35m.
Marl 2.0m dm-bdd, sh Mrl ibdd w cm-bdd arl Mic.
Marl 5.3m a/b but abund of Sst decr and Sst beds become thinner.
Marl 6.5m up to 0.5m tk beds of sh Mrl ibdd w cm to dm-bdd (3-30cm tk), bur, Glc, med to f Sst, normally graded in places. Some Sst beds have flute casts on their base. Bur in Sst extend down into Mrl.
Marl 7.2m dm-bdd sh Mrl ibdd w dm tk beds of cm-bdd, in places stybdd Mic.
Limestone ca 19.9m cm-bdd, ind, stybdd, folded Mic w a layer of small (cm-scale), pa-gy, fract, vn, rimmed Cht Nods. Nod rims enhanced by wthg. Sharp rim-Mic and rim-Cht bdies.
62.3m unexposed
BLF4
200
190
180
170
160
150
140
130
120
110
M
S

LOCALITY: Bluff Stream - Lower Gorge (36), Clarence Valley.

GRID REFERENCES

Sheet Number: 030

Base of Section: 583983

Top of Section: 582985

DATE: 29/11/84

METHOD OF MEASUREMENT: Visual estimate.

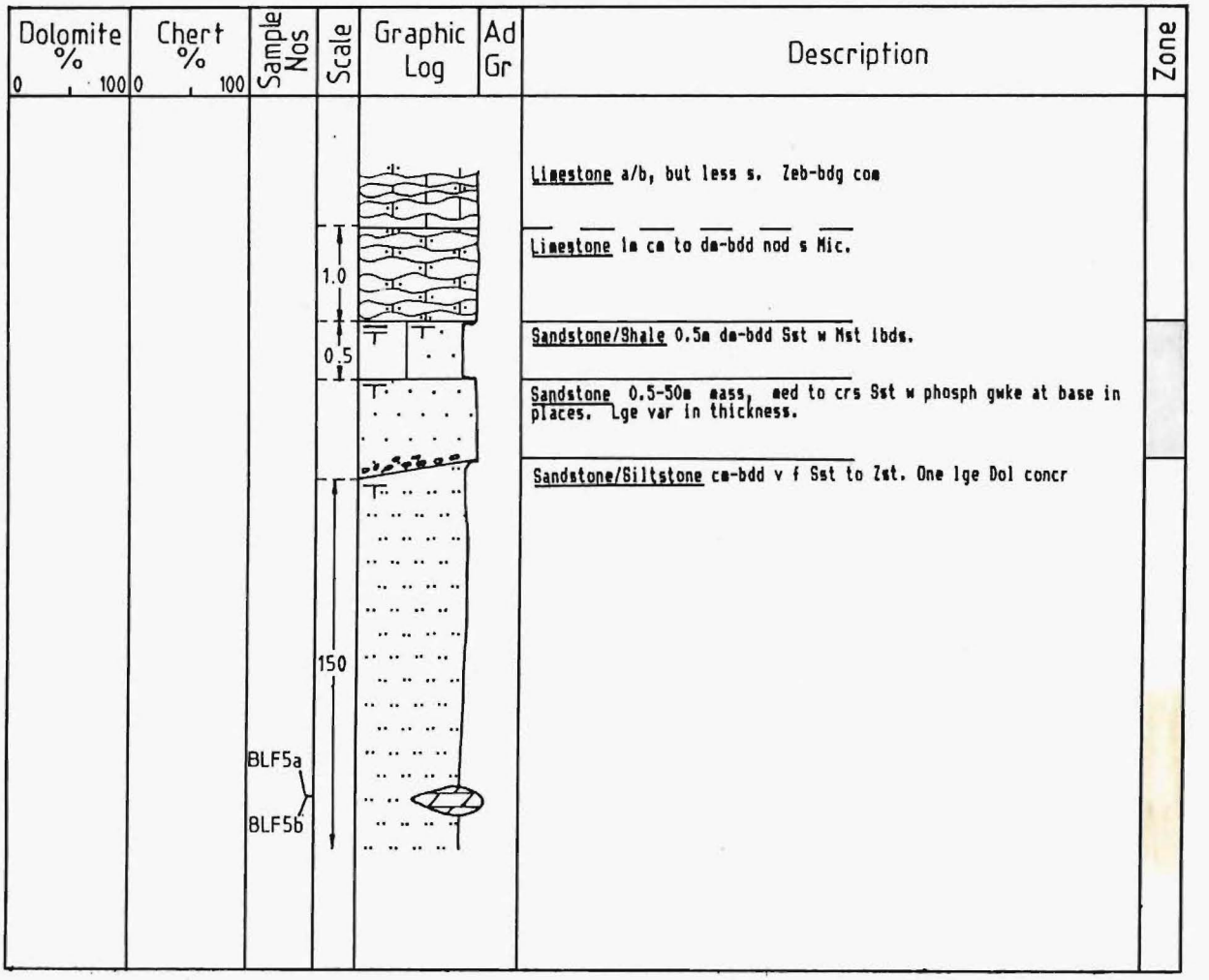

LOCALITY: Branch Stream - south tributary (29), Clarence Valley.

GRID REFERENCES

Sheet Number: 030

Base of Section: 686086

Top of Section: 983088

DATE: 8/11/84

METHOD OF MEASUREMENT: Tape and compass survey.

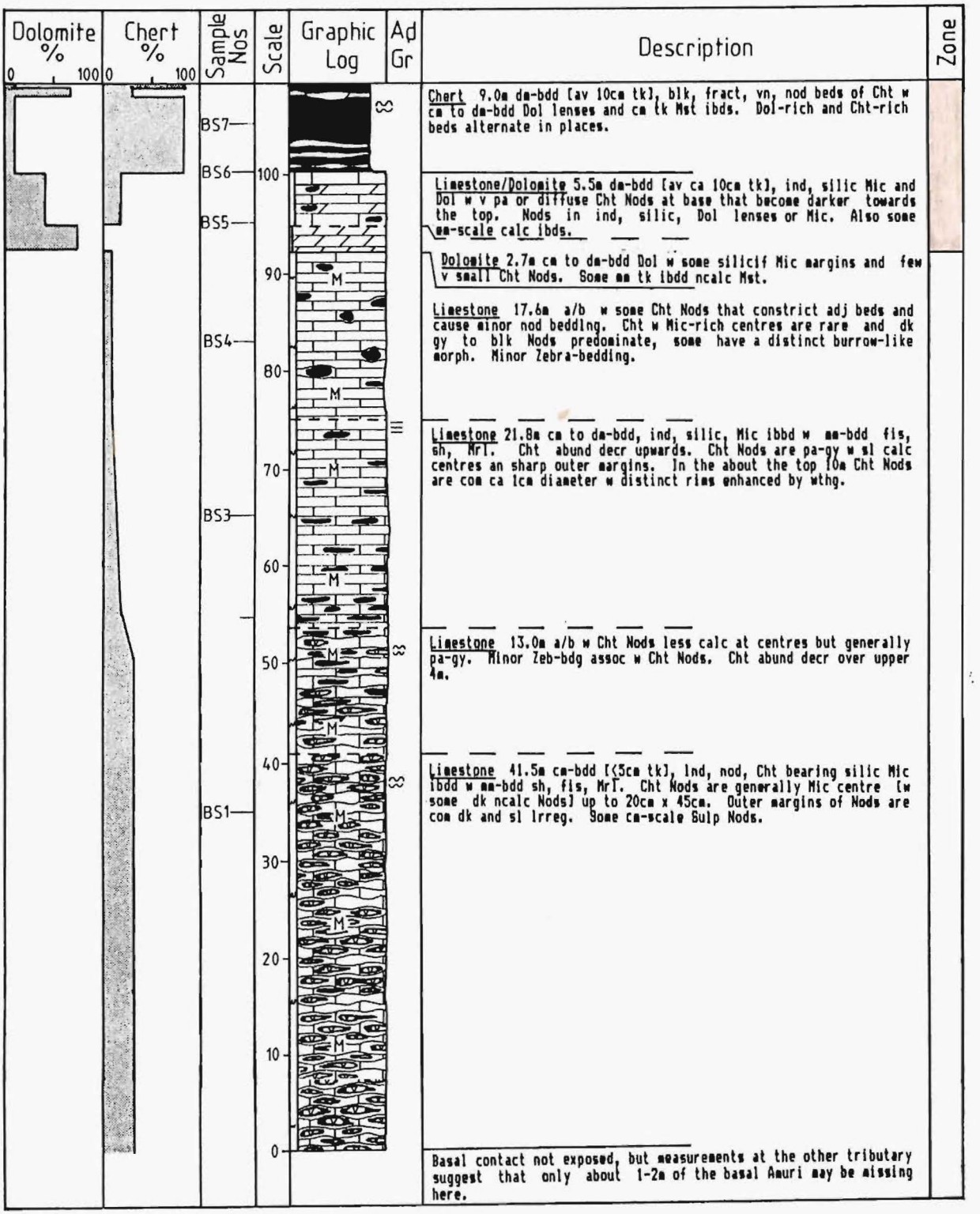

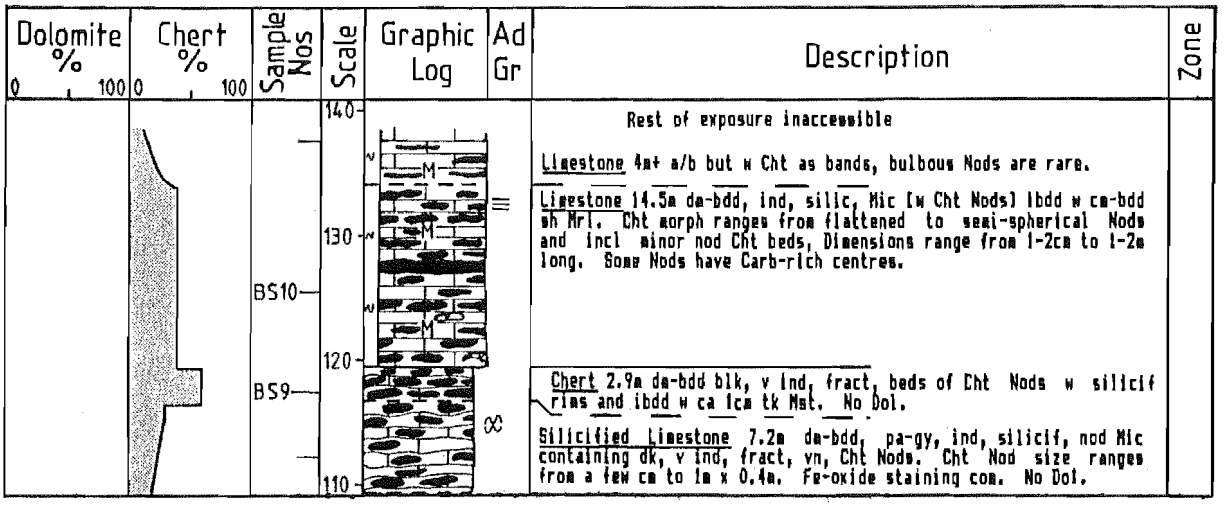
Dolomite %
0 100
Chert %
0 100
Sample Nos
Scale
Graphic Log
Ad Gr
Description
Zone
140
130
120
110
BS10
BS9
Rest of exposure inaccessible
Limestone 4m+ a/b but w Cht as bands, bulbous Nods are rare.
Limestone 14.5m da-bdd, ind, silic, Mic [w Cht Nods] lbdd w cm-bdd sh Mrl. Cht morph ranges from flattened to semi-spherical Nods and incl minor nod Cht beds, Dimensions range from 1-2cm to 1-2m long. Some Nods have Carb-rich centres.
Chert 2.9m dm-bdd blk, v ind, fract, beds of Cht Nods w silicif rims and lbdd w ca 1cm tk Mst. No Dol.
Silicified Limestone 7.2m dm-bdd, pa-gy, ind, silicif, nod Mic containing dk, v ind, fract, vn, Cht Nods. Cht Nod size ranges from a few cm to 1m x 0.4m. Fe-oxide staining com. No Dol.

LOCALITY: Branch Stream - middle tributary (28), Clarence Valley.

GRID REFERENCES

DATE: 6-7/11/84

Sheet Number: 030

Base of Section: 694093

Top of Section: 692096

METHOD OF MEASUREMENT: Visual estimate for lower sandstone, tape and compass survey for the rest.

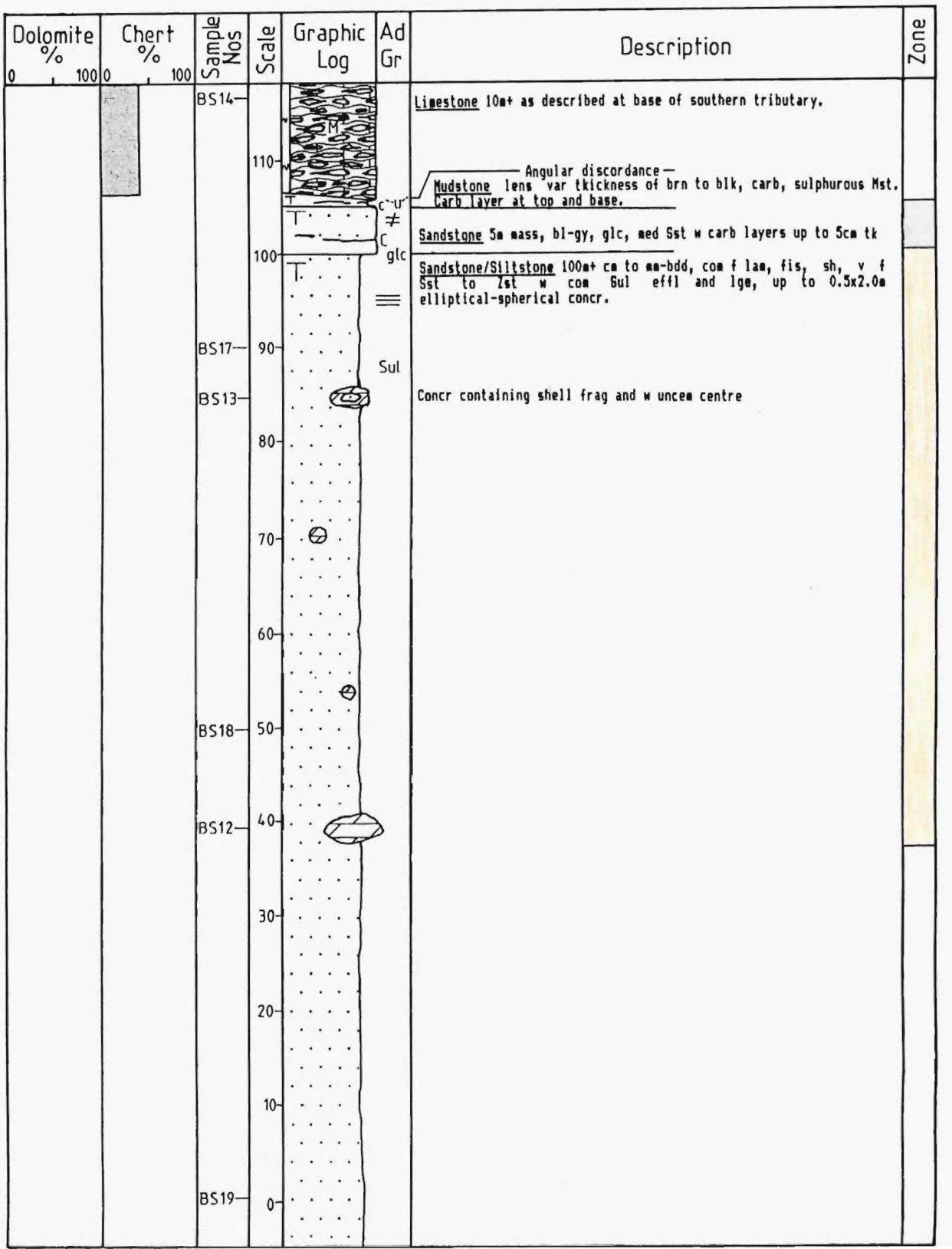

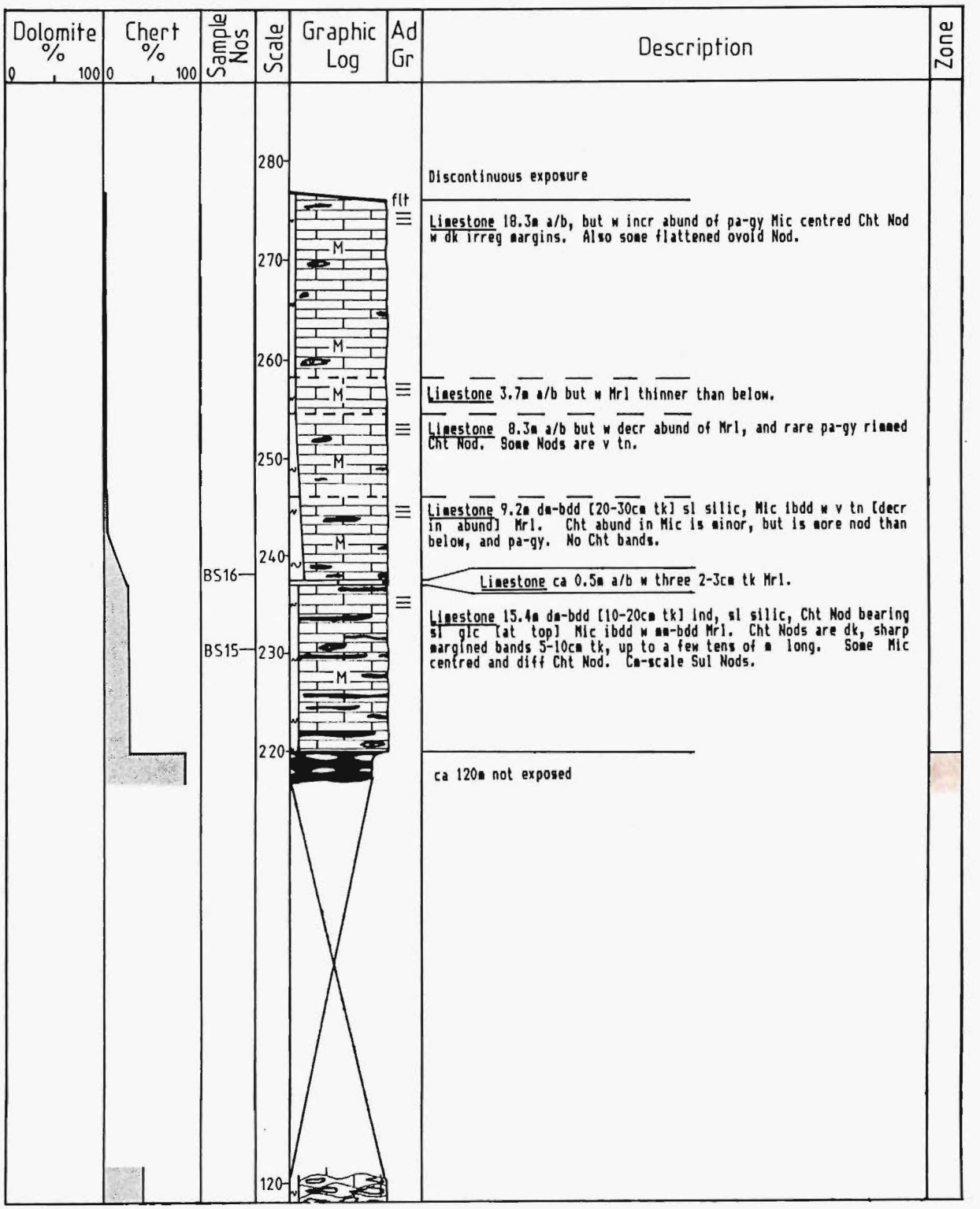
Dolomite %
0
100
Chert %
0
100
Sample Nos
Scale
Graphic Log
Ad Gr
Description
Zone
280
270
260
250
240
230
220
120
BS16
BS15
flt
M
Discontinuous exposure
Limestone 18.3m a/b, but w incr abund of pa-gy Mic centred Cht Nod w dk irreg margins. Also some flattened ovoid Nod.
Limestone 3.7m a/b but w Mrl thinner than below.
Limestone 8.3m a/b but w decr abund of Mrl, and rare pa-gy rimmed Cht Nod. Some Nods are v tn.
Limestone 9.2m dm-bdd [20-30cm tk] sl silic, Mic ibdd w v tn [decr in abund] Mrl. Cht abund in Mic is minor, but is more nod than below, and pa-gy. No Cht bands.
Limestone ca 0.5m a/b w three 2-3cm tk Mrl.
Limestone 15.4m dm-bdd [10-20cm tk] ind, sl silic, Cht Nod bearing sl glc [at top] Mic ibdd w mm-bdd Mrl. Cht Nods are dk, sharp margined bands 5-10cm tk, up to a few tens of m long. Some Mic centred and diff Cht Nod. Cm-scale Sul Nods.
ca 120m not exposed

LOCALITY: Chancet Rocks (10) - 3 km north of Flaxborne River mouth.

GRID REFERENCES

Sheet Number: P29

Base of Section: 092298

Top of Section: 092298

DATE: 18/11/85

METHOD OF MEASUREMENT: Tape and compass survey.

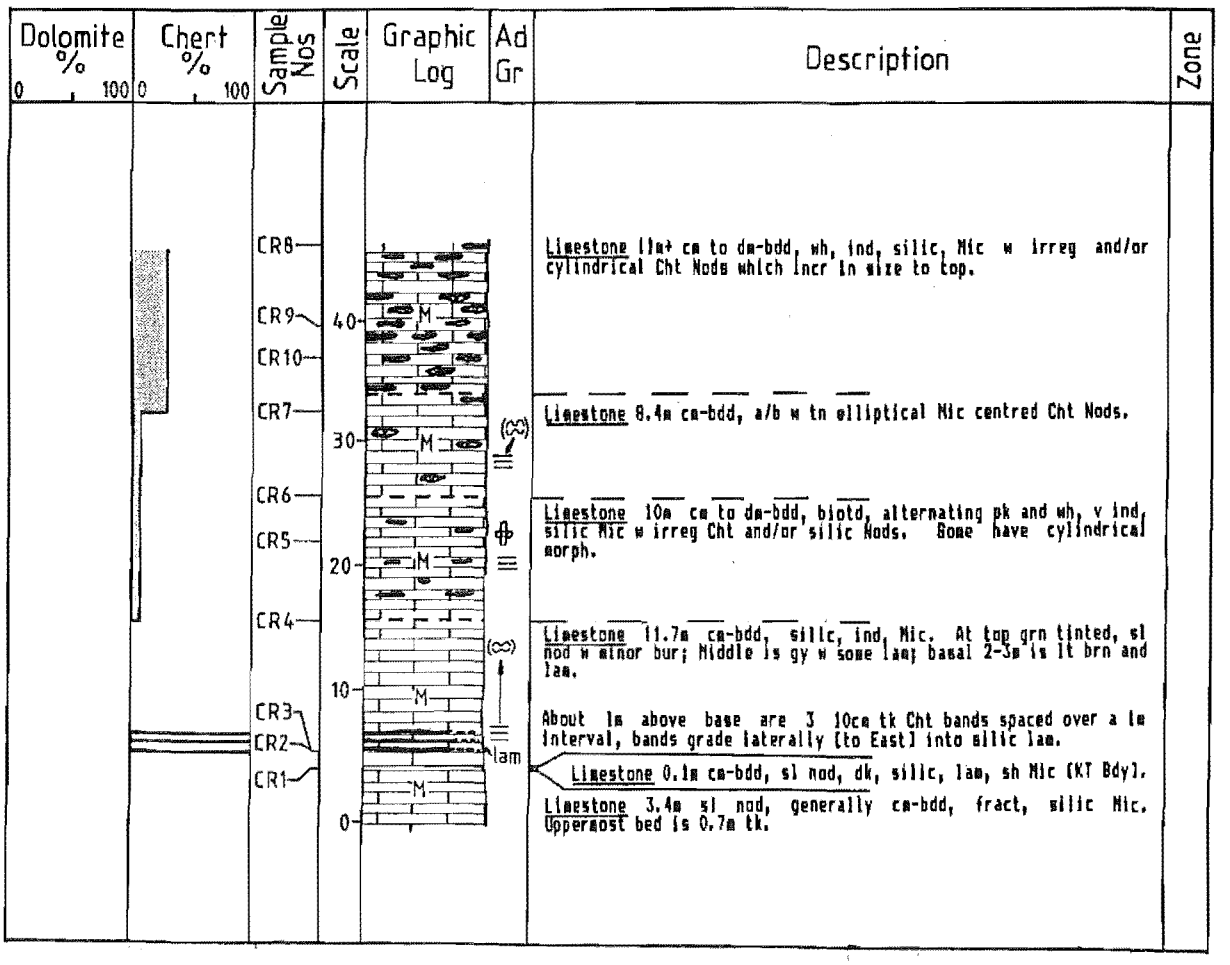

LOCALITY: Dead Horse Gully (34) - southern tributary of Muzzle Stream, Clarence Valley.

GRID REFERENCES

Sheet Number: 030

Base of Section: 604014

Top of Section: 601017

DATE: 12/11/84

METHOD OF MEASUREMENT: Tape and compass survey.

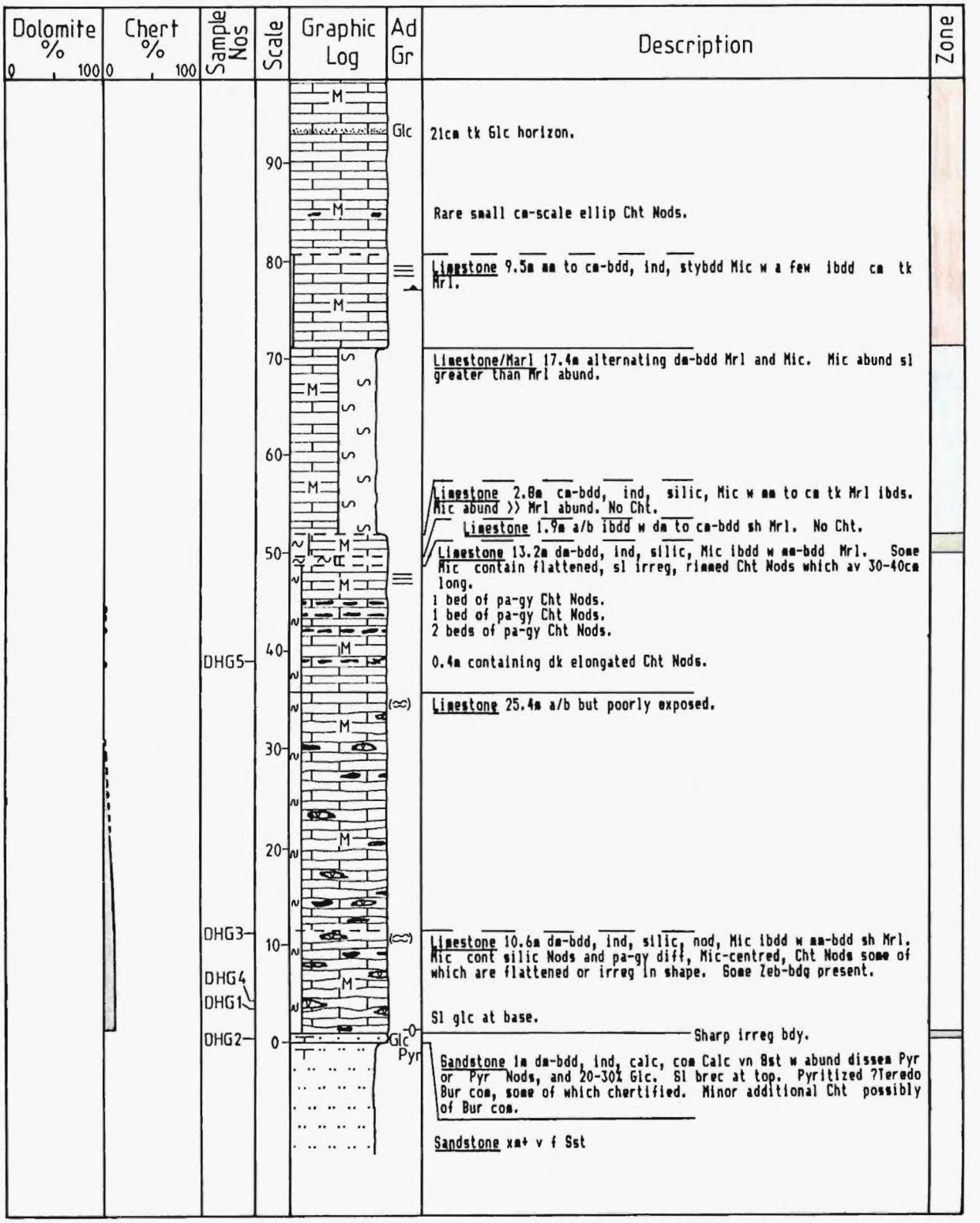

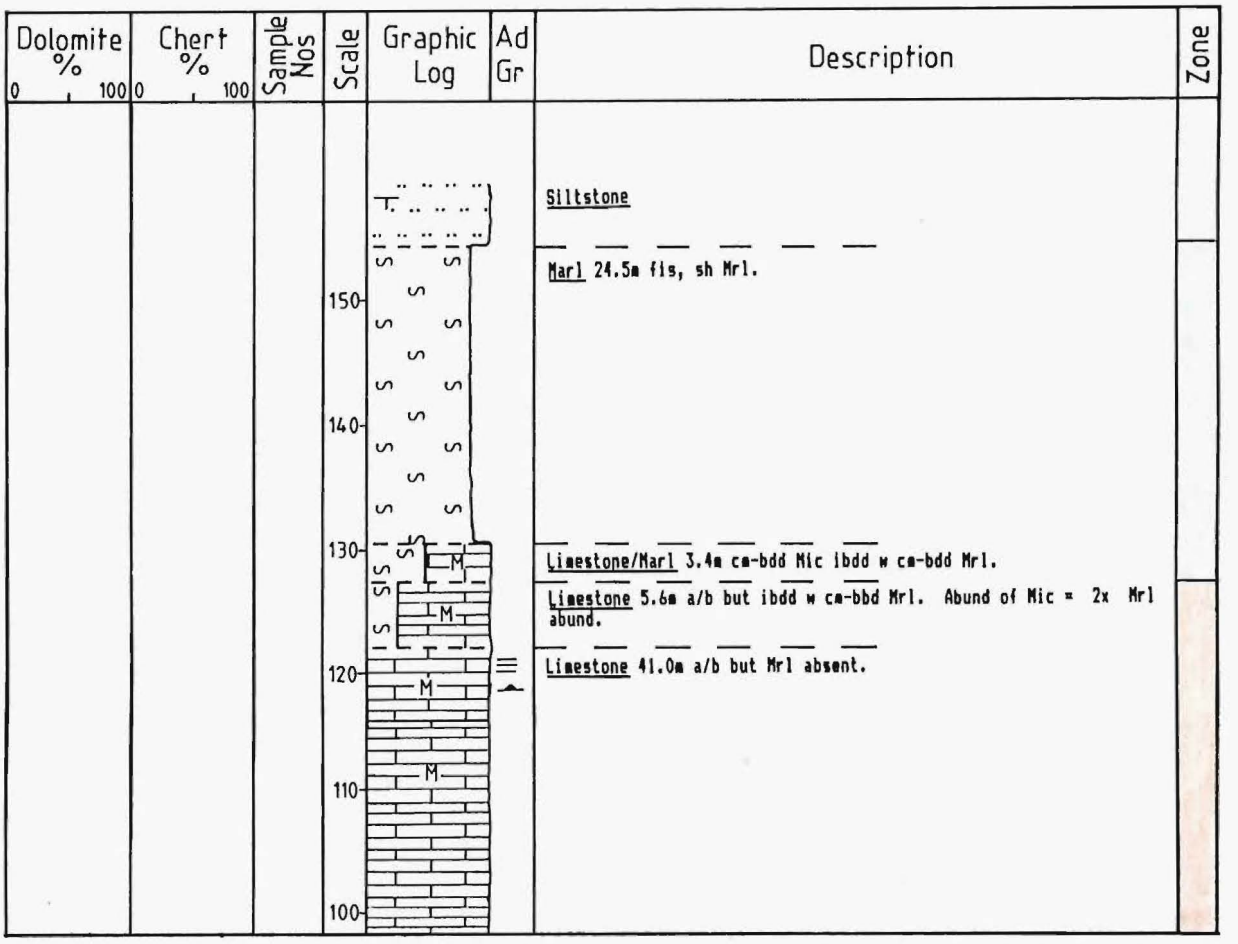
Dolomite %
0 100
Chert %
0 100
Sample Nos
Scale
Graphic Log
Ad Gr
Description
Zone
150
140
130
120
110
100
Siltstone
Marl 24.5m fis, sh Mrl.
Limestone/Marl 3.4m cm-bdd Mic ibdd w cm-bdd Mrl.
Limestone 5.6m a/b but ibdd w cm-bbd Mrl. Abund of Mic = 2x Mrl abund.
Limestone 41.0m a/b but Mrl absent.

LOCALITY: Dee Stream - southern tributary (27), Clarence Valley.

GRID REFERENCES

Sheet Number: P30

Base of Section: 711114

Top of Section: 706118

DATE: 23-24/10/84

METHOD OF MEASUREMENT: Tape and compass survey.

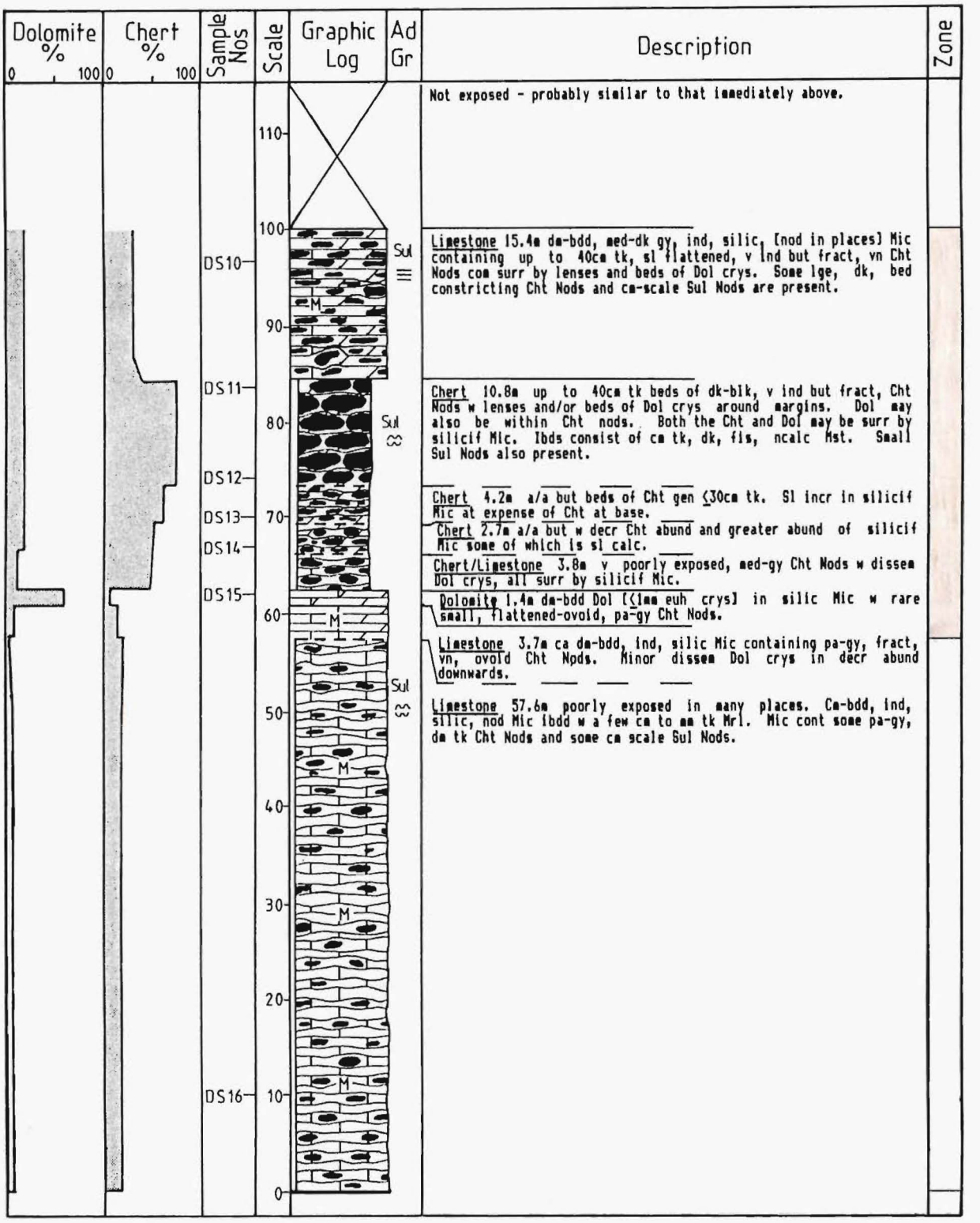

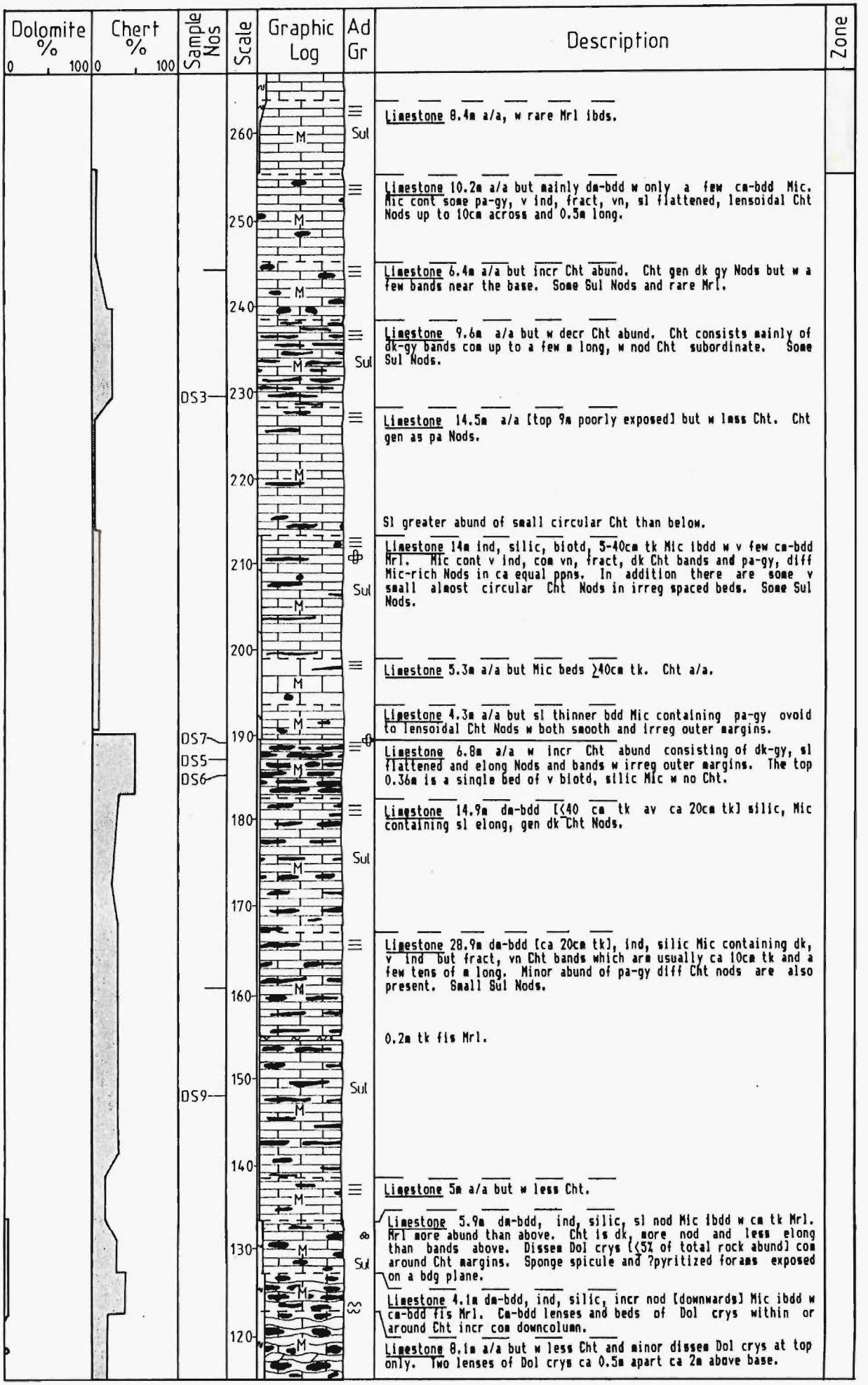
Dolomite %
0 100
Chert %
0 100
Sample Nos
Scale
Graphic Log
Ad Gr
Description
Zone
260
250
240
230
220
210
200
190
180
170
160
150
140
130
120
DS3
DS7
DS5
DS6
DS9
Sul
Limestone 8.4m a/a, w rare Mrl ibds.
Limestone 10.2m a/a but mainly dm-bdd w only a few cm-bdd Mic. Mic cont some pa-gy, v ind, fract, vn, sl flattened, lensoidal Cht Nods up to 10cm across and 0.5m long.
Limestone 6.4m a/a but incr Cht abund. Cht gen dk gy Nods but w a few bands near the base. Some Sul Nods and rare Mrl.
Limestone 9.6m a/a but w decr Cht abund. Cht consists mainly of dk-gy bands com up to a few m long, w nod Cht subordinate. Some Sul Nods.
Limestone 14.5m a/a [top 9m poorly exposed] but w less Cht. Cht gen as pa Nods.
Sl greater abund of small circular Cht than below.
Limestone 14m ind, silic, biotd, 5-40cm tk Mic ibdd w v few cm-bdd Mrl. Mic cont v ind, com vn, fract, dk Cht bands and pa-gy, diff Mic-rich Nods in ca equal ppns. In addition there are some v small almost circular Cht Nods in irreg spaced beds. Some Sul Nods.
Limestone 5.3m a/a but Mic beds ≥40cm tk. Cht a/a.
Limestone 4.3m a/a but sl thinner bdd Mic containing pa-gy ovoid to lensoidal Cht Nods w both smooth and irreg outer margins.
Limestone 6.8m a/a w incr Cht abund consisting of dk-gy, sl flattened and elong Nods and bands w irreg outer margins. The top 0.36m is a single bed of v biotd, silic Mic w no Cht.
Limestone 14.9m dm-bdd [<40 cm tk av ca 20cm tk] silic, Mic containing sl elong, gen dk Cht Nods.
Limestone 28.9m dm-bdd [ca 20cm tk], ind, silic Mic containing dk, v ind but fract, vn Cht bands which are usually ca 10cm tk and a few tens of m long. Minor abund of pa-gy diff Cht nods are also present. Small Sul Nods.
0.2m tk fis Mrl.
Limestone 5m a/a but w less Cht.
Limestone 5.9m dm-bdd, ind, silic, sl nod Mic ibdd w cm tk Mrl. Mrl more abund than above. Cht is dk, more nod and less elong than bands above. Dissem Dol crys [<5% of total rock abund] com around Cht margins. Sponge spicule and ?pyritized forams exposed on a bdg plane.
Limestone 4.1m dm-bdd, ind, silic, incr nod [downwards] Mic ibdd w cm-bdd fis Mrl. Cm-bdd lenses and beds of Dol crys within or around Cht incr com downcolumn.
Limestone 8.1m a/a but w less Cht and minor dissem Dol crys at top only. Two lenses of Dol crys ca 0.5m apart ca 2m above base.

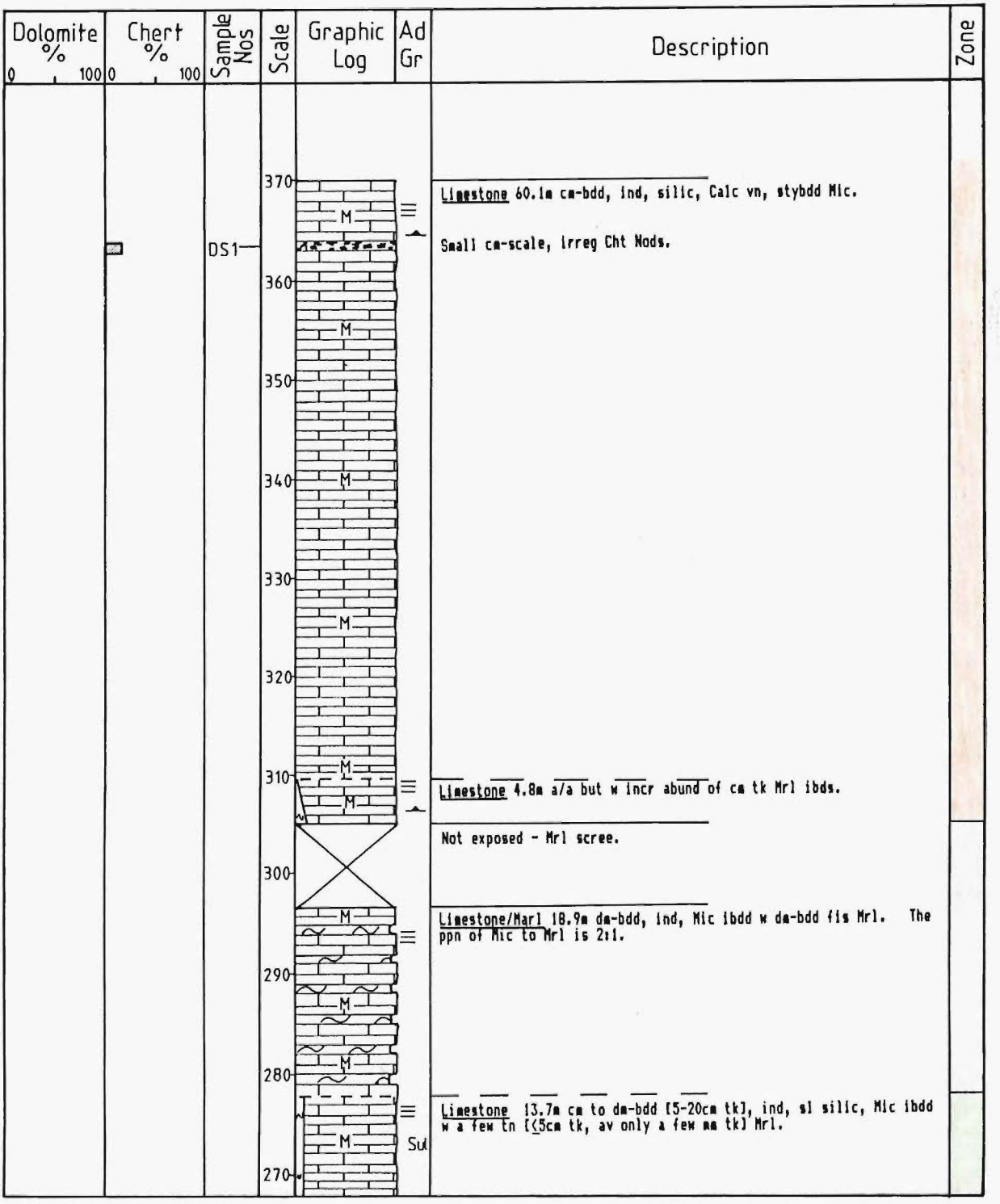
Dolomite %
0 100
Chert %
0 100
Sample Nos
Scale
Graphic Log
Ad Gr
Description
Zone
370
360
350
340
330
320
310
300
290
280
270
DS1
M
Su
Limestone 60.1m cm-bdd, ind, silic, Calc vn, stybdd Mic.
Small cm-scale, irreg Cht Nods.
Limestone 4.8m a/a but w incr abund of cm tk Mrl ibds.
Not exposed - Mrl scree.
Limestone/Marl 18.9m dm-bdd, ind, Mic ibdd w dm-bdd fis Mrl. The ppn of Mic to Mrl is 2:1.
Limestone 13.7m cm to dm-bdd [5-20cm tk], ind, sl silic, Mic ibdd w a few tn [<5cm tk, av only a few mm tk] Mrl.

LOCALITY: Dart Stream - composite section from northern (30) and southern (31), tributaries, Clarence Valley.

GRID REFERENCES

DATE: 9-10/11/84

Sheet Number: 030

Base of Section: N tributary 662059, S tributary 659059

Top of Section: N tributary 662059, S tributary 656061

METHOD OF MEASUREMENT: Visual estimate of sandstone, tape and compass survey.

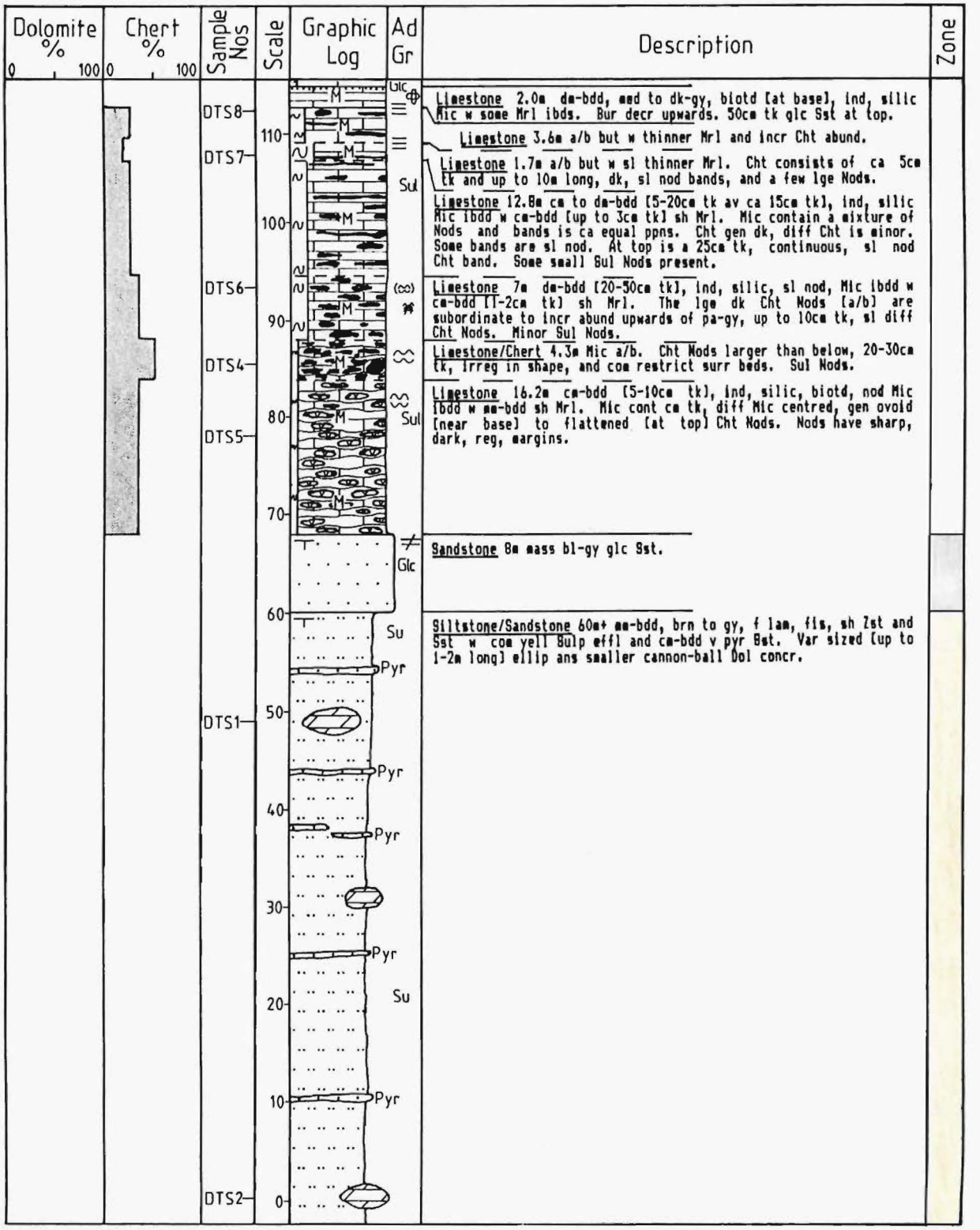

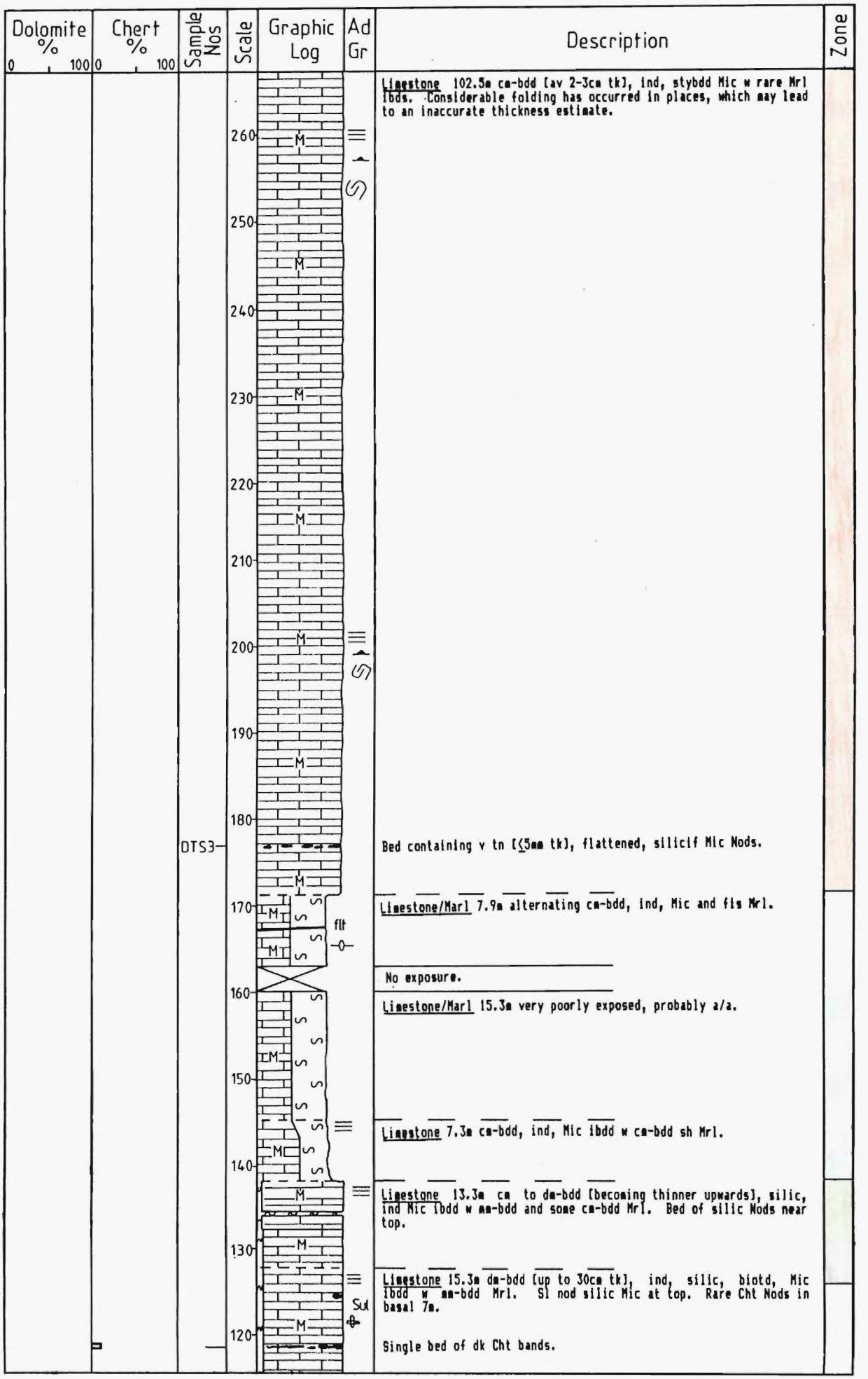
Dolomite %
0 100
Chert %
0 100
Sample Nos
Scale
Graphic Log
Ad Gr
Description
Zone
260
250
240
230
220
210
200
190
180
170
160
150
140
130
120
DTS3
flt
Sol
Limestone 102.5m cm-bdd (av 2-3cm tk), ind, stybdd Mic w rare Mrl lbds. Considerable folding has occurred in places, which may lead to an inaccurate thickness estimate.
Bed containing v tn (<5mm tk), flattened, silicif Mic Nods.
Limestone/Marl 7.9m alternating cm-bdd, ind, Mic and fis Mrl.
No exposure.
Limestone/Marl 15.3m very poorly exposed, probably a/a.
Limestone 7.3m cm-bdd, ind, Mic lbdd w cm-bdd sh Mrl.
Limestone 13.3m cm to dm-bdd (becoming thinner upwards), silic, ind Mic lbdd w mm-bdd and some cm-bdd Mrl. Bed of silic Nods near top.
Limestone 15.3m dm-bdd (up to 30cm tk), ind, silic, biotd, Mic lbdd w mm-bdd Mrl. Sl nod silic Mic at top. Rare Cht Nods in basal 7m.
Single bed of dk Cht bands.

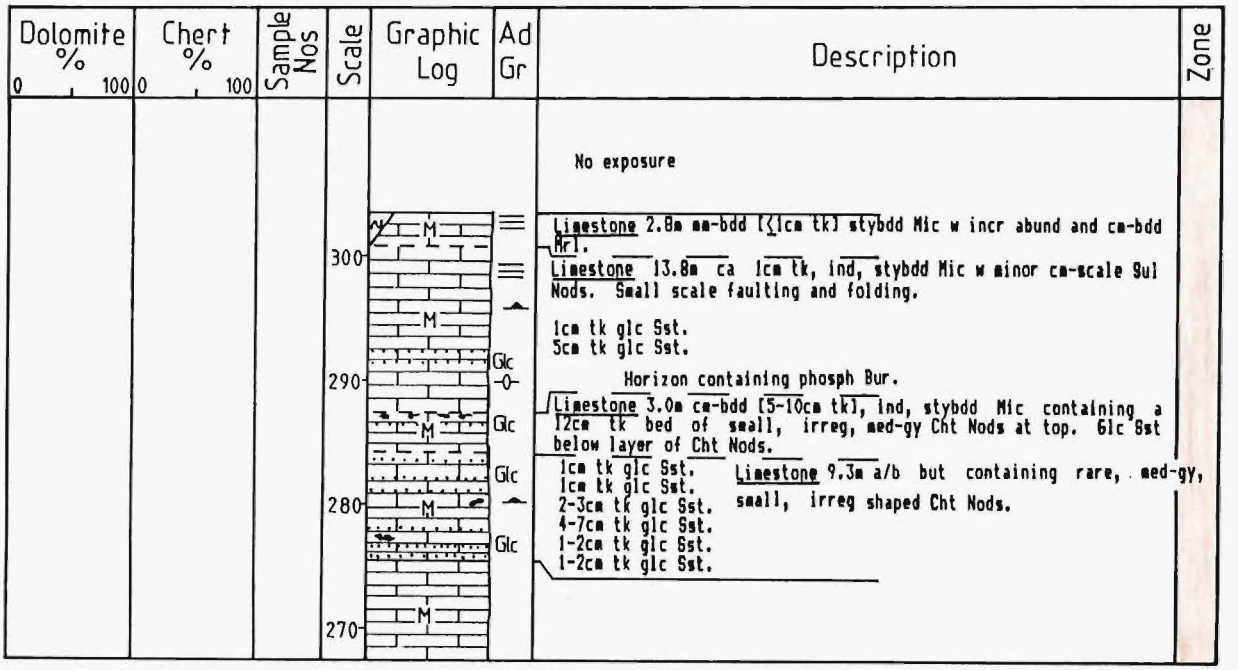

LOCALITY: Flaxbourne River Mouth (17).

GRID REFERENCES

Sheet Number: P29

Base of Section: 081285

Top of Section: 081285

DATE: 18/11/85

METHOD OF MEASUREMENT: Tape and compass survey.

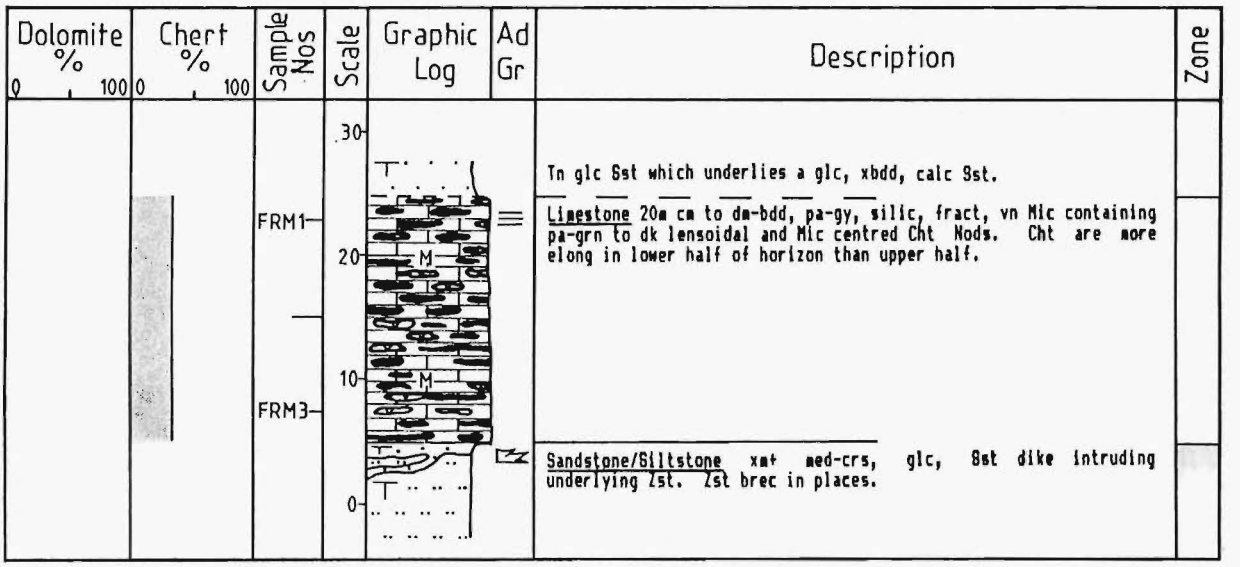

LOCALITY: Isolation Creek (20), Chalk Range – Waima River area.

GRID REFERENCES

Sheet Number: P29

Base of Section: 918229

Top of Section: 918232

DATE: 2/2/85
6/5/85

METHOD OF MEASUREMENT: Tape and compass survey, visual estimate of lower sandstone.

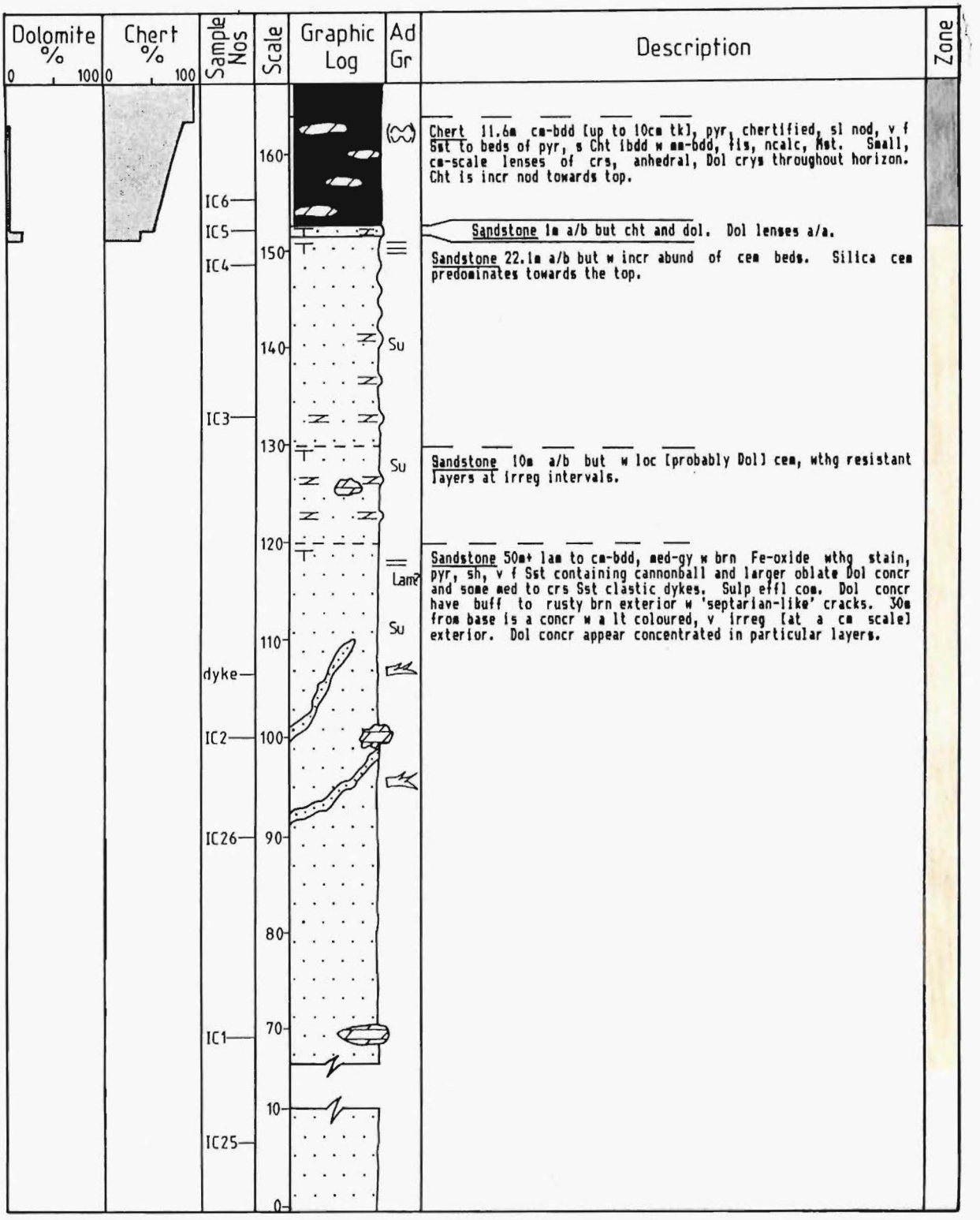

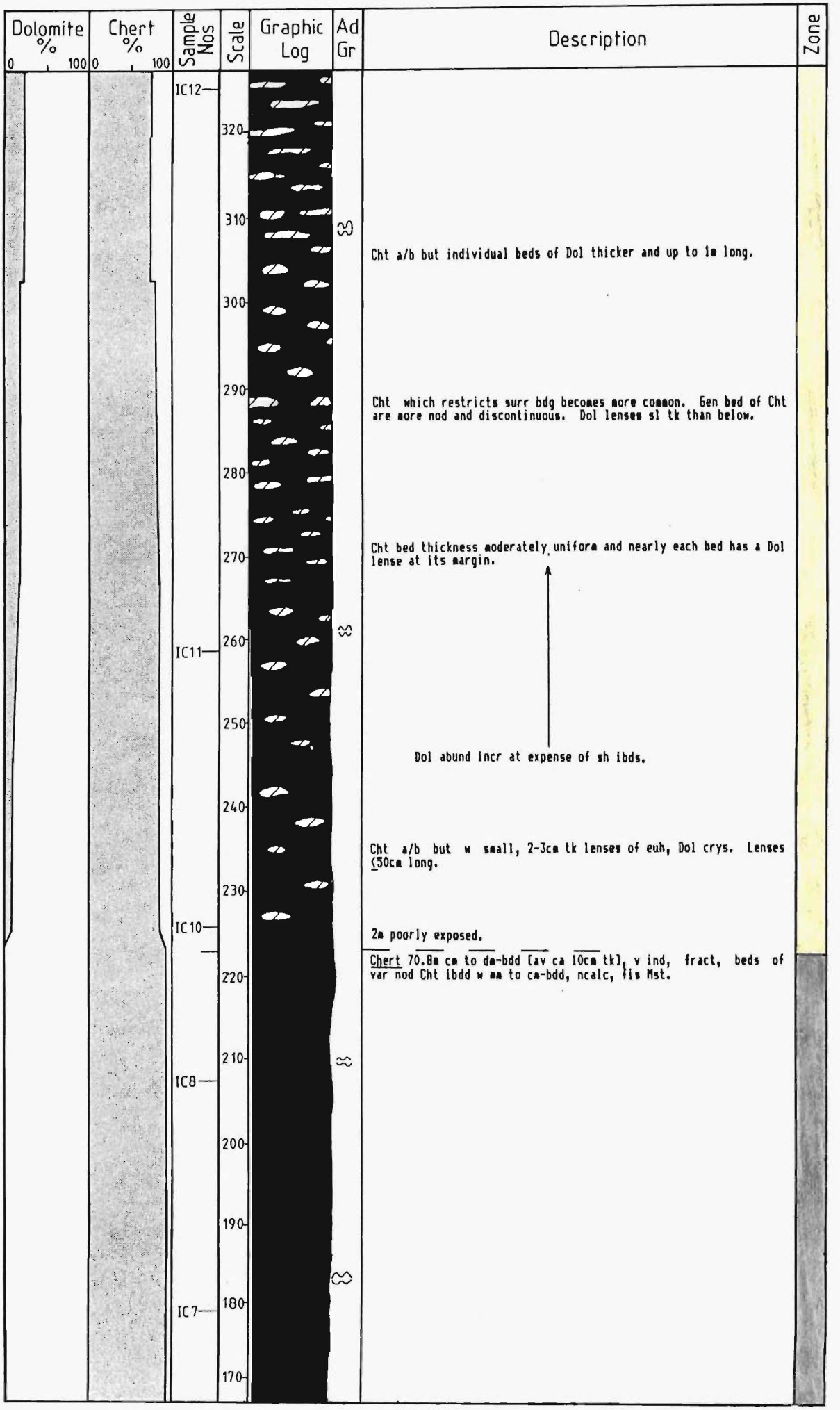
Dolomite %
0
100
Chert %
0
100
Sample Nos
IC12
IC11
IC10
IC8
IC7
Scale
320
310
300
290
280
270
260
250
240
230
220
210
200
190
180
170
Graphic Log
Ad Gr
Description
Cht a/b but individual beds of Dol thicker and up to 1m long.
Cht which restricts surr bdg becomes more common. Gen bed of Cht are more nod and discontinuous. Dol lenses sl tk than below.
Cht bed thickness moderately uniform and nearly each bed has a Dol lense at its margin.
Dol abund incr at expense of sh ibds.
Cht a/b but w small, 2-3cm tk lenses of euh, Dol crys. Lenses ≤50cm long.
2m poorly exposed.
Chert 70.8m cm to dm-bdd [av ca 10cm tk], v ind, fract, beds of var nod Cht ibdd w mm to cm-bdd, ncalc, fis Mst.
Zone

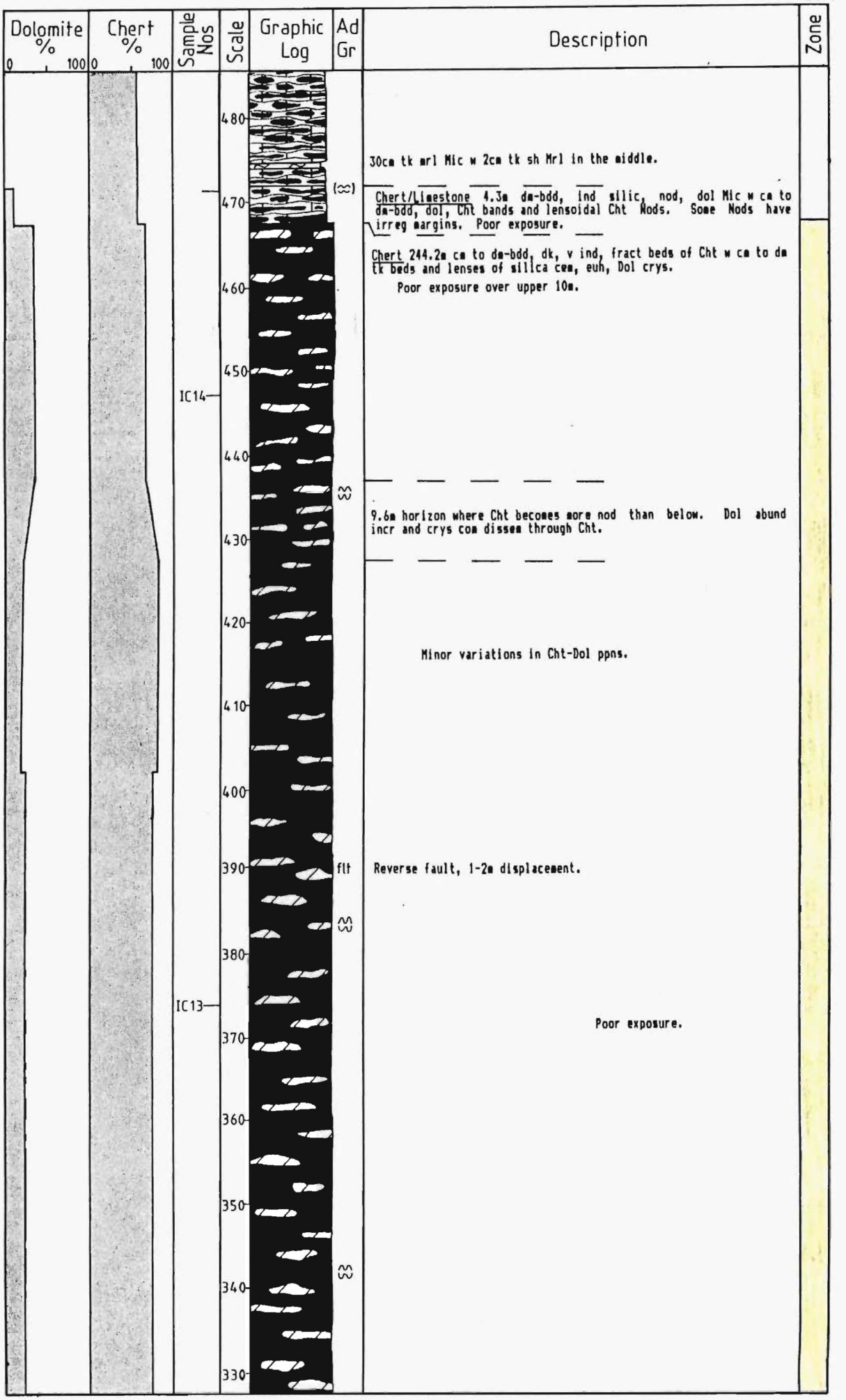
Dolomite %
0
100
Chert %
0
100
Sample Nos
Scale
Graphic Log
Ad Gr
Description
Zone
480
470
460
450
440
430
420
410
400
390
380
370
360
350
340
330
IC14
IC13
30cm tk mrl Mic w 2cm tk sh Mrl in the middle.
Chert/Limestone 4.3m dm-bdd, ind silic, nod, dol Mic w cm to dm-bdd, dol, Cht bands and lensoidal Cht Nods. Some Nods have irreg margins. Poor exposure.
Chert 244.2m cm to dm-bdd, dk, v ind, fract beds of Cht w cm to dm tk beds and lenses of silica cem, euh, Dol crys.
Poor exposure over upper 10m.
9.6m horizon where Cht becomes more nod than below. Dol abund incr and crys com dissem through Cht.
Minor variations in Cht-Dol ppns.
flt
Reverse fault, 1-2m displacement.
Poor exposure.

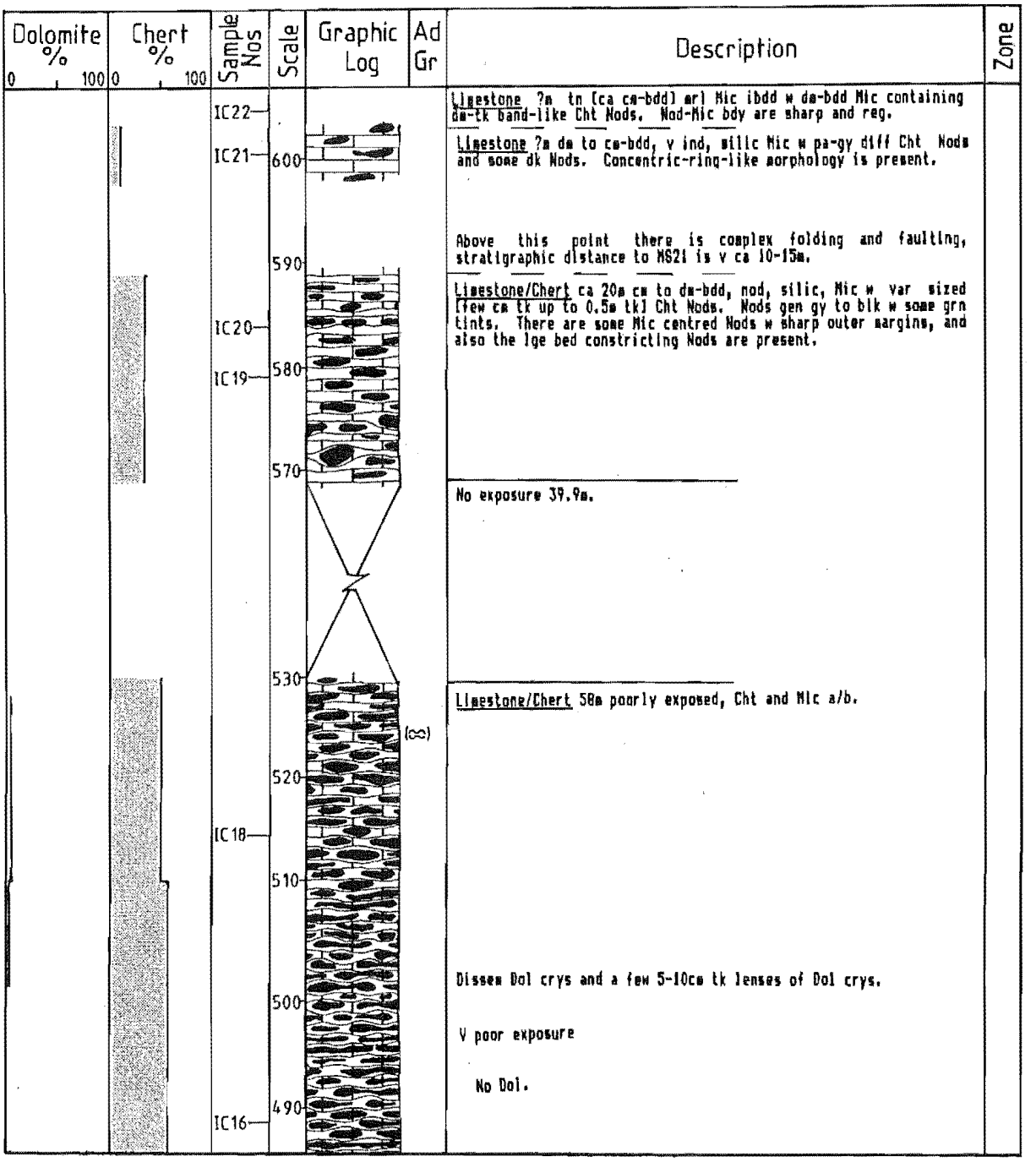
Dolomite %
0 100
Chert %
0 100
Sample Nos
Scale
Graphic Log
Ad Gr
Description
Zone
IC22
IC21
IC20
IC19
IC18
IC16
600
590
580
570
530
520
510
500
490
(∞)
Limestone ?m tn (ca cm-bdd) mr) Mic ibdd w dm-bdd Mic containing dm-tk band-like Cht Nods. Nod-Mic bdy are sharp and reg.
Limestone ?m dm to cm-bdd, v ind, silic Mic w pa-gy diff Cht Nods and some dk Nods. Concentric-ring-like morphology is present.
Above this point there is complex folding and faulting, stratigraphic distance to NS21 is v ca 10-15m.
Limestone/Chert ca 20m cm to dm-bdd, nod, silic, Mic w var sized (few cm tk up to 0.5m tk) Cht Nods. Nods gen gy to blk w some grn tints. There are some Mic centred Nods w sharp outer margins, and also the lge bed constricting Nods are present.
No exposure 39.9m.
Limestone/Chert 58m poorly exposed, Cht and Mic a/b.
Dissem Dol crys and a few 5-10cm tk lenses of Dol crys.
V poor exposure
No Dol.

LOCALITY: Lab Rocks (4), Kaikoura Peninsula.

GRID REFERENCES

Sheet Number: 031

Base of Section: 675656

Top of Section: 683656

DATE: 11/4/84
5/4/85

METHOD OF MEASUREMENT: Tape and compass survey, estimate of folded lithologies.

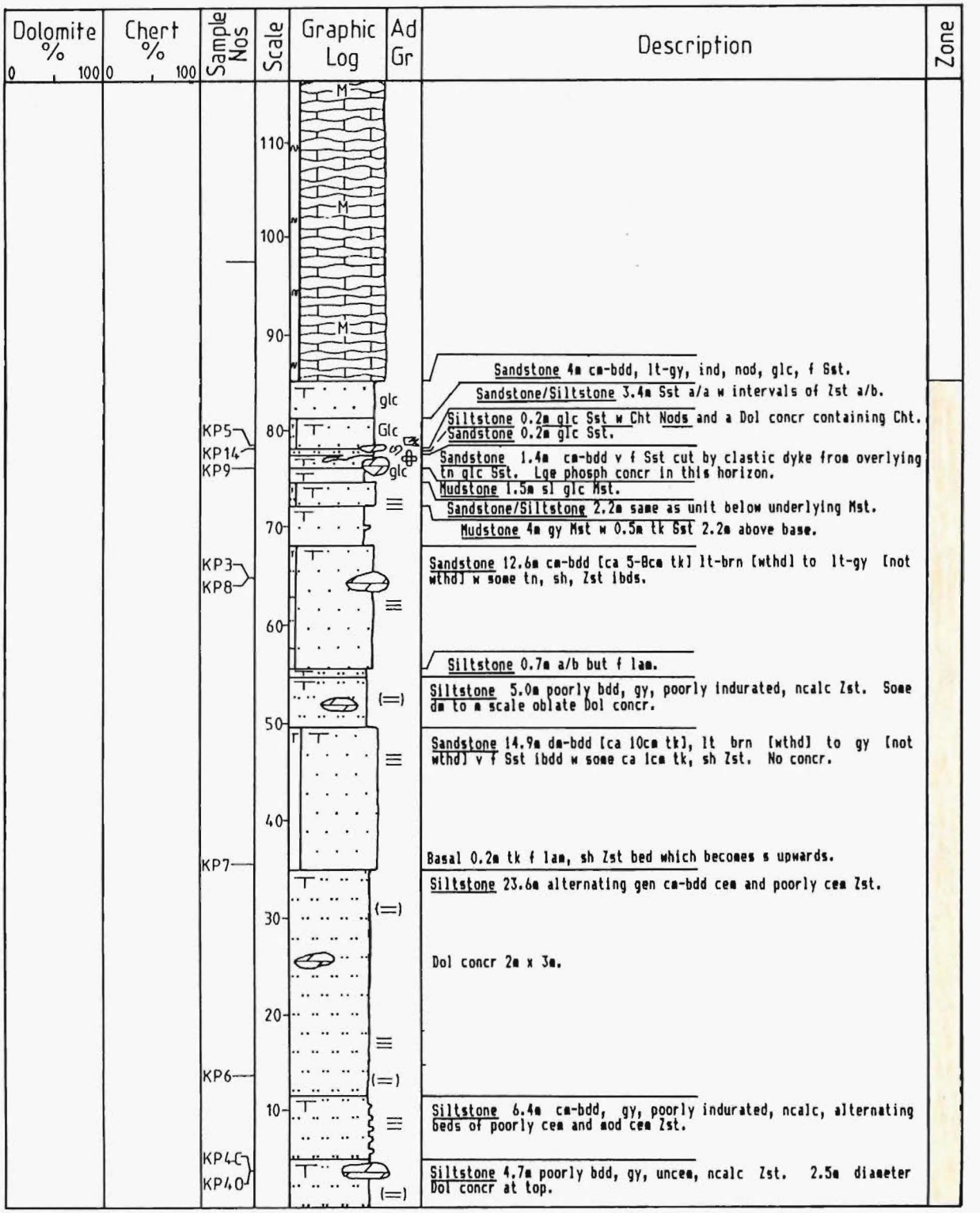

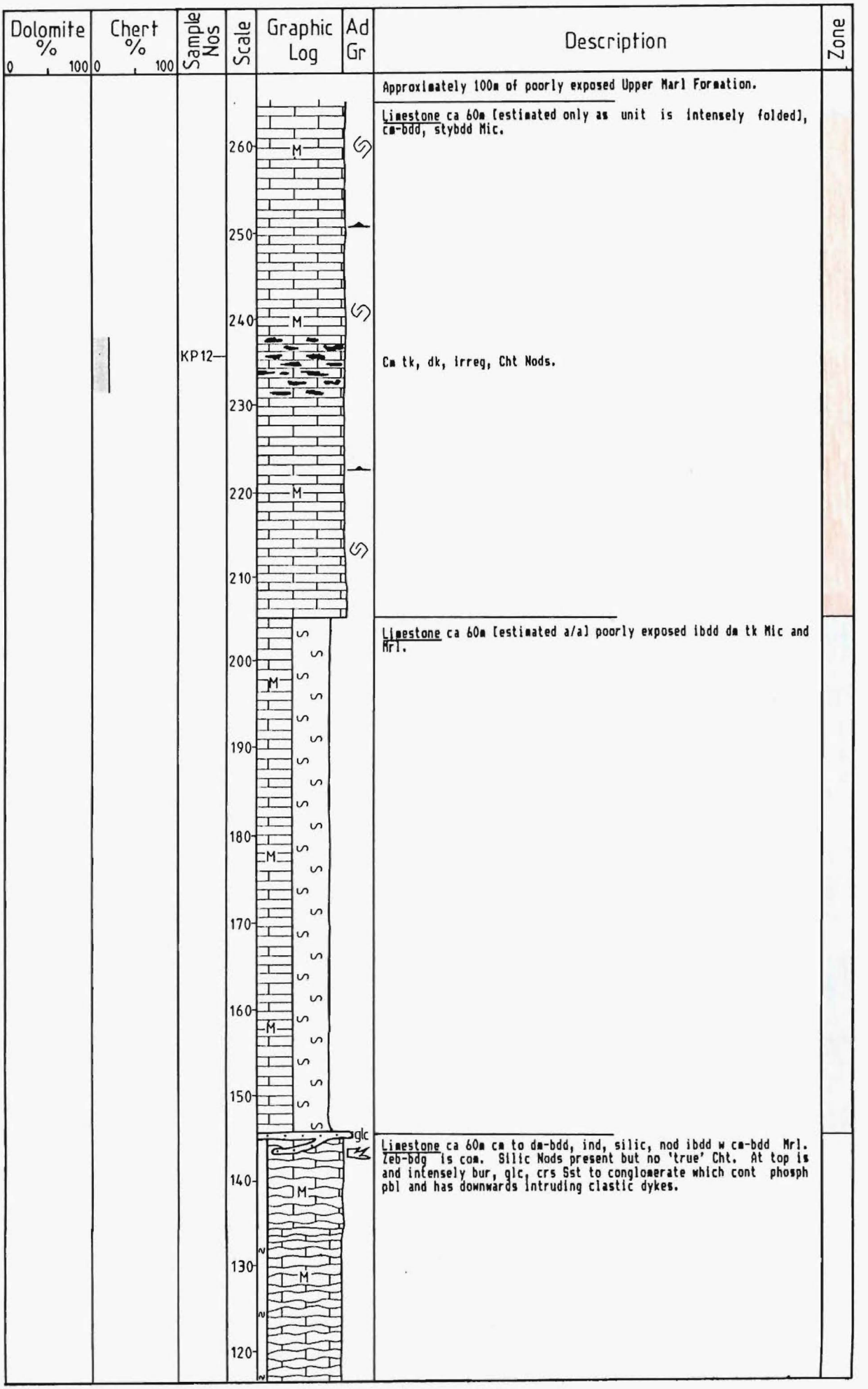
Dolomite %
0 100
Chert %
0 100
Sample Nos
Scale
Graphic Log
Ad Gr
Description
Zone
Approximately 100m of poorly exposed Upper Marl Formation.
Limestone ca 60m (estimated only as unit is intensely folded), cm-bdd, stybdd Mic.
KP12
Cm tk, dk, irreg, Cht Nods.
Limestone ca 60m (estimated a/a) poorly exposed ibdd dm tk Mic and Mrl.
glc
Limestone ca 60m cm to dm-bdd, ind, silic, nod ibdd w cm-bdd Mrl. Zeb-bdg is com. Silic Nods present but no 'true' Cht. At top is and intensely bur, glc, crs Sst to conglomerate which cont phosph pbl and has downwards intruding clastic dykes.
260
250
240
230
220
210
200
190
180
170
160
150
140
130
120
M
S

LOCALITY: South Bay (3), Kaikoura Peninsula.

GRID REFERENCES

Sheet Number: 031
Base of Section: 661647
Top of Section: 665644

DATE: 19/4/84
5/4/85

METHOD OF MEASUREMENT: Tape and compass survey, estimate of folded lithologies.

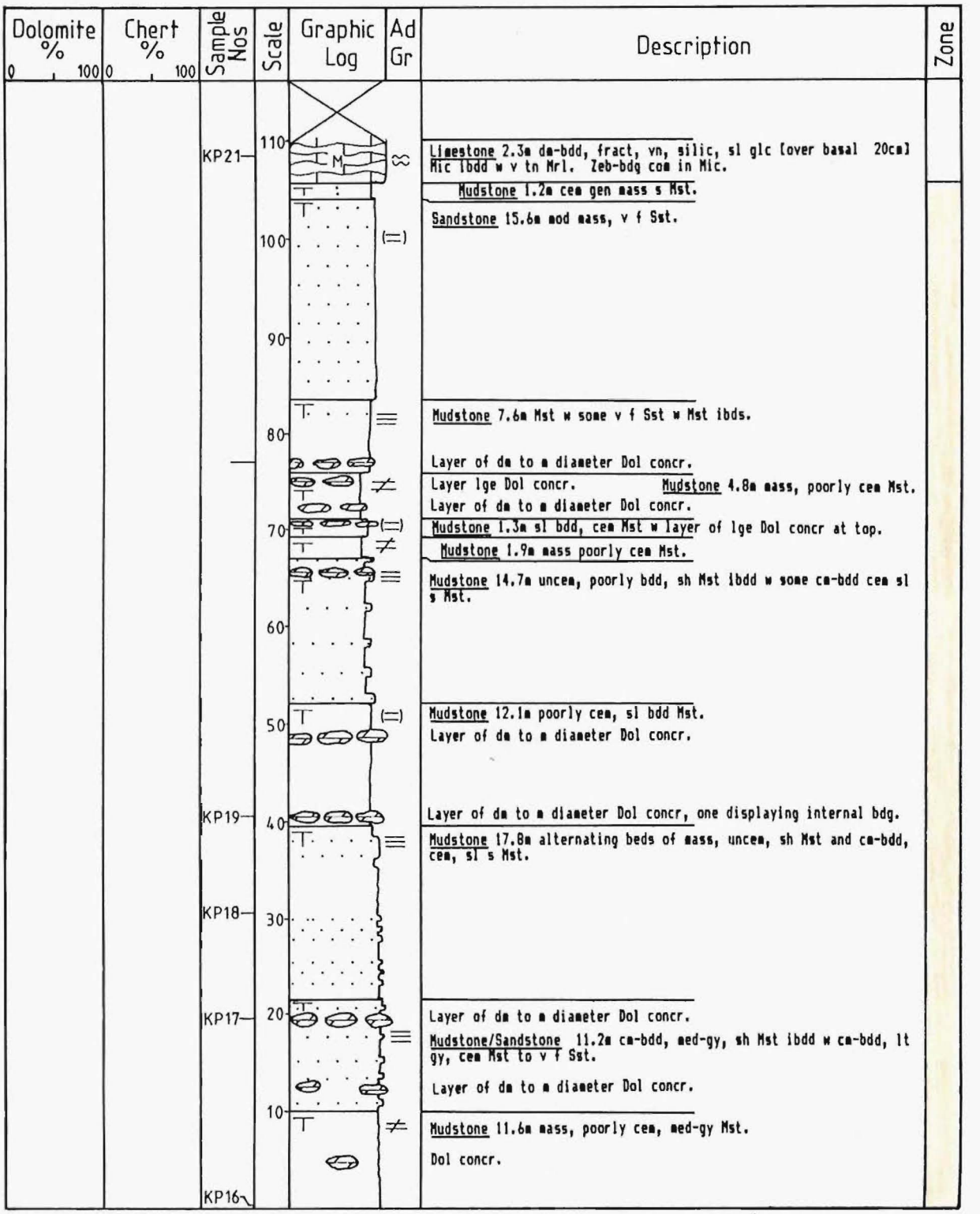

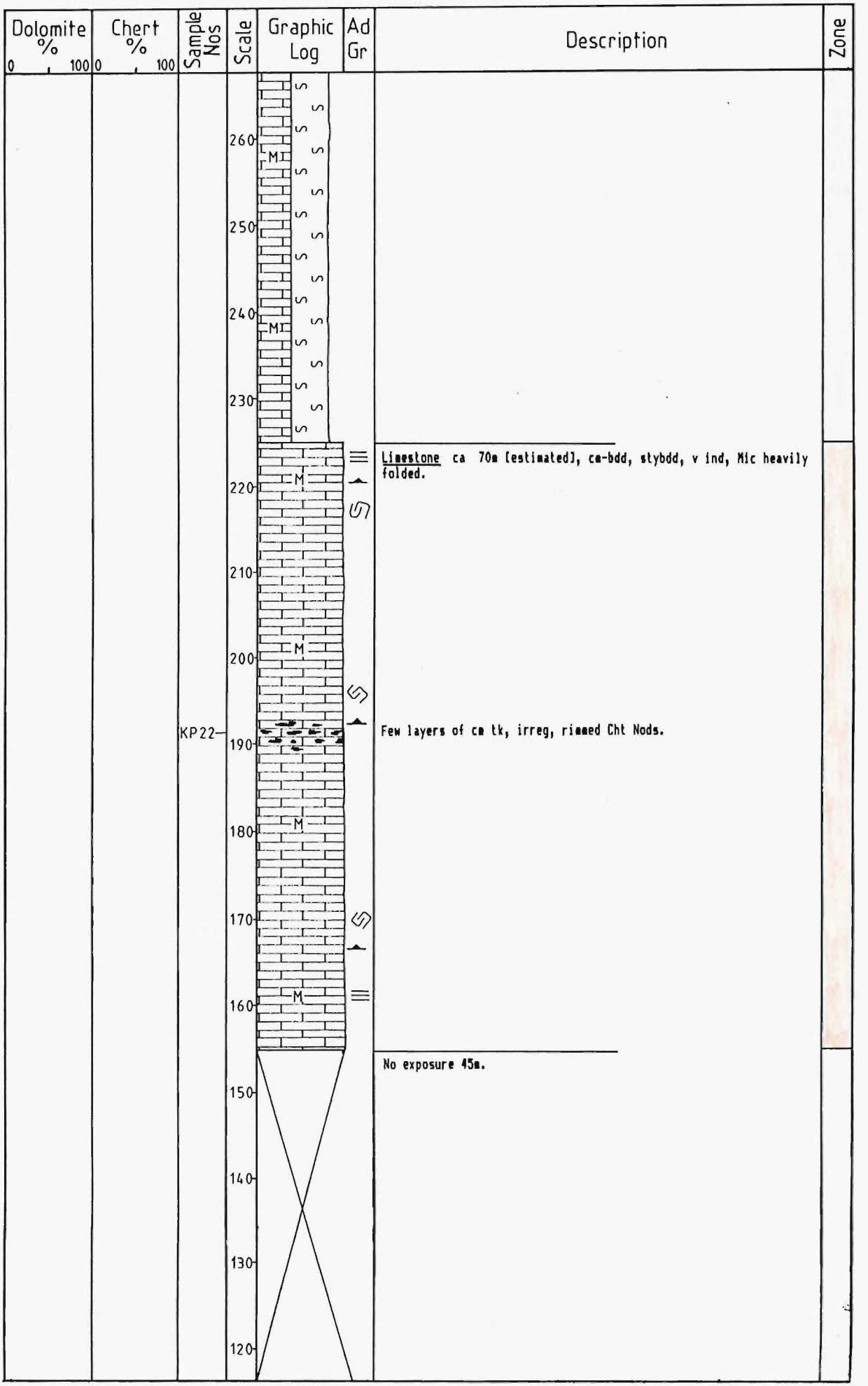
Dolomite %
0 100
Chert %
0 100
Sample Nos
Scale
Graphic Log
Ad Gr
Description
Zone
260
250
240
230
220
210
200
190
180
170
160
150
140
130
120
KP22
Limestone ca 70m (estimated), cm-bdd, stybdd, v ind, Mic heavily folded.
Few layers of cm tk, irreg, rimmed Cht Nods.
No exposure 45m.

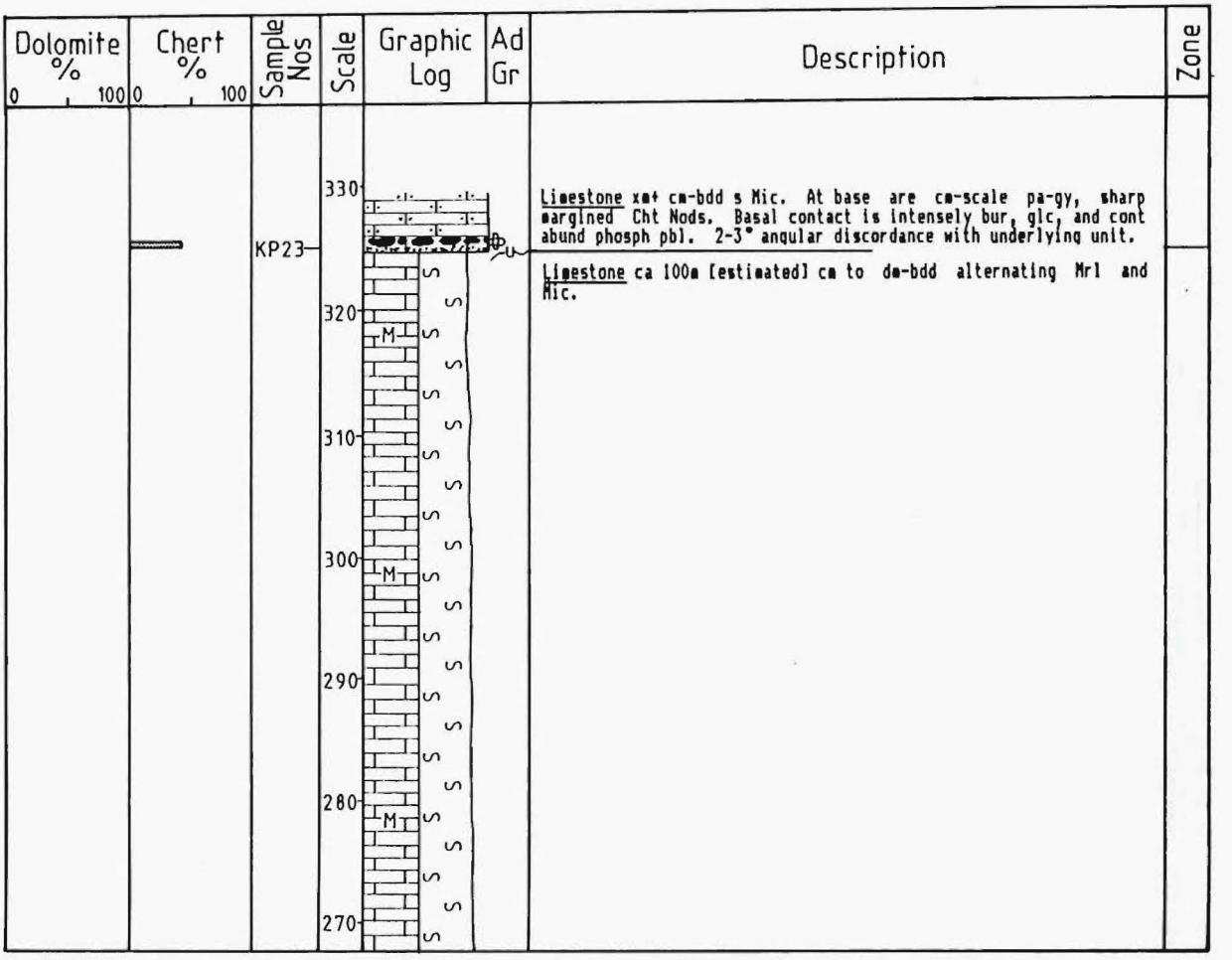
Dolomite %
0
100
Chert %
0
100
Sample Nos
Scale
Graphic Log
Ad Gr
Description
Zone
330
320
310
300
290
280
270
KP23
M
M
M
S
Limestone xmt cm-bdd s Mic. At base are cm-scale pa-gy, sharp margined Cht Nods. Basal contact is intensely bur, glc, and cont abund phosph pbl. 2-3° angular discordance with underlying unit.
Limestone ca 100m [estimated] cm to dm-bdd alternating Mrl and Mic.

LOCALITY: Limburn Steam (26), Clarence Valley.

GRID REFERENCES

Sheet Number: P30

Base of Section: 744140

Top of Section: 744142

DATE: 21/10/84

METHOD OF MEASUREMENT: Tape and compass survey.

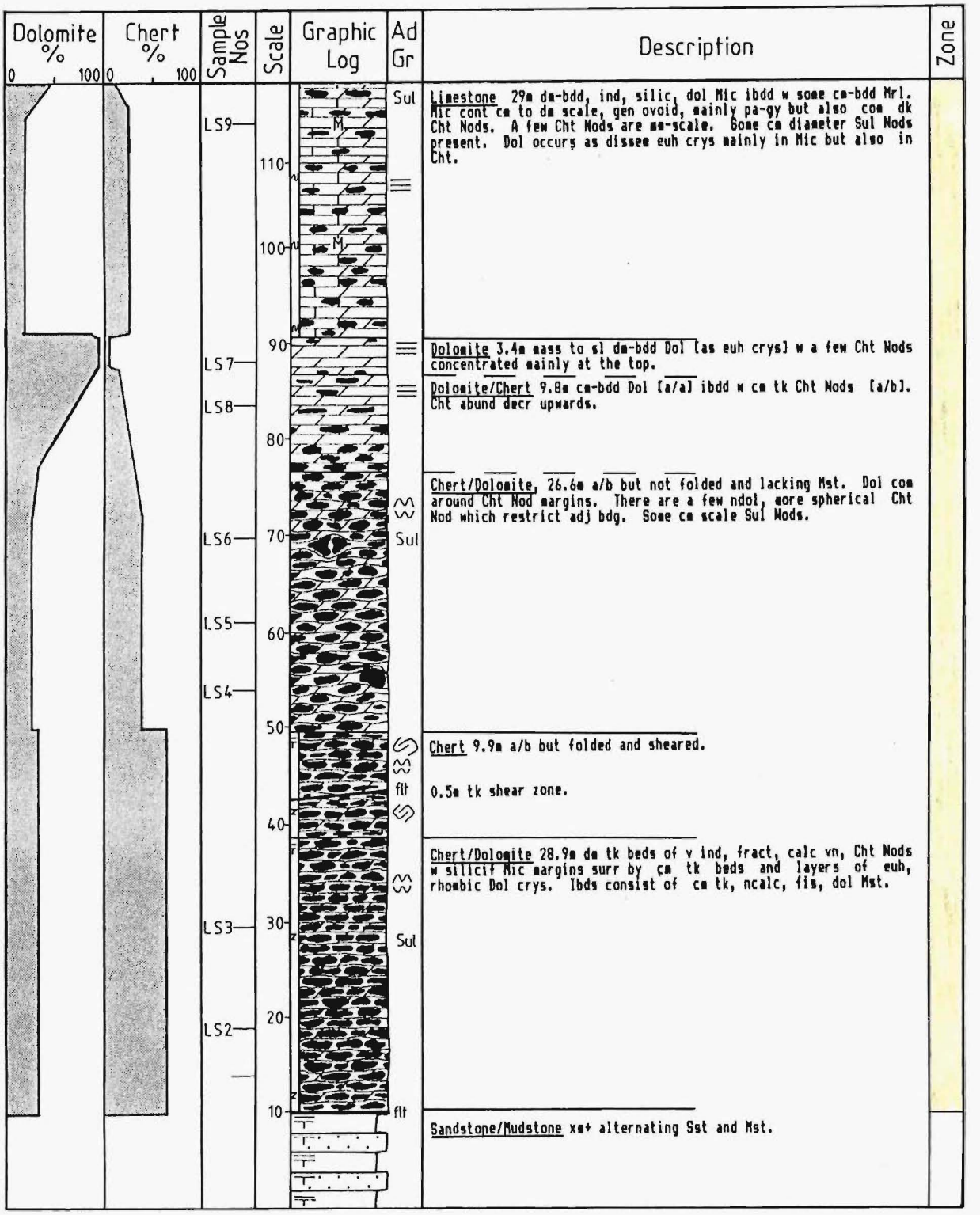

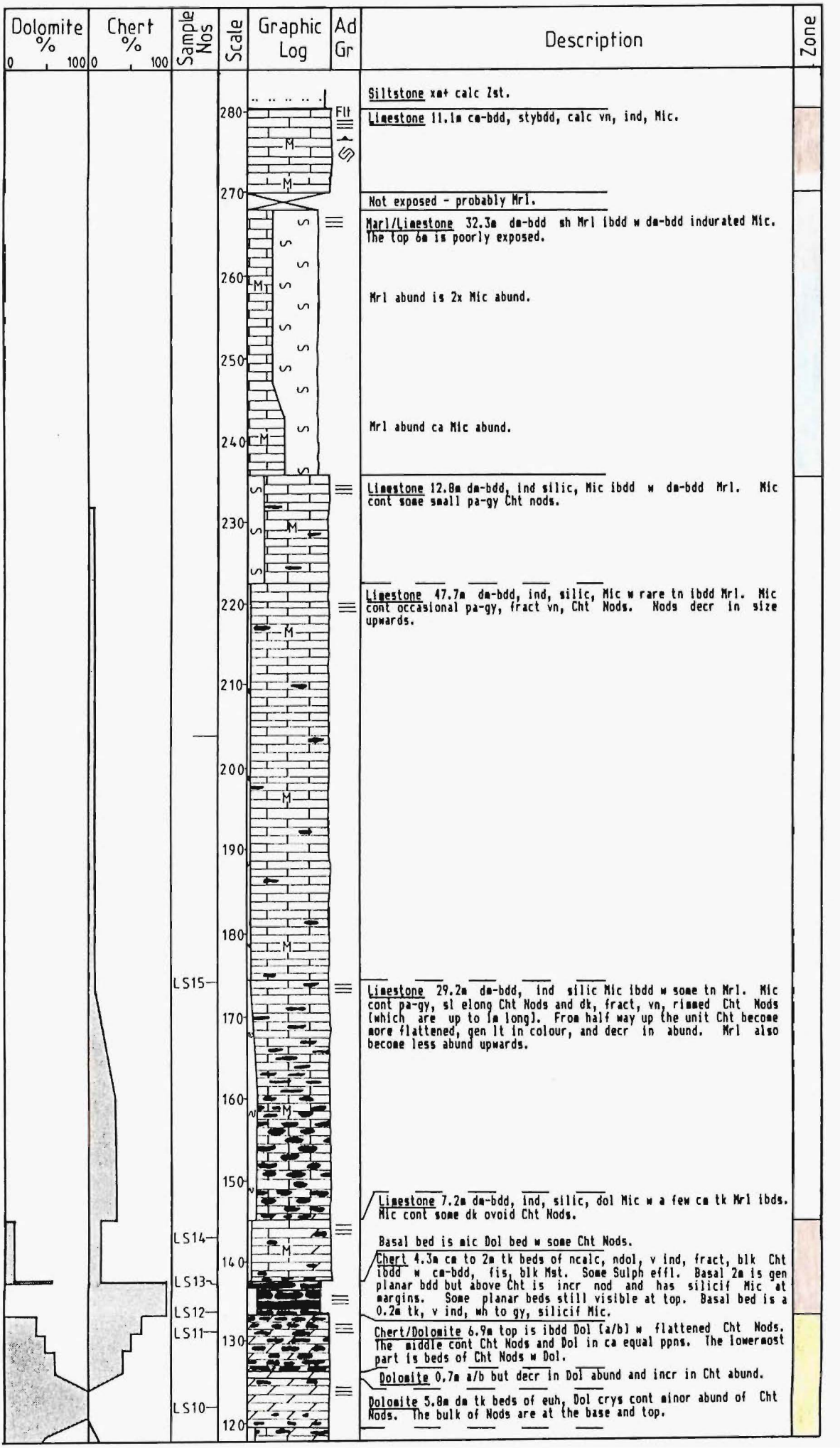
Dolomite %
0 100
Chert %
0 100
Sample Nos
Scale
Graphic Log
Ad Gr
Description
Zone
Siltstone xmt calc lst.
Limestone 11.1m cm-bdd, stybdd, calc vn, ind, Mic.
Not exposed - probably Mrl.
Marl/Limestone 32.3m dm-bdd sh Mrl ibdd w dm-bdd indurated Mic. The top 6m is poorly exposed.
Mrl abund is 2x Mic abund.
Mrl abund ca Mic abund.
Limestone 12.8m dm-bdd, ind silic, Mic ibdd w dm-bdd Mrl. Mic cont some small pa-gy Cht nods.
Limestone 47.7m dm-bdd, ind, silic, Mic w rare tn ibdd Mrl. Mic cont occasional pa-gy, fract vn, Cht Nods. Nods decr in size upwards.
Limestone 29.2m dm-bdd, ind silic Mic ibdd w some tn Mrl. Mic cont pa-gy, sl elong Cht Nods and dk, fract, vn, rimmed Cht Nods (which are up to 1m long). From half way up the unit Cht become more flattened, gen lt in colour, and decr in abund. Mrl also become less abund upwards.
Limestone 7.2m dm-bdd, ind, silic, dol Mic w a few cm tk Mrl ibds. Mic cont some dk ovoid Cht Nods.
Basal bed is mic Dol bed w some Cht Nods.
Chert 4.3m cm to 2m tk beds of ncalc, ndol, v ind, fract, blk Cht ibdd w cm-bdd, fis, blk Mst. Some Sulph effl. Basal 2m is gen planar bdd but above Cht is incr nod and has silicif Mic at margins. Some planar beds still visible at top. Basal bed is a 0.2m tk, v ind, wh to gy, silicif Mic.
Chert/Dolomite 6.9m top is ibdd Dol (a/b) w flattened Cht Nods. The middle cont Cht Nods and Dol in ca equal ppns. The lowermost part is beds of Cht Nods w Dol.
Dolomite 0.7m a/b but decr in Dol abund and incr in Cht abund.
Dolomite 5.8m dm tk beds of euh, Dol crys cont minor abund of Cht Nods. The bulk of Nods are at the base and top.
LS15
LS14
LS13
LS12
LS11
LS10

LOCALITY: Mt Alexander - eastern limb of Puhi Puhi Syncline (8).

GRID REFERENCES

DATE: 4/4/84

Sheet Number: P31

Base of Section: 754883

Top of Section: 751884

METHOD OF MEASUREMENT: Tape and compass survey, visual estimate of uppermost 80 m.

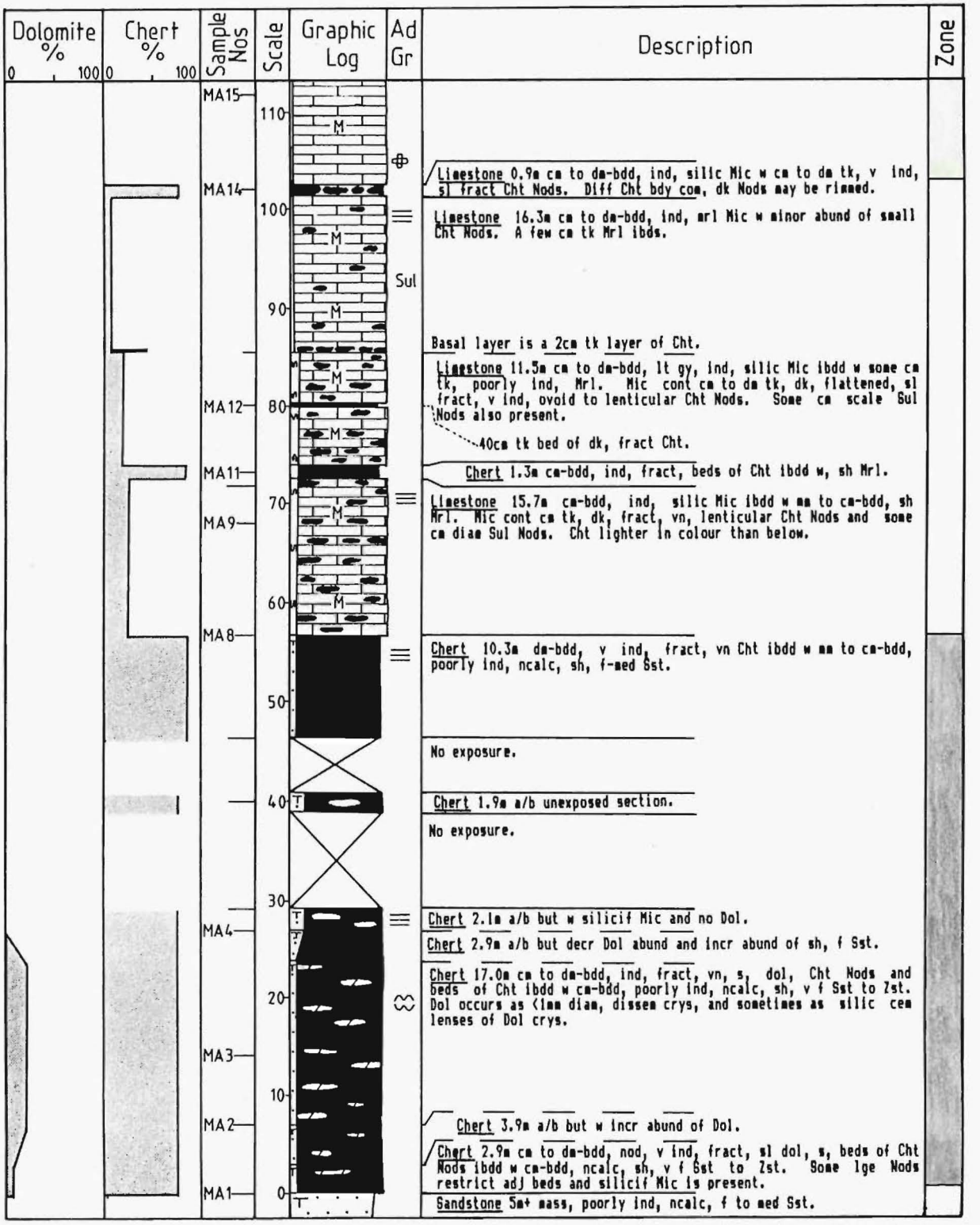

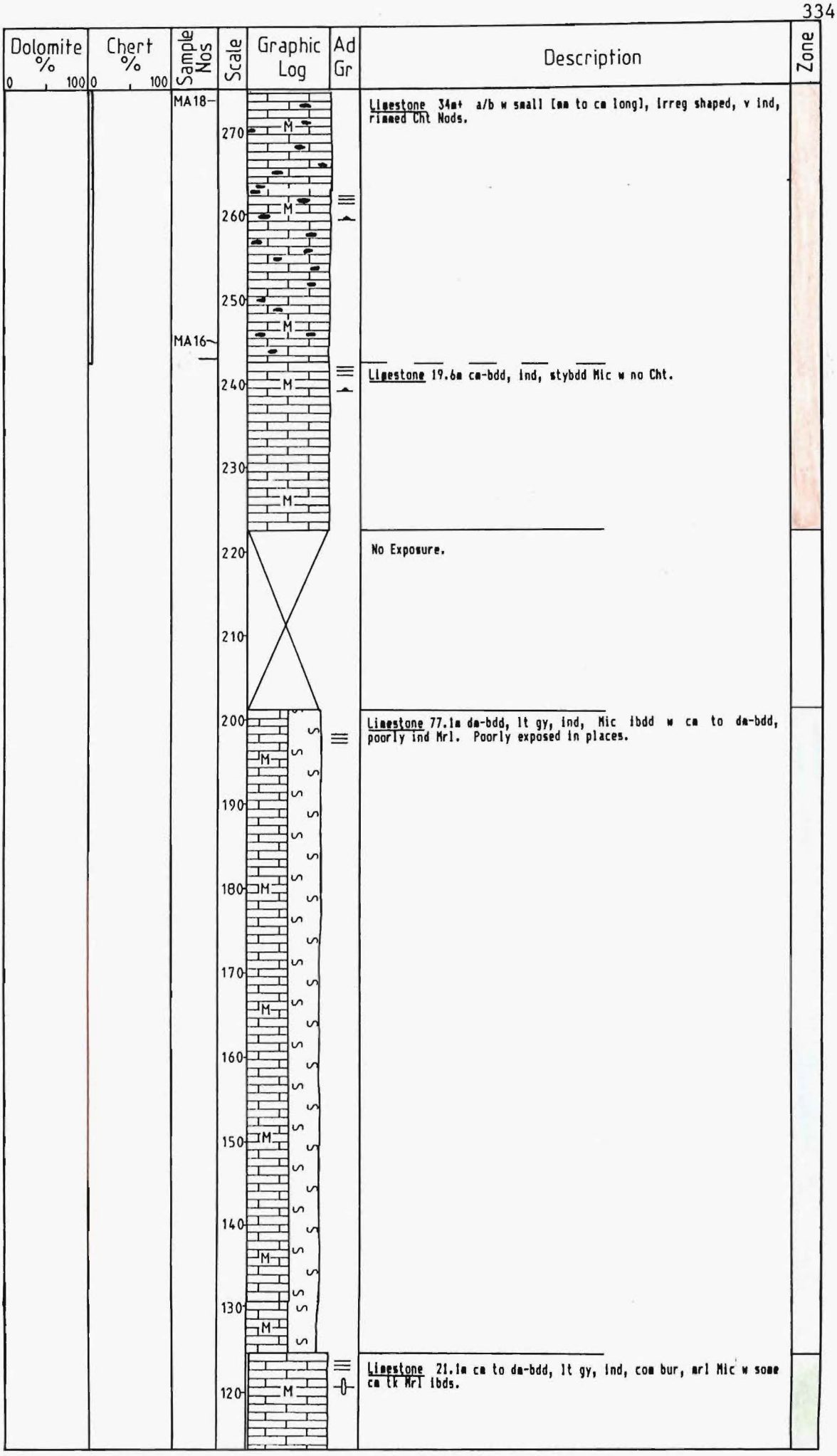
Dolomite %
0 100
Chert %
0 100
Sample Nos
MA18
MA16
Scale
270
260
250
240
230
220
210
200
190
180
170
160
150
140
130
120
Graphic Log
Ad Gr
Description
Zone
Limestone 34m+ a/b w small [mm to cm long], irreg shaped, v ind, rimmed Cht Nods.
Limestone 19.6m cm-bdd, ind, stybdd Mic w no Cht.
No Exposure.
Limestone 77.1m dm-bdd, lt gy, ind, Mic ibdd w cm to dm-bdd, poorly ind Mrl. Poorly exposed in places.
Limestone 21.1m cm to dm-bdd, lt gy, ind, com bur, arl Mic w some cm lk Mrl ibds.

LOCALITY: Mead Stream - main channel and middle tributary (24), Clarence Valley.

GRID REFERENCES

Sheet Number: P30

Base of Section: 765163

Top of Section: 763164

DATE: 16-17/10/84

METHOD OF MEASUREMENT: Tape and compass survey.

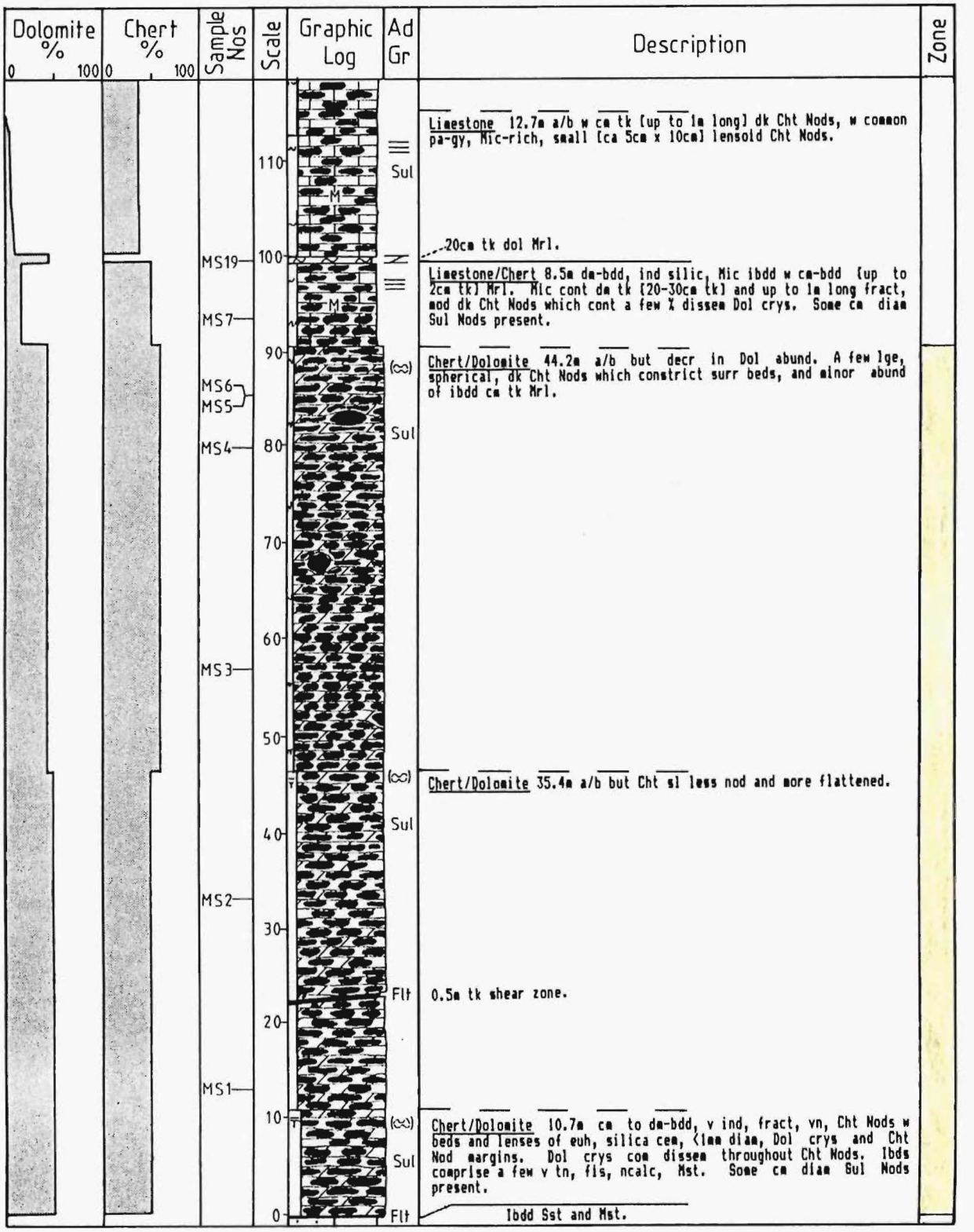

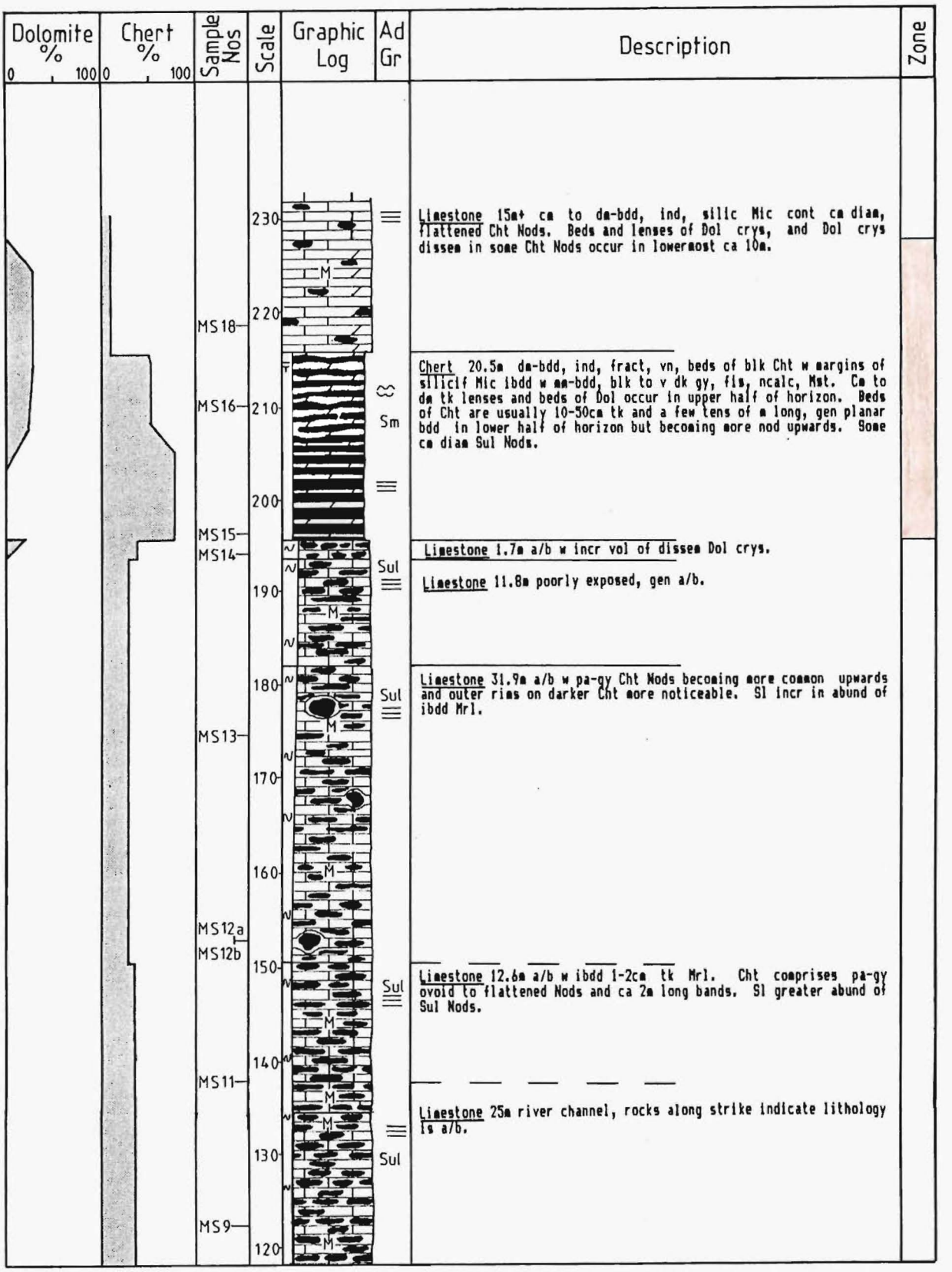
Dolomite %
0 100
Chert %
0 100
Sample Nos
Scale
Graphic Log
Ad Gr
Description
Zone
MS18
MS16
MS15
MS14
MS13
MS12a
MS12b
MS11
MS9
230
220
210
200
190
180
170
160
150
140
130
120
Sm
Sul
Sul
Sul
Sul
Limestone 15m+ cm to dm-bdd, ind, silic Mic cont cm diam, flattened Cht Nods. Beds and lenses of Dol crys, and Dol crys dissem in some Cht Nods occur in lowermost ca 10m.
Chert 20.5m dm-bdd, ind, fract, vn, beds of blk Cht w margins of silicif Mic ibdd w mm-bdd, blk to v dk gy, fis, ncalc, Mst. Cm to dm tk lenses and beds of Dol occur in upper half of horizon. Beds of Cht are usually 10-50cm tk and a few tens of m long, gen planar bdd in lower half of horizon but becoming more nod upwards. Some cm diam Sul Nods.
Limestone 1.7m a/b w incr vol of dissem Dol crys.
Limestone 11.8m poorly exposed, gen a/b.
Limestone 31.9m a/b w pa-gy Cht Nods becoming more common upwards and outer rims on darker Cht more noticeable. Sl incr in abund of ibdd Mrl.
Limestone 12.6m a/b w ibdd 1-2cm tk Mrl. Cht comprises pa-gy ovoid to flattened Nods and ca 2m long bands. Sl greater abund of Sul Nods.
Limestone 25m river channel, rocks along strike indicate lithology is a/b.

LOCALITY: Mead Stream - southern tributary (25), Clarence Valley.

GRID REFERENCES

Sheet Number: P30

Base of Section: 765163

Top of Section: 763164

DATE: 18-20/10/84

METHOD OF MEASUREMENT: Tape and compass survey.

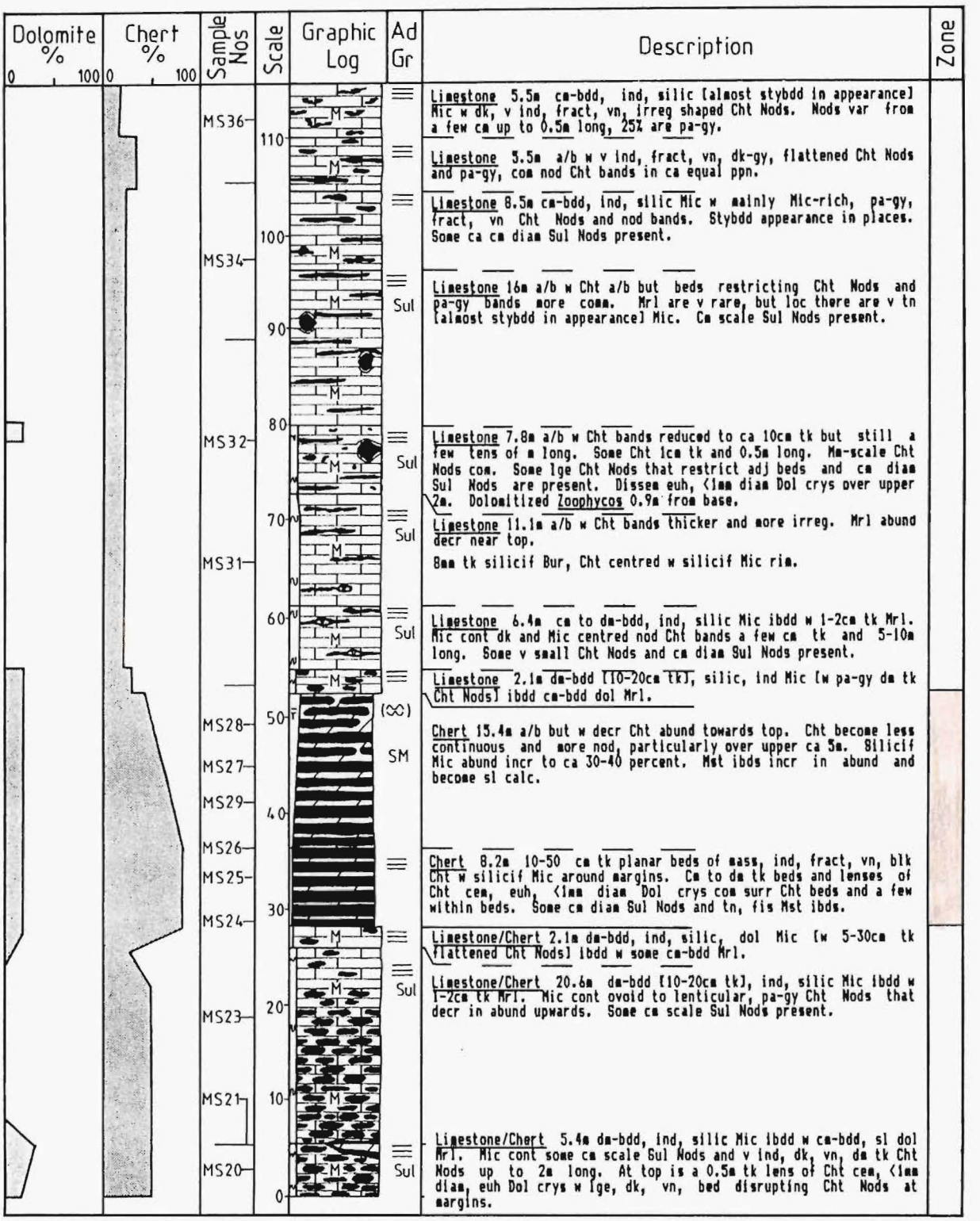

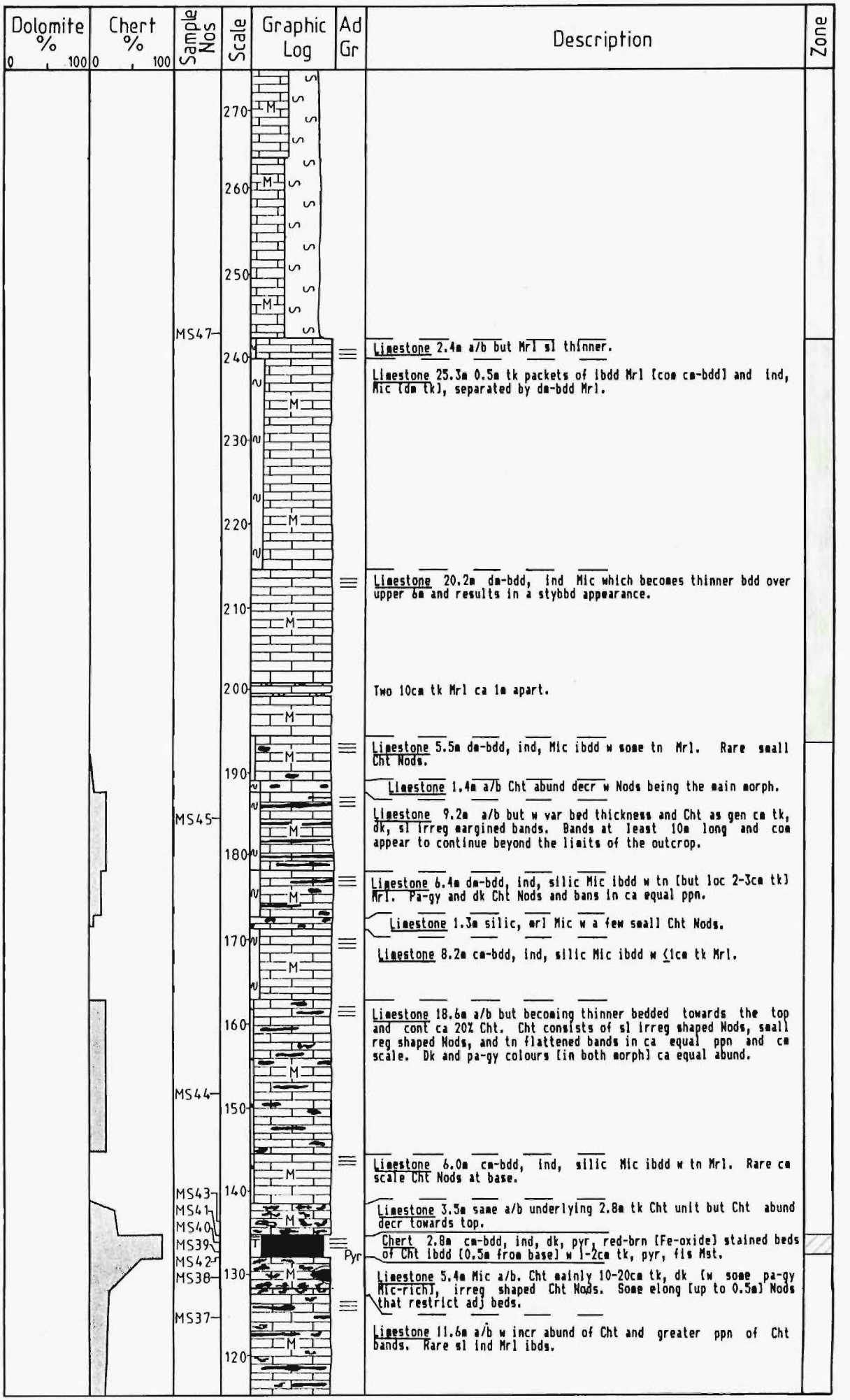
Dolomite %
0 100
Chert %
0 100
Sample Nos
Scale
Graphic Log
Ad Gr
Description
Zone
270
260
250
240
230
220
210
200
190
180
170
160
150
140
130
120
MS47
MS45
MS44
MS43
MS41
MS40
MS39
MS42
MS38
MS37
Pyr
Limestone 2.4m a/b but Mrl sl thinner.
Limestone 25.3m 0.5m tk packets of ibdd Mrl [com cm-bdd] and ind, Mic [dm tk], separated by dm-bdd Mrl.
Limestone 20.2m dm-bdd, ind Mic which becomes thinner bdd over upper 6m and results in a stybbd appearance.
Two 10cm tk Mrl ca 1m apart.
Limestone 5.5m dm-bdd, ind, Mic ibdd w some tn Mrl. Rare small Cht Nods.
Limestone 1.4m a/b Cht abund decr w Nods being the main morph.
Limestone 9.2m a/b but w var bed thickness and Cht as gen cm tk, dk, sl irreg margined bands. Bands at least 10m long and com appear to continue beyond the limits of the outcrop.
Limestone 6.4m dm-bdd, ind, silic Mic ibdd w tn [but loc 2-3cm tk] Mrl. Pa-gy and dk Cht Nods and bans in ca equal ppn.
Limestone 1.3m silic, mrl Mic w a few small Cht Nods.
Limestone 8.2m cm-bdd, ind, silic Mic ibdd w <1cm tk Mrl.
Limestone 18.6m a/b but becoming thinner bedded towards the top and cont ca 20% Cht. Cht consists of sl irreg shaped Nods, small reg shaped Nods, and tn flattened bands in ca equal ppn and cm scale. Dk and pa-gy colours [in both morph] ca equal abund.
Limestone 6.0m cm-bdd, ind, silic Mic ibdd w tn Mrl. Rare cm scale Cht Nods at base.
Limestone 3.5m same a/b underlying 2.8m tk Cht unit but Cht abund decr towards top.
Chert 2.8m cm-bdd, ind, dk, pyr, red-brn [Fe-oxide] stained beds of Cht ibdd [0.5m from base] w 1-2cm tk, pyr, fis Mst.
Limestone 5.4m Mic a/b. Cht mainly 10-20cm tk, dk [w some pa-gy Mic-rich], irreg shaped Cht Nods. Some elong [up to 0.5m] Nods that restrict adj beds.
Limestone 11.6m a/b w incr abund of Cht and greater ppn of Cht bands. Rare sl ind Mrl ibds.

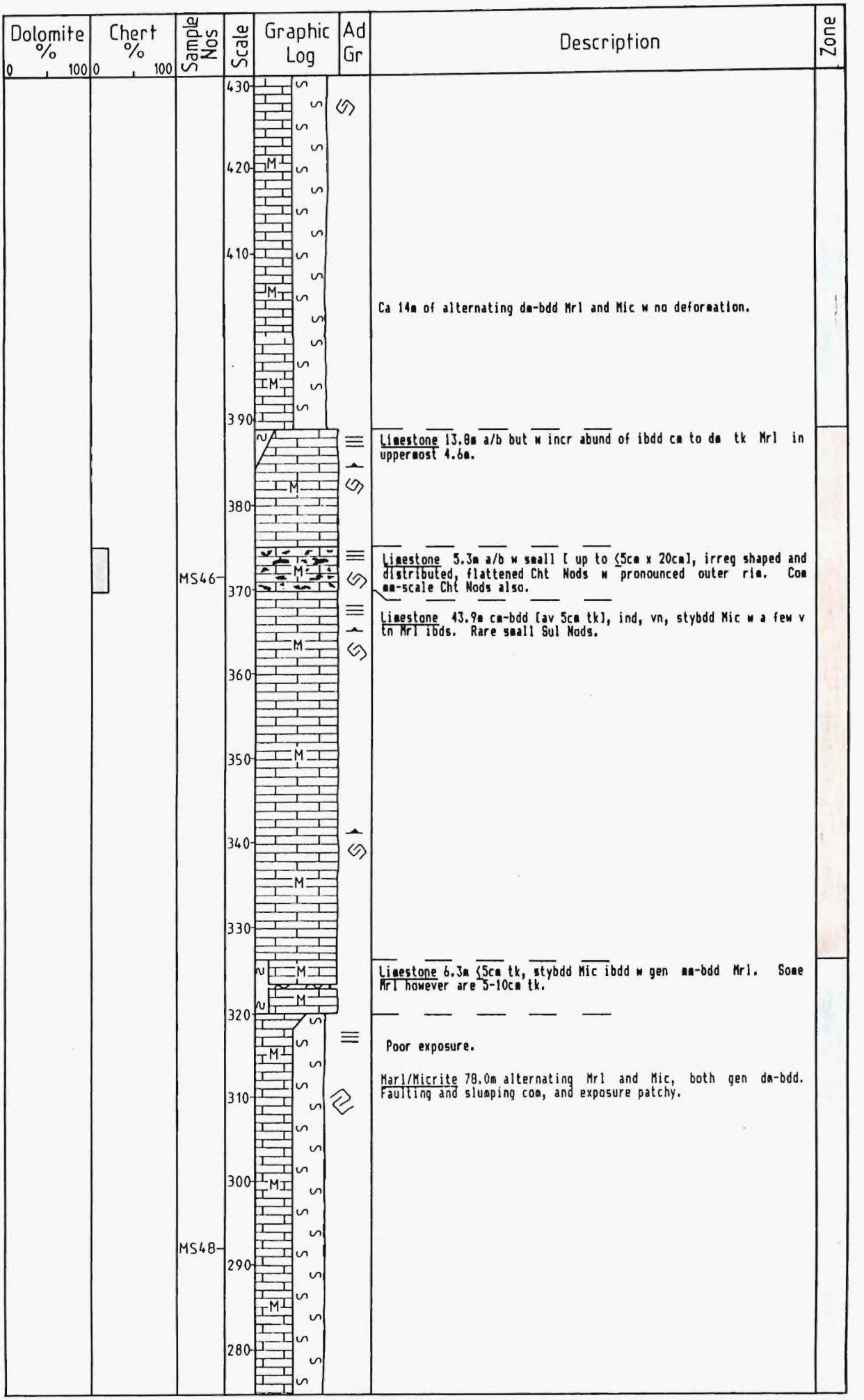
Dolomite %
0 100
Chert %
0 100
Sample Nos
Scale
Graphic Log
Ad Gr
Description
Zone
430
420
410
390
380
370
360
350
340
330
320
310
300
290
280
MS46
MS48
M
Ca 14m of alternating dm-bdd Mrl and Mic w no deformation.
Limestone 13.8m a/b but w incr abund of ibdd cm to dm tk Mrl in uppermost 4.6m.
Limestone 5.3m a/b w small [up to <5cm x 20cm], irreg shaped and distributed, flattened Cht Nods w pronounced outer rim. Com mm-scale Cht Nods also.
Limestone 43.9m cm-bdd [av 5cm tk], ind, vn, stybdd Mic w a few v tn Mrl ibds. Rare small Sul Nods.
Limestone 6.3m <5cm tk, stybdd Mic ibdd w gen mm-bdd Mrl. Some Mrl however are 5-10cm tk.
Poor exposure.
Marl/Micrite 78.0m alternating Mrl and Mic, both gen dm-bdd. Faulting and slumping com, and exposure patchy.

Dolomite % 0 – 100	Chert % 0 – 100	Sample Nos	Scale	Graphic Log	Ad Gr	Description	Zone
			500	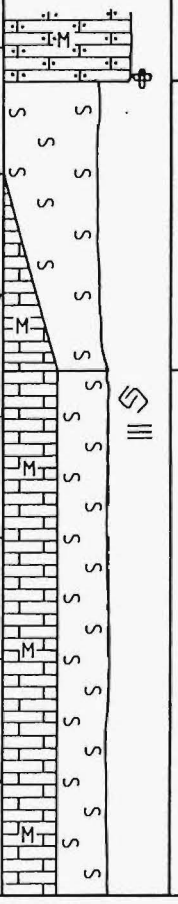		Limestone xwt cm to dm-bdd, s brn to gy glc Lst w bur base.	
						Marl 23.3m dm tk Mic in Mrl. Abund of Mic >> Mrl. No Mic in uppermost 7m.	
			490				
			480				
			470			Marl/Limestone 85.0m ibdd gen dm tk Mic and Marl, com slumped and folded. Patchy exposure.	
			460				
			450				
			440				

LOCALITY: Muzzle Stream, Clarence Valley. Composite section from various localities along the northern tributary (32).

GRID REFERENCES

Sheet Number: 030

Base of Section: 623023

Top of Section: 623045

DATE: 13/11/84

METHOD OF MEASUREMENT: Visual estimates.

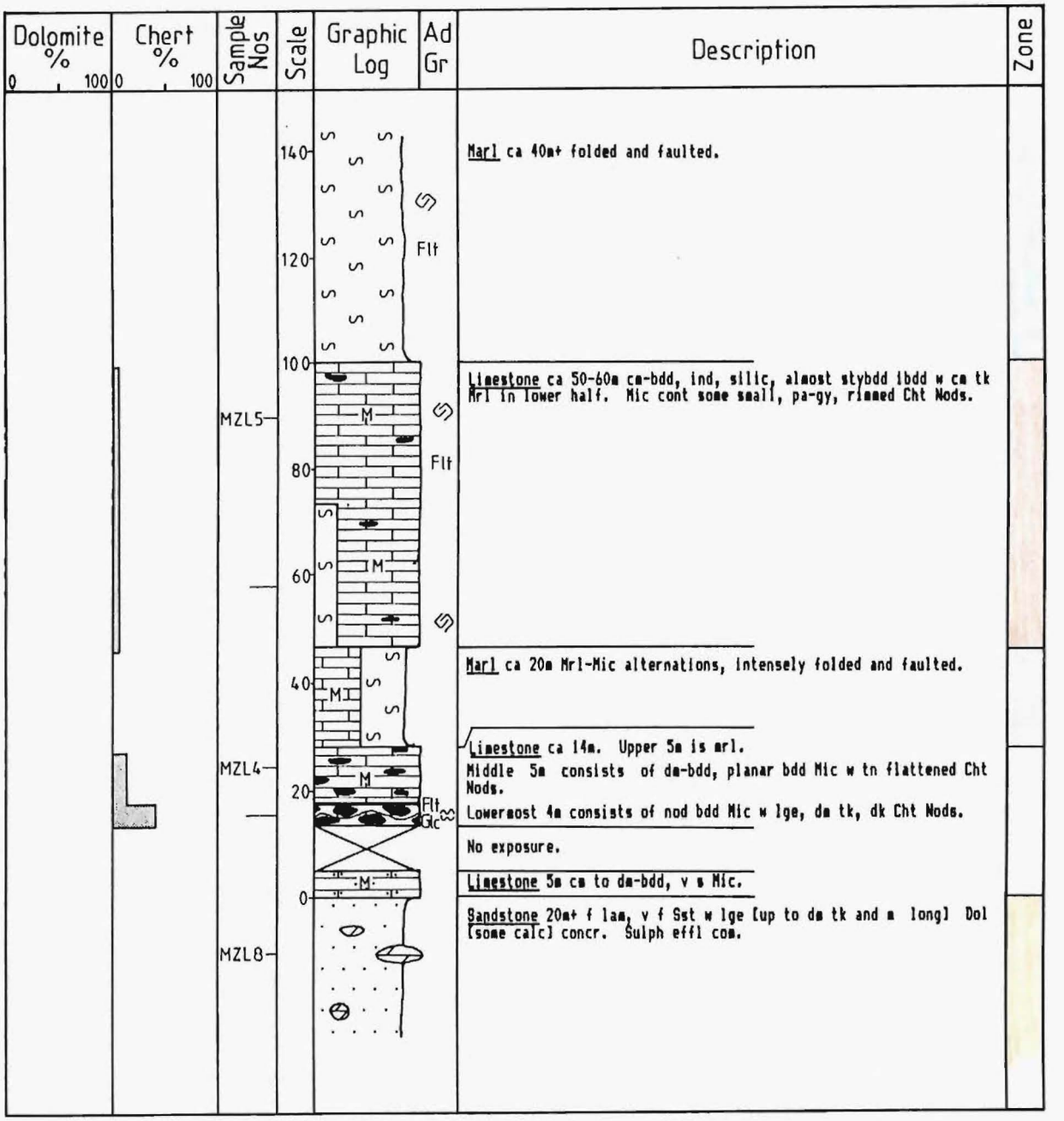

LOCALITY: Muzzle Stream - southern branch (33), Clarence Valley.

GRID REFERENCES

Sheet Number: 030

Base of Section: 616020

Top of Section: 616020

DATE: 12/11/84

METHOD OF MEASUREMENT: Tape and compass survey.

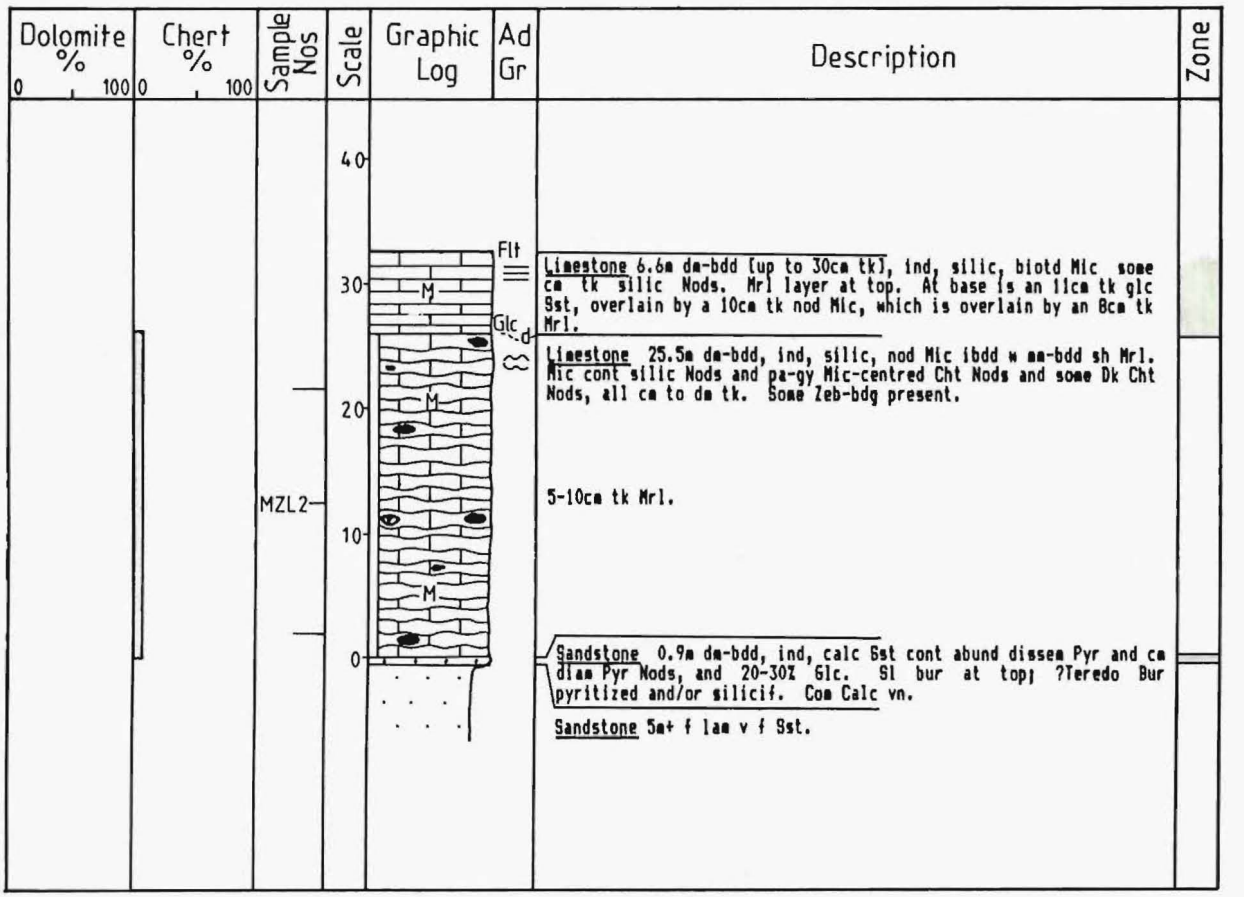

LOCALITY: Puhi Puhi River (5), near the Puhi Puhi River bridge, southern end of the Puhi Puhi Syncline.

GRID REFERENCES

Sheet Number: P31

Base of Section: 710814

Top of Section: 711818

DATE: 21-24/4/04

METHOD OF MEASUREMENT: Tape and compass survey, visual estimate of folded lithologies.

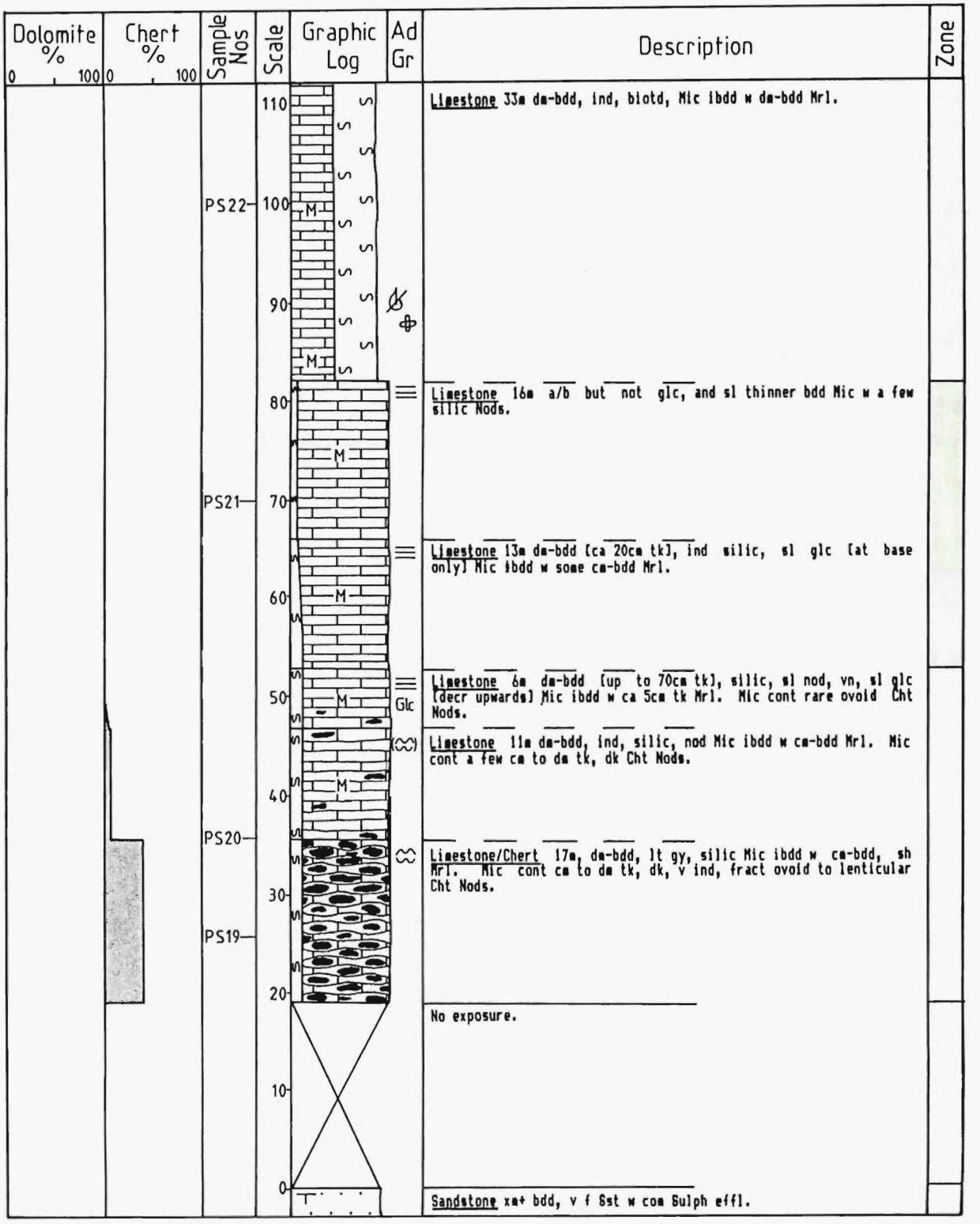

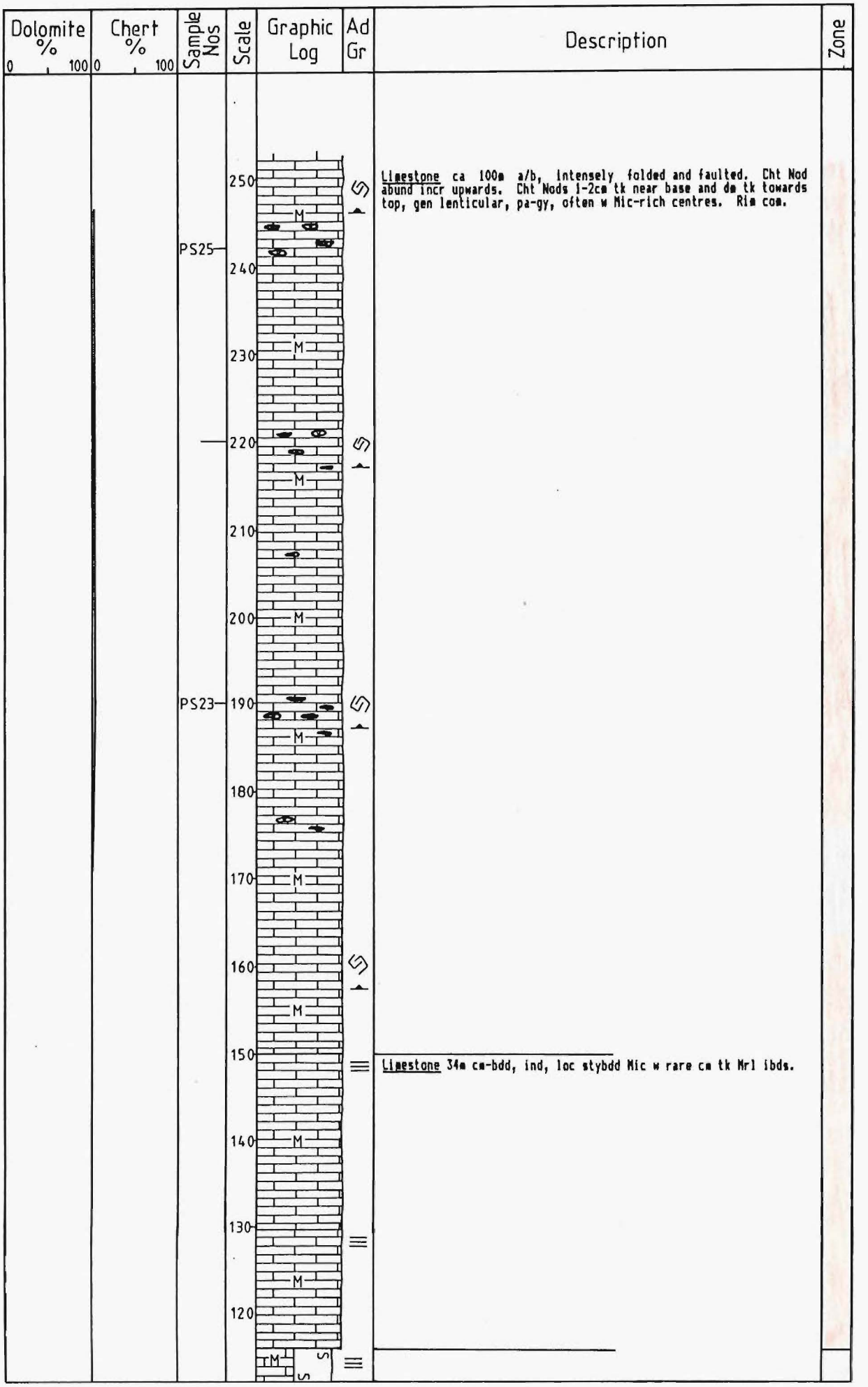
Dolomite %
0
100
Chert %
0
100
Sample Nos
Scale
Graphic Log
Ad Gr
Description
Zone
PS25
PS23
250
240
230
220
210
200
190
180
170
160
150
140
130
120
M
S
Limestone ca 100m a/b, intensely folded and faulted. Cht Nod abund incr upwards. Cht Nods 1-2cm tk near base and dm tk towards top, gen lenticular, pa-gy, often w Mic-rich centres. Rim com.
Limestone 34m cm-bdd, ind, loc stybdd Mic w rare cm tk Mrl ibds.

LOCALITY: Jordan Stream - Puhi Puhi River confluence (7), western limb of the Puhi Puhi Syncline.

GRID REFERENCES

Sheet Number: P31
Base of Section: 723848
Top of Section: 723848

DATE: 23/4/84

METHOD OF MEASUREMENT: Tape and compass survey, visual estimate of basal sandstone.

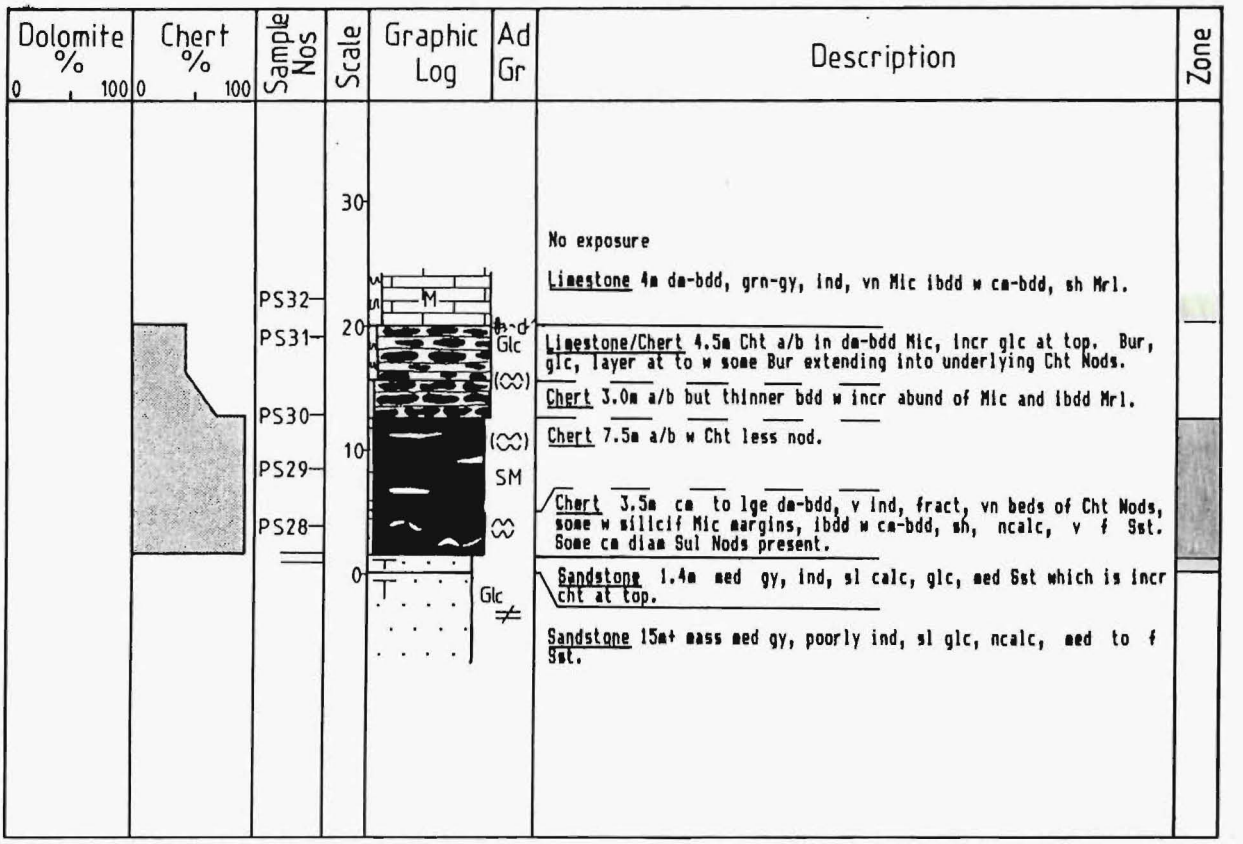

LOCALITY: Swale Stream (23), Coverham.

GRID REFERENCES

DATE: 4/5/85

Sheet Number: P30

Base of Section: 804187

Top of Section: 792198

METHOD OF MEASUREMENT: Tape and compass survey.

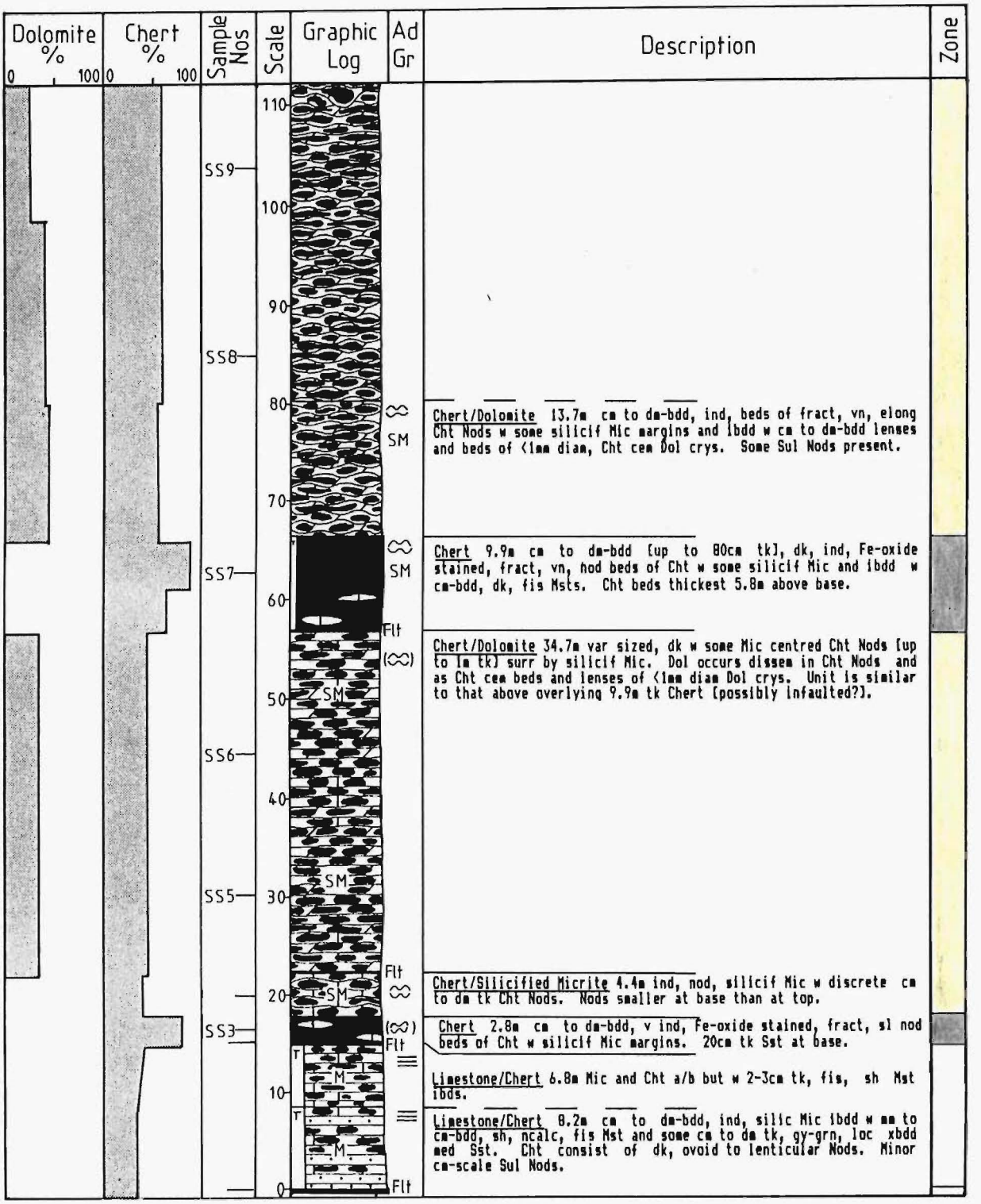

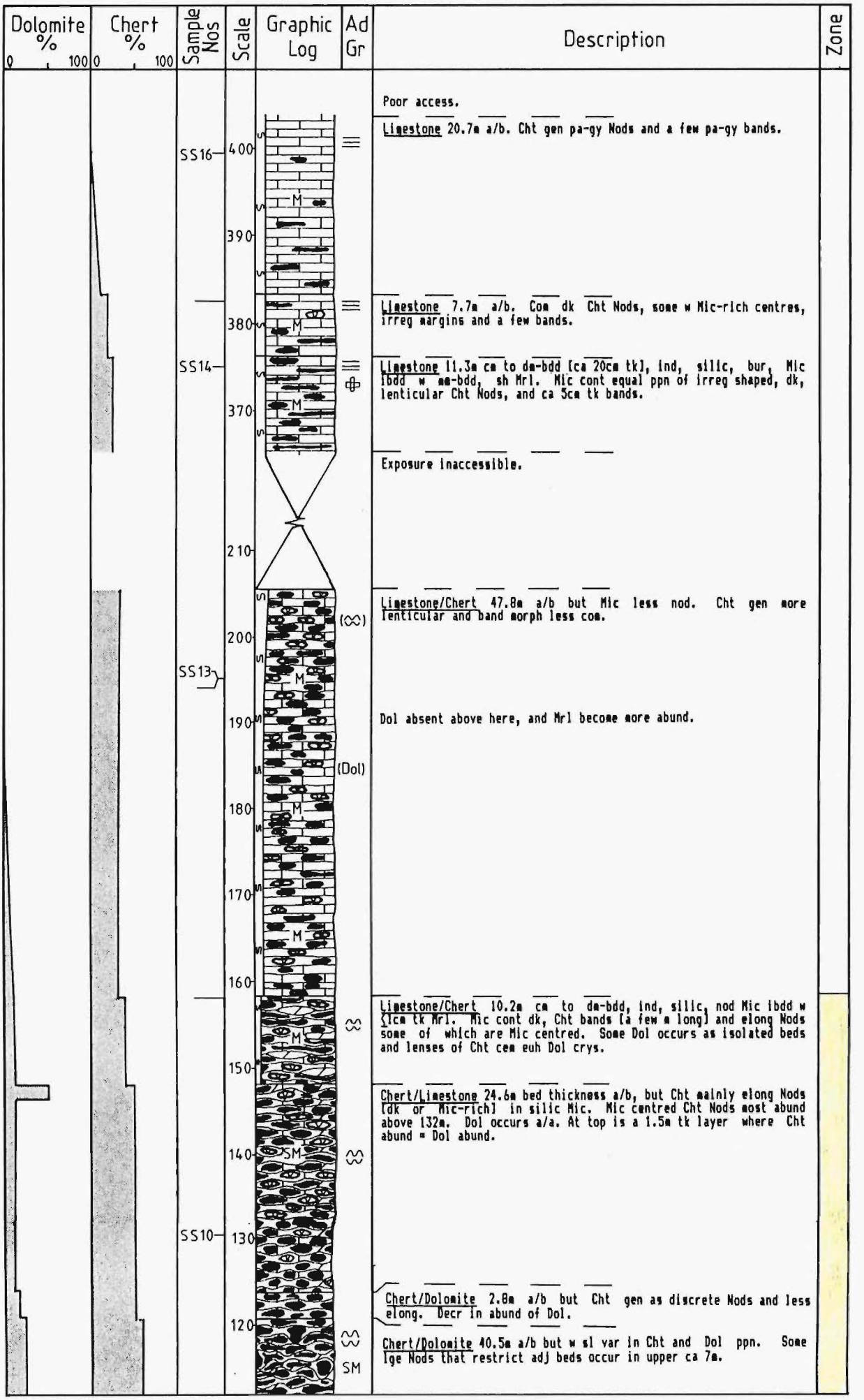
Dolomite %
0 100
Chert %
0 100
Sample Nos
Scale
Graphic Log
Ad Gr
Description
Zone
SS16
SS14
SS13
SS10
400
390
380
370
210
200
190
180
170
160
150
140
130
120
M
SM
(Dol)
Poor access.
Limestone 20.7m a/b. Cht gen pa-gy Nods and a few pa-gy bands.
Limestone 7.7m a/b. Com dk Cht Nods, some w Mic-rich centres, irreg margins and a few bands.
Limestone 11.3m cm to dm-bdd [ca 20cm tk], ind, silic, bur, Mic ibdd w mm-bdd, sh Mrl. Mic cont equal ppn of irreg shaped, dk, lenticular Cht Nods, and ca 5cm tk bands.
Exposure inaccessible.
Limestone/Chert 47.8m a/b but Mic less nod. Cht gen more lenticular and band morph less com.
Dol absent above here, and Mrl become more abund.
Limestone/Chert 10.2m cm to dm-bdd, ind, silic, nod Mic ibdd w <1cm tk Mrl. Mic cont dk, Cht bands [a few m long] and elong Nods some of which are Mic centred. Some Dol occurs as isolated beds and lenses of Cht cem euh Dol crys.
Chert/Limestone 24.6m bed thickness a/b, but Cht mainly elong Nods [dk or Mic-rich] in silic Mic. Mic centred Cht Nods most abund above 132m. Dol occurs a/a. At top is a 1.5m tk layer where Cht abund = Dol abund.
Chert/Dolomite 2.8m a/b but Cht gen as discrete Nods and less elong. Decr in abund of Dol.
Chert/Dolomite 40.5m a/b but w sl var in Cht and Dol ppn. Some lge Nods that restrict adj beds occur in upper ca 7m.

LOCALITY: South Wharanui Point (14), 200 m south of Woodside Creek mouth, Kaikoura Coast.

GRID REFERENCES

Sheet Number: P30
Base of Section: 999184
Top of Section: 999184

DATE: 30/1/85

METHOD OF MEASUREMENT: Tape and compass survey.

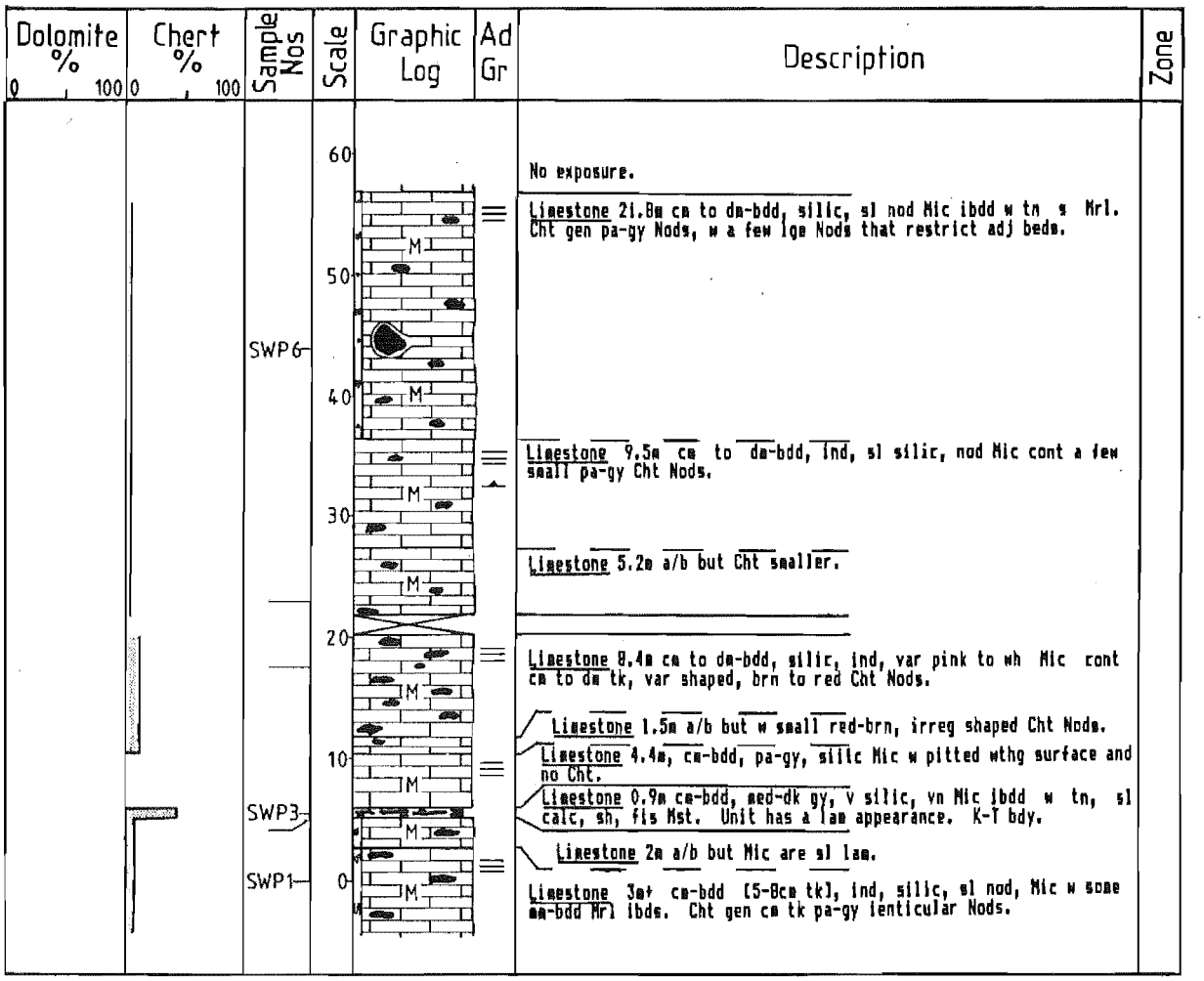

LOCALITY: Waipapa Bay - railway cutting and Mororimu Stream (10), Kaikoura Coast.

GRID REFERENCES

Sheet Number: P31
Base of Section: 816876
Top of Section: 817876

DATE: 6/4/84

METHOD OF MEASUREMENT: Tape and compass survey.

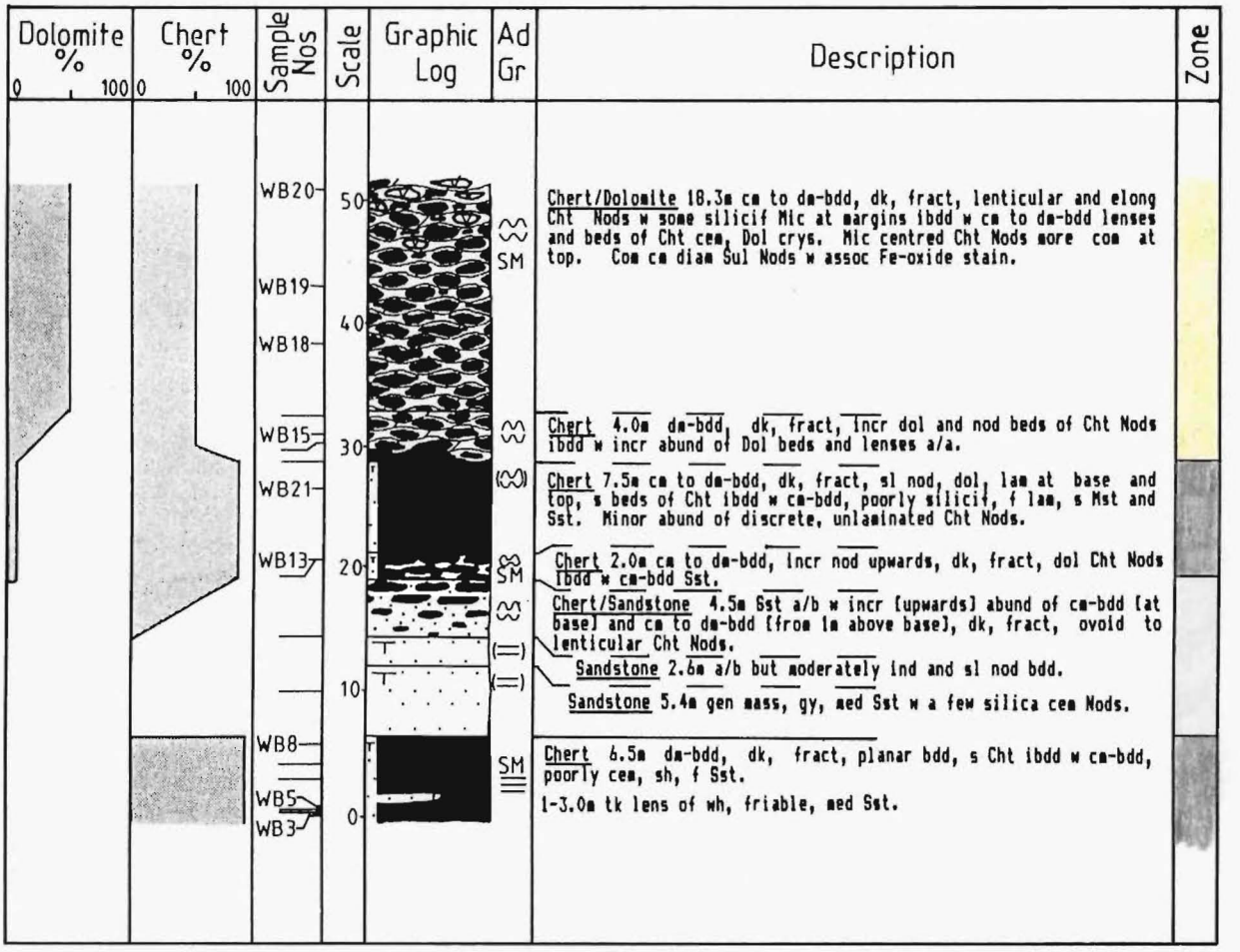

LOCALITY: Woodside Creek - lower gorge (13).

GRID REFERENCES

Sheet Number: P30

Base of Section: 988193

Top of Section: 990194

DATE: 27/1/85

METHOD OF MEASUREMENT: Tape and compass survey.

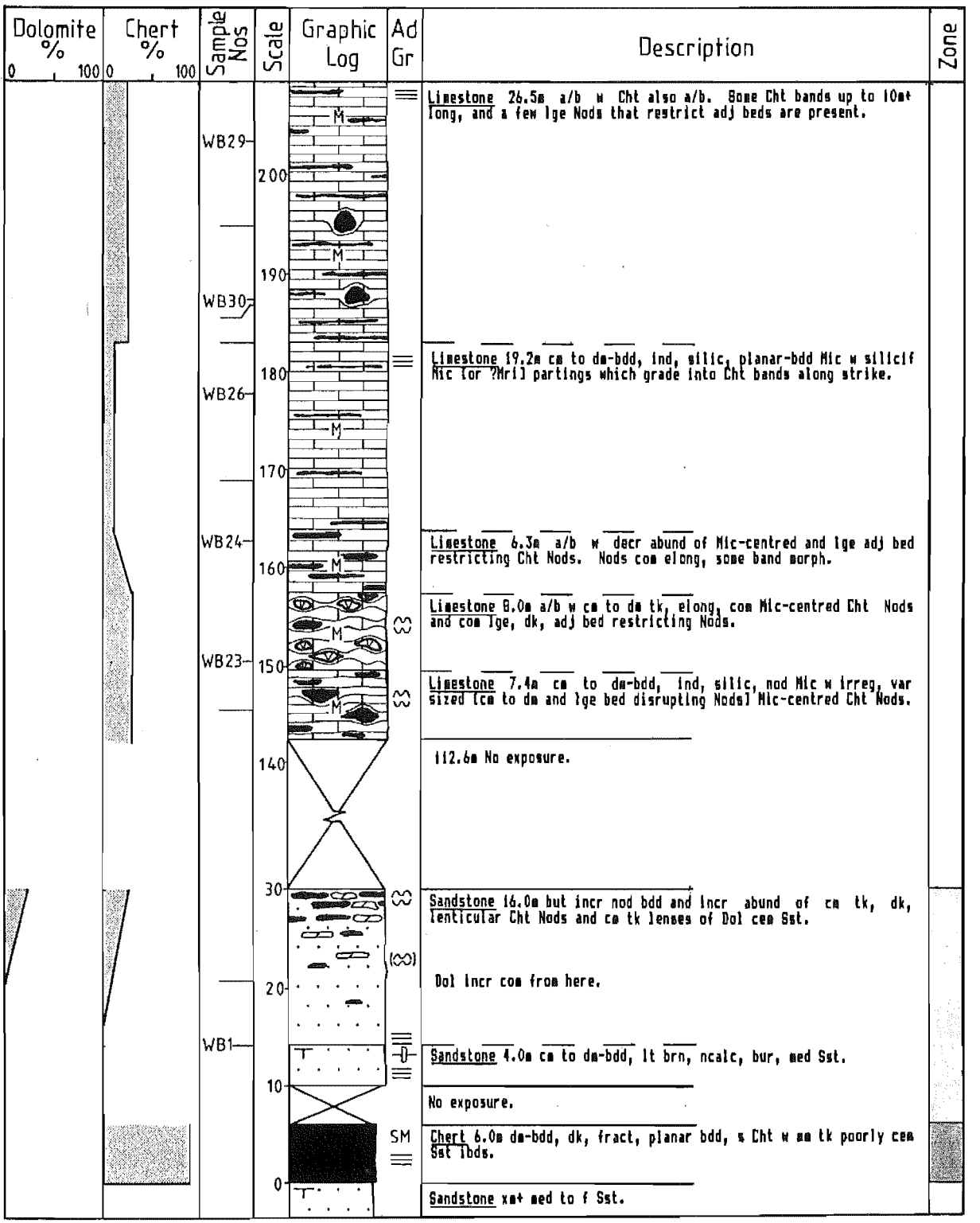

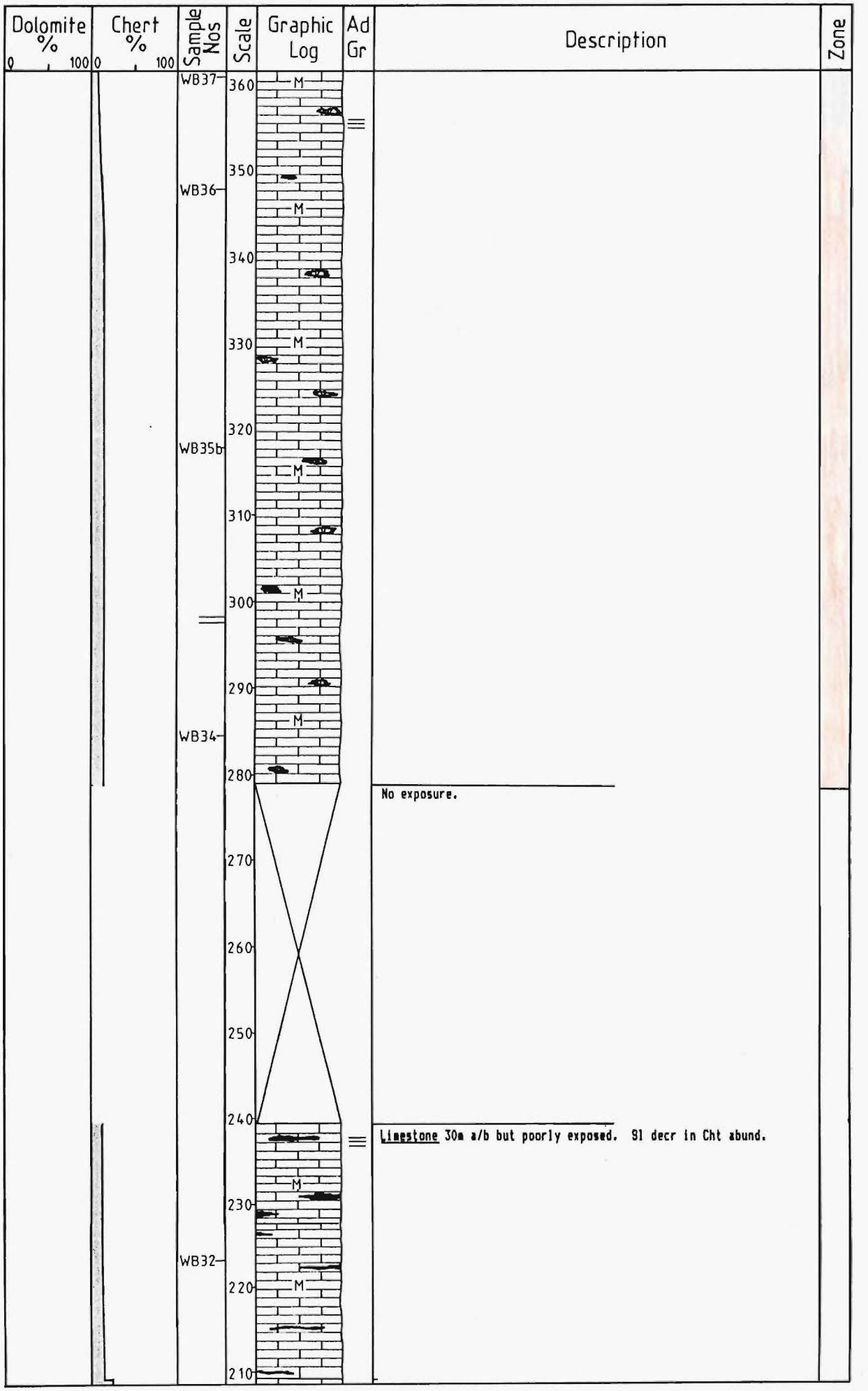
Dolomite %
0
100
Chert %
0
100
Sample Nos
WB37
WB36
WB35b
WB34
WB32
Scale
360
350
340
330
320
310
300
290
280
270
260
250
240
230
220
210
Graphic Log
M
Ad Gr
Description
No exposure.
Limestone 30m a/b but poorly exposed. Sl decr in Cht abund.
Zone

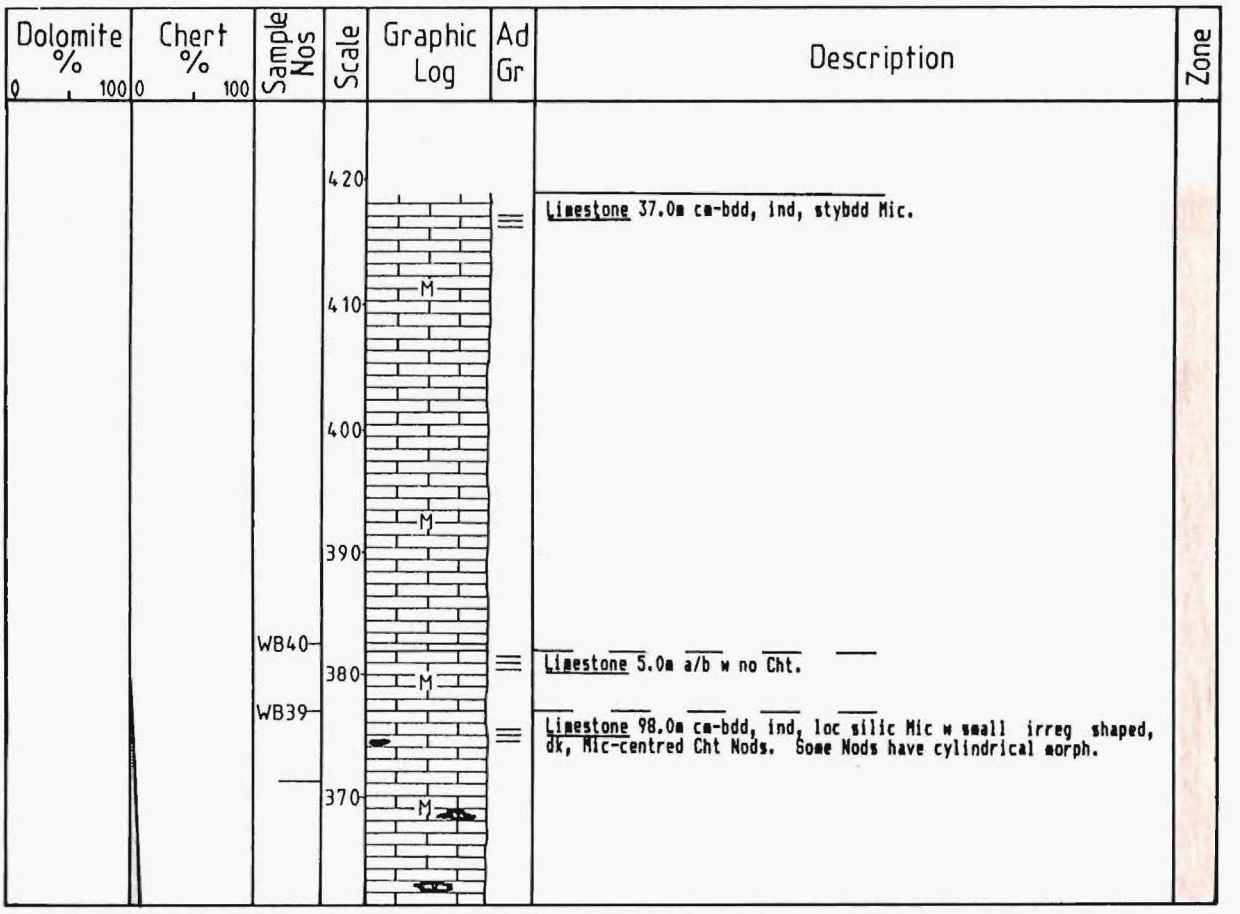
Dolomite %
0 100
Chert %
0 100
Sample Nos
Scale
Graphic Log
Ad Gr
Description
Zone
420
410
400
390
380
370
M
WB40
WB39
Limestone 37.0m cm-bdd, ind, stybdd Mic.
Limestone 5.0m a/b w no Cht.
Limestone 98.0m cm-bdd, ind, loc silic Mic w small irreg shaped, dk, Mic-centred Cht Nods. Some Nods have cylindrical morph.

LOCALITY: Waipapa Bay - beach platform (11).

GRID REFERENCES

Sheet Number: P31

Base of Section: 816874

Top of Section: 821879

DATE: 6-7/4/84

METHOD OF MEASUREMENT: Tape and compass survey.

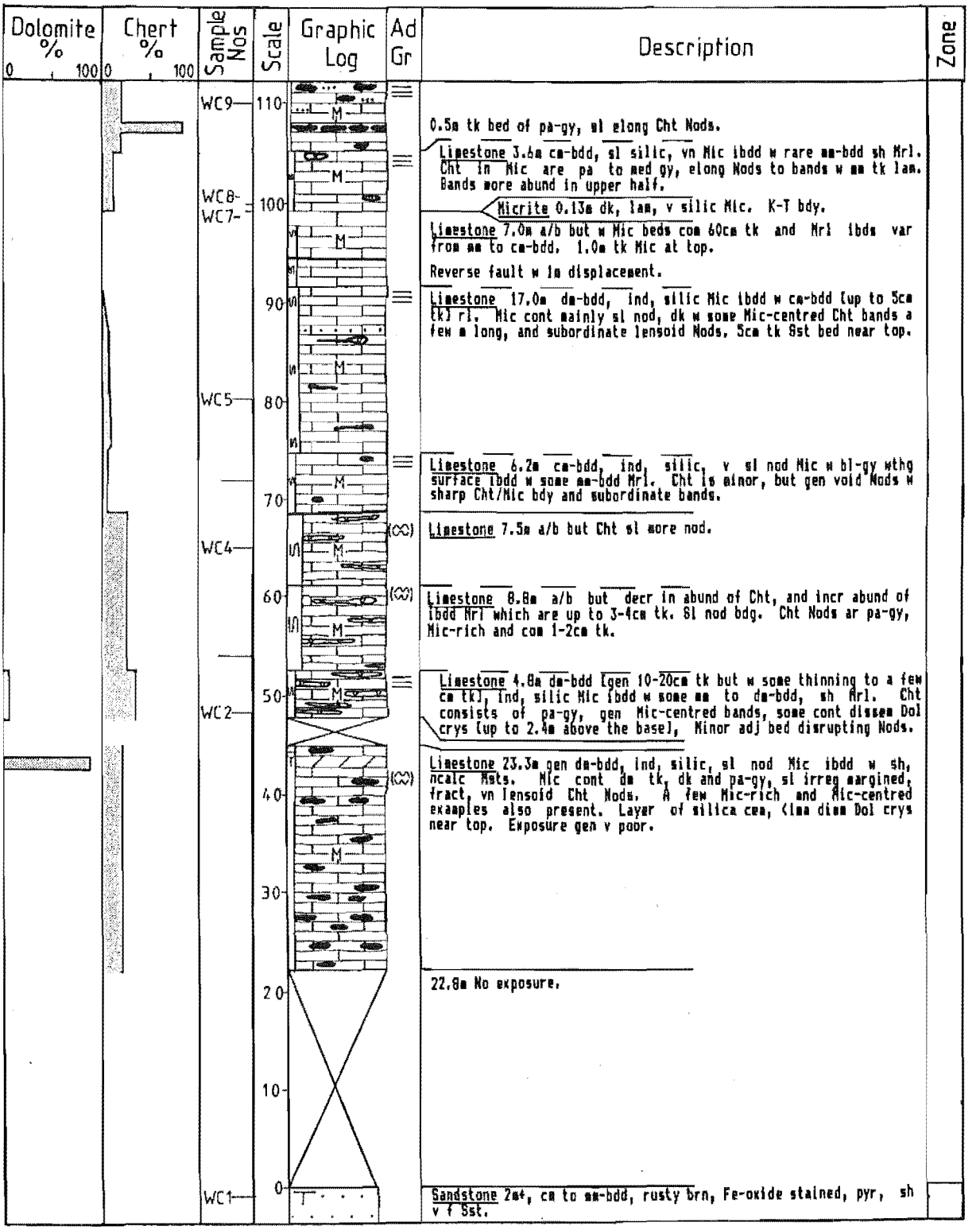

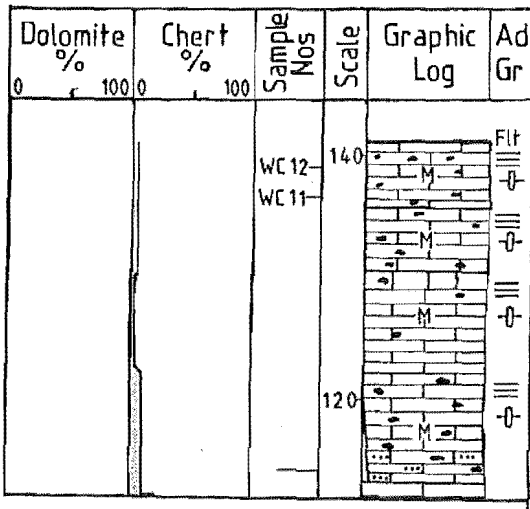

Description	Zone
No exposure.	
Limestone 5.3m a/b but Mic pink to red. Chertified Bur (dk red) w silicif Mic rim (lt red to pink) v com.	
limestone 5.0m a/b w pitted wthg surface, probably silicif Bur a/a.	
Limestone 8.5m m-bdd (up to 3m tk w dm-bdd subunits), pink, ind, jointed, silic Mic w rare lbdd Mrl.	
Limestone 9.0m dm-bdd, red to pink, silic Mic lbdd w decr abund of (m Mrl. Mic cont v small (cm diam) ovoid Cht which may be chertified Bur a/a.	
Lowermost 2m cont mm to cm scale Sst lenses in base of Mic beds.	
Limestone 1.1m cm-bdd (av 5cm tk), silic, vn Mic lbdd w <1cm tk, dk, sh Mrl.	
Limestone 7.2m a/b but w sl incr in thickness if Mic beds. Cht gen along Nods, diff margined, Mic-centred or both. Sst lenses (a/a) in base if Mic beds at top.	

LOCALITY: Wharekiri Stream (9), north end of Puhi Puhi Syncline.

GRID REFERENCES

Sheet Number: P30

Base of Section: 752914

Top of Section: 751913

DATE: 14/11/85

METHOD OF MEASUREMENT: Tape and compass survey.

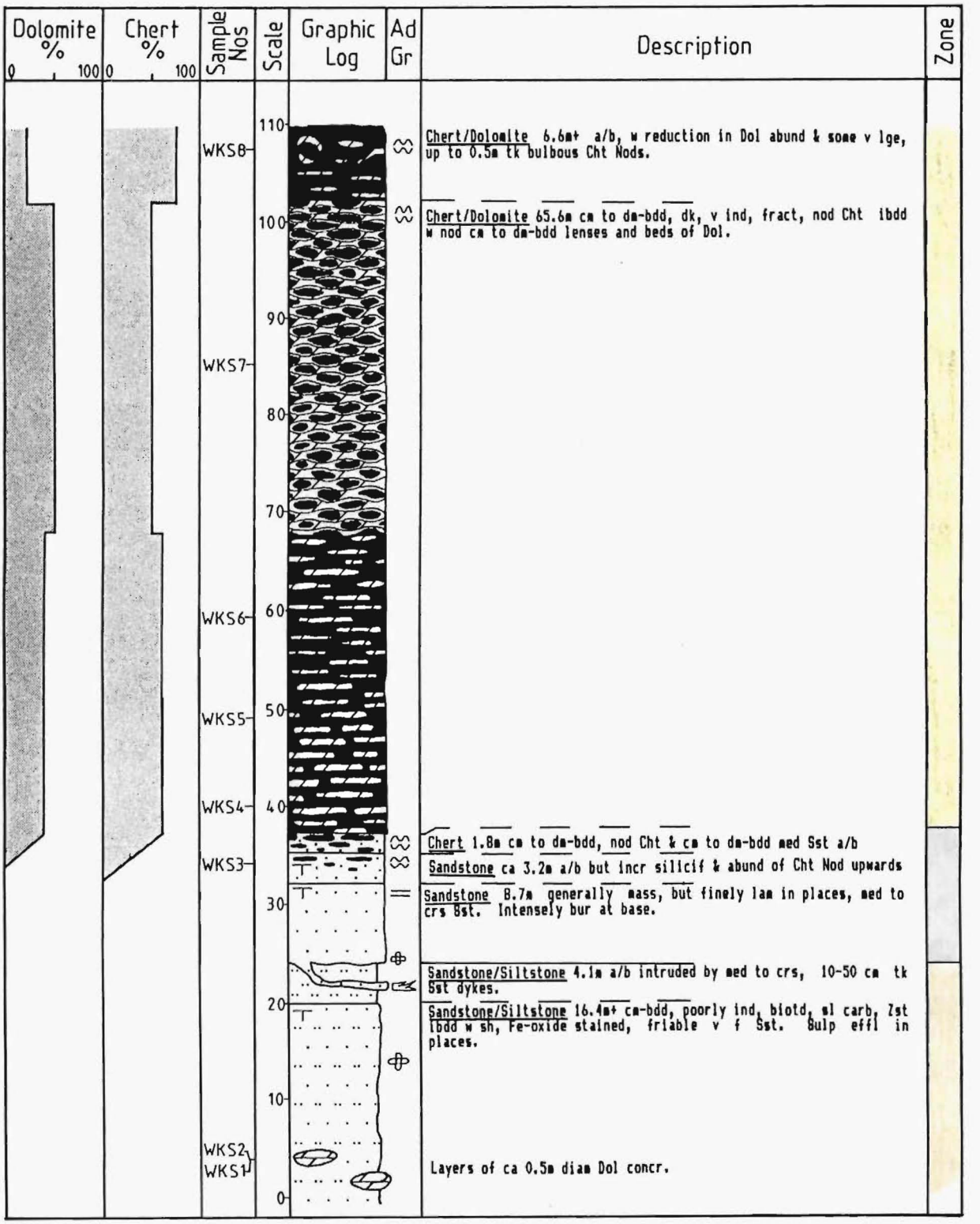

LOCALITY: Wharanui Point (15), 500 m north of Woodside Creek mouth, Kaikoura Coast.

GRID REFERENCES

Sheet Number: P30
Base of Section: 008195
Top of Section: 008195

DATE: 30/1/85

METHOD OF MEASUREMENT: Tape and compass survey.

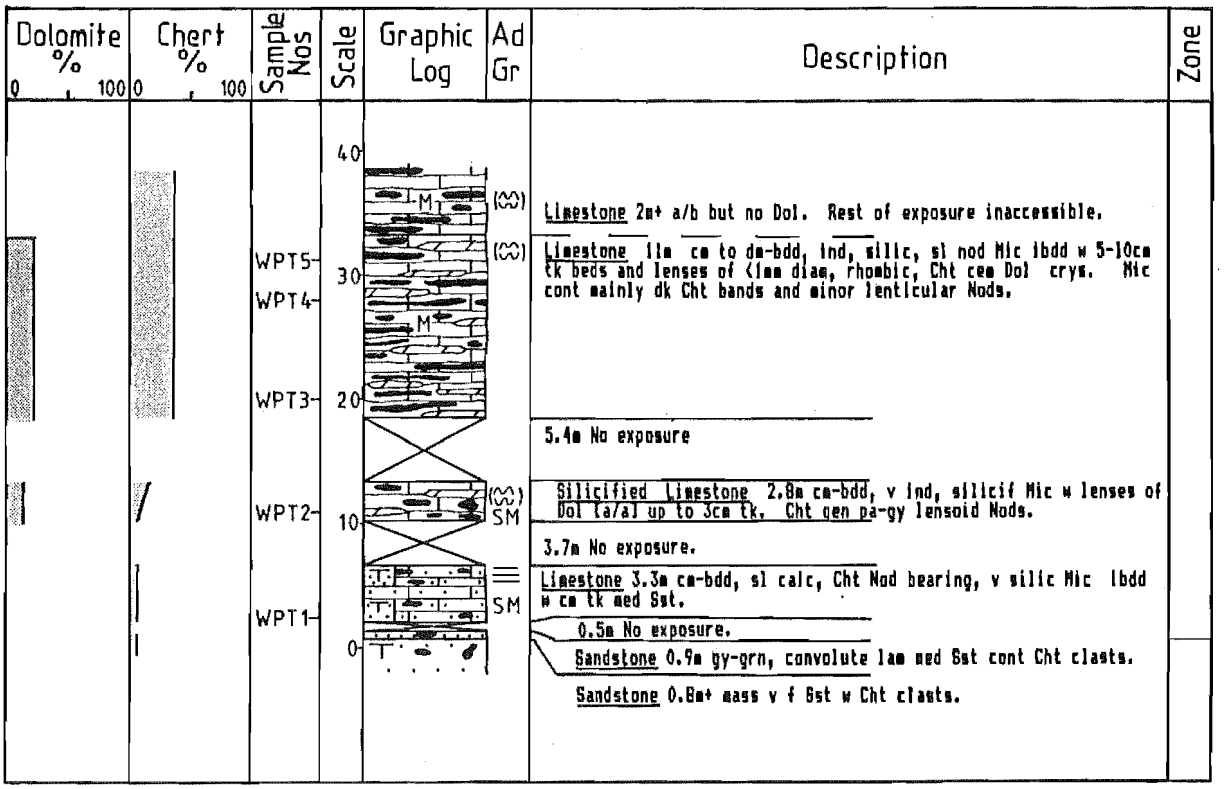

LOCALITY: Waima River (21), north of Chalk Range.

GRID REFERENCES

Sheet Number: P29

Base of Section: 909244

Top of Section: 909244

DATE: 1/2/85

METHOD OF MEASUREMENT: Direct measurement of thickness.

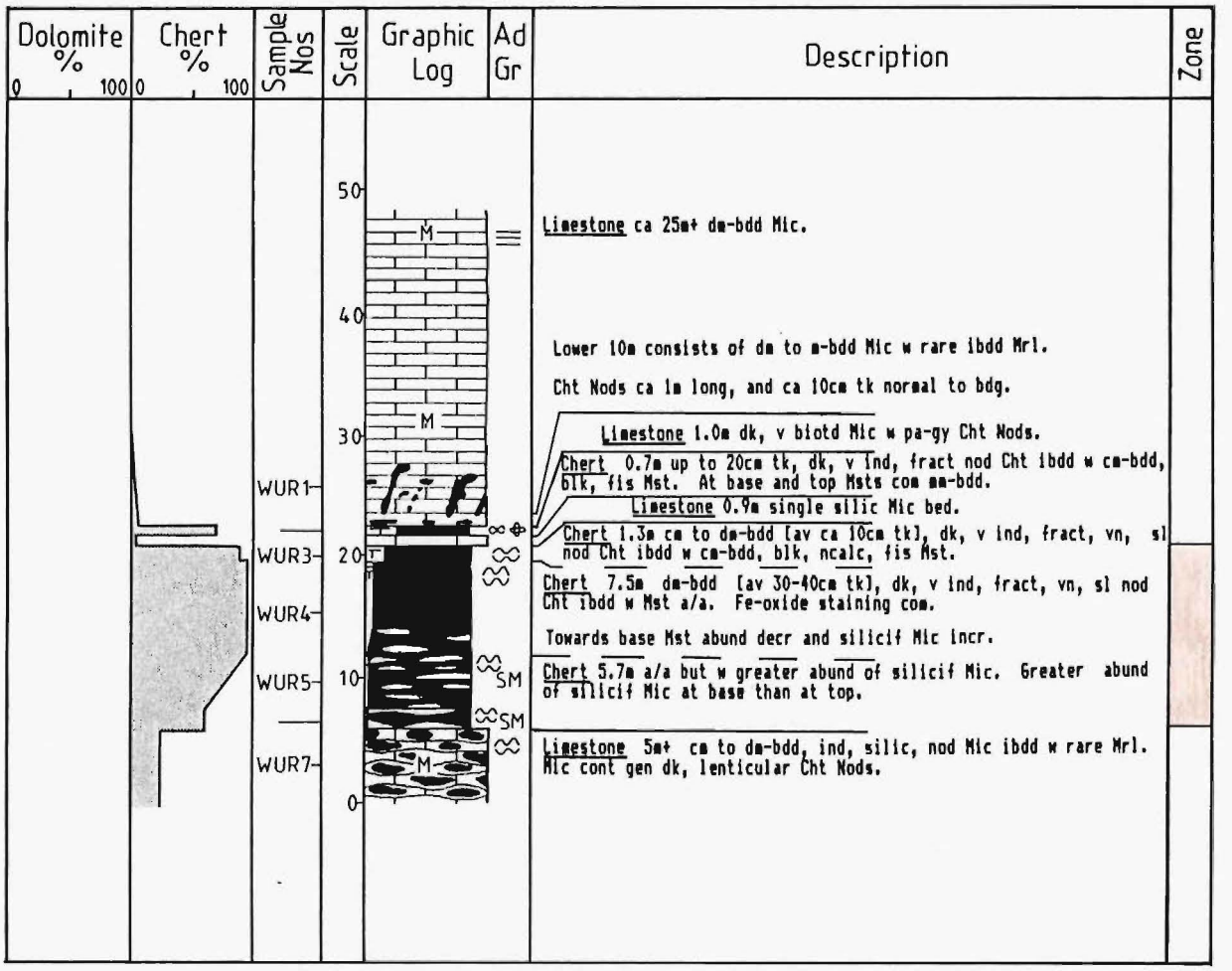

APPENDIX 3

DESCRIPTION OF PETROGRAPHY, MINERALOGY, AND GEOCHEMISTRY OF LIMESTONES

A3.1. X-RAY MINERALOGY AND PETROGRAPHY

A3.1.1. X-RAY MINERALOGY

Noncarbonate Fraction

The x-ray diffraction mineralogy of Amuri Limestone Group micrites and marls from the Upper and Lower Marl Formations was detailed by Fergusson (1985). Further investigations were also made by Morris (1987). Insoluble clay fractions consist of well crystallized smectite and illite, with some quartz identified as chert (Fergusson 1985). From some Lower and Upper Marl samples, minor quantities of clinoptilolite and barite have also been found (Fergusson 1985, Morris 1987).

The few clay mineral analyses of marls in this study show smectite (001) peaks at about 12Å [Figure A3.1]. Small illite-muscovite peaks are also obtained in some instances. Quartz (100) and (101) reflections are also common.

In micrite whole rock and HCl insoluble residue fractions, clay minerals are not detected. This may reflect very low clay mineral concentrations in micrites, or peaks are swamped by the abundant quartz found in most samples.

Carbonate Fraction

Aragonite and high-Mg calcite are absent from the Amuri Limestone Group. The calcite peaks for both marls and micrites are all in the range 3.04-3.05Å, with the secondary reflection at 3.85-3.87Å (Chave 1952, Goldsmith *et al.* 1961). All major peaks are sharp but the 3.87Å peak is sometimes slightly broadened [Figure A3.2].

A3.1.2. THIN SECTION PETROGRAPHY

Limestone beds are composed primarily of calcilutites: fossiliferous micrites to sparse biomicrites. Fossils are mostly planktonic foraminifera, with subordinate benthonic forms [Figure A3.3]. Fragmented fossil material is common. The abundance of obvious bioclastic material ranges from 5-20 percent, with an average of about 10 percent. Rare

Figure A3.1 XRD trace showing a broad smectite peak. Small illite peaks at 10-11Å may be masked by the smectite reflection (Sample MS19, 9ø fraction).

Figure A3.2 Micrite (whole rock) XRD trace (sample MS10). No clay mineral peaks are observed.

A3.1

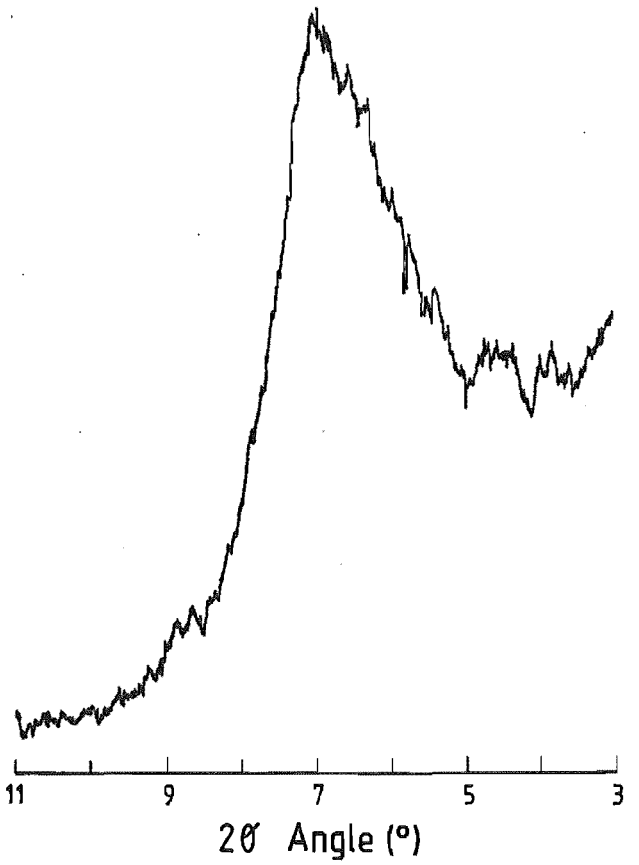
11
9
7
5
3
2θ Angle (°)

A3.2

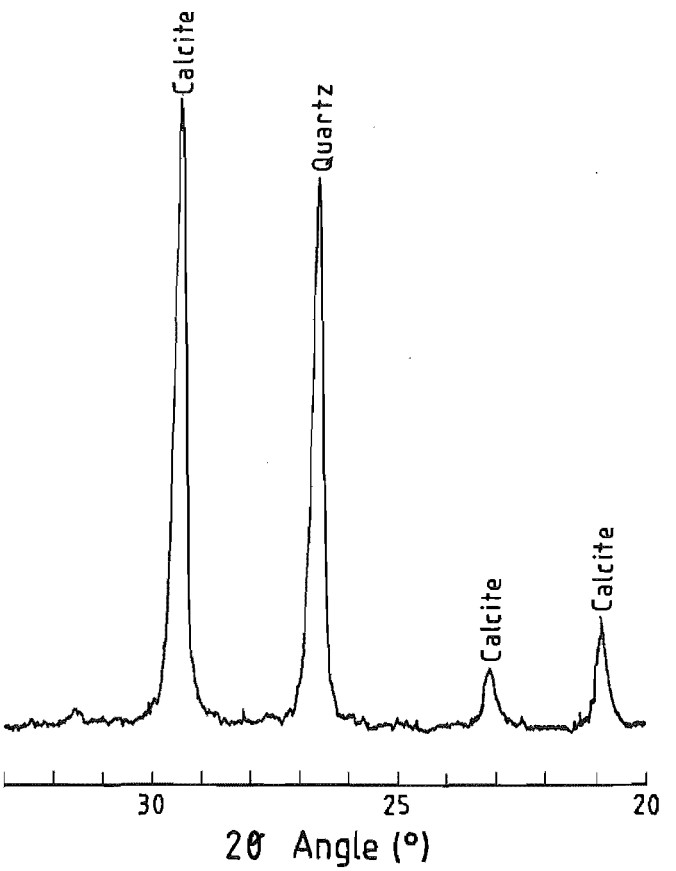
Calcite
Quartz
Calcite
Calcite
30
25
20
2θ Angle (°)

sponge spicules are seen in a few samples, but no other siliceous microfossils are identified. Non-fossiliferous grains include minor very fine silt size detrital quartz and muscovite. Some of the quartz grains have calcite embayments. Pyrite is seen in all micrites. The pyrite is mostly finely disseminated, and may be surrounded by, or associated with, reddish-brown Fe-oxide (?haematite/limonite) staining. In pink micrites little pyrite is observed but there is abundant Fe-oxide. Rare pyrite grains are commonly surrounded by Fe-oxide. Sparry calcite veins are common in all micrites.

Evidence of primary bedding in some samples is provided by the alignment of fragmented skeletal material, and occasionally by an apparent alignment of pyrite. Foraminiferal chambers contain either micrite, sparry calcite, or a combination of both. Pyrite partly or completely fills some chambers. Intact chambers show little evidence of deformation.

There is minimal petrographic variation in micrites throughout the CL and LL Zones. ML Zone micrites however, tend to display poorer microfossil preservation.

A3.2. SCANNING ELECTRON MICROSCOPY (SEM)

In heavily chertified or dolomitized parts of the sequence, virtually none of the original limestone texture remains. Samples from stratigraphically above, or laterally beyond, the greatest development of chert and dolomite, were examined to document initial limestone components. Veined samples were avoided.

Figure A3.4 shows typical micrite textures, found in ML, CL and LL Zones. Calcite recrystallization is a common feature and tends to be most extensive in the CL Zone. The range of calcite crystal sizes is bimodal in a number of samples [Figure A3.4a], with coarser crystals clustered together. This clustering of coarse crystals may reflect growth into voids (Steinen 1978). Other samples are relatively heterogeneous [Figure A3.4b], consisting of recrystallized calcite, fossils and fossil fragments, and small platy particles which may be micarb (Matter 1974). These micarb particles are thought to be structural elements or fragments thereof from coccolithophorids, or possibly foraminifera (Matter 1974). In samples such as Figures A3.4a and A3.4b, differentiation of authigenic

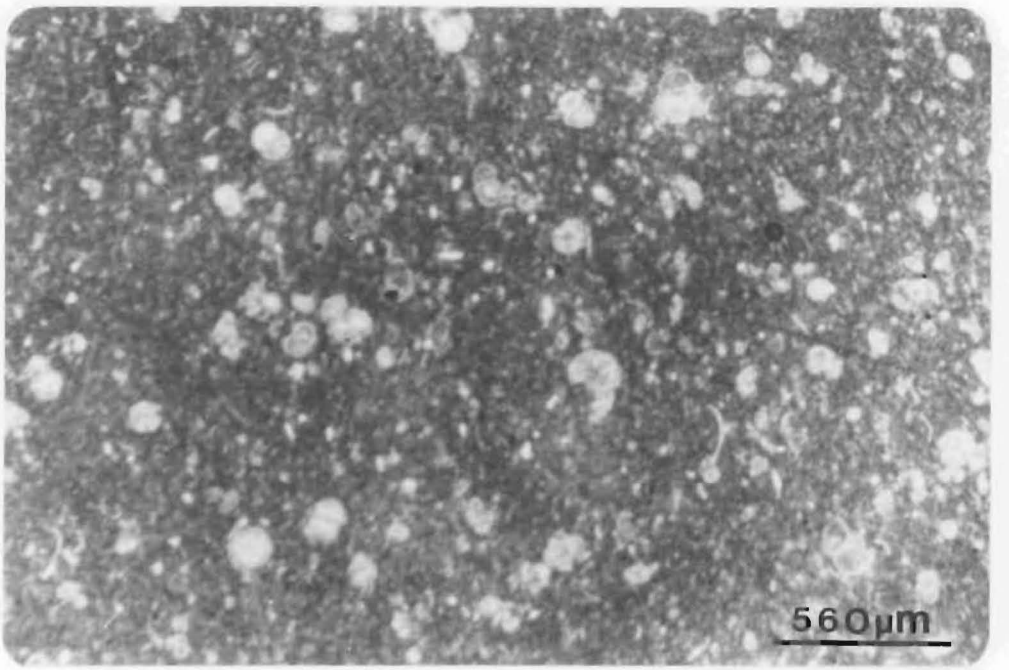

Figure A3.3 Thin section micrograph of a calcilutite, LL Zone, Mt Alexander (Plane polarized light, sample MA15).

silica (which may pseudomorph calcite crystals) from recrystallized calcite is difficult, because the small crystal sizes commonly encountered preclude identification by SEM-EDAX analysis. Generally, microporosity in these micrites appears low, and is estimated to be less than 15 percent.

Foraminiferal tests and test fragments nearly always display evidence of varying degrees of dissolution and/or recrystallization [Figure A3.4c,d,e]. Chambers may be filled with spar or microspar [Figure A3.4e]. In samples from Oaro (2) cristobalite lepispheres are found [Figure A3.4c,d]. Lepispheres were not found in any other micrite samples.

Nannofossils are not as common as expected. Those observed are mostly coccolithophorids [Figure A3.4f]. Like the forminifera, they display varying degrees of recrystallization. Micarb particles are associated with these nannofossils.

None of the limestone samples examined by SEM revealed any siliceous microfossils or nannofossils.

Although biogenic micrite (such as fossil fragments or micarb) are abundant, there is a large proportion of carbonate which appears to have a secondary origin. Interlocking euhedral carbonate grains are common and many small biogenic fragments are overgrown.

A3.3. MAJOR AND TRACE ELEMENT GEOCHEMISTRY OF MARLS AND MICRITES

Marl-micrite compositions are summarized in Table A3.1. This data, plus analyses from Morris (1987), show marls to contain higher concentrations of Fe, Na, K, Mg, and Sr than micrites. Manganese concentrations in marls are either similar to, or slightly lower than, in the micrites. The stable isotopic compositions display only small difference. $\delta^{18}O$ analyses become more positive stratigraphically upwards. All carbonates are low-Mg calcites, and also have low levels of Fe and Mn. The (HCl) insoluble residue content of marls is usually 1.3 to 2.0 times that in micrites. The higher insoluble residue content in sample MS9 micrite than in the adjacent marl is probably a result of the relatively greater quantity of authigenic silica in the micrite. For comparative purposes further micrite analyses are included with dolomite analyses [Appendix 5].

Figure A3.4 SEM micrographs of typical limestone textures.
(a) Bimodal distribution of crystal sizes with coarse crystals clustered together (sample WB 40, ML Zone).
(b) Relatively homogeneous mixture of calcite crystal sizes (ranging from a few microns up to about 15 m). The arrows indicate coccolithophorids (sample HBOA1, ML Zone).
(c,d) Recrystallization of foraminiferal test. The box in (c) shows the position of (d). In this particular example rhombic calcite crystals, and blades and lepispheres of cristobalite are present (sample HBOA1, ML Zone).
(e) Infilling of ?foraminifer chamber with sparry calcite (sample WB40, ML Zone).
(f) Overgrowth and thickening of coccolithophorid plates (sample PS32, LL Zone).

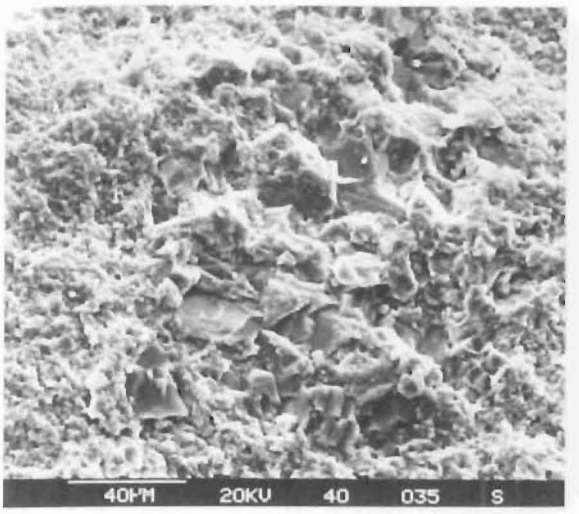
40µM 20KV 40 035 S

a

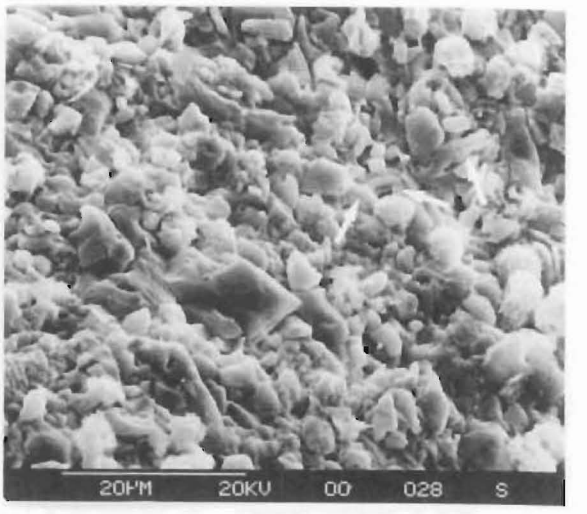
20µM 20KV 00 028 S

b

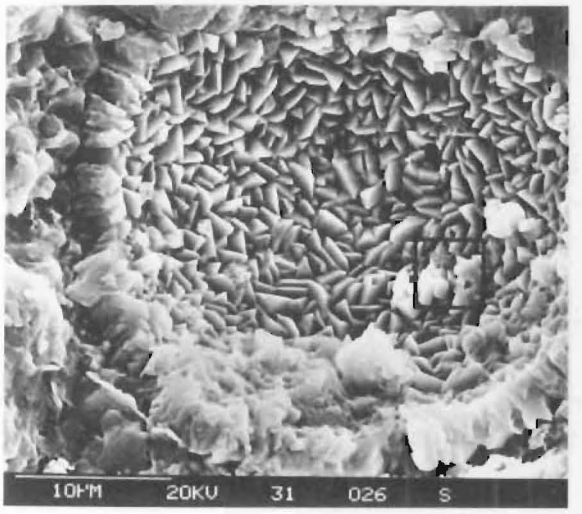
10µM 20KV 31 026 S

c

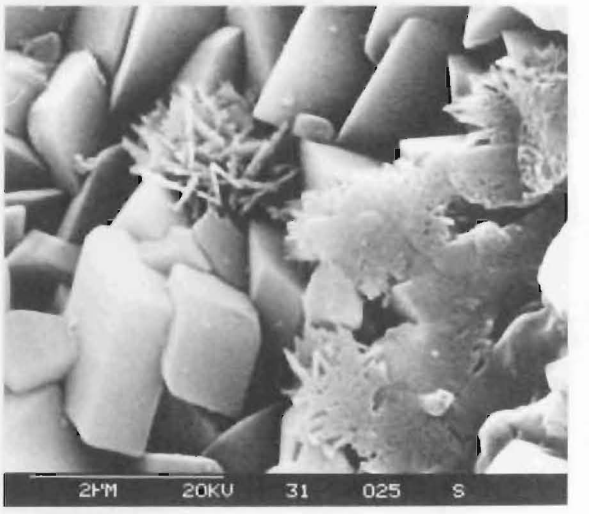
2µM 20KV 31 025 S

d

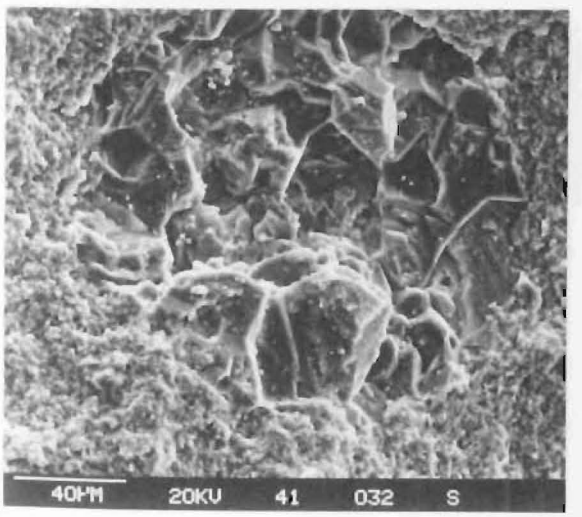
40µM 20KV 41 032 S

e

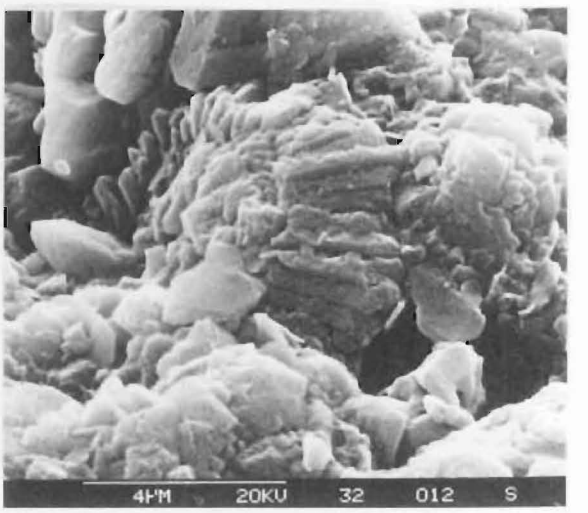
4µM 20KV 32 012 S

f

Table A3.1. Composition of marl-micrite pairs. "JM" samples were supplied by J.C. Morris.

		Carb	IR	Mn	Fe	Na	K	Mg	Ca	Sr	O-18	C-13	$MgCO_3$	$CaCO_3$	$FeCO_3$
		Wt%	Wt%	ppm	ppm	ppm	ppm	ppm	ppm	ppm	%.PDB	%.PDB	Mole%	Mole%	Mole%
JM 30/40	Marl										-1.66	+1.65			
UM Zone	Micrite										-1.62	+1.76			
MS48	Marl	63.2	36.8	589	3650	1410	6049	650	330636	1059			0.32	98.90	0.78
LM Zone	Micrite	77.4	22.6	634	3254	1300	1394	387	324405	865			0.19	99.09	0.71
JM 30/3	Marl										-3.49	+1.38			
LM Zone	Micrite										-3.29	+0.94			
MS47	Marl	62.6	37.4	489	3158	1504	6733	675	351423	1460			0.31	99.05	0.64
LM Zone	Micrite	81.6	18.4	612	2174	1259	1177	291	324246	844			0.01	99.51	0.48
JM 30/14	Marl										-6.31	+1.19			
LCM Sub	Micrite										-5.40	+1.18			
MS10	Marl	43.4	56.6	408	5480	1582	7916	4961	334177	761	-5.54	+1.38	2.36	96.50	1.14
CL Zone	Micrite	55.6	44.4	395	1242	1485	3570	4010	381682	691	-5.90	+1.73	1.70	98.07	0.23
MS9	Marl	72.3	27.7	470	1532	1374	2667	3963	332944	690			1.92	97.76	0.32
CL Zone	Micrite	57.0	43.0	433	1318	1486	4090	7243	331977	677	-5.87	+1.45	3.46	96.26	0.27

APPENDIX 4

DESCRIPTION OF PETROGRAPHY, MINERALOGY, AND GEOCHEMISTRY OF DETRITAL SEDIMENTS

A4.1. X-RAY MINERALOGY

A4.1.1. WOOLSHED CONCRETION (WC) ZONE

Mudstones of the WC Zone, and lower in the Woolshed Formation, throughout the field area generally contain the same suite of minerals: quartz, cristobalite, sparse feldspars, micas and clay minerals.

Whole rock x-ray diffraction (XRD) traces [Figure A4.1a] from oriented grain mounts show the predominant mineral to be quartz, marked by the two major peaks (100) at 4.27-4.25Å and (101) at 3.43Å. With the exception of Kaikoura Peninsula samples, these two peaks are usually sharp and larger than peaks for other minerals, suggesting greater abundance and/or good crystal ordering. A small cristobalite peak (101) at 4.04Å is found in some samples.

Clay size fraction (air dried) separates [Figure A4.1b] contain kaolinite (100) at 7.14Å, and muscovite/illite with sharp narrow peaks at 10.05Å and 5.01Å. Other muscovite/illite peaks are assigned at 5.01Å, 4.53Å, and 3.13Å respectively. Also present in samples is a relatively broad peak at about 12.3Å. On glycolation this peak shifted to 17.7Å. It probably represents Na-smectite. Some whole rock samples have a peak at 16.06Å which is also assigned to smectite.

Jarosite, commonly observed in outcrops, is not found on any XRD traces, nor are pyrite or Fe-oxides.

XRD traces of samples from both South Bay (3) and Lab Rocks (4) differ from other localities [Figure A4.2] in one respect. Quartz peaks tend to be broader and not as sharp. In addition, there is a major cristobalite (101) peak at 4.04-4.05Å. The peak at about 4Å becomes more intense stratigraphically upwards on both sides of the Peninsula (3,4). Thin section examination [Section A4.2.1] shows quartz to be the dominant detrital mineral throughout the Lab Rocks section (4). However, at South Bay (3) the cristobalite peak increases in size such that at the top of the Woolshed Formation the 4.26Å quartz peak is progressively reduced to a small shoulder on the cristobalite reflection. Tada and Iijima (1983) attribute a peak at about 4.03Å to a tridymite (200) reflection which is often masked by the quartz (100) peak. Comparison of the traces in Tada

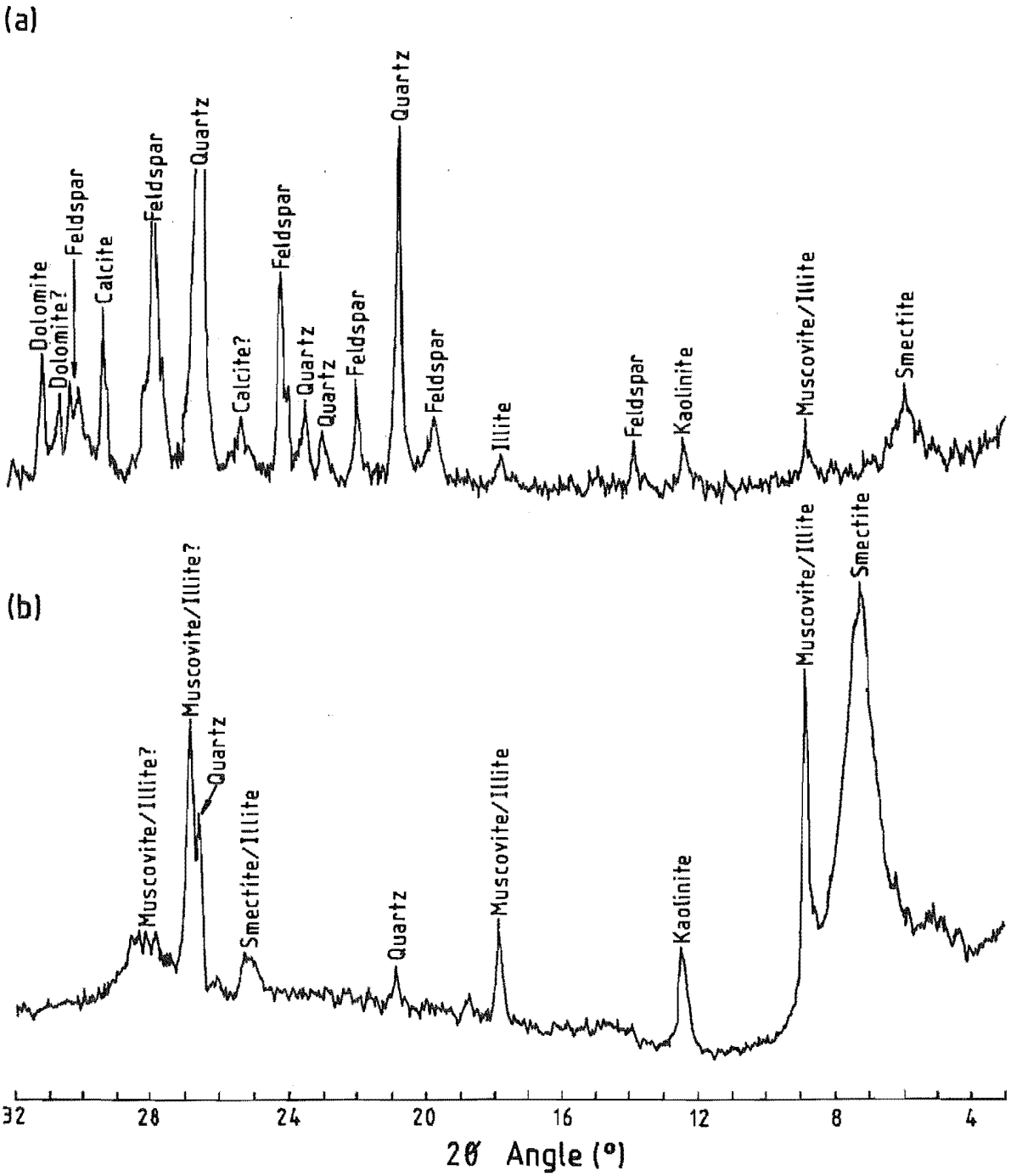

Figure A4.1 Typical XRD traces from WC Zone mudstone (sample WKS2).
(a) Whole rock XRD trace.
(b) XRD trace of the <4ø size fraction.

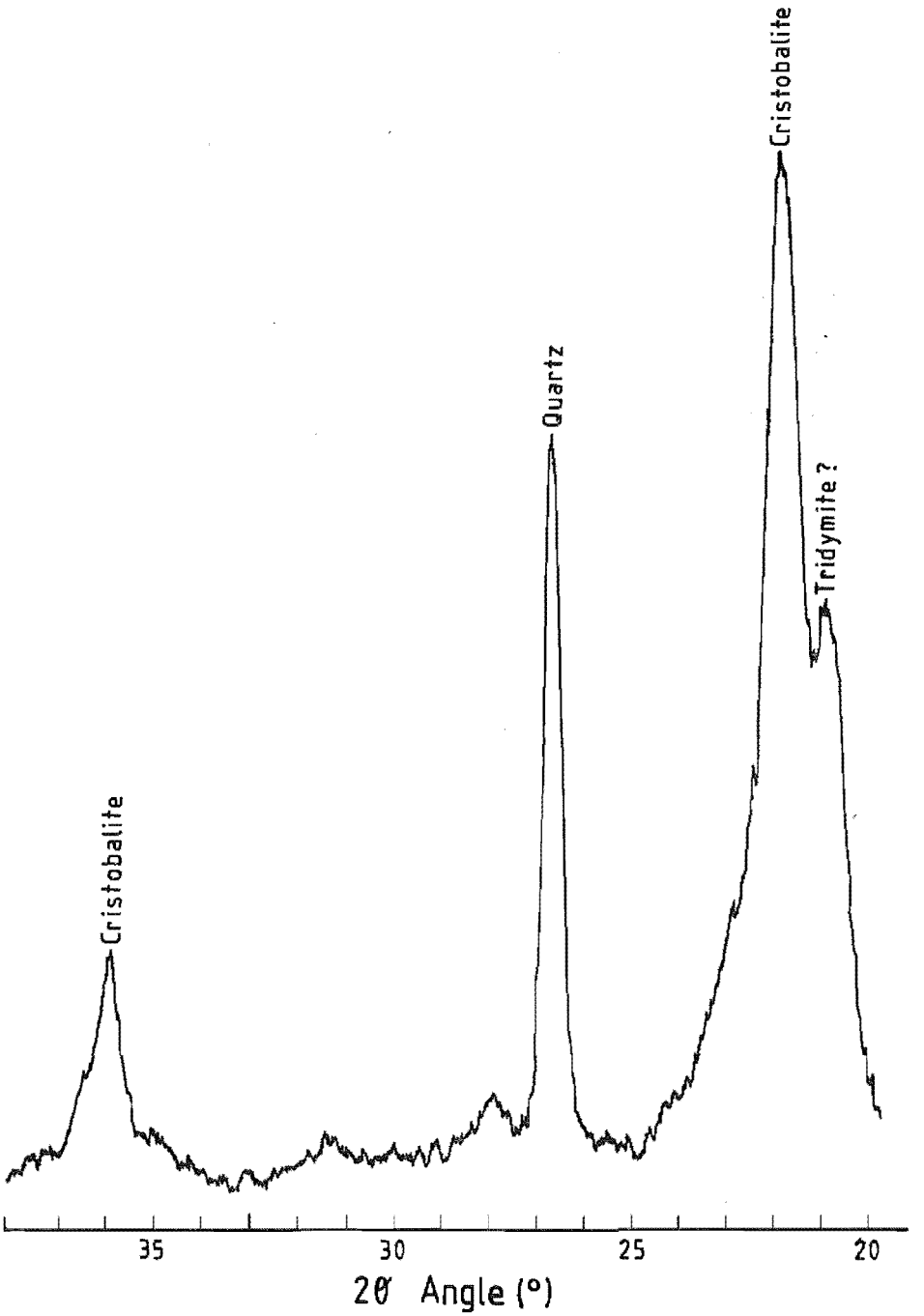

Figure A4.2 Whole rock XRD trace from WC Zone mudstone from Kaikoura Peninsula (sample KP18).

and Iijima (1983) with the range of d-spacings of the cristobalite (101) face, indicate that the material should be classified as opal-CT according to the scheme of Jones and Segnit (1971).

The highly indurated nature of the concretions precluded any attempts to disaggregate samples. Removal of the carbonate cement may have damaged some clay minerals, hence analyses were performed on whole rock powders. The detrital mineralogy consists dominantly of quartz with minor cristobalite and ?feldspar. Micas and clay minerals were not detected, probably because they are in quantities below levels of detection. However, micas can be seen in thin section [see Section A4.2.1].

Despite the micritic appearance of fillings in borings in the concretions at Lab Rocks, they contain only quartz and cristobalite.

A4.2. THIN SECTION PETROGRAPHY

A4.2.1. WOOLSHED CONCRETION (WC) ZONE

Woolshed Formation samples [Figure A4.3] contain a brown to red muddy matrix composed of clay minerals and Fe-oxides. Framework grains consist of very fine sand to silt grains made up of angular to subangular detrital quartz and rare feldspar, thin $\leq$100 μm long mica (muscovite) flakes, plus rare glauconite and rock fragments. Opaque minerals are common, and probably comprise mainly pyrite. A preferred orientation or planar fabric of micas is evident [Figure A4.3], in all sections, resulting in a strial (Lewis 1984, Table 5) fabric. Burrows particularly near the top of the unit are commonly filled with chert [Figure A4.3]. Some chert-filled foraminifera are also present.

Figure A4.4 is from the upper part of the WC Zone, Isolation Creek (20), which is both silica cemented and dolomitic. The silica cement, identified by XRD as quartz and cristobalite, is at least in part cryptocrystalline. The dolomite crystals are very large (up to 1 mm in some cases), dispersed in a matrix, very irregular, and anhedral. These crystals form the 'pod-like' aggregates near the top of the WC Zone at Isolation Creek (20). Although there is no obvious zoning some crystals show undulatory extinction. The extinction pattern can result from intergrown crystals, but in other instances it is definitely within a

single crystal.

The abundance of silt-sized detrital grains in different concretions varies from approximately 1-5% to as high as 10 percent. Some grains, particularly quartz, have dolomite embayments suggesting partial replacement or dissolution. The original mudstone texture seen in the surrounding lithology commonly cannot be seen within concretions. Micas tend to be randomly oriented. Glauconite is extremely rare. Some detrital grains are wedged between dolomite crystals, whereas other grains have been completely engulfed [see Figure A5.3 for similar features].

A4.2.2. CLAVERLEY SANDSTONE (CS) ZONE

The detrital mineralogy is detailed by Morris (1987), who classified the Claverley Sandstone as a subfeldsarenite with some glauconite and lithic fragments.

A4.3. SCANNING ELECTRON MICROSCOPY (SEM)

Detrital grains in the WC Zone consist of micas, and smooth quartz or feldspar [Figure A4.5]. The smooth faceted grains are similar in some respects to those observed in Figure A6.22d. The grains have been identified as quartz or feldspar on the basis of their abundance, and the lack of XRD evidence of any other major detrital mineral. Overgrowths on calcite grains are another possibility, although calcite is rare in the Woolshed Formation. If they were calcite overgrowths they may now be silicified. The cristobalite in the mudstones is probably part of the fine, platy groundmass between the larger grains.

A4.4. GEOCHEMICAL ANALYSES

A detailed characterization of unchertified Woolshed and Claverley sediments is beyond the scope of this thesis, so only a brief survey was carried out for comparison with chert data. Results are summarized in Table A4.1.

A4.4.1. MAJOR ELEMENTS

Compared with the Woolshed Formation, the Claverley Sandstone contains

Figure A4.3 Chertified burrow in Woolshed Formation mudstone, Woodside Creek (CPL = crossed polarized light, sample WC1). There is a definite strial fabric present, particularly in the lower right hand corner of the photograph.

Figure A4.4 Thin section micrograph of chertified, dolomitic WC Zone mudstone, Isolation Creek (CPL, sample IC3). The large, irregular dolomite crystal (d) has disrupted the sediment fabric.

Figure A4.5 SEM micrograph of smooth ?detrital grains, WC Zone mudstone, Kaikoura Peninsula. The material between grains probably contains cristobalite (sample KP17).

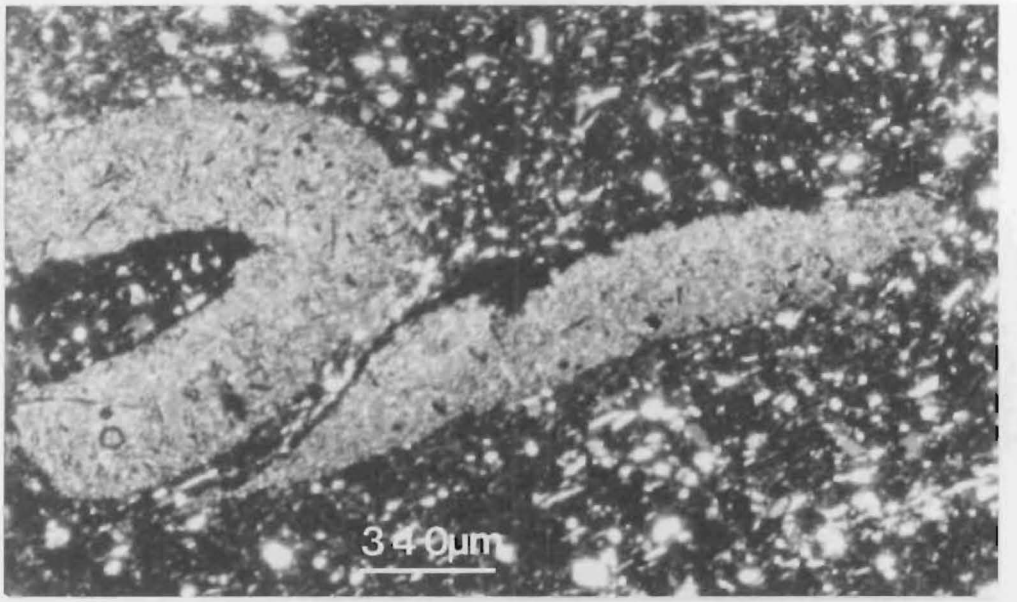

A4.3

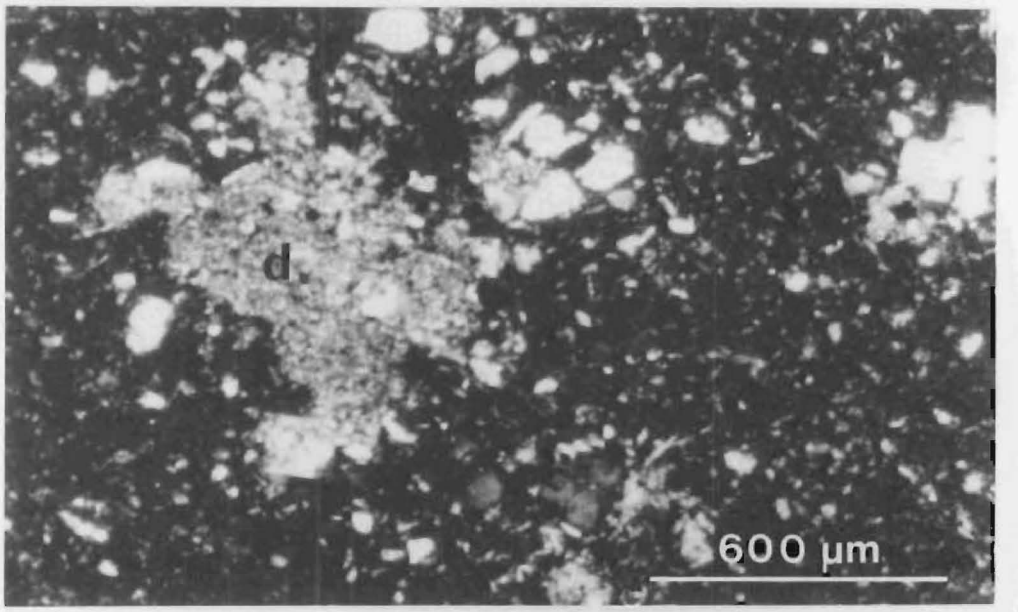

A4.4

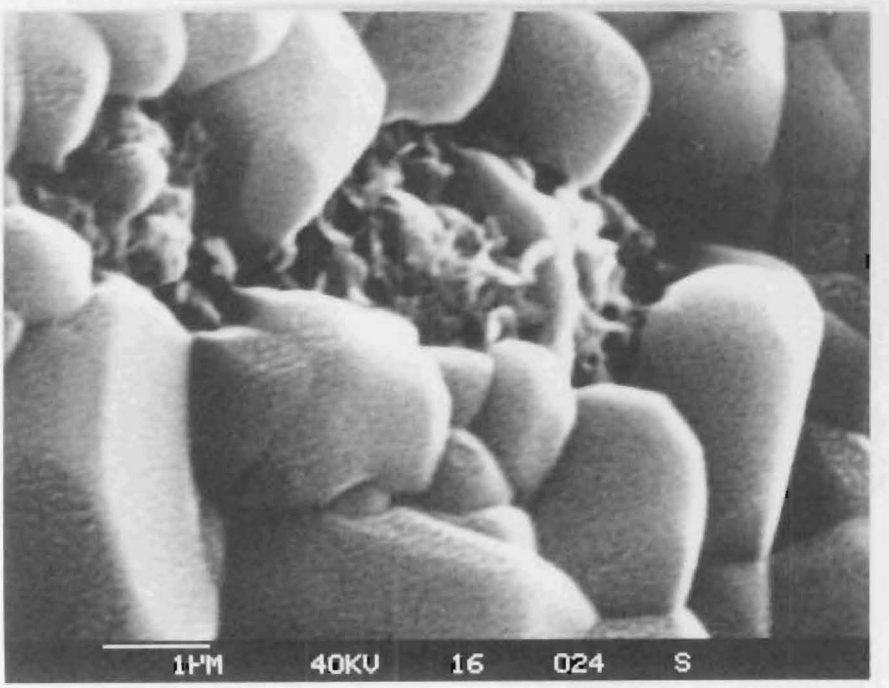

A4.5

Table A4.1 Major (weight% oxide) and trace element (ppm) analyses for Woolshed Formation (N = 15) and Claverley Sandstone (N = 2) samples.

	Woolshed Formation		Claverley Sandstone	
	Mean	S.Dev	Mean	S.Dev
SiO_2	83.84	5.98	89.11	0.61
TiO_2	0.34	0.11	0.19	0.01
Al_2O_3	7.34	2.72	5.51	0.25
Fe_2O_3	1.86	0.88	0.62	0.31
MnO	0.03	0.02	0.03	0.02
MgO	0.99	0.38	0.39	0.18
CaO	0.16	0.09	0.08	0.02
Na_2O	1.28	0.61	1.92	0.10
K_2O	1.36	0.47	1.08	0.11
LOI	2.54	0.86	1.65	0.11
P_2O_5	0.07	0.02	<0.05	-
V	61	29	23	8
Cr	43	13	15	5
Ni	20	16	<5	-
Zn	62	35	14	11
Ga	9	3	5	1
Rb	56	15	26	4
Sr	71	39	50	4
Y	12	6	5	1
Zr	116	46	109	4
Nb	6	1	<5	-
Ba	603	523	303	69
Ce	33	15	13	4
Nd	19	7	<10	-
La	16	9	6	4
Pb	9	2	5	1
Th	4	2	<1	-

more SiO_2, possibly Na_2O and K_2O, but less of every other major element (as a result of the dilution effect by SiO_2). The sandstone also has a lower loss on ignition. Both lithologies have very low P_2O_5 contents, usually at or just above detection limits ($\leq$0.05 weight%).

A4.4.2. TRACE ELEMENTS

The Woolshed Formation contains generally higher concentrations of trace elements than the Claverley Sandstone. In the Claverley Sandstone Th, Nb, Nd, and Ce are at detection limits. Although these elements are of low concentration in the mudstones only Nb is near detection limits. Barium concentrations in Woolshed Formation sediments are similar to those in the Claverley Sandstone.

APPENDIX 5

DESCRIPTION OF PETROGRAPHY, MINERALOGY, AND GEOCHEMISTRY OF DOLOMITES

A5.1. X-RAY DIFFRACTION MINERALOGY

A5.1.1. DIFFRACTION MINERALOGY OF DOLOMITE

The dominant carbonate mineral in concretions is dolomite. The dolomite (104) reflection is usually sharp at 2.90-2.89Å [Figure A5.1]. The 2.19Å reflection is also relatively sharp. Reflections at 2.41Å, 2.54Å, 2.67Å and 3.69Å all show limited line broadening. Samples from Dart (30) and Muzzle (32) Streams are exceptions containing calcite reflections at 3.03Å, 3.87Å, 2.09Å, 1.91Å, and 1.87Å. At Dart Stream (30) calcite is the dominant carbonate mineral in concretions. The 3.03Å peak indicates that they are low-Mg calcites (Chave 1952, Goldsmith *et al*. 1961). Isolation Creek (20) concretions although mainly dolomitic, also contain some calcite.

Despite their different occurrence and texture, the dolomite reflections of samples in the CD Zone and the LCM Subzone are similar in shape to those encountered in WC Zone concretions.

A5.1.2. DOLOMITE ORDERING

The degree of cation ordering can be determined from the (0012) and (015) reflections. The latter peak is used in this study and compared with the work of Goldsmith and Graf (1958, Figure 2). Increased order results in a lowered d-value; that is an increase of half a degree 2θ (Goldsmith and Graf 1958). In addition, progressive ordering increases the (015) peak height relative to the (110) and (006) peaks on either side (Goldsmith and Graf 1958, Gaines 1974). Reflections from samples in this study, compared with those shown in Goldsmith and Graf (1958, Figure 2), indicate a moderate to high degree of ordering.

A5.2. THIN SECTION PETROGRAPHY

A5.2.1. WOOLSHED CONCRETION (WC) ZONE

The detrital composition of the concretions is described in Section A4.2.1.

Dolomite in the concretions comprises an intergrown mesh of crystals

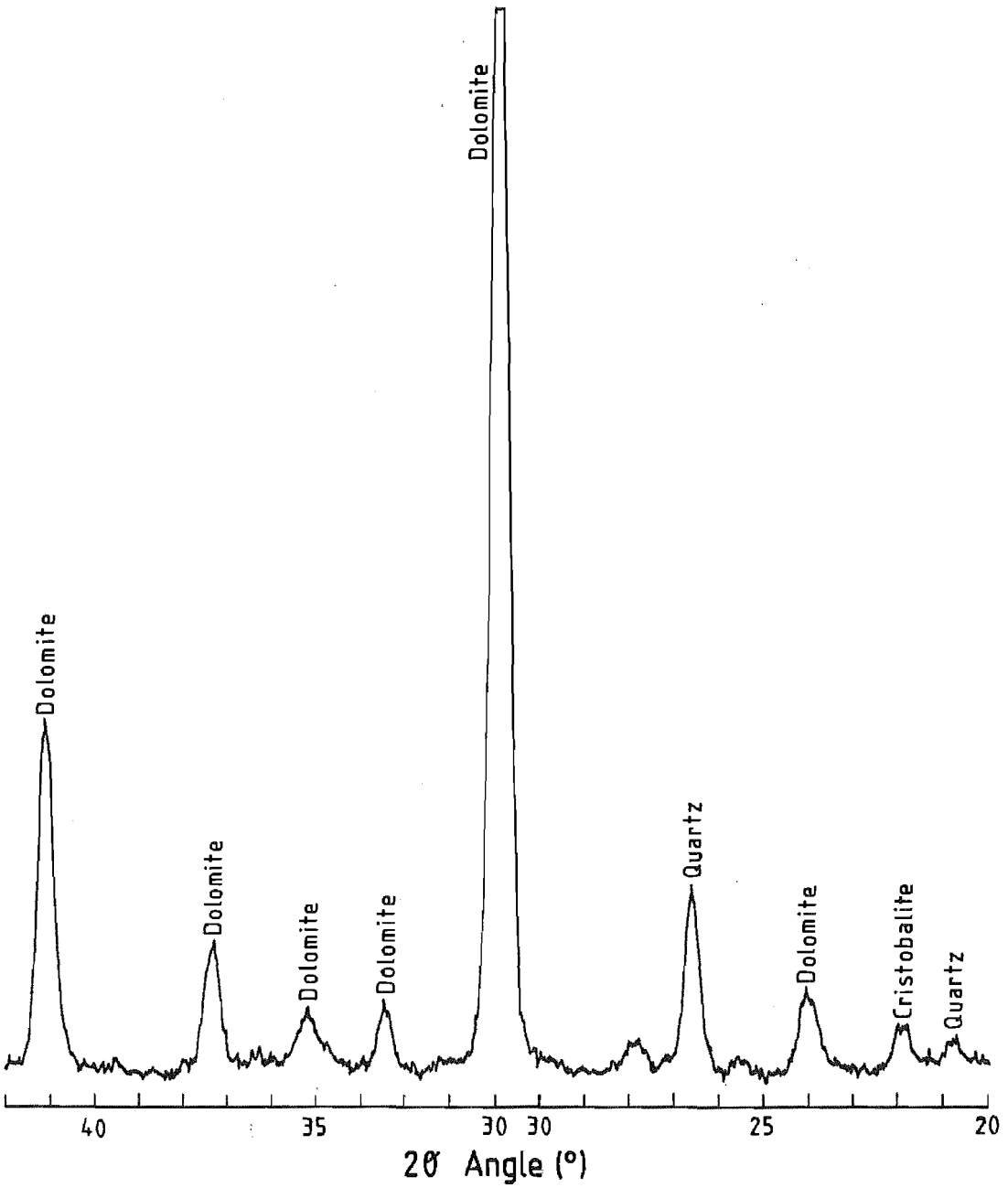

Figure A5.1 Dolomite XRD trace from a WC Zone concretion, South Bay, Kaikoura Peninsula (sample KP19).

Figure A5.2 Thin section micrographs of a dolomite concretion in the WC Zone, Lab Rocks, Kaikoura Peninsula (sample KP3).
(a) Concretion centre (CPL, sample KP3/3).
(b) Concretion margins (CPL, sample KP3/10).
(c) Inclusions (PPL, sample KP3/10). Most inclusions (arrows) are fluid filled, although pyrite may also be present.

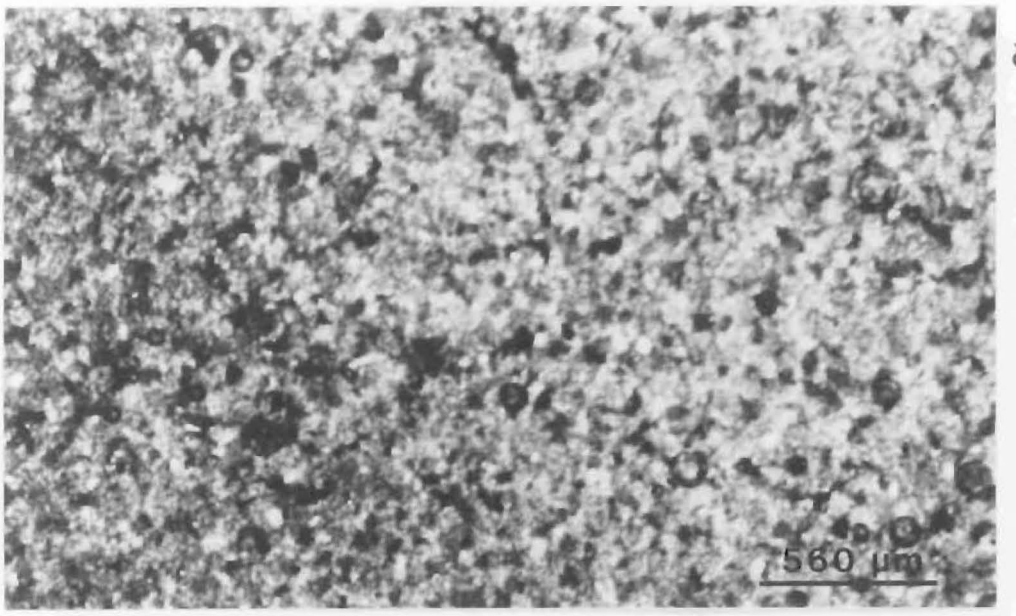

a

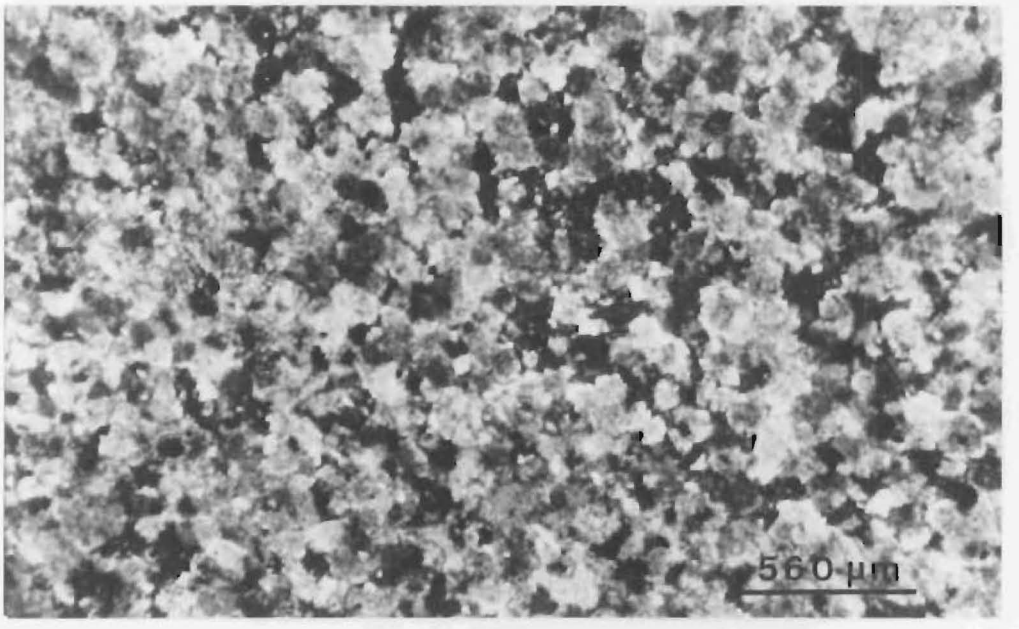

b

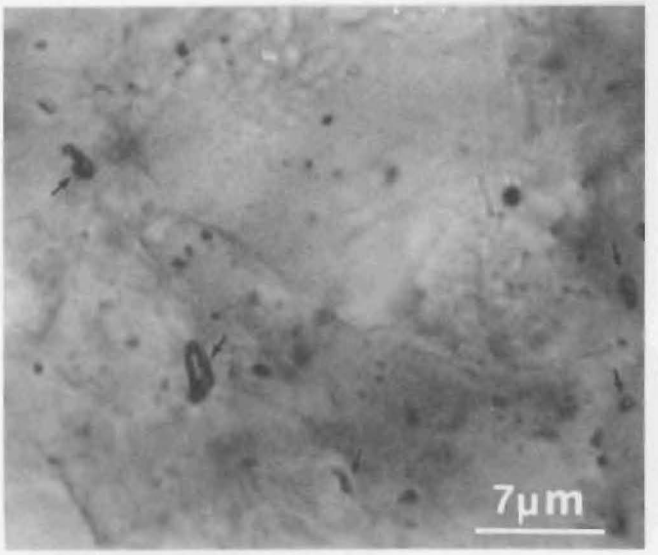

c

[Figure A5.2]. In some cases individual crystals cannot easily be resolved making textural classification difficult. Textures and crystal sizes of dolomites vary within and between concretions. One detailed cross section was obtained from a broken concretion (KP3) at Lab Rocks (4). Dolomite crystals at the centre of this concretion measure ≤20 μm, [Figure A5.2a] and are anhedral, whereas at the outer margin crystals are generally larger (of the order of 100-150 μm) and tend to be more subhedral [Figure A5.2b]. Thus the texture observed may be dependent upon the position sampled within the concretion. As the bulk of samples obtained are from the outer parts of concretions the observed texture and crystal size ranges may not necessarily be representative of concretions as a whole. Crystal sizes in all concretions sampled do not usually exceed 150 μm. Inclusions are found in most crystals; some are opaque minerals but most appear to be fluid [Figure A5.2c].

A5.2.2. CLAVERLEY SANDSTONE (CS) ZONE

Dolomite in the sandstone from Waipapa Bay (10,11) consists of disseminated, up to 500 μm across, subhedral to anhedral rhombic crystals [Figure A5.3]. Most are matrix supported textures, but crystal supported textures occur locally. Where subhedral crystals are intergrown straight compromise boundaries (Bathurst 1975) are common. Anhedral crystals produce very irregular intercrystalline boundaries. No concentric zoning is evident in plane polarized light (PPL) or crossed polarized light (CPL), but in CPL crystals display a segmental extinction which approximately coincides with crystal growth sectors (henceforth referred to as sector-like extinction). Both pyrite and fluid inclusions are distributed throughout crystals in no recognizable pattern. The distribution of relatively inclusion-rich and inclusion-poor crystals is apparently random. Crystals rich in inclusions may be adjacent to, or intergrown with, inclusion poor examples.

The matrix around dolomite crystals consists of silt to very fine sand (subfeldsarenite, Morris 1987), and silicified clay sized material. Detrital grains are generally found at the margins of dolomite crystals. Detrital grains may also be contained within dolomite crystals [Figure A5.3]. Some detrital grains adjacent to or within dolomite crystals show some corrosion, in the form of dolomite embayments.

A5.2.3. BASAL CHERT (BC) ZONE

Dolomite at the base of the BC Zone at Isolation Creek (20) consists of pods of crystals; the crystals are similar to those in Figure A4.4]. Dolomite in the lowermost BC Zone at Mt Alexander (8) consists of disseminated rhombs rather than the aggregates seen at Isolation Creek. The rhombs measure 200-300 μm and are dominantly subhedral. Under CPL most crystals show straight extinction. Most crystals have margins that are serrated or ragged. Serrated margins appear to be governed by crystal cleavage, whereas ragged margins have an irregular appearance that may be the result of minor dissolution. As in the CS Zone, inclusions are dominantly fluid, of similar size and are dispersed throughout crystals.

The matrix consists dominantly of chert (i.e. microcrystalline or cryptocrystalline quartz), along with pyrite and detrital quartz and micas.

A5.2.4. CHERT AND DOLOMITE (CD) ZONE

Dolomite in the CD Zone at Isolation Creek (20), Mead (24) and Limburn (26) Streams is similar. Crystals are dominantly subhedral, measure 300-400 μm across, and show a crystal-supported fabric [Figure A5.4]. Euhedral crystals are common in some thin sections. Intercrystalline boundaries are commonly arcuate or irregular, although straight compromise boundaries are locally evident. Dolomite rhombs disseminated in chert nodules are anhedral to subhedral, often with serrated crystal margins. Disseminated crystals are generally smaller than those in dolomite beds, with the size difference being as much as 50% in some cases.

In PPL, zonation is delineated by inclusion patterns [Figure A5.4]. Crystal centres are generally inclusion rich, and margins are inclusion poor. Such crystals are termed cloudy-centre clear-rim (CCCR) dolomite (Murray 1960). Rhombs disseminated in chert display the same zonation. However, some disseminated dolomite from the top of the CD Zone at Limburn Stream appears to have three zones [Figure A5.5].

The intercrystalline matrix of dolomite beds comprises quartz chert (<20 μm) containing opaque minerals (commonly pyrite), minor detrital quartz, and mica. Although some detrital or opaque minerals occur within

Figure A5.3 Dolomitic chertified sandstone, BC Zone, Waipapa Bay (CPL, sample WB13). Note the presence of detrital grains usually at crystal margins, although some may be contained within crystals.

Figure A5.4 CCCR dolomite, CD Zone, Isolation Creek (PPL, sample IC11). Note the finely disseminated pyrite grains (some of which are arrowed) in the intercrystalline chert matrix.

Figure A5.5 Rhombic dolomite crystal surrounded by chert, CD Zone, Limburn Stream (CPL, sample LS8). The inclusion-rich centre is surrounded by an inclusion-poor zone. Some inclusions are also concentrated at crystal margins. Above the dolomite crystal is a quartz filled foraminifer chamber (f). Pyrite is common in the chert.

Figure A5.6 Thin section micrograph showing the relationship between inclusion and extinction patterns in a CCCR dolomite, CD Zone, Mead Stream (CPL, sample MS4).

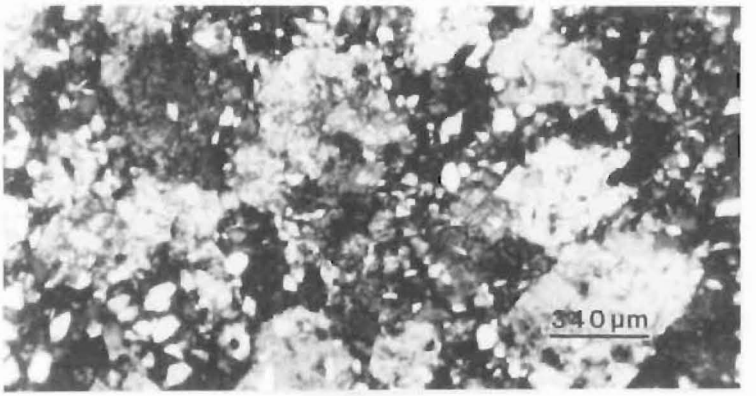

A5.3

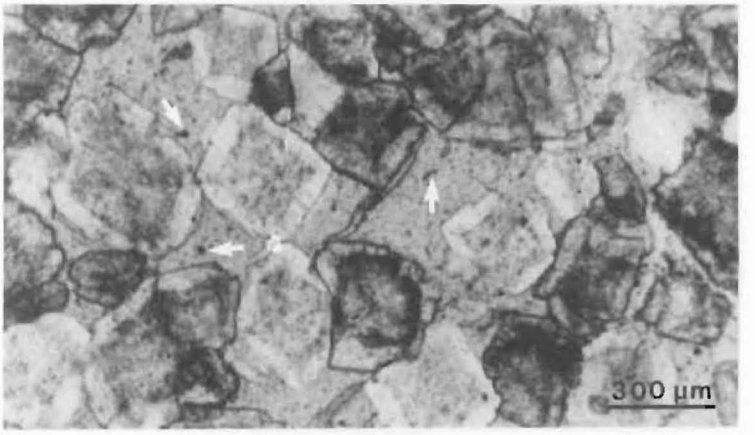

A5.4

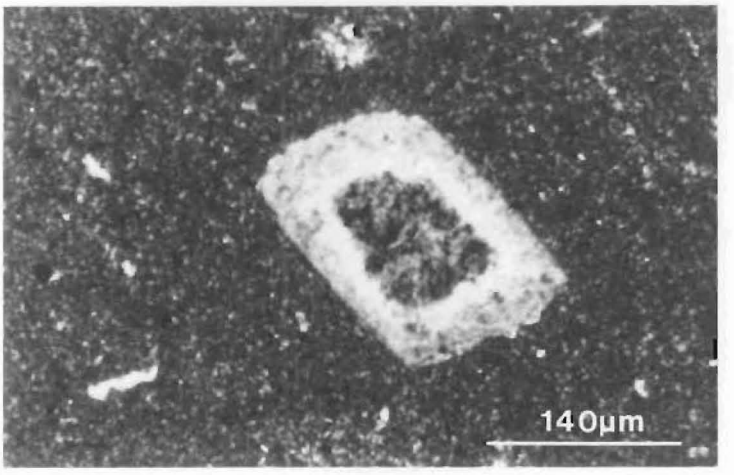

A5.5

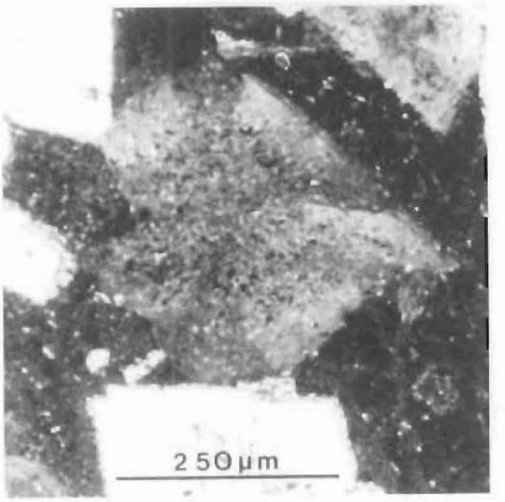

A5.6

dolomite crystals, they are more commonly found at crystal margins or in the matrix. Some foraminiferal chambers are filled with coarse quartz. Near the top of the CD Zone at Mead Stream (24), the matrix comprises predominantly micrite, with quartz chert filling pores and foraminiferal chambers.

Waipapa Bay (10) and Wharekiri (9) Stream dolomites contain more detrital material than those described above, although dimensions of crystals are the same. Waipapa Bay (10) samples lack the concentric zoning of inclusions, and have considerably fewer inclusions than other CD Zone dolomites. The detrital component in the Wharekiri (9) samples is less than in Waipapa Bay samples. At both localities detrital grains can be seen within crystals and at crystal margins.

Wharanui Point (15) samples tend to be subhedral to euhedral, with a mixture of irregular and some straight compromise boundaries where crystals are intergrown. Although predominantly crystal-supported, matrix-supported textures are common. Crystal dimensions are of the order of 300-400 μm. The volume of inclusions is much reduced compared with dolomites from inland sections. No CCCR dolomite is found. Where inclusions are sufficiently abundant they are arranged in planes, diagonally across crystals. The inter-crystalline matrix is primarily micrite with some quartz chert, minor detrital quartz, and micas. Voids in the matrix are generally filled with quartz chert. In matrix-supported samples most foraminifera are filled with micrite and sparry calcite.

Dolomite Extinction Patterns

All dolomite crystals in the CD Zone show to a greater or lesser extent a sector-like extinction pattern [Figure A5.6]. Dark zones of extinction are separated by lighter zones that crudely approximate crystal growth faces. Inclusions do not affect the extinction pattern. Not all crystals exhibit the complete pattern, as the orientation of the crystal with respect to the thin section seems to determine how much of the pattern is observed.

Dolomite Inclusion Patterns

Inclusions in dolomite crystals are dominantly translucent, with minor

Figure A5.7 Fluid inclusions in dolomite crystals (PPL). All micrographs are at the same scale.
(a,b) Inclusions in CD Zone dolomite (sample IC11).
(c,d) Inclusions in LCM Subzone dolomite (sample MS28). Although inclusions are generally cylindrical (see a,b), irregular shapes are also common with some forming aggregates as in (d). Large dark patches may be pyrite.

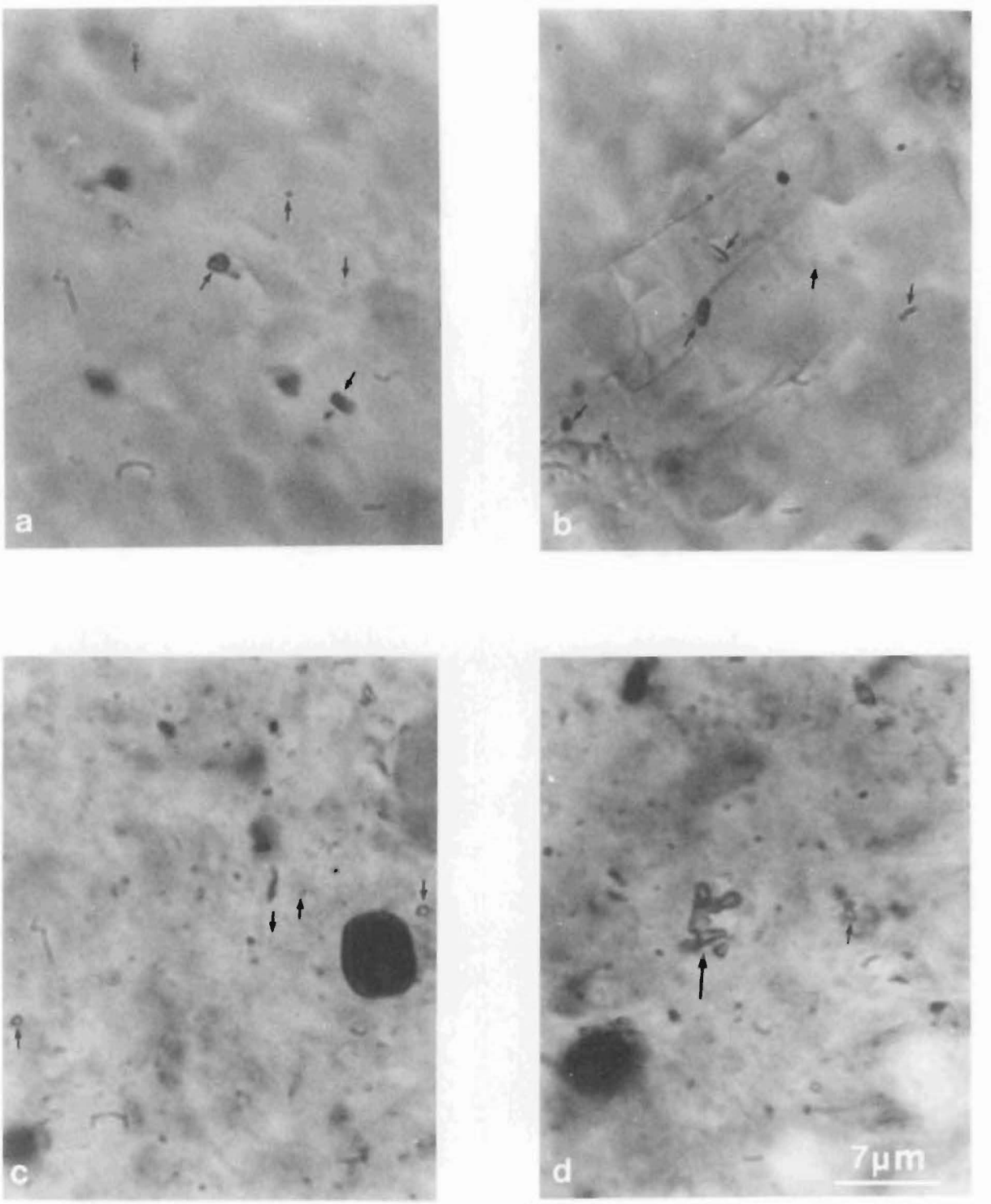
a
b
c
d
7µm

sulphides [Figure A5.7]. The translucent inclusions contain fluid in which air bubbles are occasionally visible. Inclusion morphologies are mainly cylindrical [Figure A5.7a,b,c], occasionally they form 'aggregates' [Figure A5.7d]. More irregular shapes may also be seen. In some crystals inclusions appear to be oriented parallel to cleavages, although the majority display no preferred orientation. In PPL about half the inclusions appear red-pink and the rest are blue, due probably to dispersion effects.

A5.2.5. LOWER CHERT MEMBER (LCM) SUBZONE

The dolomite crystals within the Lower Chert Member itself tend to be slightly larger (approximately 400 μm) than those in the CD Zone, and generally crystal-supported. Crystals are generally subhedral, sometimes anhedral, with margins that are irregular on the scale of a few microns. Margin irregularities are most pronounced in samples from Mead Stream (25) where they can be very ragged [Figure A5.8]. As in the chert [Section A6.2.5] there is a greater abundance of detrital material than in the CD Zone. Detrital grains tend to be concentrated between and at the margins of dolomite crystals, but rarely within crystals. Chert is the dominant intercrystalline material. Under PPL abundant finely disseminated pyrite is visible.

Despite careful examination of both CD Zone and LCM Subzone dolomite thin sections, only one example showed the effect of microfossils on dolomite crystal growth [Figure A5.9]. Usually such microfossils are very small and restricted to the intercrystalline matrix. Despite having undergone some alteration itself, the foraminiferal test has inhibited the growth of three dolomite crystals.

Dolomite Extinction Patterns

The sector-like extinction patterns observed in CD Zone dolomite is better developed in LCM Subzone dolomite crystals [Figure A5.8b,d]. Light and dark zones of extinction coincide in part with the inclusion patterns. Where planes of inclusions are divided into two, and are contained within a single extinction segment, the extinction between the two planes is no different from the rest of the segment.

Figure A5.8 Thin section micrographs showing the relationship between planar inclusion and extinction patterns in LCM Subzone dolomite crystals, Mead Stream (sample MS25). The intercrystalline matrix is chert.

(a) PPL micrograph.

(b) CPL micrograph of (a). Note the raggedness of crystal margins (arrows) common to LCM Subzone dolomite crystals.

(c) PPL micrograph. Examples of pyrite are denoted with the letter 'P'.

(d) CPL micrograph of (c). Silt sized detrital grains are common; some examples are arrowed.

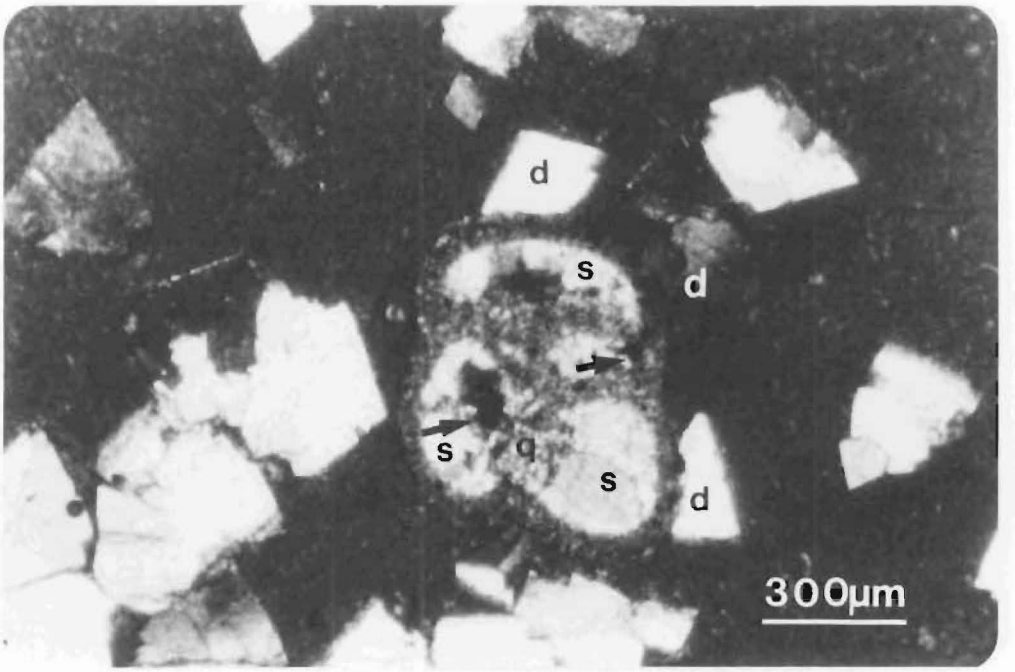

Figure A5.9 Foraminifer in the basal dolomite bed of the LCM Subzone, Branch Stream (CPL, sample BS5). Test walls contain micrite, pyrite and some microspar. Chambers are filled with sparry calcite (s), microquartz (q) and pyrite (arrows). Growth of dolomite crystals (d) has been inhibited by the foraminifer.

Dolomite Inclusion Patterns

The ubiquitous CCCR dolomite of the CD Zone is absent from dolomite beds associated with or within the Lower Chert Member. Inclusions in Mead Stream (25) samples are arranged in diagonal planar patterns [Figure A5.8a,c]. At crystal centres there is often a square shaped aggregate of inclusions. At higher magnification, some planar patterns are constructed of two separate planes of inclusions. Unfortunately, crystal orientation with respect to the plane of the thin section determines how much of the pattern is visible in each crystal. The composition of the inclusions is the same as in the CD Zone [Figure A5.7c,d], with sulphides constituting a minor proportion. There appears to be no preferential orientation of inclusions.

The inclusion patterns described above are best developed in the Mead Stream (25) area and within the Lower Chert Member proper, as opposed to the dolomite immediately above and below which is included in the LCM Subzone [see Section A2.6 and 2.2.8]. The paucity of inclusions in dolomite from the Lower Chert Member at Dee Stream makes discernment of patterns tenuous. However, dolomite from above the Lower Chert Member (but included in the LCM Subzone) contains definite planar patterns. Although somewhat ambiguous, there is a predominant planar pattern in LCM Subzone dolomite from Branch Stream (29).

A5.3. CATHODOLUMINESCENCE PETROGRAPHY

Cathodoluminescence petrography was undertaken in an attempt to clarify the relationship between inclusion and extinction patterns in CD Zone and LCM Subzone dolomites. In addition, it was hoped that it would provide more information on the growth history of dolomite crystals. Concretionary dolomites were not studied because of their small crystal size and the limited resolution of the available luminescence microscope. Within any given polished section the luminescence pattern is the same for all crystals irrespective of orientation.

A5.3.1. CAUSES OF CATHODOLUMINESCENCE

Cathodoluminescence in carbonates is thought to be activated mainly by Mn^{2+} and quenched by Fe^{2+} (Sommer 1972a, Nickel 1978, Pierson 1981,

Fairchild 1983, Machel 1985). As little as 100 ppm Mn^{2+} is required to activate luminescence, whereas Fe^{2+} begins to quench luminescence at concentrations of the order of 10,000 ppm. Dolomites containing less than 100 ppm Mn^{2+}, or more than 15,000 ppm Fe^{2+} will not luminesce (Pierson 1981). More recent evidence suggests minimum values of 20-40 ppm Mn^{2+} for luminescence activation, and approximately 30 ppm Fe^{2+} for luminescence quenching (Machel 1985). Precisely how Fe^{2+} quenches luminescence is not fully understood (Pierson 1981). The Fe^{2+}, and perhaps the Mn^{2+}, are thought to occupy Mg^{2+} sites in the dolomite crystal lattice (Sommer 1972a,b, Pierson 1981).

There appears to be no universal relationship between cathodoluminescence intensity and Mn^{2+} concentration. Concentrations inferred from luminescence depend on the instrument set-up and therefore are only relative (Machel 1985). As pointed out by Frank *et al.* (1982), luminescence intensity is controlled by Fe/Mn ratios rather than absolute values. In addition there are other factors that affect luminescence. Elements such as the rare earths and Zn^{2+} may also be activators. The effect of luminescence sensitizors must also be considered. Sensitizors promote the luminescence of activators. Thus the observed colours could correspond to associations of trace elements (be they activators, sensitizors, or quenchers) and/or lattice defects, rather than one activator and quencher. Assignment of colours to particular trace elements or relative proportions thereof is not always possible without suitable spectroscopic analysis (Machel 1985). Commonly, Fe and Mn are considered to the exclusion of other elements, which may in part be due to lack of adequate data.

A5.3.2. CHERT AND DOLOMITE (CD) ZONE

Where inclusions are absent, luminescence patterns, or zones, in dolomite crystals are concentric and parallel to crystal margins. In inclusion-rich parts of the crystal there is no distinct pattern at all [Figure A5.10]. The marginal concentric zonation parallels all faces on crystals regardless of crystal shape, or the presence of re-entrant angles and other crystal facets. Some crystals display an almost complete absence of any pattern. No relationship is apparent between the presence and absence of concentric luminescence zonation and stratigraphy.

Figure A5.10 Cathodoluminescence in CD Zone dolomite crystals from Isolation Creek (sample IC13). Concentric luminescence is visible only in the inclusion-free margins.
(a) PPL micrograph.
(b) Cathodoluminescence micrograph.

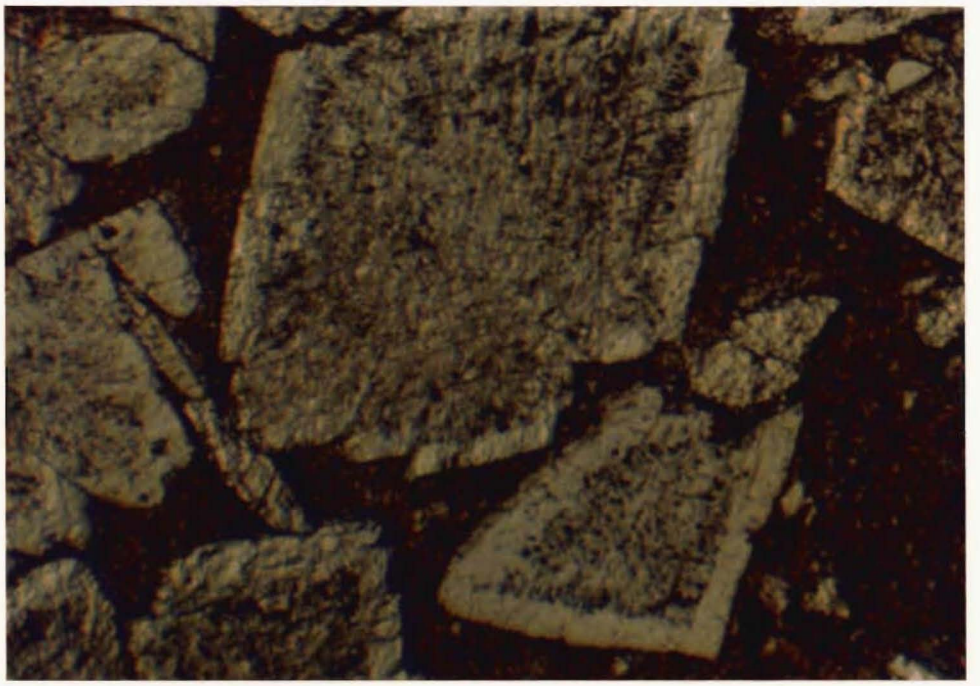

a

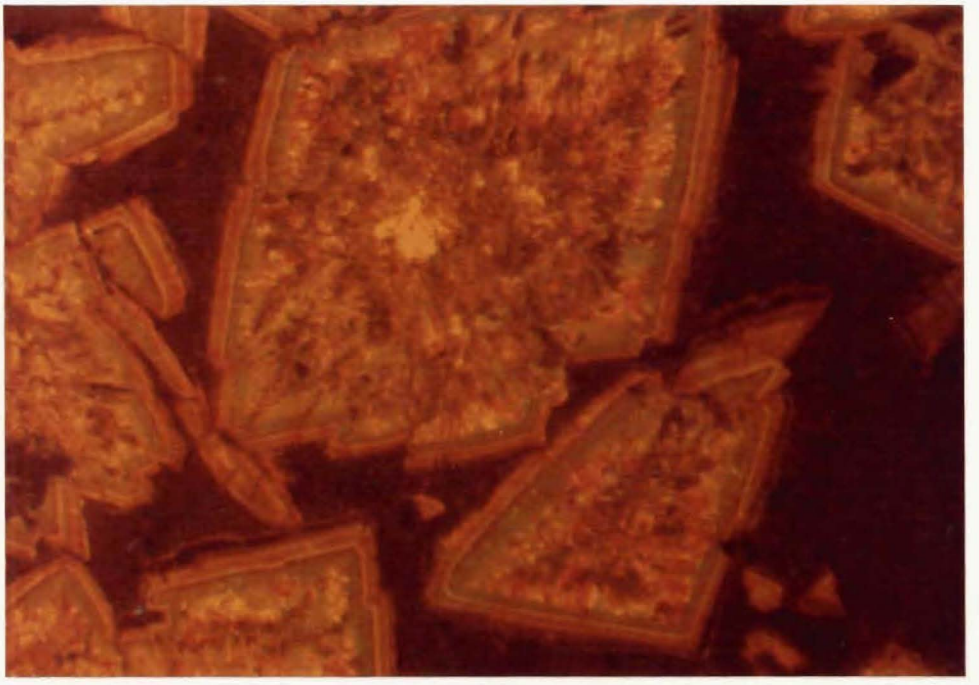

b

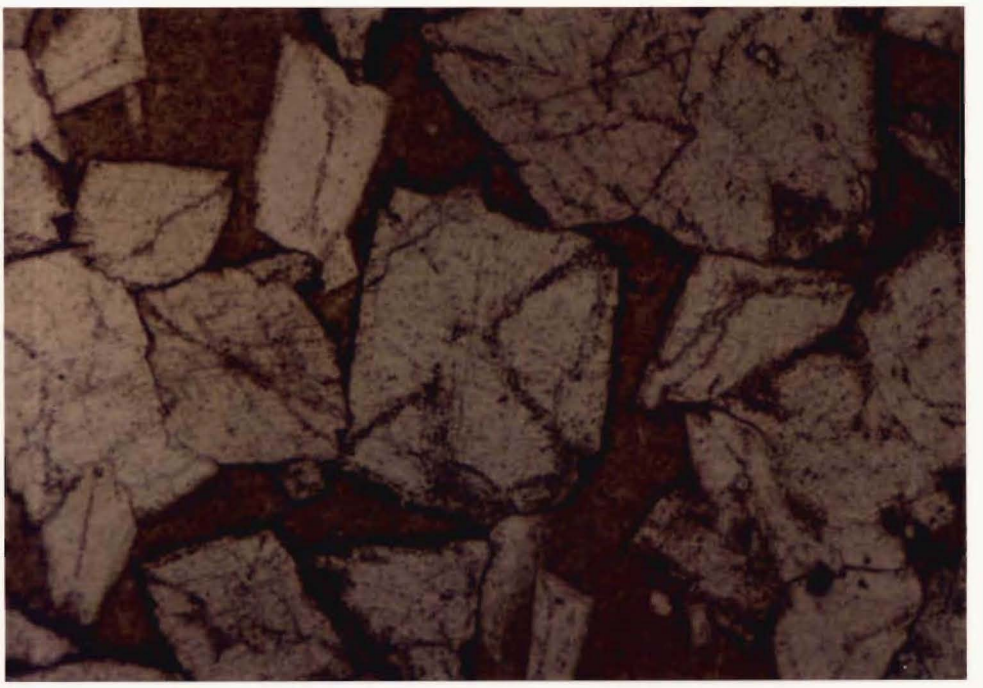

a

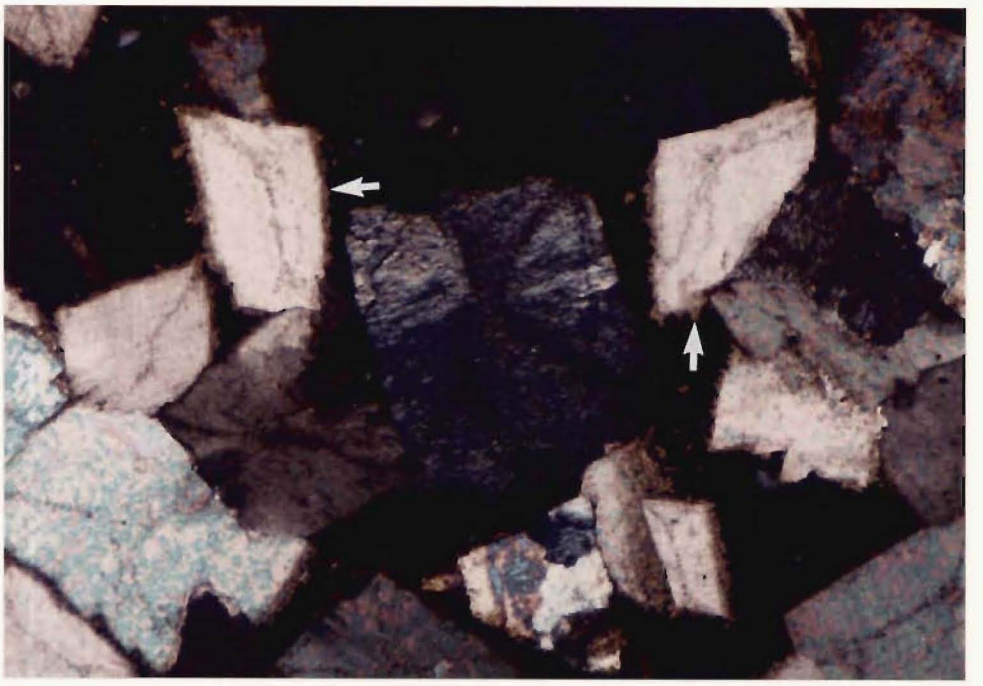

b

340μm

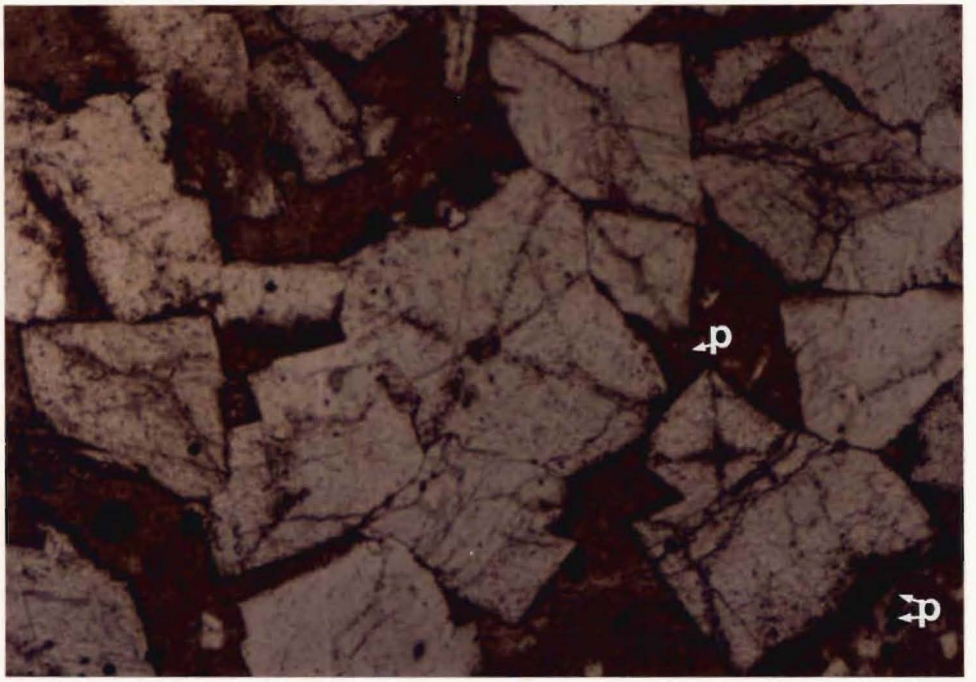

c

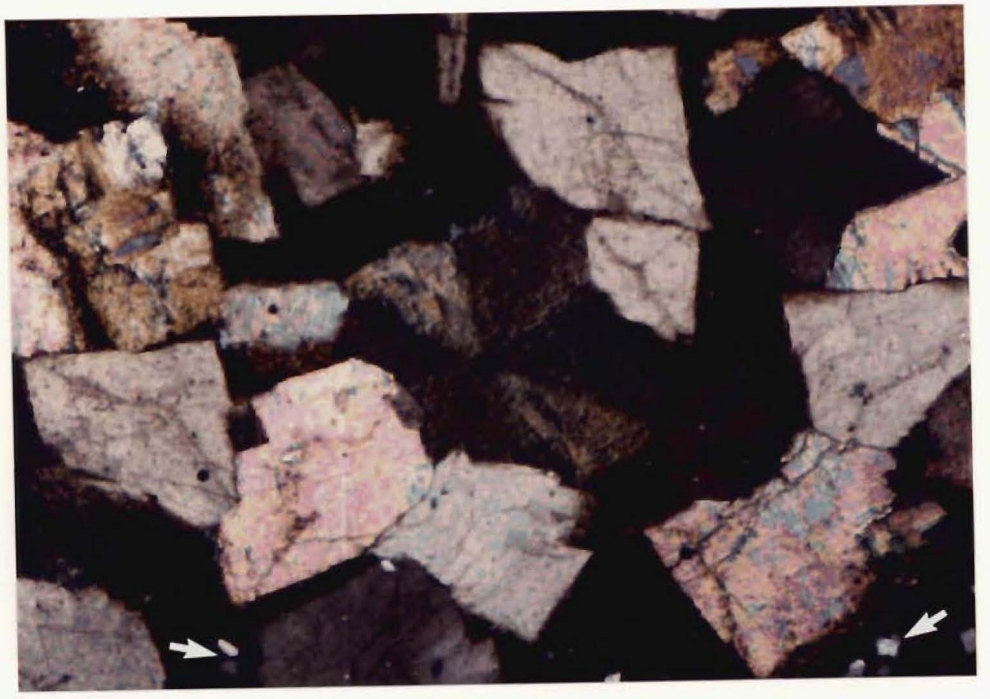

d

340µm

A5.3.3. LOWER CHERT MEMBER (LCM) SUBZONE

Some form of concentric zonation is apparent in all dolomites in the LCM Subzone. The zonation may be weakly, moderately, or well developed. As in the CD Zone there is no recognizable stratigraphic or geographic relationship with zonation patterns.

The two most weakly developed luminescence patterns are shown in Figure A5.11. The crystal in Figure A5.11a is from a dolomite bed about 12 m below the Lower Chert Member. The brighter centre is surrounded by a barely detectable darker zone, and a brighter margin. Figure A5.11b is a crystal from within the Lower Chert Member. The bulk of the crystal comprises a darker central zone surrounded by a slightly brighter zone. Planar inclusion patterns and intergrowth with other crystals disrupt the luminescence zonation [Figure A5.11b].

Moderately developed patterns of high luminescence intensity [Figure 5.12] show much better definition between light and dark zones than is evident in weakly developed patterns. In Figure A5.12a the bright centre has a different shape to the present crystal margins, whereas the multiple concentric zonation in Figure A5.12b parallels crystal faces.

Figure A5.13 shows a very well developed concentric zonation, parallel to crystal faces, but disrupted by inclusions. There is some evidence that growth faces were initially different. One internal face is not parallel to the present crystal margin. Intergrowth of a small 'parasitic' crystal on the right hand face terminates some of the zonation. Within the parasitic crystal, zonation is crystal face parallel.

A5.4. SCANNING ELECTRON MICROSCOPY (SEM)

A5.4.1. WOOLSHED CONCRETION (WC) ZONE

Concretionary dolomite crystals are quite different from Amuri Limestone Group dolomites [Section A5.4.2.]. Rhombic forms although still recognizable, are much finer and more intergrown. In many cases the boundaries between the dolomite crystals and surrounding matrix are difficult to detect [Figure A5.14a,b,c]. Commonly the dolomite is only recognized on the basis of the presence of rhombohedral cleavage patterns

Figure A5.11 Two examples of weakly developed cathodoluminescence zonation in LCM Subzone dolomite crystals.
(a) High intensity luminescence with a slightly darker band indicated by the arrows (Limburn Stream, sample LS10).
(b) Low intensity luminescence. The arrows indicate where intergrowth with another crystal has interfered with luminescence banding. Planar inclusion patterns also disrupt the luminescence pattern (Mead Stream, sample MS29).

Figure A5.12 Two examples of moderately developed cathodoluminscence zonation in dolomite crystals from the LCM Subzone, Dee Stream.
(a) High intensity luminescence, basal dolomite bed (sample DS15).
(b) Low intensity luminescence, upper LCM Subzone, above the Lower Chert Member (sample DS10). The blue luminescence is detrital quartz.

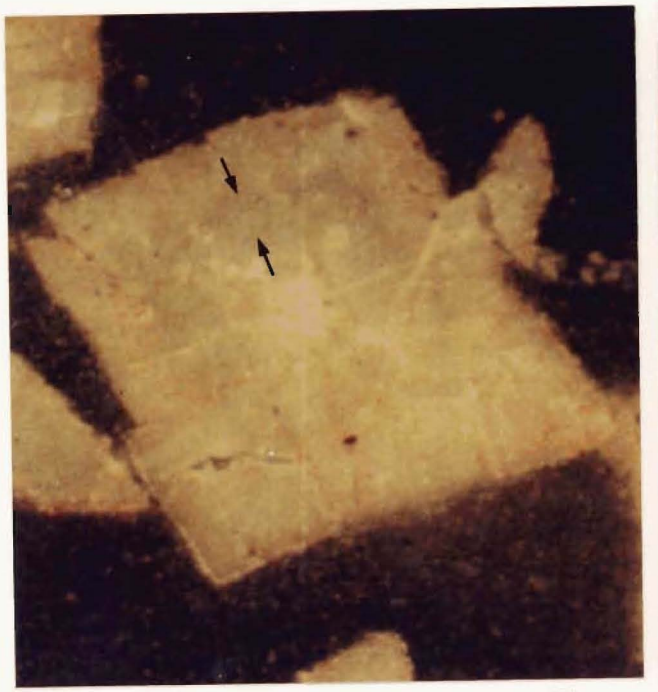

a

A5.11

b

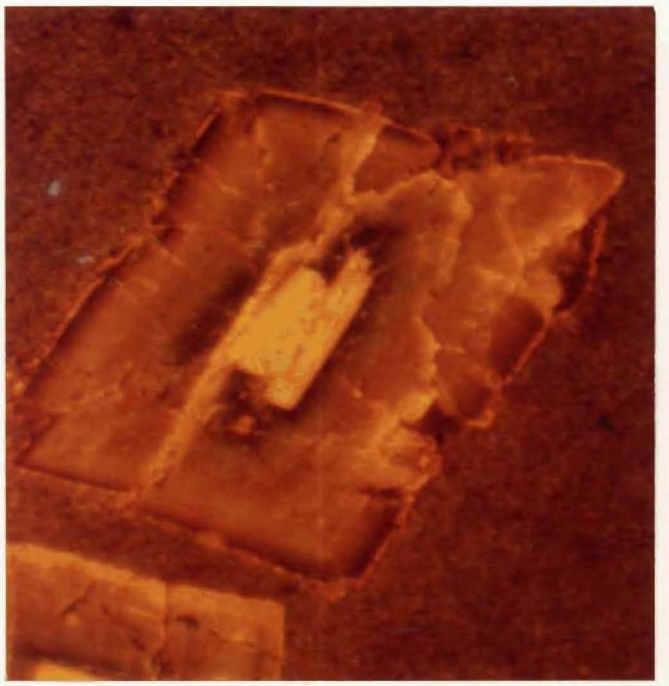

a

A5.12

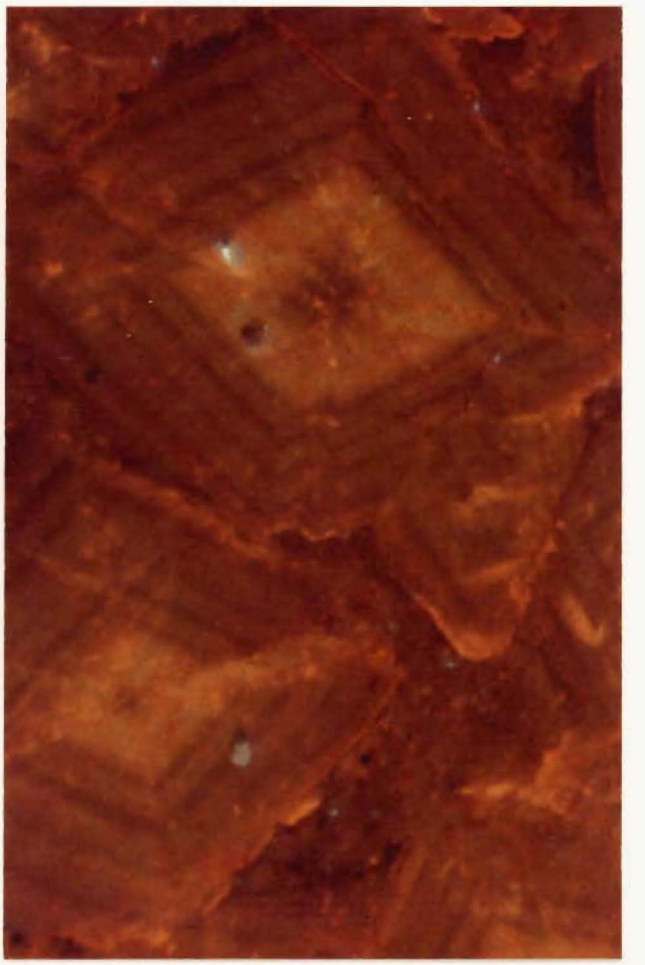

b

Figure A5.13 Well developed cathodoluminescence zonation in dolomite crystals from the LCM Subzone, Mead Stream (sample MS26). Note the dislocations (D) in crystal faces and re-entrant angles (R) at crystal apices. The arrow indicates an episode on non-crystal-face-parallel growth.

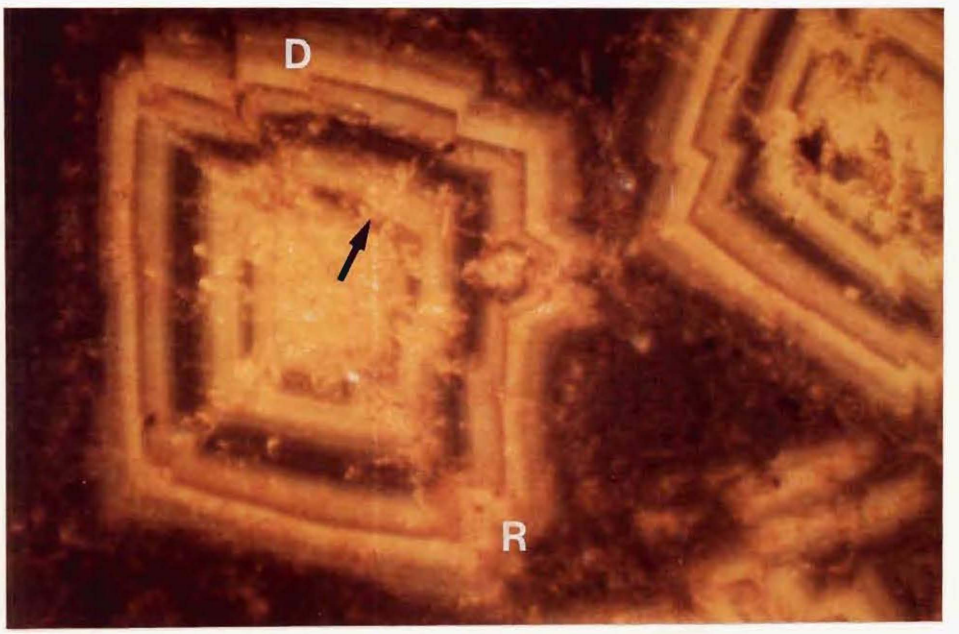
D
R

Figure A5.14 SEM micrographs of examples of concretions from the WC Zone.
(a,b,c) Intergrown dolomite crystals in mudstone matrix. In such examples discernment of intercrystalline (dolomite) boundaries is difficult (sample KP17, South Bay, Kaikoura Peninsula).
(d) Example of intergrown rhombic dolomite crystals. The box in (c) delineates the field of view.
(e,f) Foraminifer test preserved in a concretion, Lab Rocks, Kaikoura Peninsula (sample KP3/8). The box in (e) shows the field of view in (f). Despite fracturing (e), the calcite crystals appear relatively unaltered (f).

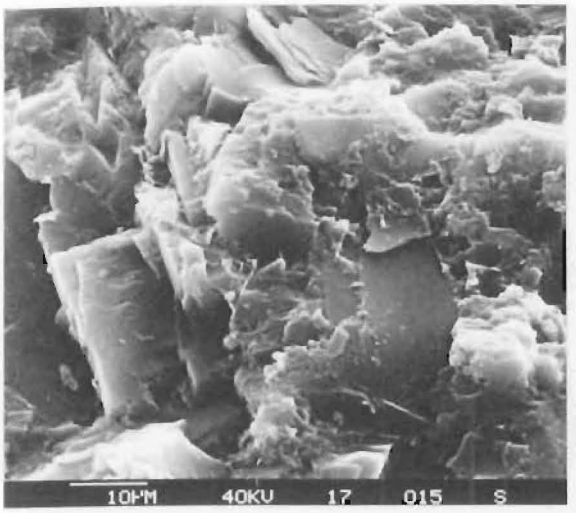
10µM 40KV 17 015 S

a

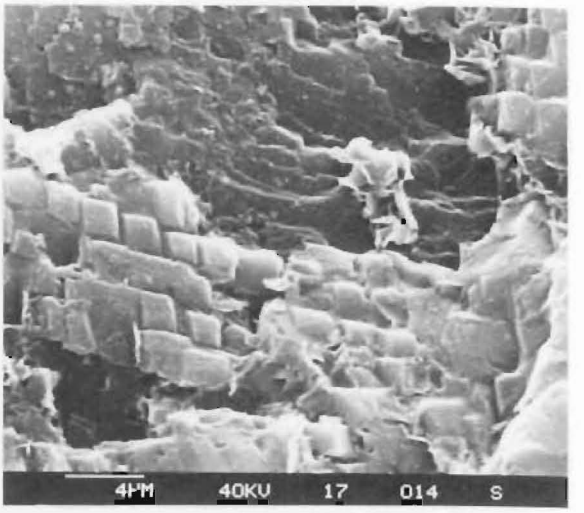
4µM 40KV 17 014 S

b

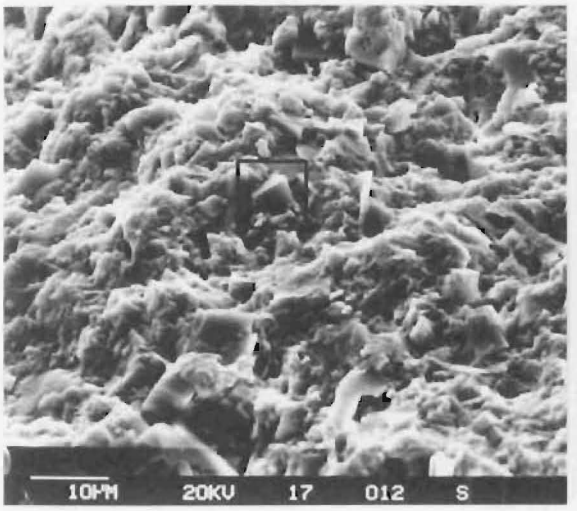
10µM 20KV 17 012 S

c

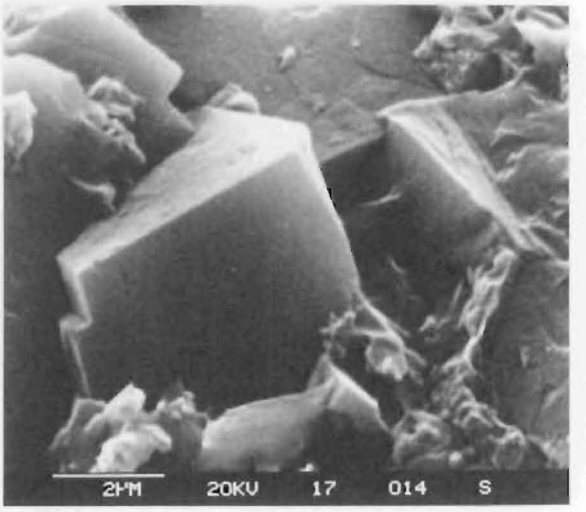
2µM 20KV 17 014 S

d

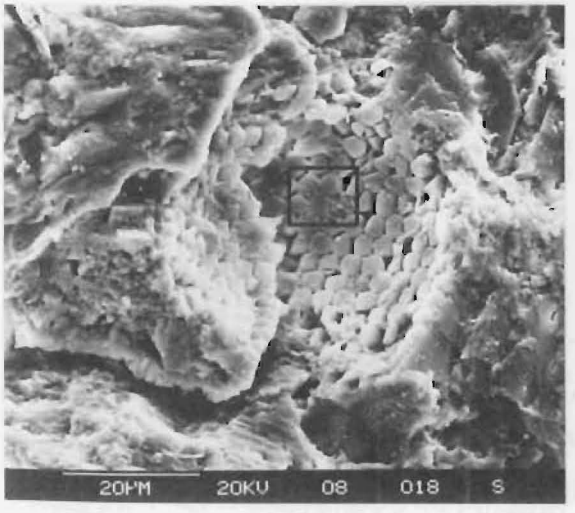
20µM 20KV 08 018 S

e

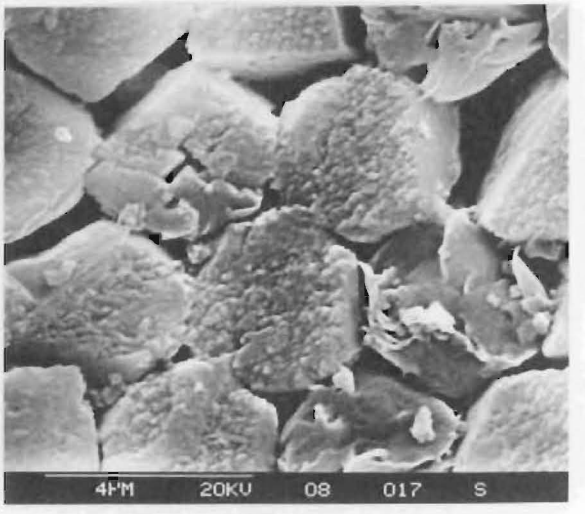
4µM 20KV 08 017 S

f

Figure A5.15 SEM micrographs of Amuri dolomite.

(a) Intergrown dolomite rhombs, CD Zone, Waipapa Bay (sample WB19).

(b) Intergrown dolomite rhombs, CD Zone, Isolation Creek (sample IC14).

(c) Straight compromise dolomite-dolomite crystal boundary (arrows), CD Zone, Wharanui Point (sample WPT4).

(d) Dolomite-chert boundary, CD Zone, Wharanui Point (sample WPT4).

(e) Pores in a dolomite crystal (some arrowed) from the CD Zone, Limburn Stream (sample LS2).

(f) Dolomite intercrystalline chert matrix (M) following etching with HCl, LCM Subzone, Dee Stream (sample DS11).

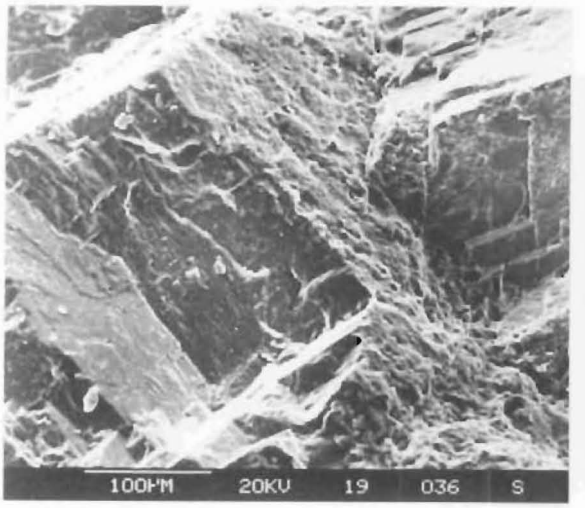
100µM 20KV 19 036 S

a

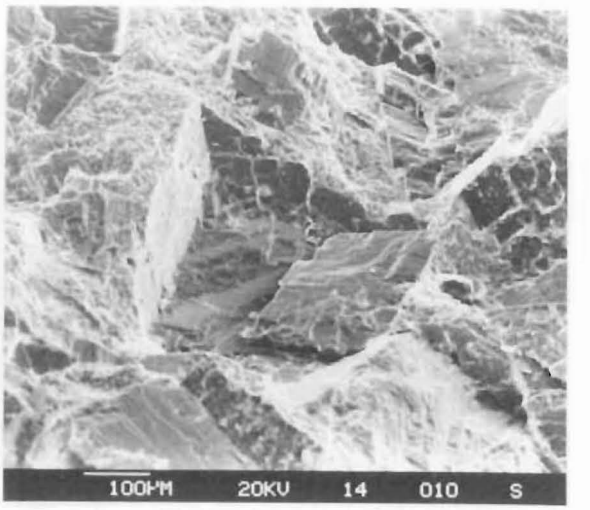
100µM 20KV 14 010 S

b

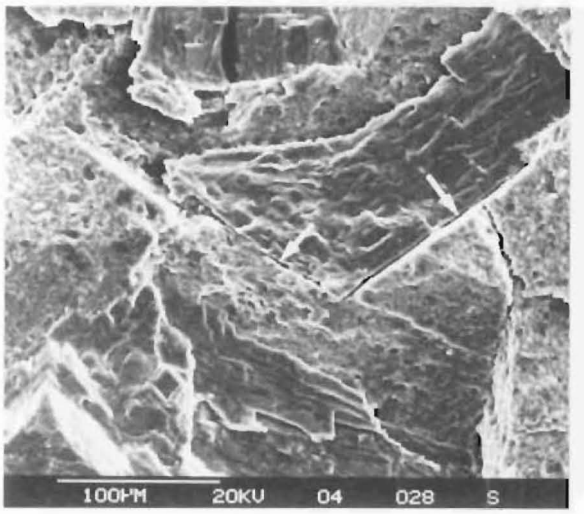
100µM 20KV 04 028 S

c

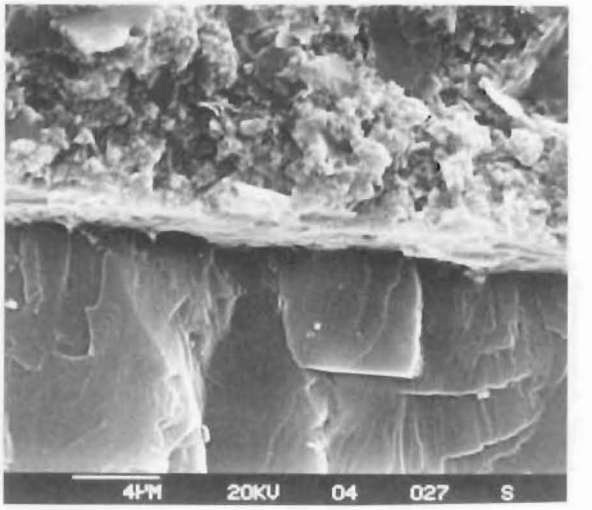
4µM 20KV 04 027 S

d

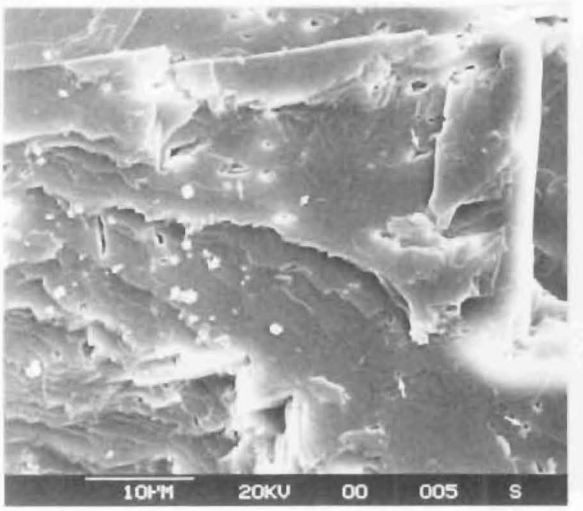
10µM 20KV 00 005 S

e

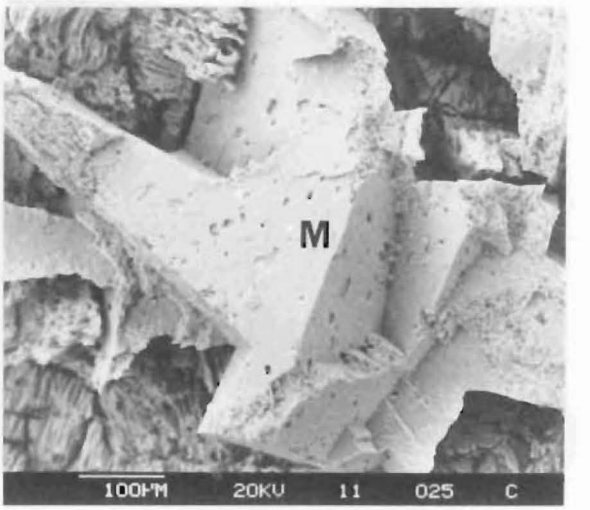
M
100µM 20KV 11 025 C

f

and intergrown rhombic forms [Figure A5.14b,d]. Foraminifera [Figure A5.14e,f], where present, tend to display less recrystallization than foraminifera in the Amuri Limestone Group.

A5.4.2. AMURI LIMESTONE GROUP

The SEM features described here are common to both CD Zone and LCM Subzone samples. Dolomite crystals have good rhombohedral cleavage, sharp boundaries with the surrounding chert, and are commonly intergrown [Figure A5.15a,b,c,d]. Small pores or cavities found in some samples probably represent fluid inclusions [Figure A5.15e]. In thin section the intercrystalline groundmass of dolomite beds, is either chert or dark silicified muddy material. Examination of the groundmass following HCl treatment reveals a porous 'swiss cheese' texture, with minor evidence of fabric lineation [Figure A5.15f]. The pores may result from either remnant original porosity or unchertified carbonate, or a combination thereof.

A sample from Wharanui Point (15) contains hexagonal crystals, commonly with orthorhombic style cruciform twinning [Figure A5.16a,b,c]. The crystals are also common in the surrounding matrix, where the cruciform twinning is best developed [Figure A5.16d]. Initially the cruciform twining and pseudohexagonal shape, plus the pink colour of the micrites at this locality, suggested the mineral to be goethite. However, SEM-EDAX analysis shows the crystals to consist mainly of Ca and S, which combined with crystal morphology, means they are probably anhydrite. These crystals were not detected by XRD or seen in thin section.

A5.5. GEOCHEMICAL AND INSOLUBLE RESIDUE ANALYSES

A5.5.1. SUMMARY OF WHOLE ROCK ANALYSES

Whole-rock carbonate analyses were performed on samples which are entirely micrite or dolomite as determined by XRD analysis. Micrites are included here for comparative purposes. The results are summarized in Table A5.1 with the raw data listed in Appendices 9 and 10. Concentrations of Ca and Mg are discussed in terms of $MgCO_3$ and $CaCO_3$ mole percent, unless otherwise stated. Calculations of mole% carbonate include $FeCO_3$ as well as $MgCO_3$ and $CaCO_3$. All carbon and oxygen isotope values are quoted in

Figure A5.16 SEM micrographs of anhydrite crystals in the CD Zone from Wharanui Point (sample WPT3).

(a) Low magnification view. The positions of (b) and (c) are indicated.

(b) Single crystal intergrown with dolomite.

(c) Two crystals intergrown with dolomite showing hexagonal crystal habit.

(d) Interpenetrating anhydrite twins in chert matrix adjacent to the dolomite crystal shown in (a).

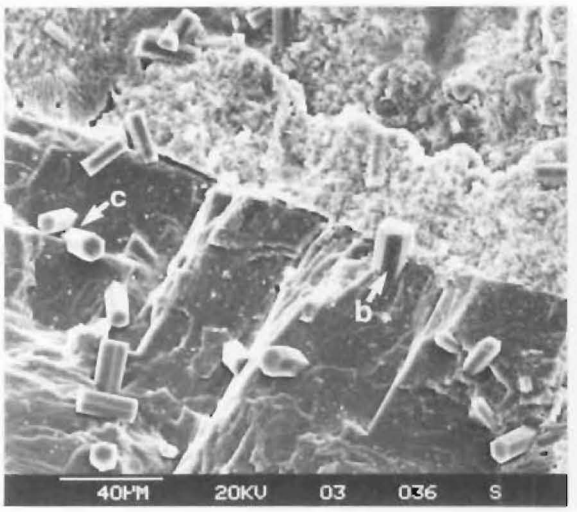
c
b
40UM 20KV 03 036 S

a

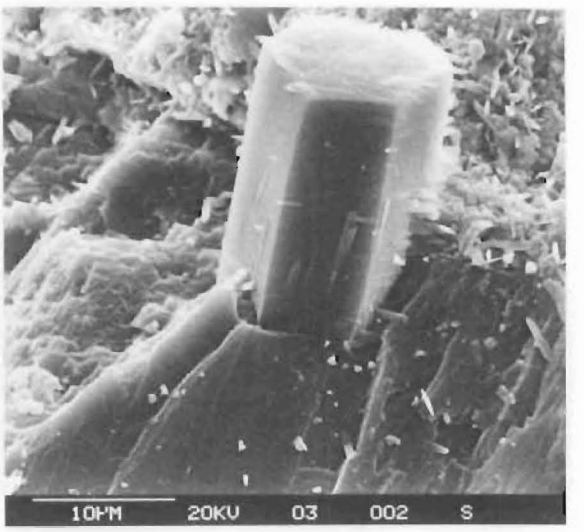
10UM 20KV 03 002 S

b

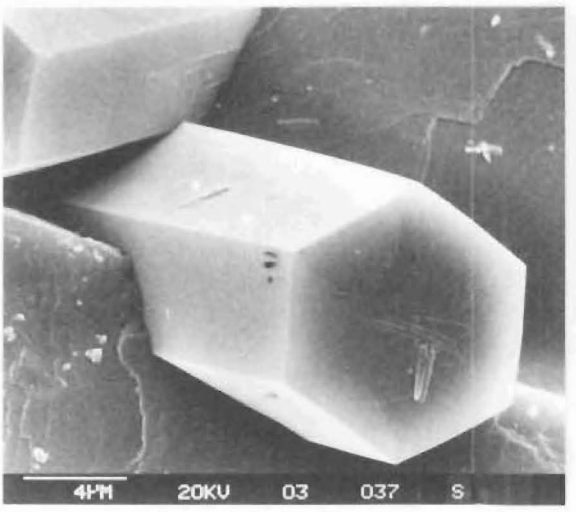
4UM 20KV 03 037 S

d

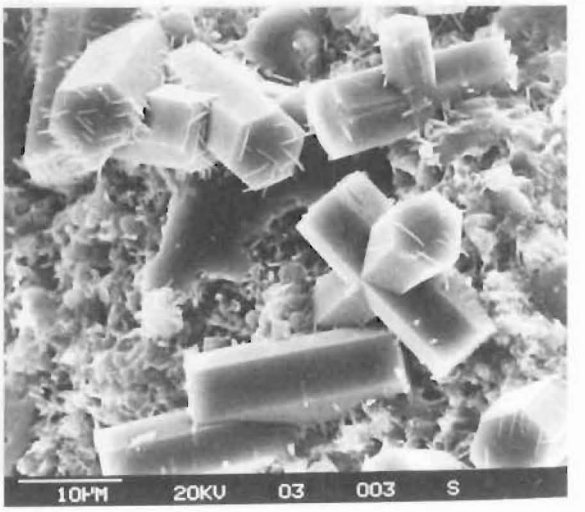
10UM 20KV 03 003 S

e

Table A5.1. Summary of geochemical data for carbonate phases. Where no range is specified only one sample was analyzed. The two calcite dominated concretions are not included in the Mg and Ca range for WC Zone samples. The number of samples considered for each lithology is as follows: WC Zone dolomite = 24, LCM Subzone dolomite = 16, CD Zone dolomite = 16, Micrites (all units combined) = 41, Marls = 4, K-T boundary = 4, Dolomitic shales (from the WC Zone, samples IC5 and IC6) = 2.

		Carb	IR	Mn	Fe	Na	K	Mg	Ca	Sr	O-18	C-13	$MgCO_3$	$CaCO_3$	$FeCO_3$
		Wt%	Wt%	ppm	ppm	ppm	ppm	ppm	ppm	ppm	‰PDB	‰PDB	Mole%	Mole%	Mole%
K-T	Minimum	31.6	62.4	1562	2757	1890	6575	1441	313087	875	-3.91	+1.76	0.60	98.11	0.82
Boundary	Maximum	37.6	68.4	1816	5602	2786	13296	2930	392540	1085	-4.96	+1.98	1.34	99.11	0.55
	Mean	34.0	66.0	1698	4099	2262	8991	2186	353059	1013	-4.30	+1.87	0.97	98.54	1.01
Marls	Minimum	43.4	27.7	408	1532	1374	5841	650	330636	690	-6.30	+1.19	0.31	96.50	0.32
	Maximum	72.3	56.6	589	5480	1582	2667	4961	351423	1460	-1.66	+1.65	2.36	99.05	1.14
	Mean	60.4	39.7	489	3455	1468	7916	2562	337295	993	-5.11	+1.40	1.23	98.05	0.72
Micrites	Minimum	10.8	6.2	31	305	200	361	132	261487	540	-6.90	-1.16	0.01	96.26	0.06
	Maximum	93.8	89.2	2374	3254	5397	15357	7243	381682	1314	-1.32	+3.04	3.46	99.77	0.71
	Mean	58.1	41.9	508	1576	1584	3838	1630	339099	904	-4.36	+1.25	0.63	99.05	0.32
LCM Subzone	Minimum	57.7	12.0	73	1803	570	1477	72090	210948	221	-4.25	+1.31	31.86	50.20	0.32
Dolomite	Maximum	88.0	42.3	1111	6806	810	7355	127219	252027	558	-2.75	+3.33	49.14	67.51	1.17
	Mean	72.2	27.8	528	3785	657	3561	108637	224981	385	-3.65	+2.35	43.84	55.49	0.66
CD Zone	Minimum	15.4	14.7	213	811	214	1325	12112	166734	103	-1.89	-5.82	28.19	43.81	0.13
Dolomite	Maximum	85.4	84.6	8547	14238	1904	15819	137065	351131	869	-6.82	+3.35	55.13	69.76	2.19
	Mean	59.0	41.0	918	3648	758	4643	114283	217198	243	-4.01	+0.73	48.84	53.38	0.65
Dolomitic	Minimum										-6.01	-46.89			
Mudstones	Maximum										-5.66	-36.67			
	Mean	69.4	30.6	712	1026	536	2681	126379	202014	207	-5.83	-41.78	50.68	49.14	0.18
WC Zone	Minimum	21.5	10.8	623	715	541	2087	7000	175338	175	-6.79	-32.74	39.30	37.40	0.15
Dolomite	Maximum	89.2	78.5	9543	57662	1930	10407	130484	321479	1423	+3.75	+8.36	53.01	51.54	20.00
	Mean	75.2	24.8	2724	204451	1327	4912	106069	209706	710	-2.16	-2.53	47.46	48.11	4.48

the per mil (‰) notation with respect to PDB (Hoefs 1980).

A5.5.2. STRATIGRAPHIC RELATIONSHIPS

All elemental profiles are plotted in Figure A5.17 [Map pocket] and stable isotopes are plotted in Figure A5.23 [Map pocket]. Only profiles for Isolation Creek and Clarence Valley sections have been plotted because overall they best display geographical, lithological, and geochemical interrelationships. Similar trends are seen at other localities.

Insoluble Residues

Table A5.1 and Figure A5.17a show that micrites and CD Zone dolomites contain higher average insoluble residue than LCM Subzone dolomites and WC Zone concretions. Average insoluble residue is marginally higher in the LCM Subzone than in the concretions. The range of values for the concretions is more restricted than for the micrites or the CD Zone dolomites.

Insoluble residue profiles [Figure A5.17a] and frequency distributions [Figure A5.18] show relatively wide variations both within and between units at different localities. There appears to be no definite relationship between lithology and the insoluble residue content. No trends or profile characteristics can be correlated from one section to another.

Composition of Insoluble Residue

The insoluble residues are divided into those from micrite, dolomite bed (CD Zone and LCM Subzone samples are grouped together as compositional differences are minor), concretion, marl, and K-T boundary samples. Results are summarized in Table A5.2.

With the exception of Ba, micrite insoluble residues fall in the range of values for cherts from the CD and CL Zones [c.f. Table A6.1]. The red micrite residue from Woodside Creek (13, sample WC12) contains more Fe_2O_3 than either associated cherts or other micrite insoluble residues. The composition of insoluble residues from dolomite concretions are within the compositional range of Woolshed Formation shales [Table A4.1].

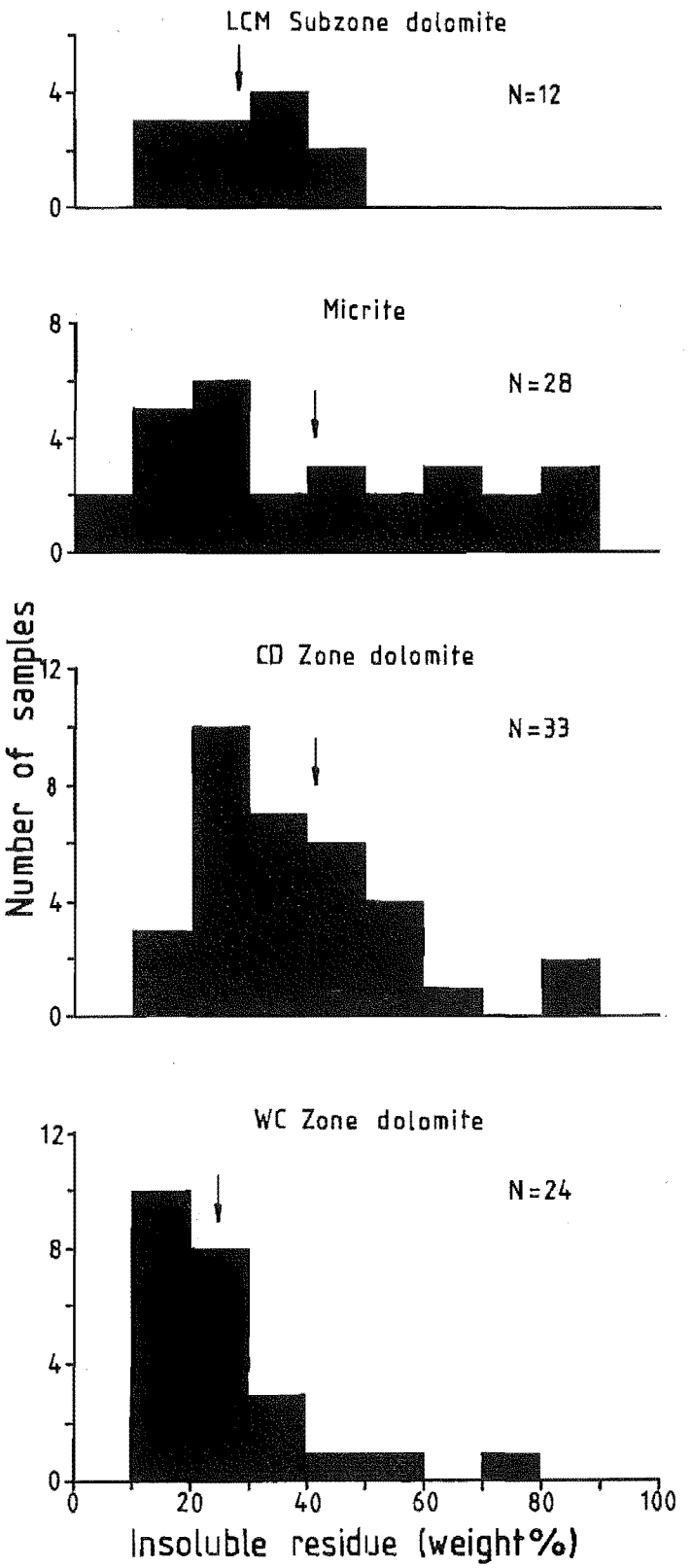

Figure A5.18 Histogram of weight% insoluble residue for dolomites and micrites. The arrows indicate mean values.

Table A5.2 Summary of elemental composition of insoluble residues from WC Zone dolomite, CD Zone and LCM Subzone (Amuri) dolomite, micrites, marls, and the K-T boundary. The marl analyses were obtained from Fergusson (1985). P_2O_5 is not included because it is below detection limits in all cases. Major elements are quoted as weight% oxide and minor elements are quoted as ppm.

	WC Zone Dolomite	Amuri Dolomite	Marls	Micrite	K-T Bdy
SiO_2	80.27	86.86	67.63	91.26	90.28
TiO_2	0.43	0.29	0.54	0.14	0.19
Al_2O_3	8.56	5.71	15.54	3.08	4.26
Fe_2O_3	1.36	1.14	4.50	0.82	0.85
MnO	0.03	<0.01	<0.01	0.02	<0.01
MgO	1.13	0.93	2.18	0.46	0.63
CaO	0.53	0.15	1.83	0.21	0.24
Na_2O	1.21	0.28	<0.10	0.21	0.22
K_2O	1.44	1.82	1.82	0.45	0.68
LOI	4.10	1.35	5.32	1.79	2.24
V	68	41	15	-	38
Cr	48	30	12	-	25
Ni	11	11	14	-	22
Zn	19	18	16	-	17
Ga	13	8	3	4	7
Rb	79	58	21	35	30
Sr	64	28	242	563	68
Y	5	5	2	11	4
Zr	191	50	44	39	42
Nb	7	7	6	5	<5
Ba	385	620	5736	-	721
Ce	<10	<10	<10	-	<10
Nd	<10	<10	<10	-	<10
La	5	9	<2	-	4
Pb	7	5	4	7	5
Th	<1	<1	<1	4	2

Dolomite bed insoluble residue contents differ from other Amuri Limestone Group insoluble residues. Regardless of whether they are in the LCM Subzone or the CD Zone, they contain greater concentrations of most major and trace elements than micrite insoluble residues, or CL and CD Zone cherts. Losses on ignition from dolomite bed samples are about the same as in cherts and micrite insoluble residues, but SiO_2 is lower. With the exception of SiO_2, concentrations are lower than in marls and WC Zone concretions. K-T boundary insoluble residue compositions are similar to those from micrites.

Calcium and Magnesium

Profiles of $CaCO_3$ and $MgCO_3$ [Figure A5.17b] are mirror images of each other and $FeCO_3$ seldom exceeds 2 mole percent. Major variations reflect the presence or absence of dolomite. $MgCO_3$ concentrations in micrites never exceed 5 mole percent.

As well as differences between micrites and dolomites, there are variations within dolomite units. Micrites display much less intra-lithologic variation than dolomites. Ranges for dolomite $CaCO_3$ and $MgCO_3$ are in excess of 10 mole percent [Figure A5.19]. The concentrations in both concretions (excluding the calcite samples from Dart Stream) and dolomite beds tend to be Mg-rich, or at least near to stoichiometric dolomite composition. LCM Subzone dolomites tend to contain higher $CaCO_3$ concentrations than CD Zone dolomites [Figure A5.19].

Whole-rock analyses of CD Zone dolomites show that just over half the samples are Mg-rich. Microprobe analyses however, [Section A5.5.3] show that most are $CaCO_3$-rich on a single crystal scale. Some of this discrepancy can be explained in terms of analytical method; some non-lattice Mg (possibly from fluid inclusions or, perhaps leached from clay minerals) may have been included. With a few exceptions (e.g. Wharanui Point samples) The single crystal data support the observation that CD Zone dolomites tend to contain more Mg than LCM Subzone dolomite. Essentially therefore, Amuri Limestone Group dolomites tend to be Ca-rich.

At Mead Stream (24,25), Isolation Creek (20) and Limburn Stream (26) there is a gradual decrease in $MgCO_3$ in CD Zone dolomites with increasing stratigraphic height [Figure 5.17b]. Mead Stream (25) LCM Subzone

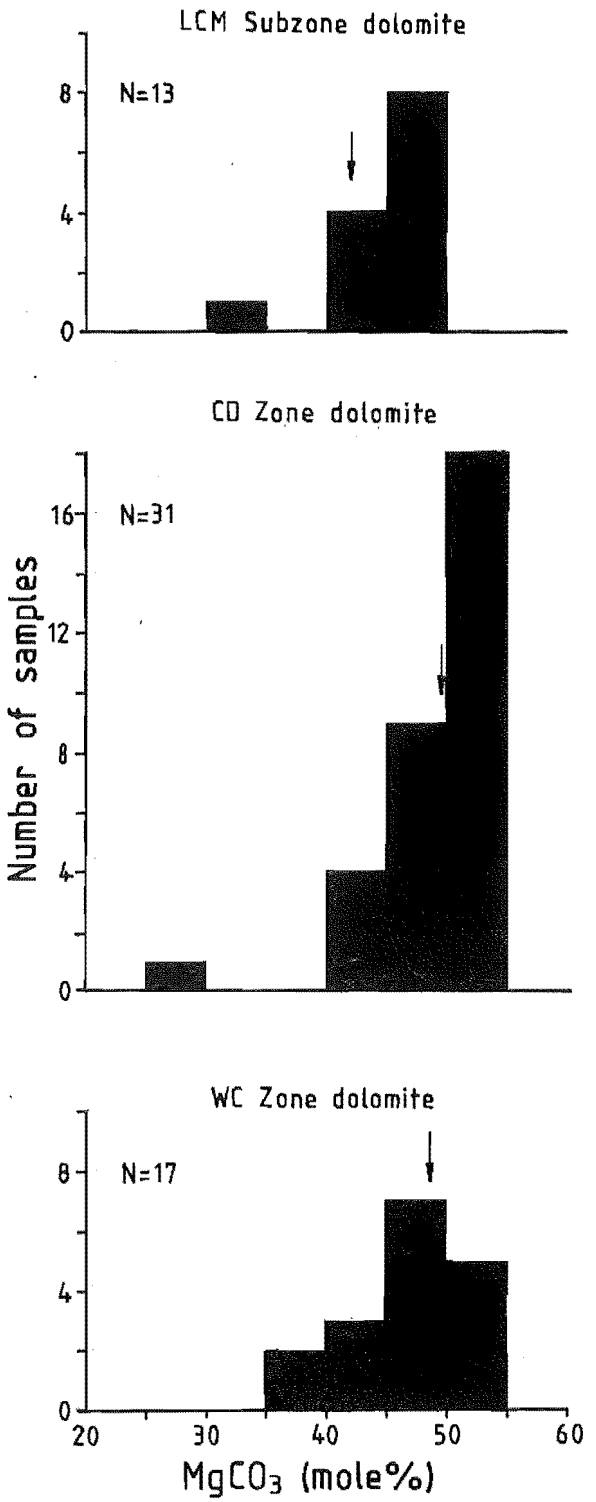

Figure A5.19 Histogram of mole% $MgCO_3$. The arrows indicate mean values. Micrites are not included as they all contain less than 5 mole% $MgCO_3$. The three calcite concretions are not included in the WC Zone dolomite.

dolomites show a similar trend. Such variations are not observed at Wharekiri Stream (9) however, where the stratigraphic interval is much reduced and encompasses only part of the CD Zone. Other sections do not contain enough samples to enable resolution of similar vertical trends.

Strontium

The Sr profiles [Figure A5.17c] show an overall increase stratigraphically upwards at Mead (24,25) and Limburn (26) Streams, but not at Isolation Creek (20). The three basal CD Zone samples at Mead Stream (24,25) show a slight decrease in concentration upwards, despite the overall trend. Although concentration ranges for the LCM Subzone and CD Zone are similar, two thirds of CD Zone samples contain less than 200 ppm Sr. All the LCM Subzone samples contain more than 200 ppm but less than 600 ppm Sr. The bulk of the micrites are in the range 600-1200 ppm which is slightly above the range (400-700 ppm) of ancient limestones (Kinsman 1969). The range of Sr concentrations in all Amuri Limestone Group dolomites is approximately 50% less than in Amuri Limestone Group calcites.

Frequency distributions [Figure A5.20] confirm the differences between diagenetic units but indicate some overlap in concentration ranges [see also Table A5.1]. Concretions have a very broad spread of values compared with the small ranges of both the LCM Subzone and the CD Zone. All micrites are included in one group however, although the few ML Zone samples tended to have Sr concentrations of about 1000 ppm, that is near the top of the micrite range.

Veizer (1983) states that among ancient dolostones the 'early' diagenetic, fine grained, layered, usually hypersaline types contain more Sr (100-1000 ppm) than the 'later' diagenetic, coarse grained, limpid, massive varieties (30-100 ppm). Although they are unlikely to be hypersaline, dolomites in this study fit the first category in terms of concentration.

Iron and Manganese

Plotted against stratigraphic position [Figure A5.17d], neither element shows an overall trend, although Fe displays a wide variation in concentrations. Seventy-one percent of the dolomite concretion samples

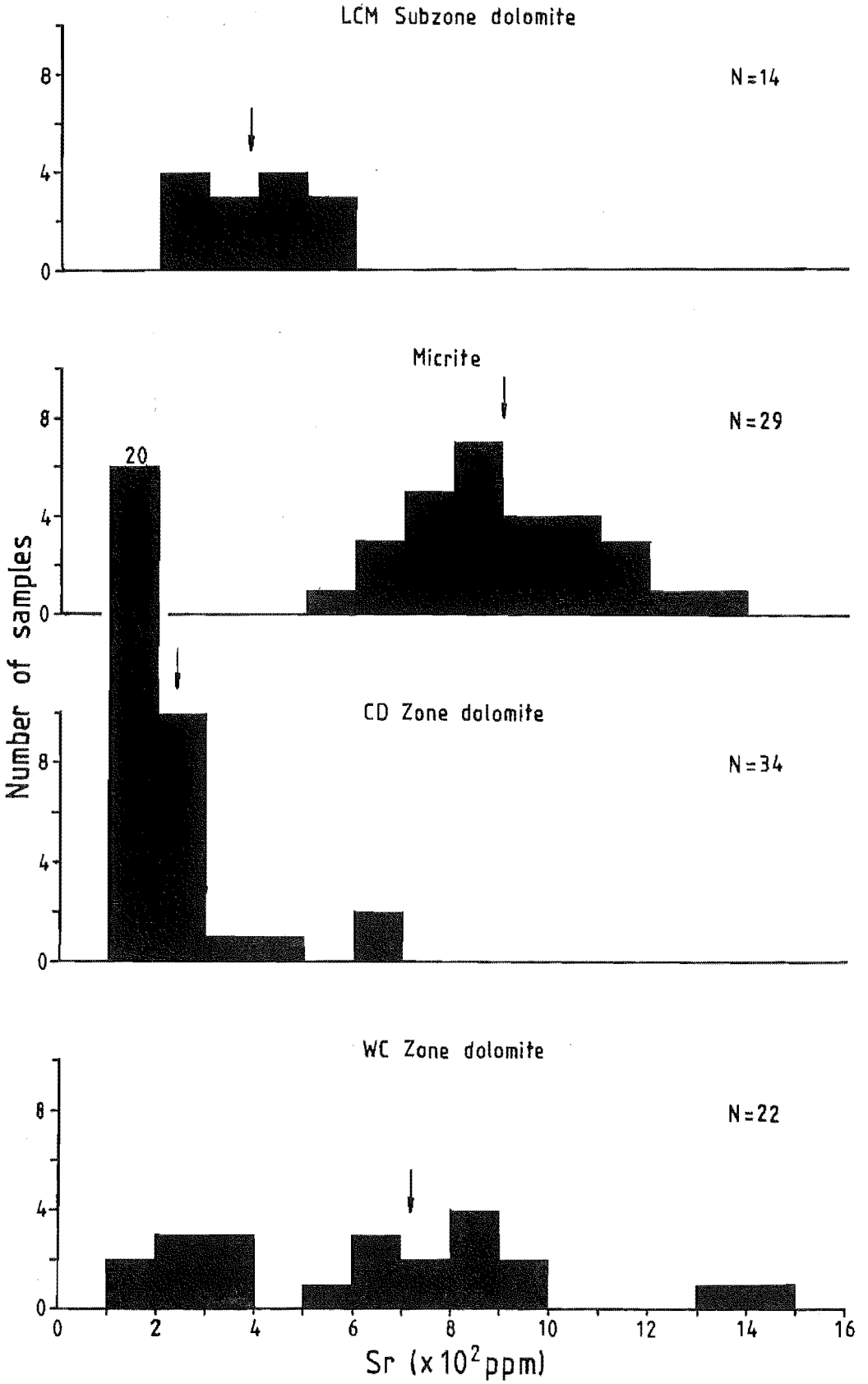

Figure A5.20 Histogram of Sr concentration in dolomites and micrites. Mean values are indicated by arrows.

are ferroan (more than 2 mole% $FeCO_3$). With the exception of two CD Zone samples all other dolomites analyzed are non-ferroan. There are no ferroan calcites. In terms of the diagenetic units the concretions display the greatest spread of both Mn and Fe values [Figure A5.21]. In general all carbonates contain less Mn than Fe.

Manganese concentrations [Figure A5.21a] in Amuri Limestone Group micrites and dolomites are moderately well clustered around the sample means, although the CD Zone contains a few extreme values. Manganese distributions in the micrites and the CD Zone dolomites are approximately the same. Means for the Amuri Limestone Group units are similar, although the CD Zone mean is slightly higher than the rest due to the few extreme values. The bulk of samples contain less than 1500 ppm Mn. Less than 50% of the concretions fall within the range of the Amuri Limestone Group samples. The concretions are overall more Mn-rich.

Iron analyses [Figure A5.21b] show greater differences between units than Mn. All micrites and approximately 72% of the CD Zone dolomites contain less than 4000 ppm Fe. Just under half the LCM Subzone analyses are below 4000 ppm with the rest ranging up to 7000 ppm. Thus overall micrites and CD Zone dolomites (excluding the three extreme values) have similar Fe contents. LCM Subzone dolomites tend to have slightly higher Fe concentrations than the micrites or CD Zone dolomites. Virtually all concretions contain more than 5000 ppm Fe, which is a marked enrichment compared with Amuri Limestone Group samples.

The three high Fe samples in the CD Zone are also high in Mn. They all come from the Wharanui Point locality and are associated with pink micrites.

Sodium and Potassium

As with Fe and Mn there is a high degree of variation stratigraphically, both between and within units. Sodium shows a slight overall increase upwards both at Isolation Creek and Mead Stream, but no such trend is found at Limburn Stream [Figure A5.17e]. The K profile is more ambiguous, but there is a slight suggestion of an overall decrease in K at Mead and Limburn Streams. Frequency distributions [Figure A5.22] show the dolomite in the CD Zone and the LCM Subzone to have generally lower Na

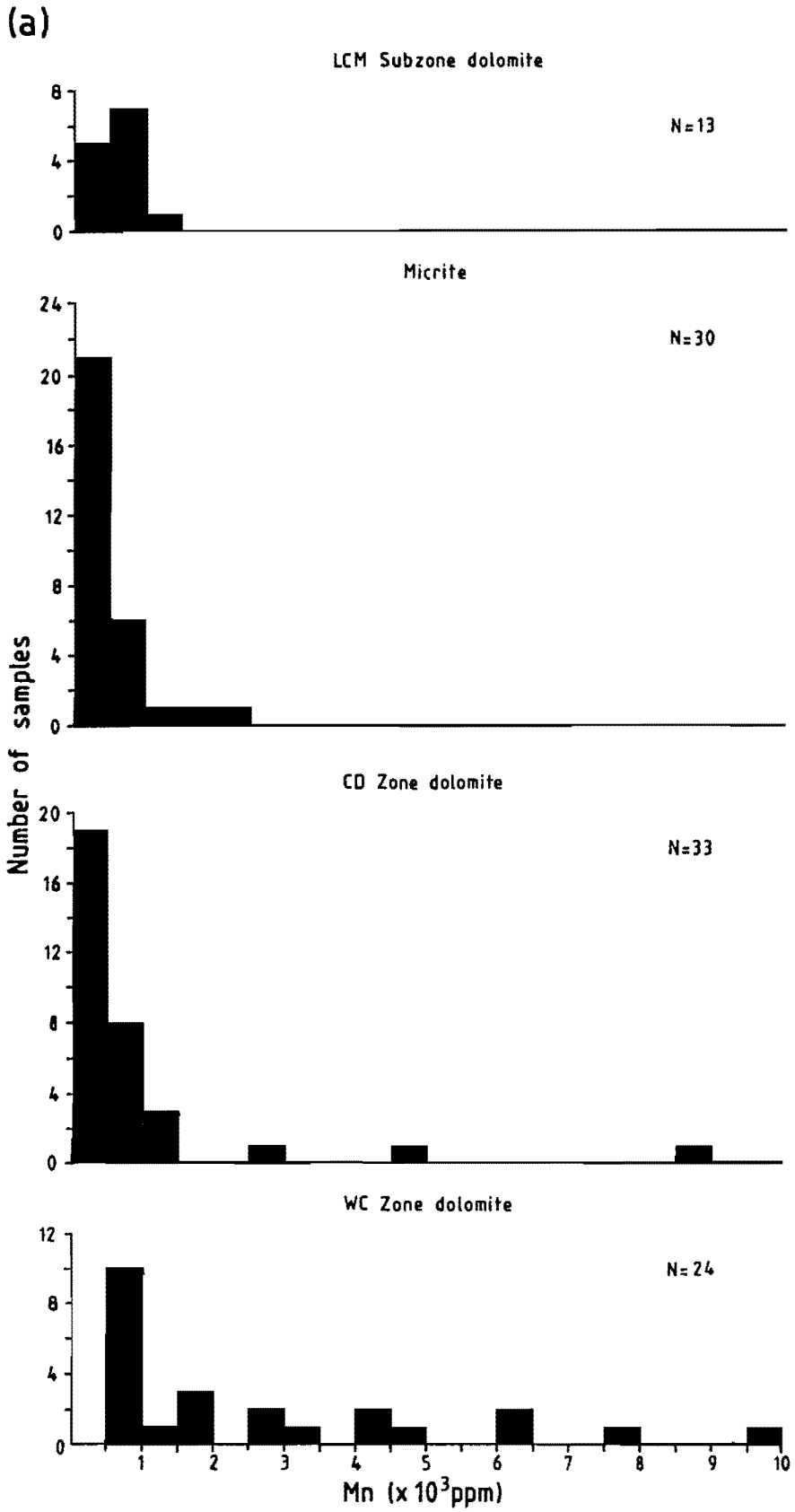

Figure A5.21 Histogram of Mn (a) and Fe (b) concentrations in dolomites and micrites. Mean values are indicated by arrows.

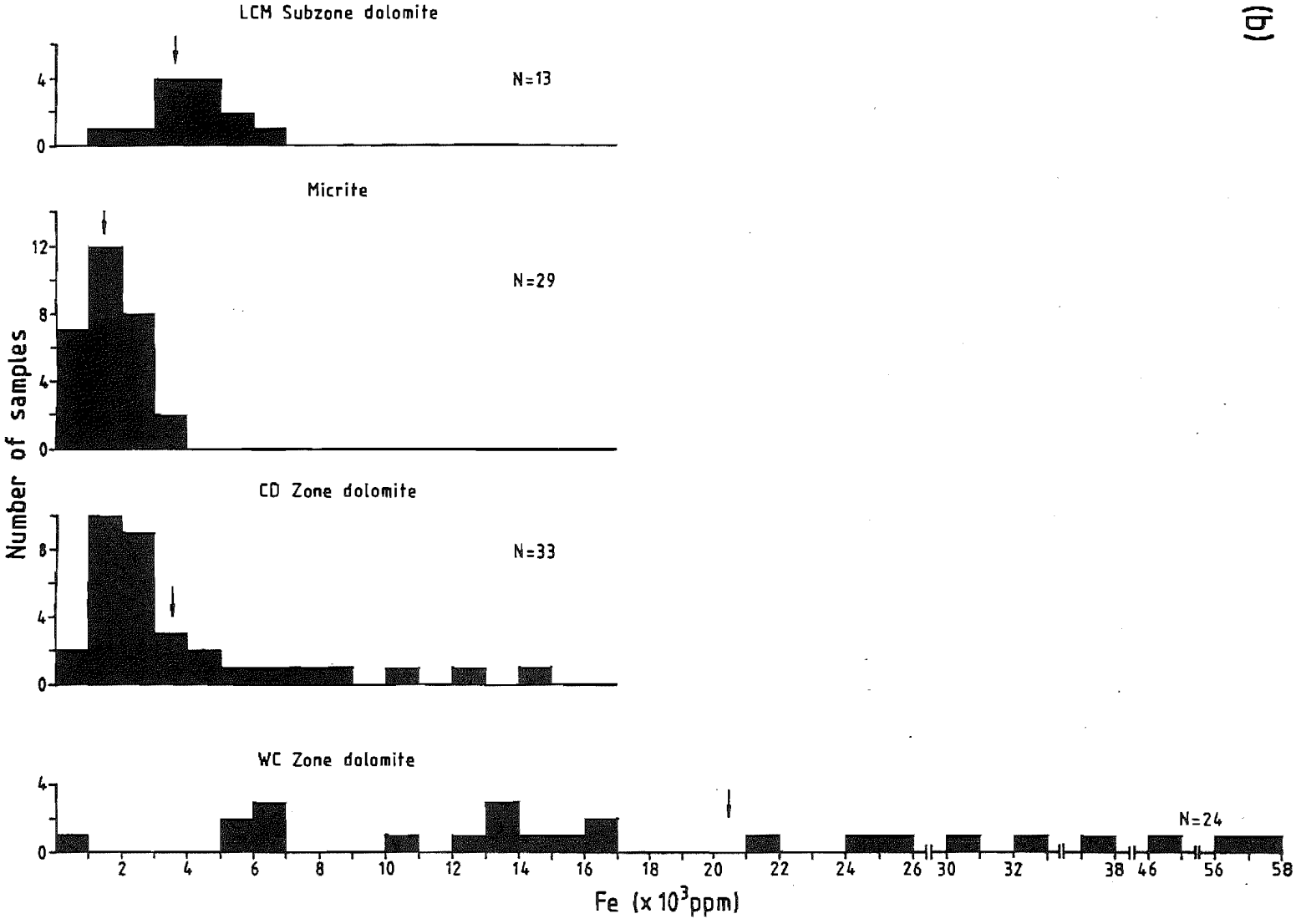
LCM Subzone dolomite
N=13
Micrite
N=29
CD Zone dolomite
N=33
WC Zone dolomite
N=24
Number of samples
Fe (x 10³ppm)

(b)

igure A5.22 Histogram of Na (a) and K (b) concentrations in dolomites and micrites with mean values shown by the arrows. The vertical line in (a) is the boundary between seawater and hypersaline carbonate environments (from Veizer *et al*. 1977).

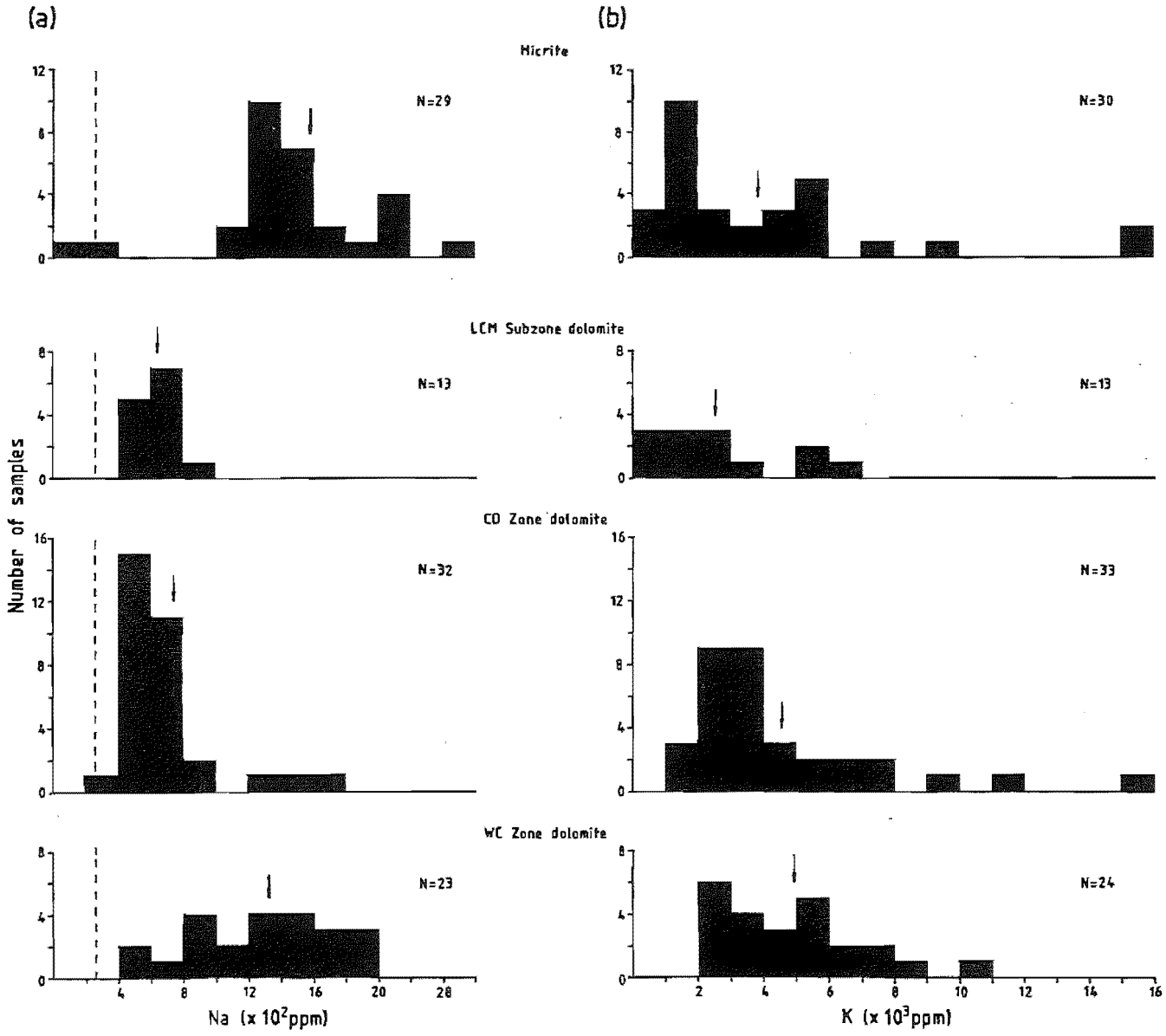
(a)
(b)
Micrite
N=29
N=30
LCM Subzone dolomite
N=13
N=13
CO Zone dolomite
N=32
N=33
WC Zone dolomite
N=23
N=24
Number of samples
Na (x 10²ppm)
K (x 10³ppm)

concentrations than marls or micrites. Concretions contain more Na than Amuri Limestone Group dolomites but similar concentrations to the micrites. Concentrations of K for all carbonate units are roughly the same [Figure A5.22b], although the ranges display slightly more variation. All samples contain more K than Na. As noted for other elements the concentrations of both K and Na are higher in marls than in adjacent micrites.

Stable Oxygen Isotopes

Profiles of $\delta^{18}O$ [Figure A5.23a] display little down-profile variation, with only a hint of an overall down-profile decrease at Mead Stream (24,25) and Isolation Creek (20). In any given profile the range of variation is about 3-4·/..$_{PDB}$. Although overall trends are poorly defined, within the CD Zone and to a lesser extent the LCM Subzone, there are more definite down-profile decreases in $\delta^{18}O$, particularly at Isolation Creek. The lack of such a trend in micrites may be the result the limited sampling at individual localities.

The ranges and means of $\delta^{18}O$ for all Amuri Limestone Group micrites and dolomites are similar [Figure A5.24]. All have a range of about 6 per mil. Some concretions are more ^{18}O enriched than Amuri Limestone Group samples. The range for concretions is about 11 per mil.

LCM Subzone dolomites are progressively depleted in O^{18} from Branch Stream to Mead Stream, that is towards the centre of the depositional basin. In some cases mean $\delta^{18}O$ values for micrites below the LCM Subzone are higher than for samples from above the LCM Subzone. No regional trends are apparent. Inspection of $\delta^{18}O$ profiles [Figure A5.23a] shows minor differences in ranges of values at different localities, but in no definite geographic pattern.

Stable Carbon Isotopes

Profiles of $\delta^{13}C$ [Figure A5.23b] for Amuri Limestone Group carbonates display no identifiable stratigraphic trends. Down-profile variability is less than for $\delta^{18}O$. The ^{13}C compositions of concretions display marked differences between samples, and some significant differences compared to Amuri Limestone Group dolomites are also observed. The range of

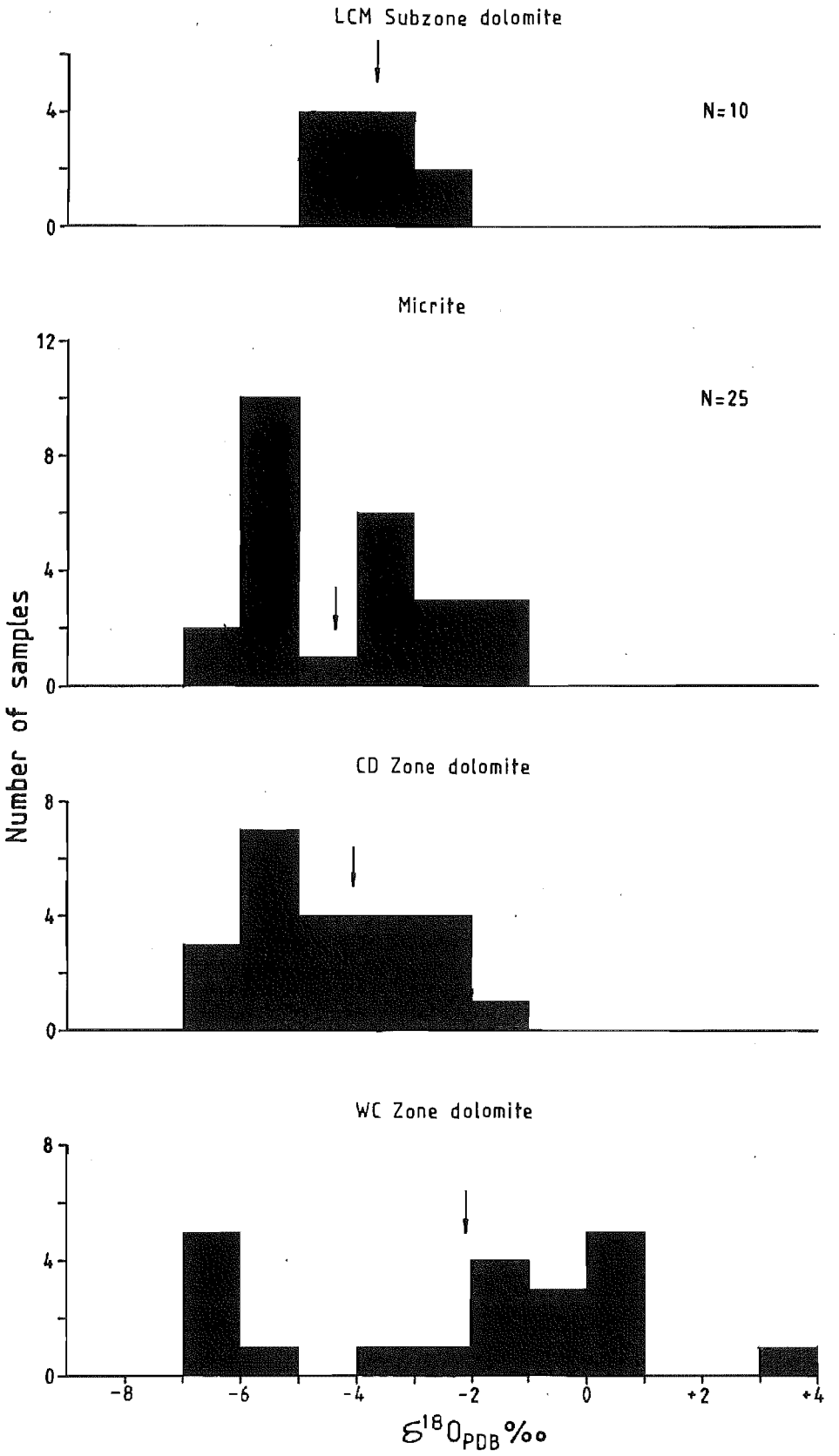

Figure A5.24 Histogram of $\delta^{18}O$ for dolomites and micrites. Arrows indicate mean values.

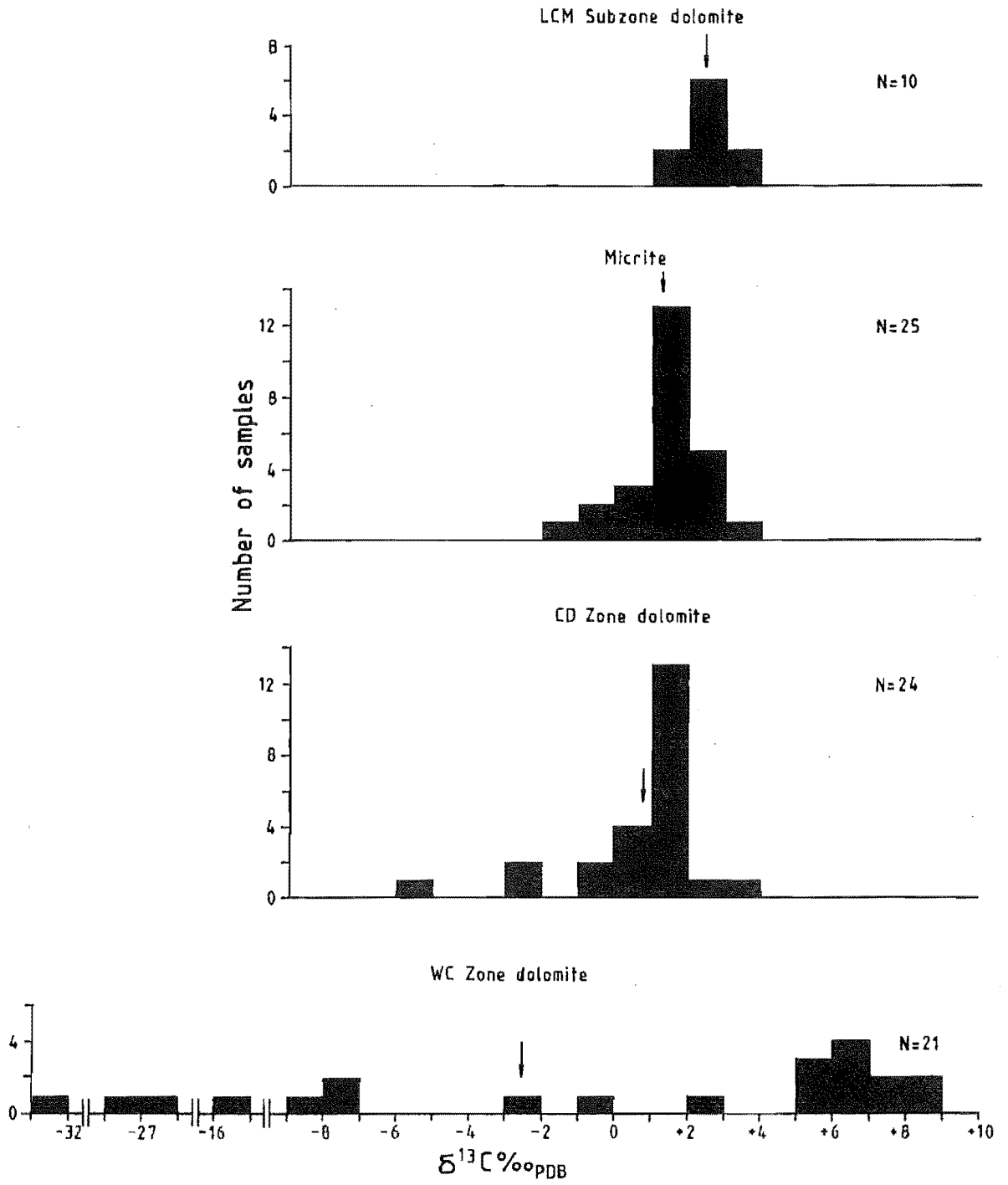

Figure A5.25 Histogram of $\delta^{13}C$ for dolomites and micrites. Arrows indicate mean values.

compositions [Figure A5.25] for all Amuri Limestone Group samples is similar, although about 1‰ higher in the LCM Subzone. $\delta^{13}C$ for concretions extends over a 42‰ range, whereas all but one Amuri Limestone Group sample is in a 7‰ range. The broad $\delta^{13}C$ range follows the similarly broad ranges for elemental concentrations in concretions.

A5.5.3. SINGLE CRYSTAL ANALYSES

Whole rock analyses implicitly assume a homogeneity in crystal composition. Petrographic and cathodoluminescence studies demonstrate that compositional homogeneity is not necessarily the case. Therefore, single crystal analyses were performed to check whole rock analyses, and to determine what, if any, chemical variations may contribute to observed petrographic and cathodoluminescence characteristics.

Crystal size limitations meant that only CD Zone and LCM Subzone dolomites could be analyzed (concretionary dolomite crystals are too small). Within the limitations of the probe, points were selected in the same relative positions in each crystal [see Figure A5.26]. It is acknowledged that there are errors implicit in recording the position of analyzed points because the microprobe did not have a means of photographing or otherwise accurately fixing the position of a point analysis.

The results are summarized in Table A5.3, with a full list in Appendix 10. Calcium and Mg were above detection limits. Strontium, Na, and K were not detected at all. Iron and Mn were only occasionally detected despite cathodoluminescence indicating their presence in varying proportions. Detection limits for Fe and Mn appeared to be about 1000 ppm (which is above the range of values obtained for dolomites analyzed by Reeder and Prosky 1986, and Reeder and Grams 1987). This lack of sensitivity of microprobes for carbonate trace analysis was noted by Veizer *et al.* (1978). Wavelength dispersive analysis (WDS) is more sensitive than energy dispersive analysis (EDS) and may have improved the sensitivity and detection limits. EDS was persevered with because WDS scans did not detect Sr, Na, or K in any samples, and because of time restrictions.

Inter-sample Variations

The mean crystal compositions [Table A5.3] confirm the LCM Subzone and CD

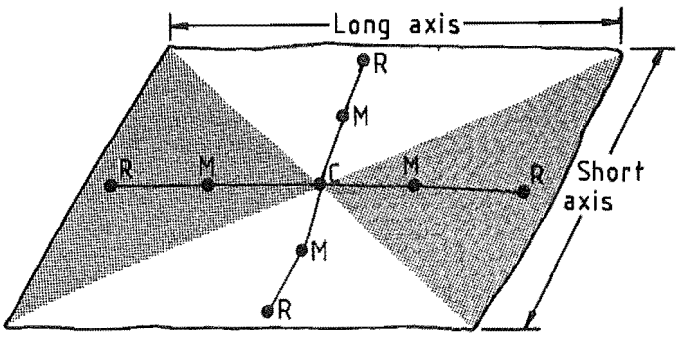

Figure A5.26 Typical location of points for microprobe analysis of dolomite crystals. C = core, M = middle or midpoint, R = rim. The same relative positions were used on all crystals regardless of size. The stippled area approximates to extinction segments seen in thin section [e.g. Figures A5.6 and A5.8].

Table A5.3 Means for all microprobe analyses of dolomite crystals. Except in sample WPT3, Mn and Fe are rarely detected in more than 3 or 4 points in a number of crystals in any given sample.

	SAMPLE	MgCO3 Mole%	CaCO3 Mole%	Mn ppm	Fe ppm
LCM	DS15	43.53	56.32	-	6038
Subzone	DS10	44.36	55.59	1162	1329
	LS11	44.23	55.77	-	-
	MS18	42.69	56.70	-	3627
	MS21	43.53	56.27	-	1793
	MS26	44.51	55.49	-	-
	MS28	42.90	56.44	-	4206
	MS29	44.25	55.54	-	2168
CD	IC12	47.39	52.59	-	1119
Zone	IC13	47.90	52.00	-	2728
	LS2	49.36	50.64	-	-
	LS7	43.76	56.24	-	-
	MS2	48.42	51.56	-	1679
	MS4	44.41	55.55	-	2938
	WB15	46.54	53.46	-	-
	WB18	46.50	53.48	-	1329
	WC2	42.74	56.65	4994	1714
	WPT3	41.14	56.02	6447	8802

Zone dolomites to be calcium rich. Comparison of mean values show that CD Zone dolomites tend to be nearer stoichiometric compositions than LCM Subzone samples. Despite overestimating $MgCO_3$ and $CaCO_3$ both by about 2 mole%, it is concluded that the whole rock results are reasonable determinations of dolomite chemistry.

Intra-Crystal Variations

$CaCO_3$ decreases from cores to margins and $MgCO_3$ shows the reverse trend [Figure A5.27]. Samples from Isolation Creek (20) and Waipapa Bay (10) show the opposite trend. Iron and Mn follow the $CaCO_3$ trend. Variations in Fe and Mn approximating the cathodoluminescence patterns [Sections A5.3.2 and A5.3.3] were not detected in any samples.

It was hoped that single crystal analyses would show whether the sector-like extinction segments seen in LCM Subzone and CD Zone dolomite crystals is compositionally controlled. Transects across long and short crystal axes display only minor differences, with both axes showing the same general trends. The minor differences can be explained in terms of analytical uncertainty. Therefore the compositional cause for the extinction segments remains equivocal.

Inter-Crystal Variations

Frequency distributions of composition [Figure A5.28] are similar for all crystal cores, midpoints, and rims. $MgCO_3$ and $CaCO_3$ distributions are generally bimodal in midpoint and rim sites. The range of core, midpoint, and rim compositions are more or less the same, despite variations between points in any given crystal.

A5.5.4. COMPOSITIONAL VARIATIONS WITHIN A SINGLE CONCRETION

Composition is likely to vary in different parts of a concretion because concretion formation was not instantaneous. Variations document changes in the chemical environment during formation. Unfortunately only one concretion, found at Lab Rocks (2), Kaikoura Peninsula, could be sampled adequately in both longitudinal and cross section.

The results are summarized in Figure A5.29 [map pocket]. The raw data is

Figure A5.27 Microprobe transects for some Amuri Limestone Group dolomites. The bar at the right of each graph indicates the estimated analytical uncertainty. ND = not detected, solid line = long crystal axis, and the dashed line = short crystal axis.

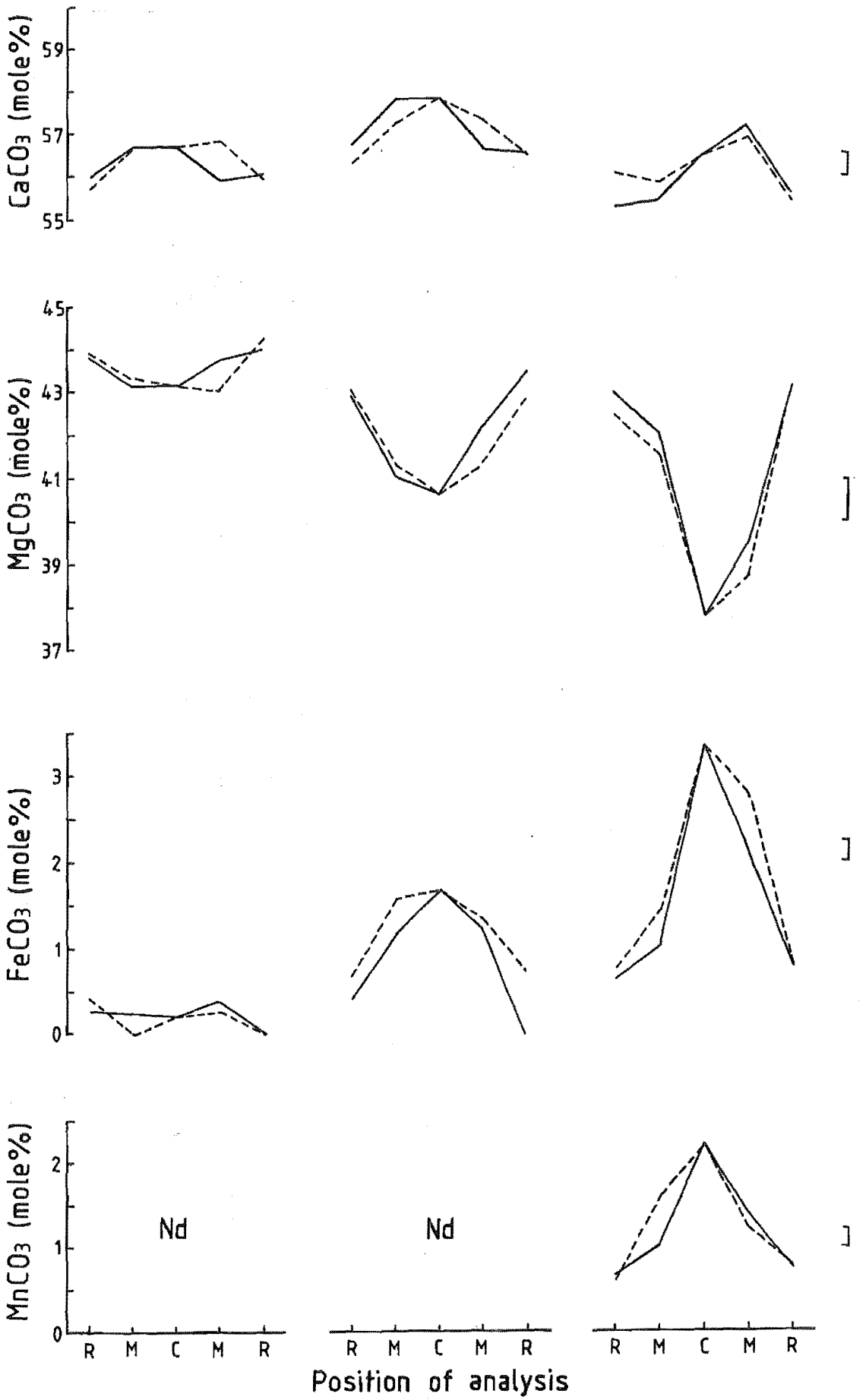
CaCO3 (mole%)
59
57
55
MgCO3 (mole%)
45
43
41
39
37
FeCO3 (mole%)
3
2
1
0
MnCO3 (mole%)
2
1
0
Nd
Nd
R M C M R
R M C M R
R M C M R
Position of analysis

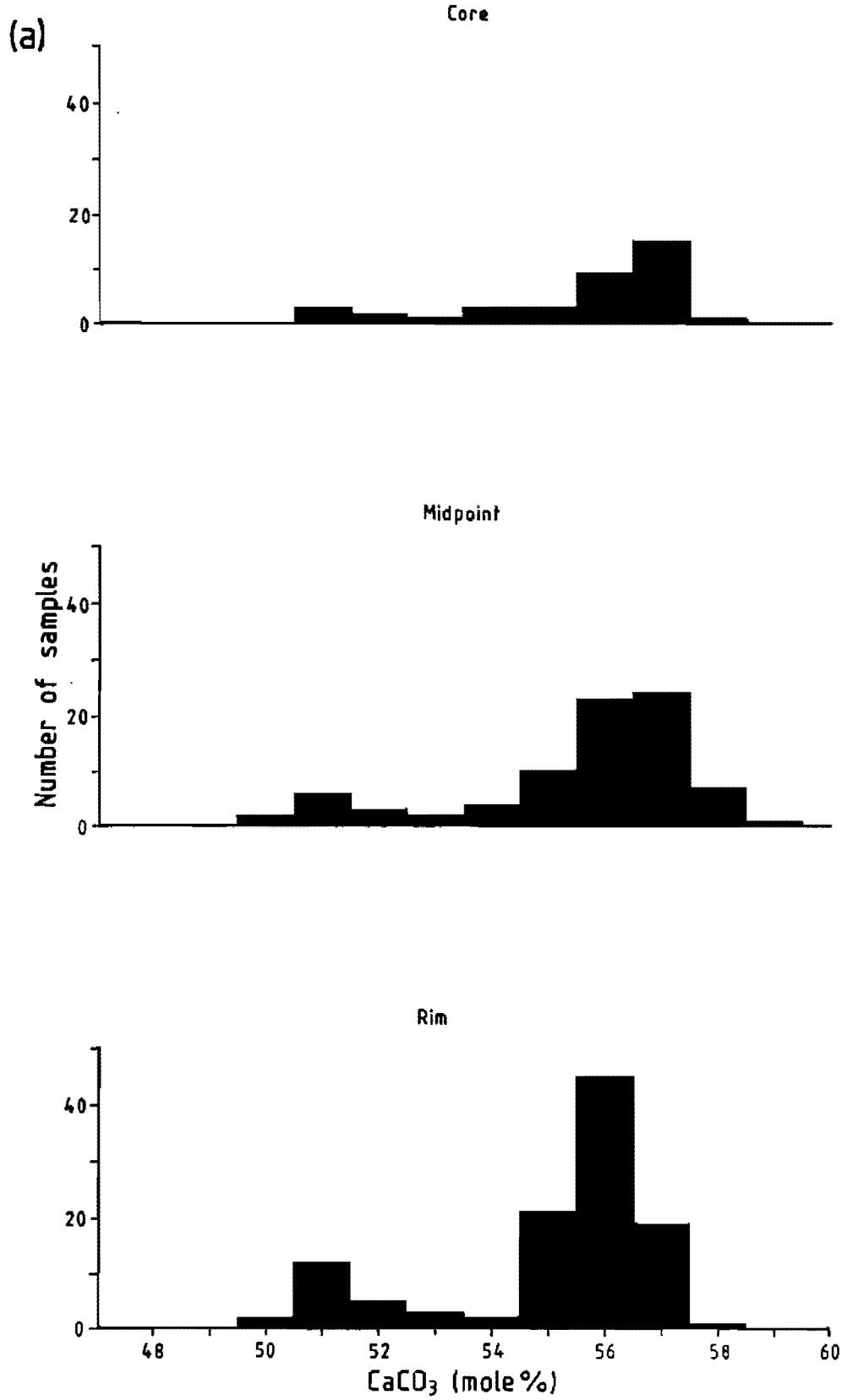

Figure A5.28 Histograms of mole% $CaCO_3$ (a), $MgCO_3$ (b), and $FeCO_3$ (c) in crystal cores, midpoints, and rims.

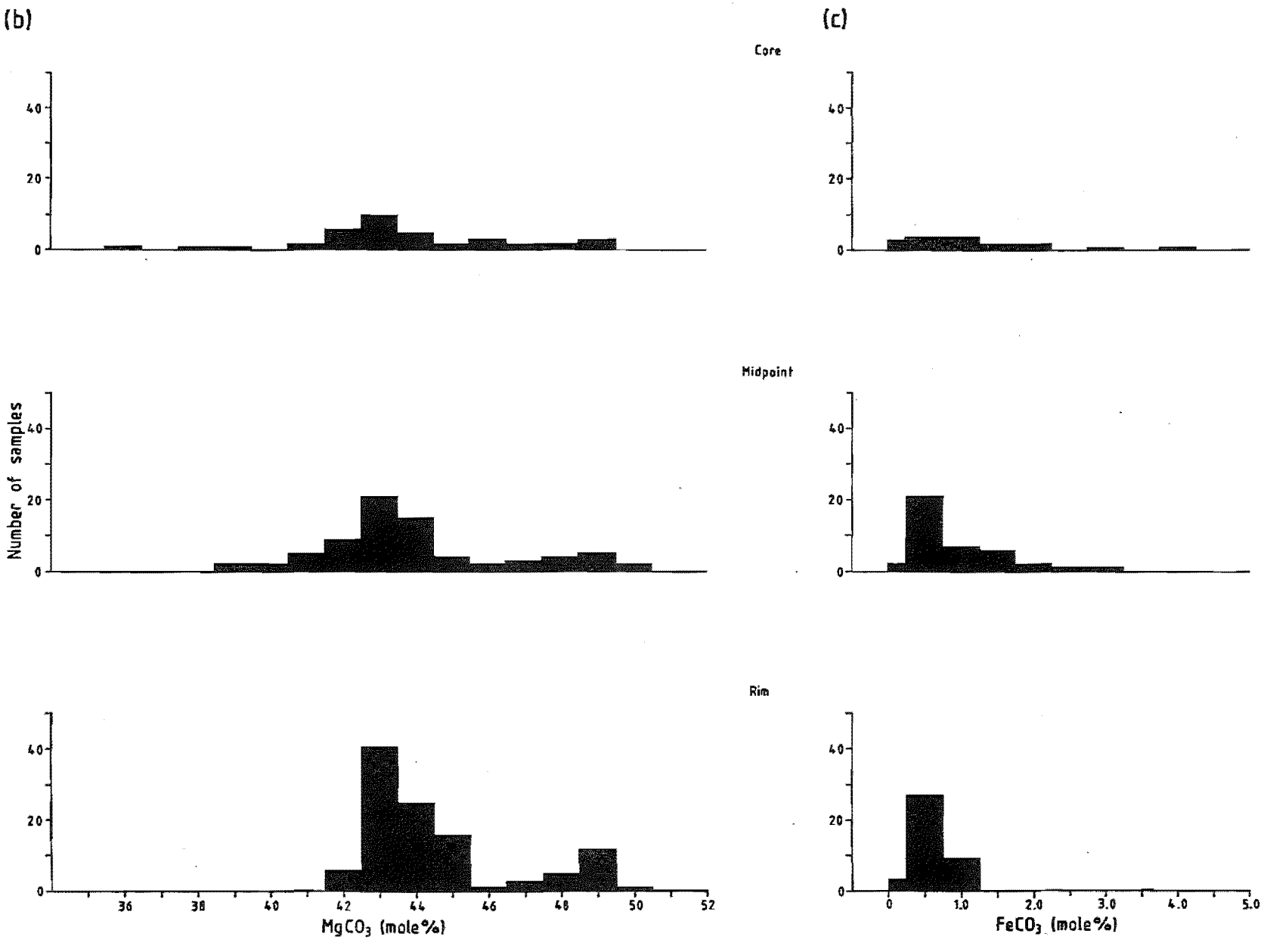
(b)
(c)
Core
Midpoint
Rim
Number of samples
0
20
40
36
38
40
42
44
46
48
50
52
$MgCO_3$ (mole%)
0
1.0
2.0
3.0
4.0
5.0
$FeCO_3$ (mole%)

given in Appendix 9. The salient features observed in Figure A5.29 are:

i) The distribution of elements and isotopes is in some cases more complex than a simple concentric increase or decrease towards the concretion margins.

ii) There is a suggestion for some analyses that there may be more than one centre of nucleation.

iii) Insoluble residue, $\delta^{13}C$, Mn, Fe [Figure A5.29b,f,g,i], increase from the apparent nucleation centres.

iv) Strontium, $\delta^{18}O$, $MgCO_3$, and $CaCO_3$ contours [Figure A5.29c,d,e,h] are slightly more complex than for other analyses, although they appear to have similar centres.

v) There is no unique contour pattern that fits all analyses.

APPENDIX 6

DESCRIPTION OF PETROGRAPHY, MINERALOGY, AND GEOCHEMISTRY OF CHERTS

A6.1. X-RAY DIFFRACTION MINERALOGY

A6.1.1. MICRITE INSOLUBLE RESIDUES AND CHERT

Cristobalite [Figure A6.1a] is found in micrites from Chancet Rocks (18), Thomson's Gully (19), Oaro (2), Haumuri Bluffs (1), and Kaikoura Peninsula (3,4) micrites.

The Chancet Rocks (18) cristobalite occurs in one sample 15 m above the base of the section in siliceous micrites. In all other samples at this locality, both above and below (including the K-T boundary), the dominant silica mineral is quartz. The two Thomson's Gully (19) samples are from a chert bed which may be a lateral equivalent of the Chancet Rocks (18) sample. If so, it forms a horizon of cristobalite sandwiched between quartz-dominated lithologies. Under the Jones and Segnit (1971) scheme, the cristobalitic samples are classified as containing opal-CT.

Haumuri Bluffs (1) and Oaro (2) XRD traces show both quartz and cristobalite reflections. The Mead Hill Formation at Kaikoura Peninsula (3,4) also contains opal-CT reflections. Despite the presence of quartz, opal-CT is the dominant silica phase.

All other micrite insoluble residue and chert XRD traces, regardless of field characteristics or apparent origin, are composed exclusively of quartz, with no detectable cristobalite [Figure A6.1b]. Clay minerals were not detected.

A6.1.2. QUARTZ CRYSTALLINITY

Determination of quartz crystallinity (Murata and Norman 1976) is based on the resolution of the quartz d(212) reflection [Figure A6.2]. The crystallinity is essentially a function of crystal size up to about 1 μm diameter. Poorly crystallized quartz has a crystallinity index of <1, with well crystallized quartz being from 8-10. Moderate to good crystallinity is in the range 3-8 (Murata and Norman 1976).

The crystallinity index was measured on 67 selected chert and silica samples. All samples show low crystallinity [Figure A6.2]. The bulk of samples (45%) have indices of 1-2; 33% have indices <1, the remainder are

Figure A6.1 Whole rock XRD traces of chert.
(a) Opal-CT chert (sample TG4).
(b) Quartz chert (sample MS3).

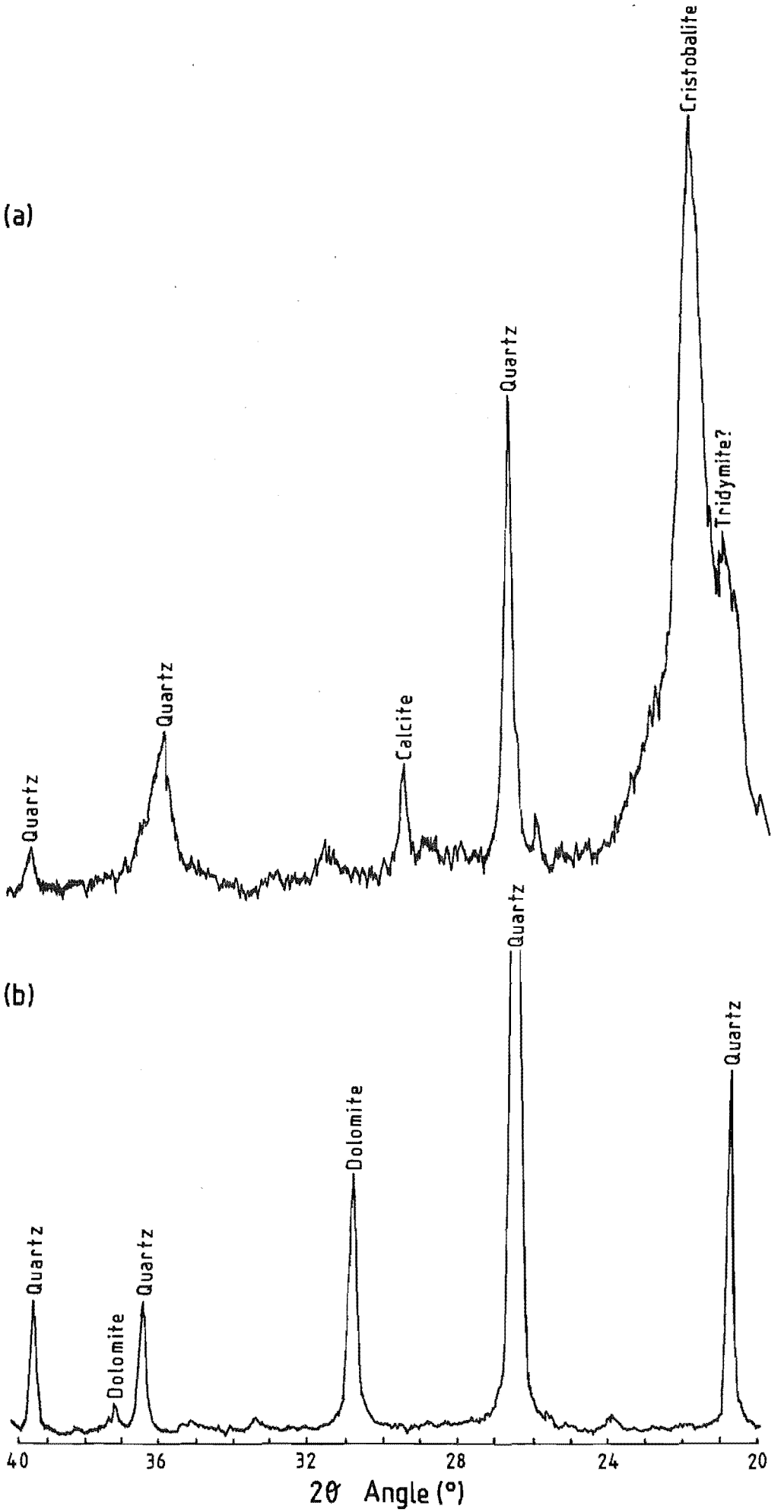
(a)
Quartz
Quartz
Calcite
Quartz
Cristobalite
Tridymite?
(b)
Quartz
Dolomite
Quartz
Dolomite
Quartz
Quartz
40
36
32
28
24
20
2θ Angle (°)

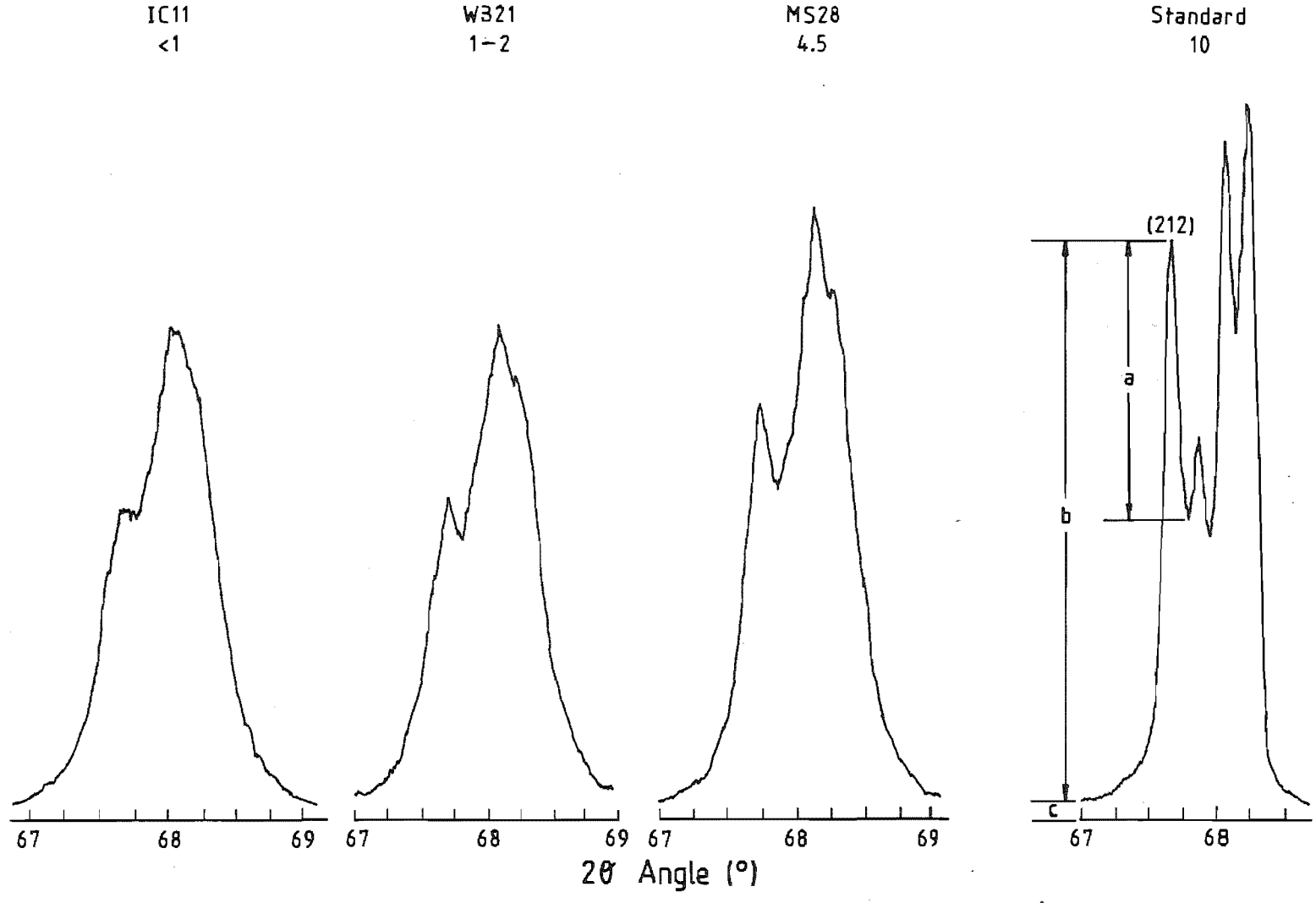

Figure A6.2 Typical quartz crystallinity traces and determined crystallinities of chert and micrite insoluble residues compared to an igneous quartz standard. The crystallinity is determined from the following equation (Murata and Norman 1976): Crystallinity = 10.a.F/b; where F = scaling factor.

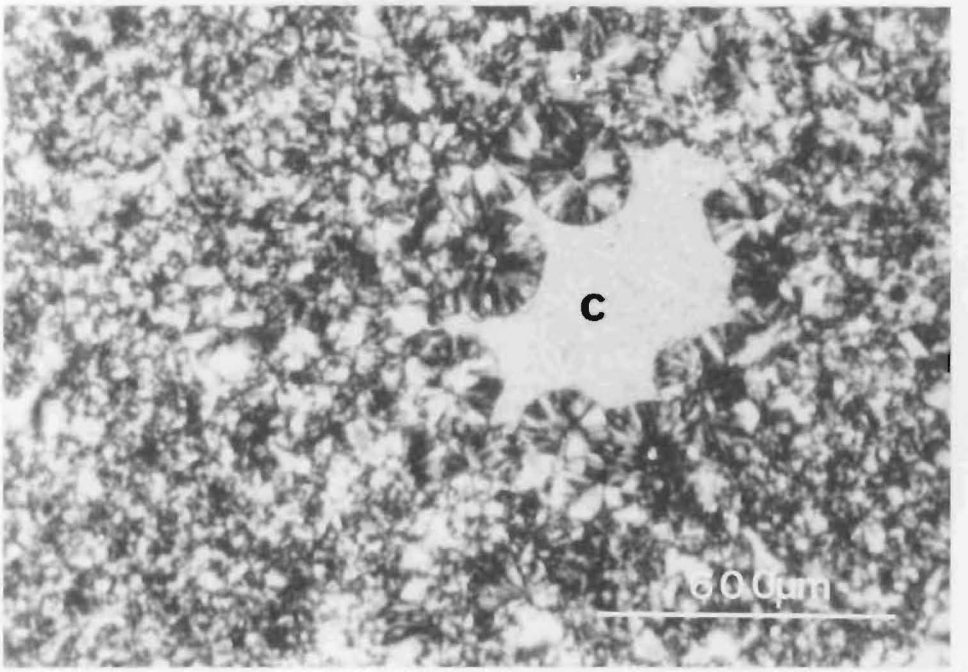

Figure A6.3 Thin section micrograph of a chertified burrow from the CS Zone, Dead Horse Gully (CPL, Sample DHG2). Chalcedony forms spherulitic bodies around the margins of the single sparry calcite (c) crystal. The rest of the chert consists of a mixture of quartz and chalcedony.

>2. Half the samples with an index of <1 have only a single large peak instead of the usual quintuplet, and no (212) peak. Samples with high detrital contents (e.g. a sample from the UCM Subzone with a crystallinity of 4.9) have higher crystallinities than nondetrital-mineral bearing samples. There is little difference between cherts and insoluble residues from adjacent micrites.

A6.2. THIN SECTION PETROGRAPHY

Petrographic nomenclature for chert is as outlined in Keene (1975):

i) Chalcedony - cryptocrystalline, optically fibrous.
ii) Microquartz - <20 μm.
iii) Megaquartz - >20 μm.

A6.2.1. CLAVERLEY SANDSTONE (CS) ZONE

At Dead Horse Gully, chert in the Claverley Sandstone is confined to burrows. Burrow chert is coarser (up to 100 μm) than chert from nodules in the Amuri, and consists of chalcedony and microquartz [Figure A6.3]. Micrite, microspar, chalcedony and microquartz surround the burrow. Minor void-filling cement is seen around some detrital grains. Non-burrow chert at other localities, such as at Waipapa Bay, [Figure A2.8], is the same as that described in more detail in the Amuri Limestone Group [see Sections A6.2.2 to A6.2.7].

A6.2.2. BASAL CHERT (BC) ZONE

Epoxy mounts of chert fragments from Isolation Creek (20) show that the detrital-rich cherts of the lower BC Zone have much in common with siliceous parts of the WC Zone, despite their different appearance in outcrop. In plane polarized light (PPL) samples are generally pale-reddish brown, and detrital mineral composition, grainsize (<150 μm), grain shape, and mica fabric [Figure A6.4a] is similar to that in the Woolshed Formation. Within a given sample the abundance of detrital material is variable between fragments. Elongate pyrite crystals often show some alignment parallel to micas. In crossed polarized light (CPL) chert embayments are also seen in some detrital grains. The matrix is composed of microcrystalline to cryptocrystalline quartz or chalcedony. Large veins which are common, contain quartz that is considerably coarser

Figure A6.4 Thin section micrographs of detrital-rich BC Zone chert displaying a well developed strial fabric.
(a) Upper BC Zone, Isolation Creek (PPL, sample IC6). The opaque minerals are pyrite; also note the clay seam subparallel to bedding.
(b) Upper BC Zone, Isolation Creek (CPL, sample IC8). Detrital grains are smaller than in (a), and there is a slightly greater abundance of micas. The ovoid structures (arrows) may be recrystallized foraminiferal chambers.

Figure A6.5 Thin section (CPL) micrographs of CD Zone chert.
(a) Microcrystalline to cryptocrystalline quartz and disseminated pyrite, Isolation Creek (sample IC11).
(b) Coarser quartz filling a ?foraminiferal chamber (f); note the large pyrite grains (arrows), Wharekiri Stream (sample WKS7).

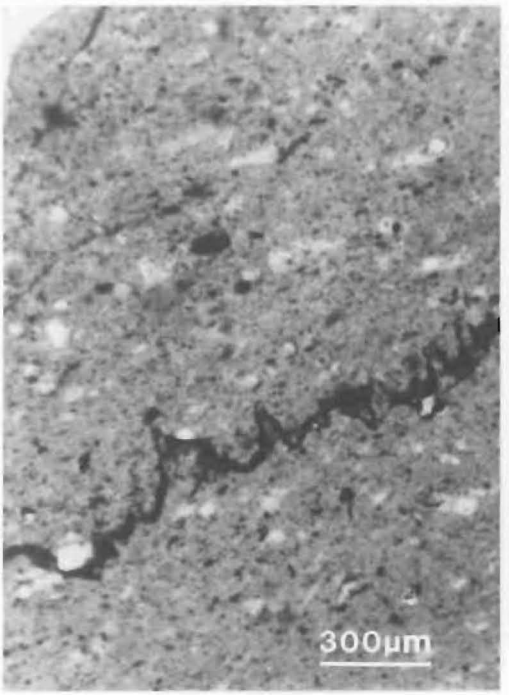

a

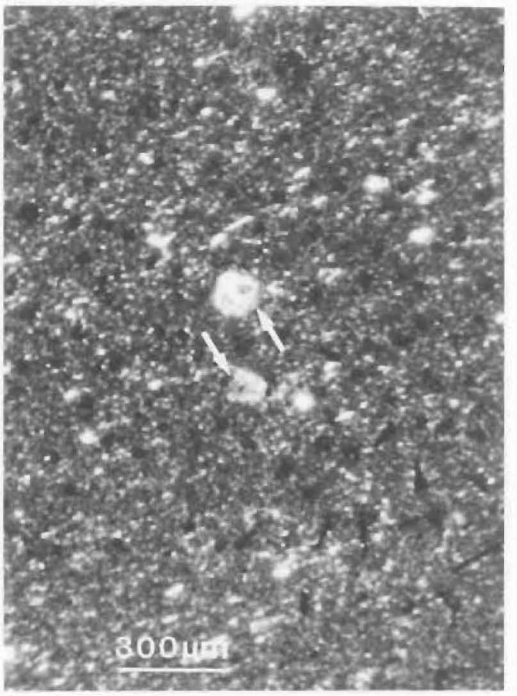

b

A6.4

a

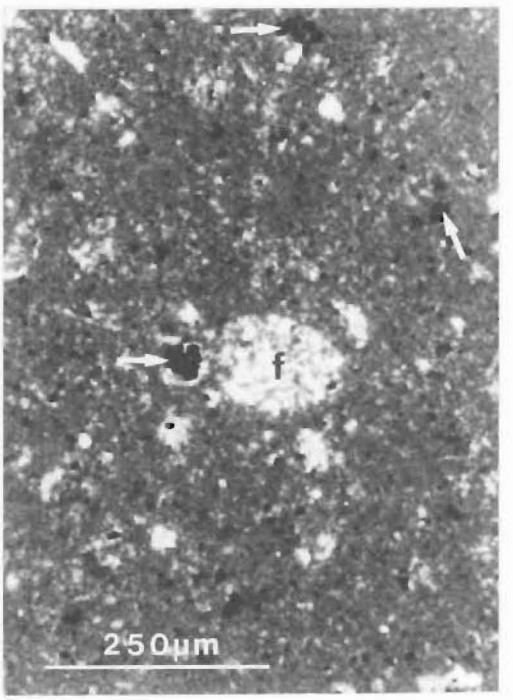

b

A6.5

than the surrounding matrix. One sample [Figure A6.4a] contains a reddish-brown clay seam. No burrows, or material of recognizable biogenic origin is observed.

Samples from the upper BC Zone (referred to in the field as detrital-poor cherts) contain a high detrital mineral content and a well defined strial fabric [Figure A6.4b]. The abundance and size of detrital grains is less than in the underlying detrital-rich cherts. In addition, there are a number of ovoid-lenticular structures, which contain either quartz coarser than the surrounding chert, or in some examples chalcedony. These resemble foraminiferal chambers, although some of the larger and more elongate examples may be chertified burrows. A few may be benthonic foraminifera. Such features are more abundant than in the Woolshed Formation and the lower BC Zone.

A6.2.3. CHERT AND DOLOMITE (CD) ZONE

In PPL the chert is a very pale brown with common pyrite patches or crystals a few microns across. The chert is dominantly microquartz [Figure A6.5a]. Coarser microquartz fills what appear to be foraminiferal chambers [Figure A6.5b]. The chambers vary in shape from circular to ovoid and some are filled with chalcedony. One arenaceous foraminifer was observed.

The abundance of detrital material is considerably less than in the BC Zone, and it decreases in grain size and abundance towards the top of the CD Zone. The size of authigenic quartz is greater than in the BC Zone. The paucity of detrital components means there is no recognizable fabric, although in some instances a preferred orientation of pyrite can be discerned in PPL.

A6.2.4. CHERT AND LIMESTONE (CL) ZONE

Generally, micrites become progressively less siliceous stratigraphically upwards. Chertification in micrite-rich thin sections shows a progressive and often patchy replacement of the fine grained micrite by microquartz [Figure A6.6]. Foraminifera tend to show less chertification than in underlying Zones, and filling of sedimentary pores with silica decreases stratigraphically upwards, and towards the margins of the Mead Hill

Figure A6.6 Thin section micrographs of cherty CL Zone micrite. Both micrographs are at the same scale.
(a) Upper CL Zone, Mead Stream (CPL, sample MS45). The micrite is preferentially chertified by microquartz. Dark areas are relatively micrite rich. Foraminifera are relatively unaffected by silicification and are filled with sparry calcite.
(b) CL Zone, Chancet Rocks (CPL, sample CR6). The large structures containing coarsely crystalline quartz are replaced foraminifera, some containing remnant sparry calcite (s). Irregular patches of microquartz are scattered throughout the micrite matrix. Note the relative lack of pyrite compared to A6.6a.

Figure A6.7 Chert filled foraminifera, CL Zone, Mead Stream (CPL, sample MS31). The foraminiferal chamber contains length-fast chalcedony (ch), microquartz (q), and microspar (s), with pyrite (arrows) adjacent to the test. Length-slow chalcedony has replaced test walls. Chalcedony has filled most of the test except that adjacent to the microspar.

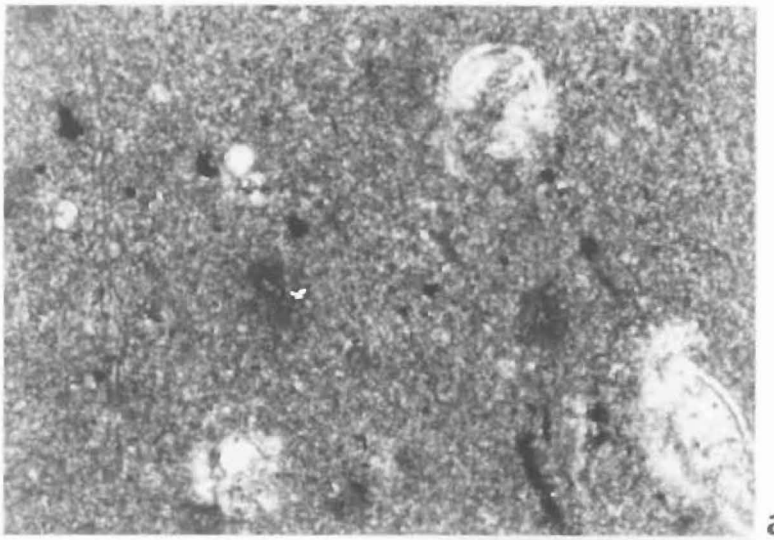

a

A6.6

b

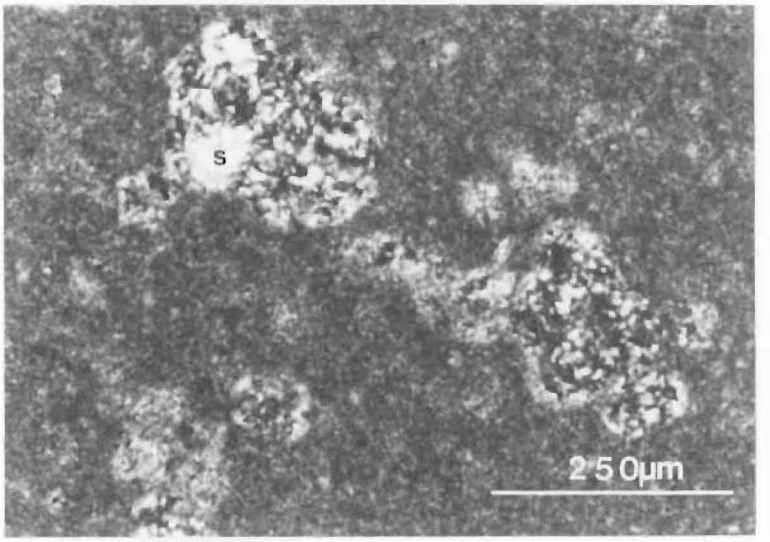

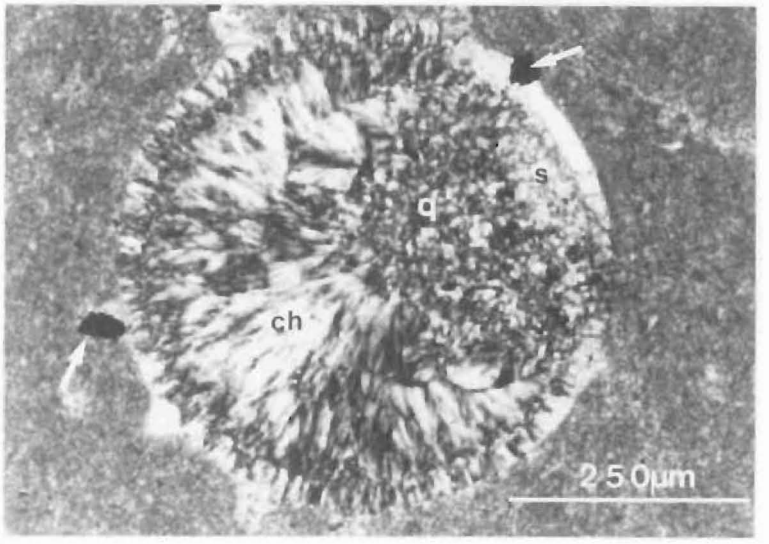

A6.7

Formation basin. For example, thin sections from the top of the CL Zone at Mead Stream are very similar to those from the top of the much thinner CL Zone at Dart Stream. Foraminifera may consist entirely of calcite with minor opaques, even when enclosed in chert nodules. Disseminated pyrite is seen in all thin sections. Despite the dominance of Fe-oxides in pink micrites [Section A3.1.2], pink cherts also contain concentrations of pyrite.

Replacement of foraminifera in micrites shows considerable variation throughout the CL Zone. Examples illustrated in Figures A6.6a and A6.6b, although not always as spectacular, may be found throughout the CL Zone. Foraminiferal chambers, recognized in underlying zones as containing only quartz, here may contain any combination of sparry calcite, micrite, pyrite and quartz varieties. The quartz can be either microquartz, megaquartz, or fibrous chalcedony [Figure A6.7]. Other samples contain chertified foraminiferal walls but chambers filled with spar or micrite. Pyrite may occur in either carbonate or silica infills. Generally chalcedony that fills foraminiferal chambers is length fast. Wall replacement chalcedony is length slow, probably due to a crystallographic control by the calcite it has replaced.

In chert nodules most of the quartz is microcrystalline. Coarser microquartz, and in some cases megaquartz is found as foraminiferal wall replacement or chamber fill. Figure A6.8 shows a variety of foraminifera replacement by quartz in chert nodules. Some foraminifera have not been replaced at all, remaining calcitic yet surrounded by dense microcrystalline quartz [Figure A6.9].

The boundaries between chert nodules and the surrounding micrite consist of a transition zone [Figure A6.10], which is a mixture of quartz and micrite. The contact between the chert proper and the transition zone is diffuse, whereas between the transition zone and the micrite it is sharper. In diffuse-margin micrite-rich chert described in the field, the transition zone may be a few centimetres thick. In such a case the actual chert/micrite boundary cannot be detected in a single thin section, and is often difficult to pinpoint at all.

Growth-ring morphologies [Figure A6.11] consist of a series of semi-concentric preferentially silicified bands (similar features have

Figure A6.8 Thin section (CPL) micrographs of CL Zone chert texture and foraminifera replacement. Disseminated pyrite is common to all samples.

(a) Replacement of foraminiferal walls by quartz coarser than in surrounding chert. Some micrite (s) has remained unchertified (Mead Stream, sample MS36).

(b) Quartz chert filling and surrounding foraminiferal chambers. Test walls however, are still composed mainly of calcite. (Mead Stream, MS36).

(c) Complete replacement by quartz of both foraminiferal chambers and test walls. Note the megaquartz vein (v) at bottom left (Waipapa Bay, sample WB26).

(d) Foraminiferal chamber filled with megaquartz with test walls consisting of calcite (Mead Stream, sample MS31).

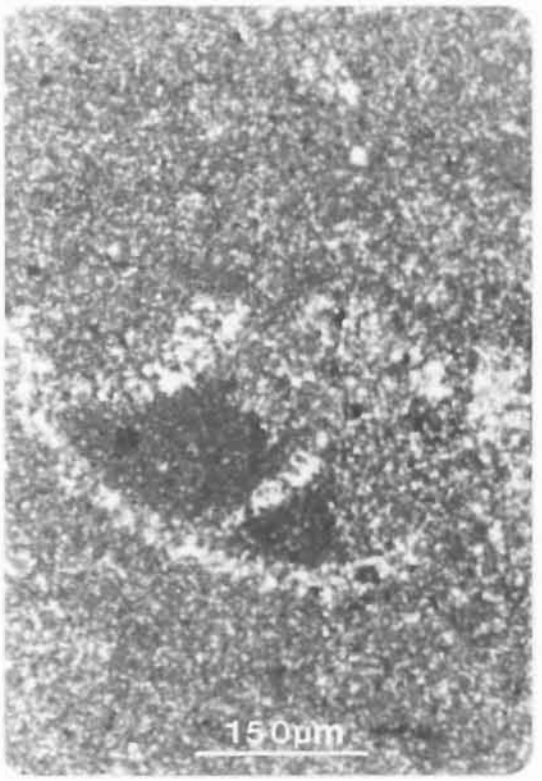

a

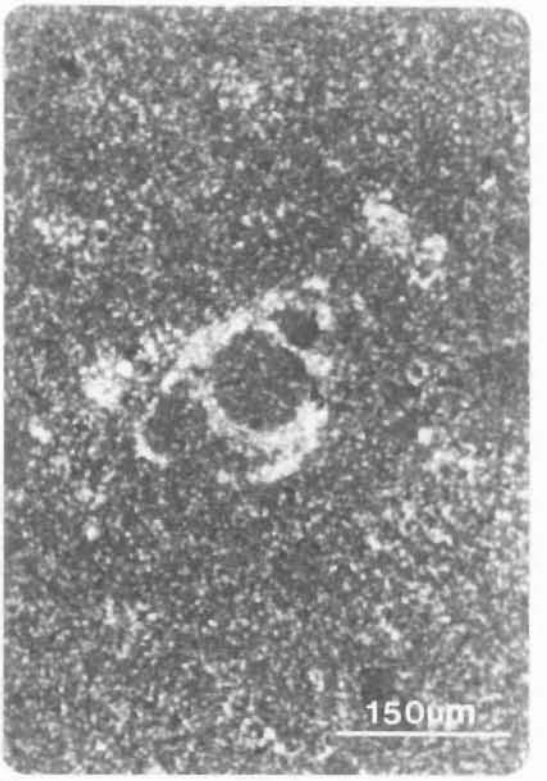

b

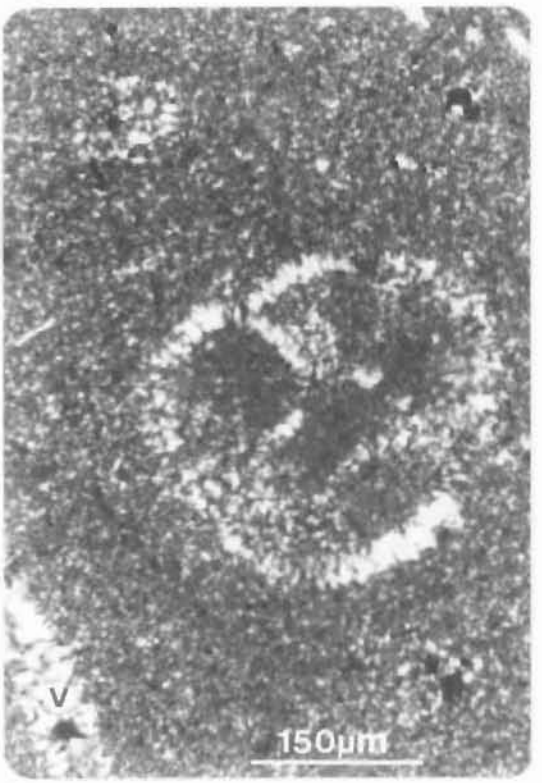

c

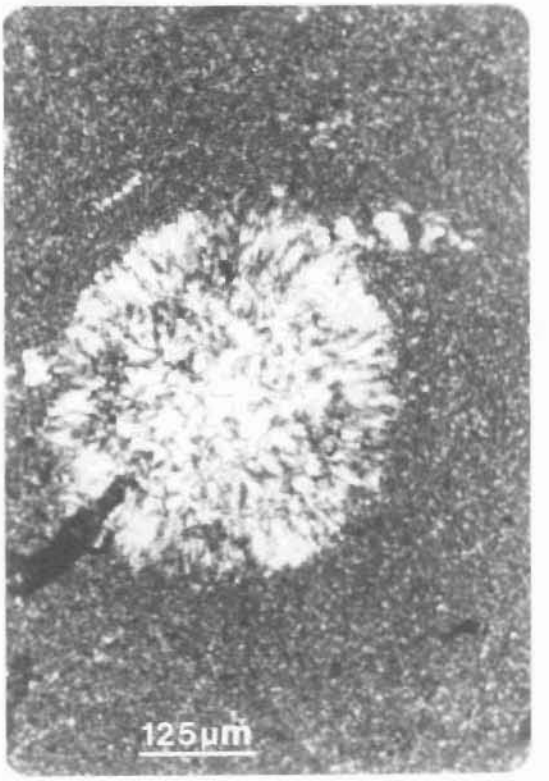

d

Figure A6.9 Chert in a nodule from the CL Zone, Dee Stream (CPL, sample DS9). Foraminifera contain micrite and spar despite complete chertification of the surrounding matrix.

Figure A6.10 Chert (c)/micrite (m) boundary (B), Mead Stream (CPL, sample MS46). Although this is a ML Zone sample, it is the same as chert/micrite boundaries in the CL Zone.

Figure A6.11 Thin section micrograph of 'growth-ring'-like morphology, CL Zone, Isolation Creek (CPL, sample IC21). The arrow indicates the assumed direction of silicification, that is away from the nodule centre.

A6.9

A6.10

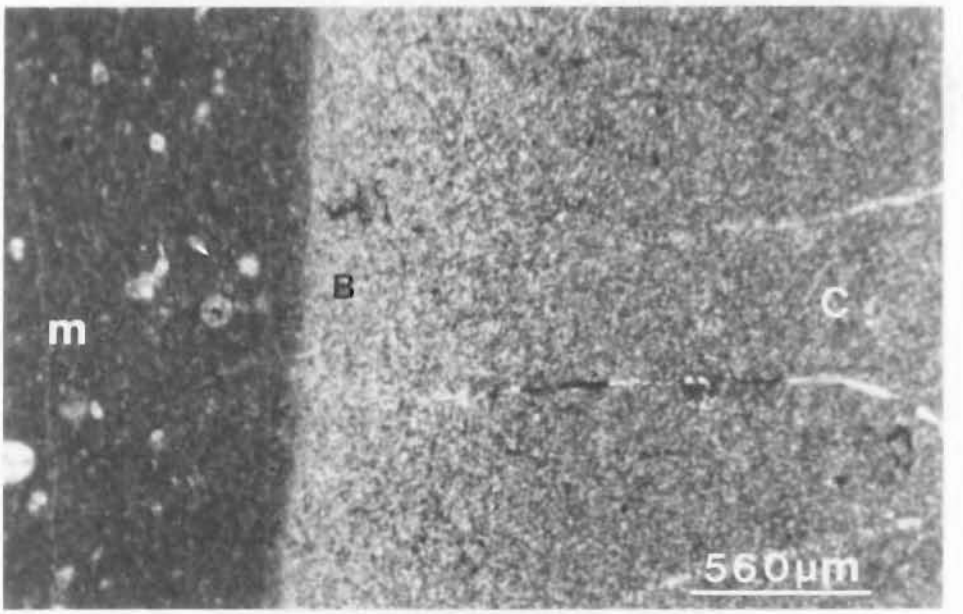

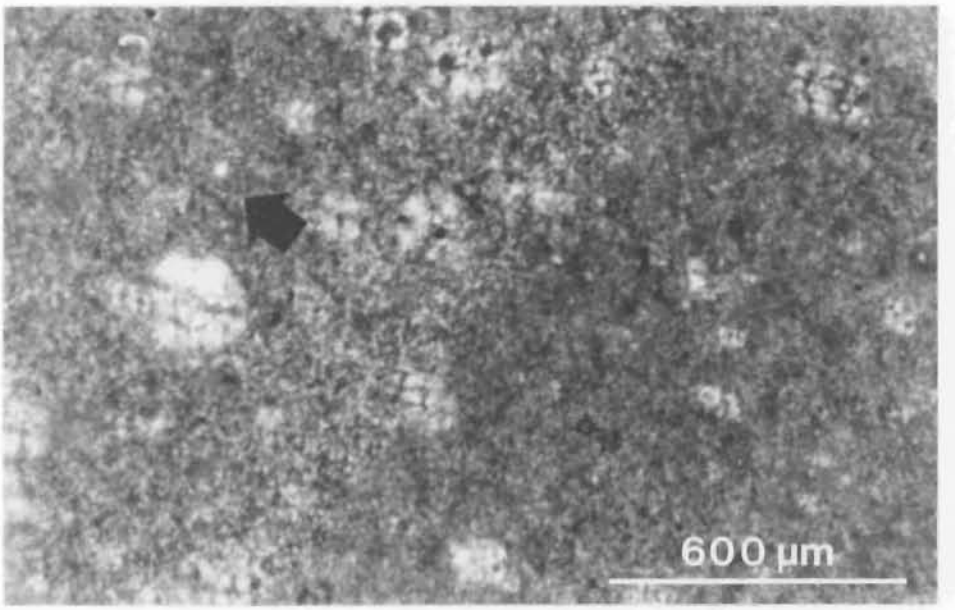

A6.11

also been described from DSDP cherts, e.g. Keene 1975). Chert-micrite boundaries are sharper towards nodule centres, but are more diffuse further away from centres. Patchy silicification between bands is common.

In thin section preserved *Zoophycos* burrows can be distinguished by a difference in micrite colour (in PPL), and by slight increases in opaque and detrital mineral contents [Figure A6.12]. The opaques (mainly pyrite, which in some cases appears to have oxidized to ?limonite) are aligned parallel to burrow walls.

Some thin sections of the K-T boundary sediments were examined for features significant with respect to chertification. Without exception the samples were laminated, siliceous, sparsely fossiliferous mudstones. Also present are minor silt sized detrital quartz, micas and abundant opaques. Fossils consist of foraminifera. No unusual silicification features were observed.

Veins in chert nodules consist of either megaquartz [Figure A6.8c], or chalcedony [Figure A6.13]. Width is often variable with some 1-2 mm across. In micrite-rich cherts veins may also consist of coarse sparry calcite, or even mixtures of quartz and calcite where a calcite vein joins a quartz vein.

Zebra-beds [Figure A6.14], consist of commonly arcuate, 2-3 mm thick veins in siliceous micrite. The vein margins consist of chalcedony with the fibres approximately perpendicular to vein walls. Some bundles of fibres radiate in a fan like manner. Commonly the central part of the vein is occupied by large sparry calcite crystals and occasionally by microcrystalline quartz. Calcite in veins is commonly optically continuous for the entire length of the vein in thin section.

Brecciated samples [Figure A6.15] have a similar but more chaotic appearance to the zebra-beds. Veins anastomose irregularly, are commonly broader than veins associated with zebra-beds, and contain relatively abundant microcrystalline quartz. Veins broken after formation may be seen 'floating' in the sparry calcite. Two layers of chalcedony are commonly found around fragments of micrite [Figure A6.15]. The first is 20-30 μm thick, surrounded by another about 150 μm thick.

Figure A6.12 Thin section micrographs of a *Zoophycos* burrow, CL Zone, Mead Stream (sample DS7).
(a) PPL. Note the colour difference and pyrite concentration both in and outside the burrow confines. Some pyrite is associated with Fe-oxides.
(b) CPL. Chert appears more or less evenly distributed throughout the sample regardless of burrowing.

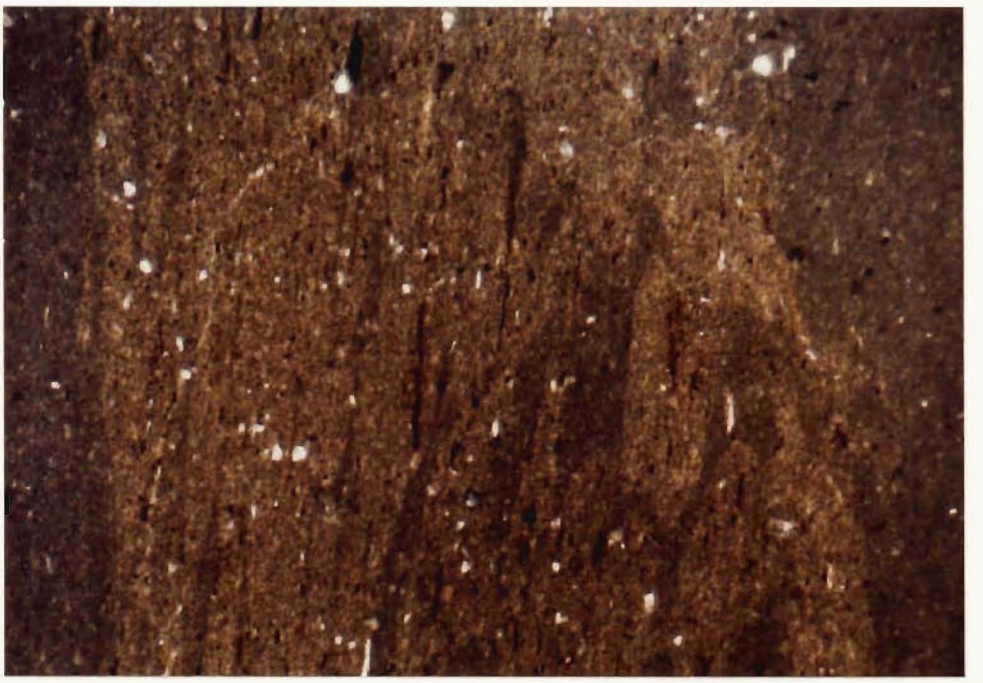

a

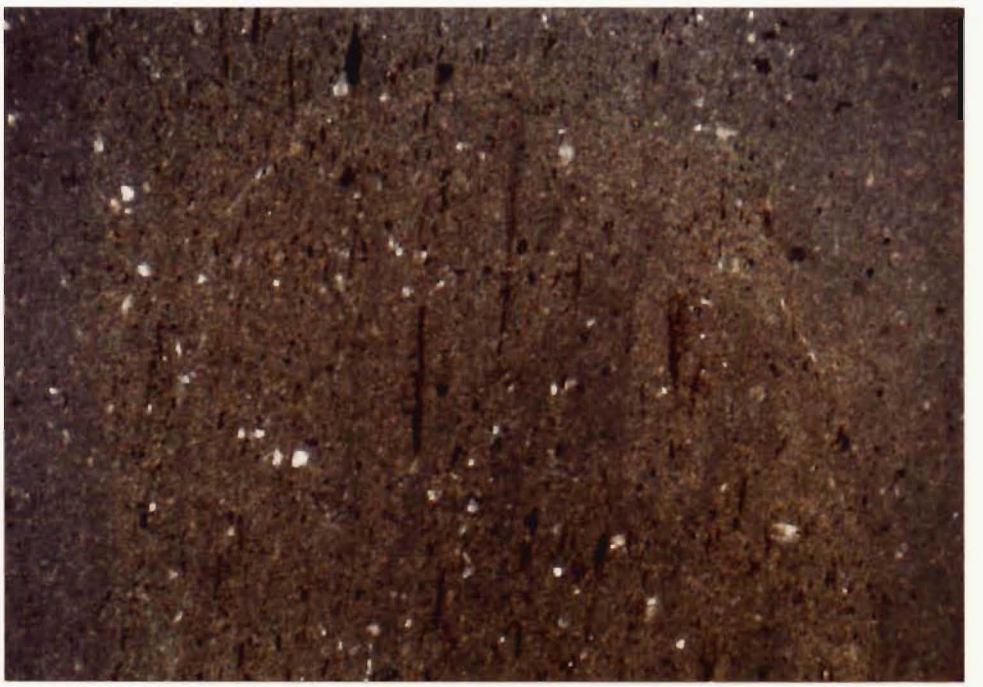

b

560µm

Figure A6.13 Chalcedony vein, CL Zone, Dart Stream (CPL, sample DTS8).

Figure A6.14 Thin section micrograph of a zebra-bed, CL Zone, Dead Horse Gully (CPL, sample DHG1). The arrows indicate the chalcedony margins separated by a large sparry calcite crystal (s). Siliceous micrite occurs on either side of the vein.

Figure A6.15 Thin section micrograph of brecciated chert, CL Zone, Kaikoura Peninsula (CPL, sample KP1). The large, dark, angular chunks of micrite contain detrital silt. The arrows indicate the thin chalcedony layer 'coating' the micrite. Large sparry calcite crystals (s) commonly separate chalcedony-surrounded chunks of micrite.

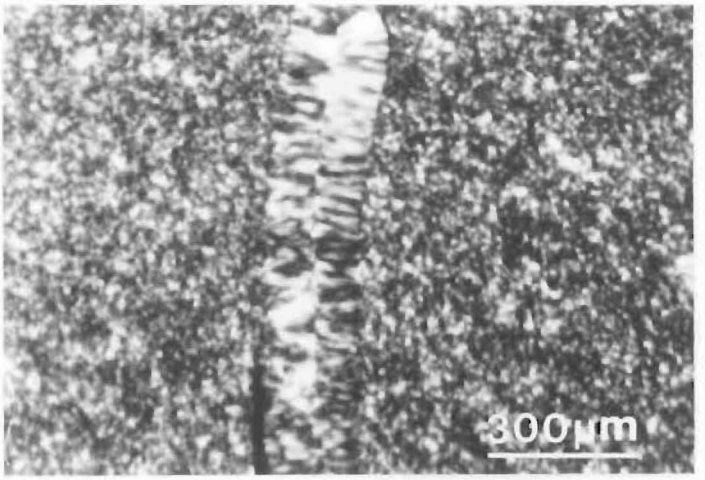

A6.13

A6.14

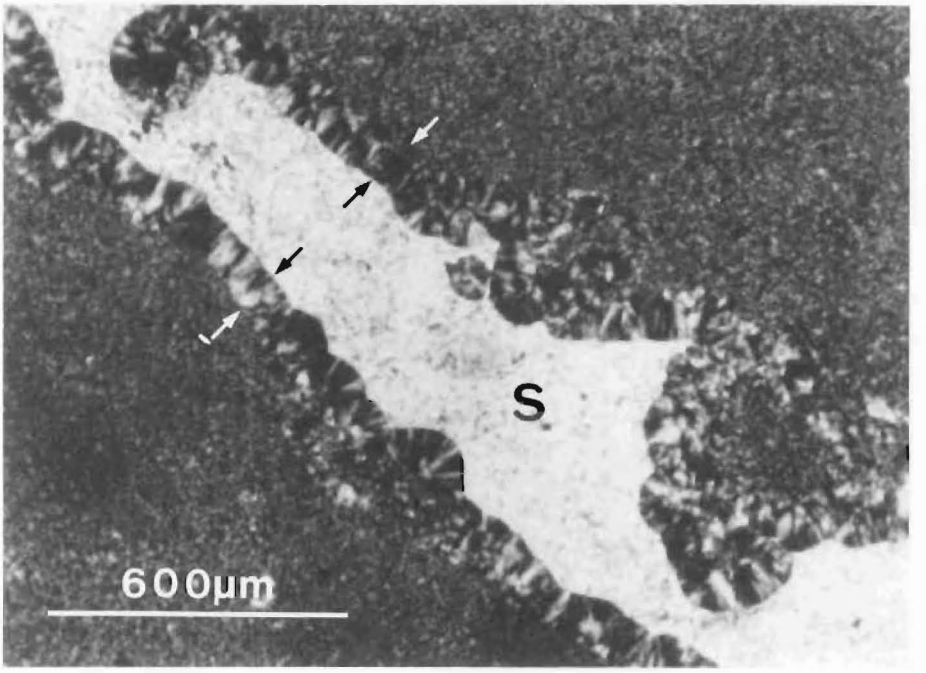

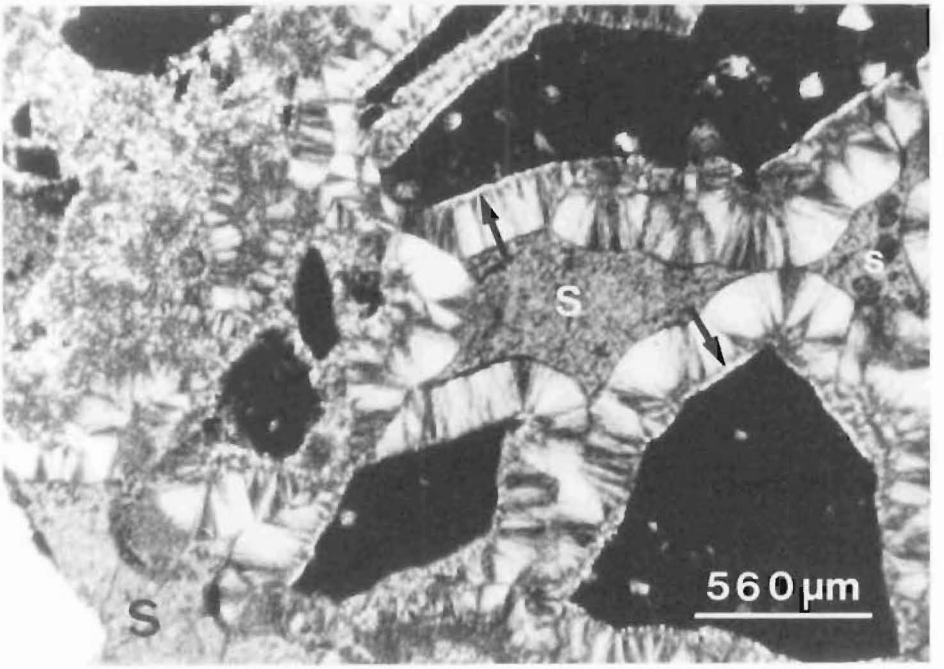

A6.15

A6.2.5. LOWER CHERT MEMBER (LCM) SUBZONE

Chert in thin sections is generally the same as that described in the CD and CL Zones, but with a slightly greater detrital and opaque mineral component. The result is evidence of a strial (Lewis 1985, Table 5) fabric which is observed as far south as Dart Stream (31). The large bed of chert in the Waima River (21) has negligible detrital minerals and lacks evidence of a fabric. An agglutinated foraminifera was found in one Branch Stream (29) sample.

A6.2.6. UPPER CHERT MEMBER (UCM) SUBZONE

Thin sections from the UCM Subzone consist of 10-15%, moderately sorted, subangular, silt to very fine sand grains in a chertified muddy matrix. Detrital grains are primarily quartz, rock fragments and mica [Figure A6.16]. Detrital quartz grains tend to have sharp but irregular margins and may be embayed. Opaque minerals, probably pyrite, and reddish-brown Fe-oxide (?haematite/limonite) staining is common, and a number of phosphatized grains are present. Some radiolaria show little evidence of dissolution. Parallel orientation of both detrital (particularly mica) and opaque grains gives these samples a distinctly strial fabric. Coarser grained authigenic quartz occurs in ovoid, slightly flattened bodies that could be recrystallized radiolaria.

A6.2.7. MIDDLE LIMESTONE (ML) ZONE

ML Zone cherts consist of microquartz as described in underlying formations [e.g. Figures A6.5 and A6.10]. Chert-filled foraminifera increase in abundance towards chert nodules. A transitional zone, or rim [Figure A6.17], usually 2-5 mm thick occurs between 'true' chert and the micrite. It consists of chertified micrite and contains a greater abundance of chert filled foraminifera than the rest of the micrite.

A6.3. SCANNING ELECTRON MICROSCOPY (SEM)

The observed texture depends to some extent upon the fracture surface under observation [Figure A6.18]. Multiple fragments from some samples were examined, and where possible examination of more than one surface from a particular sample was undertaken. A few samples are massive on all

Figure A6.16 Thin section micrograph of the UCM Subzone, Mead Stream (CPL, sample MS41). Note the high concentration of detrital grains. Also present are siliceous microfossils: radiolaria (R) and ?sponge spicules (s).

Figure A6.17 Thin section micrograph of a chert/micrite boundary, ML Zone, Kaikoura Peninsula (CPL, sample KP12). C = quartz chert, sm = silicified micrite, and m = siliceous micrite.

Figure A6.18 Variation in SEM chert texture on fracture surfaces of two different fragments of the same sample (sample DS12).
(a) 'Massive' texture.
(b) 'Crystalline' texture.

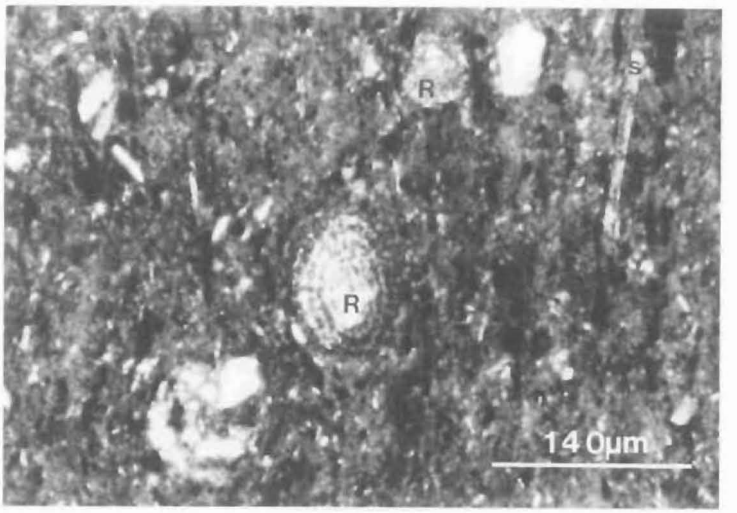

A6.16

A6.17

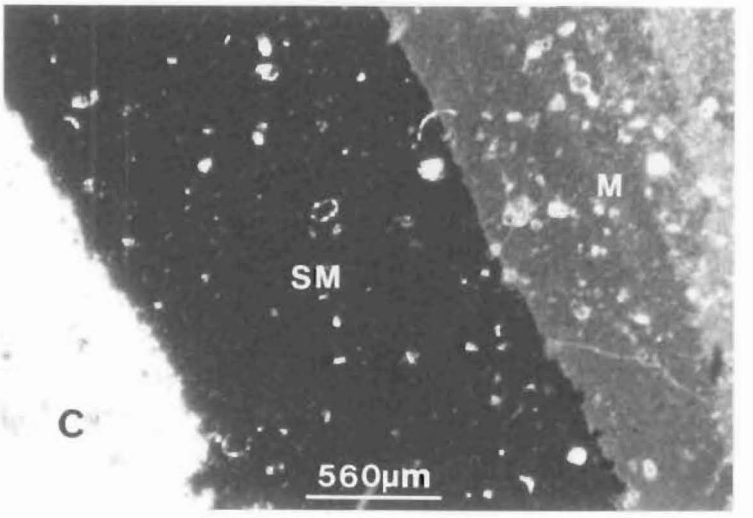

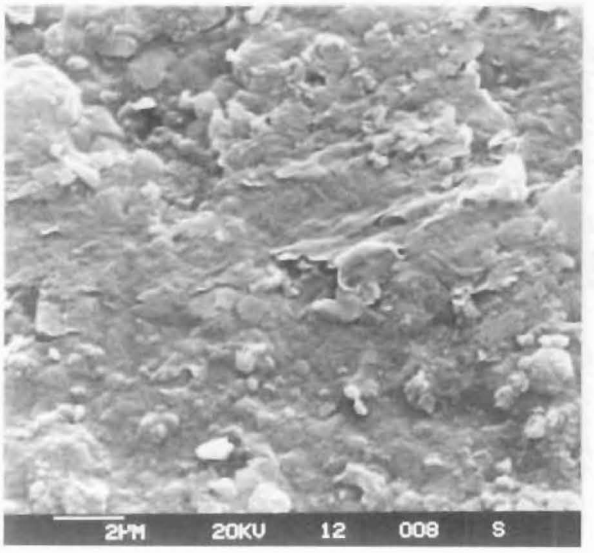

a

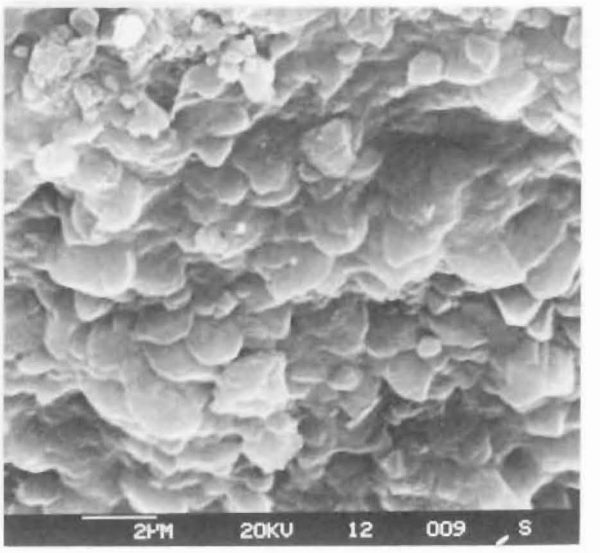

b

A6.18

surfaces.

Chert sampled in the BC, CD, and CL Zones consists of blocky to prismatic crystals [Figure A6.19], as well as massive textures [Figure A6.18a]. Crystal dimensions range from 2-10 μm. A single micrograph may contain the entire size range [Figure A6.19e]. Specific morphologies tend to predominate in some samples, although many samples contain varied morphologies. There is no apparent systematic variation in size and shape of crystals, either stratigraphically or geographically. The comparison of two adjacent cherts, one thought to be *in situ* and another which disrupts the surrounding bedding and may have been redeposited [such as seen in Figures A2.17 or A2.25], showed no textural differences.

Most of the chert in the LCM Subzone is similar to that described in the rest of the Mead Hill Formation. However, some samples display a form of preferred orientation [Figure A6.20a,b]. Samples from the vertical chert structures [Figure A2.29] display a preferred orientation also [Figure A6.20c,d]. The laminated chert at Waipapa Bay [Figure A2.11] displays distinct lamination at a microscopic scale [Figure A6.20e].

All chert fragments commonly contain spherical, often aggregated cavities which are recognizable as replaced, mainly planktonic foraminifera [Figure A6.21a,b,c]. The quartz replacing test walls is usually slightly coarser than that in the surrounding matrix. Chamber infillings tend to vary in grain size, with usually prismatic crystals but greater intercrystalline porosity than chert outside chambers. Framboidal pyrite is seen inside a few examples [Figure 6.21d]. There are no positively identifiable siliceous microfossils, and nothing recognizable as coccolithophorids are seen.

In addition to obviously recognizable biogenic material, there are rare irregularly shaped pits [Figure A6.21e]. Their internal surface texture is the same as that of the exterior. One porous chert [Figure A6.21f] occurs near the top of the sequence at Waipapa Bay. The pores consist of irregular pits, up to 0.5 μm, randomly distributed throughout the chert surface.

The cristobalite samples from Chancet Rocks (18) and Thomson's Gully (19) display massive and platy textures on most surfaces [Figure A6.22].

Figure A6.19 Typical SEM chert textures.
(a) Intergrown tabular quartz crystals, BC Zone, Isolation Creek (sample IC8).
(b) Euhedral quartz crystals, BC Zone, Mt Alexander (sample MA3).
(c) More or less rhombic quartz crystals, BC Zone, Mt Alexander (sample MA4).
(d,e) Mixtures of textures shown in (a,b,c) with variations in crystal face development, CD Zone, Limburn Stream (samples LS12 and LS2 respectively).
(f) Massive texture with some euhedral and tabular crystals in cavities, LCM Subzone, Dee Stream (sample DS15).

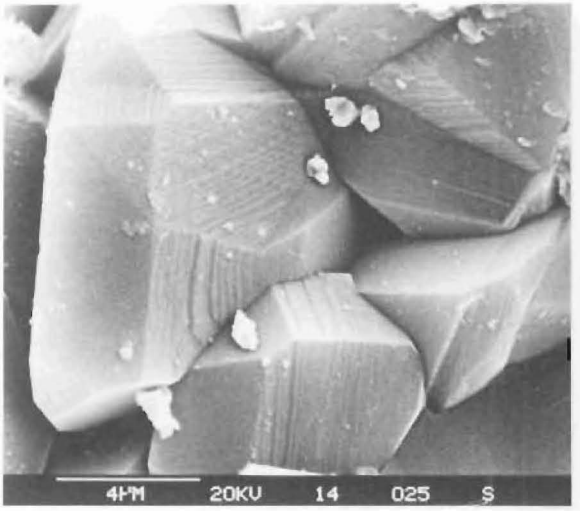
4μM 20KV 14 025 S

a

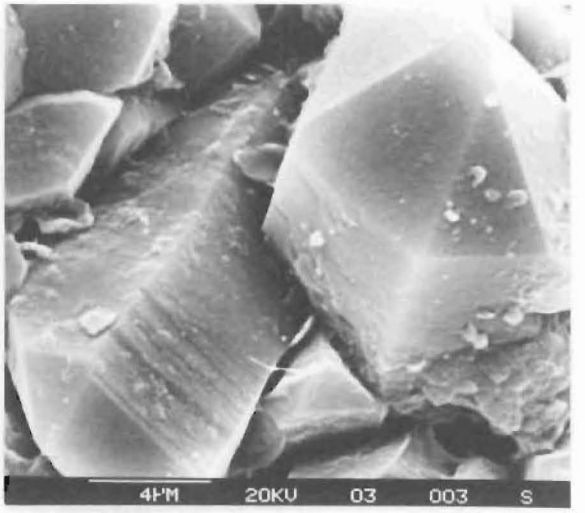
4μM 20KV 03 003 S

b

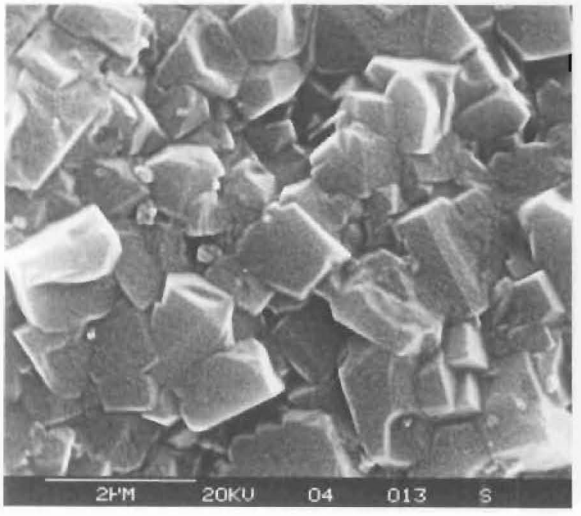
2μM 20KV 04 013 S

c

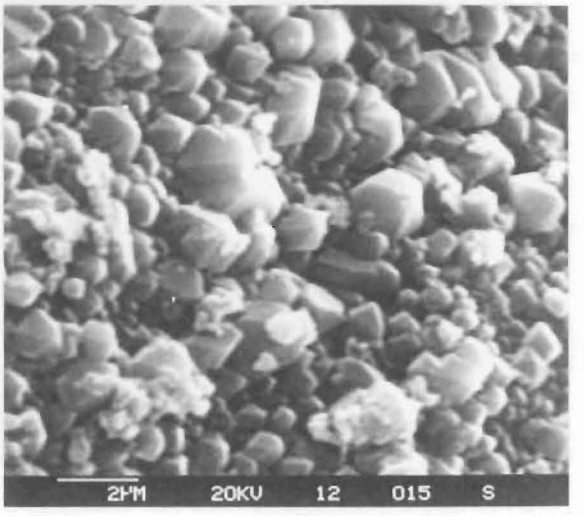
2μM 20KV 12 015 S

d

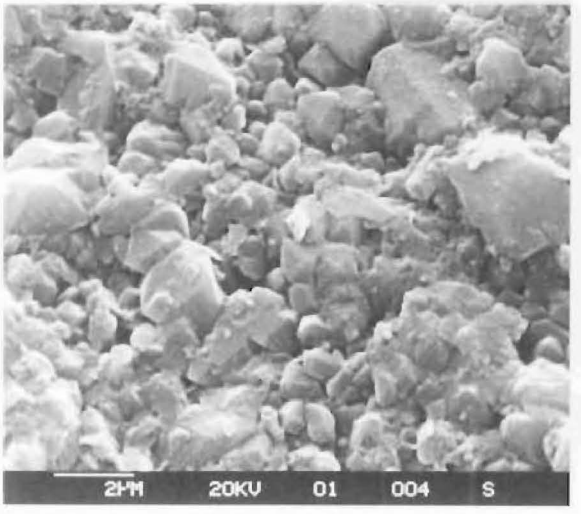
2μM 20KV 01 004 S

e

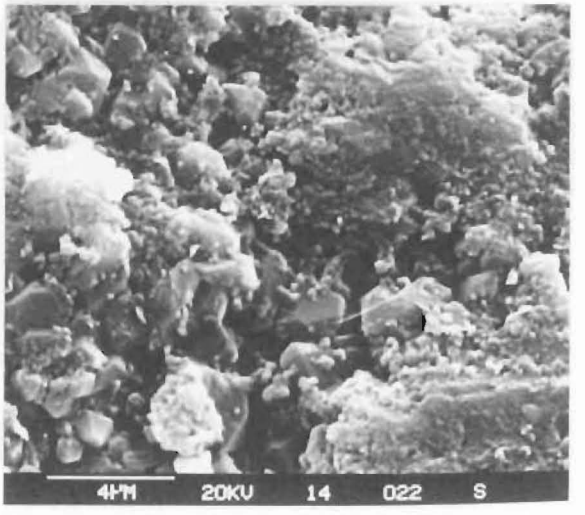
4μM 20KV 14 022 S

f

Figure A6.20 SEM micrographs of preferred orientation in chert.
(a) LCM Subzone, Waima River (sample WUR4).
(b) LCM Subzone, Mead Stream (sample MS25).
(c,d) Two different surfaces from a single fragment of a vertical chert structure, CL Zone, Waima River (sample WUR1).
(e) Laminated chert (seen in Figure A2.11), BC Zone, Waipapa Bay (sample WB21).

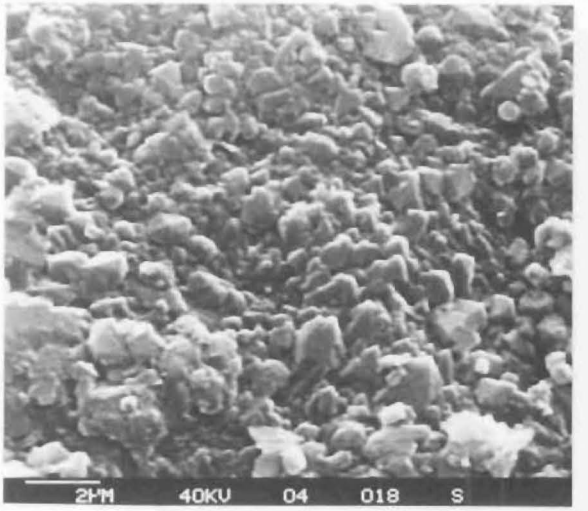
2µM 40KV 04 018 S

a

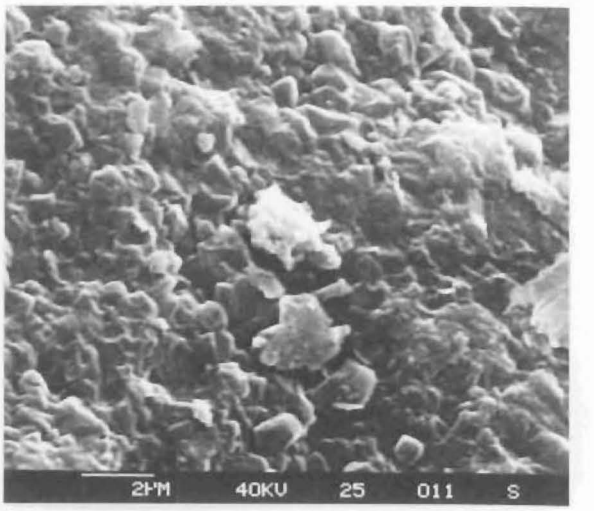
2µM 40KV 25 011 S

b

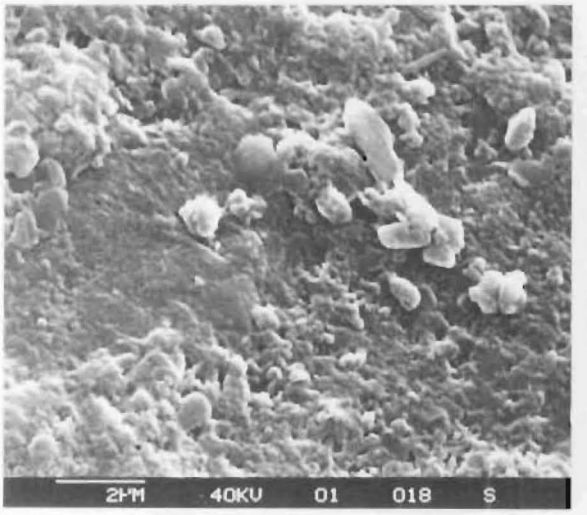
2µM 40KV 01 018 S

c

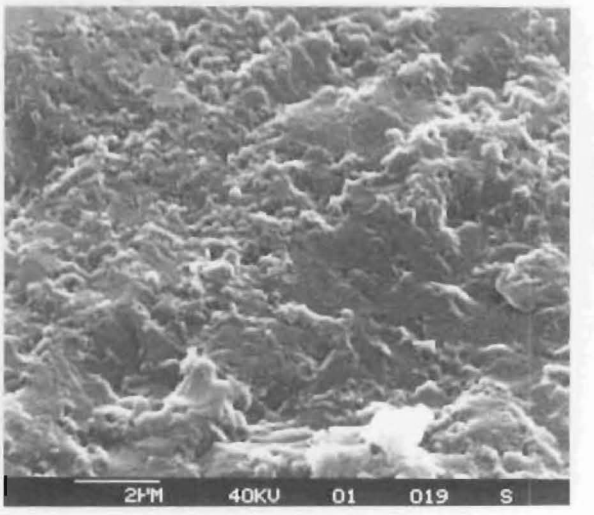
2µM 40KV 01 019 S

d

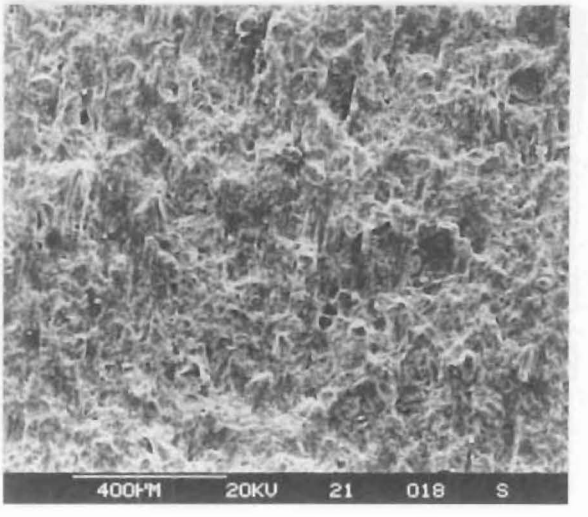
400µM 20KV 21 018 S

e

Figure A6.21 SEM micrographs of pore structures and chertified foraminifera.

(a) Single recrystallized foraminiferal chamber, BC Zone, Waipapa Bay (sample WB4).

(b,c) Recrystallization of multiple chambers, BC Zone, Waipapa Bay (b, sample WB4) and UCM Subzone, Mead Stream (c, sample MS39).

(d) Chertified foraminiferal chamber containing pyrite framboids (arrows), CL Zone, Mead Stream (sample MS34).

(e) Irregularly shaped pits, CL Zone, Puhi Puhi River (sample PS19).

(f) Porous chert containing a large number of irregularly shaped pits, ML Zone, Waipapa Bay (sample WB36).

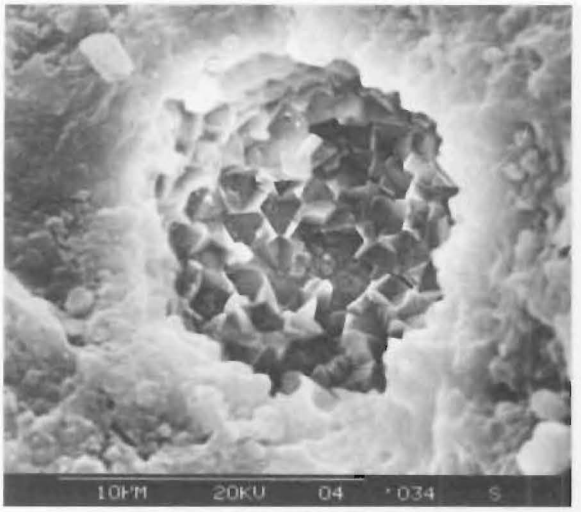
10µM 20KV 04 034 S

a

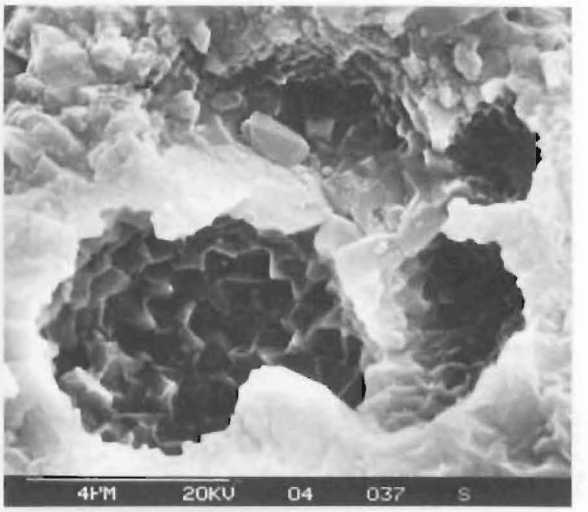
4µM 20KV 04 037 S

b

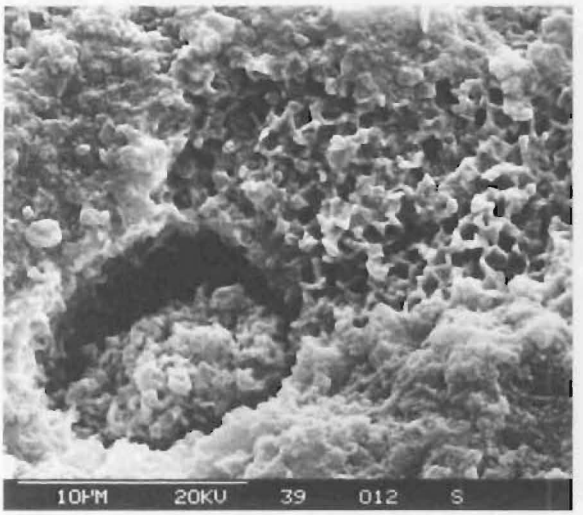
10µM 20KV 39 012 S

c

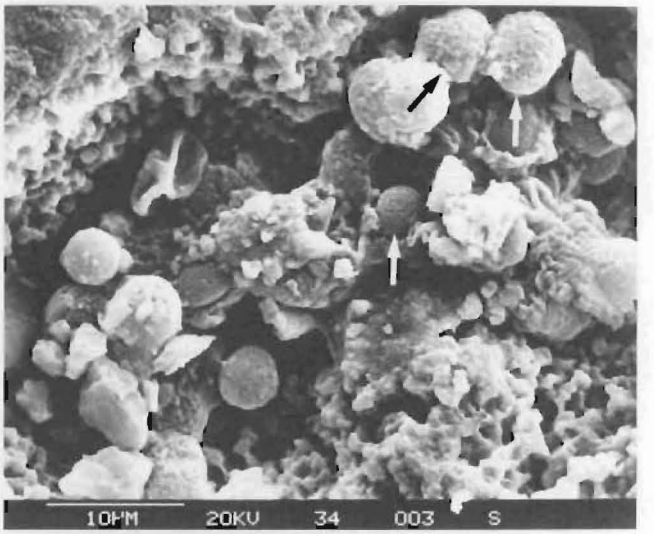
10µM 20KV 34 003 S

d

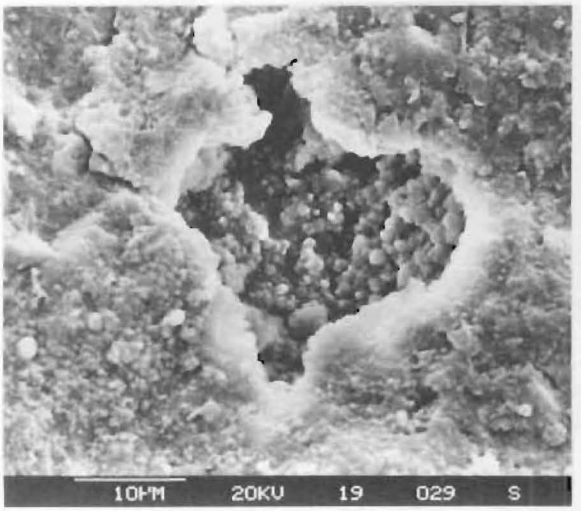
10µM 20KV 19 029 S

e

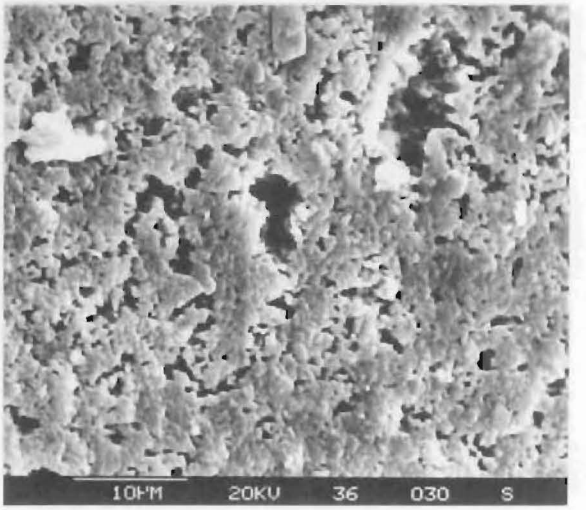
10µM 20KV 36 030 S

f

Opal-CT lepispheres and plates [Figure A6.22a,b,c] are common in or adjacent to cavities in the Thomson's Gully samples. The Chancet Rocks samples contained prominent rounded grains [Figure A6.22d] of either quartz or calcite.

Essentially the bulk of SEM characteristics are common to all cherts in the Amuri Limestone Group. The are no features specific to any particular diagenetic zone.

A6.4. GEOCHEMICAL ANALYSES

Results are summarized in Table A6.1. Geochemical profiles are plotted in Figures A6.23 and A6.25 [map pocket].

A6.4.1. MAJOR ELEMENTS

Generally the chert contains in excess of 90% SiO_2, about 1% Al_2O_3, with other major elements usually in concentrations of less than 1% each [Table A6.1a]. P_2O_5 is consistently below detection limits (0.05%) in all analyses. With the exception of the UCM Subzone, a high proportion of MgO and MnO analyses are close to, or below detection limits (0.1% and 0.01% respectively). Although some Na_2O and CaO analyses are below detection limits (0.1% and 0.01% respectively), the bulk are at least twice as high. TiO_2 is present in all units to levels usually greater than four times the detection limits, and K_2O is present to levels about ten times higher than detection limits (both have detection limits of 0.01%). Except in the UCM Subzone, all major element analyses other than SiO_2, Al_2O_3 and losses on ignition, comprise less than 2% of the total major element composition. Chert colour and morphology do not correlate in any way with major element composition.

Intra-nodule Variations

The bulk of the chert nodules are exposed in cross section, seldom in plan section, and rarely in plan section that can be adequately sampled. At one Muzzle Stream (32) locality, a large accessible chert nodule measuring 1.1 m by 2.9 m is exposed on a bedding plane. Five samples from various parts of the nodule were analyzed. The amount of variation between each sample is within the limits of analytical uncertainty. As described in

Figure A6.22 SEM micrographs of cristobalite and rounded grains.
(a,b) Cristobalite displaying platy or bladed morphology, CL Zone, Thomson's Gully (sample TG4).
(c) Cristobalite lepispheres in a cavity, CL Zone, Thomson's Gully (sample TG4).
(d) Rounded grain morphologies, CL Zone, Chancet Rocks (sample CR4).

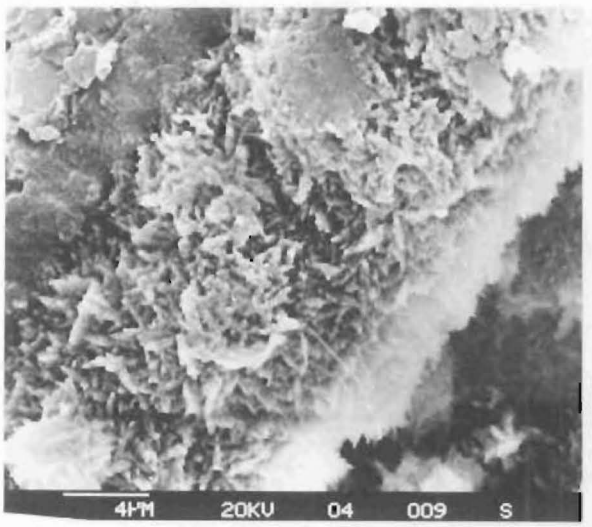
4µM 20KV 04 009 S

a

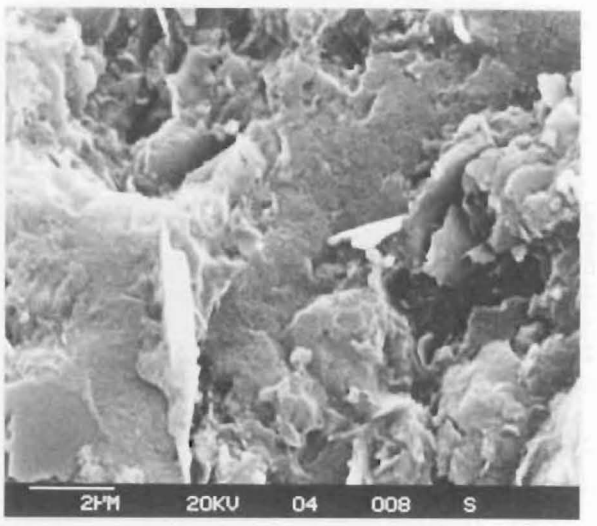
2µM 20KV 04 008 S

b

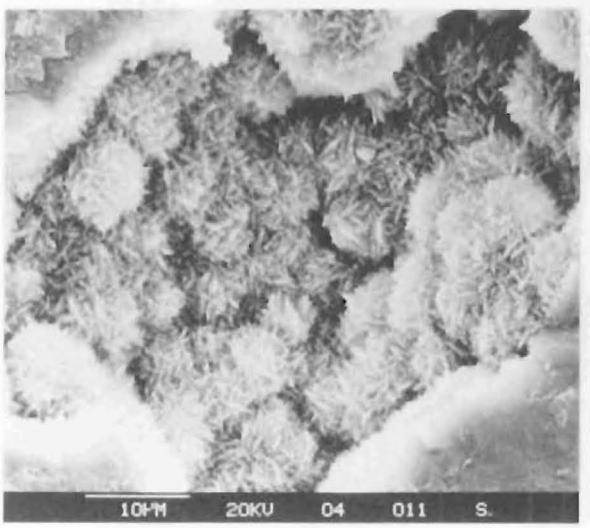
10µM 20KV 04 011 S.

c

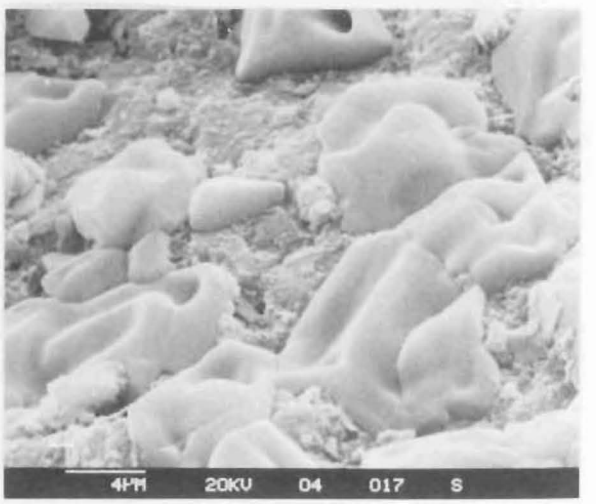
4µM 20KV 04 017 S

d

Table A6.1a Summary of major element analyses (weight% oxide) for cherts. Figures in brackets indicate the number of samples analyzed. Where minimum values are below detection limits mean values may be artificially high. Detection limits are listed in Table A1.3.

		SiO_2	TiO_2	Al_2O_3	Fe_2O_3	MnO	MgO	CaO	Na_2O	K_2O	LOI	P_2O_5
ML	Maximum	98.84	0.10	2.14	0.31	0.05	0.26	0.36	0.23	0.60	1.90	<0.05
Zone	Minimum	94.79	0.02	0.20	0.04	<0.01	<0.10	<0.01	<0.10	0.04	0.50	
(19)	Mean	97.30	0.04	0.79	0.12	0.02	0.11	0.09	0.13	0.16	1.09	
UCM	Maximum	92.39	0.17	3.19	0.75	0.05	0.46	0.75	0.36	0.62	4.13	<0.05
Subzone	Minimum	89.47	0.11	2.33	0.70	<0.05	0.40	0.05	0.25	0.43	1.68	
(3)	Mean	90.56	0.14	2.87	0.72	0.03	0.42	0.29	0.29	0.54	2.75	
LCM	Maximum	97.81	0.14	2.73	0.69	0.05	0.32	0.19	0.46	0.67	1.82	<0.05
Subzone	Minimum	92.83	0.03	0.58	0.11	<0.01	<0.10	<0.01	<0.10	0.12	0.04	
(17)	Mean	95.99	0.07	1.24	0.26	0.02	0.13	0.06	0.22	0.27	1.16	
CL	Maximum	98.91	0.25	4.92	1.05	0.05	0.85	0.18	0.38	1.53	2.81	<0.05
Zone	Minimum	87.66	0.02	0.20	0.04	<0.01	<0.10	<0.01	<0.10	0.05	0.00	
(84)	Mean	96.85	0.05	1.00	0.18	0.02	0.13	0.06	0.15	0.20	2.81	
CD	Maximum	98.39	0.17	4.86	0.64	0.05	0.45	0.42	1.57	0.99	1.60	<0.05
Zone	Minimum	89.45	0.03	0.50	0.05	<0.01	<0.10	<0.01	<0.10	0.11	0.52	
(28)	Mean	96.18	0.07	1.47	0.26	0.02	0.16	0.06	0.22	0.35	1.10	
BC	Maximum	97.59	0.14	3.42	0.83	0.05	0.41	0.19	0.93	0.78	1.71	<0.05
Zone	Minimum	92.59	0.03	0.82	0.05	<0.01	<0.10	<0.01	<0.10	0.16	0.72	
(17)	Mean	95.59	0.08	1.67	0.31	0.02	0.15	0.05	0.28	0.37	1.11	

Table A6.1b Summary of trace element analyses (in ppm) for cherts.

		V	Cr	Ni	Zn	Ga	Rb	Sr	Y	Zr	Nb	Ba	Ce	Nd	La	Pb	Th
ML	Maximum	23	8	11	9	22	13	354	3	120	<5	7237	<10	13	33	5	<1
Zone	Minimum	<5	<5	<5	<2	<2	<1	11	<1	<5		111		<10	<2	2	
	Mean	6	<5	6	3	3	5	90	<1	18		1694		<10	4	4	
UCM	Maximum	56	64	23	40	3	27	175	26	42	<5	3585	23	14	15	4	<1
Subzone	Minimum	39	33	16	12	2	17	134	5	24		1600	<10	<10	<2	2	
	Mean	48	53	20	23	3	22	153	13	35		2756	15	11	7	3	
LCM	Maximum	53	38	29	57	3	24	61	23	170	<5	1715	25	15	12	276	<1
Subzone	Minimum	5	5	<5	3	<2	3	6	<1	6		126	<10	<10	<2	2	
	Mean	16	12	7	15	2	10	32	4	22		812	11	<10	3	20	
CL	Maximum	45	28	32	27	6	57	277	5	54	<5	11289	120	13	9	7	<1
Zone	Minimum	<5	<5	<5	<2	<2	<1	8	<1	3		55	<10	<10	<2	2	
	Mean	8	7	6	6	<2	7	54	2	13		1097	11	<10	<2	4	
CD	Maximum	19	17	15	24	4	26	55	6	113	<5	590	11	17	5	5	<1
Zone	Minimum	<5	<5	<5	<2	<2	3	4	<1	5		62	<10	<10	<2	2	
	Mean	9	7	5	6	<2	11	25	2	18		243	<10	<10	<2	4	
BC	Maximum	25	23	11	44	5	26	121	6	63	<5	1158	<10	12	37	6	3
Zone	Minimum	<5	<5	<5	<2	<2	2	15	<1	10		117		<10	<2	<1	<1
	Mean	11	9	6	9	2	12	45	2	25		387		<10	6	4	1

Section A6.4.3, similar findings are common in nodule cross sections. From this it would seem that the spot samples used for the bulk chemistry are representative of bulk nodule composition. The same reasoning applies to the trace element composition.

Stratigraphic Relationships

For the same reasons outlined in Section A5.5.2, description of stratigraphic variations for both major and trace elements is confined to Isolation Creek and Clarence Valley sections.

The very low concentrations of MnO, CaO, MgO, in particular, and to some extent Na_2O and TiO_2, result in poor reproducibility [Table A1.3]. Therefore some of the stratigraphic variation can be explained in terms of analytical uncertainty. Stratigraphic variations in composition are best displayed by SiO_2, Fe_2O_3, Al_2O_3, and to some extent by K_2O and loss on ignition.

Profiles [Figure A6.23] show that SiO_2 and the other major element analyses vary antipathetically. The detrital-rich units (UCM Subzone, the lower BC Zone, and to some extent the lower LCM Subzone) contain less SiO_2 and more Fe_2O_3 and Al_2O_3 than other cherts. Loss on ignition (not plotted) shows much less stratigraphic variation, which with an analytical uncertainty of 10-20% means the real stratigraphic variation is minor. The loss on ignition for the UCM is about twice that of other cherts.

Compositional differences between the UCM Subzone and other cherts are readily apparent in Figure A6.23. Differences between other units are poorly defined. Frequency distributions of Al_2O_3 [Figure A6.24] and Fe_2O_3, and to a lesser extent K_2O, show an overall upward decrease from the BC Zone to the CD Zone. The LCM Subzone has more compositional similarity to the BC Zone, and the ML Zone is similar to the CL Zone. In general however, differences between all units except the UCM Subzone are minor. Most samples from each zone are confined to restricted compositional ranges.

A6.4.2. TRACE ELEMENTS

With the exception of Ba, concentrations of individual trace elements are

Figure A6.24 Histogram of Al_2O_3 concentration in all cherts. Fe_2O_3 displays a similar pattern.

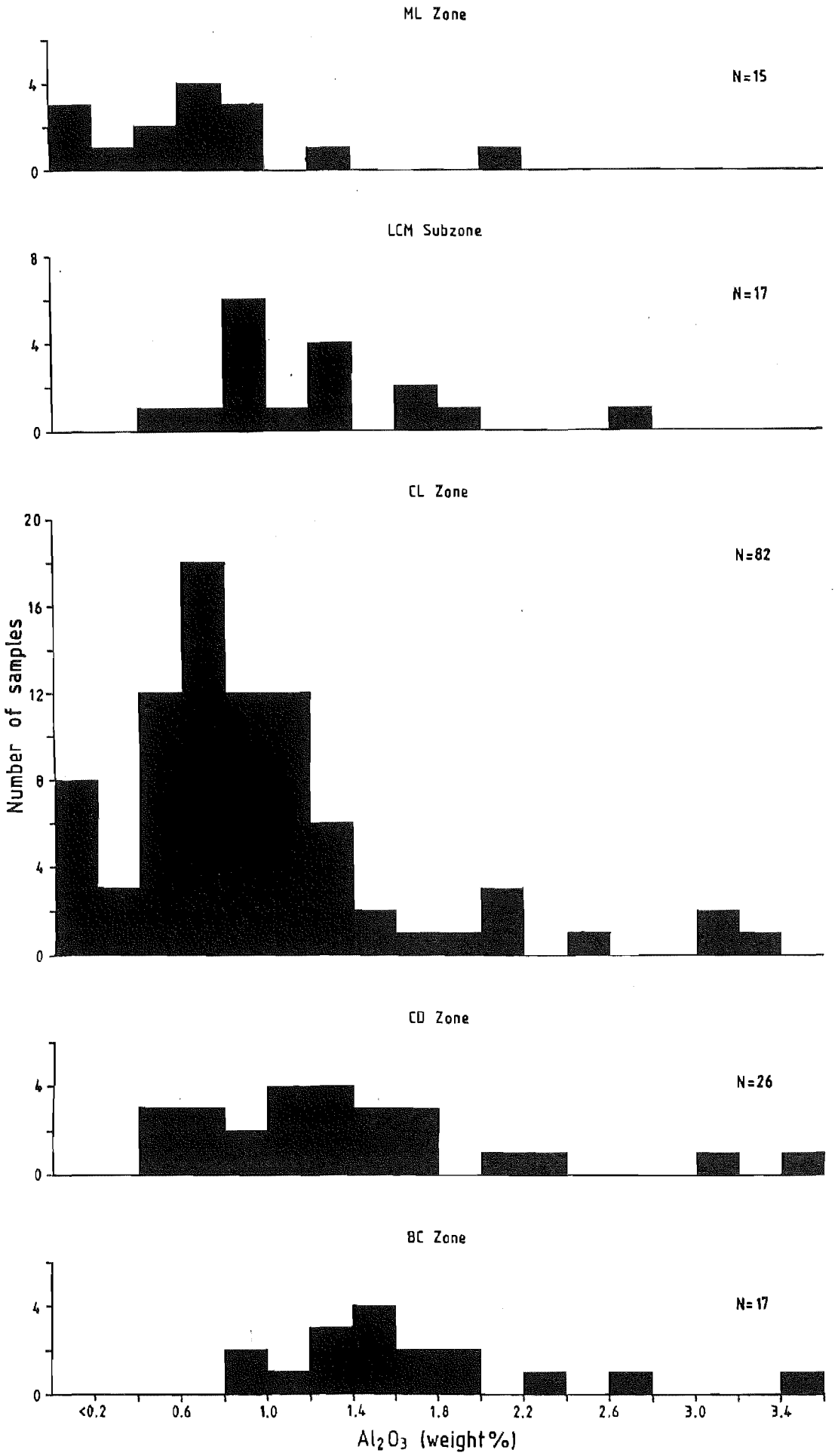
ML Zone
N=15
LCM Subzone
N=17
CL Zone
N=82
CD Zone
N=26
BC Zone
N=17
Number of samples
0
4
8
12
16
20
<0.2
0.6
1.0
1.4
1.8
2.2
2.6
3.0
3.4
Al2O3 (weight%)

frequently less than 50 ppm and nearly always less than 100 ppm [Table A6.1b]. Lanthanum, Th, Ga, Nb, Nd, and Ce are at or below detection limits. Nickel, Pb, Y, and to some extent Zn, Cr, and V, are usually only a few ppm above detection limits (Detection limits are: 2 ppm for Ga and Zn; 1 ppm for Th, Pb, and Y; 5 ppm for Nb, Ni, Cr, and V; 10 ppm for Nd and Ce.). Strontium, Rb, and Zr concentrations are usually less than 500 ppm and Ba is usually in excess of 100 ppm.

Stratigraphic Variations

Trace element concentrations in the UCM Subzone are generally higher than in any other unit. Barium, Zr, Rb, Sr, V, Cr, and Zn profiles are shown in Figure A6.25. There are considerable variations in Rb, Zr, Ba, and Sr abundances. There is less variation in V, Cr, and Zn. As seen in major element profiles there are no distinct trends, except for the high concentrations in the UCM Subzone and for some elements in the LCM Subzone. The shape of Sr, Ba, and Zr profiles is similar, as are those for V, Cr, and Zn, but the profiles of Sr, Ba, and Rb differ. The Zr profile has similarities to both sets of profiles.

Trace element ranges in each unit show considerable overlap. There is a slight suggestion from frequency distributions that the BC and ML Zone, and LCM Subzone cherts contain marginally greater trace element abundances than CD and CL Zone cherts. The CL and ML Zones contain proportionally the greatest number of Ba analyses in excess of 2000 ppm and Sr analyses in excess of 70 ppm.

A6.4.3 PARTITIONING OF ELEMENTS BETWEEN CHERT AND MUDSTONE PARTINGS

Four sets of comparative chert/mudstone parting analyses have been performed:

i) LS2 - a chert nodule with noncalcareous overlying and underlying mudstones, from the CD Zone, Limburn Stream (26).

ii) MS10 - a chert nodule with adjacent siliceous micrite, and the overlying marl, CL Zone, Mead Stream (24). Carbonate was removed by treatment with dilute HCl.

iii) WUR3 - a chert bed plus the overlying and underlying mudstones from the LCM Subzone, Waima River (21).

iv) MS41 - a chert bed plus adjacent overlying and underlying mudstones

from the UCM Subzone, Mead Stream (24).

Results are summarized in Figure A6.26 [map pocket] with detailed analyses included in Appendix 11. P_2O_5 (not plotted) is consistently below detection limits except in WUR3 mudstone partings. Elements such as Nb and Th are usually below detection in cherts but not in mudstones. Both MnO and CaO are close to detection limits. Loss on ignition in mudstones is nearly always higher than in the adjacent chert. SiO_2 decreases into mudstone partings whereas all other elements increase. The amount of variation between mudstones and cherts varies from sample to sample. The siliceous micrite residue is slightly lower is SiO_2, and higher in other elements (except Fe_2O_3) than the adjacent chert nodule. Sample WUR3 shows virtually no cross-sectional variation within the chert bed.

The range of major element concentrations in MS41 mudstone partings, and LS2 marl insoluble residue, are similar to concentration ranges for Woolshed Formation mudstones. Strontium, Ba, V, Cr, and Rb are slightly more abundant in Woolshed Formation mudstones however. Other trace elements are more comparable. Mudstones from WUR3 generally contain lower SiO_2, and greater abundances of trace and other major elements than the Woolshed Formation shales.

A6.4.4. OPAL-CT VERSUS QUARTZ CHERTS

A summary of the three opal-CT chert analyses is provided in Table A6.2. Since opal-CT is rare in the Amuri Limestone Group cherts only limited comparisons with quartz cherts can be made. SiO_2 concentrations are lower than in quartz cherts, but opal-CT samples have higher losses on ignition, major and trace element concentrations. They are compositionally similar to the UCM Subzone but contain less V, Cr, Zn, and Ni. Much higher concentrations of all elements except SiO_2 are found in cristobalite cemented Woolshed Formation.

A6.4.5. OXYGEN ISOTOPES

A limited number of samples for $\delta^{18}O$ analysis were selected from Isolation Creek (20) and Mead Stream (24,25) to cover the range of chert zones. In addition, a further 3 samples were analyzed from units at Dee Stream (27) to investigate geographic variation. All the cherts were in the range

Table A6.2 Average major (weight% oxide) and trace (ppm) element analyses for opal-CT samples CR4, TG3, and TG4.

SiO_2	91.27	LOI	2.07	Y	<1
TiO_2	0.14	P_2O_5	<0.05	Zr	41
Al_2O_3	2.93	V	20	Nb	<5
Fe_2O_3	0.73	Cr	17	Ba	3968
MnO	<0.01	Ni	11	Ce	<10
MgO	0.35	Zn	13	Nd	<10
CaO	0.15	Ga	<2	La	<2
Na_2O	<0.10	Rb	20	Pb	<2
K_2O	0.40	Sr	168	Th	<1

Table A6.3 $\delta^{18}O$ analyses of cherts and coexisting calcites (‰$_{SMOW}$). Samples are arranged in approximate stratigraphic order.

MS45	28.5	27.0
MS42	28.0	
DS5	28.6	
MS32	29.0	25.4
MS29	27.5	
DS12	28.9	
MS12a	27.9	23.9
DS16	28.4	
MS2	26.8	

26.8-29.0·/..$_{SMOW}$, with a mean of 28.2·/.. [Table A6.3]. The estimated analytical error is about 1.0 per mil. There is minimal evidence of stratigraphic variation, indicating a uniform isotopic composition for the sequence. There are no detectable variations along strike either. The two detrital-rich samples, particularly from the UCM Subzone, have essentially the same $\delta^{18}O$ signature as detrital-poor carbonate replacement cherts.

The $\delta^{18}O$ of calcite in three calcareous cherts is lower than the $\delta^{18}O$ of the silica [Table A6.3] but within the range of micrites [Table A3.1]. The chert $\delta^{18}O$ range is also within that of dolomites and micrites [Table A5.1].

Effect of Detrital Minerals

Detrital quartz (and clay minerals) incorporated in cherts have lower $\delta^{18}O$ values than authigenic quartz, thus lowering the bulk ^{18}O composition (Jones and Knauth 1979). Of the Amuri Limestone Group cherts analyzed, only the samples from the UCM and LCM Subzones contained any significant detrital quartz. Using a mass balance argument, with an assumed detrital quartz $\delta^{18}O$ = 10·/..$_{SMOW}$ (Jones and Knauth 1979), then 2% detrital quartz in the LCM would cause a 0.4·/.. decrease in $\delta^{18}O$ in a chert with a bulk composition of 29 per mil. Comparatively more alteration may have occurred to UCM Subzone results; assuming about 70% authigenic quartz would cause a reduction of about 6 per mil. The amount of detrital material in the UCM Subzone is considerably less than 70% [Section A6.2.6]. Therefore mass balance calculations indicate that the contribution of $\delta^{18}O$ from detrital sources can be ignored.

APPENDIX 7

LITERATURE REVIEW

A7.1. INTRODUCTION

Detailed accounts of the literature on chert and dolomite genesis are major undertakings. As well as being beyond the scope of this thesis, such reviews have been performed by previous authors. Therefore this section provides only an overview of previous work.

A7.2. DOLOMITES AND DOLOMITIZATION

Detailed critical discussions of dolomites and dolomitization can be found in a number of review papers, which include: Land (1980, 1983a,b), Morrow (1982a,b), Machel and Mountjoy (1986), Hardie (1987), Gunatilaka (1987), plus collected symposium proceedings such as Zenger *et al.* (1980). Discussions may also be found in most sedimentary geology textbooks (e.g. Pettijohn 1975, Friedman and Sanders 1978, Blatt *et al.* 1980). Probably by necessity, these books tend to oversimplify concepts, commonly 'bandwagoning' the current fashionable theory or theories; for example Blatt *et al.* (1980) concentrate on the reflux and mixed-water models.

The following sections give brief resumes of conditions postulated for dolomite formation, and dolomitization models, obtained from the above sources (particularly Morrow 1982a,b, and Machel and Mountjoy 1986).

A7.2.1. DOLOMITIZATION CONDITIONS

There is still some debate over primary versus secondary dolomite. Attempts to precipitate dolomite directly have met with only limited success (Chilingar *et al.* 1979), although some claim to have produced dolomite-like materials (e.g. Deelman 1975). There are claims of primary dolomite precipitation from environments such as the Persian Gulf (Chilingar *et al.* 1979), and from lakes (Müller *et al.* 1972). However, the bulk of field and petrographic evidence suggest that most ancient and modern dolomites are of replacement origin.

Some of the major problems involved in the investigation of dolomitization processes are derived from the inability to synthesize dolomite at earth surface temperatures, and an incomplete understanding of the chemistry of dolomite formation. It is currently known that dolomite is thermodynamically stable at earth surface conditions, and that the

conversion of aragonite or calcite to dolomite is thermodynamically favoured (Morrow 1982a). The basic thermodynamic requirement for dolomitization is that the ion activity product of the dolomite solution is greater than the equilibrium constant for the dolomitization reaction (Hardie 1987). The equilibrium constant depends on the temperature, plus the crystal chemistry and cation order of the dolomite. Pressure has a much smaller effect than temperature (Hardie 1987). However, there are a number of kinetic factors which can affect dolomitization; these are (summarized from Morrow 1982a, Machel and Mountjoy 1986):

1) The impedance of the segregation of Mg^{2+} and Ca^{2+} ions into their respective layers in the dolomite lattice due to rapid crystallization from supersaturated, concentrated solutions.
2) The greater hydration energy of Mg^{2+} compared with Ca^{2+} tends to favour the formation of Ca-rich phases. The rate determining step in dolomitization may involve dehydration of cations on crystal surfaces.
3) Low CO_3^{2-} activities may inhibit precipitation of Mg-carbonates because there would be very few cations available to penetrate the hydration barrier on crystal surfaces. The barrier is caused by hydrated Mg^{2+}.
4) The dilution of solutions will essentially reduce the degree of supersaturation.
5) Clay minerals may promote dolomitization by acting as nucleation sites, or by providing Mg^{2+} from clay mineral transformations during later diagenesis.
6) Dissolved SO_4^{2-} ions are thought to inhibit dolomitization, but the exact mechanism is unknown.
7) Organic material may inhibit the precipitation of dolomite; the mechanism of which is as yet unknown. However, because organic matter is a food source for certain bacteria (i.e. urease producing, uric acid fermenting, and sulphate reducing forms), it can promote dolomitization.
8) The rate of precursor carbonate dissolution may determine the rate of dolomitization.
9) Dissociation rates of complexes containing Ca^{2+}, Mg^{2+}, and CO_3^{2-} may govern their availability for the dolomitization reaction. Thus the rate of dolomitization may depend on the slowest dissociation rate in the system.
10) The rate of Mg^{2+} diffusion to the reaction site will govern how much and/or how fast the dolomite will nucleate and form.

In different environments these factors have relatively greater or lesser effects, and may interact or counteract each other (Machel and Mountjoy 1986). Morrow (1982a,b) suggests that the three major factors in dolomitization are:

i) The Mg/Ca ratio of the solution. Increases in the Mg/Ca ratio favour the uptake of Mg^{2+} in the precipitation of Mg-Ca carbonates.

ii) The ionic strength and salinity of the solution. Alterations to the ionic strength and salinity of solutions alter the supersaturation conditions, for example in mixtures of fresh groundwater and marine water, calcite becomes undersaturated and dolomite remains supersaturated (Badiozamani 1973).

iii) The CO_3^{2-}/Ca ratio of the solution. Increasing the CO_3^{2-} activity means there are a greater number of anions with sufficient energy to penetrate the hydration shield of Mg^{2+} on crystal surfaces.

Consideration of these chemical criteria, combined with field and petrographic evidence has lead to the development of a series of dolomitization models, which are summarized (mainly from Morrow 1982b, and Machel and Mountjoy 1986) in following sections.

A7.2.2. DOLOMITE STOICHIOMETRY

Dolomite Ordering

Perfectly ordered, ideal dolomite contain Ca and Mg in equal (stoichiometric) proportions, and in alternating planes (Land 1985). Disordered forms have a random arrangement of cations. In theory, the degree of disorder in dolomite is independent of the composition. Therefore degrees of disorder may occur in either stoichiometric or non-stoichiometric dolomites.

Ideal dolomite is the most stable form in which $CaCO_3$ and $MgCO_3$ may combine in the sedimentary environment (Land 1985). Phases such as those analyzed in this study, which are Ca-rich or partly disordered are essentially metastable with respect to ideal dolomite. Compositional and/or structural changes enable the attainment of more stable states. How, when and if dolomites will convert to stable forms is difficult to determine from the available data (see discussion in Land 1985).

In the past, dolomite nomenclature has been based on lattice ordering as

determined by XRD analysis. Graf and Goldsmith (1956, p184) proposed the term *protodolomite* for *"single phase rhombohedral carbonates which deviate from the composition of the dolomite that is stable in a given environment, or are imperfectly ordered, or both, but would transform to dolomite if equilibrium were established."* The definition was modified by Gaines (1977) to include those dolomites which have a high degree of cation order. This author also introduced an additional term, *pseudodolomite*, to be applied to rhombohedral carbonates approximating dolomite compositions where cation order was equivocal. The definition was based on the argued similarity between natural and synthetic dolomites. It should be remembered that artificial synthesis of low temperature dolomites has to date not been particularly successful. This scheme implies that dolomites from this study would be termed protodolomite. Land (1980) rejects the terms protodolomite and pseudodolomite on the grounds that if the material is not ordered it is not dolomite. All naturally occurring dolomites are ordered to some degree. Disordered phases are usually restricted to laboratory products. Land (1980, 1985) argues that all naturally occurring dolomites that display any ordering are termed dolomite. This argument is also favoured by Gidman (1978) and Deelman (1978), and the author of this thesis.

Influences on Dolomite Stoichiometry

Morrow (1982b) reviewed the relationship between salinity and Mg/Ca ratios in various dolomitizing environments [see Section A7.2.5]. With one exception most dolomitizing environments require Mg/Ca ratios in excess of 1:1. In addition he adds a requirement for high CO_3^{2-}/Ca^{2+} ratios. Dolomitization of calcite is the thermodynamically favoured reaction in seawater in which the Mg/Ca ratio is far in excess of 1:1 (Blatt *et al* 1980). Sediment pore waters from DSDP cores generally have lower concentrations of Ca values than Mg (Mottl *et al.* 1983, Hesse 1986, and others) also resulting in Mg/Ca ratios greater than 1:1. Morrow (1978b) claims that solutions with high Mg/Ca ratios favour the precipitation of stoichiometric dolomite, whereas low Mg/Ca ratio solutions favour Ca-rich dolomite formation. For example, in lakes the Mg content of carbonates has been related to the range of Mg/Ca ratios in the precipitating solution (Müller *et al.* 1972). Uptake of Mg^{2+} from high Mg/Ca solutions is favoured probably because there are a greater number of Mg^{2+} ions relative to Ca^{2+} ions in solution that have the adequate energy to shed

their water of hydration, and therefore be incorporated into the crystal lattice (Morrow 1982a). Solutions of very low salinity will precipitate stoichiometric dolomite regardless of the Mg/Ca ratio. Other authors believe that reduction in salinity is a means for making dolomitization a more favourable process. The Mg/Ca ratio remains high but competition from other ions for lattice sites is reduced (Folk and Land 1975).

However, despite the Mg/Ca ratio of a dolomitizing solution at near surface conditions and its salinity commonly being cited as critical factors in dolomite genesis (Chilingar 1956, Badiozamani 1973, Deelman 1975, Folk and Land 1975, Morrow 1978a,b, Gaines 1980), there is still debate as to the relative importance of the Mg/Ca ratio. Kinetic effects such as reaction rates must also be considered. For example, rapid crystallization tends to favour formation of calcium-rich phases (Morrow 1982a). The reason suggested by Morrow is that Ca^{2+} ions (which are less hydrated than Mg^{2+} ions) are more readily incorporated into the carbonate lattice and will also occupy Mg^{2+} sites. If crystallization is rapid then there is less time for Mg^{2+} ions to displace Ca^{2+} ions from Mg lattice sites. In addition, factors such as alkalinity and inhibition by SO_4^{2-} [see 3) and 7) in Section A7.2.1] are also important (e.g. Lippman 1973, Baker and Kastner 1981).

More recently experimental evidence has shown that dolomitization of $CaCO_3$ consists of two distinct stages; an induction stage (time until nucleation and growth of detectable amounts), and a nucleation stage (Sibley *et al.* 1987). The induction stage is identified as a critical part of the $CaCO_3$ to dolomite transformation. Long induction stages, which are characteristic of dolomite precipitation, are thought to explain characteristics such as the selective crystallization of fine grained $CaCO_3$, and the association of modern dolomites and brines with a high Mg/Ca ratio (e.g. De Deckker and Last 1988), and seawater with a high HCO_3^- content. Metastable phases persist where the induction stage has not been exceeded. Experiments showed that increases in the Mg/Ca ratio can decrease the length of the induction stage and may thereby produce more stoichiometric dolomite (Sibley *et al.* 1987). Reduced induction stages may be caused by sulphate reduction, reduced temperature, and increased HCO_3^- concentration. An increase in the induction stage may be caused by increasing the reactant crystal size, and the primary carbonate mineralogy being calcite rather than aragonite (Sibley *et al.* 1987).

The stoichiometry of dolomite is apparently independent of the percentage of insoluble residue, percentage of dolomite in the carbonate fraction of the rock, recrystallization, and crystal size (Lumsden and Chimahusky 1980). Sperber *et al.* (1984) however, suggests that there may be some relationship with crystal size.

A number of workers note a general trend towards more stoichiometric dolomite with age (Lumsden and Chimahusky 1980, Sperber *et al.* 1984). Calcian dolomite is metastable (Sperber *et al.* 1984, Land 1980, 1985), and with time alters towards more stoichiometric compositions. Compositional changes are brought about subsequent to formation by interaction with different pore fluids at elevated temperatures and pressures during later burial (Lumsden and Chimahusky 1980). Thus, stratigraphically related dolomites may show increasing $MgCO_3$ (nearness to stoichiometric composition) down profile due to processes not necessarily operating at the time of formation. There is some debate as to whether the transformation of calcian dolomite to stoichiometric dolomite is accomplished by multiple recrystallizations (Land 1980), or by a single dissolution-precipitation event (Sperber *et al.* 1984). Whichever is the case the availability of Mg^{2+} probably governs to what extent the transformation takes place (Sperber *et al.* 1984).

A7.2.3. SOURCES OF MAGNESIUM FOR DOLOMITIZATION

High-Mg Calcite

High-Mg Calcite is a commonly considered Mg^{2+} source for dolomitization (Chilingar *et al.* 1979). Fairbridge (1957) suggested high-Mg calcite as a crystallization nucleus. Another suggestion was that dissolution of Mg-calcite provided Mg^{2+} directly for dolomitization (Peterson 1962, Goodell and Garman 1969, Matsumoto and Iijima 1980). If high-Mg calcite is present, its higher solubility than calcite means the degree of dolomite saturation increases. Mg-calcite will also cause an increase in the Mg/Ca ratio of interstitial water, favouring dolomite stability (Sass 1965).

Adsorbed Magnesium

Baker and Kastner (1981), and Baker and Burns (1985) calculated that a

maximum of 6 weight% (of the sediment) dolomite could be produced from Mg^{2+} adsorbed onto clay minerals under the following conditions:

i) 1 Mg^{2+} ion adsorbed per square nanometre of the clay surface.

ii) A surface area of solid of 200 m^2/gm.

iii) A porosity of 75 percent.

Baker and Burns (1985) concluded from hemipelagic sediments at DSDP site 479, that ion exchange could not produce a rock with more than 1-2% dolomite. Site 479 contains principally muddy diatomaceous oozes, and probably contains a relatively high proportion of clay minerals. Considerable quantities of Mg^{2+} may be adsorbed onto biogenic silica. The process is diffusion controlled and requires a break in sedimentation for significant amounts to be adsorbed (Donnelly and Merrill 1977). These authors claim the adsorption process to be inoperative in the absence of carbonate, but suggest that it may cause some pore water Mg^{2+} gradients. Kent and Kastner (1985) argue that Mg^{2+} adsorption onto amorphous silica is insignificant. Mg^{2+} in the form of a hydroxyl compound (probably sepiolite), is important and is a requirement for the transformation of opal-A to opal-CT (Kastner *et al.* 1977). At temperatures of the order of 200°C experiments indicate that Mg^{2+} is rapidly consumed during the transformation, reducing the Mg/Ca ratio of the solution (Kastner *et al.* 1977). Between 25°C and 150°C, Mg^{2+} in the form of a hydroxide compound enhanced the opal-A to opal-CT transformation (Kastner *et al.* 1977, 1984, Kastner and Gieskes 1983). Therefore, during early diagenesis biogenic silica would be a sink rather than a source of Mg^{2+}. Most early dolomite may have formed before this transformation (Compton and Siever 1986) implying that dolomite formation may control the silica transformation. Magnesium ions taken up by opal-CT are released in the transformation to quartz, and may promote late stage dolomitization (Baker and Kastner 1981, Kastner *et al.* 1984). Contrary to the above discussion, Compton and Siever (1986) suggest that if Mg^{2+} adsorbed on diatoms is significant, then the maximum Mg^{2+} release into interstitial waters would be during the opal-A to opal-CT transformation. If this is the case, it may be important during contemporaneous chertification and dolomitization.

Organic Matter

Gebelein and Hoffman (1973) noted the association of stromatolites and dolomite and postulated that dolomite precipitation may be affected by organic material. They found that ashed mat-forming blue-green algae

contained 25-65 weight% Mg. Decay or oxidation of the organic matter may release this Mg however, reasonably large quantities of organic matter would be required to significantly affect dolomitization. Assuming 2.5 weight% organic matter in a sediment, Baker and Burns (1985) conclude that such an Mg source is negligible; a conclusion supported by Compton and Siever (1986).

Despite the generally low Mg input, organic material may still affect the dolomitization process. From work on subsurface waters from oil field brines Kharaka *et al.* (1986) suggest that although organic species form soluble complexes with metals they may not be quantitatively significant. Instead, organic material may indirectly control the concentrations of metals by controlling the Eh and pH. The Eh and pH control can effect various reactions which in turn influence precipitation and dissolution reactions. Davies *et al.* (1975) concluded that live organic material may govern the pH and when decaying can alter the alkalinity. Some organic fractions may inhibit aragonite precipitation which Davies *et al.* suggested nullifies the kinetic barriers to dolomite formation. Dolomitization in organic rich sediments does not necessarily require solid carbonate (Baker and Kastner 1981). In such conditions the HCO_3^- source is from SO_4^{2-} reduction, and methanogenesis or fermentation of organic matter.

Lattice-Bound Mg in Clay Minerals

Kahle (1965) suggested that clay minerals may be important in the dolomitization process. Murray (1960) stated that preferential growth of dolomite euhedra had been found in muds. Zen (1959) suggested an equilibrium exists between clay minerals and other sedimentary components. Structural transformations, such as changes to the mineral lattice, may take place at near surface conditions. Thus clay minerals may provide Mg^{2+} ions that are structurally bound, and in addition may act as nucleation sites for dolomitization. Mg^{2+} may be released from the interlattice positions of chlorite, vermiculite, and montmorillonite (smectite) (Kahle 1965).

Although exchangeable cations may be insignificant, lattice-bound Mg may be more important. Conversion of smectite to illite is common and involves a significant volume of clay and produces large volumes of Fe^{2+},

Mg^{2+}, Ca^{2+}, Na^{+} and Si^{4+} (McHargue and Price 1982). A number of factors control the smectite-illite transformation, including temperature, pressure, smectite composition, and age (McHargue and Price 1982, Boles and Franks 1979, Perry and Hower 1970 and references therein). Temperature is thought to be more important than the pressure in these reactions (Perry and Hower 1970). The process may occur at temperatures of the order of 50°C (Lahann 1980). The bulk of the Mg^{2+} (and Fe^{2+}) is released at temperatures above 100°C, with Si^{4+} being the dominant cation released between 50°C and 100°C (Figure 9, Boles and Franks 1979). Therefore clay minerals are probable Mg^{2+} sources for late stage dolomitization.

Seawater

Probably the most significant source of Mg for early dolomitization is seawater. The concentration of Mg^{2+} in seawater is a little over three times that of Ca^{2+} (in ppm, Brownlow 1979), and equal to 55 moles/m^3 (Compton and Siever 1986). Compton and Siever (1986) suggest four mechanisms for supplying seawater to the site of dolomite formation:

i) Advection of pore water from sediment compaction.
ii) Diffusion of Mg^{2+} from overlying seawater in response to a concentration gradient created by dolomite precipitation.
iii) Convection of pore water due to the density gradient created by temperature and salinity gradients.
iv) Externally impressed flow due to a pressure gradient.

Baker and Burns (1985) compared the advective and diffusive fluxes of Mg^{2+} in seawater into a sediment. Using DSDP data incorporating sediment and pore water compositions and equations for advection and diffusion (Berner 1980), they concluded that the bulk of Mg^{2+} for dolomitization of the upper sediment column is supplied by seawater diffusion. Compton and Siever (1986) used a different approach for dolomite from the Monterey Formation in California. These authors showed that in addition to diffusion small amounts (1-2 volume %) of dolomite may be explained by advective processes. From the amount of Mg^{2+} present in dolomite from the Monterey Formation they calculated the relative contributions from convection, advection and diffusion. Using selected DSDP sites they showed that all the early dolomite in the Monterey could potentially be formed from Mg^{2+} diffused from overlying seawater. The Mg^{2+} flux

magnitude is proportional to the dolomite reaction rate and inversely proportional to the sediment accumulation rate. Reaction rates will increase with increased supersaturation, abundance of calcite and organic matter, and geothermal gradient (Compton and Siever 1986). Burns and Baker (1987) came to a similar conclusion for another part of the Monterey Formation. Externally impressed flow due to a pressure gradient is either ruled out (Compton and Siever 1986) or not considered (Baker and Burns 1985). Externally impressed flow would most likely be driven by terrestrial groundwaters flowing through the sediments creating a hydrostatic head. Such a system would result in meteoric water interaction (which for reasons outlined elsewhere is thought unlikely to have occurred in the sediments in this study). Convection is also likely to be insignificant. Compton and Siever (1986) showed that from Rayleigh number evaluation that convection in diatomaceous sediments is rare at shallow burial. It probably requires deeper burial and high geothermal gradients.

A7.2.4. SUMMARY OF DOLOMITE FABRIC CLASSIFICATION

A number of authors have developed classification schemes for recrystallization textures and fabrics in carbonate rocks. One of the earliest (Folk 1959) describes the respective styles of recrystallization of matrix and allochems in limestones.

Friedman (1965) devised a scheme where fabrics are classified as either equigranular or inequigranular. Strangely, Friedman makes no mention of the Folk (1959) system whatsoever in his discussion of earlier schemes. In the Friedman scheme, terms for inequigranular fabrics are based upon those used in igneous and metamorphic petrology. The scheme as proposed is listed below.

Equigranular Fabrics

Xenotopic - The majority of crystals are anhedral
Hypidiotopic - The majority of crystals are subhedral
Idiotopic - The majority of crystals are euhedral

All three terms are specifically for diagenetically altered carbonate rocks or chemically precipitated sediments. The classification recognizes the importance of crystal shape, a feature not recognized in the Folk

(1959) scheme.

Inequigranular Fabrics

Porphyrotopic - Large crystals (porhyrotopes) are enclosed in a finer grained matrix (c.f. porphyritic, porphyroblastic).

Poikilotopic - Crystals are of more than one size with smaller crystals of one mineral type enclosed in larger crystals of another mineral type (c.f. poikilitic, poikiloblastic).

These terms are restricted to carbonate rocks which have undergone recrystallization and to sediments formed by precipitation. There is no reference to grain shape, only grain size. Logically one would expect that crystal shape terms could also be used for inequigranular fabrics.

Gregg and Sibley (1984) modified the Friedman (1965) scheme to produce a classification for dolomites [Figure A7.1]. The term hypidiotopic is discarded and dolomites are classified as either idiotopic (subhedral to euhedral rhombic crystals), or xenotopic (anhedral crystals). This classification has the advantage that it overcomes the lack of grain shape terms for inequigranular fabrics as noted in the Friedman scheme. The terms idiotopic and xenotopic have since been amended to planar and nonplanar respectively (Sibley and Gregg 1987). The terms are derived from the shape of the crystal boundaries. They propose that xenotopic (nonplanar) dolomite textures result from replacement by dolomite above a critical roughening temperature (CRT) of approximately 50°C which Shukla (1986) suggests may be as low as 35°C. The original xenotopic-idiotopic terminology is thought preferable because the terms planar, and non-planar, do not really relate to the overall crystal shape. In addition the term planar may lead to confusion as it is used in this thesis to describe the inclusion patterns.

Another modified version of the original Friedman scheme was produced by Randazzo and Zachos (1983/1984). Like the Friedman scheme, fabrics are either equigranular or inequigranular. Equigranular fabrics include sutured and sieve mosaic and peloidal fabrics; and, inequigranular fabrics include porphyrotopic, poikilotopic, fogged and spotted mosaics [Figure A7.2]. The degree of dolomitization is equated with fabric; porphyrotopic dolomite is an early stage whereas contact rhomb and intergrown mosaics represent progressively later stages [Figure A7.2]. Two types of

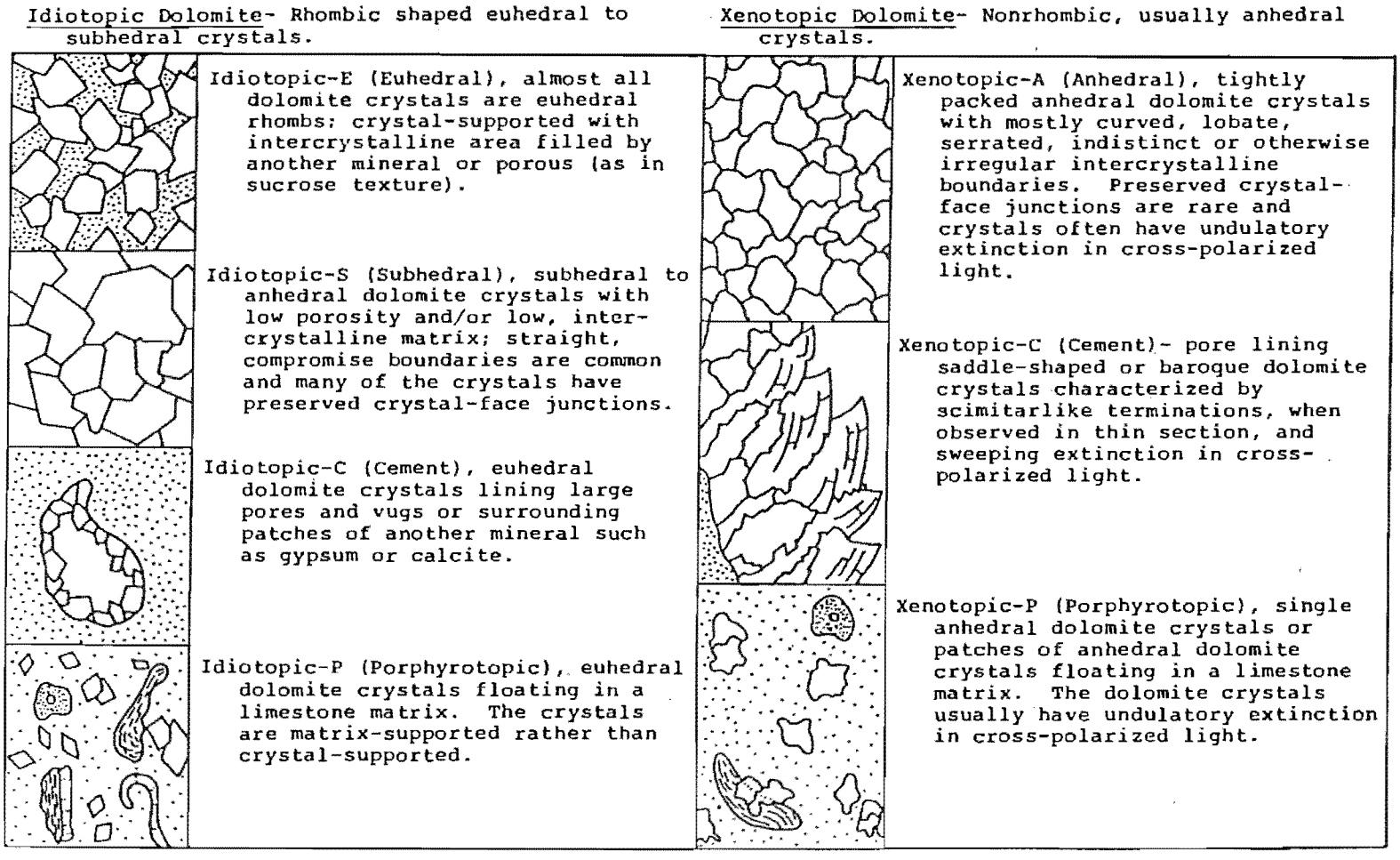

Figure A7.1 Dolomite textural classification scheme (Gregg and Sibley 1984, Figure 6).

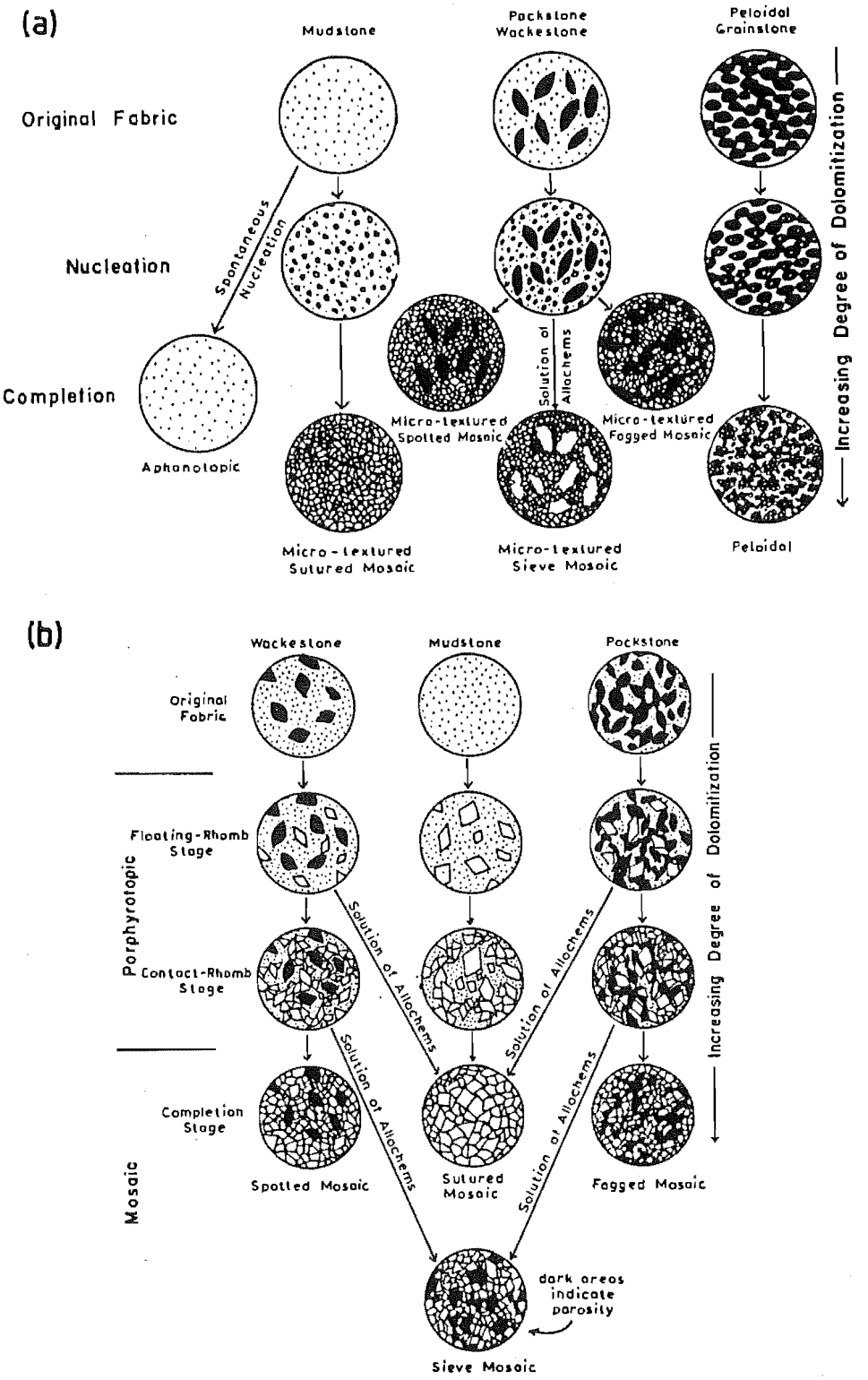

Figure A7.2 Homogeneous (a) and heterogeneous (b) dolomitization fabrics (Randazzo and Zachos 1983/1984, Figure 7 and 8).

dolomitization are postulated; heterogeneous and homogeneous. Homogeneous dolomitization is envisaged as single staged and relatively fast, and results in aphanotopic, peloidal and mosaic fabrics. Heterogeneous dolomitization causes the multistage development of porphyrotopic and some mosaic fabrics.

A7.2.5. DOLOMITIZATION MODELS.

Hypersaline Lagoon and Reflux Models.

Selected References

Adams and Rhodes (1960)
Blatt *et al.* (1980)
Deffeyes *et al.* (1964, 1965)
Illing *et al.* (1965)
McKenzie *et al.* (1980)
Murray (1969)
Patterson and Kinsman (1982)
Pierre *et al.* (1984).

Mechanism and Environment

Reflux and hypersaline models of dolomitization are envisaged to occur in environments such as the Canary Islands, San Andres and Bonaire islands in the Caribbean, and the Trucial Coast in the Persian Gulf. Evaporation causes seawater to increase in density as it passes across a hypersaline shelf lagoon. The dense brine thus formed sinks, and infiltrates the underlying sediment moving seawards by seepage (i.e. reflux) through seaward dipping beds. Mg^{2+} for dolomitization is supplied by the brine, and transported by the cycle of normal seawater replenishment of the lagoon, and brine seepage. Dolomitization apparently occurs after precipitation of gypsum, as a result of the increase in the Mg/Ca ratio of the brine.

In sabkhas in the Persian Gulf, for example, the optimum dolomite forming area is usually between the high intertidal and supratidal zones, and is commonly less than 1 km wide. Dolomite formation is essentially similar to that described above however, some authors suggest that evaporative pumping may occur (e.g. McKenzie *et al.* 1980). In such a situation landward migration of seawater through the sediments occurs to replace water lost through evaporation. Although the direction of fluid flow is opposite to that for seepage reflux, the same brine concentration effects

result in increased Mg/Ca ratios and dolomite precipitation. Thus dolomitization in sabkhas is essentially the reflux model modified by evaporative pumping (Morrow 1982b).

Mixed Water and Coorong Models

Selected References

Badiozamani (1973)
Baum *et al.* (1985)
Choquette and Steinen (1980)
Folk and Land (1975)
Hanshaw *et al* (1971)
Land (1973)
Land *et al.* (1975)
Muir *et al.* (1980)
Rosen *et al.* (1989)
Taberner and Santisteban (1989)
von der Borch (1976)
von der Borch and Jones (1976)
von der Borch and Lock (1979)
von der Borch *et al.* (1975)
Ward and Halley (1985)
Xun and Fairchild (1987)

Mechanism and Environment

The mixed water model is also referred to as the 'Dorag' or dilution model. In this model dolomite may form in any environment where fresh and saline waters mix. There are essentially two types of mixed water environment (Machel and Mountjoy 1986): i) the inland model for a confined artesian aquifer mixing with saline water, and, ii) coastal models for unconfined shallow aquifers mixing with seawater. Dolomitization according to the inland model may occur at tens to hundreds of metres depth within the sediment (e.g. Hanshaw *et al.* 1971).

Magnesium ions for dolomitization are provided by the saline water, with the transport of ions driven by groundwater flow. Essentially when saline and freshwater mix the Mg/Ca ratio is reduced, and rates of crystallization are slower. The solution will remain supersaturated with respect to dolomite but undersaturated with respect to calcite, resulting in reduced competition between Ca and Mg for lattice sites. The required segregation of ions to produce dolomite is more readily accomplished in dilute solutions and during slower crystallization.

The Coorong model is simply a modification of the mixed water model, developed from studies of ephemeral lakes on the South Australia coast.

During the wet season the lakes are filled by groundwater seepage, which may evaporate either partially or completely in the dry season. Dolomite forms in either the landward lakes under the influence of continental groundwaters, or, in the zone where seawater and groundwater mix. The source of the Mg^{2+} for the Coorong lakes is somewhat uncertain. However, it is believed to be derived from either seawater, or, groundwaters which have weathered volcanic rocks. The Mg^{2+} transport mechanism is thought to be by way of groundwater flow.

Burial Compaction Model

Selected References

Gregg (1985)
Jodry (1969)
Lee and Friedman (1987)
Mattes and Mountjoy (1980)
Usdowski (1968)
Zenger (1983)

Mechanism and Environment

When shales are compacted, expelled Mg^{2+} bearing pore waters may pass through, and dolomitize adjacent limestones. The Mg^{2+} is derived from clay mineral reactions [see Section A7.2.3]. Faults or unconformities may be important as pathways for migrating fluids. It is thought that the higher temperatures experienced at depth may reduce the kinetic inhibitory effects commonly found in near surface conditions.

Solution Cannibalization and Pressure Solution

Solution cannibalization (Goodell and Garman 1969, Kendall 1977) and pressure solution (Wanless 1979, 1983) derive Mg^{2+} from pre-existing Mg-calcite. In the case of solution cannibalization, the result is precipitation of both dolomite and low-Mg calcite at relatively shallow burial depths. During deeper burial, dolomite forms by pressure solution of Mg-calcite and precipitation along solution seams. The precipitated dolomite acts essentially as an insoluble residue. The problem with this model is that it is uncertain how Mg-calcite can be preserved at deep burial depths.

Lacustrine Dolomite

The lacustrine dolomite forming environment is essentially a version of sabkha or Coorong type environments, but without the influence of seawater. Lakes in which dolomite form tend to have high salinity and alkalinity (e.g. De Dekker and Last 1988), and Mg/Ca ratios in excess of 12 (Müller *et al.* 1972). This is also an environment where primary dolomite precipitation may occur.

Dolomite From Normal Seawater

Recently, a number of authors have documented dolomite formation from normal marine water (e.g. Saller 1984, Baker and Burns 1985, Compton and Siever 1986, Carballo *et al.* 1987). These dolomites precipitate early in the upper few tens of metres of the sediment column, and are associated with bacterial degradation of organic matter (Lippman 1973, Compton 1988). These dolomites have been termed *organogenic* by Compton (1988). The model was developed from the study of organic-rich DSDP sediments (Baker and Burns 1985, Compton and Siever 1986, Compton 1988), and from experimental investigations of the inhibitory effects of SO_4^{2-} on dolomite precipitation (Baker and Kastner 1981). As well as the supply of reactants (Ca^{2+}, Mg^{2+}, HCO_3^-) to nucleation sites, the presence or absence of dissolved SO_4^{2-} is thought to significantly affect dolomite formation. The source of the SO_4^{2-} is usually seawater. According to Baker and Kastner (1981), dissolved SO_4^{2-} at concentrations of less than 5% of that found in normal seawater can effectively inhibit the dolomitization of calcite. Dolomite formation in DSDP sediments occurs only where there is sulphate reduction. Pore waters containing SO_4^{2-}, adequate carbonate and Mg^{2+} do not contain any dolomite (Baker and Burns 1985). Degradation of organic matter by sulphate reducing bacteria can cause dolomite precipitation by simultaneously reducing SO_4^{2-} concentrations and increasing carbonate alkalinity (Lippman 1973, Compton 1988). Magnesium ions are supplied by seawater diffusion into the sediment (Compton and Siever 1986). Although a precursor carbonate is not a prerequisite, the presence of calcite (or aragonite) enhances dolomitization by providing a source of Ca^{2+} and CO_3^{2-} (Compton 1988).

In contrast, experimental precipitation of mineral analogues of dolomite suggest that sulphate may not in fact inhibit dolomitization (Morrow and

Ricketts 1986). Although isostructural with dolomite, mineral analogue precipitation may not be governed by the same factors as 'true' dolomite precipitation, which may explain the lack of similar inhibitory effects. More recently, De Dekker and Last (1988) found dolomite precipitating in lakes of high salinity, Mg/Ca ratio, and alkalinity, and moderate levels of dissolved sulphate. In such cases other factors may 'override' sulphate inhibition. Much more work is required on the problem, as the mechanism of inhibition is as yet not fully understood. However, it seems likely that there is some critical SO_4^{2-} concentration below which dolomite may form in a given environment.

Support for the concept of organic associated dolomite comes from an unexpected source. Although human success at synthesizing dolomite at near surface conditions is limited, mans best friend appears to have succeeded. A domestic dog (which received only limited acknowledgement for its contribution) produced a urolith of pure dolomite in its bladder (Mansfield 1980). The dolomite formed in an (obviously) organic environment, at a temperature of about 38°C and at one atmosphere pressure, and in less than eight months. This suggests that ordered dolomite can form over short periods of time, in organic-rich environments, at earth surface conditions (Mansfield 1980).

Tectonic and Hydrothermal Dolomite

These dolomites are commonly related to faults or hydrothermal ore bodies. They are usually saddle dolomites, which formed at temperatures in excess of 100°C (Machel and Mountjoy 1986).

A7.3. CHERT AND CHERTIFICATION

A7.3.1. INTRODUCTION

As is the case for dolomites there is a considerable quantity of literature. Not surprisingly much of the modern literature deals with oceanic cherts because 40% of DSDP cores drilled encountered siliceous rocks.

A number of reviews of aspects of chert and silica distribution in oceanic sediments have been produced: Ramsey (1973), Davies and Supko (1973),

Greenwood (1973), Wise and Weaver (1974), Calvert (1977), Riech and von Rad (1979a,b), Kastner (1981), Pisciotto (1981a). In addition there are reviews of chert and silica which cover general aspects of their diagenesis, for example Pettijohn (1975), Dapples (1979), Blatt *et al.* (1980). Summaries of chemical aspects of silica diagenesis are found in Iler (1979), Williams and Crerar (1985), Williams *et al.* (1985), and Blatt (1987). Compilation volumes containing papers on various aspects of silica and silica sedimentation include Ireland (1959), McBride (1979), Garrison and Douglas *et al.* (1981), and Iijima *et al.* (1983).

A7.3.2. CONCEPTS OF SILICA DEPOSITION

Deposition of silica by way of direct precipitation from seawater as a silica gel (Tarr 1917) was one of the earliest mechanisms postulated. Colloidal silica was supposedly carried to the sea by streams, and flocculated in seawater via an electrolytic mechanism (Tarr 1917). So-called "contraction phenomenon" in cherts were alleged to have been caused by crystallization from silica gels (Taliaferro 1934). Barton (1918) and van Tuyl (1918) both suggested that chert may replace carbonate soon after deposition, but still invoked direct precipitation of silica from seawater, contemporaneously with limestone deposition. Keller (1941) reaffirmed direct seawater origin despite the presence of biogenic siliceous fossils. He did however, suggest direct precipitation was augmented by diagenetic replacement. There is now very little support for the 'gel' theory for marine cherts. No silica gels have as yet been reported from oceanic sediments (Dapples 1979). In addition x-ray diffraction and SEM work suggest that no gel phase exists in the conversion of opal-A to chert (Weaver and Wise 1972). Most authors now recognize the bulk of chert formation (particularly in carbonates) occurs after deposition of the host sediment.

Evidence, principally from DSDP cores, indicates there to be two means of generating quartz chert; i) conversion of amorphous opal to quartz, and, ii) the direct precipitation of quartz. From work on the Monterey Formation in California, Bramlette (1946) was probably first to recognize that amorphous (biogenic) opal converted to opaline claystone (porcelanite - Taliaferro 1934). The generally accepted conversion sequence is opal-A to opal-CT to quartz and chalcedony (Heath and Moberly 1971, Berger and von Rad 1972, von Rad and Rösch 1972, 1974, Weaver and

Wise 1972, Wise *et al.* 1972, Wise and Weaver 1974, Keene 1975, von Rad *et al.* 1978, Riech and von Rad 1979a,b, Riech 1980 and many others), and is commonly referred to as the maturation theory (Wise and Weaver 1974). Originally the maturation theory was thought to follow a solid-solid state transformation (Ernst and Calvert 1969), it is now commonly accepted to follow a solution-precipitation mechanism (Stein and Kirkpatrick 1976). The opal-CT phase commonly forms spherules (Wise *et al.* 1972) called lepispheres (Weaver and Wise 1972, Oehler 1975). The direct precipitation of quartz was proposed by Lancelot (1973), and may apply particularly to chalcedony. Many authors (e.g. Lancelot 1973, Keene 1975) suggest that cherts many form from a combination of amorphous opal maturation and direct quartz precipitation.

Although the bulk of chert that formed in marine conditions is post-depositional in origin, direct inorganic precipitation in nonmarine environments has been reported by Eugster (1969). Lakes in Kenya apparently precipitate chert in association with magadiite ($NaSi_{12}O_{13}(OH)_3.3H_2O$, Eugster 1969).

Theories for the origin and genesis of chert have not been 'structured' in to specific models, as is the case for dolomitization. Chert formation and the silicification of sediments is thought to occur in environments similar to those in which dolomites form, for example fresh and saline water mixing zones (Knauth 1979, Knauth and Epstein 1976, Meyers and James 1978, Astin 1987). Jones and Knauth (1979) suggest that the Arkansas Novaculite formed in evaporitically influenced to deep burial environments. The influence of organic matter reactions and the association with burrowing is now commonly stressed (e.g. Namy 1974, Bromley *et al.* 1975, Kelts and McKenzie 1982, Bromley and Ekdale 1984, Clayton 1986, Kolodny 1986). There is a myriad of DSDP reports of chert associated with normal marine conditions. It is therefore to some extent surprising that few authors document or discuss the paragenesis of chert and dolomite. The few examples found include chertification which preceded dolomitization (Dapples 1959), the 'freezing' of dolomitization by silicification (Dietrich *et al.* 1963), and multiple silicification and dolomitization events (Swett 1965). Jacka (1974) reported the precipitation of dolomite associated with the advance of a silicification front. The geochemical factors involved in the early formation of chert and dolomite (and phosphorite) were outlined by Kastner *et al.* (1984).

A7.3.3. GEOCHEMISTRY OF SILICA DEPOSITION

The factors which affect the deposition of silica; that is the solubility and dissolution rates of silica which in turn are governed by the ionic strength of the solution, pH, temperature, pressure and surface area effects, have been investigated or reviewed by a number of authors (e.g. Siever 1962, Mizutani 1966, 1967, 1970, 1977, Calvert 1974, Ernst and Calvert 1969, Hurd and Theyer 1975, 1977, Dapples 1979, Hurd and Birdwhistle 1983, Kastner *et al.* 1977, Kastner 1981, Murata *et al.* 1977, Pisciotto 1981a,b, Stein and Kirkpatrick 1976, Williams and Crerar 1985, Williams *et al.* 1985, and others).

The transformation of initially deposited opal-A to opal-CT and finally to quartz was suggested to occur via a zero-order solid-solid transformation (Ernst and Calvert 1969). A combination of solid reaction and solution-precipitation has also been suggested (Mizutani 1966, 1967). The experimental data of Ernst and Calvert (1969) was later explained in terms of nucleation and growth reactions (Stein and Kirkpatrick 1976). Oxygen isotope studies (e.g. Murata *et al.* 1977) support the Stein and Kirkpatrick theory. The current general view is of transformation via dissolution-precipitation reactions.

The properties of the original sediment govern the diagenetic evolution of SiO_2 (Greenwood 1973, Lancelot 1973, Keene 1975, Kastner *et al.* 1977, Riech 1979, Riech and von Rad 1979a, Karpoff *et al.* 1981, Williams and Crerar 1985, and others). The transformation reactions are controlled mainly by the aqueous solubility of the phases, with the solubility being a function of crystal structure, particle size and shape (Iler 1979, Williams *et al.* 1985, Williams and Crerar 1985). When pH increases the solubility of silica increases (Williams and Crerar 1985). Increases in temperature also increase the solubility of silica (Williams *et al.* 1985). In addition temperature effects decrease the relative degree of supersaturation while increasing concentration, and increase reaction rates (Ernst and Calvert 1969, Stein and Kirkpatrick 1976, Williams and Crerar 1985). Increases in pressure can increase solubility but these effects are small compared to temperature effects (Williams and Crerar 1985).

Opal-A

Opal-A may be precipitated either biogenically or inorganically. Biogenic precipitation is probably enzyme catalyzed (Calvert 1974, Iler 1979, Williams and Crerar 1985). Inorganic deposition may occur from alkaline solutions supersaturated with respect to opal-A. In low temperature situations supersaturation is achieved by evaporation, and/or decreases in pH and temperature (Williams and Crerar 1985).

Opal-CT

Dissolved opal-A reprecipitates as opal-CT rather than quartz in saline waters because of deposition of silica polymers. These polymers form the more open ring structures of opal-CT (Williams and Crerar 1985). In the presence of carbonates, the transformation of opal-A to opal-CT is enhanced (Greenwood 1973, Lancelot 1973, Calvert 1974, Keene 1975, Kastner *et al.* 1977, and others). Nucleation of a magnesium hydroxide compound with Mg^{2+}:OH^- ratio of about 1.2, attracts silanol groups and acts as sites for opal-CT nucleation (Kastner *et al.* 1977). (The term silanol is used for any OH^- group attached to silicon (Iler 1979)). Silanol groups at silica polymer exteriors have a negative surface charge (Iler 1979). The surface positive charge of magnesium hydroxides when bridged between colloidal silica will cause flocculation. Flocculation also occurs at the point of zero charge at a pH of about two (Williams and Crerar 1985). Other possibilities for deposition include the catalysis of monomeric silica precipitation and polymerization, and following condensation reactions, monomeric and low weight oligomeric silica can precipitate preferentially at metal hydroxide surfaces (Williams and Crerar 1985).

Diffusion, complexation, adsorption, and neoformation may affect the degree of supersaturation (Williams and Crerar 1985). Oceans are normally undersaturated with respect to silica (Williams *et al.* 1985). SiO_2 in interstitial waters from the south Pacific range from 6-788 ppm, which is in excess of amorphous silica saturation levels only. In sediments concentrations are higher at depth than at the top of the sediment pile (Calvert 1968). At the sediment/water interface levels are similar to the overlying ocean, indicating diffusive loss from the sediments (Calvert 1968, Williams *et al.* 1985). Considering the low permeabilities and diffusion rates of biogenic siliceous sediments, this mechanism may have

limited effect (Williams *et al.* 1985). In sediments with lower levels of supersaturation and higher permeabilities, diffusion may be more important. Uptake of dissolved SiO_2 by clay and/or zeolite neoformation (e.g. Riech 1979), and adsorption by clays (Siever and Woodford 1973) can reduce silica concentrations to below saturation levels. The extent of adsorption depends on the specific surface of the adsorbing solids, their abundance, and the adsorbent/liquid ratio (Williams *et al.* 1985). The amount of SiO_2 depletion will depend upon the dissolved silica concentration in relation to other cations essential for clay mineral formation, and upon the relative rates of clay mineral (or zeolite) nucleation and growth. For depletion to occur, the rate of opal-CT formation should be less than the rate of formation of other authigenic phases (Williams *et al.* 1985). In fact neoformation is capable of completely suppressing authigenic silica precipitation. Similarly rates of complexation relative to silica precipitation and dissolution, and concentrations of multivalent cations will govern the effects of complexation on silica saturation (Fournier and Marshall 1983, Williams *et al.* 1985). Complexation with sulphate may be significant at increasing temperatures and pH (Fournier and Marshall 1983), although it may be diminished by sulphate reduction.

The rate of opal-A to opal-CT transformation is decreased by the presence of detrital minerals (Isaacs 1981, 1982, Williams *et al.* 1985), probably through silica adsorption.

Progressive burial causes the reordering of opal-CT resulting in progressive decreases in the opal-CT d(101) d-spacing (Murata and Nakata 1974, Mizutani 1977, Mitsui and Taguchi 1977, Isaacs 1981, Pisciotto 1981b). Debate exists as to whether this reordering process is a solid-solid (Mizutani 1977) or dissolution-precipitation (Williams *et al.* 1985) process. Isotopic evidence (Murata *et al.* 1977) has been interpreted as indicating a solid-solid transformation. However, solid state diffusion at temperatures below 100°C is likely to be too slow (Williams and Crerar 1985). More recent evidence suggests that evolved forms of opal-A are partially composed of minuscule opal-CT crystallites which grow with time and increased temperature. The growth is analogous to the Murata and Norman (1976) model for improved quartz crystallinity (Williams and Crerar 1985).

Quartz

Factors that govern opal-CT nucleation will also affect quartz precipitation. While retarding the transformation of opal-A to opal-CT, clay minerals enhance the conversion of opal-CT to quartz (Isaacs 1981, 1982). Detrital minerals have a similar effect (Williams and Crerar 1985). Nevertheless, study of DSDP sediments indicates that overall the transformation from opal-A to quartz is faster in pure carbonate than in clay-rich sediments (Keene 1975, Kastner *et al.* 1977).

When solutions are undersaturated with respect to opal-A or opal-CT, quartz precipitates by deposition of silica monomers (Williams and Crerar 1985). The direct precipitation of quartz in calcareous sediments probably occurs in this manner. Any process described previously that reduces silica concentrations below opal-A and opal-CT saturation will assist quartz precipitation. The lack of Al and other metallic cations (except Ca and Na), plus the high permeability in carbonates apparently favour direct quartz precipitation (Lancelot 1973). Hydrothermal syntheses showed that chalcedonic quartz may form directly from opal-A (e.g. Oehler 1976).

Newly precipitated quartz is usually poorly ordered (Murata and Norman 1976), that is it has poor crystallinity. In time the crystallinity improves as a result of slow recrystallization from cryptocrystalline to microcrystalline quartz (Williams and Crerar 1985).

A7.3.4. SOURCES OF SILICA

The most commonly cited source of silica is from siliceous organisms (Thomson 1919, Bramlette 1946, Heath and Moberly 1971, von Rad and Rösch 1972, Heath 1973, 1974, Lancelot 1973, Ramsey 1973, Weaver and Wise 1974, Wise and Weaver 1974, von Rad and Rösch 1974, Funk 1975, Keene 1975, Kastner *et al.* 1977, Riech and von Rad 1979a,b, Riech 1980, Hein *et al.* 1981, 1983, Coniglio 1987 and many others). In order of decreasing importance the organisms are diatoms, radiolaria, sponges, and silicoflagelates (Kastner 1981). Although the view is not universally held, it has been suggested that inorganic precipitation from seawater is unlikely due to the dominance of biogenic silica uptake (Heath 1974).

Volcanic and hydrothermal origins of silica have also been proposed. Origins of this sort have been derived from the association of chert with clinoptilolite and smectite (Calvert 1971, 1974, 1977) in sediments. Amorphous silica associated with Fe-rich deposits have also been described (Kastner 1981 and references therein). Commonly mixed volcanic and biogenic sources are inferred from either field relationships or geochemistry and petrography (e.g. Barrett 1981, Yamamoto 1981, Iijima and Utada 1983, Yamamoto 1987, Pollock 1987).

Buurman (1976) suggests that hydroxide adsorbed SiO_2 may also be an important silica source, and Keene and Kastner (1974) suggest that clay mineral transformations can be significant sources of silica. Other potential sources include silica produced by pressure solution of sand or silt grains (Houseknecht 1988), or feldspar and mica dissolution (Hurst and Irwin 1982).

APPENDIX 8

SAMPLE NUMBERS AND ANALYSES PERFORMED

All grid references are quoted from the metric NZMS 260 (1:50,000) series topographic maps. The metric sheets for eastern Marlborough have not as yet been published so grid references were obtained from NZMS 1 (1:63,630) series maps overprinted with the metric grid.

Samples are quoted according to Canterbury University, Geology Department thesis number. The location of sample sites is given in Figure 1.2, and the stratigraphic relationship of samples is given in Section A2.9. Abbreviations used in the table are as follows:

AAS/AES	Atomic absorption/emission spectroscopy
Cat Lum	Cathodoluminescence analysis
C Min	X-ray diffraction analysis of clay size fraction
C13	^{13}C analysis
Mic Pro	Microprobe analysis
O18	^{18}O analysis
SEM	Scanning Electron Microscopy
T Sec	Petrographic thin section
XRD	X-ray diffraction analysis
XRF	X-ray fluorescence

Field No	Univ No	Grid Reference	Whole Rock Analyses			Chert/Insoluble Residue/Mudstone Analyses			Carbonate Analyses					
			XRD	C Min	T Sec	SEM	XRF	O18	Qtz Cry	Thin Sect	SEM	Cat Lum	AAS AES	Mic Pro	C13 O18
BLF2	12825	030 576999	X		X		X			X					X
BLF3	12826	030 566999	X				X								
BLF4	12827	030 579002	X				X		X						
BLF5a	12828	030 583983	X							X	X		X		X
BLF5b	12829	030 583983	X							X			X		X
BS1	12830	030 685086	X				X						X		X
BS3	12831	030 685086	X				X								
BS4	12832	030 684087	X				X								
BS5	12833	030 684088	X				X			X			X		X
BS7	12834	030 684088	X		X		X								X
BS9	12835	030 684088	X		X		X								

Field No	Univ No	Grid Reference	Whole Rock Analyses			Chert/Insoluble Residue/Mudstone Analyses				Carbonate Analyses					
			XRD	C Min	T Sec	SEM	XRF	O18	Qtz Cry	Thin Sect	SEM	Cat Lum	AAS AES	Mic Pro	C13 O18
BS10	12836	O30 684088	X												X
BS12	12837	O30 694093	X							X			X		X
BS13	12838	O30 694094	X							X	X		X		X
BS14	12839	O30 694094	X		X		X								
BS16	12840	O30 692095	X										X		
BS17	12841	O30 694094	X	X			X								
BS18	12842	O30 694093	X	X			X								
BS19	12843	O30 694093	X	X			X								
CR1	12844	P29 092298	X		X		X			X			X		X
CR2	12845	P29 092298	X				X								X
CR3	12846	P29 092298	X				X								
CR4	12447	P29 092298	X			X	X		X						
CR5	12848	P29 092298	X				X								
CR6	12849	P29 092298	X		X		X			X			X		X
CR7	12850	P29 092298	X				X								
CR8	12851	P29 092298	X				X								
CR9	12852	P29 092298	X				X								
CR10	12853	P29 092298	X				X		X						
DHG1	12854	O30 604014			X										
DHG2	12855	O30 604014	X		X		X								
DHG3	12856	O30 604014	X				X						X		X
DHG4	12857	O30 604014	X				X								
DHG5	12858	O30 603015	X				X								
DS1	12859	P30 706117	X				X						X		
DS3	12860	P30 708116	X		X		X			X					X
DS5	12861	P30 709115	X			X	X	X							X
DS7	12862	P30 709115	X				X			X			X		
DS9	12863	P30 709115	X		X		X		X				X		X
DS10	12864	P30 709115	X		X		X			X		X	X	X	X
DS11	12865	P30 709115	X				X			X	X		X		X
DS12	12866	P30 709115	X			X	X	X	X						

Field No	Univ No	Grid Reference	Whole Rock Analyses			Chert/Insoluble Residue/Mudstone Analyses				Carbonate Analyses					
			XRD	C Min	T Sec	SEM	XRF	O18	Qtz Cry	Thin Sect	SEM	Cat Lum	AAS AES	Mic Pro	C13 O18
DS14	12867	P30 709115	X				X								
DS15	12868	P30 709115	X			X	X					X	X	X	X
DS16	12869	P30 711114	X			X		X					X		X
DTS1	12870	O30 662059	X							X	X		X		X
DTS2	12871	O30 662059	X										X		X
DTS3	12872	O30 658060	X												X
DTS4	12873	O30 662059	X		X	X	X		X						
DTS5	12874	O30 662059	X				X		X						X
DTS6	12875	O30 662059	X				X		X						
DTS7	12876	O30 662059	X										X		
DTS8	12877	O30 662059	X		X	X	X		X						
FRM3	12878	P29 081285	X				X								
HB5	12879	O32 523500	X				X			X			X		
HBOA1	12880	O32 516536	X				X			X	X		X		
IC1	12881	P29 917228	X							X			X		X
IC2	12882	P29 917228	X												X
IC3	12883	P29 916229	X		X					X					X
IC4	12884	P29 916229	X		X		X		X						
IC5	12885	P29 916229	X			X	X						X		X
IC6	12886	P29 916229	X				X								
IC7	12887	P29 916229	X				X								
IC8	12888	P29 916229	X		X	X	X								
IC10	12889	P29 916229	X			X	X		X				X		X
IC11	12890	P29 917230	X		X	X	X		X	X		X	X		X
IC12	12891	P29 917230	X			X	X		X			X	X	X	X
IC13	12892	P29 917230	X		X		X					X	X	X	
IC14	12893	P29 917230	X			X			X		X		X		X
IC16	12894	P29 918230	X		X		X			X					X
IC18	12895	P29 918231	X				X			X			X		

Field No	Univ No	Grid Reference	Whole Rock Analyses			Chert/Insoluble Residue/Mudstone Analyses			Carbonate Analyses						
			XRD	C Min	T Sec	SEM	XRF	O18	Qtz Cry	Thin Sect	SEM	Cat Lum	AAS AES	Mic Pro	C13 O18
IC19	12896	P29 918232	X				X								
IC20	12897	P29 918232	X				X								
IC21	12898	P29 918232			X										
IC24	12899	P29 918232	X				X								
IC25	12900	P29 918229					X								
IC26	12901	P29 917228													
KP1	12902	O31 664668			X										
KP3	12903	O31 676657	X				X			X	X		X		X
KP4	12904	O31 675656	X										X		X
KP6	12905	O31 675656	X				X								
KP7	12906	O31 675656	X				X								
KP8	12907	O31 676657	X				X								
KP9	12908	O31 676657	X				X				X		X		
KP12	12909	O31 681658	X		X		X		X	X					
KP14	12910	O31 676657	X										X		
KP16	12911	O31 661647	X			X	X								
KP17	12912	O31 661647	X				X				X		X		X
KP18	12913	O31 661647	X				X								
KP19	12914	O31 661647	X								X		X		X
KP21	12915	O31 661645	X										X		X
KP22	12916	O31 663644	X				X								X
KP23	12917	O31 665644	X				X								X
LS2	12918	P30 744140	X				X		X		X		X	X	X
LS3	12919	P30 744140	X										X		
LS4	12920	P30 744140	X		X		X			X			X		
LS5	12921	P30 744140	X		X	X	X		X						
LS6	12922	P30 744140	X		X					X			X		X
LS7	12923	P30 744140	X				X					X	X	X	X
LS8	12924	P30 744140	X		X		X			X			X		
LS9	12925	P30 744141	X				X						X		
LS10	12916	P30 744141	X				X					X	X		X

Field No	Univ No	Grid Reference	Whole Rock Analyses			Chert/Insoluble Residue/Mudstone Analyses				Carbonate Analyses				
			XRD	C Min	T Sec	SEM	XRF	O18	Qtz Cry	Thin Sect	SEM	Cat Lum	AAS AES	Mic Pro	C13 O18
LS11	12927	P30 744141	X				X					X	X	X	
LS12	12928	P30 744141	X		X	X	X								
LS13	12929	P30 744141	X		X	X	X		X						
LS14	12930	P30 744141	X										X		
LS15	12931	P30 744141	X				X								
MA1	12932	P31 754883	X		X	X	X		X		X				
MA2	12933	P31 754883	X										X		X
MA3	12934	P31 754883	X		X	X	X			X	X				
MA4	12935	P31 754883	X			X	X		X						
MA8	12936	P31 754883	X				X								
MA11	12937	P31 753883	X				X								
MA12	12938	P31 753883	X				X		X						
MA14	12939	P31 753883	X		X		X		X						
MA15	12940	P31 753883	X				X			X			X		X
MA16	12941	P31 752884	X		X		X						X		
MA18	12942	P31 751884	X		X	X	X			X	X				
MS1	12943	P30 765163	X				X		X			X	X		X
MS2	12944	P30 765163	X			X	X	X	X			X	X	X	
MS3	12945	P30 764163	X	X			X						X		
MS4	12946	P30 764163	X							X		X		X	
MS5	12947	P30 764163	X												X
MS6	12948	P30 764163	X							X			X		X
MS7	12949	P30 764163	X		X	X	X		X	X					X
MS9	12950	P30 764163	X	X			X		X				X		X
MS10	12951	P30 763163	X		X		X		X	X			X		X
MS11	12952	P30 763163	X		X		X								
MS12	12953	P30 763163	X			X	X	X	X						
MS13	12954	P30 763163	X				X		X						
MS14	12955	P30 763164	X				X		X				X		
MS15	12956	P30 763164	X		X										
MS16	12957	P30 763164	X							X					
MS18	12958	P30 763164	X				X		X				X	X	

Field No	Univ No	Grid Reference	Whole Rock Analyses			Chert/Insoluble Residue/Mudstone Analyses			Carbonate Analyses					
			XRD	C Min	T Sec	SEM	XRF	O18	Qtz Cry	Thin Sect	SEM	Cat Lum	AAS AES	Mic Pro	C13 O18
MS19	12959	P30 764162	X	X									X		X
MS21	12960	P30 761160	X		X							X	X	X	
MS23	12961	P30 761160	X										X		
MS24	12962	P30 760161	X				X		X			X	X		X
MS25	12963	P30 760161	X		X	X				X					
MS26	12964	P30 760161	X	X	X		X					X	X	X	
MS27	12965	P30 760161	X				X								
MS28	12966	P30 760161	X		X	X	X		X			X		X	
MS29	12967	P30 760161	X		X		X	X	X	X		X	X	X	X
MS31	12968	P30 760161	X		X		X		X	X			X		
MS32	12969	P30 760161	X				X	X							
MS34	12970	P30 759161	X		X	X	X		X	X					X
MS36	12971	P30 759161	X		X					X					
MS37	12972	P30 759161	X				X								
MS38	12973	P30 759161	X		X		X		X	X					X
MS39	12974	P30 759161	X	X	X	X									
MS40	12975	P30 759161	X	X	X										
MS41	12976	P30 759161	X	X	X		X		X						
MS42	12977	P30 759161	X				X	X							
MS43	12978	P30 759161	X				X		X				X		
MS44	12979	P30 759161	X		X		X								
MS45	12980	P30 759161	X		X		X	X							
MS46	12981	P30 756163	X		X		X		X				X		X
MS47	12982	P30 756161											X		
MS48	12983	P30 756162											X		
MZL2	12984	030 616020	X				X								
MZL4	12985	030 619021	X				X		X						
MZL5	12986	030 623045	X				X								
MZL8	12987	030 624025	X										X		X
NP1	12988	P29 063258	X				X								
NP2	12989	P29 063258	X		X		X								
NP3	12990	P29 063258	X				X								

Field No	Univ No	Grid Reference	Whole Rock Analyses			Chert/Insoluble Residue/Mudstone Analyses			Carbonate Analyses					
			XRD	C Min	T Sec	SEM	XRF	O18	Qtz Cry	Thin Sect	SEM	Cat Lum	AAS AES	Mic Pro	C13 O18
NP4	12991	P29 063258	X				X								
PS19	12992	P31 710814	X		X		X		X						
PS20	12993	P31 710814	X				X		X						
PS21	12994	P31 710815	X				X								
PS22	12995	P31 710816	X				X						X		X
PS23	12996	P31 711817	X				X								
PS25	12997	P31 711818	X				X								
PS28	12998	P31 723848	X				X								
PS29	12999	P31 723848	X			X	X		X						
PS30	13000	P31 723848	X				X								
PS31	13001	P31 723848	X			X	X		X						
PS32	13002	P31 723848	X			X	X								
SS3	13003	P30 804187	X				X								
SS5	13004	P30 804187	X				X						X		
SS6	13005	P30 803187	X				X						X		X
SS7	13006	P30 803187	X				X								
SS8	13007	P30 802197	X				X						X		X
SS9	13008	P30 802197	X										X		
SS10	13009	P30 801189	X				X						X		
SS14	13010	P30 792198	X				X								
SS16	13011	P30 792198	X				X								
SWP1	13012	P30 999184	X				X								
SWP3	13013	P30 999184	X				X								
SWP6	13014	P30 999184	X				X								
TG1	13015	P29 079304	X				X						X		X
TG2	13016	P29 079304	X				X								
TG3	13017	P29 083300	X			X	X								
TG4	13018	P29 083300	X			X	X								

Field No	Univ No	Grid Reference	Whole Rock Analyses			Chert/Insoluble Residue/Mudstone Analyses			Carbonate Analyses						
			XRD	C Min	T Sec	SEM	XRF	O18	Qtz Cry	Thin Sect	SEM	Cat Lum	AAS AES	Mic Pro	C13 O18
WB1	13019	P31 816874	X				X								
WB3	13020	P31 816876	X		X	X	X		X						
WB5	13021	P31 816876	X			X	X								
WB8	13022	P31 816876	X		X		X		X						
WB13	13023	P31 816876	X		X	X	X				X	X			
WB14	13024	P31 816876	X			X				X	X		X	X	
WB18	13025	P31 816876	X		X		X		X	X			X	X	X
WB19	13026	P31 816876	X		X		X		X	X	X		X		
WB20	13027	P31 816876	X		X	X	X		X	X	X				
WB21	13028	P31 816876	X		X	X	X		X						
WB23	13029	P31 819875	X		X		X		X						X
WB24	13030	P31 819875	X		X		X								
WB26	13031	P31 819876	X		X	X	X		X						
WB29	13032	P31 819876	X		X		X								
WB30	13033	P31 819876	X		X	X									X
WB32	13034	P31 820877	X		X		X						X		
WB35b	13035	P31 821878	X		X		X			X			X		
WB36	13036	P31 821878	X		X	X				X	X				
WB37	13037	P31 821878	X		X		X			X					
WB39	13038	P31 821879	X				X								
WB40	13039	P31 821879	X				X			X	X		X		X
WC1	13040	P30 988193	X				X								
WC2	13041	P30 989194	X				X		X					X	
WC3	13042	P30 989194	X												X
WC4	13043	P30 989194	X				X						X		
WC5	13044	P30 989194	X				X		X						
WC7	13045	P30 990194	X		X		X		X	X			X		X
WC8	13046	P30 990194	X				X		X				X		X
WC9	13047	P30 990194	X				X								
WC11	13048	P30 990194	X				X								
WC12	13049	P30 990194	X				X			X			X		X
WC17	13050	P30 935192	X				X								
WC19	13051	P30 987191	X				X								

Field No	Univ No	Grid Reference	Whole Rock Analyses			Chert/Insoluble Residue/Mudstone Analyses			Carbonate Analyses						
			XRD	C Min	T Sec	SEM	XRF	O18	Qtz Cry	Thin Sect	SEM	Cat Lum	AAS AES	Mic Pro	C13 O18
WKS1	13052	P30 752914	X				X						X		
WKS2	13053	P30 752914	X	X			X								
WKS3	13054	P30 752914	X				X								
WKS4	13055	P30 752914	X				X						X		X
WKS5	13056	P30 752913	X				X						X		X
WKS6	13057	P30 751913	X				X		X				X		X
WKS7	13058	P30 751913	X		X		X			X			X		X
WKS8	13059	P30 751913	X				X		X						
WPT1	13060	P30 008195	X				X								
WPT2	13061	P30 008195	X		X		X			X			X		
WPT3	13062	P30 008195	X		X	X	X			X	X	X	X	X	
WPT4	13063	P30 008195	X		X		X			X	X		X		
WPT5	13064	P30 008195	X				X								
WUR1	13065	P29 909244	X			X	X		X						
WUR3	13066	P29 909244	X				X								
WUR4	13067	P29 909244	X		X	X	X								
WUR5	13068	P29 909244	X		X	X	X								
WUR7	13069	P29 909244	X		X		X								
TLCO	13070	J41 447680	X				X								
STFDR	13071	P30 884146	X				X		X						

APPENDIX 9

WHOLE ROCK CARBONATE DATA

A9.1. MAJOR ELEMENT, TRACE ELEMENT, AND STABLE ISOTOPE DATA FROM CARBONATE PHASES

A9.1.1. WC ZONE DOLOMITE

SAMPLE	Mn ppm	Fe ppm	Na ppm	K ppm	Mg ppm	Ca ppm	Sr ppm	O-18 ‰.PDB	C-13 ‰.PDB	$MgCO_3$ Mol%	$CaCO_3$ Mol%	$FeCO_3$ Mol%
BLF5a	2503	57662	900	10407	97041	202520	636	-1.53	+5.35	39.61	50.14	10.25
BLF5b	1502	32361	880	2590	115774	185517	1072	-2.16	+8.23	47.76	46.42	5.81
BS12	2674	46844	725	3473	113636	184249	602	-3.77	-0.39	46.23	45.47	8.30
BS13	4236	24159	550	6321	108883	209326	232	-6.01	-15.05	44.20	51.54	4.27
DTS1	4275	715	1253	2087	68355	321479	319	-6.44	-32.74	3.38	96.46	.15
DTS2	6488	37960	1213	2367	7000	316594	359	-6.42	-7.38	.00	92.08	7.92
IC1	9543	30708	955	2470	13685	299566	501	-6.26	-7.06	6.56	87.04	6.40
IC2								-6.79	-27.62			
IC2								-6.13	-26.95			
IC3								-5.66	-46.89			
IC5	712	1026	536	2681	126379	202014	207	-6.01	-36.67	50.68	49.14	.18
KP3/10	1039	16060	1330	3559	122989	211251	665	+0.11	+8.36	47.65	49.64	2.71
KP3/2	994	12068	1580	4267	122589	199445	869	+0.51	+5.74	49.27	48.62	2.11
KP3/3	687	6988	1230	2710	118226	201083	863	+0.04	+6.10	48.61	50.14	1.25
KP3/4	699	13034	1530	4345	122753	191941	1079	-0.92	+7.29	50.13	47.55	2.32
KP3/5	1008	15389	1570	7004	122802	198649	710			49.12	48.20	2.68
KP3/6	623	5673	1779	6690	119269	198540	760			49.25	49.73	1.02
KP3/7	816	16219	1650	5987	120647	201283	963	-1.07	+6.44	48.30	48.88	2.83
KP3/8	888	10403	1770	4574	121816	196999	800	+0.12	+5.21	49.55	48.61	1.84
KP3/9	684	6741	1860	5457	125514	199827	1031	+3.75	+6.77	50.28	48.55	1.18
KP4c	4750	13772	1870	9921	117297	189659	175	-1.79	-8.64	49.22	48.27	2.52
KP4m	3477	14199	1690	2831	97029	187514	263	-1.73	-3.23	44.72	52.43	2.85
KP14B	1022	6550	1474	3390	122098	196076	937			50.06	48.77	1.17
KP17	6460	56691	17600	5763	93446	197016	336	-0.66	+2.66	39.33	50.29	10.38
KP19	901	13978	1930	5151	128471	186895	1332	+0.18	+6.38	42.45	37.45	20.10
KP9	1525	5264	1380	5264	120077	197473	896			49.59	49.47	.95
MZL8	1517	21408	865	3700	130484	175338	1423	-0.57	+7.34	53.01	43.21	3.79

SAMPLE	Mn ppm	Fe ppm	Na ppm	K ppm	Mg ppm	Ca ppm	Sr ppm	O-18 %.PDB	C-13 %.PDB	$MgCO_3$ Mol%	$CaCO_3$ Mol%	$FeCO_3$ Mol%
WKS1	7062	25988	541	7560	115765	184708	215			48.41	46.85	4.73

A9.1.2. AMURI LIMESTONE GROUP DOLOMITE

BS5	316	4638	810	7355	98866	232563	459	-3.12	+2.03	40.86	58.30	.83
BS7								-3.21	+2.72			
DS10	367	4297	598	2644	109069	224749	245	-4.28	+2.18	44.11	55.13	.76
DS11	387	1803	689	1890	116769	215216	221	-2.75	+3.28	47.07	52.62	.32
DS11	387	1803	689	1890	116769	215216	221	-2.87	+3.33	47.07	52.62	.32
DS15	501	3014	780	2256	72090	252027	558	-3.73	+2.14	31.86	67.56	.58
DS15	501	3014	780	2256	72090	252027	558	-3.41	+2.37	31.86	67.56	.58
DS16	246	2694	1720	9915		300875	670	-3.96	+1.56		99.36	.64
DS16	246	2694	1720	9915		300875	670	-4.87	+1.47		99.36	.64
IC10	1344	2152	556	4594	128868	186170	222	-5.43	-2.87	53.09	46.52	.39
IC11	730	1343	551	2032	124845	201474	320	-5.06	+3.35	50.42	49.35	.24
IC12	366	7730	659	11223	125973	198981	178	-5.13	-0.20	50.38	48.27	1.35
IC13	295	4449	563	7561	126776	201329	197			50.54	48.69	.77
IC14	350	3997	595	6619	124201	212889	190	-3.14	+0.89	48.69	50.62	.68
IC16								-6.20	+1.41			
IC18	471	2886	673	2838	109679	214066	279			45.55	53.93	.52
LS2	730	2556	649	2874	127194	194189	117	-4.56	+1.42	51.69	47.86	.45
LS3	420	1882	618	4152	132635	182229	138			54.36	45.30	.34
LS4	387	6021	570	7201	126937	180036	103			53.17	45.74	1.10
LS6	361	1977	640	1325	12112	213987	196	-3.68	+2.66	48.72	50.95	.34
LS7	403	4333	800	5031	97170	235849	289	-4.38	+1.87	40.13	59.09	.78
LS8	366	1778	640	2383	117141	211593	146	-6.73	+0.87	47.57	52.12	.31
LS10	469	3071	620	3536	118915	213077	268	-4.52	+1.31	47.66	51.80	.54
LS11	627	3941	590	4706	127219	214264	348			49.14	50.20	.66
LS14	763	2076	570	1712	107408	222800	421			44.12	55.51	.37
MA2	368	5634	614	6956	127250	166734	106			55.13	43.81	1.06
MS1	608	1837	530	3172	125718	198678	144	-5.48	+1.52	50.89	48.78	.32
MS2	436	1831	560	4173	128687	178538	133	-4.08	+1.65	54.12	45.54	.34

SAMPLE	Mn ppm	Fe ppm	Na ppm	K ppm	Mg ppm	Ca ppm	Sr ppm	O-18 %.PDB	C-13 %.PDB	$MgCO_3$ Mol%	$CaCO_3$ Mol%	$FeCO_3$ Mol%
MS3	511	1481	600	3173	123413	201869	127	-5.12	+1.36	50.07	49.67	.26
MS5								-2.81	+1.67			
MS6	411	2237	700	1905	109018	232098	215	-5.20	+1.46	43.47	56.14	.39
MS7								-5.15	+1.87			
MS14	73	5014	586	3765	119785	227409	463			46.09	53.07	.84
MS18	787	6806	650	6976	106347	236217	319			41.90	56.93	1.17
MS21	544	4050	620	1477	113256	223295				45.22	54.08	.70
MS24	580	4167	680	6662	119573	214259	445	-4.25	+2.33	47.57	51.71	.72
MS26	1111	3784	600	2720	116837	210948	512			47.41	51.92	.66
MS29	513	5290	590	3566	114556	220650	348	-4.31	+1.84	45.70	53.39	.92
SS5	1152	2105	582	3070	129963	195344	163			52.12	47.52	.37
SS6	798	2552	565	3530	123359	219010	275	-2.41	+1.35	47.94	51.63	.43
SS8	765	848	627	3116	123442	198234	170	-1.89	+1.41	50.58	49.27	.15
SS9	1016	1208	577	2518	116961	212454	225			47.48	52.31	.21
SS10	685	2586	586	2150	112942	219654	246			45.67	53.87	.46
WB15	516	3058	653	3426	119604	206545	227			48.58	50.88	.54
WB18	405	2480	583	3947	122258	212205	197			48.51	51.07	.43
WB19	277	3407	590	3945	127028	202802	188			50.50	48.91	.59
WKS4	213	8667	1280	2515	137065	201494	246	-3.13	-5.82	52.11	46.46	1.43
WKS5	395	1089	582	2279	132672	189893	116	-6.82	-2.33	53.43	46.38	.19
WKS6	324	811	594	1778	128041	203621	103	-2.78	+0.23	50.86	49.01	.13
WKS7	299	1123		3475	131523	192472	155	-2.15	+0.08	52.87	46.93	.20
WPT2	8547	12363	931	2928	110619	214407	172			44.96	52.85	2.19
WPT3	4585	10261	1540	5271	97481	222715	289			41.13	56.99	1.88
WPT4	2784	14238	214	15819	85161	347500	411			28.19	69.76	2.05

A9.1.3. AMURI LIMESTONE GROUP MICRITE

BS1	198	2359	2200	9039	132	337963	1014	-5.84	+1.19	.06	99.44	.50
BS10								-5.51	+3.04			
BS16	484	1650	1352	2480	506	338595	886			.25	99.41	.35
CR2								-3.47	+0.36			

SAMPLE	Mn ppm	Fe ppm	Na ppm	K ppm	Mg ppm	Ca ppm	Sr ppm	O-18 %.PDB	C-13 %.PDB	$MgCO_3$ Mol%	$CaCO_3$ Mol%	$FeCO_3$ Mol%
CR6	1109	2242	2530	5526	2285	348465	762	-4.03	+1.71	1.06	98.48	.45
DHG3	317	2699	1670	1331		361975	885	-5.13	+0.03		99.47	.53
DS1	313	1164	1260	848		344380	1167				99.76	.24
DS3								-5.78	+1.23			
DS5								-5.89	+2.37			
DS7	449	2049	1645	4333	429	349727	1177			.20	99.38	.42
DS9	272	1438	1014	4242	2142	339386	1158	-5.87	+2.07	1.03	98.67	.30
DTS3								-3.03	+1.4			
DTS5								-6.90	-0.47			
DTS7	146	1683	2020	2684		348726	1069				99.65	.35
HB5	31	535	422	15357	250	345094	1314			.12	99.77	.11
HBOA1	118	305	200	7240	748	349048	908			.35	99.59	.06
KP21	598	2533	5397	15198	1458	338512	996	-1.81	-0.22	.70	98.77	.53
KP22								-1.75	+1.39			
KP23								-1.32	-1.16			
LS9	304	1366	1904	5712	5588	351131	869			2.55	97.18	.27
LS15	662	857	1287	1161	2561	337957	684	-4.62	+1.91	1.23	98.59	.18
MA15	525	1403	1519	1209	647	330041	957	-3.38	+0.96	.32	99.52	.16
MA16	212	1071	1190	361	407	339516	1025			.20	99.58	.23
MS9	433	1318	1486	4090	7243	331977	677	-5.87	+1.45	3.46	96.26	.27
MS10	395	1242	1485	3570	4010	381682	691	-5.90	+1.73	1.70	98.07	.23
MS23	315	1592	1544	5238	2110	303993	727			1.13	98.50	.37
MS31	272	714	1270	1280	2205	353680	773			1.02	98.84	.14
MS34								-3.87	+1.59			
MS38								-6.43	+2.19			
MS43	187	2162	1430	1605	1439	338413	894			.69	98.85	.45
MS46	343	1256	1340	960		360288	1220	-2.82	+1.77		99.75	.25
MS47	612	2174	1259	1177	291	324246	844			.01	99.51	.48

SAMPLE	Mn ppm	Fe ppm	Na ppm	K ppm	Mg ppm	Ca ppm	Sr ppm	O-18 %.PDB	C-13 %.PDB	$MgCO_3$ Mol%	$CaCO_3$ Mol%	$FeCO_3$ Mol%
MS48	634	3254	1300	1394	387	324405	865			.19	99.09	.71
PS22	454	1305	1242	1183	1099	334380	879	-3.21	+1.38	.54	99.18	.28
WB22								-5.08	+1.33			
WB32	207	779	1520	3572	1698	356140	723			.78	99.07	.16
WB35b	178	859	1246	1073	269	261487	632			.17	99.60	.23
WB40	277	1059	2050	2620	526	340274	910	-2.44	+2.02	.25	99.52	.22
WC4	2374	2326	2200	5656		350542	1083				99.53	.47
WC8	1684	3076	1570	5514		327091	748	-5.55	+1.98		99.33	.67
WC12	938	597	1290	1356	683	335882	540	-3.43	+2.10	.33	99.54	.13

A9.1.4. AMURI LIMESTONE GROUP MARL

MS9	470	1532	1374	2667	3963	332944	690			1.92	97.76	.32
MS10	408	5480	1582	7916	4961	334177	761	-5.54	+1.38	2.36	96.50	1.14
MS19	926	5877	926	2489	136358	215255	196	-4.56		50.60	48.45	.95
MS47	489	3158	1504	6733	675	351423	1460			.31	99.05	.64
MS48	589	3650	1410	6049	650	330636	1059			.32	98.90	.78

A9.1.5. K-T BOUNDARY

CR1	1562	2757	2786	13296	2930	353549	1085	-3.91	+1.98	1.34	98.11	.55
TG1	1816	3937	2110	6575		313087	1080	-4.02	+1.86		99.11	.89
WC7	1717	5602	1890	7103	1441	392540	875	-4.96	+1.76	.60	98.40	1.01

A9.2. WEIGHT% CARBONATE AND INSOLUBLE RESIDUE

A9.2.1. WC ZONE DOLOMITE

SAMPLE	Carb wt%	IR wt%	SAMPLE	Carb wt%	IR wt%	SAMPLE	Carb wt%	IR wt%
BLF5a	46.32	53.68	KP3/10	86.50	13.50	KP14B	86.91	13.09
BLF5b	68.68	31.32	KP3/2	85.84	14.16	KP17	76.40	23.60
KP3/3	89.21	10.79	KP19	79.61	20.39			

SAMPLE	Carb wt%	IR wt%	SAMPLE	Carb wt%	IR wt%	SAMPLE	Carb wt%	IR wt%
BS12	66.15	33.85	KP3/4	85.51	14.49	KP9	88.70	11.30
BS13	76.31	23.69	KP3/5	80.19	19.81			
KP3/6	85.38	14.62	MZL8	62.47	37.53			
DTS1	77.63	22.37	KP3/7	82.56	17.44			
DTS2	79.59	20.41	KP3/8	84.45	15.55	WKS1	59.12	40.88
KP3/9	79.17	20.83						
IC1	78.60	21.40	KP4c	21.49	78.51			
IC5	69.37	30.63	KP4m	78.27	21.73			

A9.2.2. AMURI LIMESTONE GROUP DOLOMITE

BS5	59.73	40.27	LS4	53.87	46.13	SS5	64.24	35.76
LS6	65.20	34.80	SS6	72.42	27.58			
DS10	76.65	23.35	LS7	38.53	61.47	SS8	72.27	27.73
DS11	88.02	11.98	LS8	68.87	31.13	SS9	85.35	14.65
DS11	88.02	11.98	LS10	67.39	32.61	SS10	82.37	17.63
DS15	61.97	38.03	LS11	63.84	36.16			
DS15	61.97	38.03	LS14	85.13	14.87	WB15	79.38	20.62
DS16	18.23	81.77				WB18	71.11	28.89
DS16	18.23	81.77	MA2	61.67	38.33	WB19	66.96	33.04
IC10	51.99	48.01	MS1	76.04	23.96	WKS4	15.40	84.60
IC11	73.77	26.23	MS2	54.49	45.51	WKS5	49.52	50.48
IC12	43.60	56.40	MS3	72.84	27.16	WKS6	70.56	29.44
IC13	71.99	28.01	MS6	81.77	18.23	WKS7	47.46	52.54
IC14	67.68	32.32	MS14	74.26	25.74			
IC18	53.03	46.97	MS18	57.69	42.31	WPT2	77.93	22.07
MS21	80.57	19.43	WPT3	54.83	45.17			
LS2	61.25	38.75	MS24	65.38	34.62	WPT4	47.87	52.13
LS3	54.45	45.55	MS26	80.62	19.38			

A9.2.3. AMURI LIMESTONE GROUP MICRITE

BS1	10.75	89.25	LS9	17.99	82.01	PS22	88.43	11.57
LS15	76.71	23.29						
CR6	40.76	59.24				WB32	70.62	29.38
MA15	72.85	27.15	WB35b	81.33	18.67			

SAMPLE	Carb wt%	IR wt%	SAMPLE	Carb wt%	IR wt%	SAMPLE	Carb wt%	IR wt%
DS1	78.18	21.82	MA17	92.25	7.75	WB40	81.58	18.42
DS7	38.33	61.67						
DS9	60.20	39.80	MS9	57.02	42.98	WC4	15.47	84.53
MS10	55.57	44.43	WC8	39.65	60.35			
DTS7	10.76	89.24	MS23	30.76	69.24	WC12	78.99	21.01
MS31	81.22	18.78						
HB5	43.80	56.20	MS43	58.42	41.58			
HBOA1	93.75	6.25	MS46	69.32	30.68			
MS47	81.62	18.38						
KP21	21.87	78.13	MS48	77.41	22.59			

A9.2.4. AMURI LIMESTONE GROUP MARL AND K-T BOUNDARY

Marl

MS9	72.26	27.74
MS10	43.38	56.62
MS19	84.66	15.34
MS47	62.63	37.37
MS48	63.15	36.85

K-T Boundary

CR1	32.80	67.20
TG1	31.63	68.37
WC7	37.56	62.44

A9.3. MAJOR ELEMENT ANALYSES OF INSOLUBLE RESIDUES

SAMPLE	SiO_2	TiO_2	Al_2O_3	Fe_2O_3	MnO	MgO	CaO	Na_2O	K_2O	LOI	P_2O_5	TOTAL

A9.3.1. WC ZONE DOLOMITE

KP3/1	76.11	0.55	10.79	1.63	0.07	1.33	0.43	1.36	1.83	4.50	<0.05	98.60
KP3/9	75.43	0.54	10.67	1.42	0.05	1.64	0.87	1.35	1.77	5.59	<0.05	99.35
KP3/10	72.95	0.57	11.13	2.03	0.03	1.74	1.01	1.43	1.87	6.02	0.06	98.83
KP17	78.33	0.47	9.70	1.66	0.01	0.85	0.27	1.81	1.63	3.57	<0.05	98.36
WKS1	98.52	0.04	0.53	0.06	<0.01	<0.10	0.09	<0.10	0.10	0.83	<0.05	100.24

A9.3.2. AMURI LIMESTONE GROUP DOLOMITE

BS5	88.55	0.22	4.53	1.40	<0.01	0.70	0.13	0.24	0.99	0.37	<0.05	97.15

SAMPLE	SiO_2	TiO_2	Al_2O_3	Fe_2O_3	MnO	MgO	CaO	Na_2O	K_2O	LOI	P_2O_5	TOTAL
DS15	92.29	0.15	2.89	0.27	<0.01	0.38	0.09	0.32	0.97	1.26	<0.05	98.65
IC10	93.53	0.13	2.15	0.77	<0.01	0.51	0.23	<0.10	0.69	0.80	<0.05	98.85
IC13	82.13	0.41	7.71	1.70	0.02	1.16	0.12	0.63	2.48	1.47	<0.05	97.85
LS7	95.08	0.12	2.23	0.37	<0.01	0.23	0.06	0.10	0.75	1.06	<0.05	100.01
LS10	90.86	0.24	4.45	0.42	<0.01	0.41	0.07	0.29	1.89	1.51	<0.05	100.14
MS1	84.11	0.35	7.03	1.83	<0.01	1.19	0.15	0.27	2.10	0.67	<0.05	97.71
MS14	82.25	0.38	8.25	1.31	<0.01	1.24	0.20	0.37	2.93	2.26	<0.05	99.19
MS29	72.92	0.58	12.12	2.20	<0.01	2.52	0.32	0.21	3.54	2.71	<0.05	97.13

A9.3.3. AMURI LIMESTONE GROUP MICRITE

CR4	91.25	0.13	3.10	0.90	<0.01	0.43	0.15	0.33	0.45	2.81	<0.05	99.59
DS7	94.55	0.11	1.86	0.33	0.03	0.15	0.08	0.18	0.36	1.34	<0.05	98.99
MA15	91.09	0.14	3.04	0.58	<0.01	0.41	0.06	0.23	0.38	1.76	<0.05	97.76
MA18	96.43	0.05	0.84	0.11	<0.01	<0.10	0.05	<0.10	0.08	0.72	<0.05	98.34
MS43	96.57	0.07	1.44	0.37	0.03	<0.10	0.06	<0.10	0.25	1.04	<0.05	99.91
PS21	90.22	0.12	2.30	0.30	<0.01	0.17	0.05	<0.10	0.31	1.21	<0.05	94.68
PS22	96.75	0.06	1.21	0.15	<0.01	0.12	0.03	<0.10	0.11	1.01	<0.05	99.45
PS32	82.22	0.30	6.75	2.06	0.04	1.57	0.47	0.51	1.30	3.16	<0.05	98.39
WB32	97.08	0.06	1.21	0.20	<0.01	0.13	0.04	<0.10	0.18	1.50	<0.05	100.39
WB39	92.48	0.12	3.02	0.51	0.04	0.49	0.27	0.14	0.34	1.71	<0.05	99.09
WB40	86.72	0.17	4.20	0.82	<0.01	0.73	0.26	<0.10	0.49	1.74	<0.05	95.18
WC12	87.14	0.23	5.02	2.41	0.03	0.62	0.40	0.72	0.75	2.42	<0.05	99.75

A9.4.4. K-T BOUNDARY

CR1	89.06	0.21	5.01	0.90	<0.01	0.67	0.27	0.21	0.70	2.48	<0.05	99.55
NP2	87.37	0.26	5.66	1.49	<0.01	0.99	0.29	0.19	1.01	2.20	<0.05	99.48
TG1	93.01	0.15	3.25	0.56	<0.01	0.42	0.23	0.18	0.47	1.96	<0.05	100.25

SAMPLE	SiO_2	TiO_2	Al_2O_3	Fe_2O_3	MnO	MgO	CaO	Na_2O	K_2O	LOI	P_2O_5	TOTAL
WC7	91.66	.15	3.11	.43	.02	.43	.17	.29	.53	2.30	<0.05	99.09

A9.4. TRACE ELEMENT ANALYSES OF INSOLUBLE RESIDUES

SAMPLE	V	Cr	Ni	Zn	Ga	Rb	Sr	Y	Zr	Nb	Ba	Ce	Nd	La	Pb	Th
A9.4.1. WC ZONE DOLOMITE																
KP3/1	67	49	9	18	12	76	57	4	17	8	391	10	<10	3	7	1
KP3/3	77	56	19	20	16	95	66	4	213	9	441	<10	<10	3	13	<1
KP3/8	75	50	14	18	15	93	65	5	197	9	441	<10	<10	4	8	<1
KP3/9	60	46	12	14	12	75	74	3	144	7	356	<10	<10	2	5	<1
KP3/10	77	53	10	21	12	81	64	5	279	7	390	<10	<10	<2	7	2
KP17	60	42	7	21	11	65	58	7	280	5	335	<10	<10	15	6	1
WKS1	59	38	5	20	13	66	64	9	206	7	343	<10	13	6	6	2
A9.4.2. AMURI LIMESTONE GROUP DOLOMITE																
BS5	33	22	13	11	6	37	28	3	40	5	418	<10	<10	<2	6	<1
DS15	22	16	<5	4	4	26	20	3	30	<5	302	<10	<10	8	4	<1
IC10	17	15	8	12	11	65	25	7	21	<5	246	<10	<10	<2	8	<1
IC13	55	38	8	19	10	83	27	8	91	9	827	10	<10	9	5	<1
LS7	16	12	<5	19	3	20	17	3	20	<5	306	<10	11	<2	3	<1
LS10	28	21	5	5	5	41	22	5	42	<5	720	<10	11	22	3	<1
MS1	47	35	21	18					63	8	453	<10	12	5		
MS14	69	47	12	50	10	76	46	8	66	7	1205	<10	<10	17	3	<1
MS29	78	61	26	26	18	117	42	8	81	12	1100	<10	<10	12	9	<1
A9.4.3. AMURI LIMESTONE GROUP MICRITE																
CR4	16	14	12	11	3	20	131	3	30	<5	2700	<10	<10	<2	3	<1

SAMPLE	V	Cr	Ni	Zn	Ga	Rb	Sr	Y	Zr	Nb	Ba	Ce	Nd	La	Pb	Th
DS7	10	13	13	16	<2	13	263	2	33	<5	6335	<10	<10	<2	4	<1
MA15	18	15	17	18	<2	19	676	2	46	<5	11474	<10	<10	<2	3	<1
MA18	<5	<5	11	5	<2	4	354	1	23	<5	7237	<10	<10	33	2	<1
MS43	20	12	8	21	2	9	75	2	15	<5	953	10	<10	<2	5	<1
PS21	<5	6	34	16	<2	20	507	2	74	<5	13145	<10	<10	<2	3	<1
PS22	<5	<5	5	4	<2	7	211	1	15	<5	5042	<10	<10	<2	4	<1
PS32	29	23	20	29	3	52	225	4	82	6	6037	<10	<10	2	6	<1
WB32	8	<5	6	2	<2	7	31	2	13	<5	89	<10	<10	24	4	<1
WB39	14	9	<5	7	<2	19	249	2	46	<5	6739	<10	<10	<2	5	<1
WB40	16	10	17	5	<2	24	253	3	64	<5	11951	<10	<10	<2	3	<1
WC12	21	26	23	53	5	34	178	4	82	9	4119	<10	<10	2	5	<1

A9.4.4. K-T BOUNDARY

CR1	38	23	12	12	9	29	58	4	42	<5	507	<10	14	5	5	<1
NP2	59	33	32	29	9	43	64	6	63	6	739	10	<10	6	5	<1
TG1	28	18	40	21	4	20	75	5	29	5	730	<10	<10	<2	5	<1
WC7	26	26	<5	6	6	26	74	3	34	<5	906	<10	<10	<2	5	<1

APPENDIX 10

DOLOMITE SINGLE CRYSTAL DATA

Analyzed (wt% oxide) and derived (mole% carbonate and ppm cation) are supplied for each point. Crystals and the location of points on each crystal are numbered consecutively. Each microprobe analysis is designated as a core (C), midpoint (M), or rim (R) site [see Figure A5.26]. In some cases the point analysis location with respect to cores, midpoints or rims was uncertain or not recorded. Such points are indicated by '?'.

Sample	Cryst No	Probe Pos	MnO	FeO	MgO	CaO	$MnCO_3$ mole%	$FeCO_3$ mole%	$MgCO_3$ mole%	$CaCO_3$ mole%	Mn (ppm)	Fe (ppm)
DS15	1	1-M			18.10	31.42			44.49	55.51		
		2-M			17.37	30.26			44.40	55.60		
		3-R			17.39	29.97			44.66	55.34		
		4-M			17.65	31.91			43.48	56.52		
	2	1-C			18.32	33.28			43.37	56.63		
		2-R			19.11	32.58			44.93	55.07		
	3	1-C		1.37	18.13	34.38		1.76	41.57	56.67		9582
		2-M			18.40	34.79			42.39	57.61		
		3-R			19.22	33.03			44.73	55.27		
		4-M			19.13	32.86			44.75	55.25		
		5-R			18.60	34.27			43.02	56.98		
		6-R			18.84	33.78			43.69	56.31		
	4	1-C			18.47	33.80			43.19	56.81		
		2-M			18.35	34.41			42.59	57.41		
		3-R			18.85	33.67			43.78	56.22		
		4-M		0.18	18.41	33.64		0.24	43.12	56.64		1259
		5-R			19.03	33.93			43.83	56.17		
	5	1-C		1.04	17.70	32.97		1.39	42.16	56.45		7274
		2-M			18.14	33.64			42.86	57.14		
		3-R			18.72	33.43			43.79	56.21		
		4-M			18.54	33.72			43.34	56.66		
		5-R			18.64	33.74			43.45	56.55		
DS10	1	1-R			19.58	34.99			43.77	56.23		
		2-M			19.41	33.01			44.99	55.01		
		3-R		0.22	19.38	32.54		0.29	45.18	54.53		1539
	2	1-R		0.16	19.38	32.92		0.21	44.93	54.86		1119
		2-R			18.83	32.73			44.45	55.55		
		3-R			19.09	32.86			44.69	55.31		

Sample	Cryst No	Probe Pos	MnO	FeO	MgO	CaO	$MnCO_3$ mole%	$FeCO_3$ mole%	$MgCO_3$ mole%	$CaCO_3$ mole%	Mn (ppm)	Fe (ppm)
DS10	3	1-M			18.63	32.91			44.05	55.95		
		2-R			19.60	33.65			44.76	55.24		
		3-M			18.63	33.01			43.98	56.02		
	4	1-R			18.71	33.42			43.78	56.22		
		2-R	0.15		19.17	33.30	0.20		44.38	55.42	1162	
		3-R			18.54	33.77			43.30	56.70		
IC12	1	1-C			21.30	32.94			47.35	52.65		
		2-R			19.65	33.30			45.08	54.92		
		3-M			19.60	33.96			44.53	55.47		
	2	1-R			21.57	31.20			49.02	50.98		
		3-C			21.58	31.99			48.41	51.59		
	3	1-R			19.78	33.51			45.09	54.91		
		2-M			21.94	31.00			49.61	50.39		
		3-C			19.84	32.59			45.85	54.15		
		4-R			20.21	32.61			46.30	53.70		
	4	1-R			22.55	30.10			51.03	48.97		
		2-M		0.16	20.81	30.00		0.21	49.00	50.78		1119
IC13	1	1-R			18.71	32.13			44.75	55.25		
		2-M			20.04	30.62			47.66	52.34		
		3-C			20.63	30.29			48.65	51.35		
		4-M			20.87	30.87			48.47	51.53		
	2	1-R			20.98	30.22			49.12	50.88		
		2-M			21.15	30.58			49.03	50.97		
		3-C			20.95	30.17			49.13	50.87		
		4-M			19.98	31.02			47.26	52.74		
		5-R			21.14	30.09			49.43	50.57		
	3	1-C		0.30	20.71	30.02		0.40	48.78	50.83		2098
		2-M		0.74	19.78	30.07		0.99	47.31	51.70		5176
		3-M		0.29	19.61	30.83		0.39	46.76	52.85		2028
		4-R			20.65	30.39			48.59	51.41		
		5-M			19.73	32.76			45.59	54.41		
		6-R			20.67	30.14			48.82	51.18		
	4	1-C			19.48	30.05			47.42	52.58		
		2-M			21.18	29.95			49.59	50.41		

Sample	Cryst No	Probe Pos	MnO	FeO	MgO	CaO	$MnCO_3$ mole%	$FeCO_3$ mole%	$MgCO_3$ mole%	$CaCO_3$ mole%	Mn (ppm)	Fe (ppm)
IC13		3-R		0.23	20.69	30.18		0.30	48.67	51.03		1609
		4-M			20.56	30.36			48.51	51.49		
		5-R			18.74	32.61			44.43	55.57		
LS2	1	4-?			20.41	29.26			49.25	50.75		
		5-R			20.90	30.08			49.15	50.85		
		6-?			21.17	29.59			49.88	50.12		
	2	1-?			20.74	30.28			48.79	51.21		
		3-?			20.76	29.85			49.17	50.83		
		4-R			21.16	29.33			50.09	49.91		
	3	1-?			20.76	29.85			49.17	50.83		
LS7	1	1-?			19.12	34.10			43.82	56.18		
		2-?			19.18	33.63			44.24	55.76		
	2	1-?			19.10	34.15			43.76	56.24		
		2-?			17.94	34.18			42.20	57.80		
	3	1-?			18.67	33.41			43.74	56.26		
		2-?			18.77	32.39			44.63	55.37		
	4	1-?			19.58	33.17			45.09	54.91		
		2-?			17.16	32.18			42.59	57.41		
LS11	1	1-C			19.60	34.57			44.09	55.91		
		2-M			19.05	32.66			44.79	55.21		
		3-R			18.76	33.91			43.49	56.51		
		4-M			19.17	34.02			43.94	56.06		
		5-R			19.24	33.13			44.69	55.31		
	2	1-?			19.17	33.71			44.17	55.83		
		2-?			19.58	33.05			45.18	54.82		
		3-?			18.43	32.81			43.86	56.14		
		4-?			19.35	34.03			44.16	55.84		
	3	1-C			19.15	33.10			44.59	55.41		
		2-M			18.99	33.43			44.14	55.86		
		3-R			19.02	33.78			43.92	56.08		
		4-?			19.05	33.81			43.94	56.06		
MS2	1	1-R			21.66	30.84			49.42	50.58		
		2-C		0.24	20.76	30.03		0.32	48.87	50.82		1679
		5-R			21.44	31.24			48.84	51.16		

Sample	Cryst No	Probe Pos	MnO	FeO	MgO	CaO	$MnCO_3$ mole%	$FeCO_3$ mole%	$MgCO_3$ mole%	$CaCO_3$ mole%	Mn (ppm)	Fe (ppm)
MS2	2	1-C			20.61	30.95			48.09	51.91		
		2-M			21.24	30.96			48.83	51.17		
		3-R			21.32	30.72			49.12	50.88		
		4-R			19.83	30.98			47.10	52.90		
		5-R			21.13	30.84			48.80	51.20		
		6-R			20.89	30.99			48.39	51.61		
		7-R			21.19	31.21			48.57	51.43		
	3	1-R			20.80	31.64			47.77	52.23		
		2-R			21.06	31.19			48.43	51.57		
		3-R			20.85	31.68			47.79	52.21		
	4	2-M			21.28	30.78			49.02	50.98		
		3-M			20.29	31.29			47.42	52.58		
		4-?			21.17	31.51			48.31	51.69		
MS4	1	1-C			19.79	34.54			44.35	55.65		
		2-M			19.20	33.70			44.21	55.79		
		3-R			18.83	34.43			43.21	56.79		
	2	1-C			19.02	32.47			44.90	55.10		
		4-R		0.42	19.06	33.35		0.54	44.05	55.41		2938
	3	3-R			18.68	33.62			43.60	56.40		
		5-R			18.71	33.66			43.61	56.39		
	4	1-?			18.28	33.52			43.14	56.86		
		2-?			18.98	33.60			44.00	56.00		
		3-?			18.87	33.34			44.05	55.95		
		4-?			18.52	33.55			43.43	56.57		
	5	1-?			19.06	31.81			45.46	54.54		
		2-?			20.21	30.68			47.82	52.18		
		3-?			18.60	33.42			43.64	56.36		
		4-?			20.33	31.31			47.46	52.54		
		5-?			18.68	33.47			43.71	56.29		
MS18	1	1-C		0.40	18.84	34.53		0.51	42.93	56.56		2798
		2-M		0.49	18.31	35.39		0.62	41.59	57.79		3427
		3-R		0.44	19.40	34.15		0.56	43.89	55.55		3078
		4-M		0.31	18.55	34.62		0.40	42.53	57.07		2168
		5-R		0.33	18.78	34.30		0.42	43.05	56.52		2308
	2	1-C		1.69	17.71	34.65		2.18	40.65	57.17		11820

Sample	Cryst No	Probe Pos	MnO	FeO	MgO	CaO	$MnCO_3$ mole%	$FeCO_3$ mole%	$MgCO_3$ mole%	$CaCO_3$ mole%	Mn (ppm)	Fe (ppm)
MS18		2-M		0.70	18.15	35.00		0.90	41.53	57.57		4896
		3-R		0.38	18.76	34.33		0.49	42.98	56.54		2658
		4-M		0.76	18.37	33.96		0.99	42.51	56.50		5316
		5-R			18.65	33.71			43.49	56.51		
		6-R		0.23	18.41	34.22		0.30	42.68	57.03		1609
	3	1-C		0.82	17.80	33.61		1.08	41.96	56.96		5735
		2-M			18.51	33.75			43.28	56.72		
		3-R		0.36	19.06	33.22		0.47	44.18	55.35		2518
		4-M		0.23	18.61	33.98		0.30	43.11	56.59		1609
		5-R		0.32	18.56	33.67		0.42	43.22	56.36		2238
	4	1-C		0.85	17.81	34.08		1.11	41.63	57.26		5945
		2-R		0.91	18.29	34.19		1.18	42.16	56.66		6365
		3-M		0.41	17.70	34.55		0.54	41.39	58.08		2868
		4-R		0.33	18.90	33.97		0.43	43.44	56.13		2308
		5-R		0.21	18.80	33.40		0.27	43.79	55.93		1469
		6-M		0.40	18.69	33.51		0.52	43.46	56.02		2798
		7-R		0.32	18.39	34.46		0.41	42.43	57.16		2238
MS21	1	1-C		0.16	19.06	34.84		0.20	43.13	56.67		1119
		2-M		0.31	19.29	34.30		0.39	43.72	55.89		2168
		3-R			18.98	33.63			43.98	56.02		
		4-M		0.19	18.75	34.32		0.24	43.08	56.68		1329
		5-R		0.21	18.95	33.71		0.27	43.76	55.96		1469
		6-M			18.85	34.34			43.30	56.70		
		7-R		0.33	19.23	33.90		0.42	43.92	55.66		2308
		8-M		0.20	18.71	34.38		0.26	42.97	56.77		1399
		9-R			19.35	34.05			44.15	55.85		
		10-?		0.23	19.14	34.12		.29	43.70	56.00		1609
	2	1-C			18.91	34.60			43.19	56.81		
		2-M		0.18	19.66	35.27		0.22	43.58	56.20		1259
		3-R		0.24	19.74	32.95		0.31	45.31	54.38		1679
		4-M		0.30	19.16	33.94		0.38	43.82	55.80		2098
		5-R			19.06	34.38			43.54	56.46		
		6-M		0.19	19.08	33.55		0.25	44.06	55.69		1329
		7-R			19.10	34.12			43.78	56.22		
	3	1-C		0.26	19.08	34.99		0.33	42.99	56.68		1819
		2-M			18.22	34.48			42.37	57.63		

Sample	Cryst No	Probe Pos	MnO	FeO	MgO	CaO	$MnCO_3$ mole%	$FeCO_3$ mole%	$MgCO_3$ mole%	$CaCO_3$ mole%	Mn (ppm)	Fe (ppm)
MS21		3-R		0.33	19.35	33.42		0.43	44.42	55.15		2308
		4-M		0.33	19.56	34.07		0.42	44.22	55.37		2308
		5-R			18.56	34.22			43.00	57.00		
		6-M			18.79	34.07			43.41	56.59		
		7-R			18.37	34.45			42.59	57.41		
	4	1-C		0.23	18.71	34.87		0.29	42.61	57.09		1609
		2-M		0.37	18.87	34.39		0.47	43.08	56.44		2588
		3-R			18.99	34.44			43.41	56.59		
		4-M		0.24	18.53	34.33		0.31	42.75	56.94		1679
		5-R		0.18	19.39	33.18		0.23	44.74	55.03		1259
		6-M		0.39	19.01	34.00		0.50	43.53	55.97		2728
		7-R			19.14	34.69			43.42	56.58		
MS26	1	1-?			19.02	34.34			43.52	56.48		
		2-?			19.28	32.77			45.01	54.99		
		3-?			19.34	32.86			45.02	54.98		
MS28	1	1-C		0.62	18.77	32.98		0.81	43.83	55.36		4337
		2-M		0.69	18.61	34.05		0.89	42.81	56.30		4826
		3-R		0.48	18.26	32.85		0.64	43.33	56.03		3357
		4-R		0.64	18.40	33.74		0.83	42.78	56.39		4476
		5-R		0.30	18.33	34.14		0.39	42.59	57.02		2098
	2	2-R			19.52	33.49			44.78	55.22		
		3-R		0.16	19.25	33.30		0.21	44.48	55.31		1119
		4-R		0.40	18.36	33.99		0.52	42.68	56.80		2798
		5-R			19.43	33.13			44.93	55.07		
		6-?		0.18	18.73	33.63		0.23	43.55	56.21		1259
	3	1-C		1.23	17.03	33.69		1.65	40.61	57.75		8603
		2-M		0.90	17.49	34.25		1.18	41.04	57.77		6295
		3-R		0.31	18.46	33.96		0.40	42.88	56.71		2168
		4-M		1.20	17.71	34.11		1.57	41.28	57.15		8393
		5-R		0.53	18.41	33.58		0.69	42.97	56.34		3707
		6-M		1.01	17.58	33.91		1.33	41.34	57.33		7064
		7-R		0.57	18.41	33.81		0.74	42.78	56.48		3987
		8-M		0.94	18.08	33.73		1.23	42.19	56.58		6575
		9-R			18.78	33.90			43.52	56.48		
	4	1-C		0.66	18.22	34.34		0.86	42.10	57.04		4616
		2-M		0.51	18.32	34.18		0.66	42.43	56.91		3567

Sample	Cryst No	Probe Pos	MnO	FeO	MgO	CaO	$MnCO_3$ mole%	$FeCO_3$ mole%	$MgCO_3$ mole%	$CaCO_3$ mole%	Mn (ppm)	Fe (ppm)
MS28		3-M		0.86	18.14	34.13		1.12	42.03	56.85		6015
		4-R		0.57	18.34	34.16		0.74	42.44	56.82		3987
		5-R		0.19	19.54	33.32		0.24	44.82	54.94		1329
		6-R		0.28	18.12	33.73		0.37	42.61	57.02		1958
		7-R			19.07	33.06			44.52	55.48		
MS29	1	1-?			19.43	34.05			44.25	55.75		
		2-?			19.97	33.80			45.11	54.89		
		3-?		0.26	20.43	35.32		0.32	44.45	55.24		1819
	2	1-?			19.20	33.95			44.03	55.97		
		2-?			19.45	34.35			44.06	55.94		
		3-?		0.25	19.45	34.19		0.32	44.04	55.65		1749
		4-?			19.89	33.13			45.51	54.49		
	3	1-M		0.51	19.89	33.55		0.65	44.90	54.45		3567
		2-R			19.11	34.69			43.38	56.62		
		3-R		0.29	18.98	33.83		0.37	43.67	55.96		2028
		4-M			19.63	33.80			44.69	55.31		
		5-?		0.37	19.09	33.90		0.48	43.72	55.81		2588
	4	1-R			19.36	33.87			44.29	55.71		
		2-R		0.30	19.41	33.24		0.39	44.65	54.97		2098
		4-R			19.41	33.77			44.43	55.57		
		5-M		0.21	19.25	34.42		0.27	43.64	56.09		1469
		6-M		0.41	18.98	33.34		0.53	43.96	55.51		2868
	5	1-R			19.28	34.10			44.02	55.98		
		2-M		0.28	19.32	34.47		0.35	43.65	55.99		1958
		3-R		0.24	19.96	33.89		0.30	44.90	54.80		1679
		4-R		0.29	19.57	34.49		0.37	43.95	55.68		2028
WB15	1	1-R			19.15	30.78			46.39	53.61		
		2-?			18.50	31.78			44.74	55.26		
		3-?			18.37	31.55			44.75	55.25		
	2	1-R			19.38	30.69			46.76	53.24		
		2-C			19.13	31.13			46.09	53.91		
	3	1-R			20.53	29.76			48.97	51.03		
		2-C			20.11	30.22			48.07	51.93		
WB18	1	1-C			19.99	33.08			45.67	54.33		

Sample	Cryst No	Probe Pos	MnO	FeO	MgO	CaO	$MnCO_3$ mole%	$FeCO_3$ mole%	$MgCO_3$ mole%	$CaCO_3$ mole%	Mn (ppm)	Fe (ppm)
WB18		2-M			20.95	31.08			48.39	51.61		
		3-R			21.58	30.57			49.55	50.45		
		4-M			19.89	32.59			45.92	54.08		
		5-R			20.89	30.88			48.48	51.52		
	2	1-C			18.23	33.43			43.14	56.86		
		2-M		0.19	19.63	31.80		0.25	46.08	53.67		1329
		3-R			20.18	31.56			47.07	52.93		
		4-M			18.57	33.13			43.81	56.19		
	3	1-R			20.96	30.46			48.91	51.09		
		2-M			19.15	33.01			44.66	55.34		
		3-C			20.88	33.68			46.31	53.69		
WC2	1	1-C	0.40	0.18	18.52	33.80	0.53	0.23	42.92	56.32	3100	1259
		2-M	0.21		17.46	32.48	0.29		42.66	57.05	1627	
		3-R	0.68		17.69	32.21	0.94		42.90	56.16	5269	
		4-R	0.67		17.83	32.75	0.91		42.70	56.39	5192	
		5-M			18.06	33.22			43.06	56.94		
		6-R	0.84		17.28	32.84	1.15		41.77	57.07	6509	
	2	1-R	0.76		17.77	32.49	1.04		42.76	56.20	5889	
		2-R	0.67		17.62	32.41	0.92		42.66	56.41	5192	
		3-R	0.69		17.82	32.45	0.94		42.90	56.16	5347	
		4-R	0.74		17.79	32.69	1.01		42.65	56.34	5734	
		5-M	0.17		18.28	32.75	0.23		43.61	56.16	1317	
		6-C			18.00	32.53			43.49	56.51		
	3	1-C	0.26	0.31	17.67	31.77	0.36	0.43	43.28	55.94	2015	2168
		2-M			17.64	32.77			42.82	57.18		
		3-R	0.84		17.90	32.37	1.15		42.98	55.87	6509	
		4-R	0.75		17.16	32.49	1.04		41.91	57.05	5812	
		5-M			17.77	32.80			42.98	57.02		
		6-M			18.14	33.25			43.15	56.85		
	4	1-R	0.76		17.46	31.92	1.06		42.75	56.19	5889	
		2-M			17.88	33.39			42.69	57.31		
		5-M			17.85	32.12			43.60	56.40		
		6-R	0.84		17.54	32.28	1.16		42.55	56.29	6509	
	5	2-M	0.66		17.89	32.83	0.90		42.73	56.37	5114	
		3-C			18.22	33.19			43.30	56.70		
		4-M			17.75	33.47			42.45	57.55		

Sample	Cryst No	Probe Pos	MnO	FeO	MgO	CaO	$MnCO_3$ mole%	$FeCO_3$ mole%	$MgCO_3$ mole%	$CaCO_3$ mole%	Mn (ppm)	Fe (ppm)
WC2		5-R	0.84		17.40	31.91	1.17		42.63	56.20	6509	
		6-M	0.82		15.78	32.31	1.18		39.98	58.84	6354	
WPT3	1	1-R	0.56	0.60	18.24	33.10	0.75	0.79	42.73	55.74	4339	4197
		2-M	0.88	1.27	17.47	33.50	1.17	1.67	40.85	56.31	6819	8883
		3-C	1.59	3.06	15.04	32.79	2.19	4.16	36.48	57.17	12321	21403
	2	1-M	1.01	1.82	17.29	32.41	1.36	2.42	40.99	55.23	7826	12730
		2-R	0.41	0.59	17.97	32.86	0.55	0.79	42.63	56.04	3177	4127
		3-R	0.48	0.57	18.24	32.74	0.64	0.75	43.05	55.55	3719	3987
		4-M	0.76	0.84	17.71	32.83	1.02	1.12	41.95	55.91	5889	5875
	3	1-C	1.57	2.79	15.36	32.00	2.19	3.83	37.63	56.35	12166	19514
		2-M	1.03	1.60	16.43	33.11	1.40	2.15	39.39	57.06	7981	11191
		3-R	0.55	0.57	18.06	32.44	0.74	0.76	42.99	55.51	4262	3987
		4-M	0.74	1.23	17.64	32.38	1.00	1.64	41.97	55.39	5734	8603
		5-R	0.48	0.82	18.05	32.36	0.65	1.09	42.93	55.33	3719	5735
		6-M	1.17	2.03	15.95	32.59	1.61	2.77	38.73	56.89	9066	14199
		7-M	0.89	1.06	17.28	32.32	1.22	1.43	41.52	55.83	6897	7414
		8-R	0.56	0.59	17.71	32.54	0.76	0.79	42.42	56.03	4339	4127
		9-R	0.53	0.58	17.76	31.74	0.73	0.79	43.10	55.38	4107	4057
	4	1-R	0.60	0.55	18.03	31.87	0.82	0.74	43.35	55.09	4649	3847
		2-M	0.68	0.95	16.89	32.15	0.94	1.30	41.27	56.48	5269	6645
		3-C	1.12	2.09	15.95	31.71	1.57	2.89	39.33	56.21	8679	14618
		4-M	1.03	1.56	16.09	32.14	1.44	2.15	39.58	56.83	7981	10911

APPENDIX 11

WHOLE ROCK CHERT AND DETRITAL SEDIMENT DATA

A11.1. MAJOR AND TRACE ELEMENT ANALYSES OF CHERT

An '*' following a sample number indicates values are an average of replicate analyses.

A11.1.1. MAJOR ELEMENTS (Weight% oxide)

SAMPLE	SiO_2	TiO_2	Al_2O_3	Fe_2O_3	MnO	MgO	CaO	Na_2O	K_2O	LOI	P_2O_5	TOTAL
BLF2	96.70	0.05	0.82	0.17	<0.01	<0.10	0.08	0.17	0.14	1.11	<0.05	99.32
BLF3	96.54	0.05	0.77	0.18	<0.01	0.10	0.04	0.15	0.13	1.20	<0.05	99.20
BLF4	97.99	0.03	0.59	0.09	0.04	<0.10	0.17	<0.10	0.10	0.50	<0.05	99.51
BS1	97.53	0.06	1.09	0.19	0.05	<0.10	0.05	<0.10	0.24	1.06	<0.05	100.25
BS3	96.65	0.07	1.32	0.31	0.03	0.13	0.05	0.11	0.30	1.20	<0.05	100.17
BS4	98.14	0.02	0.44	0.05	0.03	<0.10	0.02	<0.10	0.11	1.14	<0.05	99.98
BS7	92.83	0.14	2.73	0.69	0.03	0.24	0.08	0.33	0.67	1.38	<0.05	99.13
BS9	96.39	0.06	1.16	0.21	0.05	<0.10	0.05	0.22	0.27	1.90	<0.05	100.38
BS14	97.25	0.06	1.11	0.20	0.03	<0.10	0.03	0.23	0.23	1.30	<0.05	100.51
CR2	96.56	0.04	0.67	0.07	0.01	<0.10	0.03	0.15	0.10	1.15	<0.05	98.83
CR3	95.82	0.04	0.89	0.06	<0.01	<0.10	0.06	0.19	0.13	1.32	<0.05	98.59
CR4*	91.24	0.13	3.12	0.90	<0.01	0.40	0.15	0.25	0.44	2.64	<0.05	99.29
CR5	96.98	0.04	0.77	0.24	<0.01	0.11	0.07	0.22	0.14	1.36	<0.05	99.94
CR6	96.45	0.04	1.06	0.29	<0.01	0.10	0.06	<0.10	0.16	1.09	<0.05	99.31
CR7	96.37	0.04	0.82	0.16	0.02	<0.10	0.16	0.22	0.15	1.39	<0.05	99.42
CR8	97.27	0.02	<0.20	<0.05	<0.01	<0.10	0.01	0.18	0.06	0.95	<0.05	98.88
CR9	97.73	0.02	<0.20	<0.05	0.01	<0.10	0.02	<0.10	0.06	1.02	<0.05	99.28
CR10	98.82	0.02	<0.20	<0.05	<0.01	<0.10	0.01	<0.10	0.07	0.79	<0.05	100.19
DHG2	95.34	0.05	0.99	0.48	<0.01	0.13	0.04	0.26	0.19	0.66	<0.05	98.17
DHG3	97.29	0.05	0.97	0.10	0.03	<0.10	0.09	0.11	0.16	1.37	<0.05	100.26
DHG4	97.53	0.04	0.60	0.12	<0.01	<0.10	0.03	0.24	0.10	1.06	<0.05	99.78
DHG5	97.46	0.03	<0.20	<0.05	<0.01	<0.10	0.05	0.12	0.06	0.83	<0.05	98.94
DS1	95.64	0.05	0.92	0.09	<0.01	<0.10	0.33	0.14	0.12	1.15	<0.05	98.52
DS3*	96.00	0.05	1.25	0.15	0.03	<0.10	0.12	0.16	0.21	1.36	<0.05	99.41
DS5	97.89	0.04	0.78	0.13	0.05	<0.10	0.04	0.20	0.17	1.19	<0.05	100.52
DS7	97.09	0.06	1.09	0.17	0.04	<0.10	0.07	0.26	0.23	1.34	<0.05	100.44
DS9*	97.68	0.03	0.66	0.05	0.04	<0.10	0.10	<0.10	0.13	0.92	<0.05	99.73

SAMPLE	SiO_2	TiO_2	Al_2O_3	Fe_2O_3	MnO	MgO	CaO	Na_2O	K_2O	LOI	P_2O_5	TOTAL
DS11	95.50	0.06	1.17	0.23	<0.01	0.12	0.09	0.14	0.30	0.95	<0.05	98.61
DS12	97.18	0.05	0.86	0.25	<0.01	<0.10	0.02	0.13	0.19	0.99	<0.05	99.79
DS14	95.94	0.05	0.91	0.21	<0.01	<0.10	0.05	0.11	0.23	1.22	<0.05	98.84
DS16	96.57	0.07	1.45	0.27	0.03	0.18	0.06	0.13	0.40	0.57	<0.05	99.74
DTS4	96.42	0.06	1.29	0.31	0.04	<0.10	0.04	0.23	0.28	0.97	<0.05	99.72
DTS5	96.74	0.07	1.29	0.32	0.03	<0.10	0.05	0.11	0.29	1.03	<0.05	100.01
DTS6	96.29	0.06	1.33	0.22	0.03	<0.10	0.17	0.31	0.23	1.13	<0.05	99.76
DTS8	98.26	0.03	0.50	0.07	0.04	<0.10	0.03	<0.10	0.09	1.03	<0.05	100.21
FRM3	95.85	0.05	0.99	0.12	<0.01	<0.10	0.03	0.28	0.18	1.80	<0.05	99.37
HB5	94.95	0.09	1.67	0.53	<0.01	0.18	0.17	0.15	0.23	1.29	<0.05	99.28
IC6	93.16	0.13	2.72	0.83	0.04	0.41	0.19	0.39	0.64	1.19	<0.05	99.72
IC7	95.75	0.08	1.41	0.46	0.03	0.25	0.06	0.23	0.37	0.72	<0.05	99.37
IC8	95.81	0.08	1.57	0.57	0.03	0.23	0.06	0.22	0.42	0.75	<0.05	99.75
IC11	96.52	0.06	1.19	0.40	0.03	0.24	0.15	0.18	0.30	1.50	<0.05	100.59
IC12	95.81	0.07	1.72	0.45	<0.01	0.36	0.14	0.10	0.43	0.85	<0.05	99.98
IC13	94.26	0.07	1.37	0.36	<0.01	0.45	0.42	0.22	0.37	1.43	<0.05	99.02
IC16	97.56	0.05	0.88	0.14	0.01	<0.10	0.04	0.20	0.21	0.93	<0.05	100.07
IC18	96.33	0.06	0.97	0.16	0.02	0.11	0.04	0.28	0.21	0.95	<0.05	99.16
IC19	98.45	0.03	<0.20	<0.05	<0.01	<0.10	0.04	0.13	0.05	0.81	<0.05	99.85
IC20	87.66	0.25	4.92	1.05	<0.01	0.85	0.11	0.36	1.53	1.89	<0.05	98.65
IC24	96.85	0.04	0.72	0.19	<0.01	<0.10	<0.01	0.22	0.15	0.78	<0.05	99.02
KP12	98.02	0.02	0.35	0.04	0.02	<0.10	0.03	<0.10	0.07	1.35	<0.05	99.90
KP22	98.84	0.02	<0.20	<0.05	<0.01	<0.10	0.03	<0.10	0.04	0.98	<0.05	100.19
KP23	98.32	0.04	<0.20	0.06	<0.01	<0.10	0.03	<0.10	0.07	1.09	<0.05	99.95
LS4	98.14	0.03	0.58	0.10	0.05	<0.10	0.02	<0.10	0.14	0.84	<0.05	99.98
LS5	98.39	0.03	0.50	0.07	0.03	<0.10	0.03	0.13	0.11	1.34	<0.05	100.61
LS8	98.18	0.04	0.62	0.07	0.02	<0.10	0.03	<0.10	0.16	1.07	<0.05	100.31
LS9	96.43	0.08	1.47	0.11	0.01	<0.10	0.06	0.19	0.47	1.31	<0.05	100.22
LS11	96.98	0.08	1.34	0.19	<0.01	0.22	0.04	<0.10	0.35	1.22	<0.05	100.43
LS12	97.81	0.04	0.58	0.11	<0.01	<0.10	<0.01	<0.10	0.14	0.78	<0.05	99.55
LS13	96.94	0.07	1.23	0.20	<0.01	<0.10	0.03	0.11	0.28	1.03	<0.05	99.95
LS15	98.91	0.03	<0.20	0.06	<0.01	<0.10	0.03	<0.10	0.12	1.15	<0.05	100.86

SAMPLE	SiO_2	TiO_2	Al_2O_3	Fe_2O_3	MnO	MgO	CaO	Na_2O	K_2O	LOI	P_2O_5	TOTAL
MA1b	95.71	0.09	1.73	0.25	<0.01	0.18	0.04	<0.10	0.36	0.92	<0.05	99.38
MA1a	95.42	0.11	1.85	0.23	<0.01	0.12	0.04	0.17	0.41	1.09	<0.05	99.45
MA3	97.59	0.05	0.89	0.24	0.03	0.10	0.04	0.24	0.20	1.10	<0.05	100.48
MA4	96.54	0.07	1.32	0.27	<0.01	<0.10	0.03	0.15	0.31	1.10	<0.05	99.89
MA8	95.16	0.10	1.88	0.19	0.05	<0.10	0.09	0.39	0.41	1.71	<0.05	100.06
MA12	96.86	0.05	0.76	0.08	<0.01	<0.10	0.07	<0.10	0.12	0.76	<0.05	98.77
MA14	96.52	0.07	1.26	0.23	<0.01	<0.10	0.07	<0.10	0.19	0.96	<0.05	99.42
MA16	97.80	0.04	0.61	0.06	<0.01	<0.10	0.03	<0.10	0.07	1.03	<0.05	99.69
MS1	95.76	0.08	1.51	0.37	0.02	0.17	0.04	0.10	0.41	1.07	<0.05	99.57
MS2	97.56	0.04	0.68	0.15	0.04	<0.10	0.02	0.12	0.16	0.95	<0.05	99.81
MS3	97.15	0.08	1.23	0.22	<0.01	<0.10	0.03	0.15	0.34	0.73	<0.05	100.03
MS7	96.41	0.08	1.46	0.29	0.02	0.16	0.06	<0.10	0.40	0.77	<0.05	99.76
MS9	97.15	0.08	1.23	0.22	<0.01	<0.10	0.03	0.15	0.34	0.73	<0.05	100.03
MS11	98.15	0.03	0.53	<0.05	0.03	<0.10	0.02	<0.10	0.12	0.77	<0.05	99.77
MS12a	98.42	0.03	0.61	0.08	0.03	<0.10	0.03	0.18	0.13	0.57	<0.05	100.17
MS12b	97.57	0.06	1.13	0.14	0.02	0.11	0.06	<0.10	0.33	0.70	<0.05	100.17
MS13	97.53	0.07	1.02	0.10	<0.01	<0.10	0.03	<0.10	0.26	1.05	<0.05	100.09
MS14	97.93	0.05	1.01	0.11	<0.01	<0.10	0.04	0.17	0.23	0.97	<0.05	100.62
MS18	96.15	0.06	1.15	0.11	<0.01	<0.10	0.08	<0.10	0.27	1.57	<0.05	99.51
MS24	95.36	0.08	1.39	0.22	0.02	<0.10	0.03	0.16	0.38	0.80	<0.05	98.51
MS26	96.53	0.05	0.96	0.20	<0.01	<0.10	0.03	0.21	0.21	1.03	<0.05	99.29
MS27	96.68	0.06	1.21	0.23	<0.01	<0.10	0.04	0.25	0.26	1.30	<0.05	100.13
MS28	96.93	0.04	0.86	0.11	<0.01	<0.10	0.03	0.21	0.18	1.00	<0.05	99.45
MS29	97.17	0.05	0.96	0.14	<0.01	<0.10	0.04	0.26	0.20	0.04	<0.05	99.00
MS31	98.50	0.02	0.36	0.05	<0.01	<0.10	0.04	<0.10	0.08	0.83	<0.05	99.97
MS32*	98.52	0.02	0.34	<0.05	<0.01	<0.10	0.04	<0.10	0.06	0.70	<0.05	99.99
MS34	98.07	0.03	0.53	0.07	0.02	<0.10	0.05	<0.10	0.13	0.80	<0.05	99.75
MS37*	98.49	0.02	0.30	0.14	0.02	<0.10	0.03	<0.10	0.07	0.76	<0.05	99.98
MS38	97.86	0.03	0.59	0.14	0.02	<0.10	0.04	0.13	0.12	1.51	<0.05	100.48
MS42	89.83	0.15	3.10	0.75	0.03	0.46	0.06	0.25	0.57	2.44	<0.05	97.66
MS43	96.77	0.04	0.68	0.12	0.04	<0.10	0.04	<0.10	0.14	1.03	<0.05	98.97
MS44	97.38	0.06	0.86	0.21	0.03	<0.10	0.07	0.15	0.19	0.97	<0.05	99.98
MS45	96.66	0.04	0.79	0.14	0.03	<0.10	0.05	<0.10	0.15	0.43	<0.05	98.44
MS46	96.35	0.05	1.10	0.12	0.01	0.16	0.36	0.18	0.13	0.94	<0.05	99.42
MZL2	97.86	0.04	0.71	0.09	0.03	<0.10	0.05	0.11	0.11	0.87	<0.05	99.91
MZL4a	98.80	0.04	0.46	0.13	0.02	<0.10	0.05	<0.10	0.08	0.80	<0.05	100.45

SAMPLE	SiO_2	TiO_2	Al_2O_3	Fe_2O_3	MnO	MgO	CaO	Na_2O	K_2O	LOI	P_2O_5	TOTAL
MZL4b	97.70	0.03	0.43	0.05	0.02	<0.10	0.04	0.23	0.07	0.67	<0.05	99.22
MZL4c	98.13	0.03	0.61	0.08	0.03	<0.10	0.07	0.10	0.09	0.80	<0.05	100.02
MZL4d	97.72	0.04	<0.20	0.10	<0.01	<0.10	0.04	<0.10	0.08	0.86	<0.05	99.45
MZL4e	98.51	0.04	0.50	0.13	<0.01	<0.10	0.03	<0.10	0.08	1.02	<0.05	100.35
MZL5	97.80	0.04	0.81	0.04	0.04	<0.10	0.17	<0.10	0.11	0.67	<0.05	99.76
NP1	97.85	0.03	0.51	0.10	<0.01	<0.10	0.02	<0.10	0.09	0.95	<0.05	99.61
NP3	100.97	0.05	0.95	0.16	<0.01	<0.10	0.04	<0.10	0.17	1.00	<0.05	103.45
NP4	98.08	0.05	0.78	0.21	0.02	<0.10	0.03	0.14	0.16	0.86	<0.05	100.45
PS19	95.21	0.10	1.90	0.30	<0.01	0.10	0.06	0.22	0.33	1.10	<0.05	99.33
PS20	94.08	0.10	2.18	0.45	<0.01	0.16	0.10	0.38	0.36	0.97	<0.05	98.79
PS23	94.79	0.10	2.14	0.29	<0.01	0.26	0.07	<0.10	0.22	1.81	<0.05	99.77
PS25	97.86	0.03	0.64	0.08	0.04	<0.10	0.10	<0.10	0.09	1.03	<0.05	99.95
PS28	96.81	0.06	1.24	0.23	0.05	<0.10	0.05	0.39	0.20	1.14	<0.05	100.26
PS29	96.13	0.07	1.33	0.23	<0.01	0.10	0.04	0.19	0.22	1.25	<0.05	99.58
PS30	95.49	0.09	1.65	0.34	<0.01	0.18	0.09	0.24	0.28	1.09	<0.05	99.47
PS31	94.09	0.10	2.10	0.39	<0.01	0.17	0.11	0.32	0.37	1.24	<0.05	98.92
SS3	94.96	0.11	1.79	0.38	<0.01	0.12	0.02	<0.10	0.45	1.09	<0.05	99.02
SS5	97.03	0.06	0.88	0.12	<0.01	<0.10	0.02	<0.10	0.21	1.14	<0.05	99.60
SS6	96.83	0.06	0.89	0.18	<0.01	<0.10	0.03	<0.10	0.22	1.40	<0.05	99.67
SS7	95.35	0.09	1.49	0.43	<0.01	0.13	0.02	0.13	0.38	1.11	<0.05	99.12
SS8	95.45	0.07	1.12	0.46	<0.01	0.13	0.02	0.33	0.27	0.89	<0.05	98.75
SS10	97.70	0.04	0.51	0.07	<0.01	<0.10	0.01	<0.10	0.11	1.06	<0.05	99.57
SS13	96.14	0.06	0.95	0.12	<0.01	<0.10	0.03	<0.10	0.20	1.02	<0.05	98.67
SS14	96.77	0.04	0.71	0.10	<0.01	<0.10	0.07	<0.10	0.14	0.90	<0.05	98.80
SS16	97.92	0.04	0.51	0.06	<0.01	<0.10	0.09	<0.10	0.10	0.58	<0.05	99.34
SWP1	97.22	0.05	0.79	0.12	<0.01	<0.10	0.08	<0.10	0.13	1.51	<0.05	100.05
SWP3	96.62	0.06	1.35	0.17	0.04	<0.10	0.07	0.26	0.21	1.37	<0.05	100.22
SWP6	96.87	0.05	1.05	0.16	0.02	<0.10	0.12	<0.10	0.18	1.07	<0.05	99.64
TG2	97.75	0.04	0.65	0.08	<0.01	<0.10	0.05	<0.10	0.12	1.20	<0.05	99.96
TG3	91.35	0.11	2.14	0.41	<0.01	0.21	0.11	<0.10	0.29	1.15	<0.05	95.80
TG4	92.51	0.18	3.33	0.63	<0.01	0.38	0.18	<0.10	0.46	1.84	<0.05	99.60

SAMPLE	SiO_2	TiO_2	Al_2O_3	Fe_2O_3	MnO	MgO	CaO	Na_2O	K_2O	LOI	P_2O_5	TOTAL
WB3	94.79	0.07	1.53	0.20	<0.01	0.11	0.02	0.23	0.34	1.23	<0.05	98.53
WB5	96.30	0.06	1.33	0.25	0.03	0.10	0.03	0.24	0.31	1.40	<0.05	100.06
WB8	97.54	0.04	0.82	<0.05	<0.01	<0.10	<0.01	0.15	0.16	0.82	<0.05	99.60
WB13	94.69	0.10	2.27	0.32	<0.01	0.14	0.05	0.49	0.45	1.14	<0.05	99.67
WB18	89.45	0.17	4.86	0.53	<0.01	0.32	0.08	1.57	0.99	1.00	<0.05	99.00
WB19	93.74	0.12	2.00	0.39	<0.01	0.18	0.04	0.25	0.54	1.13	<0.05	98.39
WB20	96.55	0.06	1.07	0.23	<0.01	<0.10	0.03	0.16	0.27	1.02	<0.05	99.48
WB21	92.59	0.14	3.42	0.34	<0.01	0.15	0.06	0.93	0.78	0.97	<0.05	99.40
WB23	96.60	0.06	1.17	0.13	<0.01	<0.10	0.08	0.12	0.22	1.50	<0.05	99.96
WB24	94.07	0.12	2.52	0.46	<0.01	0.24	0.05	0.32	0.63	1.10	<0.05	99.47
WB26	97.78	0.03	<0.20	0.06	<0.01	<0.10	0.03	<0.10	0.10	0.89	<0.05	99.45
WB29	97.76	0.02	0.41	0.05	<0.01	<0.10	0.03	<0.10	0.07	1.10	<0.05	99.55
WB35b	98.19	0.02	<0.20	<0.05	<0.01	<0.10	0.07	<0.10	0.06	0.90	<0.05	99.62
WB37	98.63	0.02	<0.20	<0.05	<0.01	<0.10	0.07	<0.10	0.60	0.89	<0.05	100.11
WC2	96.22	0.06	1.11	0.38	<0.01	<0.10	0.06	0.11	0.29	1.14	<0.05	99.44
WC4	97.04	0.05	1.10	0.10	0.04	<0.10	0.09	0.18	0.22	1.17	<0.05	100.07
WC5	98.35	0.03	0.48	0.04	0.04	<0.10	0.04	0.17	0.10	0.98	<0.05	100.23
WC8	97.42	0.04	0.89	0.09	0.03	<0.10	0.06	0.16	0.15	0.00	<0.05	98.94
WC9	96.43	0.05	1.09	0.16	0.02	<0.10	0.06	0.27	0.18	1.23	<0.05	99.55
WC11	97.82	0.03	0.68	0.18	0.02	<0.10	0.05	0.17	0.10	0.80	<0.05	99.95
WC17*	92.39	0.11	2.33	0.71	0.05	0.40	0.75	0.26	0.43	1.94	<0.05	100.28
WKS3	96.36	0.11	1.85	0.23	<0.01	0.17	0.04	0.27	0.42	1.18	<0.05	100.65
WKS4	92.14	0.15	3.13	0.64	<0.01	0.30	0.04	0.40	0.65	0.97	<0.05	98.43
WKS5	97.18	0.06	1.06	0.18	<0.01	0.10	0.01	<0.10	0.20	0.52	<0.05	99.42
WKS6	97.87	0.04	0.62	0.18	<0.01	<0.10	<0.01	<0.10	0.13	0.81	<0.05	99.72
WKS7	96.25	0.04	0.76	0.18	<0.01	<0.10	<0.01	0.14	0.13	0.81	<0.05	98.41
WKS8	95.08	0.11	1.79	0.39	<0.01	0.17	0.02	0.32	0.40	0.56	<0.05	98.84
WPT1	98.06	0.03	0.77	0.04	0.04	<0.10	0.02	0.16	0.14	1.27	<0.05	100.59
WPT2	97.25	0.04	1.04	0.10	0.03	<0.10	0.03	0.21	0.19	1.37	<0.05	100.35
WPT3	96.90	0.05	0.70	0.10	<0.01	<0.10	0.07	<0.10	0.14	1.46	<0.05	99.27
WPT4	96.69	0.06	1.23	0.19	0.03	0.11	0.04	0.22	0.29	1.60	<0.05	100.48
WPT5	95.87	0.09	1.73	0.32	0.03	0.16	0.06	0.20	0.43	1.30	<0.05	100.19
WUR1	98.78	0.03	0.36	0.05	0.02	<0.10	0.03	0.13	0.07	0.67	<0.05	100.22
WUR3*	94.18	0.10	1.76	0.44	0.03	0.22	0.14	0.41	0.30	1.74	0.07	99.38

SAMPLE	SiO_2	TiO_2	Al_2O_3	Fe_2O_3	MnO	MgO	CaO	Na_2O	K_2O	LOI	P_2O_5	TOTAL
WUR4	97.11	0.03	0.67	0.17	0.03	<0.10	0.09	<0.10	0.12	1.67	<0.05	100.05
WUR5	96.94	0.06	0.95	0.12	<0.01	<0.10	0.03	<0.10	0.20	1.32	<0.05	99.72
WUR7	97.95	0.03	0.67	0.07	0.04	<0.10	0.07	0.19	0.12	0.80	<0.05	99.94
CR1	89.06	0.21	5.01	0.90	<0.01	0.67	0.27	0.21	0.70	2.48	<0.05	99.55
TG1	93.01	0.15	3.25	0.56	<0.01	0.42	0.23	0.18	0.47	1.96	<0.05	100.25
WC7	91.68	0.15	3.11	0.43	0.02	0.43	0.17	0.29	0.53	2.31	<0.05	99.09

A11.1.2. TRACE ELEMENTS (ppm)

SAMPLE	V	Cr	Ni	Zn	Ga	Rb	Sr	Y	Zr	Nb	Ba	Ce	Nd	La	Pb	Th
BLF2	<5	<5	<5	5	<2	6	29	1	8	<5	98	<10	<10	<2	4	<1
BLF3	<5	<5	<5	3	<2	5	30	1	10	<5	81	<10	<10	<2	2	<1
BLF4	<5	<5	<5	2	<2	3	36	2	13	<5	695	<10	<10	<2	4	<1
BS1	5	<5	<5	5	2	9	26	2	11	<5	190	<10	<10	<2	4	<1
BS3	<5	5	<5	2	<2	11	26	1	15	<5	480	<10	<10	<2	4	<1
BS4	<5	<5	<5	<2	<2	3	11	1	7	<5	1163	<10	<10	<2	5	<1
BS7	21	15	<5	5	3	24	42	2	31	<5	994	<10	<10	<2	5	<1
BS9	23	6	<5	9	<2	9	21	2	14	<5	355	<10	<10	<2	4	<1
BS14	5	6	<5	3	2	10	24	1	13	<5	198	<10	<10	<2	5	<1
CR2	<5	<5	10	<2	3	2	24	<1	8	<5	160	<10	13	<2	4	<1
CR3	<5	<5	<5	<2	4	4	36	2	9	<5	234	<10	12	<2	4	<1
CR4*	16	14	12	11	3	20	131	3	30	<5	2700	<10	<10	<2	3	<1
CR5	<5	<5	<5	2	<2	5	33	2	8	<5	363	<10	12	<2	3	<1
CR6	8	6	6	5	<2	7	35	1	17	<5	442	<10	12	<2	4	<1
CR7	<5	20	<5	4	2	6	30	<1	10	<5	241	<10	<10	<2	2	<1
CR8	<5	<5	<5	<2	<2	<1	35	1	26	<5	680	<10	<10	<2	4	<1
CR9	<5	<5	<5	<2	<2	<1	17	1	16	<5	350	<10	<10	<2	3	<1
CR10	<5	<5	<5	3	3	1	28	<1	14	<5	859	<10	<10	<2	3	<1
DHG2	6	6	<5	4	<2	8	17	<1	12	<5	169	<10	<10	<2	5	<1
DHG3	<5	<5	<5	5	2	6	36	2	12	<5	373	<10	<10	<2	5	<1
DHG4	<5	<5	<5	5	<2	3	20	<1	6	<5	181	<10	<10	<2	4	<1
DHG5	<5	<5	<5	<2	<2	1	9	<1	8	<5	55	<10	<10	<2	4	<1

SAMPLE	V	Cr	Ni	Zn	Ga	Rb	Sr	Y	Zr	Nb	Ba	Ce	Nd	La	Pb	Th
DS1	<5	<5	<5	3	<2	6	268	1	17	6	5078	<10	<10	<2	4	<1
DS3*	<5	5	5	8	<2	7	154	1	20	<5	2529	<10	<10	<2	4	<1
DS5	10	7	<5	2	<2	5	39	1	8	<5	422	<10	<10	<2	3	<1
DS7	8	10	6	8	<2	7	78	3	12	<5	1214	<10	10	<2	4	<1
DS9*	8	6	<5	4	2	4	31	2	6	<5	414	<10	<10	<2	3	<1
DS11	11	7	<5	17	<2	10	19	2	8	<5	431	10	<10	<2	4	<1
DS12	10	6	<5	20	<2	8	20	1	6	<5	460	<10	<10	<2	5	<1
DS14	11	<5	<5	13	<2	7	16	2	6	<5	302	<10	<10	<2	3	<1
DS16	9	7	<5	12	<2	12	26	1	15	5	607	<10	<10	<2	4	<1
DTS4	<5	<5	<5	5	<2	9	27	1	12	<5	382	<10	<10	<2	5	<1
DTS5	6	7	<5	4	<2	10	34	1	14	<5	324	<10	<10	<2	4	<1
DTS6	7	<5	<5	5	<2	8	45	1	13	<5	1020	<10	<10	<2	4	<1
DTS8	<5	<5	<5	7	2	3	12	<1	<5	<5	217	<10	<10	<2	3	<1
FRM3	<5	<5	<5	3	4	6	18	2	14	<5	228	<10	<10	<2	2	<1
HB5	14	8	11	9	<2	13	65	<1	15	<5	335	<10	<10	<2	3	<1
IC6	25	23	9	44	3	21	39	6	40	<5	673	<10	<10	5	5	<1
IC7	18	12	6	24	<2	13	49	4	19	<5	394	<10	<10	3	4	1
IC8	19	12	<5	23	2	15	34	5	16	<5	387	10	<10	3	6	<1
IC11	14	9	<5	16	<2	10	31	4	12	<5	348	11	<10	3	4	1
IC12	11	8	<5	24	2	12	28	6	11	<5	590	<10	11	5	4	<1
IC13	12	9	<5	16	<2	12	40	4	13	<5	459	<10	<10	2	3	<1
IC16	8	6	<5	7	2	7	13	2	7	<5	477	<10	<10	<2	3	<1
IC18	<5	<5	<5	9	<2	7	16	3	10	<5	500	<10	<10	<2	3	<1
IC19	13	<5	5	7	<2	5	23	1	6	<5	760	<10	<10	<2	3	<1
IC20	45	28	32	27	5	57	131	4	40	6	3068	<10	<10	<2	7	<1
IC24	<5	<5	<5	<2	<2	<1	47	<1	<5	<5	458	<10	<10	<2	4	<1
KP12	6	5	<5	3	<2	3	86	1	11	<5	1561	<10	<10	<2	3	<1
KP22	<5	<5	<5	<2	<2	1	14	1	<5	<5	147	<10	<10	<2	3	<1
KP23	5	<5	<5	<2	<2	2	15	2	11	<5	<10	<10	<10	<2	3	<1
LS4	9	5	<5	<2	<2	4	5	1	6	<5	82	<10	<10	<2	3	<1
LS5	7	5	<5	2	2	3	4	1	5	<5	67	<10	<10	<2	3	<1
LS8	9	6	<5	2	<2	5	6	1	7	<5	97	<10	<10	<2	3	<1

SAMPLE	V	Cr	Ni	Zn	Ga	Rb	Sr	Y	Zr	Nb	Ba	Ce	Nd	La	Pb	Th
LS9	12	10	<5	<2	<2	14	19	1	13	<5	398	<10	<10	<2	3	<1
LS11	8	5	<5	8	<2	11	19	1	11	<5	330	<10	10	<2	2	<1
LS12	11	7	<5	3	2	4	6	1	7	<5	126	<10	<10	<2	3	<1
LS13	9	6	<5	3	<2	10	21	1	11	<5	422	<10	<10	<2	4	<1
LS15	<5	<5	<5	5	2	3	8	1	<5	<5	214	<10	<10	<2	3	<1
MA1b	10	9	<5	6	<2	13	65	1	24	<5	430	<10	<10	11	4	<1
MA1a	12	11	<5	4	2	15	63	2	26	<5	424	<10	<10	20	4	<1
MA3	6	5	5	4	2	7	44	2	12	5	290	<10	<10	2	4	1
MA4	6	12	11	7	3	11	54	1	17	<5	393	<10	<10	<2	3	<1
MA8	7	7	<5	<2	<2	15	121	1	28	5	1158	<10	<10	<2	4	<1
MA12	<5	<5	<5	2	<2	5	258	2	25	<5	11289	<10	<10	<2	3	<1
MA14	8	6	7	10	<2	9	210	1	18	<5	4031	<10	<10	9	2	<1
MA16	<5	<5	<5	<2	<2	2	295	<1	13	<5	6053	<10	<10	<2	2	<1
MS1	13	9	<5	8	2	24	14	2	15	<5	235	<10	<10	<2	4	<1
MS2	10	6	<5	7	<2	5	11	1	6	<5	126	<10	<10	<2	4	<1
MS3	6	<5	<5	9	<2	6	6	1	7	<5	96	<10	<10	<2	3	<1
MS7	13	10	<5	14	2	13	17	1	15	<5	541	<10	<10	<2	4	<1
MS9	6	6	<5	10	<2	11	28	1	12	<5	335	<10	<10	<2	5	<1
MS11	7	5	<5	<2	<2	3	13	1	4	<5	137	<10	<10	<2	3	<1
MS12a	8	5	<5	4	<2	4	13	2	5	<5	184	<10	<10	<2	3	<1
MS12b	11	8	<5	5	<2	10	22	2	12	<5	234	<10	<10	<2	3	<1
MS13					<2	9	21	2							3	<1
MS14	10	7	<5	6	3	7	22	1	8	<5	253	<10	<10	<2	4	<1
MS18	10	8	<5	3	2	10	39	2	9	<5	599	<10	<10	<2	4	<1
MS24	10	7	<5	7	<2	13	34	1	9	<5	209	<10	<10	<2	5	<1
MS26	10	9	<5	5	<2	7	35	1	9	<5	582	<10	<10	<2	4	<1
MS27	19	9	<5	6	<2	10	52	1	10	<5	932	<10	<10	<2	3	<1
MS28	12	6	<5	6	<2	6	33	1	7	<5	630	<10	<10	<2	3	<1
MS29	10	6	<5	3	<2	8	42	1	170	<5	840	<10	<10	<2	276	<1
MS31	7	4	<5	9	2	2	22	1	4	<5	452	<10	<10	<2	3	<1
MS32*	6	4	<5	2	<2	1	22	1	3	<5	510	<10	<10	<2	4	<1
MS34	5	6	<5	2	<2	5	63	1	7	<5	2780	<10	<10	<2	2	<1
MS37*	7	5	<5	3	<2	2	25	2	5	<5	584	<10	<10	<2	4	<1
MS38	10	8	<5	4	<2	3	46	1	7	<5	1053	<10	<10	<2	4	<1
MS42	56	63	23	17	3	23	175	7	39	<5	3585	13	<10	5	2	<1
MS43	8	8	<5	5	2	5	54	1	7	<5	541	<10	<10	<2	4	<1

SAMPLE	V	Cr	Ni	Zn	Ga	Rb	Sr	Y	Zr	Nb	Ba	Ce	Nd	La	Pb	Th
MS44	9	8	5	3	2	6	57	2	11	<5	564	<10	<10	<2	3	<1
MS45	9	7	12	4	<2	5	66	2	8	<5	621	<10	<10	<2	5	<1
MS46	7	5	<5	4	<2	5	235	3	21	<5	3642	<10	<10	<2	3	<1
MZL2	<5	<5	<5	4	<2	4	30	1	6	<5	77	<10	<10	<2	4	<1
MZL4a	6	6	<5	2	<2	3	21	<1	7	<5	62	<10	<10	<2	3	<1
MZL4b	<5	<5	<5	2	<2	2	21	<1	6	5	59	<10	<10	<2	3	<1
MZL4c	5	<5	<5	3	<2	3	28	3	<5	<5	96	<10	<10	<2	4	<1
MZL4d	7	6	<5	3	<2	3	25	<1	9	<5	66	<10	10	<2	3	<1
MZL4e	<5	<5	<5	8	<2	3	30	<1	6	<5	91	<10	<10	<2	3	<1
MZL5	<5	<5	<5	<2	2	4	82	1	12	<5	196	<10	<10	<2	5	<1
NP1	<5	<5	<5	2	<2	2	110	<1	13	<5	3892	<10	<10	<2	3	<1
NP3	<5	6	<5	2	3	5	50	<1	11	<5	415	<10	<10	<2	3	<1
NP4	<5	<5	<5	4	<2	7	120	1	15	<5	4278	<10	<10	<2	3	<1
PS19	8	8	6	4	<2	12	82	2	25	<5	580	<10	<10	<2	3	<1
PS20	10	9	<5	14	2	14	95	2	29	<5	734	<10	<10	<2	4	<1
PS23	8	8	8	7	<2	11	185	2	20	<5	2006	<10	<10	<2	2	<1
PS25	<5	<5	<5	<2	<2	2	96	1	7	<5	1345	<10	<10	5	3	<1
PS28	7	6	<5	4	<2	9	50	2	15	<5	479	<10	12	<2	4	<1
PS29	7	6	8	8	<2	10	52	2	17	<5	507	<10	<10	<2	4	<1
PS30	12	9	<5	8	<2	13	68	2	21	<5	974	<10	<10	4	3	<1
PS31	23	24	7	17	<2	15	90	2	31	<5	1015	<10	<10	<2	4	<1
SS3	12	10	<5	11	<2	14	32	2	26	<5	191	<10	<10	<2	3	<1
SS5	6	<5	<5	2	<2	7	24	1	11	<5	175	<10	11	<2	3	<1
SS6	6	6	<5	3	2	8	24	1	10	<5	196	<10	<10	<2	2	<1
SS7	10	8	<5	3	3	12	31	2	19	<5	198	<10	<10	<2	4	<1
SS8	9	6	<5	6	<2	9	19	2	11	<5	206	<10	<10	<2	4	<1
SS10	<5	<5	<5	<2	<2	3	20	1	5	<5	1345	<10	<10	<2	3	<1
SS13	<5	<5	<5	8	<2	7	36	2	9	<5	1328	<10	<10	<2	4	<1
SS14	<5	<5	<5	10	2	4	87	2	6	<5	488	<10	<10	<2	4	<1
SS16	<5	<5	<5	11	3	3	53	<1	<5	<5	495	<10	<10	<2	2	<1
SWP1	<5	<5	<5	3	2	4	51	2	14	<5	985	<10	<10	<2	4	<1
SWP3	11	8	<5	13	3	9	57	2	12	<5	61	<10	<10	<2	5	<1

SAMPLE	V	Cr	Ni	Zn	Ga	Rb	Sr	Y	Zr	Nb	Ba	Ce	Nd	La	Pb	Th
SWP6	<5	<5	<5	5	<2	7	56	2	23	<5	2291	<10	<10	<2	5	<1
TG2	<5	<5	<5	<2	3	4	24	1	6	<5	131	<10	<10	<2	4	<1
TG3	<5	10	10	13	<2	15	277	3	40	<5	8489	<10	<10	<2	4	<1
TG4	38	28	12	16	<2	25	134	5	54	<5	714	13	<10	6	4	<1
WB3	8	6	8	3	<2	10	23	2	30	<5	179	<10	<10	<2	3	<1
WB5	7	5	<5	2	<2	16	45	2	16	<5	148	<10	<10	<2	3	<1
WB8	<5	<5	6	<2	5	2	15	2	10	<5	117	<10	11	37	<1	<1
WB13	12	8	9	8	<2	14	36	2	41	<5	287	<10	<10	<2	4	<1
WB18	19	13	<5	9	5	30	59	4	113	<5	400	<10	<10	<2	5	1
WB19	12	9	<5	7	2	17	31	2	25	<5	249	<10	<10	12	4	<1
WB20	<5	5	7	3	3	8	22	1	14	<5	183	<10	13	<2	3	<1
WB21	14	8	6	3	3	19	39	3	63	<5	332	<10	10	<2	4	<1
WB23	<5	<5	<5	9	<2	8	52	2	10	<5	273	<10	<10	<2	3	<1
WB24	14	12	8	12	2	19	42	1	35	<5	318	<10	<10	<2	4	<1
WB26	<5	<5	12	<2	2	2	17	2	<5	<5	177	<10	11	9	3	<1
WB29	5	5	<5	2	<2				5	<5	341	<10	<10	<2		<1
WB35b	<5	<5	<5	<2	<2	1	22	1	<5	<5	111	<10	<10	<2	4	<1
WB37	<5	<5	8	<2	<2	2	33	1	<5	<5	256	<10	12	<2	3	<1
WC2	<5	<5	<5	6	3	10	36	2	18	<5	182	<10	<10	<2	4	<1
WC4	<5	6	<5	<2	<2	7	62	2	23	<5	1954	<10	<10	<2	4	<1
WC5	<5	<5	<5	<2	<2	2	47	<1	21	<5	4203	<10	<10	<2	5	<1
WC8	<5	<5	<5	4	3	5	58	<1	10	<5	399	<10	<10	<2	3	<1
WC9	<5	<5	<5	<2	<2	7	108	<1	25	<5	4201	<10	<10	<2	5	<1
WC11	<5	<5	<5	3	<2	3	59	1	18	<5	1344	<10	<10	<2	4	<1
WC17*	39	33	21	40	2	17	134	26	24	<5	1600	23	14	15	4	1
WKS3	13	12	<5	7	3	18	51	3	39	<5	348	<10	10	<2	4	<1
WKS4	17	17	<5	8	3	22	50	3	48	<5	355	<10	14	<2	4	<1
WKS5	6	<5	<5	<2	<2	6	27	1	13	<5	201	<10	17	<2	4	<1
WKS6	<5	<5	<5	2	<2	4	20	<1	5	<5	129	<10	16	<2	3	<1
WKS7	<5	<5	<5	3	<2	5	28	<1	7	<5	200	<10	11	<2	5	<1
WKS8	11	<5	6	3	2	17	41	2	23	<5	461	<10	<10	<2	5	<1
WPT1	<5	<5	<5	<2	3	4	16	<1	12	<5	62	<10	<10	<2	4	<1
WPT2	<5	<5	15	<2	4	7	35	2	14	<5	107	<10	<10	<2	5	<1

SAMPLE	V	Cr	Ni	Zn	Ga	Rb	Sr	Y	Zr	Nb	Ba	Ce	Nd	La	Pb	Th
WPT3	5	5	<5	<2	3	13	37	<1	21	<5	182	<10	<10	<2	4	<1
WPT4	<5	<5	<5	2	<2	10	33	1	21	<5	426	<10	<10	<2	4	<1
WPT5	6	<5	<5	4	2	15	45	2	21	<5	151	<10	<10	<2	3	<1
WUR1	<5	<5	<5	<2	<2	1	10	3	10	<5	358	<10	<10	<2	4	<1
WUR3*	27	25	11	26	<2	13	52	17	20	<5	1579	<10	<10	9	4	<1
WUR4	10	8	<5	12	<2	4	22	2	6	<5	1133	<10	<10	<2	4	<1
WUR5	13	13	5	19	<2	3	12	1	19	<5	1623	<10	<10	<2	2	<1
WUR7	7	5	<5	7	<2	20	36	1	8	<5	649	<10	<10	<2	4	<1
CR1	38	23	12	12	9	29	58	4	42	<5	507	<10	14	5	5	<1
TG1	28	18	40	21	4	20	75	5	29	5	730	<10	<10	<2	5	<1
WC7	26	26	<5	6	6	26	74	3	34	<5	906	<10	<10	<2	5	<1

A11.2. QUARTZ CRYSTALLINITY

A '-' indicates no identifiable (212) peak, and 'sm' denotes a silicified micrite.

BLF4	-	-	-	MA14	2.1	2.2	2.6	MZL4	1.2	1.2	
CR4	-	-	-	MS1	1.7	1.6	1.8	PS19	0.9	-	
CR10	1.3	1.1	1.3	MS2	1.7	2.5	2.3	PS20	1.2	1.2	
DS9	1.2	1.1	-	MS7	1.6	1.8	0.7	PS29	2.4	1.5	-
DS12	1.7	2.1	2.4	MS9	1.7	2.6	2.1	PS31	-	-	-
DTS4	0.9	0.7		MS10	1.0	0.6		STFDR	-	-	-
DTS5	0.9	0.9		MS10sm	0.7	0.8		TG4	-	-	-
DTS6	1.6	-		MS12a	1.1	1.6	1.2	WB3	3.0	1.3	2.0
DTS8	-	-	-	MS12b	1.7	2.4	2.8	WB8	2.1	1.6	1.4
IC4	3.2	3.3	2.6	MS13	0.8	1.3	1.3	WB13	1.8	1.6	1.8
IC10	2.0	1.9	-	MS14	1.9	1.1	1.4	WB18	3.3		
IC11	0.9	1.3	-	MS18	1.4	1.1	1.3	WB19	1.0	1.0	
IC12	1.7	1.6	1.8	MS24	1.2	1.7		WB20	1.2	2.3	2.3
IC14	3.0	3.4	3.3	MS28	4.4	4.6	5.1	WB21	1.6	2.0	1.8
KP12	-	-	-	MS29	1.1	1.2	1.0	WB23	-	-	-
LS2	1.5	0.9		MS31	-	0.9		WC2	0.9		
LS5	0.9	1.1		MS34	3.4	3.3	3.6	WC5	1.2	1.6	1.0
LS13	1.3	1.8	1.9	MS38	1.3	1.1	0.9	WC8	0.4	0.6	
MA1a	1.5	1.4	1.6	MS41	1.4	1.6	2.3	WKS6	1.0	-	

MA1b	1.5	1.2	MS43	1.1	1.5	WKS8	2.5	2.5	1.4
MA4	0.7		MS43sm	1.7	2.1	WUR1	0.5	1.5	
MA12	1.7	-	MS46	0.4					

A11.3. MAJOR AND TRACE ELEMENT ANALYSES OF INTERBEDDED CHERT AND MUDSTONE

A11.3.1. MAJOR ELEMENTS (Weight% oxide)

SAMPLE	LITHOLOGY	SiO2	TiO2	Al2O3	Fe2O3	MnO	MgO	CaO	Na2O	K2O	LOI	P2O5	TOTAL
LS2	Upper Shale	76.06	0.44	8.33	6.92	0.03	1.23	0.05	0.35	2.34	1.83	<0.05	97.60
	Chert	95.62	0.09	2.22	0.21	0.03	0.28	0.06	0.10	0.64	1.28	<0.05	100.55
	Lower Shale	85.44	0.33	7.07	1.28	0.05	1.04	0.06	0.32	1.90	2.64	<0.05	100.13
MA11a	Shale	83.95	0.34	7.37	1.62	<0.01	1.27	0.09	1.01	1.55	2.30	<0.05	99.51
MA11b	Chert	97.51	0.06	1.04	0.24	<0.01	<0.10	0.03	<0.10	0.19	0.89	<0.05	100.04
MS41	Upper Shale	80.95	0.35	6.72	1.71	0.05	1.17	0.09	0.45	1.36	5.56	<0.05	98.45
	Chert	89.47	0.17	3.19	0.70	0.01	0.41	0.05	0.36	0.62	4.13	<0.05	99.13
	Lower Shale	80.79	0.33	6.35	1.30	0.03	0.91	0.09	0.50	1.26	6.69	<0.05	98.28
WUR3	Upper Shale	74.44	0.42	8.43	3.19	0.03	2.76	1.30	0.59	2.06	5.97	0.56	99.74
	Upper Chert	95.25	0.12	1.85	0.35	0.03	0.16	0.03	0.39	0.36	1.82	<0.05	100.35
	Middle Chert	94.11	0.09	1.75	0.53	0.02	0.32	0.19	0.37	0.26	1.63	0.10	99.36
	Lower Chert	93.18	0.09	1.70	0.43	0.05	0.20	0.18	0.46	0.27	1.77	0.10	98.43
	Lower Shale	69.48	0.53	10.88	3.54	0.05	2.73	1.39	0.47	3.14	7.01	0.59	99.81
MS10	Marl	77.99	0.59	9.71	1.77	0.02	1.58	0.27	0.57	3.28	3.11	<0.05	98.91
	Silic Mic	93.32	0.14	3.00	0.39	0.03	0.35	0.10	0.36	1.06	1.75	<0.05	100.49
	Chert	97.47	0.05	0.95	0.19	0.02	<0.10	0.07	<0.10	0.21	1.20	<0.05	100.27

A11.3.2. TRACE ELEMENTS (ppm)

SAMPLE	V	Cr	Ni	Zn	Ga	Rb	Sr	Y	Zr	Nb	Ba	Ce	Nd	La	Pb	Th
LS2	95	53	14	73	14	93	40	11	96	<5	1739	11	<10	10	5	<1
	15	11	<5	5	2	18	18	2	19	<5	289	<10	<10	<2	4	<1
	60	34	<5	25	11	67	24	7	59	9	449	<10	<10	5	5	3

SAMPLE	V	Cr	Ni	Zn	Ga	Rb	Sr	Y	Zr	Nb	Ba	Ce	Nd	La	Pb	Th
MA11a	132	70	28	83	11	71	118	6	96	5	1834	17	<10	11	5	3
MA11b	9	7	<5	6	<2	7	95	1	9	<5	458	<10	<10	<2	3	<1
MS41	115	114	44	47	9	62	218	10	80	<5	4065	13	<10	5	4	2
	49	64	16	12	3	27	151	5	42	<5	3083	<10	<10	<2	3	1
	108	125	28	28	5	56	347	11	87	<5	6911	19	<10	5	3	<1
WUR3	199	150	70	168	15	92	136	78	92	6	1864	92	63	53	9	12
	27	22	8	10	<2	16	61	23	25	<5	1463	<10	<10	12	4	<1
	28	25	14	35	<2	12	47	14	17	<5	1715	14	10	8	5	<1
	25	28	10	34	<2	12	47	15	17	<5	1559	14	<10	8	3	1
	196	163	45	149	22	129	227	69	103	6	2848	80	54	47	10	13
MS10	102	61	<5	27	16	118	60	10	115	12	1472	14	<10	4	6	2
	23	14	<5	10	4	26	46	2	24	<5	610	<10	<10	<2	5	<1
	12	11	<5	4	3	7	23	2	14	<5	604	<10	<10	<2	4	<1

A11.4. MAJOR AND TRACE ELEMENT ANALYSES OF DETRITAL SEDIMENTS

A11.4.1. MAJOR ELEMENTS (Weight% oxide)

SAMPLE	SiO_2	TiO_2	Al_2O_3	Fe_2O_3	MnO	MgO	CaO	Na_2O	K_2O	LOI	P_2O_5	TOTAL
Woolshed Formation												
BS17	73.96	0.54	12.59	3.17	0.04	1.56	0.15	2.19	2.02	3.65	0.07	99.95
BS18	75.70	0.49	11.86	2.89	0.02	1.32	0.13	2.20	1.82	3.93	0.08	100.45
BS19	83.88	0.37	7.99	1.82	<0.01	0.96	0.14	1.22	1.28	2.52	0.06	100.23
IC4	86.87	0.25	5.59	1.28	0.04	0.93	0.24	0.66	2.02	1.59	0.05	98.51
IC5	86.54	0.30	5.90	1.30	0.05	0.84	0.06	0.75	1.13	1.98	<0.05	98.85
IC25	83.85	0.37	8.05	2.18	0.01	1.05	0.05	1.22	1.37	2.49	0.05	100.70
IC26	80.10	0.45	10.04	2.54	0.02	1.45	0.19	1.42	1.76	1.95	0.06	99.98
KP6	80.51	0.35	7.53	2.21	0.08	0.97	0.25	1.53	1.37	3.40	0.11	98.32
KP7	77.44	0.40	9.35	3.49	0.05	1.23	0.23	2.21	1.51	2.04	0.07	98.02
KP8	79.87	0.40	8.64	2.26	0.06	1.25	0.24	1.67	1.55	3.55	0.09	99.54
KP16	83.23	0.32	6.77	1.08	0.04	0.90	0.15	2.10	1.19	4.08	0.11	99.96

SAMPLE	SiO_2	TiO_2	Al_2O_3	Fe_2O_3	MnO	MgO	CaO	Na_2O	K_2O	LOI	P_2O_5	TOTAL
KP18	92.07	0.15	3.10	0.90	0.02	0.41	0.10	0.87	0.57	2.47	<0.05	100.70
MA11a	83.95	0.34	7.37	1.62	<0.01	1.27	0.09	1.01	1.55	2.30	<0.05	99.51
WC19	83.88	0.37	8.03	1.92	0.02	0.93	0.35	0.97	1.29	2.52	0.08	100.35
WKS2	97.54	0.09	1.78	0.24	<0.01	0.13	0.04	0.15	0.37	0.97	<0.05	101.33
Claverley Sandstone												
WB1	89.54	0.18	5.33	0.40	<0.01	0.26	0.06	1.99	1.00	1.57	<0.05	100.34
WB3	88.68	0.20	5.69	0.84	0.04	0.51	0.09	1.85	1.16	1.72	<0.05	100.79

A11.4.2. TRACE ELEMENTS (ppm)

SAMPLE	V	Cr	Ni	Zn	Ga	Rb	Sr	Y	Zr	Nb	Ba	Ce	Nd	La	Pb	Th
Woolshed Formation																
BS17	78	55	18	104	13	76	96	15	174	8	1037	43	21	22	11	8
BS18					13	71	73	15							9	7
BS19	61	41	16	84	9	55	71	13	119	5	496	38	23	16	9	5
IC4	45	40	11	62	7	10	61	1	77	<5	464	18	16	10	4	<1
IC5	48	36	6	14	7	45	38	5	96	5	773	<10	<10	3	6	<1
IC25	59	48	9	59	10	60	40	12	100	7	554	29	16	14	11	5
IC26	73	47	23	98	12	75	59	24	131	<5	525	49	29	22	13	5
KP6	53	50	37	72	9	52	62	20	117	6	332	53	28	33	8	5
KP7	59	42	16	61	9	57	64	13	125	5	327	44	19	23	11	5
KP8	57	47	23	83	10	59	56	15	107	7	285	49	27	26	10	5
KP16	31	29	<5	12	7	46	50	7	95	<5	164	<10	<10	4	6	3
KP18	19	18	6	20	3	22	38	5	36	<5	122	15	<10	4	5	<1
MA11a	132	70	28	83	11	71	118	6	96	5	1834	17	<10	11	5	3
WC19	54	35	20	65	12	60	175	14	110	9	827	40	20	17	8	5

SAMPLE	V	Cr	Ni	Zn	Ga	Rb	Sr	Y	Zr	Nb	Ba	Ce	Nd	La	Pb	Th
WKS2	65	40	<5	18	11	62	62	10	236	8	343	34	23	16	7	4
Claverley Sandstone																
WB1	17	11	<5	6	5	29	52	5	106	<5	254	<10	<10	3	5	1
WB3	28	18	5	21	4	23	47	4	111	5	352	15	<10	8	4	1